frontiers | Research Topics

The synaptic basis of neuropathology

Edited by
Fereshteh S. Nugent, Alfredo Kirkwood, Carl R. Lupica and P. Jesper Sjöström

Published in
Frontiers in Synaptic Neuroscience

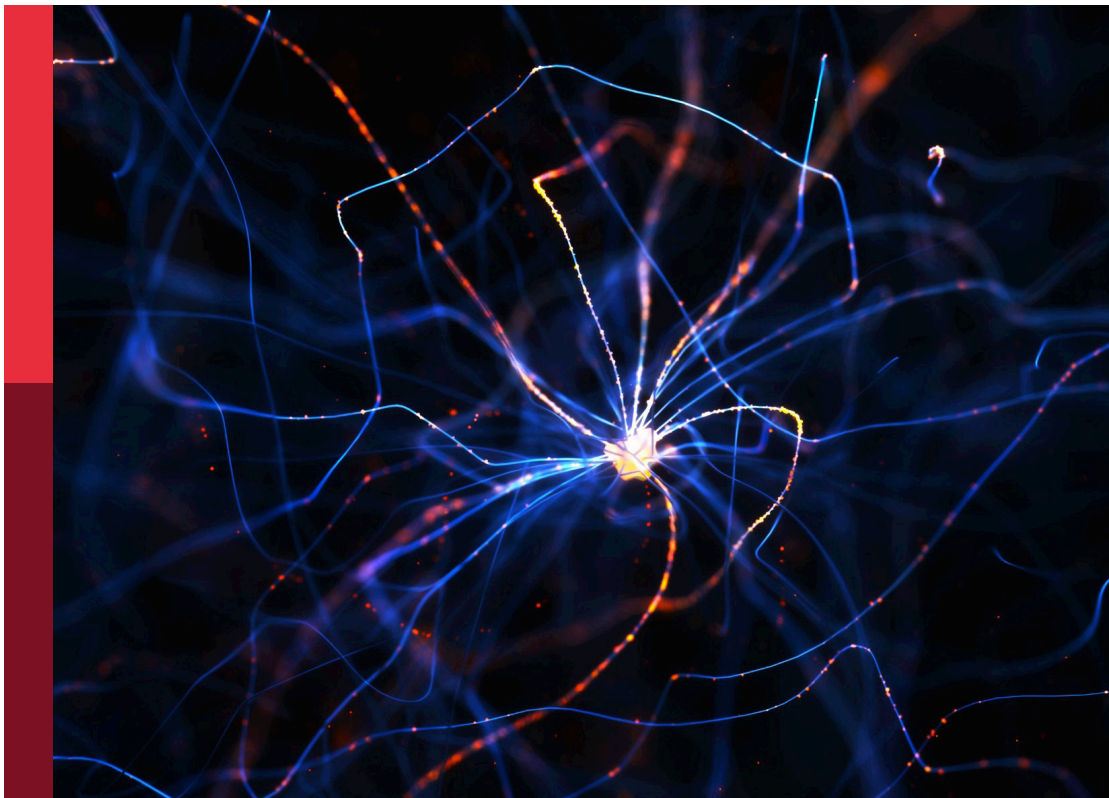

ISSN 1664-8714
ISBN 978-2-83251-978-3
DOI 10.3389/978-2-83251-978-3

About Frontiers

Frontiers is more than just an open access publisher of scholarly articles: it is a pioneering approach to the world of academia, radically improving the way scholarly research is managed. The grand vision of Frontiers is a world where all people have an equal opportunity to seek, share and generate knowledge. Frontiers provides immediate and permanent online open access to all its publications, but this alone is not enough to realize our grand goals.

Frontiers journal series

The Frontiers journal series is a multi-tier and interdisciplinary set of open-access, online journals, promising a paradigm shift from the current review, selection and dissemination processes in academic publishing. All Frontiers journals are driven by researchers for researchers; therefore, they constitute a service to the scholarly community. At the same time, the *Frontiers journal series* operates on a revolutionary invention, the tiered publishing system, initially addressing specific communities of scholars, and gradually climbing up to broader public understanding, thus serving the interests of the lay society, too.

Dedication to quality

Each Frontiers article is a landmark of the highest quality, thanks to genuinely collaborative interactions between authors and review editors, who include some of the world's best academicians. Research must be certified by peers before entering a stream of knowledge that may eventually reach the public - and shape society; therefore, Frontiers only applies the most rigorous and unbiased reviews. Frontiers revolutionizes research publishing by freely delivering the most outstanding research, evaluated with no bias from both the academic and social point of view. By applying the most advanced information technologies, Frontiers is catapulting scholarly publishing into a new generation.

What are Frontiers Research Topics?

Frontiers Research Topics are very popular trademarks of the *Frontiers journals series*: they are collections of at least ten articles, all centered on a particular subject. With their unique mix of varied contributions from Original Research to Review Articles, Frontiers Research Topics unify the most influential researchers, the latest key findings and historical advances in a hot research area.

Find out more on how to host your own Frontiers Research Topic or contribute to one as an author by contacting the Frontiers editorial office: frontiersin.org/about/contact

The synaptic basis of neuropathology

Topic editors

Fereshteh S. Nugent — Uniformed Services University, United States
Alfredo Kirkwood — Johns Hopkins University, United States
Carl R. Lupica — National Institute on Drug Abuse (NIH), United States
P. Jesper Sjöström — McGill University, Canada

Citation

Nugent, F. S., Kirkwood, A., Lupica, C. R., Sjöström, P. J., eds. (2023). *The synaptic basis of neuropathology.* Lausanne: Frontiers Media SA. doi: 10.3389/978-2-83251-978-3

Table of contents

frontiers | Frontiers in Synaptic Neuroscience

TYPE Editorial
PUBLISHED 13 October 2022
DOI 10.3389/fnsyn.2022.1043480

OPEN ACCESS

EDITED AND REVIEWED BY
Atsuo Fukuda,
Hamamatsu University School of Medicine, Japan

*CORRESPONDENCE
Carl R. Lupica
clupica@nih.gov
P. Jesper Sjöström
jesper.sjostrom@mcgill.ca

RECEIVED 13 September 2022
ACCEPTED 29 September 2022
PUBLISHED 13 October 2022

CITATION
Nugent FS, Kirkwood A, Lupica CR and Sjöström PJ (2022) Editorial: The synaptic basis of neuropathology. *Front. Synaptic Neurosci.* 14:1043480. doi: 10.3389/fnsyn.2022.1043480

Editorial: The synaptic basis of neuropathology

Fereshteh S. Nugent[1], Alfredo Kirkwood[2], Carl R. Lupica[3]* and P. Jesper Sjöström[4]*

[1]F. Edward Hébert School of Medicine, Uniformed Services University, Bethesda, MD, United States, [2]Department of Neuroscience, Mind/Brain Institute, Johns Hopkins University, Baltimore, MD, United States, [3]National Institute on Drug Abuse Intramural Research Program, National Institutes of Health, Baltimore, MD, United States, [4]Brain Repair and Integrative Neuroscience Program, Department of Medicine, Department of Neurology and Neurosurgery, Centre for Research in Neuroscience, The Research Institute of the McGill University Health Centre, Montreal General Hospital, Montreal, QC, Canada

KEYWORDS

synapse, plasticity, electrophysiology, microscopy, synaptic dysfunction, GABAergic, glutamatergic

Editorial on the Research Topic
The synaptic basis of neuropathology

Introduction

A growing body of evidence points to malfunctioning synapses and plasticity as key contributors to neuropathology, leading to the idea that there may be a synaptic basis for brain disease (Lüscher and Isaac, 2009; Kilgard, 2012). For example in epilepsy, recurring excessive neuronal activity in the healthy brain can recruit plasticity and result in a pathologically increased susceptibility for seizures (Cela and Sjöström). Both presynaptic (Van Battum et al., 2015; Perrone-Capano et al., 2021) and postsynaptic compartments (Kasai et al., 2021) have been implicated in neuropathology, including autism, amyotrophic lateral sclerosis, Alzheimer's disease, and schizophrenia. Since different synapse types have distinct forms of short and long-term plasticity (Blackman et al.; Larsen and Sjöström, 2015), approaching major brain disease as synaptic neuropathology may increase the likelihood of finding new and more specific treatments. For example, blocking calcium-permeable but not calcium-impermeable AMPA receptors of the cochlea can protect from excitotoxicity due to acoustic overexposure without impairing hearing (Walia et al.).

Here, we organized a Research Topic to highlight the latest advancements in the field of synaptic disease. These articles describe the state of the art by outlining recent developments and major accomplishments.

Papers in this collection

Synapses, plasticity, and learning

Although it is widely accepted that AMPA receptor trafficking is key for expression of long-term potentiation (LTP) at Schaffer collateral synapses to CA1 pyramidal neurons (Díaz-Alonso and Nicoll, 2021), the involvement of specific AMPA receptor domains remains unclear. To address the requirement of GluA1 AMPA receptor subunit in the developmental expression of LTP, Liu et al. used their newly generated knock-in mouse line (GluA1^{C2KI}; Zhou et al., 2018), where the C-terminal domain (CTD) of endogenous GluA1 is replaced by that of GluA2. Unlike the global or conditional genetic deletion of GluA1, the expression of the GluA1 subunit still occurs in these mice, which limits the aberrant formation of AMPA receptor complexes. Using wildtype and GluA1^{C2KI} mouse slices, they showed that the CTD of GluA1 contributed differentially to different forms of LTP.

The Kv family of voltage-gated potassium channels (VGKC) plays an important role in spike generation and propagation in the brain. Several heterozygous mutations in KCNA2, the gene encoding KV1.2 VGKC, have been identified in patients with severe epilepsy (Syrbe et al., 2015; Masnada et al., 2017; Nilsson et al., 2022). For example, in VGKC antibody-associated encephalopathy, high titers of patient-derived autoantibodies against VGKC complex may increase pathogenicity (Vincent et al., 2004). In this collection, Kirschstein et al. investigated in rats the pathogenic effects of patient-derived antisera against Kv1.2 and the VGKC-associated protein contactin-associated protein-2 (CASPR2) by stereotactic antisera microinjection into rat hippocampus. At Schaffer collateral-CA1 synapses, but not medial perforant path-dentate gyrus connections, injection of anti-Kv1.2 but not anti-CASPR2 increased neurotransmitter release, which facilitated post-synaptic depolarization and boosted LTP in CA1 but not the dentate gyrus. Moreover, both anti-Kv1.2 and anti-CASPR2 sera promoted epileptic discharges and hyperexcitability in hippocampus. The authors conclude that although the cellular effects of patient-derived Kv1.2 and CASPR2 antibodies may differ, both presented pathophysiologically relevant VGKC complex-antibodies.

Emerging studies report that fear acquisition alters excitability of infralimbic cortex neurons (Soler-Cedeno et al., 2016; Bloodgood et al., 2018), even though auditory fear conditioning does not elicit infralimbic cortex synaptic plasticity (Pattwell et al., 2012; Sepulveda-Orengo et al., 2013). Rather, plasticity in infralimbic cortex occurs after extinction but not acquisition of fear learning (Pattwell et al., 2012; Sepulveda-Orengo et al., 2013). Still, in male rats, there is evidence for reduced NMDA receptor currents at connections from ventral hippocampus to infralimbic cortex after fear learning (Soler-Cedeno et al., 2016). Castillo-Ocampo et al. wondered if females showed similar plasticity, and therefore tagged these synapses with enhanced yellow fluorescent protein, EYFP. To assess NMDA receptor levels, the obligatory subunit GluN1 was labeled. Using fluorescence-activated cell sorting of infralimbic cortex synaptosomes, the authors surprisingly showed more EYFP+/GluN1+ synaptosomes with greater average expression of GluN1 in male rats after auditory fear conditioning, but not after contextual fear conditioning, indicating a plasticity that was specific to learning paradigm. However, no such NMDA receptor plasticity was found in female rats, suggesting sex-specific auditory fear conditioning mechanisms. The increasing evidence for sex-specific differences in fear learning highlights a need for reassessment since most studies to date have disregarded this possibility.

Neurodevelopment

Taurine is a free amino acid highly abundant in the CNS, particularly early in neurodevelopment, when it has been considered to be involved in trophic functions. Using cell cultures from vertebrate (rat) and invertebrate (*Lymnaea*) models, Mersman et al. examined how taurine affects neurite outgrowth, synapse formation, and synaptic transmission. In rat cell culture, immunocytochemistry revealed that taurine promotes neurite outgrowth and expression of synaptic markers. In *Lymnaea* cell cultures, electrophysiology revealed that taurine promotes formation of new functional synapses. These findings suggest the involvement of taurine in synaptic development mechanisms that are common across phyla.

The brain stem structure known as the lateral dorsal tegmental nucleus (LDT) has long been recognized for its central role in the brain's reticular activating system, where it may mediate sleep, wakefulness, and arousal (Jouvet, 1965). Later studies established that LDT cholinergic neurons, rather than glutamatergic or GABAergic cells, are especially important in this regard (Baghdoyan et al., 1987; Grant and Highfield, 1991; Kayama et al., 1992; Van Dort et al., 2015). In this respect, the LDT was envisaged to be important in regulating homeostatic autonomous brain functions, and resistant to experience-dependent plasticity. However, here Kohlmeier and Polli propose that more recent evidence supports the idea that the LDT and its associated synaptic pathways can undergo significant remodeling as a result of experience and exposure to abused drugs such as nicotine and cannabis. Thus, the authors identify altered synaptic plasticity, neuronal activity, and connectivity of the LDT resulting from prenatal or postnatal stimuli, and they argue that this may alter the LDT's impact on behavior.

Clmp is a synaptic adhesion molecule whose expression peaks neonatally. In the CNS, Clmp also associates with subunits of AMPA receptors and kainate receptors. Jang et al. analyzed the synaptic and behavioral effects of genetically ablating Clmp in synaptic function. In hippocampal CA3 neurons, Clmp deletion

increased the frequency and amplitude of miniature excitatory post-synaptic currents (mEPSCs) mediated by AMPA receptors and kainate receptors. Behaviorally, the deletion enhanced novel object recognition as well as susceptibility to kainate-induced seizures. These findings reveal that Clmp negatively regulates fast synaptic transmission with behavioral consequences.

Autism spectrum disorder

In autism spectrum disorders (ASD), learning of social behaviors and development of social skills are severely compromised (Chevallier et al., 2012). ASD-linked mutations in multiple genes converge on common molecular and cellular pathways that lead to synaptic and neural circuit dysfunction. A major signaling pathway implicated in ASD is β-catenin (Caracci et al.). In this collection, Alexander et al. generated mouse lines with either β-catenin up- or down-dysregulation in cortical glutamatergic neurons to provide direct behavioral evidence for a causal role of β-catenin dysregulation in ASD. To link β-catenin dysregulation in forebrain excitatory neurons to behavioral deficits, they utilized CamKIIα Cre driver mice during an early postnatal period critical for synapse formation and connectivity of neural circuits relevant to ASD. They found that β-catenin upregulation led to social deficits, increased repetitive behaviors, and aberrant expression of ADS-linked genes, whereas β-catenin downregulation prevented behavioral and molecular ASD phenotypes. The study suggests that the β-catenin pathway represents a point of convergence for ASD-linked genes that contribute to synaptic and circuit dysfunction and social deficits.

Cytoplasmic FMR1-interacting protein 1 (*Cyfip1*) and Synaptic Ras GTPase-activating protein 1 (*SynGAP1*) are both important for brain development and function, and there are similarities of action between *Cyfip1* and *SynGAP1* suggesting that haploinsufficiency of either causes intellectual disability or autism (Chen et al., 1998; Kushima et al., 2018). Consequently, Sahasrabudhe et al. explored whether *Cyfip1* haploinsufficiency impacted *SynGAP1* levels and localization. The authors found that in mouse hippocampus, Cyfip1 indeed regulated SynGAP1 anchoring and synaptic localization, and that the two proteins together direct actin polymerization and GAP activity at synapses. Compared to wildtype mice, *Cyfip1*$^{+/-}$ mice had reduced levels of SynGAP1 and GluA1 at synapses, whereas mGluR1/5, GluA2, and F-actin were enhanced. These findings nicely demonstrate how graded changes in levels of a specific protein can effectively be boosted locally at synapses, resulting in an overall large impact.

Banke and Barria investigated the early postnatal development of synaptic function and plasticity in Fmr1 knock-out (KO) mouse, a model of Fragile X syndrome (FXS), the leading monogenic form of ASD. Their electrophysiological measures revealed two prominent features: a large but transient enhanced GluA2 subunit expression of synaptic AMPA receptors that it is over by the 2nd postnatal week, and the virtually complete absence of LTP in the first 3 weeks of age. The results are discussed in the context of the known abnormalities in spine density and shape of Fmr1 KO mice that already manifest at that developmental stage.

Injury and inflammation

The neuropeptide corticotropin releasing factor (CRF, also known as CRH) is widely known for its stress-induced activation of the hypothalamic-pituitary-adrenal axis, but CRF also acts in the brain to directly regulate both positive and negative motivated behavioral response to stressors (Lemos et al., 2012; Lemos and Alvarez, 2020; Baumgartner et al., 2021). Persistent CRF dysregulation following mild traumatic brain injury (mTBI) has been suggested to contribute to chronic psychiatric morbidities with abnormal stress-related neuronal responses and negative affective states associated with mTBI (Fox et al., 2016; Russell et al., 2018; Kosari-Nasab et al., 2019). However, it is unclear how mTBI alters synaptic and neuronal function of CRF neurons. In this collection, Simmons et al. investigated cell-type and sub-region-specific effects of mild blast traumatic brain injury (mbTBI) on CRF neuronal and synaptic function in ventral and dorsal hypothalamic paraventricular nucleus (vPVN and dPVN) using whole-cell recordings in adult male mice a week after injury. While mbTBI did not affect neuronal excitability of CRF neurons in dPVN and vPVN sub-regions, it selectively increased spontaneous firing of dPVN CRF neurons due to mbTBI-induced GABAergic dysfunction. The authors suggest that mbTBI-induced dysregulation of non-neuroendocrine CRF pathways from the dPVN underlies anxiety-like behaviors associated with this model of mTBI (Russell et al., 2018). Their work also highlights that GABAergic synaptic inputs may be more susceptible to mTBI resulting in dysfunction of distinct central CRF neural circuits implicated in mood disorders following mTBI.

Although hot compresses are often used to treat pain and inflammation associated with peripheral nerve damage, the mechanism of this beneficial treatment is largely unknown. In a study by Chan et al. in this collection, behavioral measures and a series of molecular markers of nerve damage were obtained in rats undergoing sciatic nerve chronic constriction injury (CCI) that received either hot compress treatment or no intervention. The investigators found that 40°–42° C compresses reduced inflammation and restored sciatic nerve sensitivity, and that an increase in hyperalgesia seen after this nerve injury was also reduced along with synaptophysin, a protein that may mediate sciatic nerve pain through activation of spinal dorsal horn neurons. Hot compress treatment also dramatically reduced several proinflammatory cytokines, both at the site of injury

and in the brain. Therefore, this study supports the use of hot compresses to treat sciatic nerve pain.

Neurodegenerative disease

Contemporary research in psychiatry has re-ignited interest in the use of psychedelics to treat disorders ranging from depression to anxiety. Psychedelic drugs are agonists at serotonin type 2A receptors (5-HT2A), which are found in high concentrations in brain areas associated with attention, introspection, and memory (e.g., cerebral cortex, hippocampus, and amygdala). Here, Vann Jones and O'Kelly review the use of psychedelics in the treatment of psychiatric disorders and evaluate the hypothesis that they may also provide therapy for dementia and Alzheimer's disease. The authors discuss evidence showing that psychedelics can increase brain metabolism, decrease brain inflammation, and enhance cognitive performance in healthy human subjects, supporting this potential therapy for Alzheimer's patients.

In humans, Alzheimer's disease has a long presymptomatic phase. In contrast, most mouse models—like those based on Aβ precursor protein (APP) transgene to drive pathology *via* oligomeric amyloid-β (Aβ)—often overexpress the molecule of interest, thus greatly accelerating the process. To overcome this limitation, Hrynchak et al. studied the progression of pathology in transgenic mice expressing equal levels of mouse and human APP carrying (FAD)-linked mutations, a line that develops plaques only in old age. The analysis revealed differences across brain regions. Increasing concentrations of Aβ lowered spine density and changed spine morphology in hippocampal CA1 neurons but had no effect in neocortical pyramidal cells.

Synaptic degeneration occurs early in many neurodegenerative pathologies such as Huntington's and Parkinson's diseases (Cheng et al., 2010; Milnerwood and Raymond, 2010), but the mechanisms of synaptic dysfunction and loss are not well-understood. Mounting evidence has implicated Wnt deficiency in adult synaptic degeneration as well as in neurodegenerative diseases (Galli et al., 2014; Liu et al., 2014). To manipulate Wnt signaling in mouse striatum, Galli et al. induced expression of the Wnt antagonist Dickkopf-1. This led to a loss of inhibitory synapses on striatal medium spiny neurons and affected the synaptic transmission of D2 striatal medium spiny neurons. Conversely, turning off Dickkopf-1 to reactivate Wnt resulted in complete recovery of inhibitory and dopamine synapse numbers. Although Wnt signaling has not yet been directly linked to Parkinson's or Huntington's, the findings of Galli et al. highlight Wnt as a promising therapeutic target for brain repair in these neuropathologies.

With a similar rationale, Iuliano et al. performed electron microscopy and biochemical analyses of synaptic proteins and lipids in mouse models of Huntington's disease to identify several pre and postsynaptic molecules whose distribution and concentrations were altered. Their study strengthens the idea that the Huntington's mutation causes age-dependent disruption of the localization and composition of synaptic proteins and lipids that are key to synaptic function. Their findings furthermore support the notion these changes in Huntington's mice reflect those in patients that ultimately lead to cognitive and psychiatric pathology.

Concluding remarks

By providing a thorough overview, this Research Topic sheds light on recent progress made in the synaptic disease field as well as on its future challenges. We hope this collection will inform and inspire future research on the synaptic basis of neuropathology.

Author contributions

FN, AK, CL, and PS wrote the manuscript. All authors contributed to the article and approved the submitted version.

Funding

FN was supported by the National Institutes of Health (NIH)—National Institute of Neurological Disorders and Stroke (NIH/NINDS) Grant#R21 NS120628. AK was supported by RO1-EY012124, PO-AG009973, and RO1-EY025922. CL was supported by DA000599 and the National Institutes of Health, National Institute on Drug Abuse Intramural Research Program. PS was supported by FRQS *Chercheurs-Boursiers* Senior 9 Award #254033.

Acknowledgments

Authors thank Alanna Watt for help and useful discussions.

Conflict of interest

The authors declare that the research was conducted in the absence of any commercial of financial relationships that could be construed as a potential conflict of interest.

Publisher's note

Author disclaimer

The opinions and assertions contained herein are the private opinions of the authors and are not to be construed as official or reflecting the views of the Uniformed Services University of the Health Sciences or the Department of Defense or the Government of the United States.

References

Baghdoyan, H. A., Rodrigo-Angulo, M. L., McCarley, R. W., and Hobson, J. A. (1987). A neuroanatomical gradient in the pontine tegmentum for the cholinoceptive induction of desynchronized sleep signs. *Brain Res.* 414, 245–261. doi: 10.1016/0006-8993(87)90005-9

Baumgartner, H. M., Schulkin, J., and Berridge, K. C. (2021). Activating corticotropin-releasing factor systems in the nucleus accumbens, amygdala, and bed nucleus of stria terminalis: incentive motivation or aversive motivation? *Biol. Psychiatry* 89, 1162–1175. doi: 10.1016/j.biopsych.2021.01.007

Bloodgood, D. W., Sugam, J. A., Holmes, A., and Kash, T. L. (2018). Fear extinction requires infralimbic cortex projections to the basolateral amygdala. *Transl. Psychiatry* 8:60. doi: 10.1038/s41398-018-0106-x

Chen, H. J., Rojas-Soto, M., Oguni, A., and Kennedy, M. B. (1998). A synaptic Ras-GTPase activating protein (p135 SynGAP) inhibited by CaM kinase II. *Neuron* 20, 895–904. doi: 10.1016/S0896-6273(00)80471-7

Cheng, H. C., Ulane, C. M., and Burke, R. E. (2010). Clinical progression in Parkinson disease and the neurobiology of axons. *Ann. Neurol.* 67, 715–725. doi: 10.1002/ana.21995

Chevallier, C., Kohls, G., Troiani, V., Brodkin, E. S., and Schultz, R. T. (2012). The social motivation theory of autism. *Trends Cogn. Sci.* 16, 231–239. doi: 10.1016/j.tics.2012.02.007

Díaz-Alonso, J., and Nicoll, R. A. (2021). AMPA receptor trafficking and LTP: carboxy-termini, amino-termini and TARPs. *Neuropharmacology* 197:108710. doi: 10.1016/j.neuropharm.2021.108710

Fox, L. C., Davies, D. R., Scholl, J. L., Watt, M. J., and Forster, G. L. (2016). Differential effects of glucocorticoid and mineralocorticoid antagonism on anxiety behavior in mild traumatic brain injury. *Behav. Brain Res.* 312, 362–365. doi: 10.1016/j.bbr.2016.06.048

Galli, S., Lopes, D. M., Ammari, R., Kopra, J., Millar, S. E., Gibb, A., et al. (2014). Deficient Wnt signalling triggers striatal synaptic degeneration and impaired motor behaviour in adult mice. *Nat. Commun.* 5:4992. doi: 10.1038/ncomms5992

Grant, S. J., and Highfield, D. A. (1991). Extracellular characteristics of putative cholinergic neurons in the rat laterodorsal tegmental nucleus. *Brain Res.* 559, 64–74. doi: 10.1016/0006-8993(91)90287-6

Jouvet, M. (1965). Paradoxical sleep–a study of its nature and mechanisms. *Prog. Brain Res.* 18, 20–62. doi: 10.1016/S0079-6123(08)63582-7

Kasai, H., Ziv, N. E., Okazaki, H., Yagishita, S., and Toyoizumi, T. (2021). Spine dynamics in the brain, mental disorders and artificial neural networks. *Nat. Rev. Neurosci.* 22, 407–422. doi: 10.1038/s41583-021-00467-3

Kayama, Y., Ohta, M., and Jodo, E. (1992). Firing of 'possibly' cholinergic neurons in the rat laterodorsal tegmental nucleus during sleep and wakefulness. *Brain Res.* 569, 210–220. doi: 10.1016/0006-8993(92)90632-J

Kilgard, M. P. (2012). Harnessing plasticity to understand learning and treat disease. *Trends Neurosci.* 35, 715–722. doi: 10.1016/j.tins.2012.09.002

Kosari-Nasab, M., Sadeghi, T., Bashiri, H., Shokouhi, G., and Salari, A. A. (2019). The blockade of corticotropin-releasing factor 1 receptor attenuates anxiety-related symptoms and hypothalamus-pituitary-adrenal axis reactivity in mice with mild traumatic brain injury. *Behav. Pharmacol.* 30, 220–228. doi: 10.1097/FBP.0000000000000450

Kushima, I., Aleksic, B., Nakatochi, M., Shimamura, T., Okada, T., Uno, Y., et al. (2018). Comparative analyses of copy-number variation in autism spectrum disorder and schizophrenia reveal etiological overlap and biological insights. *Cell Rep.* 24, 2838–2856. doi: 10.1016/j.celrep.2018.08.022

Larsen, R. S., and Sjöström, P. J. (2015). Synapse-type-specific plasticity in local circuits. *CONB* 35, 127–135. doi: 10.1016/j.conb.2015.08.001

Lemos, J. C., and Alvarez, V. A. (2020). The upside of stress: a mechanism for the positive motivational role of corticotropin releasing factor. *Neuropsychopharmacology* 45, 219–220. doi: 10.1038/s41386-019-0510-9

Lemos, J. C., Wanat, M. J., Smith, J. S., Reyes, B. A., Hollon, N. G., Van Bockstaele, E. J., et al. (2012). Severe stress switches CRF action in the nucleus accumbens from appetitive to aversive. *Nature* 490, 402–406. doi: 10.1038/nature11436

Liu, C. C., Tsai, C. W., Deak, F., Rogers, J., Penuliar, M., Sung, Y. M., et al. (2014). Deficiency in LRP6-mediated Wnt signaling contributes to synaptic abnormalities and amyloid pathology in Alzheimer's disease. *Neuron* 84, 63–77. doi: 10.1016/j.neuron.2014.08.048

Lüscher, C., and Isaac, J. T. (2009). The synapse: center stage for many brain diseases. *J. Physiol.* 587, 727–729. doi: 10.1113/jphysiol.2008.167742

Masnada, S., Hedrich, U. B. S., Gardella, E., Schubert, J., Kaiwar, C., Klee, E. W., et al. (2017). Clinical spectrum and genotype-phenotype associations of KCNA2-related encephalopathies. *Brain* 140, 2337–2354. doi: 10.1093/brain/awx184

Milnerwood, A. J., and Raymond, L. A. (2010). Early synaptic pathophysiology in neurodegeneration: insights from Huntington's disease. *Trends Neurosci.* 33, 513–523. doi: 10.1016/j.tins.2010.08.002

Nilsson, M., Lindström, S. H., Kaneko, M., Wang, K., Minguez-Viñas, T., Angelini, M., et al. (2022). An epilepsy-associated $K_V1.2$ charge-transfer-center mutation impairs $K_V1.2$ and $K_V1.4$ trafficking. *Proc. Natl. Acad. Sci. U.S.A.* 119:e2113675119. doi: 10.1073/pnas.2113675119

Pattwell, S. S., Duhoux, S., Hartley, C. A., Johnson, D. C., Jing, D., Elliott, M. D., et al. (2012). Altered fear learning across development in both mouse and human. *Proc. Natl. Acad. Sci. U.S.A.* 109, 16318–16323. doi: 10.1073/pnas.1206834109

Perrone-Capano, C., Volpicelli, F., Penna, E., Chun, J. T., and Crispino, M. (2021). Presynaptic protein synthesis and brain plasticity: from physiology to neuropathology. *Prog. Neurobiol.* 202:102051. doi: 10.1016/j.pneurobio.2021.102051

Russell, A. L., Richardson, M. R., Bauman, B. M., Hernandez, I. M., Saperstein, S., Handa, R. J., et al. (2018). Differential responses of the HPA axis to mild blast traumatic brain injury in male and female mice. *Endocrinology* 159, 2363–2375. doi: 10.1210/en.2018-00203

Sepulveda-Orengo, M. T., Lopez, A. V., Soler-Cedeno, O., and Porter, J. T. (2013). Fear extinction induces mGluR5-mediated synaptic and intrinsic plasticity in infralimbic neurons. *J. Neurosci.* 33, 7184–7193. doi: 10.1523/JNEUROSCI.5198-12.2013

Soler-Cedeno, O., Cruz, E., Criado-Marrero, M., and Porter, J. T. (2016). Contextual fear conditioning depresses infralimbic excitability. *Neurobiol. Learn. Mem.* 130, 77–82. doi: 10.1016/j.nlm.2016.01.015

Syrbe, S., Hedrich, U. B. S., Riesch, E., Djémi,é, T., Müller, S., Møller, R. S., et al. (2015). De novo loss- or gain-of-function mutations in KCNA2 cause epileptic encephalopathy. *Nat. Genet.* 47, 393–399. doi: 10.1038/ng.3239

Van Battum, E. Y., Brignani, S., and Pasterkamp, R. J. (2015). Axon guidance proteins in neurological disorders. *Lancet Neurol.* 14, 532–546. doi: 10.1016/S1474-4422(14)70257-1

Van Dort, C. J., Zachs, D. P., Kenny, J. D., Zheng, S., Goldblum, R. R., Gelwan, N. A., et al. (2015). Optogenetic activation of cholinergic neurons in the PPT or LDT induces REM sleep. *Proc. Natl. Acad. Sci. U.S.A.* 112, 584–589. doi: 10.1073/pnas.1423136112

Vincent, A., Buckley, C., Schott, J. M., Baker, I., Dewar, B. K., Detert, N., et al. (2004). Potassium channel antibody-associated encephalopathy: a potentially immunotherapy-responsive form of limbic encephalitis. *Brain* 127, 701–712. doi: 10.1093/brain/awh077

Zhou, Z., Liu, A., Xia, S., Leung, C., Qi, J., Meng, Y., et al. (2018). The C-terminal tails of endogenous GluA1 and GluA2 differentially contribute to hippocampal synaptic plasticity and learning. *Nat. Neurosci.* 21, 50–62. doi: 10.1038/s41593-017-0030-z

frontiers in Synaptic Neuroscience

HYPOTHESIS AND THEORY
published: 07 February 2020
doi: 10.3389/fnsyn.2020.00003

Plasticity in the Brainstem: Prenatal and Postnatal Experience Can Alter Laterodorsal Tegmental (LDT) Structure and Function

Kristi A. Kohlmeier and Filip S. Polli†*

Department of Drug Design and Pharmacology, University of Copenhagen, Copenhagen, Denmark

OPEN ACCESS

Edited by:
Carl R. Lupica, National Institute on Drug Abuse (NIDA), United States

Reviewed by:
Daniel S. McGehee, The University of Chicago, United States
Thomas Hnasko, University of California, San Diego, United States

****Correspondence:***
Kristi A. Kohlmeier
kak1@sund.ku.dk

†Present address:
Filip S. Polli, Dorris Neuroscience Center, Department of Neuroscience, Scripps Research, La Jolla, CA, United States

Received: *01 November 2019*
Accepted: *14 January 2020*
Published: *07 February 2020*

Citation:
Kohlmeier KA and Polli FS (2020) Plasticity in the Brainstem: Prenatal and Postnatal Experience Can Alter Laterodorsal Tegmental (LDT) Structure and Function. Front. Synaptic Neurosci. 12:3. doi: 10.3389/fnsyn.2020.00003

The brainstem has traditionally been considered an area of the brain with autonomous control of mostly homeostatic functions such as heart rate, respiration, and the sleep and wakefulness state, which would preclude the necessity to exhibit the high degree of synaptic or cellular mechanisms of plasticity typical of regions of the brain responsible for flexible, executive control, such as the medial prefrontal cortex or the hippocampus. The perception that the brainstem does not share the same degree of flexibility to alter synaptic strength and/or wiring within local circuits makes intuitive sense, as it is not easy to understand how "soft wiring" would be an advantage when considering the importance of faithful and consistent performance of the homeostatic, autonomic functions that are controlled by the brainstem. However, many of the molecular and cellular requirements which underlie strengthening of synapses seen in brain regions involved in higher-level processing are present in brainstem nuclei, and recent research suggest that the view of the brainstem as "hard wired," with rigid and static connectivity and with unchanging synaptic strength, is outdated. In fact, information from studies within the last decades, including work conducted in our group, leads us to propose that the brainstem can dynamically alter synaptic proteins, and change synaptic connections in response to prenatal or postnatal stimuli, and this would likely alter functionality and output. This article reviews recent research that has provided information resulting in our revision of the view of the brainstem as static and non-changing by using as example recent information gleaned from a brainstem pontine nucleus, the laterodorsal tegmentum (LDT). The LDT has demonstrated mechanisms underlying synaptic plasticity, and plasticity has been exhibited in the postnatal LDT following exposure to drugs of abuse. Further, exposure of the brain during gestation to drugs of abuse results in alterations in development of signaling pathways in the LDT. As the LDT provides

a high degree of innervation of mesoaccumbal and mesocortical circuits involved in salience, as well as thalamocortical circuits involved in control of arousal and orientation, changes in synaptic strength would be expected to alter output, which would significantly impact behavioral state, motivated behavior and directed attention. Further, alterations in developmental trajectory within the LDT following prenatal exposure to drugs of abuse would be expected to impact on later life expression of motivation and arousal.

Keywords: drug dependency, REM sleep, mesopontine cholinergic, nitric oxide synthase, plasticity, laterodorsal tegmental nucleus

THE LATERODORSAL TEGMENTAL NUCLEUS HAS A PROMINENT ROLE IN CONTROL OF THE SLEEP AND WAKEFULNESS CYCLE (INTRODUCTION)

The laterodorsal tegmentum (LDT) is located in the pontine central gray, just below the caudal portion of the aqueduct, which connects the third and fourth ventricles. The LDT is a heterogeneous nucleus composed of cholinergic, GABAergic and glutamatergic neurons (Vincent et al., 1983; Clements and Grant, 1990; Wang and Morales, 2009). The efferent projections from the LDT stream both rostrally and caudally. Rostral projections include terminations within the thalamus, hippocampus and basal forebrain, whereas, caudal pathways terminate within several nuclei within the pons and medulla (Woolf and Butcher, 1986). Lesion studies in the 1960s revealed the critical role of the LDT in control of the states of sleep and wakefulness (Jouvet, 1965). Follow up work in the 1980s and the 1990s revealed that it was cholinergic neurons of the LDT which were vital for this function, and optogenetic studies in the 2010's have validated the important role of the cholinergic cells in this control (Baghdoyan et al., 1987; Grant and Highfield, 1991; Kayama et al., 1992; van Dort et al., 2015). The cholinergic neurons of the LDT comprise part of the reticular activating system, which is a collection of brainstem nuclei, including the locus coeruleus (LC) and dorsal raphe (DR), which collectively project to the thalamus where they participate in gating of cortical activity underlying states of wakefulness, arousal, and the stages of sleep (Baghdoyan et al., 1987; Steriade et al., 1990). In addition, the cholinergic neurons of the LDT have been shown to play a particular role in gating and controlling rapid eye movement sleep (REM sleep), which is a state when LC and DR neurons are silent (McGinty and Harper, 1976; Aston-Jones and Bloom, 1981; Mansari et al., 1989). Paradoxically, activity of a population of the cholinergic cells of the LDT is highest in REM and during wakefulness, with the lowest activity expressed during slow wave sleep (Boucetta and Jones, 2009; Boucetta et al., 2014). How activity within the same neuronal population can participate in such diametrically opposed behavioral states remains a great source of investigation, but the high activity might involve generation of cortical activity promotive of processing, encoding, and storage of waking life experiences dependent on synaptic strengthening, however, the synaptic homeostasis theory of the function of sleep posits that sleep is a time of synaptic scaling resulting in synaptic weakening (Poe, 2017; Tononi and Cirelli, 2019).

THE KNOWN ROLE OF THE LDT EXPANDS

Although outside of the scope of the early work focusing on the role of the LDT in state control, anatomical tract tracing studies showed that the LDT does not just project upstream to the thalamus, where it controls cortical neuronal firing patterns typical of alert wakefulness and REM sleep, or downstream to pontine and medullary nuclei controlling the classic, motor-related physiological sign of REM sleep, motor atonia (Sofroniew et al., 1985; Cornwall et al., 1990; Steriade et al., 1990; Jones, 1991; Imon et al., 1996). Rather, the LDT projects to a multiplicity of sites, including cortical, sensory, and limbic structures (Satoh and Fibiger, 1986; Woolf and Butcher, 1986; Cornwall et al., 1990). Many of these neuronal sites were not easily incorporated into the classic functional circuits known to play a role in control of states of wakefulness or sleep. Therefore, their presence suggested a role of the LDT beyond state control, however, the functional significance of these other projections was not studied until the mid to late 1990s. One major projection terminates in the ventral tegmental area (VTA) and the nucleus accumbens (NAc), which are central players in the mesoaccumbal and mesocortical pathways of the limbic system (**Figure 1**). Together with the prefrontal cortex, the VTA and NAc comprise the brain's reward circuitry and activity involving alterations in dopamine (DA) within the mesoaccumbal pathway in which they participate is generated by pleasurable and aversive stimuli (Di Chiara and Imperato, 1988; Damsma et al., 1992; Hansen et al., 1993; Kiyatkin and Gratton, 1994).

As the VTA was known to be important in goal-directed behavior based on seminal studies from the 1970's, identification of the projections to the mesoaccumbal pathway had raised speculation that the LDT could be involved in limbic processing of behaviorally-relevant stimuli (Cornwall et al., 1990; Oakman et al., 1995). Investigations of these projections using functional techniques were conducted. Chronoamperometry revealed that electrical stimulation of the LDT resulted in phasic rises of DA in the NAc (Forster and Blaha, 2000). An earlier study using pharmacological stimulation had demonstrated a role

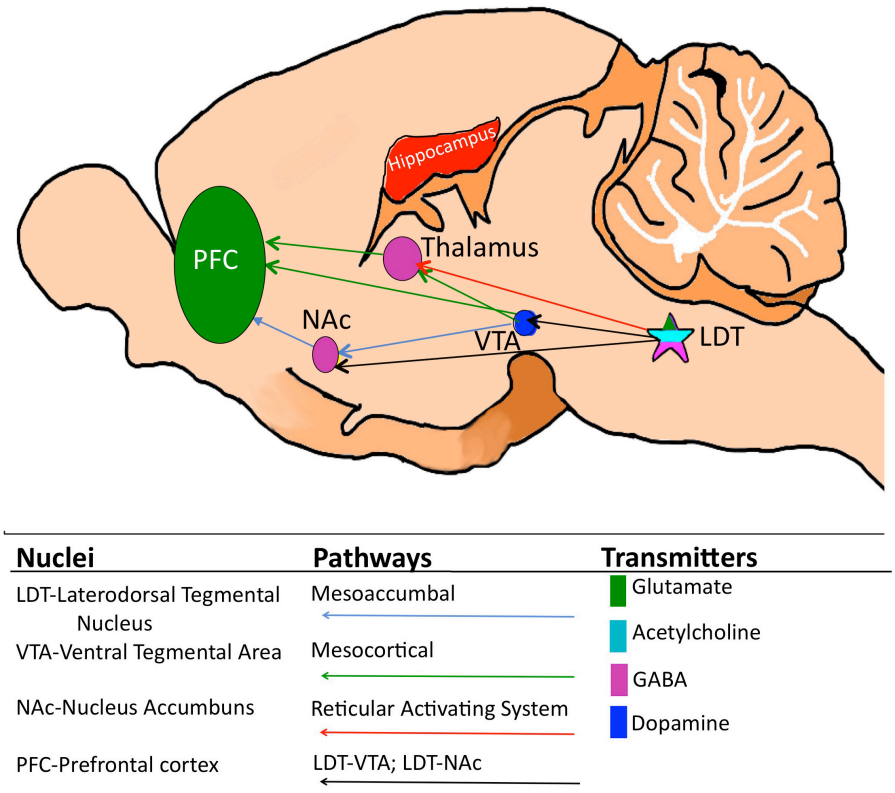

FIGURE 1 | Cartoon of the mouse brain showing relevant corticothalamic, mesoaccumbal and mesocortical pathways and, while not an exhaustive list, the relevant key neuronal phenotypes. The laterodorsal tegmentum (LDT) which is comprised of glutamate, GABA and acetylcholine-containing neurons is located in the pons and sends projections to a multiplicity of brain sites, including the thalamus, the ventral tegmental area (VTA) and the nucleus accumbens (NAc). Via these projections, the LDT governs arousal associated with learning and memory and motivated behaviors, including drug seeking behavior, as well as cortical electrical signatures of arousal.

for LDT cholinergic mechanisms in NAc DA rises (Blaha et al., 1996), which was also seen in the electrical stimulation studies, and further, contribution of a glutamatergic component sourcing from the LDT was also noted (Forster and Blaha, 2000). Investigations of the structural organization of the LDT showed that this nucleus provides glutamatergic and GABAergic synaptic inputs to neurons of the VTA and NAc (Omelchenko and Sesack, 2005; Wang and Morales, 2009). As many regions provide GABA and glutamatergic inputs to the VTA and NAc, this was not as profound as data indicating that the LDT, along with the neighboring pedunculopontine tegmentum (PPT), provides the primary cholinergic input to the mesoaccumbal region, suggesting a potential for domination of cholinergic modulation within these midbrain groups by the two acetylcholine (ACh)-containing brainstem nuclei (Cornwall et al., 1990; Oakman et al., 1995; Omelchenko and Sesack, 2005, 2006; Wang and Morales, 2009). Further, later work showed that cholinergic projections from the LDT are preferentially directed to the lateral region of the VTA, that projects to the lateral shell of the NAc (Lammel et al., 2012), which is a subregion importantly involved in motivating behaviors (Tsai et al., 2009; Witten et al., 2011; Pascoli et al., 2015). When taken together, the anatomical and physiological studies showed that the LDT-VTA-NAc pathway noted in the 1980's was functional. Interestingly, what motivational stimuli share in common, whether they are pleasurable or aversive is their ability to arouse. Once the critical role of the LDT in the reticular activating pathway, and in control of the sleep and wakefulness state was recognized, that might have presaged formulation of the hypothesis of functional influence of the LDT on motivated states earlier than anatomical studies identified the presence of the LDT-VTA-NAc pathway.

The VTA and the NAc Reward Pathway

After decades of study, the VTA-NAc pathway is now known to play a fundamental role in assignment of reward to stimuli, including reward assigned to drugs of abuse, and further, the idea that DA plays a critical role in this function is widely accepted. In the mid 1970s, findings that DA receptor blockers reduced lever press for intravenous amphetamine self-administration in rats led to the suggestion that DA plays a central role in perception and extent of reward (Yokel and Wise, 1975). Studies conducted at the end of the 1980s were among the first to present a common biochemical basis of the rewarding effects of different classes of drugs of abuse. These investigations employed microdialysis methods to measure

extrasynaptic levels of DA in different brain areas, including the NAc. Following peripheral administration of all drugs of abuse tested (amphetamine, cocaine, morphine, ethanol, and nicotine), DA levels in the NAc of freely moving rats were found to exceed basal levels by over 100% and remain elevated for hours, which exhibited a dependency upon drug concentration (Di Chiara and Imperato, 1988).

Further work showed that electrical stimulation of VTA neurons enhanced cueing effects of amphetamine (Druhan et al., 1990), while activation of type 1 DA receptors (D1) in the NAc increased cocaine self-administration and produced conditioned place preference (CPP), which is a behavioral indicator of the rewarding effects of drugs of abuse (White et al., 1991; Robledo et al., 1992). These and other studies lead researchers to propose activation of DA neurons of the VTA, with subsequent release of DA in targets in the NAc, as a central mechanism signaling rewarding effects of drugs of abuse (Di Chiara and Imperato, 1988). Reward reinforcement of behaviors required for continuation of the species, such as sex (Damsma et al., 1992), social interactions (Hansen et al., 1993), and consumption of food (Kiyatkin and Gratton, 1994), were also shown to be mediated by DA VTA-NAc signaling.

Several sources of modulation within the VTA have been shown to lead to drug-induced DA rises. Drugs of abuse exhibit a variety of pharmacological mechanisms, and rises in DA can occur via actions in the synaptic cleft, direct excitation of DA cells, and/or via activation of non-DA VTA cells (Nestler, 2005; Lüscher and Ungless, 2006; Pierce and Kumaresan, 2006). Although there is some debate as to exact proportions, GABA cells comprise the largest population of non-DA VTA cells (Johnson and North, 1992; Margolis et al., 2006), with some contribution from glutamate cells (Nair-Roberts et al., 2008; Yamaguchi et al., 2015). The non-DA cells have been shown to respond to drugs of abuse differentially dependent on drug class with a complex impact on intra VTA circuit dynamics likely affecting encoding of stimuli valence (Hnasko et al., 2012; Yan et al., 2019; Grieder et al., 2019). Drugs not abused by humans, such as imipramine and atropine, fail to induce DA rises in the NAc, while drugs with aversive properties, including κ-opioid agonists, can reduce DA levels within this region, however, interestingly, enhanced activity of DA VTA cells has also been implicated in aversion to nicotine (Di Chiara and Imperato, 1988; Grieder et al., 2019).

Recent development of optogenetic tools allowed further characterization of DA VTA neurons which has shown that they display reward-related firing patterns, and that their activity is sufficient to trigger addiction-related behaviors, the later shown even in the absence of any drug exposure (Tsai et al., 2009; Witten et al., 2011; Pascoli et al., 2015). Taken together, these studies support the conclusion that DA signaling within the NAc, sourcing from VTA neurons plays a key role in the processing of experience-driven reward. Firing of these cells encodes motivational salience which turns an organism toward, or away, from repetition of behaviors leading to acquisition of a stimulus. While this is a necessary process to encourage repetition of healthy behaviors in order to ensure our existence, when the activity is promoted by drug activity, this can be counterproductive. However, while the VTA is critical in signaling salience to natural and drug-related stimuli, it does not work in isolation to encode reward valence in motivational circuits, since DA VTA neuronal firing is strongly influenced by afferent input, which might itself be enhanced by natural or drug-related stimuli.

LDT-VTA INPUTS

In vivo and Pharmacologic Studies of Afferent Input From the LDT to the VTA

The anatomical connectivity from the LDT to the VTA suggested that the LDT likely participates in motivated and salience-related behaviors. Indeed, a functional role of the LDT-VTA pathway in addiction-related behaviors has been corroborated by several *in vivo* and *in vitro* approaches (Satoh and Fibiger, 1986; Cornwall et al., 1990; Oakman et al., 1995). Amphetamine-induced locomotion and behavioral sensitization were shown to be reduced in LDT lesioned rats, suggesting regulation by the LDT of VTA output of DA (Laviolette et al., 2000). Consistent with this, LDT stimulation in anesthetized rats increased DA release into the NAc, which was potentiated by i.p. injections of cocaine (Lester et al., 2010). These effects were attenuated by intra-VTA application of scopolamine, a blocker of mAChRs, suggesting that cholinergic projections in the LDT-VTA pathway are involved in enhancement of accumbal DA release (Lester et al., 2010). However, the role of the LDT in enhancement of DA levels in the striatum might vary depending on the drug class or exposure protocols. While LDT-lesioned rats showed attenuation of DA levels in response to morphine, enhanced DA levels was shown in the same striatal region following administration of amphetamine which was half of the concentration utilized earlier in examination of amphetamine actions in presence of LDT lesion (Forster et al., 2002). Blockade of glutamatergic AMPA receptors in a region of the brainstem encompassing the LDT, which should inhibit LDT excitability, was shown *in vivo* to attenuate reinstatement of drug seeking induced by cocaine injection, an effect also observed after intra-VTA blockage of AMPA, nAChR, and mAChR receptors, suggesting that ACh output from the LDT was involved, with perhaps a contribution from glutamatergic LDT output, and further, that excitatory glutamatergic activity within the LDT was important for drug induced behaviors (Schmidt et al., 2009). A role for glutamatergic activity in the LDT in drug-addiction-associated behaviors was also indicated by intra-LDT pharmacologic blockade of AMPA and NMDA receptors *in vivo* which attenuated cocaine CPP (Shinohara et al., 2014; Kaneda, 2019). This attenuation reached its maximum effect following intra-LDT application of carbachol, which hyperpolarizes LDT neurons when acting at mAChRs, leading to a profound inhibition (Shinohara et al., 2014; Kaneda, 2019). Finally, a study of the role of the functional significance of the LDT-VTA pathway in addiction-related behaviors and signaling provided probably the first indication that drug-related plasticity can occur in the LDT, albeit this was not the focus of the study. AMPA injection in the LDT lead to

sustained enhancements in glutamate recorded in the VTA as well as rises in DA in the NAc in amphetamine-treated rats (Nelson et al., 2007). Interestingly, significant rises in glutamate released in VTA were seen following intra LDT injection of AMPA in non-amphetamine treated controls as well (Nelson et al., 2007). While this did indicate the presence of plasticity in the LDT-VTA pathway leading to heightened LDT output to mesoaccumbal structures, an effect which was termed "LTP-like," direct evidence of the underlying cellular mechanism was not provided as this was beyond the scope of the work (Nelson et al., 2007).

Although these *in vivo* studies certainly contributed to the understanding that the LDT is involved in the circuits critical to dependency, they were technically limited by their inability to demonstrate LDT direct actions in the VTA since effects following nucleus-specific manipulations, including intra-nucleus injections, could have been indirect or included targets beyond those intended. However, evidence of direct involvement of LDT-VTA pathways in motivated behaviors and cellular activity was provided by studies employing optogenetic approaches. Specific opto-stimulation of LDT inputs into the VTA was shown to elicit CPP in mice (Lammel et al., 2012), and photoexcitation of LDT specific cholinergic projections within the VTA was associated with positive reinforcement as CPP was induced (Xiao et al., 2016). Interestingly, in a combined behavioral and optogenetic study which was notable because LDT-VTA cholinergic and glutamatergic terminals were selectively activated under the same experimental conditions allowing a direct comparison of effect, cholinergic input was found to be critical in a CPP assay for reinforcement of remaining in the conditioned chamber, however, glutamate release was determined to be involved in initial entries into the conditioned chamber, suggesting complementary, but separate functions of the two different LDT populations (Steidl et al., 2017).

While the preponderance of studies have shown a role of the LDT in reinforcement of relevant stimuli indicative of a positive valence, activity in the LDT-VTA circuits has also been shown to be involved in coding negative valence underlying aversion. The precise local circuits and pathways involved in coding aversion, however, are not fully elucidated. High doses of nicotine can be aversive (Goldberg et al., 1981, 1983; Goldberg and Spealman, 1982, 1983) which has been shown to involve stimulation of the medial habenula-interpeduncular (IPN) pathway (Fowler and Kenny, 2014). Interestingly, while an earlier study suggested distinct populations of VTA neurons involved in encoding reinforcement and avoidance, with the LDT to VTA projection involved in positive encoding and a projection from the lateral habenula to the VTA regulating aversion (Lammel et al., 2012), a later optogenetic study revealed a role of the LDT in avoidance encoding to aversive doses of nicotine that involved activation of IPN-sourced GABAergic inputs directed to phenotypically-unidentified neurons of the LDT, which projected to the VTA (Wolfman et al., 2018). Further, while not strictly an aversion-inducing stimuli, social defeat stress was associated with hyperactivity of cholinergic and glutamatergic LDT neurons which projected to the VTA, however, further studies indicated that of the two cell types, only cholinergic neurons were involved in maladaptive responses to stress (Fernandez et al., 2018). Although caution in making conclusions was noted, stimulation of LDT cholinergic afferents to DA-VTA neurons was found to enhance the increase in firing noted upon an aversive, paw pinch stimulation (Dautan et al., 2016). While it appears a role is played by GABAergic neurons of the LDT in encoding aversion to olfactory innate fear, and optogenetic activation of this cell type induced fear and anxiety-like behaviors, these actions were not believed to involve subsequent activation of the VTA, and accordingly, different pathways were suggested (Yang et al., 2016). At this time, dissection of the role played by the different LDT neuronal phenotypes in negative reinforcement and stress, as well as elucidation of the mechanisms which can explain how cholinergic, glutmatergic, and GABAergic output from the LDT to likely different populations of DA, and non-DA, cells of the VTA can be involved in encoding both positive and negative valence remain an open area of investigation.

While focus of LDT involvement in studies of motivated behaviors and the role of DA release in these behaviors has been most commonly on cholinergic and glutamatergic input from the LDT to the VTA, direct projections from the LDT to the NAc have been characterized (Dautan et al., 2014). Recently, *in vivo* optogenetic activation of cholinergic inputs sourcing from the LDT and synapsing within the NAc were found to shift preference, enhance motivation, and drive positive reinforcement in drug-related behavioral tests (Coimbra et al., 2019). This finding suggests that LDT involvement in induction of salience can occur independent of LDT modulation of VTA dopaminergic function, which raises the complexity by which the LDT can control output of the mesoaccumbal pathway.

Cellular Studies of the LDT-VTA Pathway

The effect on DA VTA cell activity and output of stimulation of the LDT-VTA pathway has been examined *in vivo* and *in vitro*, and absence or presence of activity in this pathway was found to explain some conflicting data in the literature using these two approaches. The LDT has been shown to regulate activity of DA VTA cells and the pattern of this regulation likely plays a major role in behavioral outcomes. Activation of the LDT nucleus in anesthetized rats revealed an interesting modulation of DA release into the NAc, in which three components were reliably and reproducibly evoked: (1) brief increase in DA release; (2) followed by a decreased DA release below baseline levels; and (3) a sustained DA release for several minutes, which was at levels approximately 80% higher than baseline. The blockage of nicotinic receptors (nAChRs) or ionotropic glutamate receptors in the VTA attenuated the first component, while suppression of the second component was achieved by intra-LDT blockage of muscarinic receptors (mAChRs) suggesting an autoregulatory role. Intra-VTA infusions of mAChR blockers were shown to attenuate the third, sustained component (Forster and Blaha, 2000). When taken together, these data suggested that DA levels in the NAc are selectively mediated by LDT-elicited activation of glutamatergic, nAChR, and mAChR in the VTA, as well as mAChRs on LDT neurons (Forster and Blaha, 2000).

These findings are aligned with previous data showing that both glutamatergic and cholinergic LDT neurons establish multiple, asymmetric, presumably excitatory, contacts with DA-containing VTA cells (Cornwall et al., 1990; Oakman et al., 1995). Fast, direct excitation of DA VTA cells likely occurs at demonstrated postsynaptically-located ionotropic AMPA and nACh receptors (Di Chiara and Imperato, 1988; Forster and Blaha, 2000; Lammel et al., 2012). However, ACh-stimulated excitation is also likely mediated by metabotropic mAChRs. Following earlier studies showing that the DA VTA neuronal population is one of the few in the brain expressing M_5-type mAChRs (Weiner et al., 1990), DA release was shown to be stimulated by LDT-mediated cholinergic excitation of M_5-type mAChRs (Forster and Blaha, 2000; Miller and Blaha, 2005; Lester et al., 2010). The conclusion that activation of M_5 mAChRs leads to sustained increases in DA release within the NAc is supported by a study showing that knockout mice for the M_5 mAChR failed to demonstrate the long-lasting, third component of DA release in the NAc upon LDT-activation (Forster et al., 2002), and by a more recent investigation demonstrating that pharmacological activation of M_5 receptors on VTA neurons potentiates DA release into the striatum (Shin et al., 2015). Another subtype of mAChR also plays a role in DA VTA functioning, as M_4 receptors located on LDT terminals in the VTA were shown to play an autoregulatory function, and limit release of ACh in the VTA (Zhang et al., 2002).

In vivo, behaviorally-relevant release of DA into the NAc occurs upon a burst-firing pattern, which has been shown to rely on an intact LDT, and it was this recognition that reconciled conflicts in the literature that burst firing of VTA cells could be elicited *in vivo*, but not *in vitro* (Lodge and Grace, 2006). The role of the LDT in DA VTA burst firing was reinforced, and refined by optogenetic studies showing that activation of cholinergic LDT projections can alter VTA DA firing such that ongoing firing activity can be shifted, resulting in greater intensity of bursting, presumably resulting in heightened DA output to the NAc (Dautan et al., 2016). In addition, this approach revealed that LDT cholinergic and glutamatergic neurons can modulate firing activity of both DA and non-DA VTA neurons (Dautan et al., 2016). Interestingly, behavioral actions of endogenous peptides which induce arousal, such as those important in appetite control and food seeking behavior, of which ghrelin and orexin are excellent examples, rely on cholinergic tone in the VTA for their activation of DA VTA cells, and, this tone was demonstrated to act at VTA nACh receptors (Borgland et al., 2006; Jerlhag et al., 2012). Both orexin and ghrelin have been shown to induce excitation of LDT neurons, which would be expected to trigger output from the LDT to target regions (Kohlmeier et al., 2004; Takano et al., 2009; Hauberg and Kohlmeier, 2015). In support of this conclusion, ghrelin has been shown to result in concomitant rises in ACh in the VTA and DA in the NAc (Jerlhag et al., 2012). Finally, although the VTA and DA are not incorporated into theories of sleep control circuits, optogenetic evidence suggests revision of this lack of inclusion as an active VTA counters initiation of sleep, and an inhibitory effect on REM sleep was noted (Eban-Rothschild et al., 2016), supporting the interpretation that excitatory afferent input occurs during wakefulness. From all of the studies of the LDT-VTA pathway, a picture has emerged that cholinergic and glutamatergic output from the LDT to the VTA is essential in controlling behaviorally-relevant VTA firing. Actions appear to be direct on DA VTA cells, but as non-DA VTA cells also contain ACh and glutamate receptors, and receive input from the LDT, modulation of their activity following LDT stimulation is also likely involved, but the precise contribution of LDT-stimulated activity of non-DA VTA cells in control of motivated behavior needs to be further elucidated (Mansvelder and McGehee, 2000; Mansvelder et al., 2002; Lammel et al., 2012; Dautan et al., 2014, 2016; Yan et al., 2018, 2019). When taken together, the role of the LDT in activation of mesoaccumbal, with participation also of activity within mesocortical, pathways seems to include stimulation of arousal with the likely outcome of directing orientation and focus of the individual toward the relevant, triggering environmental or internal stimulus. Interestingly, this suggests that the LDT cholinergic inputs to the VTA could exhibit projections and/or firing patterns distinct from those cholinergic LDT cells which exhibit high firing levels during REM sleep.

CELLULAR AND SYNAPTIC MECHANISMS UNDERLYING PLASTICITY

Mechanisms underlying the molecular and cellular basis of learning and memory remain one of the most popular investigative topics in neuroscience because these processes are central to shaping what an individual is, and how they are perceived by others. Understanding the underlying mechanisms of these cognitive-related processes is expected to reveal how the brain actually changes in response to day-to-day experiences. In addition, elucidation of underlying mechanisms of these operations has relevance for understanding and treating disease states which present with alterations in cognition manifested as decrements in learning and memory, such as Alzheimer's disease. Synaptic plasticity is the ability of synapses to change their efficiency and is believed to underlie learning and memory. Several different forms of synaptic plasticity are likely at the heart of re-wiring of the brain in response to experiences. Although changes in the intrinsic properties of cell membranes that govern neuronal excitability have been associated with an activity-dependent, glutamate-independent form of plasticity, coined as intrinsic plasticity (Zhang and Linden, 2003; Lisman et al., 2018; Debanne et al., 2019), functional alterations in glutamatergic receptors seem to play a more central, mechanistic role in synaptic plasticity associated with information storage in cognition-related neural centers (Diering and Huganir, 2018).

A series of electrophysiological experiments conducted in the hippocampus suggested that increases in glutamatergic synaptic strength through both pre- and postsynaptic mechanisms occur, which has been coined Long Term Potentiation (LTP). Blockade

of LTP *in vivo* has been shown to result in cognitive dysfunctions (Abel et al., 1997; Pastalkova et al., 2006; Sacktor, 2008). To date, LTP represents the best mechanistic explanation of the synaptic basis of memory (Bliss and Collingridge, 1993), and corroborates earlier predictions that activity-dependent, synaptic strengthening reflects learning and memory consolidation in the brain (Hebb, 1949). Postsynaptic NMDARs were found to drive most forms of LTP known (Bliss and Collingridge, 2013), and genetic manipulations that impair, or restrict, NMDA receptor functioning or expression induce deficits in learning and memory (Nakazawa et al., 2004). AMPAR activation represents the main mechanism of neuronal depolarization, which allows the Mg^{+2} unblocking of, and calcium signaling through, NMDARs during experience-driven activities. The activation of NMDAR-mediated events, in turn, recruits AMPARs to postsynaptic sites, in which strengthening of synaptic connections is reflected in higher amplitudes of AMPAR-mediated postsynaptic potentials and currents upon subsequent activation within that synapse (Malinow and Malenka, 2002; Kandel et al., 2013). Drugs of abuse have been well established to result in LTP at excitatory and inhibitory synapses in the VTA, which can be transient, and context specific. However, with chronic exposure, this "drug-evoked synaptic plasticity" likely contributes significantly to expression of drug-dependent behavior (for review, see Ungless et al., 2001).

Another mechanism of glutamate-related plasticity was recognized when it was discovered that some postsynaptic sites are composed of only one type of conditionally functional ionotropic glutamate receptor, the NMDAR. Due to the Mg^{+2} blockage, these synapses are not functional at resting membrane potential, as glutamate release from presynaptic sites is unable to induce appreciable levels of currents in the postsynaptic neuron upon binding to the NMDAR. These NMDAR-containing synapses which lack functional AMPAR, were termed "silent synapses" (Isaac, 2003). Silent synapses were found to be abundant during developmental stages (Durand et al., 1996; Isaac et al., 1997) however, their numbers decrease across ontogeny with a very low presence in adulthood, suggesting they play a role in brain circuit maturation. Upon continuous glutamate binding to postsynaptic NMDARs, these synapses were shown to undergo un-silencing processes through recruitment of functional AMPARs (Lee et al., 2013; Dong and Nestler, 2014; Ma et al., 2014). It has been suggested that un-silencing plays a role in establishing new synapses, rewiring brain circuits, and in contributing to LTP establishment (Malenka and Nicoll, 1997; Brecht and Feldman, 2005; Kerchner and Nicoll, 2008; Hanse et al., 2013; Dong and Nestler, 2014).

Interestingly, silent synapses can be generated *de novo* in the brain following certain experiences, such as upon exposure to drugs of abuse, where it is believed they play a role in remodeling reward-processing brain regions (Kerchner and Nicoll, 2008; Hanse et al., 2013; Whitaker et al., 2016; Beroun et al., 2018; McDevitt and Graziane, 2018). However, their appearance or activation upon drug exposure can be dependent on many factors. Acute nicotine application in hippocampal brain slices of newborn rats can activate silent synapses in CA1 neurons, whereas, chronic nicotine exposure in mice was associated with increased number of silent synapses in medium spiny neurons of the striatum (Maggi et al., 2003; Xia et al., 2017), suggesting that the outcomes of nicotine-induced alterations, and perhaps also of other drugs, on silent synapses likely depends on brain areas, drug concentration, and developmental phase at which drug exposure occurs. When taken together, silent synapses represent a powerful mechanism of metaplasticity in the brain, that can be either generated or unsilenced in a region-specific, age-dependent fashion and which appear to be dynamically controlled by drugs of abuse, which likely importantly contribute to drug-induced remodeling of reward-related circuits (Abraham and Bear, 1996; Brown et al., 2011; Lee et al., 2013; Huang et al., 2015; Dong, 2016).

EVIDENCE OF PLASTICITY AND METAPLASTICITY IN THE LDT

Given the role of LTP and silent synapses in learning and memory, induction and presence of these processes have been examined predominantly in forebrain regions with little focus on the brainstem, although AMPAR-present, silent synapses were shown postsynaptically in the nucleus tractus solitarii (Balland et al., 2008). Although plasticity in the LDT had been postulated based on behavior, microdialysis, and lesion studies (Nelson et al., 2007), and a mechanism of presynaptic plasticity was shown by recording identified cholinergic LDT neurons following chronic administration of cocaine which resulted in increases in glutamate release from presynaptic terminals that reversed after 5 days post treatment (Kurosawa et al., 2013), the ability to induce glutamate receptor-dependent postsynaptic LTP in the LDT, or the presence of NMDAR-containing silent synapses in this nucleus, had not been previously shown at the cellular level. However, recent studies from our lab have demonstrated that silent synapses are present in the LDT at juvenile stages (Polli and Kohlmeier, 2019), and further, that LTP can be induced in neurons of this nucleus.

The LDT was originally designated Ch6, based on presence of cholinergic neurons, however, this phenotype represents the minority of cells in this nucleus with GABA and glutamate neurons outweighing the numbers of cholinergic cells, and the three types exhibit some regional specificity across the rostral, medial, and caudal LDT (Wang and Morales, 2009; Luquin et al., 2018). The majority of cholinergic cells can be identified by the combination of a polygonal-shaped large soma, and presence of an A-type K^{+} current without/with a T-type Ca^{+2} current, defined as type III or II neurons, respectively (Leonard and Llinás, 1990). Small, round-shaped neurons with exclusive presence of T-type Ca^{+2} current are putatively GABAergic neurons, and are classified as type I. Glutamate cells are intermittent in size, albeit mostly smaller than cholinergic ones (Boucetta and Jones, 2009). We have recently confirmed the high-degree of correlation between soma size, and presence of A- or T-type currents, with phenotype in the LDT (Polli and Kohlmeier, 2019). In a protocol employing minimum external stimulation designed to reveal silent synapses, presence of synapses with

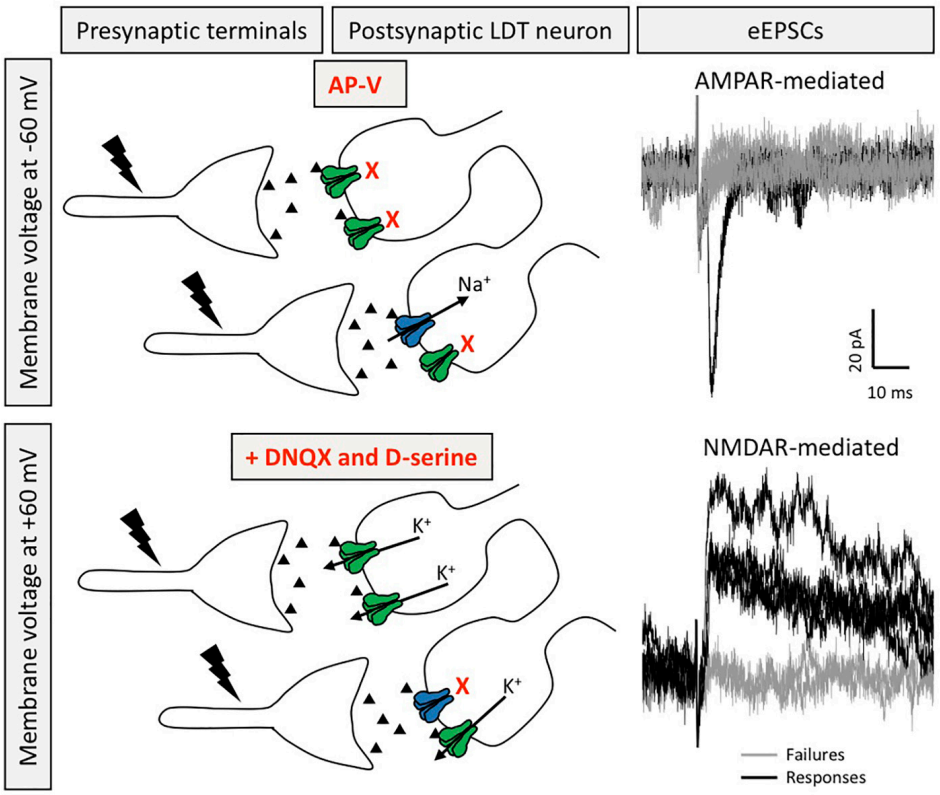

FIGURE 2 | Silent synapses are present in LDT neurons. Silent synapses were identified in *ex vivo* brain slices from juvenile mice using the minimum stimulation protocol, in which several EPSCs are evoked (0.1 Hz) at resting membrane potential in the presence of the NMDAR blocker AP-V and with QX-314 in the patch pipette to block voltage gated sodium channels in order to isolate AMPAR-mediated responses in absence of elicitation of action potentials **(top)**. After washout of AP-V, in the presence of DNQX and D-serine, the voltage command is set to a depolarized membrane potential to evoke NMDAR-mediated EPSCs recorded as outward potassium currents **(bottom)**. Silent synapses are calculated by the comparison of the failure rate between NMDAR- and AMPAR-mediated eEPSCs. Recordings in black denote eEPSCs, whereas gray traces depict failures (for both conditions). Postsynaptic receptors shown in blue are AMPAR and those in green are NMDAR.

NMDA receptors and absence of functional AMPA receptors were found in three cell types in the juvenile LDT (Polli and Kohlmeier, 2019; **Figure 2**). Further, pilot studies found that while not present in every cell examined, LDT neurons from juvenile mice can exhibit increases in synaptic strength at glutamatergic synapses upon theta-burst stimulation (TBS; **Figure 3**). Although we did not conduct a systematic study that would have allowed us to compare response proportions, this effect did appear in Type I, Type II, and Type III LDT cells. As this form of LTP was elicited by coupling the TBS protocol with depolarization of the postsynaptic neuron (see section "Methods"), this suggests the possibility of a NMDAR-dependent LTP mechanism in these cells, a hypothesis which is currently under investigation in our lab. When taken together, these published and preliminary cellular findings have led us to conclude that glutamate receptor-involved, cellular processes resulting in alterations in synaptic strength exist within all phenotypes examined within the LDT. Further experiments combining high-resolution imaging, molecular quantification of protein synthesis, and electrophysiological recordings in optogenetically-identified neuronal subtypes would provide confirmation of these data, and allow a full characterization of the processes involved in this phenomenon.

Evidence for Plasticity Induced Within the LDT by Exposure to Drugs of Abuse in the Postnatal Period

Development of drug dependency includes a large, learning component, albeit a maladaptive one. Plasticity mechanisms seen in other forms of learning have been shown in brain regions exposed to drugs of abuse and are believed to be involved in progression of drug-dependent behavior. When drugs of abuse are utilized, the entire brain is exposed and the LDT is no exception. Therefore, as plasticity is involved in the neural process leading to drug dependency, it would be of interest to know whether different classes of drugs that are abused and which have been shown to induce plasticity in midbrain and cortical regions, induce plasticity in the LDT. However, up until a few years ago, little was known regarding whether cellular actions can be engendered in the LDT by first-time, acute exposures to drugs which are commonly abused. As a step to elucidate the role the

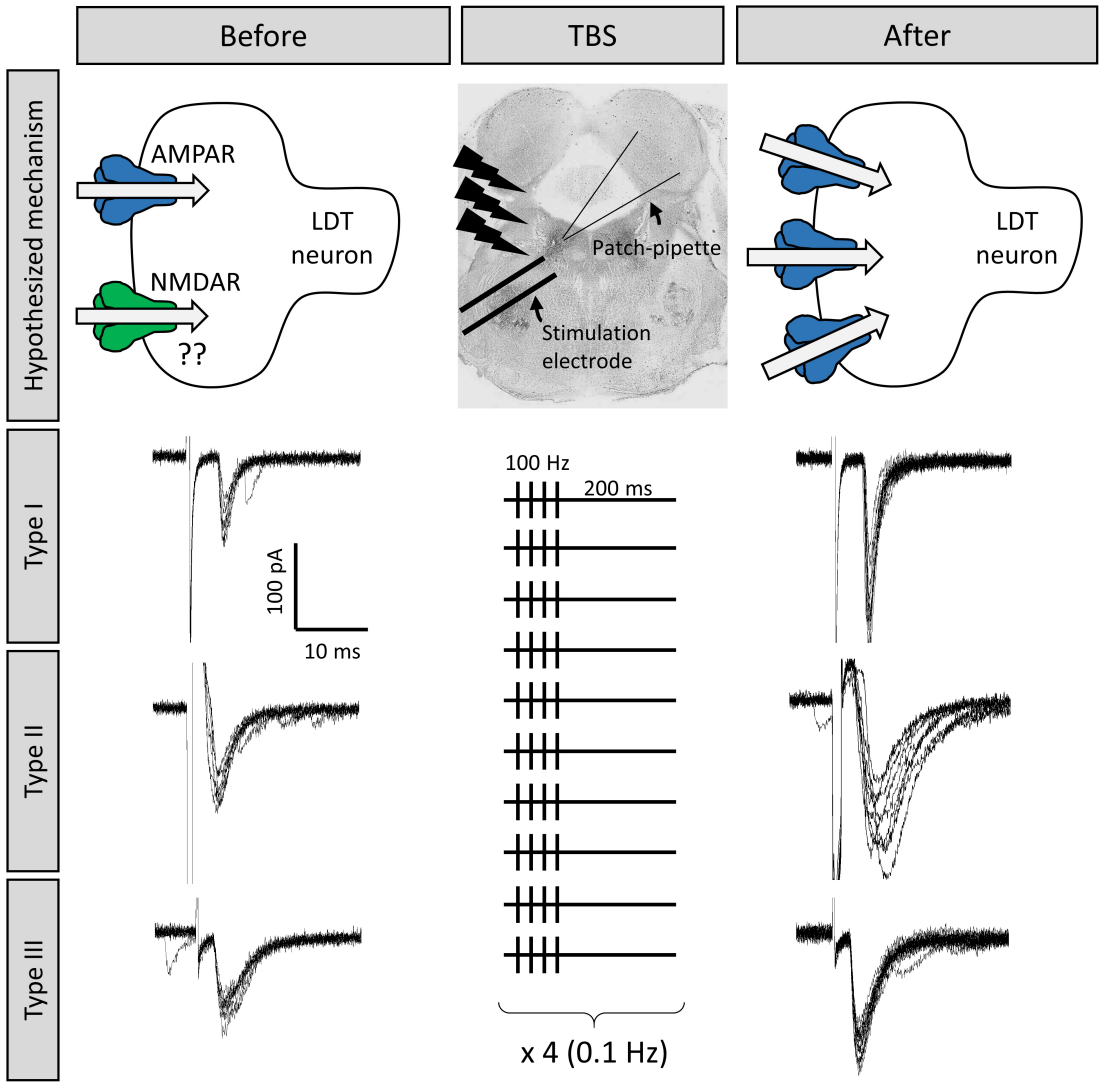

FIGURE 3 | Long term potentiation (LTP) could be induced at LDT synapses, which was an effect seen in all three cell types. Shown are the responses of three different LDT neurons representative of the three electrophysiological cell types in the LDT to electrical stimulation of nearby glutamatergic afferents The top middle panel shows the location of the stimulation electrode in the LDT. Stimulation is adjusted until inward current with similar amplitude is consistently evoked (electrophysiological traces to the left). Following a 100 Hz, theta-burst stimulation (TBS) protocol (shown in the middle panel, see section "Methods" for more details), combined with a simultaneous depolarization of the recorded cells, the amplitude of the inward current was enhanced in these cells (electrophysiological traces to the right), which was a persistent effect, indicative of LTP, likely due to insertion of AMPA receptors into the postsynaptic membrane (top images).

LDT plays in drug dependent behaviors at a cellular level, we have recently conducted *ex vivo* electrophysiological studies in order to assess the responsiveness of LDT neurons to acute exposures to different drugs of abuse associated with induction of plasticity in midbrain and cortex.

All the drugs of abuse which we tested *ex vivo* for acute cellular actions on LDT cells were shown to induce effects. Local applications of a cannabinoid 1 receptor (CB1R) agonist to cholinergic LDT cells elicited calcium release from intracellular calcium stores, and decreased the frequency of inhibitory postsynaptic currents (IPSCs) of LDT neurons, suggesting the functional presence of CB1Rs within the LDT nucleus which plays a role in induction of depolarization-induced suppression of inhibition (Soni et al., 2014). Further, acute bath application of cocaine or amphetamine was shown to elicit intracellular calcium rises in LDT neurons. This effect was abolished by prior exhaustion of intracellular calcium stores, and reduced in the presence of DA receptor antagonists (Lambert et al., 2017). In addition, nicotine excitation of LDT neurons has been demonstrated which was sufficient to induce firing, and rises in calcium in cholinergic neurons (Ishibashi et al., 2009).

As acute exposure to CB1R agonists and stimulants led to excitation of LDT cells, and since these drugs have been shown to induce plasticity in other brain regions, we have speculated that they could induce plasticity in the LDT, as there is functional evidence to support the conclusion that changes in

synaptic strength do occur in the LDT which would alter output to target regions upon exposure to stimulants. Lesion of the LDT led to reductions in amphetamine behavioral sensitization, and chemical stimulation of the LDT 2 days after systemic amphetamine administration led to increases in glutamate levels in the VTA which was suggestive of LTP-like plasticity within the LDT-VTA circuit (Nelson et al., 2007). While not examined with amphetamine, although AMPA/NMDA ratios have been shown to be altered in the mesolimbic midbrain structures by relatively short term exposures to cocaine, short and longer term exposures did not alter this ratio in the LDT as examined *ex vivo* (Kamii et al., 2015). However, a 2-week exposure to cocaine in rats did reveal heightened presynaptic release of glutamate onto cholinergic LDT neurons (Kurosawa et al., 2013). Further, the increase was shown to involve NMDA receptor activation, production of nitric oxide and likely involved glutamatergic synapses derived from the mPFC. A similar effect on inhibitory transmission was not noted. However, reductions in GABAergic inhibition were induced by noradrenaline-mediated actions on presynaptic alpha-2 adrenoreceptors, which was an action only seen in cocaine-treated animals, suggestive of drug-induced presynaptic plasticity in the LDT involving the inhibitory system (Taoka et al., 2016). Repeated administration of cocaine was also shown to lead to an increase in firing rate of cholinergic LDT neurons, that was attributed to enhancement of a persistent sodium channel, which is considered a form of intrinsic plasticity (Kamii et al., 2015). Inhibition of this sodium channel abolished cocaine-induced CPP, suggesting the heightened excitability of the cholinergic cells was critical for encoding of motivational drive (Kamii et al., 2015). When taken together, the data suggest that in drug-experienced animals, enhanced membrane excitability in combination with presynaptic facilitation of glutamatergic drive results, and output of cholinergic LDT cells is heightened which could include output from the LDT in the VTA and NAc. Although the AMPA/NMDA ratio did not alter with cocaine (Kamii et al., 2015), based on *in vivo* LDT data with amphetamine (Nelson et al., 2007), and the mechanisms underlying plasticity induced by a variety of drugs of abuse in other neuronal regions (Bellone and Luscher, 2006; Nelson et al., 2007; Yuan et al., 2013; Pascoli et al., 2015), it could be speculated that under different drug exposure protocols, changes could occur postsynaptically in glutamate receptors in the LDT which could contribute to changes in excitability. Further, the excitatory drive would be facilitated if NA input, which would presumably be high during the stress of drug-seeking behaviors in drug experienced rodents, led to decreases in GABAergic inhibition via disinhibitory mechanisms reliant on NA tone (Taoka et al., 2016). Unfortunately, to the best of our knowledge, cocaine is the only drug of abuse that has been shown to induce glutamate-receptor dependent plasticity, which has been examined for a similar effect in the LDT. However, as the glutamatergic synaptic machinery necessary for altering synaptic strength is present in the LDT, the effects of acute and chronic exposure to other drugs of abuse on glutamate-based changes in synaptic strength should be examined in the LDT. Nevertheless, we conclude that drugs of abuse lead to heightened activation of the VTA via indirect actions on the LDT, and further, we speculate that input to the reward circuitry from the LDT in response to drugs of abuse does not remain fixed, but the drug exposure shapes or leads to variations in input to the VTA or NAc, even when the stimuli remains the same, due to glutamate receptor-based, postsynaptic plasticity within synapses of the LDT.

Evidence for Plasticity Induced Within the LDT by Drugs of Abuse in the Prenatal Period

Recent studies conducted in our laboratory have provided knowledge toward understanding of the flexibility that the LDT exhibits in neuronal trajectory dependent on the environment present during development. We have exposed pregnant mice to nicotine via their drinking water and by use of prenatal nicotine exposed (PNE) offspring, monitored the functionality of the LDT postnatally with implications for a role of the LDT in negative behavioral outcomes seen in those exposed to nicotine in the prenatal period, including a higher susceptibility for development of dependency to drugs of abuse (Polli and Kohlmeier, 2018, 2019). Our focus was on alterations in the juvenile brain, as this is the riskiest time for negative behavioral outcomes if drugs of abuse are utilized during this period in ontogeny, which is an association seen in both non-prenatally exposed individuals and those exposed prenatally to nicotine during gestation. Further, this period is when great changes are occurring in LDT neuronal maturation, with pruning of synapses and loss of total cell numbers in the LDT (Ninomiya et al., 2005). Accordingly, permutations of the normal progression of these processes would have a large impact on signaling saliency within reward-related areas later in life, especially if those changes rode on top of the ontologically-associated, high risk for dependency.

Presynaptic Glutamate Release

Ionic currents resulting from activation of membrane-inserted, ionotropic receptors can be pharmacologically isolated, which allows determination of occurrence of specific neurotransmitter signaling, such as glutamate, in the form of spontaneous and miniature excitatory postsynaptic potentials (sEPSCs and mEPSCs), with mEPSCs amplitude and frequency reflecting effects of action potential-independent glutamate release. While the amplitude of such currents has been correlated with postsynaptic function of glutamate receptors, particularly AMPAR, examination of the frequency by which these currents occurs has been a common initial analysis approach to investigate alterations in the probability of glutamate release from presynaptic terminals. A higher frequency of postsynaptic currents predicts a greater degree of glutamatergic release directed to a neuron, whereas a reduced frequency of EPSCs likely reflects a reduced degree of active glutamatergic input to the recorded neuron.

In our work, we have found a reduced frequency of mEPSCs in putative cholinergic LDT neurons associated with PNE treatment, suggesting a lower probability of activity-independent glutamate release from presynaptic terminals within this nucleus (Polli and Kohlmeier, 2018). A more direct assay of presynaptic release employs a paired pulse stimulation protocol resulting in

two evoked EPSCs (eEPSCs), elicited by an external electrode placed nearby a patch-clamped, recorded neuron. Under such conditions, glutamate release probability can be estimated by the ratio between the amplitude of the first and second eEPSCs, in which an increased ratio is observed under decreased glutamate release conditions. This phenomenon is called short-term facilitation, and can be mechanistically explained by the residual calcium hypothesis, in which calcium at presynaptic terminals resulting from the first stimulation builds up with that from the second, leading to a potentiation in the number of vesicles released from presynaptic terminals, and an enhanced postsynaptic response during the second stimulation, which reveals a reduced probability of glutamate release at the first stimulus (Malinow and Malenka, 2002). By having employed this protocol in PNE male juveniles, paired pulse facilitation was found in putative cholinergic LDT neurons, which was reflected as reduced glutamate neurotransmission within these cells (Polli and Kohlmeier, 2018). These findings are consistent with the interpretation that PNE treatment results in reductions in glutamatergic drive directed to postsynaptic cholinergic neurons within the LDT, which corroborates findings of a smaller frequency of mEPSCs seen in the PNE.

AMPA Receptors

The ontological expression of ionotropic glutamate receptor subunits in the rodent brain has been well characterized for both AMPA and NMDA receptors, and identified changes in the balance of these subunits throughout the lifespan suggest they play different functional roles during development, in which their subunit switch represents a key step in the maturation of glutamate signaling (Roberts et al., 2009; Henson et al., 2012; Diering and Huganir, 2018). Among AMPARs, a central process in receptor maturation is the insertion of GluA2 subunits in the postsynaptic AMPAR during development, which contributes to the stabilization of synapses (Diering and Huganir, 2018). In contrast to what is understood about post-translational editing of mRNA coding for the other AMPAR subunits, GluA2 mRNA editing promotes a codon exchange in the pore-forming M2 segment, in which a glutamine codon in the GluA2 gene is substituted by an arginine codon (Sommer et al., 1991). This alteration has a dramatic impact on AMPAR function, as it impairs the calcium permeability of the receptor, reduces single-channel conductance, and decreases intracellular polyamine blockage (Washburn et al., 1997). Accordingly, AMPARs composed of GluA1/3/4 subunits, and lacking GluA2, display higher conductance, calcium permeability, and inward rectification of the receptor current-voltage relationship. These calcium permeable AMPARs (CP-AMPAR) are highly expressed during the first postnatal weeks within the cortex, hippocampus, and VTA (Kumar et al., 2002; Ho et al., 2007; Bellone and Mameli, 2011), but decrease in presence due to a relatively higher insertion of GluA2 subunits which occurs across age. Interestingly, a higher functional presence of the immature CP-AMPAR seems to be a common brain outcome following exposure to drugs of abuse, and has been reported after postnatal administration of cocaine, morphine, and ethanol (Bellone and Luscher, 2006; Billa et al., 2010; Purgianto et al., 2013; Hausknecht et al., 2015). We have recently reported that PNE is associated with electrophysiological alterations in AMPAR-mediated signaling in the LDT, that were suggestive of an enhanced functional presence of CP-AMPARs among putative cholinergic neurons within the LDT nucleus that was confirmed by a demonstrated greater action of the pharmacological blocker of CP-AMPAR, NASPM, on AMPAR-mediated currents in PNE LDT neurons (Polli and Kohlmeier, 2018). Thus, we concluded that PNE treatment was associated with enhanced functional presence of the immature CP-AMPAR within the large LDT neurons of juvenile mice, resulting in enhanced AMPAR-mediated signaling responsiveness, including a higher amplitude of mEPSCs.

NMDA Receptors

NMDA receptors also show PNE-associated changes in the LDT. Interestingly, the subunits affected are the same ones implicated to play a large role in TBS-induced LTP, and in drug-induced LTP in other brain regions where this has been examined. The GluN2B NMDAR subunit has been suggested to play a central role in brain mechanisms of plasticity associated with several physiological brain functions, including learning and memory (Qiu et al., 2011). Studies have demonstrated that activation of GluN2B subunits is necessary for cortical plasticity (LTP) and fear contextual memory (Zhao et al., 2005). This subunit is also involved in synaptic plasticity within the amygdala and hippocampus (Berberich et al., 2007; Miwa et al., 2008). Further, studies using transgenic mice found that the overexpression of GluN2B subunits in the forebrain induces higher activation of NMDAR and facilitates expression of hippocampal LTP, which was associated with enhanced learning and memory in several behavioral tasks (Tang et al., 1999). Complementary results were seen in aged mice, in which memory was rescued by upregulation of GluN2B subunits (Brim et al., 2013). The key role of GluN2B subunits in cognitive processes is further supported by observations of downregulation of this subunit in neurodegenerative disorders that present with cognitive dysfunctions. Lower expression of GluN2B subunits was reported in a rat model of Parkinson's disease (Dunah et al., 2000), and lower levels of this subunit were found in human postmortem brains from individuals diagnosed with Alzheimer's disease (Sze et al., 2001; Mishizen-eberz et al., 2004). In our PNE model, we reported higher functional presence of GluN2B subunits within synaptic sites in small, Type I, putatively GABAergic LDT neurons in the PNE (Polli and Kohlmeier, 2019). Given the role of the GluN2B subunit in other regions, our data suggest that these cells might undergo a potentiated form of LTP, in addition to an observed enhancement of sustained depolarization upon synaptic NMDAR activation due to actions on current kinetics conferred by the presence of GluN2B. Further, we saw a reduced functional presence of this subunit in putatively cholinergic LDT neurons (Polli and Kohlmeier, 2019), which could predict impairments or attenuated LTP induction within this cell population in PNE juveniles.

The GluN3 subunit plays a vital role in the maturation of NMDARs and supports stabilization of glutamate signaling. Expression of this subunit increases and becomes widespread during the first postnatal days, but declines to very low levels

throughout the lifespan (Pachernegg et al., 2012). In addition, this subunit is found at the postsynaptic density at PND8, but moves to perisynaptic and extrasynaptic sites shortly after and is not seen at postsynaptic domains during juvenile stages (Pérez-Otaño et al., 2006, 2016; Henson et al., 2012). GluN3A-containing NMDARs are characterized by a fast, desensitizing current and low calcium conductivity (Sasaki et al., 2002; Henson et al., 2010; Grand et al., 2018). We have reported that large, type II + III PNE LDT neurons, which likely include a majority of cholinergic neurons, displayed NMDAR kinetic activity typical of receptors containing GluN3A subunits, including reduced inward current and smaller intracellular calcium rises upon NMDA application, as well as a faster desensitization when agonist was applied in a manner designed to facilitate extrasynaptic receptor activation. While our data strongly suggested a higher functional presence of GluN3A subunits in these neurons, unfortunately, the lack of commercialized drugs that could specifically bind GluN3A sites (Pérez-Otaño et al., 2016) was a hindrance to definitively examining presence of this subunit. However, we believe that alterations in the GluN3A subunit in the PNE underlie our findings, as we were able to directly eliminate a role for the other potential subunit that could explain our data which is also found extrasynaptically, the GluN2D (Polli and Kohlmeier, 2019). As further support of our hypothesis of a heightened functional presence of GluN3A, expression of this subunit predicts GluA2-lacking AMPAR insertion at postsynaptic densities (Roberts et al., 2009; Yuan and Bellone, 2013), which is consistent with our findings of an enhanced GluA2-lacking functionality in the PNE. When taken together, we hypothesize that GluN3A subunit expression is altered in the PNE in putative cholinergic neurons. An enhanced insertion of GluN3A subunits following drug exposure would not be novel, since postnatal cocaine administration was shown to exert such alteration in DA VTA neurons (Yuan et al., 2013). Interestingly, prolonged expression of GluN3A subunits has been associated with higher liability for drug dependence, as well as cognitive and motor disabilities that have also been shown in humans to be associated with a higher risk following gestational nicotine exposure (Liu et al., 2009; Roberts et al., 2009; Spanagel, 2009; Marco et al., 2013; Yuan et al., 2013; Jin et al., 2014; Kehoe et al., 2014; Yang et al., 2015; Pérez-Otaño et al., 2016).

Silent Synapses

Exposure to drugs of abuse has been shown to reactivate plasticity mechanisms seen during development in addiction-associated brain regions, which may play a role in the formation of addiction-related memories (Dong and Nestler, 2014) as reactivation of silent synapses remodels brain circuits and alters behavior, including those which are addiction-related (Brown et al., 2011; Lee et al., 2013). Higher rates of silent synapses in the rodent brain have been associated with cocaine, alcohol, nicotine, and morphine administration, which was an effect found mostly in NAc GABAergic populations (Huang et al., 2009; Graziane et al., 2016; Xia et al., 2017; Beroun et al., 2018). Our laboratory was the first to show functional evidence that LDT neurons of juvenile mice display silent synapses (**Figure 2**), and, further, that PNE treatment has an impact on their expression. While no differences were seen in silent synapses in cholinergic neurons following PNE treatment, an increased number of silent synapses were seen in putative GABAergic LDT neurons, which parallels the enhanced silent synapses seen in inhibitory NAc neurons following postnatal drug administration (Xia et al., 2017). The higher number of silent synapses seen in putative GABAergic LDT neurons associated with PNE treatment provides indirect support of the interpretation that PNE is associated with a delayed maturation of glutamate synapses in these inhibitory neurons. Further, since it has been previously shown that brief, local applications of nicotine in Schaffer collateral-CA1 connections convert silent synapses into active ones in newborn rat brain slices (Maggi et al., 2003), and previous studies from our group have demonstrated that nicotine has a strong excitatory effect on LDT neurons during the postnatal period (Ishibashi et al., 2009), it is tempting to hypothesize that postnatal nicotine, or exposure to other dependency-inducing drugs, could unsilence these synapses in the GABAergic LDT population following PNE treatment.

Intrinsic Plasticity: PNE and the Action Potential

The intrinsic properties of neurons underlying neuronal excitability have been shown to exhibit plasticity in an activity-dependent fashion (Zhang and Linden, 2003; Lisman et al., 2018; Debanne et al., 2019). This process has been shown to occur in the LDT following postnatal chronic exposure to cocaine (Kaneda, 2019). Our studies provide further support that intrinsic plasticity can be altered by experience, as we showed that a form of intrinsic plasticity is engendered by early-life exposure to nicotine, as reflected in alterations in membrane properties and action potential kinetics of LDT neurons in the PNE (Polli and Kohlmeier, 2018). Further, PNE treatment was associated with lower activity-dependent intracellular calcium rises in putative cholinergic LDT cells of juvenile mice, assessed by single-photon calcium imaging of neurons activated by high current injection (Polli and Kohlmeier, 2018), which was an effect attributed to a reduced functionality of voltage-gated calcium channels (VGCCs). This finding is consistent with kinetic alterations seen in the action potential of the PNE LDT found in two independent studies from our laboratory (Christensen et al., 2015; Polli and Kohlmeier, 2018), as lower calcium rises mediated by VGCCs predict smaller activation of calcium-dependent potassium channels, with subsequent broadening of the action potential half-width (Bean, 2007), which were characteristics of the kinetics of the action potential observed in PNE LDT cells. Changes in VGCCs leading to reduced activity-dependent calcium predict a reduced excitability of these neurons, which parallels previous studies showing that PNE LDT neurons displayed a higher rheobase which is the amount of current necessary to induce an action potential (Christensen et al., 2015). Consistent with this, in unpublished observations, we noted that while PNE LDT neurons displayed higher inward currents upon AMPA application in the absence of TTX, a significantly smaller percentage of neurons fired action potentials following AMPAR activation in the PNE group relative to the number of cells in which AMPA

induced action potential firing in control. A lower functionality of VGCC in these neurons upon depolarization reconciles findings from earlier work from our group, in which application of AMPA was associated with reduced intracellular calcium rises in PNE LDT neurons, despite enhanced postsynaptic AMPAR-induced current amplitudes (McNair and Kohlmeier, 2015; Polli and Kohlmeier, 2018). In the earlier study, the AMPA-induced depolarization in PNE LDT neurons was likely associated with a reduced VGCC functioning, resulting in an overall lower intracellular calcium rise. Although the precise calcium channel subtype that was altered in the PNE was not elucidated, in the CNS, VGCC function mediated by different VGCC subtypes is associated with neuronal development, membrane oscillation, and neurotransmitter release, among other physiological functions (Catterall, 2011; Simms and Zamponi, 2014). Given their role in all of these processes, early life dependent changes in their properties would be expected to profoundly affect communication within the LDT and transmission to target regions.

FUNCTIONAL SIGNIFICANCE OF ALTERATIONS IN LDT DEVELOPMENT ASSOCIATED WITH PNE

In LDT neurons, PNE was associated with alterations in AMPA and NMDA receptors, reductions in glutamate release and activity-dependent intracellular calcium, changes in intrinsic properties, and reductions in firing excitability, which would certainly impact on output to target regions, such as those within the mesoaccumbal pathway. One prominent hypothesis of drug dependence is the hypodopaminergic hypothesis which posits that those with relatively lower DA tone in the mesoaccumbal circuit exhibit a heightened sensitivity to drug stimuli, and are therefore more vulnerable to the reinforcing properties of drugs of abuse. PNE has been associated with a high liability for development of drugs of abuse, and the enhanced susceptibility for development of dependency to drugs of abuse associated with these individuals has been suggested to be due to hypodopaminergic VTA functioning resulting from the early life nicotine exposure (Navarro et al., 1988; Muneoka et al., 1997, 1999; Alkam et al., 2013; Yochum et al., 2014). In support of this supposition, DA VTA neurons exhibited significant alterations in burst firing in the adolescent PNE (Dragomir et al., 2017). Changes seen within the LDT following gestational nicotine exposure would be predicted to result in differential cellular responses to postnatal exposures to nicotine, and other dependency-inducing drugs. When taken together, our findings predict that upon LDT excitation, there would be a lower cholinergic tone within the VTA in PNE individuals when compared to individuals without these alterations. Further, if the uncovering of silent synapses in the GABAergic LDT population is induced by postnatal exposure to drugs of abuse, such as nicotine, is found to occur, and if drug-induced LTP occurs in these cells, the balance of inhibitory output to GABAergic target regions within the LDT and outside the LDT would be shifted, likely resulting in a net reduction in excitatory drive directed to DA-VTA cells, which would be exacerbated in the PNE as the number of silent synapses is greater. Given the modulatory role exerted by LDT on midbrain dopaminergic and striatal functions via control over burst firing, our findings which are suggestive of reduced cholinergic output in the PNE provide a neuronal basis for the alterations in burst firing of VTA cells seen in the PNE. These changes would be expected to lead to reduced release of DA in the NAc. Therefore, dysregulation in the LDT could play a significant role in the higher risks of negative behavioral outcomes in this population.

CONCLUSION

The LDT had long been thought to be a hardwired "way station," playing a role as a faithful effector, passively transmitting information to its targets, without any meaningful alteration of the informational content of signaling received from higher-order brain regions. Review articles focused on synaptic plasticity, including those detailing the neuronal plasticity engendered by drugs of abuse, remain centered on higher order structures involved in learning and memory with little to no mention of mechanisms underlying synaptic plasticity occurring in the brainstem, nor what the functional impact of such an alteration would be (Holtmaat and Svoboda, 2009; Lüscher and Malenka, 2011; Espinosa and Stryker, 2012; Kandel et al., 2014). Further, popular textbooks reflect that higher cognitive centers, including the limbic system developed on top of the brainstem in order to allow flexible behavior likely reliant on synapse rewiring (Millers, 2010; Dietrich, 2015). However, emerging information suggests that this interpretation does not reflect the potential for synaptic flexibility of the LDT, nor that this potential for a change in the strength of wiring could play a role in higher-order, cognitive behavior. The LDT is a dynamic nucleus, capable of functional alterations depending on environment-driven experiences, such as exposure to drugs of abuse. Behavioral and lesion studies suggest that the LDT does exhibit plasticity, with heightened excitatory output upon acute exposure to drugs of abuse. Chronic exposure to drugs of abuse can elicit pre and postsynaptic changes in LDT synaptic functioning, and mechanisms associated with long-term potentiation seem to be present at LDT synapses. Prenatal exposures to drugs of abuse alter the development of excitatory and inhibitory signaling in the LDT. Discovery of the machinery necessary for altering synaptic strength in the LDT leads us to conclude that it is possible that input to the reward circuitry from the brainstem does not remain fixed in the face of stimuli, but the experience of that stimuli could shape or vary input to the VTA or NAc, even when the stimuli remains the same, due to plastic changes in the brainstem.

As environmental experiences occurring in both prenatal and postnatal life have been shown to alter its functionality, it will be important to determine the impact of such alterations on drug dependence and other aroused, attentive, and motivated behaviors associated with prenatal nicotine exposure. Additionally, how these changes impact behaviors for which the LDT is more traditionally known to play a role, such as control of the sleep and wakefulness state and arousal, also warrant

investigation. Further, additional studies should be conducted with different technical approaches such as optogenetics, electron microscopy, and characterization of early response genes and expression of exogenous molecules known to play a role in information processing-based synaptic alterations in order to confirm findings of plasticity in the LDT, as well as to determine which specific LDT neuronal subtypes can experience plastic changes. In summary, while arousal can be associated with compulsive or rote behavior, it can also be governed by flexible executive control. While such control is often believed to stem from cortical regions, we now know the brainstem could also play a role. Therefore, future studies should be conducted to provide a full characterization of the alterations in plasticity possible in the brainstem, and specifically within LDT neurons, as well as the underlying mechanisms and the behavioral consequences of plasticity-associated deficits promoted in this neural area by experiences throughout the lifespan if we are to truly understand cognitive-based processes including those leading to drug dependence and motivated and goal-directed arousal.

METHODS

Animals

Animal procedures were authorized by the Animal Welfare Committee (Danish Ministry of Justice) and in accordance with European directives for the employment of rodents in research. All experimental procedures were conducted under valid permits (2014-15-0201-00031 and 2017-15-0201-01195). Naive NMRI male mice (Taconic, Denmark) between 11 and 15 days old were employed for *ex vivo* electrophysiological recordings. Animals were kept in the cage with their maternal progenitor under 12-hour light/dark cycle with lights on at 7:00, controlled humidity (52–62%), and constant temperature (22 ± 2°C). *Ad libitum* access to food and water was provided to the moms.

Brain Slices

Brain slices were obtained as previously described (Polli and Kohlmeier, 2018, 2019). Briefly, juvenile mice were anesthetized with isoflurane and decapitated. The skull was opened, and the brain was removed in ice-cold (0–4°C) artificial cerebrospinal fluid (ACSF) containing, in Mm: NaCl 124, KCl 5, Na_2HPO_4 1.2, $CaCl_2$ 2.7, $MgSO_4$ (anhydrous) 1.2, Glucose 10, $NaHCO_3$ 26; oxygenated in 95% oxygen/5% carbogen]. Coronal slices containing the LDT (300 μm) were obtained at 0–4°C with a Leica vibratome (VT1200, Leica, Germany), heated for 15 min at 37°C, and recovered at room temperature for 1 h prior to recordings. A sagittal cut was performed along the midline of the slice to separate the two hemispheres. Slices were placed in a microscope chamber (Olympus BX51WI, Germany, Olympus Europe) constantly perfused with oxygenated ACSF at 33°C with a controlled flow rate of 1 mL/min provided by 4 Head Perfusion pump (Ole Dick, Hvidovre, Denmark). Slices were visualized on screen via a CCD camera system (PCO Sensicam, Till Photonics, Germany) attached to the microscope using Live Acquisition software 2.2.0 (TILL Photonics, United States).

Whole-Cell Patch Clamping

Thin-walled borosilicate patch pipettes (ID: 1.1 mm, OD: 1.5; Sutter Instruments, United States; 7–12 MΩ) were fabricated on a horizontal puller (Sutter Instruments P-97) and filled with an internal solution (in mM: K-gluconate 144, $MgCl_2$ 3, HEPES 10, NaGTP 0.3 and Na_2ATP 4; EGTA free; 285 mOsm). The liquid junction potential was calculated as +14.7 mV at 20°C as previously described (Neher, 1992), and no correction was made. Voltage-clamp was performed with an Axoclamp 200B amplifier (Molecular Devices, United States) connected to an analog-digital converter (Digi-Data 1440A; Axon Instruments, Molecular Devices). Signals were sampled at 20 kHz and filtered with a 5-kHz low-pass Bessel filter with a scaled output gain of five. Pipette offset correction and fast capacitance compensation were employed before each cell recording. Series resistance and capacitance compensation (70–80%) were performed to decrease the transient response which could have introduced artifacts in the recordings. Only healthy neurons, with a stable holding current <200 pA were used. Access resistance was monitored during the experiments by the application of brief 5 mV pulses at each sweep, and only data obtained from patches with an access resistance maintained stably below 30 MΩ throughout the recording were considered. A combination of neuronal size and the presence/absence of the after-hyperpolarization A-type K^+ or T-type Ca^{+2} currents were used to classify LDT neurons. A hyperpolarization voltage step (−85 mV) was followed by 7 depolarization voltage steps (−60 to −10 mV; Δ = +10 mV). To allow the employment of this protocol, QX-314 (5 μM; Alomone Labs, Israel) was added to the patch solution to block voltage-gated sodium channels. Small, round-shaped neurons with presence of T-type Ca^{+2} current, which are likely GABAergic neurons, were classified as type I. The medium/big-sized, polygonal-shaped neurons containing either A-type K^+ current (type II) or both currents (type III), were likely cholinergic cells based both on previous literature (Leonard and Llinás, 1990; Kamondi et al., 1992; Boucetta and Jones, 2009). A recent study conducted in our group showed that cholinergic neurons were types II and III, whereas 90% of non-cholinergic neurons were type I (Polli and Kohlmeier, 2019). Although the combination of size and type is not a definitive method to classify LDT neurons based on their neurotransmitter release, we believe this simple approach is reliable in distinguish cholinergic from non-cholinergic neurons, with the caveat that glutamate cells could potentially be present within all neuronal types. D-Serine (10 μM; Sigma) was included as a co-agonist of NMDARs. All data were recorded using Clampex 10.3 (Axon Instruments) and analyzed using Clampfit 10.3 (Axon Instruments). Electrophysiological data were exported as text files and imported to Igor Pro 6.2 (Wavemetrics, United States) for figure preparation.

Induction of Long-Term Potentiation

In these pilot experiments, an external bipolar electrode (0.25 mm; FHC Microelectrodes, Bowdoin, ME, United States) used for presynaptic stimulation was placed in the ventral portion of the LDT nucleus (100–300 μm from the recorded neuron). The electrode was connected to a Stimulus Isolator A365 (World

Precise Instruments, United States) with the output parameters controlled by a Pulse Stimulator Master-9 (A.M.P.I., Israel), triggered with TTL pulses generated by Clampex. 5 min after the acquisition of the whole-cell configuration (for equilibration), 10 pulses (0.033 Hz) were delivered to the slice via the stimulation electrode to record evoked excitatory postsynaptic currents (eEPSCs) with a voltage membrane command set at −60 mV, as a baseline. Intensity and duration of pulses were set to evoke EPSCs with amplitudes between 50 and 150 pA. Next, the patched neuron was depolarized to 0 mV, concomitant with the application of a theta burst stimulation (TBS) protocol, as previously described for the hippocampus (Kang et al., 1997). Four pulses (100 Hz) were injected 10 times (0.2 Hz). This protocol was repeated 4 times at 0.1 Hz frequency (see **Figure 3** for detail). Following burst stimulation, the neuronal membrane was repolarized to −60 mV and kept under this voltage until the end of the recording. Between 20 and 30 stimulations (0.033 Hz) were employed to evoke EPSCs following the TBS protocol. A single neuron was recorded for each hemisphere of LDT-containing slices.

DATA AVAILABILITY STATEMENT

The datasets generated for this study are available on request to the corresponding author.

ETHICS STATEMENT

The animal study was reviewed and approved by the Dyreforsøgstilsynet as mandated by the European Communities Council Directive (86/609/EEC).

AUTHOR CONTRIBUTIONS

Both authors did literature searching, data collection and/or interpretation, wrote and edited the manuscript.

FUNDING

The present study received support from the National Council of Research (CNPQ; Brazil) through the fellowship provided to FSP (201542/2014-5).

ACKNOWLEDGMENTS

The authors thank Astrid Sabina Kristensen for her assistance with artwork shown in **Figure 1**.

REFERENCES

Abel, T., Nguyen, P. V., Barad, M., Deuel, T. A. S., Kandel, E. R., and Bourtchouladze, R. (1997). Genetic demonstration of a role for PKA in the late phase of LTP and in hippocampus-based long-term memory. *Cell* 88, 615–626. doi: 10.1016/S0092-8674(00)81904-81902

Abraham, W. C., and Bear, M. F. (1996). Metaplasticity: plasticity of synaptic. *Trends Neurosci.* 19, 126–130. doi: 10.1016/S0304-5412(12)70253-70256

Alkam, T., Kim, H., Mamiya, T., Yamada, K., Hiramatsu, M., and Nabeshima, T. (2013). Evaluation of cognitive behaviors in young offspring of C57BL / 6J mice after gestational nicotine exposure during different time-windows. *Psychopharmacology* 230, 451–463. doi: 10.1007/s00213-013-3175-9

Aston-Jones, G., and Bloom, F. E. (1981). Activity of norepinephrine-containing locus coeruleus neurons in behaving rats anticipates fluctuations in the sleep-waking cycle. *J. Neurosci.* 1, 876–886. doi: 10.1523/jneurosci.01-08-00876.1981

Baghdoyan, H. A., Rodrigo-Angulo, M. L., McCarley, R. W., and Hobson, J. A. (1987). A neuroanatomical gradient in the pontine tegmentum for the cholinoceptive induction of desynchronized sleep signs. *Brain Res.* 414, 245–261. doi: 10.1016/0006-8993(87)90005-9

Balland, B., Lachamp, P., Kessler, J. P., and Tell, F. (2008). Silent synapses in developing rat nucleus tractus solitarii have AMPA receptors. *J. Neurosci.* 28, 4624–4634. doi: 10.1523/JNEUROSCI.5355-07.2008

Bean, B. P. (2007). The action potential in mammalian central neurons. *Nat. Rev. Neurosci.* 8, 18–20. doi: 10.1038/nrn2148

Bellone, C., and Luscher, C. (2006). Cocaine triggered AMPA receptor redistribution is reversed in vivo by mGluR-dependent long-term depression. *Nat. Neurosci.* 9, 1–6. doi: 10.1038/nn1682

Bellone, C., and Mameli, M. (2011). In utero exposure to cocaine delays postnatal synaptic maturation of glutamatergic transmission in the VTA In utero exposure to cocaine delays postnatal synaptic maturation of glutamatergic transmission in the VTA. *Nat. Neurosci.* 14, 1439–1446. doi: 10.1038/nn.2930

Berberich, S., Jensen, V., Hvalby, Ø, Seeburg, P. H., and Kohr, G. (2007).). The role of NMDAR subtypes and charge transfer during hippocampal LTP induction. *Neuropharmacology* 52, 77–86. doi: 10.1016/j.neuropharm.2006.07.016

Beroun, A., Nalberczak-Skóra, M., Harda, Z., Piechota, M., Ziółkowska, M., Cały, A., et al. (2018). Generation of silent synapses in dentate gyrus correlates with development of alcohol addiction. *Neuropsychopharmacology* 43, 1989–1999. doi: 10.1038/s41386-018-0119-114

Billa, S. K., Liu, J., Bjorklund, N. L., Sinha, N., Fu, Y., Shinnick-gallagher, P., et al. (2010). Increased insertion of glutamate receptor 2-Lacking a-Amino-3-hydroxy-5-methyl-4-isoxazole Propionic Acid (AMPA) receptors at hippocampal synapses upon repeated morphine administration. *Mol. Pharmacol.* 77, 874–883. doi: 10.1124/mol.109.060301.responses

Blaha, C. D., Allen, L. F., Das, S., Inglis, W. L., Latimer, M. P., Vincent, S. R., et al. (1996). Modulation of dopamine efflux in the nucleus accumbens after cholinergic stimulation of the ventral tegmental area in intact, pedunculopontine tegmental nucleus-lesioned, and laterodorsal tegmental nucleus-lesioned rats. *J. Neurosci.* 16, 714–722. doi: 10.1523/jneurosci.16-02-00714.1996

Bliss, T. V. P., and Collingridge, G. L. (1993). A synaptic model of memory: long-term potentiation in the hippocampus. *Nature* 361, 31–39. doi: 10.1038/361031a0

Bliss, T. V. P., and Collingridge, G. L. (2013). Expression of NMDA receptor-dependent LTP in the hippocampus: bridging the divide. *Mol. Brain* 6, 1–14. doi: 10.1186/1756-6606-6-5

Borgland, S. L., Taha, S. A., Sarti, F., Fields, H. L., and Bonci, A. (2006). Orexin a in the VTA is critical for the induction of synaptic plasticity and behavioral sensitization to cocaine. *Neuron* 49, 589–601. doi: 10.1016/j.neuron.2006.01.016

Boucetta, S., Cissé, Y., Mainville, L., Morales, M., and Jones, B. E. (2014). Discharge profiles across the sleep-waking cycle of identified cholinergic. *J. Neurosci.* 34, 4708–4727. doi: 10.1523/JNEUROSCI.2617-13.2014

Boucetta, S., and Jones, B. E. (2009). Activity Profiles of cholinergic and intermingled GABAergic and putative glutamatergic neurons in the pontomesencephalic tegmentum of urethane-anesthetized rats. *J. Neurosci.* 29, 4664–4674. doi: 10.1523/JNEUROSCI.5502-08.2009

Brecht, M., and Feldman, D. E. (2005). Map plasticity in somatosensory cortex. *Science* 310, 810–815. doi: 10.1126/science.1115807

Brim, B. L., Haskell, R., Awedikian, R., Ellinwood, N. M., Jin, L., Kumar, A., et al. (2013). Memory in aged mice is rescued by enhanced expression of the GluN2B subunit of the NMDA receptor. *Behav. Brain Res.* 238, 211–226. doi: 10.1016/j.bbr.2012.10.026

Brown, T. E., Lee, B. R., Mu, P., Ferguson, D., Dietz, D., Ohnishi, Y. N., et al. (2011). A Silent Synapse-Based Mechanism for Cocaine-Induced Locomotor Sensitization. *J. Neurosci.* 31, 8163–8174. doi: 10.1523/jneurosci.0016-11.2011

Catterall, W. A. (2011). Voltage-gated calcium channels. *Cold Spring Harb. Perspect. Biol.* 3:a003947. doi: 10.1101/cshperspect.a003947

Christensen, M. H., Nielsen, M. L., and Kohlmeier, K. A. (2015). Electrophysiological changes in laterodorsal tegmental neurons associated with prenatal nicotine exposure: implications for heightened susceptibility to addict to drugs of abuse. *J. Dev. Orig. Health Dis.* 6, 182–200. doi: 10.1017/S204017441400049X

Clements, J. R., and Grant, S. (1990). Glutamate-like immunoreactivity in neurons of the laterodorsal tegmental and pedunculopontine nuclei in the rat. *Neurosci. Lett.* 120, 70–73. doi: 10.1016/0304-3940(90)90170-e

Coimbra, B., Soares-Cunha, C., Vasconcelos, N. A. P., Domingues, A. V., Borges, S., Sousa, N., et al. (2019). Role of laterodorsal tegmentum projections to nucleus accumbens in reward-related behaviors. *Nat. Commun.* 10, 1–15. doi: 10.1038/s41467-019-11557-11553

Cornwall, J., Cooper, J. D., and Phillipson, O. T. (1990). Afferent and efferent connections of the laterodorsal tegmental nucleus in the rat. *Brain Res. Bull.* 25, 271–284. doi: 10.1016/0361-9230(90)90072-8

Damsma, G., Pfaus, J. G., Wenkstern, D., Phillips, A. G., and Fibiger, H. C. (1992). Sexual behavior increases dopamine transmission in the nucleus accumbens and striatum of male rats: comparison with novelty and locomotion. *Behav. Neurosci.* 106, 181–191. doi: 10.1037/0735-7044.106.1.181

Dautan, D., Huerta-Ocampo, I., Witten, I. B., Deisseroth, K., Bolam, J. P., Gerdjikov, T., et al. (2014). A major external source of cholinergic innervation of the striatum and nucleus accumbens originates in the brainstem. *J. Neurosci.* 34, 4509–4518. doi: 10.1523/jneurosci.5071-13.2014

Dautan, D., Souza, A. S., Huerta-ocampo, I., Valencia, M., Assous, M., Witten, I. B., et al. (2016). Segregated cholinergic transmission modulates dopamine neurons integrated in distinct functional circuits. *Nat. Neurosci.* 19, 1–14. doi: 10.1038/nn.4335

Debanne, D., Inglebert, Y., and Russier, M. (2019). Plasticity of intrinsic neuronal excitability. *Curr. Opin. Neurobiol.* 54, 73–82. doi: 10.1016/j.conb.2018.09.001

Di Chiara, G., and Imperato, A. (1988). Drugs abused by humans preferentially increase synaptic dopamine concentrations in the mesolimbic system of freely moving rats. *Proc. Natl. Acad. Sci. U.S.A.* 85, 5274–5278. doi: 10.1073/pnas.85.14.5274

Diering, G. H., and Huganir, R. L. (2018). The AMPA receptor code of synaptic plasticity. *Neuron* 100, 314–329. doi: 10.1016/j.neuron.2018.10.018

Dietrich, A. (2015). *How Creativity Happens in the Brain*. London: Springer.

Dong, Y. (2016). Silent synapse-based circuitry remodeling in drug addiction. *Int. J. Neuropsychopharmacol.* 19, 1–4. doi: 10.1093/ijnp/pyv136

Dong, Y., and Nestler, E. J. (2014). The neural rejuvenation hypothesis of cocaine addiction. *Trends Pharmacol. Sci.* 35, 374–383. doi: 10.1016/j.tips.2014.05.005

Dragomir, A., Akay, Y. M., Zhang, D., and Akay, M. (2017). Ventral tegmental area dopamine neurons firing model reveals prenatal nicotine induced alterations. *Trans. Neural Syst. Rehabil. Eng.* 25, 1387–1396. doi: 10.1109/TNSRE.2016.2636133

Druhan, J. P., Fibiger, H. C., and Phillips, A. G. (1990). Amphetamine-like stimulus properties produced by electrical stimulation of reward sites in the ventral tegmental area. *Behav. Brain Res.* 38, 175–184. doi: 10.1016/0166-4328(90)90015-7

Dunah, A. W., Wang, Y., Yasuda, R. P., Kameyama, K., Huganir, R. L., Wolfe, B. B., et al. (2000). Alterations in subunit expression, composition, and Phosphorylation of Striatal N-Methyl-D-aspartate glutamate receptors in a rat 6-Hydroxydopamine Model of Parkinson's Disease. *Mol. Pharmacol.* 352, 342–352.

Durand, G. M., Kovalchuk, Y., and Konnerth, A. (1996). Long-term potentiation and functional synapse induction in developing hippocampus. *Lett. Neurosci.* 381, 71–75. doi: 10.1038/381071a0

Eban-Rothschild, A., Rothschild, G., Giardino, W. J., Jones, J. R., and De Lecea, L. (2016). VTA dopaminergic neurons regulate ethologically relevant sleep-wake behaviors. *Nat. Neurosci.* 19, 1356–1366. doi: 10.1038/nn.4377

Espinosa, J. S., and Stryker, M. P. (2012). Development and Plasticity of the Primary Visual Cortex. *Neuron* 75, 230–249. doi: 10.1016/j.neuron.2012.06.009

Fernandez, S. P., Broussot, L., Marti, F., Contesse, T., Mouska, X., Soiza-Reilly, M., et al. (2018). Mesopontine cholinergic inputs to midbrain dopamine neurons drive stress-induced depressive-like behaviors. *Nat. Commun.* 9:4449. doi: 10.1038/s41467-018-06809-6807

Forster, G. L., and Blaha, C. D. (2000). Laterodorsal tegmental stimulation elicits dopamine efflux in the rat nucleus accumbens by activation of acetylcholine and glutamate receptors in the ventral tegmental area. *Eur. J. Neurosci.* 12, 3596–3604. doi: 10.1046/j.1460-9568.2000.00250.x

Forster, G. L., Falcon, A. J., Miller, A. D., Heruc, G. A., and Blaha, C. D. (2002). Effects of laterodorsal tegmentum excitotoxic lesions on behavioral and dopamine responses evoked by morphine and d-Amphetamine. *Lett. Neurosci.* 114, 817–823. doi: 10.1016/s0306-4522(02)00365-2

Fowler, C. D., and Kenny, P. J. (2014). Nicotine aversion: neurobiological mechanisms and relevance to tobacco dependence vulnerability. *Neuropharmacology* 76, 533–544. doi: 10.1016/j.neuropharm.2013.09.008

Goldberg, S., and Spealman, R. (1982). Maintenance and suppression of behavior by intravenous nicotine injections in squirrel monkeys. *Fed. Proc.* 41, 216–220.

Goldberg, S. R., and Spealman, R. D. (1983). Suppression of behavior by intravenous injections of nicotine or by electric shocks in squirrel monkeys: effects of chlordiazepoxide and mecamylamine. *J. Pharmacol. Exp. Ther.* 224, 334–340.

Goldberg, S. R., Spealman, R. D., Risner, M. E., and Henningfield, J. E. (1983). Control of behavior by intravenous nicotine injections in laboratory animals. *Pharmacol. Biochem. Behav.* 19, 1011–1020. doi: 10.1016/0091-3057(83)90408-2

Goldberg, S. R., Spealmand, R. D., and Goldberg, D. M. (1981). Persistent behavior at high rates maintained by intravenous self-administration of nicotine. *Science* 214, 573–575. doi: 10.1126/science.7291998

Grand, T., Abi Gerges, S., David, M., Diana, M. A., and Paoletti, P. (2018). Unmasking GluN1/GluN3A excitatory glycine NMDA receptors. *Nat. Commun.* 9:4769. doi: 10.1038/s41467-018-07236-7234

Grant, S. J., and Highfield, D. A. (1991). Extracellular characteristics of putative cholinergic neurons in the rat laterodorsal tegmental nucleus. *Brain Res.* 559, 64–74. doi: 10.1016/0006-8993(91)90287-6

Graziane, N. M., Sun, S., Wright, W. J., Jang, D., Liu, Z., Huang, Y. H., et al. (2016). Opposing mechanisms mediate morphine- and cocaine-induced generation of silent synapses. *Nat. Neurosci.* 19, 915–925. doi: 10.1038/nn.4313

Grieder, T. E., Besson, M., Maal-Bared, G., Pons, S., Maskos, U., and van der Kooy, D. (2019). Beta2 nAChRs on VTA dopamine and GABA neurons seperately mediate nicotine aversion and reward. *PNAS* 116, 25968–25973. doi: 10.1073/pnas.1908724116

Hanse, E., Seth, H., and Riebe, I. (2013). AMPA-silent synapses in brain development and pathology. *Nat. Rev. Neurosci.* 14, 839–850. doi: 10.1038/nrn3642

Hansen, S., Bergvall, A. H., and Nyiredi, S. (1993). Interaction with pups enhances dopamine release in the ventral striatum of maternal rats: a microdialysis study. *Pharmacol. Biochem. Behav.* 45, 673–676. doi: 10.1016/0091-3057(93)90523-v

Hauberg, K., and Kohlmeier, K. A. (2015). The appetite-inducing peptide, ghrelin, induces intracellular store-mediated rises in calcium in addiction and arousal-related laterodorsal tegmental neurons in mouse brain slices. *Peptides* 65, 34–45. doi: 10.1016/j.peptides.2015.01.006

Hausknecht, K., Haj-Dahmane, S., Shen, Y.-L., Vezina, P., Dlugos, C., and Shen, R.-Y. (2015). Excitatory Synaptic Function and Plasticity is Persistently Altered in Ventral Tegmental Area Dopamine Neurons after Prenatal Ethanol Exposure. *Neuropsychopharmacology* 40, 893–905. doi: 10.1038/npp.2014.265

Hebb, D. O. (1949). *The Organization of Behavior: A Neuropsychological Theory*. Hoboken, NJ: John Wiley.

Henson, M. A., Larsen, R. S., Lawson, S. N., Pérez-Otaño, I., Nakanishi, N., Lipton, S. A., et al. (2012). Genetic deletion of NR3A accelerates Glutamatergic synapse maturation. *PLoS One* 7:e42327. doi: 10.1371/journal.pone.0042327

Henson, M. A., Roberts, A. C., Pérez-Otaño, I., and Philpot, B. D. (2010). Influence of the NR3A subunit on NMDA receptor functions. *Prog. Neurobiol.* 91, 23–37. doi: 10.1016/j.pneurobio.2010.01.004

Hnasko, T. S., Hjelmstad, G. O., Fields, H. L., and Edwards, R. H. (2012). Ventral tegmental area glutamate neurons: electrophysiological properties and

projections. *J. Neurosci.* 32, 15076–15085. doi: 10.1523/JNEUROSCI.3128-12.2012

Ho, M. T., Pelkey, K. A., Topolnik, L., Petralia, R. S., Takamiya, K., Xia, J., et al. (2007). Developmental expression of Ca^{2+}-Permeable AMPA receptors underlies depolarization-induced long-term depression at mossy Fiber – CA3 pyramid synapses. *J. Neurosci.* 27, 11651–11662. doi: 10.1523/JNEUROSCI.2671-07.2007

Holtmaat, A., and Svoboda, K. (2009). Experience-dependent structural synaptic plasticity in the mammalian brain. *Nat. Rev. Neurosci.* 10, 647–658. doi: 10.1038/nrn2699

Huang, Y. H., Lin, Y., Mu, P., Lee, B. R., Brown, T. E., Wayman, G., et al. (2009). Report in vivo cocaine experience generates silent synapses. *Neuron* 63, 40–47. doi: 10.1016/j.neuron.2009.06.007

Huang, Y. H., Schlüter, O. M., and Dong, Y. (2015). Silent synapses speak up: updates of the neural rejuvenation hypothesis of drug addiction. *Neuroscientist* 21, 451–459. doi: 10.1177/1073858415579405

Imon, H., Ito, K., Dauphin, L., and McCarley, R. W. (1996). Electrical stimulation of the cholinergic laterodorsal tegmental nucleus elicits scopolamine-sensitive excitatory postsynaptic potentials in medial pontine reticular formation neurons. *Neuroscience* 74, 393–401. doi: 10.1016/0306-4522(96)00134-130

Isaac, J. T. R. (2003). Postsynaptic silent synapses: evidence and mechanisms. *Neuropharmacology* 45, 450–460. doi: 10.1016/S0028-3908(03)00229-226

Isaac, J. T. R., Crair, M. C., Nicoll, R. A., and Malenka, R. C. (1997). Silent synapses during development of thalamocortical inputs. *Neuron* 18, 269–280. doi: 10.1016/S0896-6273(00)80267-80266

Ishibashi, M., Leonard, C. S., and Kohlmeier, K. A. (2009). Implications for addiction to nicotine. *Neuropsychopharmacology* 34, 2529–2547. doi: 10.1038/npp.2009.82.Nicotinic

Jerlhag, E., Janson, A. C., Waters, S., and Engel, J. A. (2012). Concomitant release of ventral tegmental acetylcholine and accumbal dopamine by ghrelin in rats. *PLoS One* 7:e49557. doi: 10.1371/journal.pone.0049557

Jin, Z., Bhandage, A. K., Bazov, I., Kononenko, O., Bakalkin, G., Korpi, E. R., et al. (2014). Selective increases of AMPA, NMDA, and kainate receptor subunit mRNAs in the hippocampus and orbitofrontal cortex but not in prefrontal cortex of human alcoholics. *Front. Cell. Neurosci.* 8:11. doi: 10.3389/fncel.2014.00011

Johnson, S. W., and North, R. A. (1992). Two types of neurone in the rat ventral tegmental area and their synaptic inputs. *J. Physiol.* 450, 455–468. doi: 10.1113/jphysiol.1992.sp019136

Jones, B. E. (1991). Paradoxical sleep and its chemical/structural substrates in the brain. *Neuroscience* 40, 637–656. doi: 10.1016/0306-4522(91)90002-6

Jouvet, M. (1965). Paradoxical Sleep — A study of its nature and mechanisms. *Prog. Brain Res.* 18, 20–62. doi: 10.1016/S0079-6123(08)63582-63587

Kamii, H., Kurosawa, R., Taoka, N., Shinohara, F., Minami, M., and Kaneda, K. (2015). Intrinsic membrane plasticity via increased persistent sodium conductance of cholinergic neurons in the rat laterodorsal tegmental nucleus contributes to cocaine-induced addictive behavior. *Eur. J. Neurosci.* 41, 1126–1138. doi: 10.1111/ejn.12855

Kamondi, A., Williams, J. A., Hutcheon, B., and Reiner, P. B. (1992). Membrane properties of mesopontine cholinergic neurons studied with the whole-cell patch-clamp technique: implications for behavioral state control. *J. Neurophysiol.* 68, 1359–1372. doi: 10.1152/jn.1992.68.4.1359

Kandel, E. R., Dudai, Y., and Mayford, M. R. (2014). The molecular and systems biology of memory. *Cell* 157, 163–186. doi: 10.1016/j.cell.2014.03.001

Kandel, E. R., Schwartz, J. H., and Jessel, T. M. (2013). *Principles of Neural Science*. New York, NY: McGraw-Hill Companies.

Kaneda, K. (2019). Neuroplasticity in cholinergic neurons of the laterodorsal tegmental nucleus contributes to the development of cocaine addiction. *Eur. J. Neurosci.* 50, 2239–2246. doi: 10.1111/ejn.13962

Kang, H., Welcher, A. A., Shelton, D., and Schuman, E. M. (1997). Neurotrophins and time: different roles for TrkB signaling in hippocampal long-term potentiation. *Neuron* 19, 653–664. doi: 10.1016/S0896-6273(00)80378-80375

Kayama, Y., Ohta, M., and Jodo, E. (1992). Firing of 'possibly' cholinergic neurons in the rat laterodorsal tegmental nucleus during sleep and wakefulness. *Brain Res.* 569, 210–220. doi: 10.1016/0006-8993(92)90632-j

Kehoe, L. A., Bellone, C., De Roo, M., Zandueta, A., Dey, P. N., Perez-Otano, I., et al. (2014). GluN3A promotes dendritic spine pruning and destabilization during postnatal development. *J. Neurosci.* 34, 9213–9221. doi: 10.1523/jneurosci.5183-13.2014

Kerchner, G. A., and Nicoll, R. A. (2008). Silent synapses and the emergence of a postsynaptic mechanism for LTP. *Nat. Rev. Neurosci.* 9, 813–825. doi: 10.1038/nrn2501

Kiyatkin, E. A., and Gratton, A. (1994). Electrochemical monitoring of extracellular dopamine in nucleus accumbens of rats lever-pressing for food. *Brain Res.* 652, 225–234. doi: 10.1016/0006-8993(94)90231-3

Kohlmeier, K. A., Inoue, T., and Leonard, C. S. (2004). Hypocretin/orexin peptide signaling in the ascending arousal system: elevation of intracellular calcium in the mouse dorsal raphe and laterodorsal tegmentum. *J. Neurophysiol.* 92, 221–235. doi: 10.1152/jn.00076.2004

Kumar, S. S., Bacci, A., Kharazia, V., and Huguenard, J. R. (2002). A developmental switch of AMPA receptor subunits in neocortical pyramidal neurons. *J. Neurosci.* 22, 3005–3015. doi: 10.1523/jneurosci.22-08-03005.2002

Kurosawa, R., Taoka, N., Shinohara, F., Minami, M., and Kaneda, K. (2013). Cocaine exposure enhances excitatory synaptic drive to cholinergic neurons in the laterodorsal tegmental nucleus. *Eur. J. Neurosci.* 38, 3027–3035. doi: 10.1111/ejn.12296

Lambert, M. Ø, Ipsen, T. H., and Kohlmeier, K. A. (2017). Acute cocaine exposure elicits rises in calcium in arousal-related laterodorsal tegmental neurons. *Pharmacol. Res. Perspect.* 5:e00282. doi: 10.1002/prp2.282

Lammel, S., Lim, B. K., Ran, C., Huang, K. W., Betley, M. J., Tye, K. M., et al. (2012). Input-specific control of reward and aversion in the ventral tegmental area. *Nature* 491, 212–217. doi: 10.1038/nature11527

Laviolette, S. R., Priebe, R. P. M., and Yeomans, J. S. (2000). Role of the laterodorsal tegmental nucleus in scopolamine- and amphetamine-induced locomotion and stereotypy. *Pharmacol. Biochem. Behav.* 65, 163–174. doi: 10.1016/S0091-3057(99)00195-191

Lee, B. R., Ma, Y. Y., Huang, Y. H., Wang, X., Otaka, M., Ishikawa, M., et al. (2013). Maturation of silent synapses in amygdala-accumbens projection contributes to incubation of cocaine craving. *Nat. Neurosci.* 16, 1644–1651. doi: 10.1038/nn.3533

Leonard, C. S., and Llinás, R. R. (1990). "Brain cholinergic systems," in *Electrophysiology of Mammalian Pedunculopontine and Laterodorsal Tegmental Neurons in vitro: Implications for the Control of REM Sleep*, ed. M. Steriade, (Oxford: Oxford University Press).

Lester, D. B., Miller, A. D., and Blaha, C. D. (2010). Muscarinic receptor blockade in the ventral tegmental area attenuates cocaine enhancement of laterodorsal tegmentum stimulation-evoked accumbens dopamine efflux in the mouse. *Synapse* 223, 216–223. doi: 10.1002/syn.20717

Lisman, J., Cooper, K., Sehgal, M., and Silva, A. J. (2018). Memory formation depends on both synapse- specific modifications of synaptic strength and cell-specific increases in excitability. *Nat. Neurosci.* 21, 309–314. doi: 10.1038/s41593-018-0076-76

Liu, H., Lin, W., Liu, S., Wang, W., Tsai, C.-H., Wu, B.-T., et al. (2009). Genetic variation in N-Methyl- D -Aspartate receptor subunit NR3A but Not NR3B influences susceptibility to Alzheimer ' s Disease. *Dement. Geriatr. Cogn. Disord.* 28, 521–527. doi: 10.1159/000254757

Lodge, D. J., and Grace, A. A. (2006). The laterodorsal tegmentum is essential for burst firing of ventral tegmental area dopamine neurons. *Proc. Natl. Acad. Sci. U.S.A.* 103, 5167–5172. doi: 10.1073/pnas.0510715103

Luquin, E., Huerta, I., Aymerich, M. S., Mengual, E., and Integral, C. (2018). Stereological estimates of glutamatergic, GABAergic, and cholinergic neurons in the pedunculopontine and laterodorsal tegmental nuclei in the rat. *Front. Neuroanat.* 12:34. doi: 10.3389/fnana.2018.00034

Lüscher, C., and Malenka, R. C. (2011). Drug-evoked synaptic plasticity in addiction: from molecular changes to circuit remodeling. *Neuron* 69, 650–663. doi: 10.1016/j.neuron.2011.01.017

Lüscher, C., and Ungless, M. A. (2006). The mechanistic classification of addictive drugs. *PLoS Med.* 3:e437. doi: 10.1371/journal.pmed.0030437

Ma, Y., Lee, B. R., Wang, X., Guo, C., Liu, L., Cui, R., et al. (2014). Bidirectional modulation of incubation of cocaine craving by silent synapse-based remodeling of prefrontal cortex to accumbens projections. *Neuron* 83, 1453–1467. doi: 10.1016/j.neuron.2014.08.023

Maggi, L., Le Magueresse, C., Changeux, J.-P., and Cherubini, E. (2003). Nicotine activates immature "silent" connections in the developing hippocampus. *Proc. Natl. Acad. Sci.* 100, 2059–2064. doi: 10.1073/pnas.0437947100

Malenka, R. C., and Nicoll, R. A. (1997). Silent synapses speak up. *Neuron* 19, 473–476.

Malinow, R., and Malenka, R. C. (2002). AMPA rceptor tafficking and synaptic plasticity. *Annu. Rev. Neurosci.* 25, 103–126. doi: 10.1146/annurev.neuro.25.112701.142758

Mansari, M., El Sakai, K., and Jouvet, M. (1989). Unitary characteristics of presumptive cholinergic tegmental neurons during the sleep-waking cycle in freely moving cats. *Exp. Brain Res.* 76, 519–529. doi: 10.1007/bf00248908

Mansvelder, H. D., Keath, J. R., and McGehee, D. S. (2002). Synaptic mechanisms underlie nicotine-induced excitability of brain reward areas. *Neuron* 33, 905–919. doi: 10.1016/s0896-6273(02)00625-6

Mansvelder, H. D., and McGehee, D. S. (2000). Long-term potentiation of excitatory inputs to brain reward areas by nicotine. *Neuron* 27, 349–357. doi: 10.1016/s0896-6273(00)00042-8

Marco, S., Giralt, A., Petrovic, M. M., Pouladi, M. A., Martínez-Turrillas, R., Martínez-Hernández, J., et al. (2013). Suppressing aberrant GluN3A expression rescues synaptic and behavioral impairments in Huntington's disease models. *Nat. Med.* 19, 1030–1038. doi: 10.1038/nm.3246

Margolis, E. B., Lock, H., Hjelmstad, G. O., and Fields, H. L. (2006). The ventral tegmental area revisited: Is there an electrophysiological marker for dopaminergic neurons? *J. Physiol.* 577, 907–924. doi: 10.1113/jphysiol.2006.117069

McDevitt, D. S., and Graziane, N. M. (2018). Neuronal mechanisms mediating pathological reward-related behaviors: a focus on silent synapses in the nucleus accumbens. *Pharmacol. Res.* 136, 90–96. doi: 10.1016/j.phrs.2018.08.025

McGinty, D. J., and Harper, R. M. (1976). Dorsal raphe neurons: depression of firing during sleep in cats. *Brain Res.* 101, 569–575. doi: 10.1016/0006-8993(76)90480-7

McNair, L. F., and Kohlmeier, K. A. (2015). Prenatal nicotine is associated with reduced AMPA and NMDA receptor-mediated rises in calcium within the laterodorsal tegmentum: a pontine nucleus involved in addiction processes. *J. Dev. Orig. Health Dis.* 6, 225–241. doi: 10.1017/S2040174414000439

Miller, A. D., and Blaha, C. D. (2005). Midbrain muscarinic receptor mechanisms underlying regulation of mesoaccumbens and nigrostriatal dopaminergic transmission in the rat. *Eur. J. Neurosci.* 21, 1837–1846. doi: 10.1111/j.1460-9568.2005.04017.x

Millers, D. (2010). *How Our Brain Works: The Construction and Functionality of Your Brain Presented and Explained*. Bloomington IN: iUniverse.

Mishizen-eberz, A. J., Rissman, R. A., Carter, T. L., Ikonomovic, M. D., Wolfe, B. B., and Armstrong, D. M. (2004). Biochemical and molecular studies of NMDA receptor subunits NR1 / 2A / 2B in hippocampal subregions throughout progression of Alzheimer ' s disease pathology. *Neurobiol. Dis.* 15, 80–92. doi: 10.1016/j.nbd.2003.09.016

Miwa, H., Fukaya, M., Watabe, A. M., Watanabe, M., and Manabe, T. (2008). Functional contributions of synaptically localized NR2B subunits of the NMDA receptor to synaptic transmission and long-term potentiation in the adult mouse CNS. *J. Physiol.* 10, 2539–2550. doi: 10.1113/jphysiol.2007.147652

Muneoka, K., Nakatsu, T., Fuji, J.-I., Ogawa, T., and Takigawa, M. (1999). Prenatal administration of nicotine results in dopaminergic alterations in the neocortex. *Neurotoxicol. Teratol.* 21, 603–609. doi: 10.1016/s0892-0362(99)00028-8

Muneoka, K., Ogawa, T., Kamei, K., Muraoka, S., Tomiyoshi, R., Mimura, Y., et al. (1997). Prenatal nicotine exposure affects the development of the central serotonergic system as well as the dopaminergic system in rat offspring: involvement of route of drug administrations. *Dev. Brain Res.* 102, 117–126. doi: 10.1016/s0165-3806(97)00092-8

Nair-Roberts, R. G., Chatelain-Badie, S. D., Benson, E., Bolam, J. P., and Ungless, M. A. (2008). Stereological estimates of dopaminergic, GABAergic and glutamatergic neurons in the ventral tegmental area, substantia nigra and retrorubral field in the rat. *Neuroscience* 152, 1024–1031. doi: 10.1016/j.neuroscience.2008.01.046

Nakazawa, K., Mchugh, T. J., Wilson, M. A., and Tonegawa, S. (2004). NMDA receptors, place cells and hippocampal spatial memory. *Nat. Neurosci.* 5, 361–372. doi: 10.1038/nrn1385

Navarro, H. A., Seidler, F. J., Whitmore, W. L., and Slotkin, T. A. (1988). Prenatal exposure to nicotine via maternal development of catecholamine infusions: effects on development of catecholamine systems. *Pharmacol. Exp. Ther.* 244, 940–944.

Neher, E. (1992). Correction for liquid junction potentials in pathc clamp experiments. *Methods Enzymol.* 207, 123–131. doi: 10.1016/0076-6879(92)07008-C

Nelson, C. L., Wetter, J. B., Milovanovic, M., and Wolf, M. E. (2007). The laterodorsal tegmentum contributes to behavioral sensitization to amphetamine. *Neuroscience* 146, 41–49. doi: 10.1016/j.neuroscience.2007.01.027

Nestler, E. J. (2005). Is there a common molecular pathway for addiction? *Nat. Neurosci.* 8, 1445–1449. doi: 10.1038/nn1578

Ninomiya, Y., Kayama, Y., and Koyama, Y. (2005). Postnatal development of cholinergic neurons in the mesopontine tegmentum revealed by histochemistry. *Int. J. Dev. Neurosci.* 23, 711–721. doi: 10.1016/j.ijdevneu.2005.09.002

Oakman, S. A., Faris, L., Kerr, E., and Hartman, K. (1995). Distribution of Pontomesencephalic cholinergic neurons projecting to substantia nigra differs significantly from those projecting to ventral tegmental area. *J. Neurosci.* 15, 5859–5869. doi: 10.1523/jneurosci.15-09-05859.1995

Omelchenko, N., and Sesack, S. R. (2005). Laterodorsal tegmental projections to identified cell populations in the rat ventral tegmental area. *J. Comp. Neurol.* 483, 217–235. doi: 10.1002/cne.20417

Omelchenko, N., and Sesack, S. R. (2006). Cholinergic axons in the rat ventral tegmental area synapse preferentially onto mesoaccumbens dopamine neurons. *J. Comp. Neurol.* 494, 863–875. doi: 10.1002/cne.20852

Pachernegg, S., Strutz-seebohm, N., and Hollmann, M. (2012). GluN3 subunit-containing NMDA receptors: not just one-trick ponies. *Trends Neurosci.* 35, 240–249. doi: 10.1016/j.tins.2011.11.010

Pascoli, V., Terrier, J., Hiver, A., and Luscher, C. (2015). Sufficiency of mesolimbic dopamine neuron stimulation for the progression to addiction. *Neuron* 88, 1054–1066. doi: 10.1016/j.neuron.2015.10.017

Pastalkova, E., Serrano, P., Pinkhasova, D., Wallace, E., Fenton, A. A., and Sacktor, T. C. (2006). Storage of spatial information by the maintenance mechanism of LTP. *Science* 313, 1141–1144. doi: 10.1126/science.1128657

Pérez-Otaño, I., Larsen, R. S., and Wesseling, J. F. (2016). Emerging roles of GluN3-containing NMDA receptors in the CNS. *Nat. Rev. Neurosci.* 17, 623–635. doi: 10.1038/nrn.2016.92

Pérez-Otaño, I., Luján, R., Tavalin, S. J., Plomann, M., Modregger, J., Liu, X. B., et al. (2006). Endocytosis and synaptic removal of NR3A-containing NMDA receptors by PACSIN1/syndapin1. *Nat. Neurosci.* 9, 611–621. doi: 10.1038/nn1680

Pierce, R. C., and Kumaresan, V. (2006). The mesolimbic dopamine system: the final common pathway for the reinforcing effect of drugs of abuse? *Neurosci. Biobehav. Rev.* 30, 215–238. doi: 10.1016/j.neubiorev.2005.04.016

Poe, G. R. (2017). Sleep is for forgetting. *J. Neurosci.* 37, 464–473. doi: 10.1523/JNEUROSCI.0820-16.2017

Polli, F. S., and Kohlmeier, K. A. (2018). Prenatal nicotine exposure alters postsynaptic AMPA receptors and glutamate neurotransmission within the laterodorsal tegmentum (LDT) of juvenile mice. *Neuropharmacology* 137, 71–85. doi: 10.1016/j.neuropharm.2018.04.024

Polli, F. S., and Kohlmeier, K. A. (2019). Alterations in NMDAR-mediated signaling within the laterodorsal tegmental nucleus are associated with prenatal. *Neuropharmacology* 158:107744. doi: 10.1016/j.neuropharm.2019.107744

Purgianto, A., Scheyer, A. F., Loweth, J. A., Ford, K. A., Tseng, K. Y., and Wolf, M. E. (2013). Different adaptations in AMPA receptor transmission in the nucleus accumbens after short vs long access cocaine self-administration regimens. *Neuropsychopharmacology* 38, 1789–1797. doi: 10.1038/npp.2013.78

Qiu, S., Li, X., and Zhuo, M. (2011). Seminars in cell & developmental biology post-translational modification of NMDA receptor GluN2B subunit and its roles in chronic pain and memory. *Semin. Cell Dev. Biol.* 22, 521–529. doi: 10.1016/j.semcdb.2011.06.003

Roberts, A. C., Díez-García, J., Rodriguiz, R. M., López, I. P., Luján, R., Martínez-Turrillas, R., et al. (2009). Downregulation of NR3A-containing NMDARs is required for synapse maturation and memory consolidation. *Neuron* 63, 342–356. doi: 10.1016/j.neuron.2009.06.016

Robledo, P., Maldonado-lopez, R., and Koob, G. F. (1992). Role of dopamine receptors i n the nucleus accumbens i n the rewararcling properties of cocaine. *Ann. N. Y. Acad. Sci.* 5, 509–512.

Sacktor, T. C. (2008). *Chapter 2 PKMζ, LTP Maintenance, and the Dynamic Molecular Biology of Memory Storage*. Amsterdam: Elsevier.

Sasaki, Y. F., Rothe, T., Premkumar, L. S., Das, S., Cui, J., Talantova, M. V., et al. (2002). Characterization and comparison of the NR3A subunit of the NMDA receptor in recombinant systems and primary cortical neurons. *J. Neurophysiol.* 87, 2052–2063. doi: 10.1152/jn.00531.2001

Satoh, K., and Fibiger, H. C. (1986). Cholinergic neurons of the laterodorsal tegmental nucleus: efferent and afferent connections. *J. Comp. Neurol.* 253, 277–302. doi: 10.1002/cne.902530302

Schmidt, H. D., Famous, K. R., and Pierce, R. C. (2009). The limbic circuitry underlying cocaine seeking encompasses the PPTg/LDT. *Eur. J. Neurosci.* 30, 1358–1369. doi: 10.1111/j.1460-9568.2009.06904.x

Shin, J. H., Adrover, M. F., Wess, J., and Alvarez, V. A. (2015). Muscarinic regulation of dopamine and glutamate transmission in the nucleus accumbens. *PNAS* 112, 8124–8129. doi: 10.1073/pnas.1508846112

Shinohara, F., Kihara, Y., Ide, S., Minami, M., and Kaneda, K. (2014). Critical role of cholinergic transmission from the laterodorsal tegmental nucleus to the ventral tegmental area in cocaine-induced place preference. *Neuropharmacology* 79, 573–579. doi: 10.1016/j.neuropharm.2014.01.019

Simms, B. A., and Zamponi, G. W. (2014). Neuronal voltage-gated calcium channels: structure, function, and dysfunction. *Neuron* 82, 24–45. doi: 10.1016/j.neuron.2014.03.016

Sofroniew, M. V., Priestley, J. V., Consolazione, A., Eckenstein, F., and Cuello, A. C. (1985). Cholinergic projections from the midbrain and pons to the thalamus in the rat, identified by combined retrograde tracing and choline acetyltransferase immunohistochemistry. *Brain Res.* 329, 213–223. doi: 10.1016/0006-8993(85)90527-x

Sommer, B., Kohler, M., Sprengel, F., and Seeburg, P. H. (1991). RNA editing in brain controls of ion flow in glutamate-gated a determinant channels. *Cell* 67, 11–19. doi: 10.1016/0092-8674(91)90568-j

Soni, N., Satpathy, S., and Kohlmeier, K. A. (2014). Neurophysiological evidence for the presence of cannabinoid CB1 receptors in the laterodorsal tegmental nucleus. *Eur. J. Neurosci.* 40, 3635–3652. doi: 10.1111/ejn.12730

Spanagel, R. (2009). Alcoholism: a systems approach from molecular physiology to addictive behavior. *Physiol. Rev.* 89, 649–705. doi: 10.1152/physrev.00013.2008

Steidl, S., Wang, H., Ordonez, M., Zhang, S., and Morales, M. (2017). Optogenetic excitation in the ventral tegmental area of glutamatergic or cholinergic inputs from the laterodorsal tegmental area drives reward. *Eur. J. Neurosci.* 45, 559–571. doi: 10.1111/ejn.13436

Steriade, M., Curro Dossi, R., Pare, D., Datta, S., and Oakson, G. (1990). Neuronal activities in brain-stem cholinergic nuclei related to tonic activation processes in thalamocortical systems. *J. Neurosci.* 10, 2541–2559. doi: 10.1523/jneurosci.10-08-02541.1990

Sze, C., Bi, H., Filley, C. M., and Martin, L. J. (2001). N -Methyl- D -aspartate receptor subunit proteins and their phosphorylation status are altered selectively in Alzheimer ' s Disease. *J. Neurol. Sci.* 182, 151–159. doi: 10.1016/s0022-510x(00)00467-6

Takano, S., Kim, J., Ikari, Y., Ogaya, M., Nakajima, K., Oomura, Y., et al. (2009). Electrophysiological effects of ghrelin on laterodorsal tegmental neurons in rats: An in vitro study. *Peptides* 30, 1901–1908. doi: 10.1016/j.peptides.2009.07.014

Tang, Y.-P., Shimizu, E., Bube, G. R., Rampon, C., Kerchner, G. A., Zhuo, M., et al. (1999). Genetic enhancement of learning and memory in mice. *Lett. Nat.* 401, 63–69. doi: 10.1038/43432

Taoka, N., Kamiizawa, R., Wada, S., Minami, M., and Kaneda, K. (2016). Chronic cocaine exposure induces noradrenergic modulation of inhibitory synaptic transmission to cholinergic neurons of the laterodorsal tegmental nucleus. *Eur. J. Neurosci.* 44, 3035–3045. doi: 10.1111/ejn.13405

Tononi, G., and Cirelli, C. (2019). Sleep and synaptic down-selection. *Eur. J. Neurosci.* [Epub ahead of print].

Tsai, H., Zhang, F., Adamantidis, A., Stuber, G. D., Bonci, A., Lecea, L., et al. (2009). Phasic firing in dopaminergic neurons is sufficient for behavioral conditioning. *Science* 324, 1080–1084. doi: 10.1126/science.1168878.Phasic

Ungless, M. A., Whistler, J. L., Malenka, R. C., and Bonci, A. (2001). Single cocaine exposure in vivo induces long-term potentiation in dopamine neurons. *Nature* 411, 583–587. doi: 10.1038/35079077

van Dort, C. J., Zachs, D. P., Kenny, J. D., Zheng, S., and Goldblum, R. R. (2015). Optogenetic activation of cholinergic neurons in the PPT or LDT induces REM sleep. *PNAS* 112, 584–589. doi: 10.1073/pnas.1423136112

Vincent, S. R., Satoh, K., Armstrong, D. M., and Fibiger, H. C. (1983). NADPH-diaphorase: a selective histochemical marker for the cholinergic neurons of the pontine reticular formation. *Neurosci. Lett.* 43, 31–36. doi: 10.1016/0304-3940(83)90124-6

Wang, H., and Morales, M. (2009). Pedunculopontine and laterodorsal tegmental nuclei contain distinct populations of cholinergic, glutamatergic and GABAergic neurons in the rat. *Eur. J. Neurosci.* 29, 340–358. doi: 10.1111/j.1460-9568.2008.06576.x

Washburn, M. S., Numberger, M., Zhang, S., and Dingledine, R. (1997). Differential dependence on glur2 expression of three characteristic features of AMPA receptors. *J. Neurosci.* 17, 9393–9406. doi: 10.1523/jneurosci.17-24-09393.1997

Weiner, D. M., Levey, A. I., and Brann, M. R. (1990). Expression of muscarinic acetylcholine and dopamine receptor mRNAs in rat basal ganglia. *Proc. Natl. Acad. Sci. USA* 87, 7050–7054. doi: 10.1073/pnas.87.18.7050

Whitaker, L. R., Carneiro de Oliveira, P. E., McPherson, K. B., Fallon, R. V., Planeta, C. S., Bonci, A., et al. (2016). Associative learning drives the formation of silent synapses in neuronal ensembles of the nucleus accumbens. *Biol. Psychiatry* 80, 246–256. doi: 10.1016/j.biopsych.2015.08.006

White, N. M., Packard, M. G., and Hiroi, N. (1991). Place conditioning with dopamine D1 and D2 agonists injected peripherally or into nucleus accumbens. *Psychopharmacology* 103, 271–276. doi: 10.1007/bf02244216

Witten, I. B., Steinberg, E. E., Lee, S. Y., Davidson, T. J., Zalocusky, K. A., Brodsky, M., et al. (2011). Recombinase-driver rat lines: tools, techniques, and optogenetic application to dopamine-mediated reinforcement. *Neuron* 72, 721–733. doi: 10.1016/j.neuron.2011.10.028

Wolfman, S. L., Gill, D. F., Bogdanic, F., Long, K., Al-Hasani, R., McCall, J. G., et al. (2018). Nicotine aversion is mediated by GABAergic interpeduncular nucleus inputs to laterodorsal tegmentum. *Nat. Commun.* 9, 1–11. doi: 10.1038/s41467-018-04654-2

Woolf, N. J., and Butcher, L. (1986). Cholinergic systems in the rat brain: III . Projections From the Pontomesencephalic Tegmentum the Thalamus, Tectum, Basal Ganglia, and Basal Forebrain. *Brain Res. Bull.* 16, 603–637. doi: 10.1016/0361-9230(86)90134-6

Xia, J., Meyers, A. M., and Beeler, J. A. (2017). Chronic nicotine alters corticostriatal plasticity in the striatopallidal pathway mediated by NR2B-containing silent synapses. *Neuropsychopharmacology* 42, 2314–2324. doi: 10.1038/npp.2017.87

Xiao, C., Cho, J. R., Zhou, C., Treweek, J. B., Chan, K., McKinney, S. L., et al. (2016). Cholinergic mesopontine signals govern locomotion and reward through dissociable midbrain pathways. *Neuron* 90, 333–347. doi: 10.1016/j.neuron.2016.03.028

Yamaguchi, T., Qi, J., Wang, H. L., Zhang, S., and Morales, M. (2015). Glutamatergic and dopaminergic neurons in the mouse ventral tegmental area. *Eur. J. Neurosci.* 41, 760–772. doi: 10.1111/ejn.12818

Yan, Y., Beckley, N. A., Kim, V. J., and Drenan, R. M. (2019). Differential nicotinic modulation of glutamatergic and GABAergic VTA microcircuits. *eNeuro* 6, 1–12. doi: 10.1523/ENEURO.0298-19.2019

Yan, Y., Peng, C., Arvin, M. C., Jin, X.-T., Kim, V. J., Ramsey, M. D., et al. (2018). Nicotinic cholinergic receptors in VTA glutamate neurons modulate excitatory transmission. *Cell Rep.* 23, 2236–2244. doi: 10.1016/j.celrep.2018.04.062

Yang, H., Yang, J., Xi, W., Hao, S., Luo, B., He, X., et al. (2016). Laterodorsal tegmentum interneuron subtypes oppositely regulate olfactory cue-induced innate fear. *Nat. Neurosci.* 19, 283–289. doi: 10.1038/nn.4208

Yang, Z., Wang, S., Yang, J., Hodgkinson, C. A., Iarikova, P., Ma, J. Z., et al. (2015). The contribution of rare and common variants in 30 genes to risk nicotine dependence. *Mol. Psychiatry* 20, 1467–1478. doi: 10.1038/mp.2014.156

Yochum, C., Doherty-lyon, S., Hoffman, C., Hossain, M. M., Zelikoff, J. T., and Richardson, J. R. (2014). Prenatal cigarette smoke exposure causes hyperactivity and aggressive behavior: role of altered catecholamines and BDNF. *Exp. Neurol.* 254, 145–152. doi: 10.1016/j.expneurol.2014.01.016

Yokel, R. A., and Wise, R. A. (1975). Increased lever pressing for amphetamine after pimozide in rats: implications for a dopamine theory of reward. *Science (80-.).* 187, 547–549. doi: 10.1126/science.1114313

Yuan, T., and Bellone, C. (2013). Glutamatergic receptors at developing synapses: the role of GluN3A-containing NMDA receptors and GluA2-lacking AMPA receptors. *Eur. J. Pharmacol.* 719, 107–111. doi: 10.1016/j.ejphar.2013.04.056

Yuan, T., Mameli, M., O'Connor, E. C., Dey, P. N., Verpelli, C., Sala, C., et al. (2013). Expression of cocaine-evoked synaptic plasticity by GluN3A-Containing NMDA Receptors. *Neuron* 80, 1025–1038. doi: 10.1016/j.neuron.2013.07.050

Zhang, W., Basile, A. S., Gomeza, J., Volpicelli, L. A., Levey, A. I., and Wess, J. (2002). Characterization of central inhibitory muscarinic autoreceptors by the use of muscarinic acetylcholine receptor knock-out mice. *J. Neurosci.* 22, 1709–1717. doi: 10.1523/jneurosci.22-05-01709.2002

Zhang, W., and Linden, D. J. (2003). The other side of the engram: experience-driven changes in neuronal intrinsic excitability. *Nat. Neurosci.* 4, 885–900. doi: 10.1038/nrn1248

Zhao, M., Toyoda, H., Lee, Y., Wu, L., Ko, S. W., Zhang, X., et al. (2005). Roles of NMDA NR2B subtype receptor in prefrontal long-term potentiation and contextual fear memory. *Neuron* 47, 859–872. doi: 10.1016/j.neuron.2005.08.014

Conflict of Interest: The authors declare that the research was conducted in the absence of any commercial or financial relationships that could be construed as a potential conflict of interest.

frontiers in Synaptic Neuroscience

ORIGINAL RESEARCH
published: 25 March 2020
doi: 10.3389/fnsyn.2020.00013

Stereotactically Injected Kv1.2 and CASPR2 Antisera Cause Differential Effects on CA1 Synaptic and Cellular Excitability, but Both Enhance the Vulnerability to Pro-epileptic Conditions

Timo Kirschstein[1,2,3]†, Erika Sadkiewicz[1†], Gerda Hund-Göschel[1†], Juliane Becker[1], Xiati Guli[1], Steffen Müller[1], Marco Rohde[1], Dora-Charlotte Hübner[1], Hannes Brehme[2], Stephan Kolbaske[2], Katrin Porath[1], Tina Sellmann[1], Annette Großmann[4], Matthias Wittstock[2], Steffen Syrbe[5], Alexander Storch[2,3] and Rüdiger Köhling[1,3]*

[1] Oscar Langendorff Institute of Physiology, University of Rostock, Rostock, Germany, [2] Department of Neurology, University of Rostock, Rostock, Germany, [3] Center of Transdisciplinary Neurosciences Rostock, University of Rostock, Rostock, Germany, [4] Institute of Diagnostic and Intervention Radiology, University of Rostock, Rostock, Germany, [5] Clinik for Pediatric and Adolescent Medicine, University of Heidelberg, Heidelberg, Germany

OPEN ACCESS

Edited by:
Ka Wan Li,
Vrije Universiteit Amsterdam, Netherlands

Reviewed by:
Nikhil J. Pandya,
Roche (Switzerland), Switzerland
Aleksey V. Zaitsev,
Institute of Evolutionary Physiology and Biochemistry (RAS), Russia

***Correspondence:**
Timo Kirschstein
timo.kirschstein@uni-rostock.de

[†] These authors have contributed equally to this work

Received: 02 October 2019
Accepted: 06 March 2020
Published: 25 March 2020

Citation:
Kirschstein T, Sadkiewicz E, Hund-Göschel G, Becker J, Guli X, Müller S, Rohde M, Hübner D-C, Brehme H, Kolbaske S, Porath K, Sellmann T, Großmann A, Wittstock M, Syrbe S, Storch A and Köhling R (2020) Stereotactically Injected Kv1.2 and CASPR2 Antisera Cause Differential Effects on CA1 Synaptic and Cellular Excitability, but Both Enhance the Vulnerability to Pro-epileptic Conditions. Front. Synaptic Neurosci. 12:13. doi: 10.3389/fnsyn.2020.00013

Purpose: We present a case of voltage-gated potassium channel (VGKC) complex antibody-positive limbic encephalitis (LE) harboring autoantibodies against Kv1.2. Since the patient responded well to immunotherapy, the autoantibodies were regarded as pathogenic. We aimed to characterize the pathophysiological role of this antibody in comparison to an antibody against the VGKC-associated protein contactin-associated protein-2 (CASPR2).

Methods: Stereotactic injection of patient sera (anti-Kv1.2-associated LE or anti-CASPR2 encephalopathy) and a control subject was performed into the hippocampus of the anesthetized rat *in vivo*, and hippocampal slices were prepared for electrophysiological purposes. Using extra- and intracellular techniques, synaptic transmission, long-term potentiation (LTP) and vulnerability to pro-epileptic conditions were analyzed.

Results: We observed that the slope of the field excitatory postsynaptic potential (fEPSP) was significantly increased at Schaffer collateral-CA1 synapses in anti-Kv1.2-treated and anti-CASPR2-treated rats, but not at medial perforant path-dentate gyrus synapses. The increase of the fEPSP slope in CA1 was accompanied by a decrease of the paired-pulse ratio in anti-Kv1.2, but not in anti-CASPR2 tissue, indicating presynaptic site of anti-Kv1.2. In addition, anti-Kv1.2 tissue showed enhanced LTP in CA1, but dentate gyrus LTP remained unaltered. Importantly, LTP in slices from anti-CASPR2-treated animals did not differ from control values. Intracellular recordings from CA1 neurons revealed that the resting membrane potential and a single action potential were not different between anti-Kv1.2 and control tissue. However, when the

depolarization was prolonged, the number of action potentials elicited was reduced in anti-Kv1.2-treated tissue compared to both control and anti-CASPR2 tissue. In contrast, polyspike discharges induced by removal of Mg^{2+} occurred earlier and more frequently in both patient sera compared to control.

Conclusion: Patient serum containing anti-Kv1.2 facilitates presynaptic transmitter release as well as postsynaptic depolarization at the Schaffer-collateral-CA1 synapse, but not in the dentate gyrus. As a consequence, both synaptic transmission and LTP in CA1 are facilitated and action potential firing is altered. In contrast, anti-CASPR2 leads to increased postsynaptic potentials, but without changing LTP or firing properties suggesting that anti-Kv1.2 and anti-CASPR2 differ in their cellular effects. Both patient sera alter susceptibility to epileptic conditions, but presumably by different mechanisms.

Keywords: limbic encephalitis, voltage-gated potassium channel, synaptic transmission, long-term potentiation, spike frequency adaptation

INTRODUCTION

Twenty years ago, limbic encephalitis (LE) associated with antibodies against voltage-gated potassium channels (VGKC) was described as a potentially reversible autoimmune encephalitis responding to immunotherapies which was in striking contrast to the formerly known forms of paraneoplastic encephalitis associated with antibodies against intracellular antigens (Buckley et al., 2001). Since VGKC antibodies interfered with the binding of the Kv1 channel blocker dendrotoxin (Hart et al., 2002), VGKC antibodies were believed to bind Kv1 channels. However, it turned out that VGKC antibodies were raised against Kv1-channel complex proteins such as leucine-rich, glioma inactivated 1 (LGI1) and contactin-associated protein-2 (CASPR2) (Lai et al., 2010; Irani et al., 2010). Recently, a large series of sera with VGKC complex antibodies were re-analyzed and only 56% harbored antibodies against LGI1 or CASPR2 (Lang et al., 2017). Almost all of the remaining sera, called double-negative VGKC complex antibody-positive samples, had cytosolic targets, but one serum bound to live hippocampal neurons, suggesting a possible novel surface antigen (Lang et al., 2017).

In this study, we present a case with LE admitted to our emergency presenting with status epilepticus. The patient's serum was double-negative VGKC complex antibody-positive. Further analysis by a commercial laboratory revealed anti-Kv1.2, i.e., a pore-forming subunit of the VGKC Kv1. Since the patient responded well to immunotherapy, the autoantibodies were regarded as pathogenic in nature. In the hippocampus, Kv1.2 channels are particularly present in the middle molecular layer of the dentate gyrus, the CA1 stratum radiatum, and the CA1 stratum lacunosum-moleculare with the most striking immunoreactivity observed on axons and presynaptic terminals (Wang et al., 1993, 1994; Sheng et al., 1994; Monaghan et al., 2001; Gu et al., 2003; Wenzel et al., 2007; Lorincz and Nusser, 2008). Dendritic, but not somatic expression was also reported for cortical and hippocampal pyramidal cells (Sheng et al., 1994; Guan et al., 2006). In contrast, dentate granule cells appeared to be immunonegative (Sheng et al., 1994), and mossy fibers as well as CA3 pyramidal neurons seem to express Kv1.2 only during ontogenesis at immature stages (Prüss et al., 2010).

Functionally, Kv1.2 encodes a slowly activating and slowly inactivating D-type K^+ conductance when expressed in Xenopus oocytes (Stühmer et al., 1989). D-type K^+ currents in central neurons are primarily mediated by Kv1.1 and Kv1.2, both members of the Kv1 channel subfamily. They were recorded from CA1 neurons, and the activation and inactivation curves of D-type K^+ currents cross near the resting membrane potential (RMP) giving rise to a window current (Storm, 1988), hence making this current powerfully regulate the neuron's action potential threshold (Golding et al., 1999; Cudmore et al., 2010). The slow inactivation properties of Kv1 channels, in turn, contribute to spike repolarization (Mitterdorfer and Bean, 2002). Although Kv1.1 is much more widely expressed in the hippocampus than Kv1.2 (Wang et al., 1993, 1994; Veh et al., 1995; Grigg et al., 2000), Kv1.2 knock-out mice die after 15–18 days and are more prone to seizures than mice lacking Kv1.1 (Smart et al., 1998; Brew et al., 2007) supporting the view that Kv1.2 channels are crucial for hippocampal functional integrity. In this study, we injected patient sera containing anti-Kv1.2 or anti-CASPR2 into the rat hippocampus and asked whether synaptic or intrinsic properties were altered in the tissue from these rats.

MATERIALS AND METHODS

Case of Kv1.2-Associated Limbic Encephalitis

A 74-year-old male patient was admitted to our emergency with the history of at least two epileptic seizures witnessed by the prehospital emergency medical services. One of these seizures was reported to have presented with a focal onset (orofacial motor symptoms and gaze preference to the left side). Upon initial neurological assessment, he was comatose (Glasgow Coma Scale 3) most likely due to status epilepticus and presented

with tetraparesis, but accentuated at the left side. Therefore, he immediately received endotracheal intubation and mechanical ventilation. Computed tomography was inconclusive, the further clinical and paraclinical work-up revealed inflammation (leukocytes 9500/μl; C-reactive protein 90 μmol/l) which was suspected to be associated with aspiration pneumonia, but electrolytes as well as renal and hepatic function did not explain the patient's clinical situation. The subsequently performed MRI found hyperintense cortices in the right hemisphere, in particular the temporal lobe which was attributed to status epilepticus or encephalitis (**Figure 1**). The EEG showed epileptic discharges on right hemispheric leads (**Figure 1**). Hence, we started to treat the patient with levetiracetam and propofol for sedation. Analysis of the cerebrospinal fluid showed increased protein and lactate levels, but could not evidence an acute infectious inflammation (leukocytes 1/μl, lactate 4 mmol/l, protein 520 mg/l, albumin 370 mg/l, negative for intrathecal immunoglobulin synthesis, identical oligoclonal bands in CSF and serum, i.e., type IV reaction). Neurotropic viruses (HSV, VZV, CMV, and EBV) as well as lyme neuroborreliosis were also ruled out. Given the suspected LE, we tested a battery of autoantibodies and found a positive titer for antibodies against VGKCs (115 pmol/l). Unexpectedly, anti-LG1 was negative, but a novel antibody, IgG against the pore-forming subunit KCNA2 (also called Kv1.2), could be detected (titer 1:10, Euroimmun, Lübeck, Germany). The patient received five episodes of plasmapheresis, and subsequently recovered from comatose state and spontaneously opened his eyes. We received blood serum samples together with the permission to keep these samples in −20°C for further scientific studies. The patient was supplied with a percutaneous endoscopic gastrostoma as well as a tracheostoma and was successfully transferred to rehabilitation 4 weeks after admission.

Case of Anti-CASPR2 Encephalopathy

A 1-year and 8 months old boy was admitted for change of behavior with unprovoked crying, suspected pain, and severe sleeplessness. He developed treatment refractive hypertonia and general weakness. Brain MRI, whole body MRI and laboratory work-up was unremarkable. Cerebrospinal fluid analysis showed mild pleocytosis (12 leucocytes, normal protein, no oligoclonal bands). Neurotropic viruses and neuroborreliosis were ruled out. Testing for antineural antibodies revealed high titer anti-CASPR2 (1:1280) in serum only (VGKC 119 pmol/l). Electrophysiological studies with nerve conductions studies and EEG were normal. Pediatric Morvan syndrome was diagnosed and he received treatment with intravenous immunoglobulins and repeated methylprednisolone pulses which resulted in resolution of acute symptoms. At 3 years of age, he was diagnosed with autism spectrum disorder. The patient's clinical and serological findings were reported within a series of children with CASPR2 autoimmunity (Syrbe et al., 2020).

Stereotactic Intrahippocampal Serum Injection *in vivo*

Stereotactic injection of the serum from the case patients or a non-epileptic control subject into both hippocampi *in vivo* was performed as previously described (Blome et al., 2018; Kersten et al., 2019). Briefly, 75 male Wistar rats (8–10 weeks old, Charles River, Sulzfeld, Germany) were anesthetized with S-ketamine (100 mg/kg i.p.) and xylazine (15 mg/kg i.p.) and mounted on a stereotactic frame (Narishige, Tokyo, Japan). Using a Hamilton syringe (75N; Hamilton AG, Bonaduz, Switzerland) patient or control serum was slowly (10 steps of 0.5 μl every 2 min, total of 5 μl for each side) injected into the hippocampus with the following coordinates: 5.2 mm posterior, ±4.3 mm lateral, 4.8 mm deep (relative to bregma). These coordinates were obtained in previous studies (Blome et al., 2018; Kersten et al., 2019). After completing the injection, the syringe remained *in situ* for another 2 min to enable proper serum diffusion into the hippocampus. After surgery, rats were given metamizole (100–150 mg/kg) for postoperative pain control and allowed to recover in an atmosphere with enhanced oxygen fraction (4–5 l/min in an 8 l glass vessel). There was one rat (anti-Kv1.2 group) showing severe respiratory insufficiency and was thus killed during anesthesia, but no further severe morbidity or mortality was observed (overall lethality 1/98). Due to the randomization process, rats treated with anti-Kv1.2, anti-CASPR2 or control serum did not differ significantly in weight during surgery (anti-Kv1.2: 256 ± 10 g, n = 36; control: 265 ± 10 g, n = 39; anti-CASPR2: 298 ± 12 g, n = 23) or in latency between surgery and slice preparation (anti-Kv1.2: 2.6 ± 0.3 days; control: 3.1 ± 0.4 days; anti-CASPR2: 3.6 ± 0.5 days). Moreover, experimenters were blinded to the injected serum (whether anti-Kv1.2, anti-CASPR2 or control serum). In addition, we also used 11 naive, non-operated rats for input–output relations and long-term zero Mg^{2+} experiments as a second control. All procedures were performed according to national and international guidelines on the ethical use of animals (European Council Directive 86/609/EEC, approval of local authority LALLF M-V/TSD/7221.3-1.1-017/11 and M-V/TSD/7221.3-1.1-007/16), and all efforts were made to minimize animal suffering and to reduce the number of animals used.

Immunodetection of Anti-Kv1.2 in Patient Serum

The immunoreactivity of patient serum was tested by immunofluorescence and Western blot analysis. To this end, hippocampal brain slices of adult male Wistar rats were obtained and either used for immunofluorescence or Western blot. In order to increase the protein content of the IgG fraction, the patient serum was concentrated by a factor of 4 with centrifugal concentrators (Vivaspin) using a 100 kDa molecular weight cutoff filter to omit the albumin fraction. For Western blot analysis, the hippocampal tissue was homogenized in RIPA buffer to disrupt cells. The crude extract was centrifuged to yield a clear protein solution. Performing SDS gel electrophoresis, a total of 15 μg proteins were separated and blotted onto PVDF membranes (Immobilon-FL, Millipore). Overnight incubation with a commercial rabbit polyclonal anti-Kv1.2 antibody (1:1000, Alomone, #APC-010) or patient serum was followed by secondary antibody reaction (anti-human or anti-rabbit IRDye 800CW, Odyssey). Specific proteins band were

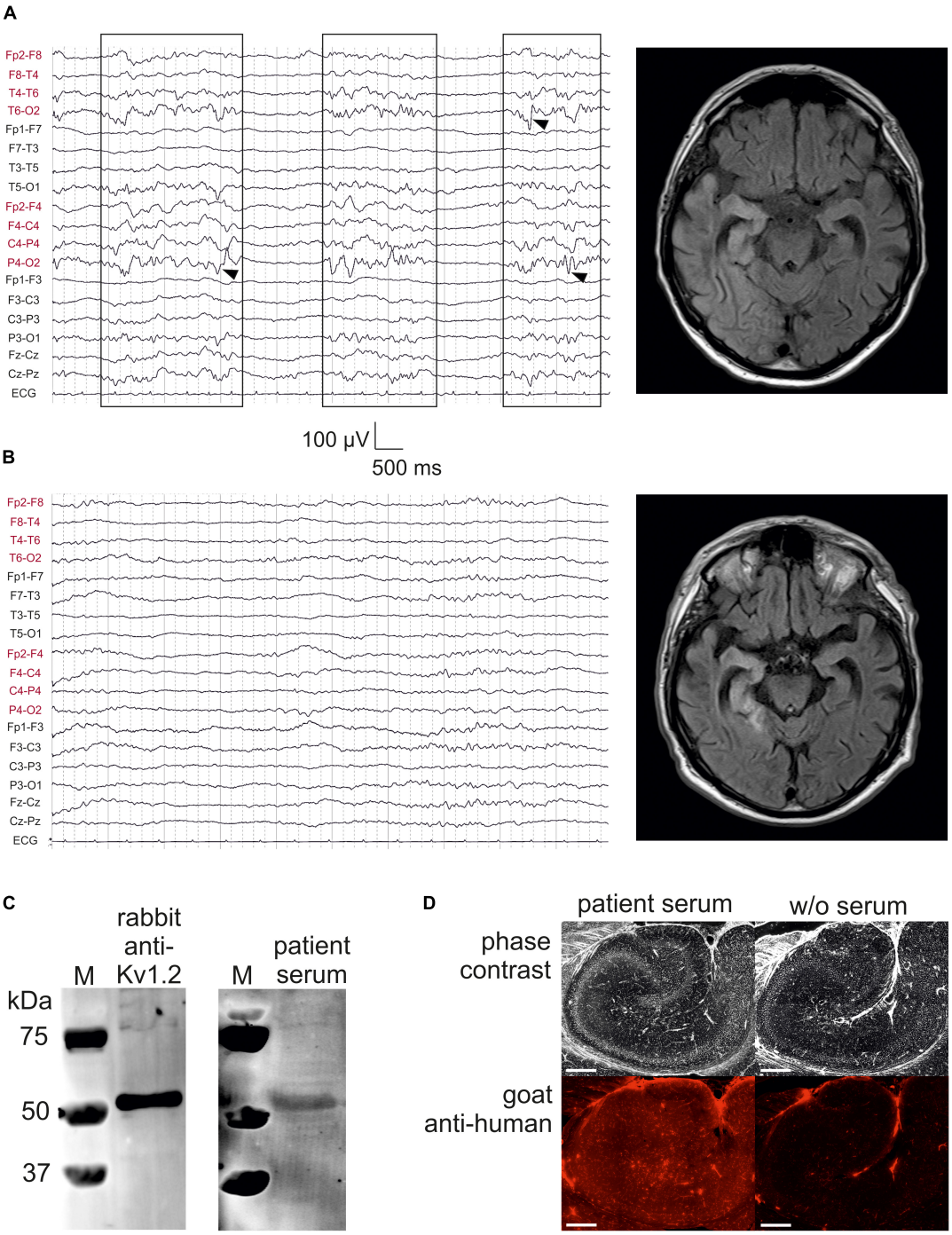

FIGURE 1 | Kv1.2-associated limbic encephalitis. **(A)** EEG and FLAIR MRI on the day of admission, but after starting sedation with propofol. There were bursts of right-sided delta activity and sharp transients (boxes with arrowheads) interrupted by nearly isoelectric lines, consistent with the hyperintensities in right temporoparietal structures involving the mesial temporal lobe. **(B)** EEG and FLAIR MRI after 7 days of treatment at the intensive care unit. Note the low-voltage burst-suppression-like pattern indicating therapeutic coma. On the MRI, hyperintensive lesions have concentrated to temporomesial structures. **(C)** Western blot analysis of rat CA1 protein lysate stained with rabbit anti-Kv1.2 (left panel) and patient serum (right panel). M, marker. **(D)** Specific binding of patient serum serum (left panel) was also confirmed as compared to negative control (w/o serum, right panel). Scale bar = 500 µm.

visualized using the Odyssey infrared imaging scanner (Li-cor). For immunofluorescence staining, the slices were fixed in 3.7% formaldehyde solution, then cryo-preserved with 30% buffered sucrose solution at 4°C overnight and finally frozen. Thin layers of 50 µm thickness were sliced using a cryo-vibratome and mounted on microscope object carriers. Immunoreaction was

carried out with or without patient serum (negative control). Fluorescence signals emerged from Cy5-coupled secondary antibodies (goat anti-human, Invitrogen) and were visualized using a Leica DMI 6000B fluorescence microscopy under identical conditions. Each image was taken in a tile scan mode to receive an overview picture from the hippocampus.

Electrophysiological Recordings and LTP Induction

Hippocampal slices were prepared 1 to 6 days after stereotactic surgery (Blome et al., 2018; Kersten et al., 2019). Briefly, rats were decapitated in deep anesthesia with diethyl ether, the brains were rapidly removed and submerged into oxygenated ice-cold dissection solution containing (in mM) 125 NaCl, 26 $NaHCO_3$, 3 KCl, 1.25 NaH_2PO_4, 0.2 $CaCl_2$, 5 $MgCl_2$ and 13 D-glucose (95% O_2, 5% CO_2; pH 7.4; 306–314 mosmol/kg). Horizontal hippocampal brain slices (400 μm) were cut using a vibratome (Campden Instruments, Loughborough, United Kingdom), and slices were then transferred into a holding chamber containing artificial cerebrospinal fluid (ACSF) containing (in mM) 125 NaCl, 26 $NaHCO_3$, 3 KCl, 1.25 NaH_2PO_4, 2.5 $CaCl_2$, 1.3 $MgCl_2$ and 13 D-glucose (306–314 mosmol/kg, bubbled with 95% O_2 and 5% CO_2 to maintain the pH at 7.4).

Synaptic transmission and plasticity were assessed by recording field excitatory postsynaptic potentials (fEPSPs) from CA1 or from the dentate gyrus. The slices were continuously bathed in oxygenated ACSF (flow rate of 2 ml/min, temperature 32 ± 1°C, npi electronic GmbH, Tamm, Germany). For stimulation of the afferent fibers (Schaffer collaterals, or medial perforant path, respectively), bipolar stimulating electrodes fabricated from teflon-insulated platinum wire electrodes (PT-2T, Science Products, Hofheim, Germany) were placed into CA1 stratum radiatum or dentate gyrus middle molecular layer, respectively. Stimuli were delivered through a stimulus isolator (A365, World Precision Instruments, Sarasota, FL, United States) triggered by a Master-8 stimulator (A.M.P.I., Jerusalem, Israel), and the stimulus intensity was routinely increased from 25 to 300 μA. For the prospective analysis of fEPSP slopes (**Figure 3C**), we adjusted the stimulus intensity in each slice to the half-maximum amplitude, which was typically around 85 μA (between 75 and 125 μA). The same procedure was done to establish the baseline stimulus intensity for LTP experiments. NMDAR-dependent LTP was induced by a paradigm consisting of 10 trains of 20 stimuli at 100 Hz (stimulus duration 100 μs, intertrain interval 800 ms, at double baseline stimulation intensity, Blome et al., 2018; Kersten et al., 2019). NMDAR-independent LTP was induced by a similar paradigm (stimulus duration 100 μs, intertrain interval 800 ms, at double baseline stimulation intensity), but in the presence of D-AP5 (50 μM). Recording electrodes filled with ACSF were placed into CA1 stratum radiatum or dentate gyrus middle molecular layer, respectively. Analog recording signals were amplified, filtered at 1 kHz by an EXT-10-2F (npi electronic GmbH, Tamm, Germany), and digitized with a Micro1401 analog-to-digital converter (Cambridge Electronic Design, Cambridge, United Kingdom) using Signal 2.16 software (Cambridge Electronic Design, Cambridge, United Kingdom). Chemicals used for physiological solutions were purchased from Sigma-Aldrich (Taufkirchen, Germany).

Intracellular recordings were performed in CA1 pyramidal cells impaled with borosilicate glass microelectrodes (80–120 MΩ, pulled with Sutter P-97 and filled with 3 M potassium acetate and 0.013 M KCl) using an SEC-10LX amplifier (npi electronic). In these recordings, RMP was determined, and action potentials were elicited by short (duration 7 ms, from +0.5 to +2.4 nA in 0.1-nA-steps, interstimulus-interval 1.1 s) or prolonged current injections (duration 600 ms, from −1.0 to +1.0 nA in 0.1-nA-steps, interstimulus interval 10 s). Action potential (AP) threshold was assessed as the voltage at the point of the steepest slope of the AP upstroke (i.e., the beginning of the upstroke). We also determined AP amplitude, AP overshoot, and AP duration at half-maximum amplitude (width at half), and the afterhyperpolarizing potential following prolonged depolarization (600 ms, +1.0 nA). Digitization at 10 kHz and offline data processing were performed with the CED package (Micro1401 analog-to-digital converter, Signal 2.16 software, all from Cambridge Electronic Design, Cambridge, United Kingdom).

Acutely Induced Epileptiform Discharges

In order to test the effect of anti-Kv1.2 on acutely induced epilepsy, we evoked spontaneous epileptic discharges by removal of Mg^{2+} from the bath. In these experiments, the extracellular electrode was placed in the upper blade of the dentate gyrus molecular layer. At the beginning of each experiment, the absence of spontaneous epileptic discharges was confirmed by recording under baseline conditions for at least 20 min. Then Mg^{2+} was omitted from the ACSF, and the recordings were maintained for further 60 min. Spontaneous epileptic events were counted in each slice for the entire recording period of 80 min. Occasionally, epileptic events consisted of more than one spike discharge. In a second approach, these polyspike discharges were analyzed individually. Further events, such as seizure-like episodes or spreading depressions, were also documented.

Statistical Analysis

Data are expressed as mean values ± the standard error of the mean (SEM) or box-whisker plots (created with SigmaStat 3.5: box = quartiles, whiskers = 10/90% percentiles). For statistical evaluation, data were first tested for normal distribution and equal variance (SigmaStat 3.5). Depending on this normality test, statistical comparisons were performed either using parametric (paired or unpaired *t*-test, ANOVA) or non-parametric tests (Mann–Whitney test) as indicated. The level of significance is indicated by asterisks ($^*P < 0.05$, $^{**}P < 0.01$).

RESULTS

We present a case with status epilepticus due to anti-Kv1.2-associated LE, presenting with lateralized delta activity as well as sharp transients, predominantly over right posterior hemispheric leads (**Figure 1A**, left panel). Bursts of focal slowing and epileptiform potentials (boxes with arrowheads in **Figure 1A**)

were interrupted by nearly isoelectric lines as a result from propofol medication in the mechanically ventilated patient (burst-suppression pattern). FLAIR MRI at this time point clearly showed high signal intensities on the right temporoparietal lobes with strong involvement of temporomesial structures (**Figure 1A**, right panel), consistent with the right-sided epileptic activity. One week later, these hyperintense lesions tended to concentrate on these temporomesial structures providing *post hoc* evidence for the LE (**Figure 1B**, right panel). The EEG at this time point showed typical burst-suppression due to therapeutic coma rather than lateralized epileptic activity (**Figure 1B**, left panel).

To test the specificity of the patient serum, we performed a Western blot analysis using rat CA1 hippocampal protein lysate immunoblotted with rabbit anti-Kv1.2 which detected a band consistent with the expected molecular weight of rat Kv1.2 (499 amino acids, 57 kDa; **Figure 1C**, left panel). When this primary antibody was replaced by concentrated albumin-free patient serum counterstained by an anti-human secondary antibody, the same band was obtained (**Figure 1C**, right panel). Importantly, there were no further bands in this blot suggesting that the predominant protein identified by the patient serum presumably represented Kv1.2. Immunohistochemistry on a rat hippocampal section confirmed that albumin-free patient serum (**Figure 1D**, left panel) showed specific binding as compared to the negative control without serum (**Figure 1D**, right panel).

Pre- and Postsynaptic Excitability and Plasticity

In this study, we aimed to study the effects of patient serum containing anti-Kv1.2 on synaptic function. To this end, we stereotactically injected serum into the hippocampus *in vivo* and obtained horizontal hippocampal brain slices 1–6 days after surgery. We studied the Schaffer collateral-CA1 synapse and the medial perforant path-dentate gyrus synapse, both typical expression sites of Kv1.2. Increasing stimulation intensities (25 to 300 μA) of the afferent fibers led to increasing excitatory postsynaptic field potentials (fEPSPs) in the respective hippocampal area (**Figure 2A**). Obviously, two-way ANOVA revealed a significant effect of stimulus intensity ($P < 0.01$ in both fields), but there was no significant interaction between stimulus intensity and animal group ($P < 0.9$ in both fields). While input–output relations did not show consistent significant differences for anti-Kv1.2 in the dentate gyrus (Tukey *post hoc* test: $P < 0.05$ between control and anti-Kv1.2, but $P = 0.429$ between naive and anti-Kv1.2), there was a consistent group effect in the CA1 area (Tukey *post hoc* test: $P = 0.01$ between anti-Kv1.2 and control as well as between anti-Kv1.2 and naive tissue, **Figure 2A**). Since we observed that the slope of the fEPSP recorded in CA1 was more negative in slices from anti-Kv1.2-treated than in control-injected rats (**Figure 2B**), we performed a further series of experiments and selected the half-maximum fEPSP of each experiment in order to determine the slope of this potential. As shown in **Figure 2C**, the negative slope of the half-maximum fEPSP in anti-Kv1.2-treated tissue was indeed significantly higher than in controls at Schaffer-collateral-CA1 synapses (anti-Kv1.2: $P < 0.05$, Student *t*-test), but not in the dentate gyrus ($P = 0.323$, Mann–Whitney *U* test). Since we aimed to compare anti-Kv1.2 effects with anti-CASPR2 effects, we used a further patient serum containing CASPR2 autoantibodies. In anti-CASPR2-treated tissue, the slope of the fEPSP was highly variable and, occasionally, we obtained fEPSPs with epileptic afterdischarges (38% of anti-CASPR2 slices, see arrowhead in rightmost traces, **Figure 2B**). Hence, the negative slope of the half-maximum fEPSP in this tissue was significantly higher than in control slices ($P < 0.001$, Mann–Whitney *U* test, **Figure 2C**) indicating enhanced synaptic transmission under both pathological conditions, but suggesting differences between anti-Kv1.2 and anti-CASPR2.

Increased fEPSP slopes may suggest a more synchronous transmitter release, for instance by an inhibitory effect of anti-Kv1.2 on presynaptic terminals, because Kv1 channels were reported to dampen presynaptic post-firing hyperexcitability (Dodson et al., 2003). One measure to address this question is to test paired-pulse plasticity. Since transmitter release probability is inversely related to the paired-pulse ratio (PPR; Zucker, 2002), we delivered paired pulses (interstimulus interval 40 ms). As expected, the PPR of fEPSP slopes in the dentate gyrus was not significantly altered (anti-Kv1.2: 89 ± 4%, $n = 16$; control: 92 ± 4%, $n = 11$; $P = 0.608$; Mann–Whitney *U* test; **Figure 2D**), but confirmed the typical paired-pulse depression in the medial perforant path (Dietrich et al., 1997). In contrast, slices from anti-CASPR2-treated animals showed paired-pulse facilitation rather than depression (110 ± 9%, $n = 9$, **Figure 2D**) which could suggest that anti-CASPR2 leads to presynaptic inhibition at medial perforant path terminals. In contrast, we obtained significantly reduced PPR of fEPSP slopes in the CA1 area from anti-Kv1.2 tissue as compared to control (anti-Kv1.2: 129 ± 7%, $n = 12$; control: 153 ± 8%, $n = 13$; $P < 0.05$, Mann–Whitney *U* test; **Figure 2D**), suggesting an increased transmitter release probability at these synapses. The PPR in anti-CASPR2 slices was only slightly reduced (133 ± 6%, $n = 16$, $P = 0.076$ versus control, Mann–Whitney *U* test; **Figure 2D**) indicating that the increased fEPSP slope in this tissue was partially due to increased presynaptic transmitter release, but may have involved other mechanisms such as network disinhibition.

So far, these data suggest that anti-Kv1.2 and anti-CASPR2 differ in their effects on Schaffer collateral presynaptic function. However, they cannot exclude that postsynaptic cells may also be altered in anti-Kv1.2 or anti-CASPR2 tissue. To control for this, we performed intracellular recordings of CA1 neurons from anti-Kv1.2, anti-CASPR2 and control rats. At first, there were no significant differences in the RMP and cellular membrane properties such as resistance and time constant between anti-Kv1.2 and controls (**Table 1**), indicating that anti-Kv1.2 did not significantly affect the leak conductance. When we applied short current injections to elicit a single action potential (duration 7 ms, interstimulus interval 1.1 s), there were again no differences in action potential characteristics (**Table 1**) arguing against major postsynaptic differences in intrinsic cellular excitability between these two groups. In contrast, cells from anti-CASPR2 tissue differed from cells recorded in control or anti-Kv1.2-treated slices (**Table 1**). It is important to note, however, that all significant

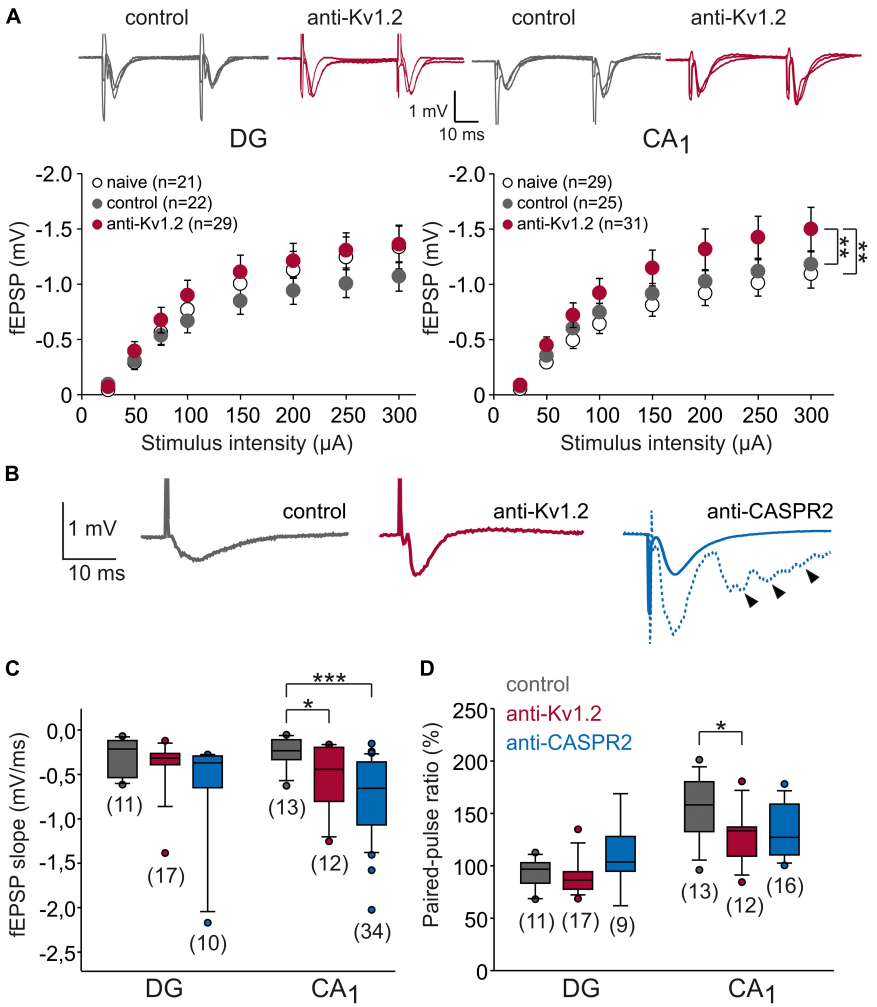

FIGURE 2 | Synaptic transmission is altered in CA1, but not the dentate gyrus. **(A)** Input–output relationships of dentate gyrus (DG) and CA1 area of the hippocampus. Sample traces were obtained by increasing stimulation intensities (100, 200, 300 µA). In CA1, but not in the dentate gyrus, fEPSPs from anti-Kv1.2 tissue (red symbols) were significantly different from those obtained in slices of control-injected (gray symbols) or non-operated rats (open symbols). Statistical comparison was performed using two-way ANOVA and Tukey *post hoc* tests (factors stimulus intensity and animal group). **(B)** Representative recordings of fEPSPs in the CA1 area showing the more negative slope in anti-Kv1.2 tissue (red trace) and anti-CASPR2 tissue (blue trace) as opposed to control-injected tissue (gray trace). Note that in anti-CASPR2 tissue, a proportion of cells showed epileptic afterdischarges at baseline (arrowheads in dashed blue trace). **(C)** Box-whisker plots of fEPSP slopes at the half-maximum size show significant differences in CA1 (*$P < 0.05$, Student *t*-test; ***$P < 0.001$, Mann–Whitney *U* test), but not in the dentate gyrus. **(D)** Box-whisker plots of paired-pulse ratio (PPR) show significant differences between anti-Kv1.2 and control in CA1 (*$P < 0.05$, Mann–Whitney *U* test), but not in the dentate gyrus.

TABLE 1 | Intrinsic CA1 pyramidal cell properties.

	Control (*n* = 9)	Anti-Kv1.2 (*n* = 11)	Anti-CASPR2 (*n* = 9)
Resting membrane potential	−58.4 ± 1.2 mV	−59.1 ± 1.6 mV	−62.5 ± 1.3 mV
Membrane resistance	45.7 ± 3.7 MΩ	43.1 ± 6.3 MΩ	39.7 ± 3.8 MΩ
Membrane time constant*	7.3 ± 0.7 ms	8.3 ± 0.6 ms	10.2 ± 0.8 ms (a)
Action potential amplitude	65.9 ± 2.0 mV	64.1 ± 2.4 mV	67.8 ± 1.3 mV
Action potential overshoot	6.6 ± 1.1 mV	4.5 ± 2.2 mV	3.3 ± 1.8 mV
Action potential width at half*	1.6 ± 0.1 ms	1.6 ± 0.1 ms	1.4 ± 0.05 ms (a,b)
Action potential threshold*	−45.1 ± 1.3 mV	−43.8 ± 2.4 mV	−51.0 ± 1.9 mV (a,b)
Afterhyperpolarizing potential*	−6.3 ± 0.9 mV	−5.9 ± 1.1 mV	−13.6 ± 1.5 mV (a,b)

Statistical comparisons were performed using ANOVA with Student–Newman–Keuls post hoc tests. Significant group effects are indicated with asterisks, the lowercase letters in parentheses indicate statistically significant differences between anti-CASPR2 and control (a), or between anti-CASPR2 and anti-Kv1.2 (b).

differences obtained (especially action potential characteristics and afterhyperpolarizing potential) are not compatible with an impaired K^+ channel function of CA1 neurons, but may rather indicate separate changes on the network level.

In addition, one unique property of Kv1.2, but not of other Kv1 channels, is the use-dependent activation (Baronas et al., 2015). Hence, we prolonged the current injection to 600 ms (500 pA) with an interstimulus interval of 10 s. Under these conditions, we observed that CA1 cells from anti-Kv1.2 showed a significantly reduced number of action potentials compared to control ($P < 0.05$, two-way ANOVA with factors current injection and animal group, followed by Tukey *post hoc* test; **Figure 3A**). Importantly, there was also a significant difference between anti-Kv1.2 and anti-CASPR2 ($P < 0.05$; **Figure 3A**), while there was no significant interaction between current injection and animal group ($P = 0.991$, two-way ANOVA). However, spike broadening was not different between all experimental groups as assessed by the action potential duration (width at half: 3rd AP relative to 1st: 168 ± 51%, $n = 11$ in anti-Kv1.2; 178 ± 59%, $n = 9$ in control; 176 ± 59%, $n = 9$ in anti-CASPR2; $P = 0.369$, one-way ANOVA).

Intriguingly, we also noticed that the first action potential occurred later in anti-Kv1.2-treated than in control tissue (see arrowheads in **Figure 3B**). This was a consistent finding, CA1 neurons from anti-Kv1.2 tissue showed significantly higher latencies to the first action potential compared to both control and anti-CASPR2 tissue ($P < 0.05$, two-way ANOVA with factors current injection and animal group, followed by Tukey *post hoc* test; **Figure 3C**). In addition, we analyzed the interspike interval duration during current injection (600 ms, +1.0 nA) and found significantly prolonged interspike intervals in cells from anti-Kv1.2-treated rats as compared to both other groups ($P < 0.01$ versus control and anti-CASPR2, two-way ANOVA with factors #interspike interval and animal group, followed by Tukey *post hoc* test; **Figure 3D**). Since the delayed firing in anti-Kv1.2 could not be attributed to an altered membrane time constant (**Table 1**), our data suggest that both pre- and postsynaptic sites may be involved in changes observed in anti-Kv1.2 tissue.

Next, we asked whether the level of achievable long-term potentiation (LTP) might be altered in anti-Kv1.2 tissue. Thus, we were interested in the propensity to activate postsynaptic NMDA receptors upon high-frequency extracellular afferent stimulation. Consistent with our previous data so far, LTP at the medial perforant path-dentate gyrus synapse was almost identical between all three groups (anti-Kv1.2: 120 ± 11%, $n = 22$; control: 120 ± 13%, $n = 20$; anti-CASPR2: 104 ± 5%, $n = 9$; **Figure 4A**), but in marked contrast, CA1-LTP in anti-Kv1.2-treated tissue (182 ± 11%, $n = 18$) was significantly higher as compared to both control (143 ± 14%, $n = 17$, $P < 0.05$, Student t-test) and anti-CASPR2 tissue (155 ± 10%, $n = 16$, $P < 0.05$, Mann–Whitney U test; **Figure 4B**). In addition, we also tested NMDAR-independent LTP at Schaffer collateral-CA1 synapses which was again significantly enhanced in slices from anti-Kv1.2-treated rats (143 ± 10%, $n = 18$; control: 109 ± 6%, $n = 15$, $P < 0.01$, Student t-test; anti-CASPR2: 106 ± 13%, $n = 15$, $P < 0.05$, Student t-test; **Figure 4C**). Taken together, these findings suggest that stereotactic injection with patient serum containing anti-Kv1.2 facilitates presynaptic transmitter release and postsynaptic depolarization at the Schaffer collateral-CA1 synapse, but not in the dentate gyrus, and as a consequence of this, both synaptic transmission and LTP in CA1 are facilitated. In contrast, patient serum containing anti-CASPR2 enhances postsynaptic responses, but rather independently of K^+ channel modulation, and does not interfere with LTP at Schaffer collateral-CA1 synapses.

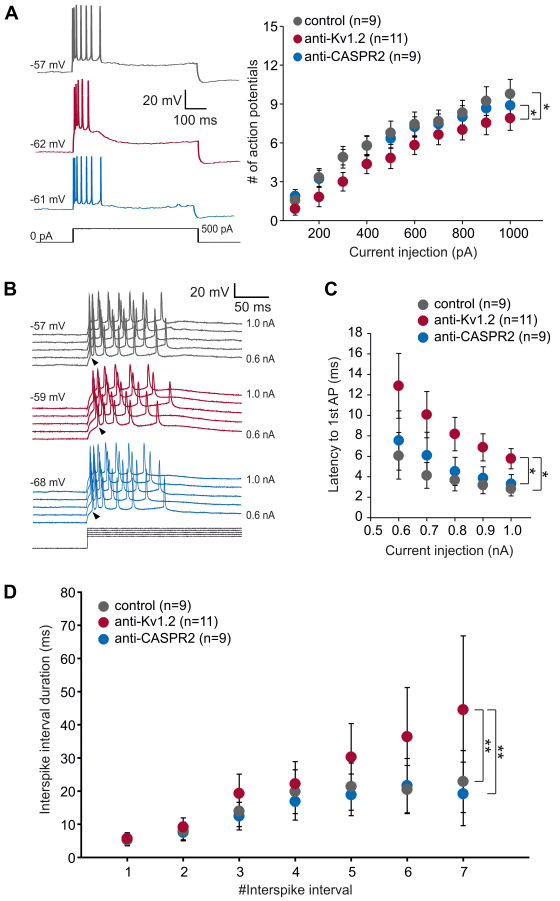

FIGURE 3 | Intrinsic properties of CA1 neurons. **(A)** Representative intracellular voltage recordings of a CA1 neuron from anti-Kv1.2 (red traces), control-injected (gray traces) and anti-CASPR2 (blue traces) animals evoked by prolonged current injection (500 pA, black trace). Two-way ANOVA and Tukey *post hoc* tests (factors current injection and animal group) detected a significant effect of animal group between anti-Kv1.2 and control (*$P < 0.05$) as well as between anti-Kv1.2 and anti-CASPR2 (*$P < 0.05$) regarding the number of action potentials elicited by depolarizing current injection (600 ms). Importantly, while there was a significant effect of current injection ($P < 0.05$), there was no significant interaction between current injection and animal group ($P = 0.991$). **(B)** Voltage recordings from CA1 neurons evoked by increasing steps of suprathreshold prolonged current injection (0.5 to 1.0 nA in 0.1-nA-steps, black traces). Arrowheads point to the onset of the first action potential which was delayed in anti-Kv1.2 tissue (red traces) as compared to control (gray traces) and anti-CASPR2 (blue traces). **(C)** The latency to the 1st AP was significantly delayed in anti-Kv1.2 tissue compared to both other groups (*$P < 0.05$, two-way ANOVA and Tukey *post hoc* test). **(D)** Interspike interval duration increases during the course of depolarization due to spike frequency adaptation. Cells from anti-Kv1.2 tissue showed significantly prolonged interspike interval durations compared to both other groups (**$P < 0.01$, two-way ANOVA and Tukey *post hoc* test).

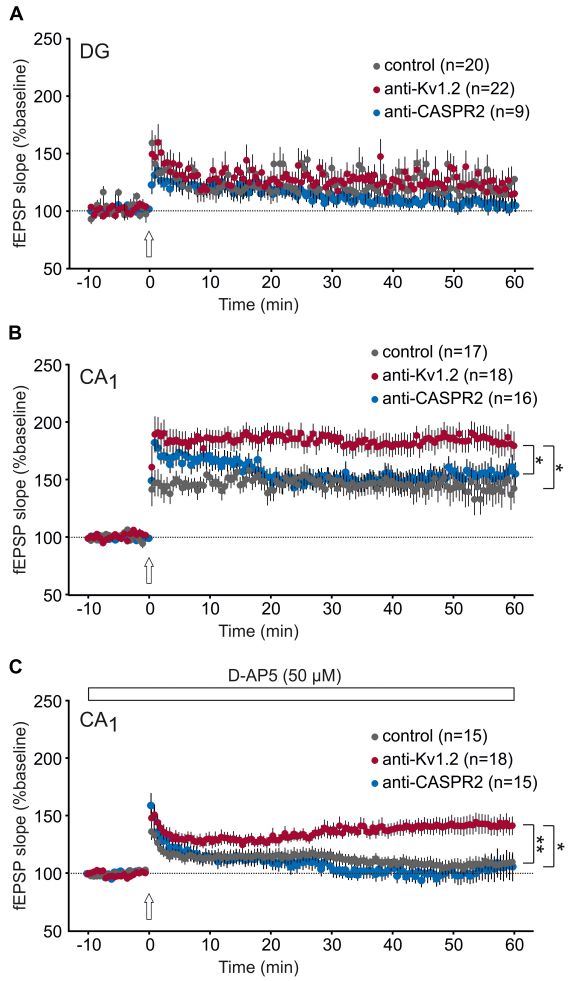

FIGURE 4 | Synaptic plasticity is enhanced in CA1, but not the dentate gyrus. **(A)** Long-term potentiation (LTP) in the dentate gyrus (DG) was not different between anti-Kv1.2, anti-CASPR2 and control slices. The arrow indicates the time-point of LTP inducing high-frequency stimulation. **(B)** LTP in the CA1 area reveals a significant increase in anti-Kv1.2 tissue compared to control (*$P < 0.05$, Student *t*-test) and anti-CASPR2 (*$P < 0.05$, Mann–Whitney *U* test). **(C)** Slices from anti-Kv1.2-treated rats also showed enhanced NMDAR-independent LTP in CA1 (**$P < 0.01$ versus control, Student *t*-test; *$P < 0.05$ versus anti-CASPR2, Student *t*-test). The entire experiment was carried out in the presence of the NMDAR blocker D-AP5 (50 µM).

Vulnerability to Epileptic Conditions

Facilitation of synaptic transmission and plasticity may imply that the tissue might be more vulnerable to hyperexcitable states. Since the anti-Kv1.2 encephalitis suffered from epilepsy, we tested the susceptibility of anti-Kv1.2-treated and anti-CASPR2-treated tissue by removal of Mg^{2+} from the bath. Under these conditions, spontaneous epileptiform potentials were elicited in all experimental groups (**Figure 5A**). In fact, there was a tendency toward more epileptic events in control tissue, albeit not significant (**Figure 5B**). While the vast majority of epileptic events consisted of a single interictal spike, we occasionally observed two or more spikes (referred to as polyspike discharges) and, intriguingly, the incidence of these polyspike discharges was markedly higher in slices from anti-Kv1.2-treated and anti-CASPR2-treated rats (**Figure 5C**). In order to quantify the development of polyspike discharges, we determined the cumulative probability of polyspike discharge incidence rates showing a trend toward a shorter latency and a higher proportion in anti-Kv1.2 tissue ($P = 0.109$, Kaplan–Meier log-rank test) and anti-CASPR2 tissue ($P = 0.05$, Kaplan–Meier log-rank test, **Figure 5D**). When only slices with polyspike discharges were analyzed, the onset of these discharges was significantly advanced in anti-Kv1.2 as compared to control ($P < 0.05$, Mann–Whitney *U* test; **Figure 5E**). These data indicate that susceptibility to epileptic conditions was altered in anti-Kv1.2 tissue. The onset of polyspike discharges in anti-CASPR2 tissue tended to be also advanced ($P = 0.095$, Mann–Whitney *U* test; **Figure 5E**), but more intriguingly, this tissue was markedly prone to seizure-like events (see blue sample traces in **Figure 5A**) which were never observed in the other groups (anti-CASPR2: 4/8 slices, $P < 0.05$ versus anti-Kv1.2 and control, Fisher's exact test).

DISCUSSION

We present a case of Kv1.2-associated LE with status epilepticus. We took advantage of testing this patient's serum by stereotactic injection into the rat hippocampus. The human Kv1.2 protein primary structure is 99.4% identical to the rat isoform (NCBI, blast analysis). Therefore, we assumed that the human antibody could bind to the rat Kv1.2 in the hippocampus, and using Western blot we showed that both a commercial rabbit anti-Kv1.2 and the patient's serum detected the same band which was consistent with the calculated molecular weight of 57 kDa for this protein. We also had the opportunity to compare this patient's serum with a serum from a case of anti-CASPR2 encephalopathy. This approach was also used with patient cerebrospinal fluid containing NMDAR or GAD65 antibodies in previous studies (Hackert et al., 2016; Würdemann et al., 2016; Blome et al., 2018; Kersten et al., 2019). Thus, we propose the intrahippocampal bolus injection of serum is also a valid model for studying patient-derived autoantibodies.

Originally, Kv1 shaker-related K^+ channels have been characterized pharmacologically by the use of dendrotoxins, relatively selective Kv1 inhibitors derived from the venom of *Dendroaspis* snakes (Dolly et al., 1984; Rehm and Lazdunski, 1988; Parcej and Dolly, 1989). Currently, seven pore-forming α-subunits Kv1.1-1.7 have been cloned (Gutman and Chandy, 1993) and studied in various heterologous expression systems revealing substantial differences in activation and inactivation kinetics (Baranauskas, 2007). In addition, auxiliary β-subunits such as Kvβ1-3 with splice variants were discovered which may modify gating properties or serve as chaperones (Rettig et al., 1994; Scott et al., 1994; England et al., 1995; Heinemann et al., 1995; Majumder et al., 1995). The complexity of gating properties, in particular of Kv1.2, is further increased by two different activation kinetics referred to as "slow" and "fast" gating channels (Rezazadeh et al., 2007) and, finally, by glycosylation of the extracellular S1-S2 linker resulting in a

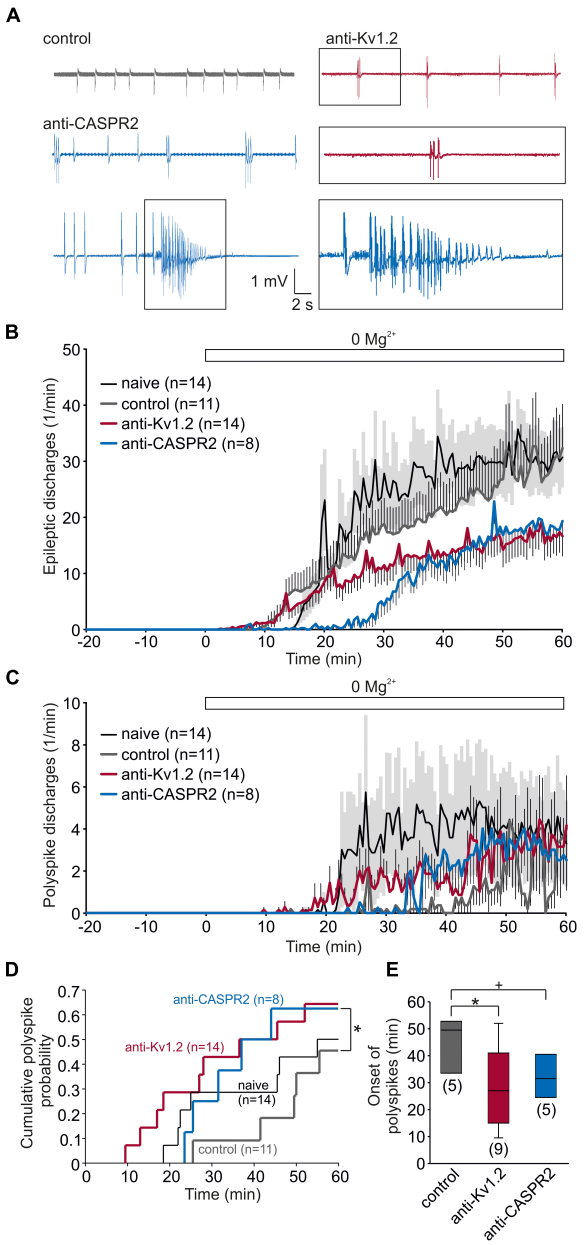

FIGURE 5 | Susceptibility to pro-epileptic conditions is altered in anti-Kv1.2 tissue. **(A)** Representative recordings from slices under pro-epileptic conditions (removal of Mg^{2+}). Note the polyspike discharge in the anti-Kv1.2 trace (red), shown enlarged in the box below. In anti-CASPR2 tissue, there were again polyspike discharges, but also seizure-like events (lowermost row, enlarged in the box). **(B)** Time course of epileptic discharges in slices from non-operated rats (black), anti-Kv1.2-treated rats (red), anti-CASPR2-treated rats (blue) and control-injected rats (gray). Mg^{2+} was omitted from the bath at time-point 0 (indicated by the open bar). SEM for anti-Kv1.2, anti-CASPR2 and control tissue is depicted as antennas; SEM for non-operated rats is depicted as a light gray area. Note that epileptic discharges in slices from anti-Kv1.2 tissue were less frequent than in both control groups. **(C)** Time course of polyspike discharges in all experimental groups. Note the difference in polyspike discharge onset between slices from anti-Kv1.2 and anti-CASPR2 or control-injected rats. **(D)** Cumulative probability plots of polyspike discharge incidence rates reveal a difference between anti-Kv1.2 and control ($P = 0.109$, *(Continued)*

FIGURE 5 | Continued
Kaplan–Meier log-rank test) as well as between anti-CASPR2 and control (*$P = 0.05$, Kaplan–Meier log-rank test). **(E)** Onset of polyspike dischargeswhen they were present. The difference in polyspike discharge onset was still significant between anti-Kv1.2 and control ($^{+}P = 0.095$, *$P < 0.05$, Mann–Whitney *U* test).

depolarizing shift in the half-maximal activation (Watanabe et al., 2007). Typical features of Kv1.2 are the low threshold (below action potential threshold) and the use-dependent activation (Baronas et al., 2015). Thus, Kv1.2 is activated before the action potential is elicited, and repetitive firing may increase Kv1.2 contribution to AP repolarization. It is well established that Kv1.2 is predominantly expressed at presynaptic terminals (Wang et al., 1993, 1994; Sheng et al., 1994; Monaghan et al., 2001; Gu et al., 2003; Wenzel et al., 2007; Lorincz and Nusser, 2008), but functional characterization of presynaptic ion channels is feasible only at highly specialized synapses such as the Calyx of Held (Rezazadeh et al., 2007). While it is actually impossible to predict the effects of antibodies against Kv1.2 at a certain synapse, the available data indicate that Kv1.2 powerfully counteracts depolarizing afterpotentials and thereby constrains transmitter release (Lambe and Aghajanian, 2001; Dodson et al., 2003).

What can we learn from the effects of the patient's antibody against Kv1.2? We found that Schaffer collateral-CA1, but not medial perforant path-dentate gyrus synapses showed an increased slope of the fEPSP suggesting higher synchronization of transmitter release. In the view of the role of Kv1.2 at presynaptic terminals, this implies the view that Kv1.2 antibodies may exert inhibitory effects on presynaptic Kv1.2 function which was confirmed by the significant reduction of the PPR. A similar finding was obtained from rats after intracerebroventricular injection of Kv1.4-antisense oligodeoxyribonucleotides which led to a reduced PPR and, in addition, impaired LTP in CA1 (Meiri et al., 1998). The latter, however, is difficult to explain, since reduced paired-pulse plasticity should imply an increase of transmitter release probability due to the reduction of presynaptic Kv1.4 channel function. Possibly, LTP in that study was reduced by a concomitant impairment of AMPA receptors as recently reported for anti-LGI1 (Petit-Pedrol et al., 2018). Nonetheless, increased release probability should facilitate postsynaptic depolarization and thereby LTP. In the present study, NMDAR-dependent and NMDAR-independent LTP both relying on postsynaptic depolarization were indeed enhanced in anti-Kv1.2-treated tissue in the present study. Interestingly, LTP in the dentate gyrus was preserved in both the present anti-Kv1.2 model and the Kv1.4-antisense rat (Meiri et al., 1998). Hence, anti-Kv1.2 appears to negatively interfere with presynaptic Kv1.2 function. However, the precise epitope of the antibody and consequently its molecular effects remain open, since antibody binding might affect activation, inactivation or even recovery from inactivation. The latter, for instance, is extremely slow in D-type K^{+} currents (Storm, 1988).

Similar to anti-Kv1.2, experiments with anti-CASPR2 showed an increased slope of the fEPSP in CA1, but not in the dentate gyrus. However, in contrast to Kv1.2, anti-CASPR2 did not

significantly reduce the PPR and, moreover, LTP values were indistinguishable from control values. These data indicate that antibodies against CASPR2 which is crucial for axonal targeting of Kv1.2 (Pinatel et al., 2017), does not seem to interfere with presynaptic Kv1.2 function. In addition, these experiments also help argue against putatively unspecific effects of the anti-Kv1.2 patient's serum, since all data on postsynaptic CA1 action potential firing properties did not differ between control and anti-CASPR2 tissues. It is, however, obvious that we cannot fully exclude that the patient's serum might contain further agents such as propofol or levetiracetam, but it is unlikely that these compounds would depress K^+ channel function. A further line of evidence against unspecific effects of anti-Kv1.2 serum derives from the differential effects of this antibody on CA1 and the dentate gyrus. In fact, it was an unexpected and intriguing finding that the changes were restricted to the Schaffer collateral-CA1 synapse. This might be explained by the high diversity of Kv1.2 channel-complexes with auxiliary β-subunits. In this sense, it is important to note that the extracellular S1-S2 linker glycosylation is a relevant regulator of Kv1.2 activation (Watanabe et al., 2007), and *N*-glycosylation was required for the epitope retrieval of patient-derived antibodies in NMDAR encephalitis (Gleichman et al., 2012). Alternatively, it is also possible that the patient's antibody binds to the VGKC-complex as a whole rather than exclusively the pore-forming α-subunit as previously shown for other VGKC-complex antibody species (Irani et al., 2010; Lai et al., 2010).

It has been shown that Kv1.2 is expressed on CA1 pyramidal cells, but not on dentate granule cells (Sheng et al., 1994; Guan et al., 2006). Therefore, Kv1.2 might contribute to the RMP as well as the action potential (AP) threshold and repolarization. Intracellular recordings from CA1 neurons, however, failed to detect differences in the RMP or AP characteristics such as threshold, amplitude or duration suggesting that Kv1.2 may only play a minor role under resting conditions. In addition, this may also reflect the predominantly dendritic expression of Kv1.2 (Sheng et al., 1994; Guan et al., 2006). In contrast, during prolonged depolarization CA1 neurons from anti-Kv1.2-treated rats showed a delayed onset of the first AP as well as reduced numbers of action potentials. Importantly, the latter finding refers to the original description of D-type K^+ currents: K^+ currents with activation thresholds below the AP threshold which therefore delayed the firing were called D-type (i.e., delay-type) (Storm, 1988). In line with this finding, the interspike interval during prolonged depolarization was significantly increased in anti-Kv1.2 tissue. It is important to note that all these findings were specific for anti-Kv1.2, since cells from anti-CASPR2-treated animals showed the same results as controls and therefore significantly differed from cells recorded in anti-Kv1.2 tissue. At first sight, the anti-Kv1.2 effects may suggest facilitated hyperpolarization rather than inhibited K^+ outward currents. This is difficult to appreciate because differential effects would have to be proposed for the same antibody. However, Kv1.2 channels can be divided into slow and fast gating channels (Rezazadeh et al., 2007), and it is uncertain to what extent gating properties observed in expression systems can be transferred to presynaptic terminals. But for the dendritic Kv1.2 channels together with the use-dependent activation of Kv1.2 (Baronas et al., 2015), it is possible that the patient's antibody shifts the slow gating channel into the fast gating one. Interestingly, both loss-of-function and gain-of-function mutations of the Kv1.2-encoding gene, KCNA2, were associated with epileptic encephalopathy (Syrbe et al., 2015). This suggests that both hyper- and hypofunction of Kv1.2 can lead to hyperexcitability.

Lastly, we also tested the tissue susceptibility to hyperexcitable states. We found that epileptic events were not significantly different between anti-Kv1.2 and both control groups. However, polyspike discharges occurred significantly earlier and with higher incidence rates in tissue from anti-Kv1.2-treated animals. Intriguingly, anti-CASPR2 tissue also showed higher rates of polyspike discharges, and, even more important, presented with seizure-like events. Together, both patient sera converted the tissue to become more vulnerable to pro-epileptic conditions. Nonetheless, the network changes in anti-Kv1.2 tissue with respect to hyperexcitability were obviously less pronounced when compared to the pre- and postsynaptic changes at Schaffer collateral-CA1 synapses as described before. This could be due to anti-Kv1.2 effects in opposite directions as observed with prolonged depolarizations in intracellular recordings, in particular with respect to hyperexcitability following both hyper- and hypofunction of KCNA2 mutations (Syrbe et al., 2015). In addition, this may also partially be attributed to the fact that Kv1.2 plays a minor role at perforant path-dentate gyrus synapses (present study) as well as at CA3 synapses (Sheng et al., 1994; Prüss et al., 2010).

What can we learn for patient care from these studies? Although it may be uncertain whether the patient's Kv1.2 antibody binds Kv1.2 directly or not, Kv1.2 appears crucial for governing excitability in the CNS. As known from knockout studies, Kv1.2 deletion is lethal within early postnatal stages, and contrasts with mild consequences of knocking out most other Kv1 channels (London et al., 1998; Smart et al., 1998; Brew et al., 2007), although Kv1.1 is much more widely expressed in the hippocampus than Kv1.2 (Wang et al., 1993, 1994; Veh et al., 1995; Grigg et al., 2000). Nonetheless, Kv1.1 and Kv1.2 are predominant target structures of autoimmune pathology in LE and Morvan syndrome (Kleopa et al., 2006). Hence, our studies can help distinguish clinically relevant autoantibodies from those representing rather as an epiphenomenon such as anti-GAD65 (Stemmler et al., 2015; Widman et al., 2015; Hackert et al., 2016). Moreover, the present study showed that anti-Kv1.2 and anti-CASPR2 differed in their cellular effects, but both led to hyperexcitability. In this sense, both patients' antibodies should be regarded as pathophysiologically relevant which is in line with previous studies on VGKC complex-antibodies (Lalic et al., 2011; Petit-Pedrol et al., 2018) and thereby give *in vitro* evidence for the clinical decision to use plasmapheresis in the present case.

DATA AVAILABILITY STATEMENT

The datasets generated for this study are available on request to the corresponding author.

ETHICS STATEMENT

The studies involving human participants were reviewed and approved by the Ethikkommission der Universität Rostock. The patients/participants provided their written informed consent to participate in this study. The animal study was reviewed and approved by the Landesamt für Lebensmittel, Landwirtschaft und Fischerei Mecklenburg-Vorpommern 7221.3-1.1-017/11 and 7221.3-1.1-007/16. Written informed consent was obtained from the individual(s) for the publication of any potentially identifiable images or data included in this article.

AUTHOR CONTRIBUTIONS

HB, SK, AG, MW, SS, and AS collected the patient data. TK, ES, GH-G, JB, XG, SM, KP, and TS performed the experiments. TK, AG, MW, SS, AS, and RK contributed conception and design of the study. TK, ES, and GH-G organized the database. TK, XG, D-CH, and KP performed the statistical analysis. TK wrote the first draft of the manuscript. AG, MW, SS, AS, and RK wrote sections of the manuscript. SM, HB, SK, and KP contributed to manuscript preparation. All authors contributed to manuscript revision, read and approved the final version of this manuscript for submission.

FUNDING

This work was supported by a grant from the Medical Faculty of the University of Rostock to TK.

ACKNOWLEDGMENTS

The authors wish to thank Hanka Schmidt, Simone Rackow, Andreas Prestel, and Bernd Memmener for excellent technical assistance.

REFERENCES

Baranauskas, G. (2007). Ionic channel function in action potential generation: current perspective. *Mol. Neurobiol.* 35, 129–150. doi: 10.1007/s12035-007-8001-0

Baronas, V. A., McGuinness, B. R., Brigidi, G. S., Kolisko, R. N. G., Vilin, Y. Y., Kim, R. Y., et al. (2015). Use-dependent activation of neuronal Kv1.2 channel complexes. *J. Neurosci.* 35, 3515–3524. doi: 10.1523/jneurosci.4518-13.2015

Blome, R., Bach, W., Guli, X., Porath, K., Sellmann, T., Bien, C. G., et al. (2018). Differentially altered NMDAR dependent and independent long-term potentiation in the CA3 subfield in a model of anti-NMDAR encephalitis. *Front. Synaptic Neurosci.* 31:26. doi: 10.3389/fnsyn.2018.00026

Brew, H. M., Gittelman, J. X., Silverstein, R. S., Hanks, T. D., Demas, V. P., Robinson, L. C., et al. (2007). Seizures and reduced life span in mice lacking the potassium channel subunit Kv1.2, but hypoexcitability and enlarged Kv1 currents in auditory neurons. *J. Neurophysiol.* 98, 1501–1525. doi: 10.1152/jn.00640.2006

Buckley, C., Oger, J., Clover, L., Tüzün, E., Carpenter, K., Jackson, M., et al. (2001). Potassium channel antibodies in two patients with reversible limbic encephalitis. *Ann. Neurol.* 50, 73–78. doi: 10.1002/ana.1097

Cudmore, R. H., Fronzaroli-Molinieres, L., Giraud, P., and Debanne, D. (2010). Spike-time precision and network synchrony are controlled by the homeostatic regulation of the D-type potassium current. *J. Neurosci.* 30, 12885–12895. doi: 10.1523/JNEUROSCI.0740-10.2010

Dietrich, D., Beck, H., Kral, T., Clusmann, H., Elger, C. E., and Schramm, J. (1997). Metabotropic glutamate receptors modulate synaptic transmission in the perforant path: pharmacology and localization of two distinct receptors. *Brain Res.* 767, 220–227. doi: 10.1016/s0006-8993(97)00579-9

Dodson, P. D., Billups, B., Rusznák, Z., Szûcs, G., Barker, M. C., and Forsythe, I. D. (2003). Presynaptic rat Kv1.2 channels suppress synaptic terminal hyperexcitability following action potential invasion. *J. Physiol.* 550, 27–33. doi: 10.1113/jphysiol.2003.046250

Dolly, J. O., Halliwell, J. V., Black, J. D., Williams, R. S., Pelchen-Matthews, A., Breeze, A. L., et al. (1984). Botulinum neurotoxin and dendrotoxin as probes for studies on transmitter release. *J. Physiol.* 79, 280–303.

England, S. K., Uebele, V. N., Kodali, J., Bennett, P. B., and Tamkun, M. M. (1995). A novel K+ channel beta-subunit (hKv beta 1.3) is produced via alternative mRNA splicings. *J. Biol. Chem.* 270, 28531–28534. doi: 10.1074/jbc.270.48.28531

Gleichman, A. J., Spruce, L. A., Dalmau, J., Seeholzer, S. H., and Lynch, D. R. (2012). Anti-NMDA receptor encephalitis antibody binding is dependent on amino acid identity of a small region within the GluN1 amino terminal domain. *J. Neurosci.* 32, 11082–11094. doi: 10.1523/jneurosci.0064-12.2012

Golding, N. L., Jung, H., Mickus, T., and Spruston, N. (1999). Dendritic calcium spike initiation and repolarization are controlled by distinct potassium channel subtypes in CA1 pyramidal neurons. *J. Neurosci.* 19, 8789–8798. doi: 10.1523/jneurosci.19-20-08789.1999

Grigg, J. J., Brew, H. M., and Tempel, B. L. (2000). Differential expression of voltage-gated potassium channel genes in auditory nuclei of the mouse brainstem. *Hear. Res.* 140, 77–90. doi: 10.1016/s0378-5955(99)00187-2

Gu, C., Jan, Y. N., and Jan, L. Y. (2003). A conserved domain in axonal targeting of Kv1 (Shaker) voltage-gated potassium channels. *Science* 301, 646–649. doi: 10.1126/science.1086998

Guan, D., Lee, J. C. F., Tkatch, T., Surmeier, D. J., Armstrong, W. E., and Foehring, R. C. (2006). Expression and biophysical properties of Kv1 channels in supragranular neocortical pyramidal neurones. *J. Physiol.* 571, 371–389. doi: 10.1113/jphysiol.2005.097006

Gutman, G. A., and Chandy, K. G. (1993). Nomenclature of mammalian voltage-dependent potassium channel genes. *Semin. Neurosci.* 5, 101–106. doi: 10.1016/s1044-5765(05)80004-1

Hackert, J. K., Müller, L., Rohde, M., Bien, C. G., Köhling, R., and Kirschstein, T. (2016). Anti-GAD65 containing cerebrospinal fluid does not alter GABAergic transmission. *Front. Cell. Neurosci.* 10:130. doi: 10.3389/fncel.2016.00130

Hart, I. K., Maddison, P., Newsom-Davis, J., Vincent, A., and Mills, K. R. (2002). Phenotypic variants of autoimmune peripheral nerve hyperexcitability. *Brain* 125(Pt. 8), 1887–1895. doi: 10.1093/brain/awf178

Heinemann, S. H., Rettig, J., Wunder, F., and Pongs, O. (1995). Molecular and functional characterization of a rat brain Kv beta 3 potassium channel subunit. *FEBS Lett.* 377, 383–389. doi: 10.1016/0014-5793(95)01377-6

Irani, S. R., Alexander, S., Waters, P., Kleopa, K. A., Pettingill, P., Zuliani, L., et al. (2010). Antibodies to Kv1 potassium channel-complex proteins leucine-rich, glioma inactivated 1 protein and contactin-associated protein-2 in limbic encephalitis, Morvan's syndrome and acquired neuromyotonia. *Brain* 133, 2734–2748. doi: 10.1093/brain/awq213

Kersten, M., Rabbe, T., Blome, R., Porath, K., Sellmann, T., Bien, C. G., et al. (2019). Novel object recognition inrats with NMDAR dysfunction in CA1 after stereotactic injection of anti-NMDAR encephalitis cerebrospinal fluid. *Front. Neurol.* 10:586. doi: 10.3389/fneur.2019.00586

Kleopa, K. A., Elman, L. B., Lang, B., Vincent, A., and Scherer, S. S. (2006). Neuromyotonia and limbic encephalitis sera target mature Shaker-type K+ channels: subunit specificity correlates with clinical manifestations. *Brain* 129, 1570–1584. doi: 10.1093/brain/awl084

Lai, M., Huijbers, M. G., Lancaster, E., Graus, F., Bataller, L., Balice-Gordon, R., et al. (2010). Investigation of LGI1 as the antigen in limbic encephalitis previously attributed to potassium channels: a case series. *Lancet Neurol.* 9, 776–785. doi: 10.1016/S1474-4422(10)70137-X

Lalic, T., Pettingill, P., Vincent, A., and Capogna, M. (2011). Human limbic encephalitis serum enhances hippocampal mossy fiber-CA3 pyramidal cell synaptic transmission. *Epilepsia* 52, 121–131. doi: 10.1111/j.1528-1167.2010.02756.x

Lambe, E. K., and Aghajanian, G. K. (2001). The role of Kv1.2-containing potassium channels in serotonin-induced glutamate release from thalamocortical terminals in rat frontal cortex. *J. Neurosci.* 21, 9955–9963. doi: 10.1523/jneurosci.21-24-09955.2001

Lang, B., Makuch, M., Moloney, T., Dettmann, I., Mindorf, S., Probst, C., et al. (2017). Intracellular and non-neuronal targets of voltage-gated potassium channel complex antibodies. *J. Neurol. Neurosurg. Psychiatry* 88, 353–361. doi: 10.1136/jnnp-2016-314758

London, B., Wang, D. W., Hill, J. A., and Bennett, P. B. (1998). The transient outward current in mice lacking the potassium channel gene Kv1.4. *J. Physiol.* 509, 171–182. doi: 10.1111/j.1469-7793.1998.171bo.x

Lorincz, A., and Nusser, Z. (2008). Cell-type-dependent molecular composition of the axon initial segment. *J. Neurosci.* 28, 14329–14340. doi: 10.1523/JNEUROSCI.4833-08.2008

Majumder, K., Debiasi, M., Wang, Z. G., and Wible, B. A. (1995). Molecular-cloning and functional expression of a novel potassium channel beta-subunit from human atrium. *FEBS Lett.* 361, 13–16. doi: 10.1016/0014-5793(95)00120-x

Meiri, N., Sun, M.-K., Segal, Z., and Alkon, D. L. (1998). Memory and long-term potentiation (LTP) dissociated: normal spatial memory despite CA1 LTP elimination with Kv1.4 antisense. *Proc. Natl. Acad. Sci. U.S.A.* 95, 15037–15042. doi: 10.1073/pnas.95.25.15037

Mitterdorfer, J., and Bean, B. P. (2002). Potassium currents during the action potential of hippocampal CA3 neurons. *J. Neurosci.* 22, 10106–10115. doi: 10.1523/jneurosci.22-23-10106.2002

Monaghan, M. M., Trimmer, J. S., and Rhodes, K. J. (2001). Experimental Localization of Kv1 Family Voltage-Gated K+ Channel α and β Subunits in Rat Hippocampal Formation. *J. Neurosci.* 21, 5973–5983. doi: 10.1523/jneurosci.21-16-05973.2001

Parcej, D. N., and Dolly, J. O. (1989). Dendrotoxin acceptor from bovine synaptic plasma membranes: binding properties, purification and subunit composition of a putative constituent of certain voltageactivated K+ channels. *Biochem. J.* 257, 899–903. doi: 10.1042/bj2570899

Petit-Pedrol, M., Sell, J., Planagumà, J., Mannara, F., Radosevic, M., Haselmann, H., et al. (2018). LGI1 antibodies alter Kv1.1 and AMPA receptors changing synaptic excitability, plasticity and memory. *Brain* 141, 3144–3159. doi: 10.1093/brain/awy253

Pinatel, D., Hivert, B., Saint-Martin, M., Noraz, N., Savvaki, M., Karagogeos, D., et al. (2017). The Kv1-associated molecules TAG-1 and Caspr2 are selectively targeted to the axon initial segment in hippocampal neurons. *J. Cell Sci.* 130, 2209–2220. doi: 10.1242/jcs.202267

Prüss, H., Grosse, G., Brunk, I., Veh, R. W., and Ahnert-Hilger, G. (2010). Age-dependent axonal expression of potassium channel proteins during development in mouse hippocampus. *Histochem. Cell. Biol.* 33, 301–312. doi: 10.1007/s00418-009-0668-z

Rehm, H., and Lazdunski, M. (1988). Purification and subunit structure of a putative K1-channel protein identified by its binding properties for dendrotoxin I. *Proc. Natl. Acad. Sci. U.S.A.* 85, 4919–4923. doi: 10.1073/pnas.85.13.4919

Rettig, J., Heinemann, S. H., Wunder, F., Lorra, C., Parcej, D. N., Dolly, J. O., et al. (1994). Inactivation properties of voltage-gated K+ channels altered by presence of beta-subunit. *Nature* 369, 289–294. doi: 10.1038/369289a0

Rezazadeh, S., Kurata, H. T., Claydon, T. W., Kehl, S. J., and Fedida, D. (2007). An activation gating switch in Kv1.2 is localized to a threonine residue in the S2-S3 LINKER. *Biophys. J.* 93, 4173–4186. doi: 10.1529/biophysj.107.116160

Scott, V. E. S., Rettig, J., Parcej, D. N., Keen, J. N., Findlay, J. B. C., Pongs, O., et al. (1994). Primary structure of a beta subunit of alpha-dendrotoxin-sensitive K+ channels from bovine brain. *Proc. Natl. Acad. Sci. U.S.A.* 91, 1637–1641. doi: 10.1073/pnas.91.5.1637

Sheng, M., Tsaur, M. L., Jan, Y. N., and Jan, L. Y. (1994). Contrasting subcellular localization of the Kv1.2 K+ channel subunit in different neurons of rat brain. *J. Neurosci.* 14, 2408–2417. doi: 10.1523/jneurosci.14-04-02408.1994

Smart, S. L., Lopantsev, V., Zhang, C. L., Robbins, C. A., Wang, H., Chiu, S. Y., et al. (1998). Deletion of the K(v)1.1 potassium channel causes epilepsy in mice. *Neuron* 20, 809–819. doi: 10.1016/s0896-6273(00)81018-1

Stemmler, N., Rohleder, K., Malter, M. P., Widman, G., Elger, C. E., Beck, H., et al. (2015). Serum from a patient with GAD65 antibody-associated limbic encephalitis did not alter GABAergic neurotransmission in cultured hippocampal networks. *Front. Neurol.* 6:189. doi: 10.3389/fneur.2015.00189

Storm, J. F. (1988). Temporal integration by a slowly inactivating K+ current in hippocampal neurons. *Nature* 336, 379–381. doi: 10.1038/336379a0

Stühmer, W., Ruppersberg, J. P., Schröter, K. H., Sakmann, B., Stocker, M., Giese, K. P., et al. (1989). Molecular basis of functional diversity of voltage gated potassium chennals in mammalian brain. *EMBO J.* 8, 3235–3244. doi: 10.1002/j.1460-2075.1989.tb08483.x

Syrbe, S., Hedrich, U. B. S., Riesch, E., Djémié, T., Müller, S., Møller, R. S., et al. (2015). De novo loss- or gain-of-function mutations in KCNA2 cause epileptic encephalopathy. *Nat. Genet.* 47, 393–399. doi: 10.1038/ng.3239

Syrbe, S., Stettner, G. M., Bally, J., Borggraefe, I., Bien, C. I., Ferfoglia, R. I., et al. (2020). CASPR2-autoimmunity in children, expanding to mild encephalopathy with hypertension. *Neurology*. [in press].

Veh, R. W., Lichtinghagen, R., Sewing, S., Wunder, F., Grumbach, I. M., and Pongs, O. (1995). Immunohistochemical localization of five members of the Kv1 channel subunits: contrasting subcellular locations and neuron-specific co-localizations in rat brain. *Eur. J. Neurosci.* 7, 2189–2205. doi: 10.1111/j.1460-9568.1995.tb00641.x

Wang, H., Kunkel, D. D., Martin, T. M., Schwartzkroin, P. A., and Tempel, B. L. (1993). Heteromultimeric K+ channels in terminal and juxtaparanodal regions of neurons. *Nature* 365, 75–79. doi: 10.1038/365075a0

Wang, H., Kunkel, D. D., Schwartzkroin, P. A., and Tempel, B. L. (1994). Localization of Kv1.1 and Kv1.2, two K channel proteins, to synaptic terminals, somata and dendrites in the mouse brain. *J. Neurosci.* 14, 4588–4599. doi: 10.1523/jneurosci.14-08-04588.1994

Watanabe, I., Zhu, J., Sutachan, J. J., Gottschalk, A., Recio-Pinto, E., and Thornhill, W. B. (2007). The glycosylation state of Kv1.2 potassium channels affects trafficking, gating, and simulated action potentials. *Brain Res.* 1144, 1–18. doi: 10.1016/j.brainres.2007.01.092

Wenzel, H. J., Vacher, H., Clark, E., Trimmer, J. S., Lee, A. L., Sapolsky, R. M., et al. (2007). Structural consequences of Kcna1 gene deletion and transfer in the mouse hippocampus. *Epilepsia* 48, 2023–2046. doi: 10.1111/j.1528-1167.2007.01189.x

Widman, G., Golombeck, K., Hautzel, H., Gross, C. C., Quesada, C. M., Witt, J. A., et al. (2015). Treating a GAD65 antibody-associated limbic encephalitis with Basiliximab: a case study. *Front. Neurol.* 6:167. doi: 10.3389/fneur.2015.00167

Würdemann, T., Kersten, M., Tokay, T., Guli, X., Kober, M., Rohde, M., et al. (2016). Stereotactic injection of cerebrospinal fluid from anti-NMDA receptor encephalitis into rat dentate gyrus impairs NMDA receptor function. *Brain Res.* 1633, 10–18. doi: 10.1016/j.brainres.2015.12.027

Zucker, R. S. (2002). Short-term plasticity. *Annu. Rev. Physiol.* 64, 355–405. doi: 10.1146/annurev.physiol.64.092501.114547

Conflict of Interest: The authors declare that the research was conducted in the absence of any commercial or financial relationships that could be construed as a potential conflict of interest.

frontiers in Synaptic Neuroscience

BRIEF RESEARCH REPORT
published: 31 March 2020
doi: 10.3389/fnsyn.2020.00014

Excessive β-Catenin in Excitatory Neurons Results in Reduced Social and Increased Repetitive Behaviors and Altered Expression of Multiple Genes Linked to Human Autism

*Jonathan Michael Alexander, Antonella Pirone and Michele H. Jacob**

Department of Neuroscience, Sackler School of Biomedical Sciences, Tufts University School of Medicine, Boston, MA, United States

Multiple human autism risk genes are predicted to converge on the β-catenin (β-cat)/Wnt pathway. However, direct tests to link β-cat up- or down-regulation with autism are largely lacking, and the associated pathophysiological changes are poorly defined. Here we identify excessive β-cat as a risk factor that causes expression changes in several genes relevant to human autism. Our studies utilize mouse lines with β-cat dysregulation in forebrain excitatory neurons, identified as cell types with a convergent expression of autism-linked genes in both human and mouse brains. We show that mice expressing excessive β-cat display behavioral and molecular changes, including decreased social interest, increased repetitive behaviors, reduced parvalbumin and altered expression levels of additional genes identified as potential risk factors for human autism. These behavioral and molecular phenotypes are averted by reducing β-cat in neurons predisposed by gene mutations to express elevated β-cat. Using next-generation sequencing of the prefrontal cortex (PFC), we identify 87 dysregulated genes that are shared between mouse lines with excessive β-cat and autism-like behaviors, but not mouse lines with reduced β-cat and normal social behavior. Our findings provide critical new insights into β-cat, Wnt pathway dysregulation in the brain causing behavioral phenotypes relevant to the disease and the molecular etiology which includes several human autism risk genes.

Keywords: autism (ASD), Wnt, β-catenin (β-catenin), prefronal cortex, parvalbumin

OPEN ACCESS

Edited by:
Dirk Feldmeyer,
Julich Research Centre, Germany

Reviewed by:
Yuchio Yanagawa,
Gunma University, Japan
Karun K. Singh,
McMaster University, Canada

****Correspondence:***
Michele H. Jacob
michele.jacob@tufts.edu

Received: *27 September 2019*
Accepted: *17 March 2020*
Published: *31 March 2020*

Citation:
Alexander JM, Pirone A, and Jacob MH (2020) Excessive β-Catenin in Excitatory Neurons Results in Reduced Social and Increased Repetitive Behaviors and Altered Expression of Multiple Genes Linked to Human Autism. Front. Synaptic Neurosci. 12:14. doi: 10.3389/fnsyn.2020.00014

BACKGROUND

Emerging evidence suggests that autism spectrum disorders (ASD) likely stem from combinatorial molecular changes that ultimately impact synaptic and circuit functions. Although genetic studies of families with ASD have identified hundreds of risk genes, typically only one mutated gene has been found per affected individual (O'Roak et al., 2012; Sanders et al., 2015; de la Torre-Ubieta et al., 2016). This disparity highlights the need for defining the associated molecular changes caused by ASD-linked risk factors to gain insights into shared pathologies and thereby identify targets for effective therapeutic intervention. Here, we show that malfunction of β-catenin (β-cat) results in reduced social and increased repetitive behavioral phenotypes and altered expression levels of multiple genes whose human orthologs have been implicated in ASD.

β-cat/Wnt has been defined as one of a small number of convergent pathways whose malfunction may predispose neurons to ASD (Gilman et al., 2011; Iossifov et al., 2012; Neale et al., 2012; O'Roak et al., 2012; Zoghbi and Bear, 2012). Several ASD-linked human gene mutations are predicted to cause up- or down-regulation of β-cat functions, including *ctnnb1* (β-cat) itself (Krumm et al., 2014; Tucci et al., 2014; Krupp et al., 2017), adenomatous polyposis coli (APC; Zhou et al., 2007), *chd8* (Durak et al., 2016), *ank3* (Kloth et al., 2017), *arx* (Cho et al., 2017), *ube3a* (Yi et al., 2017), *prickle1* (Todd and Bassuk, 2018), and *wnt1a* (Martin et al., 2013). However, direct tests for linking β-cat malfunction to autism are largely lacking and the associated pathophysiological changes are poorly defined. Our study provides new insights into the molecular etiologies of autism relevant behavioral phenotypes caused by β-cat dysregulation.

Our previous studies implicate, but do not directly test, excessive β-cat in excitatory neurons as a risk factor for altered social and repetitive behaviors and do not elucidate the associated molecular changes. We have shown that conditional knockout (cKO) of APC, the major negative regulator of β-cat, in mouse forebrain excitatory neurons, causes the expected increases in β-cat and canonical Wnt target gene expression levels, as well as behavioral phenotypes (reduced social interactions, increased repetitive behaviors), cognitive impairments and seizures (Mohn et al., 2014; Pirone et al., 2017) relevant to ASD. However, beyond regulating β-cat levels, APC has other roles critical for neuron maturation and function that are potentially relevant to normal behaviors: including its role in regulating microtubule and actin cytoskeleton dynamics (Zumbrunn et al., 2001; Akiyama and Kawasaki, 2006) and as an mRNA binding protein with several of its targets functioning in brain development (Preitner et al., 2014).

In the present study, we have used new mouse lines with direct genetic manipulation of β-cat in the presence and absence of APC. We show roles of β-cat up- and down-regulation in the brain in causing vs. averting autism relevant social and repetitive behavior phenotypes. Importantly, we identify associated molecular changes, including altered expression levels of several genes linked to autism in humans. Our findings provide critical insights into a molecular etiology of impaired social and repetitive behaviors, with relevance to human ASD-linked genes predicted to dysregulate the β-cat network.

MATERIALS AND METHODS

Animals

APC cKO ($APC^{fl/fl}$) mice were generated as previously described (Mohn et al., 2014). β-cat cOE ($ctnnb1^{fl(ex3)/+}$; Harada et al., 1999), β-cat cKO ($ctnnb1^{fl/fl}$; Wickham et al., 2019), and APC/β-cat cKOs ($APC^{fl/fl}$/$ctnnb1^{fl/fl}$) mice were generated with the identical CamKIIα-Cre-93 recombinase carrying line (Rios et al., 2001). For all experiments, 2–3 month-old mice of both sexes were used. Littermate controls (Cre negative) were pooled from all lines. Mice of all genotypes were born at Mendelian ratios and showed no deficits in body weight or survivability until the age of testing (although 5% of APC/β-cat cKO mice showed hydrocephaly and were excluded from experiments). All procedures were approved by the Tufts University Institutional Animal Care and Use Committee in accordance with National Institutes of Health guidelines.

Biochemical Experiments

Western blots and quantitative PCR were performed as previously described (Mohn et al., 2014). Primers for *pvalb* qPCR are: (Fwd) ATCAAGAAGGCGATAGGA GCC (Rev) GGCCAGAAGCGTCTTTGTT. Antibodies used are anti-β-catenin (mouse, 1:2,000, Invitrogen, RRID:AB_2533039), anti-APC (rabbit, 1:1,000, Abcam, RRID:AB_301806), anti-parvalbumin (rabbit, 1:1,000, Swant, RRID:AB_2631173), anti-HSP90 (rabbit, 1:1,000, Cell Signaling, RRID:AB_2233331), and anti-GAPDH (mouse, 1:10,000, Millipore, RRID:AB_2107445).

λ-Phosphatase treatment was performed as previously described (Humrich et al., 2003). Briefly, β-cat cOE and littermate control hippocampi were homogenized in λ-phosphatase buffer containing protease inhibitor cocktail. λ-phosphatase (10,000 U/ml) and magnesium cocktail was added to 100 ug of total protein and incubated at 370C for 1 h (untreated samples did not receive λ-phosphatase but were prepared in the same fashion). Fifty microgram of protein was resolved on a 3–8% gel (Invitrogen) and immunoblots used HSP90 as a loading control.

Behavioral Assays

Mice were housed on a reversed 12-h light/dark cycle, and handled 5 min daily for a week before behavioral testing. Three chamber test and marble burying were performed as previously described (Mohn et al., 2014). For the repetitive circling assay, mice were removed from their home cage and placed in an empty shoebox cage containing no nestlet. The mice were videotaped for 15 min and were scored by a blinded observer. Criteria for circling behavior was a minimum of two bouts of at least three consecutive, unidirectional, fast circling motions within a restricted area (i.e., circling the outside edge of the cage was not considered circling behavior) during a period of 15 min.

Spine Density

Fluorescent labeling of neurons for synaptic spine density was done as previously described (Staffend and Meisel, 2011). Neurons were imaged by confocal microscopy (Nikon A1R laser confocal scanning microscope with 63× objective; 3× zoom). Dendritic spines were reconstructed (Imaris software), and spine density was calculated.

Next-Generation Sequencing

Library preparation, sequencing, and initial expression analysis was performed by the Tufts University Core Facility Genomics lab. Briefly, the quality of input RNA samples was assessed on Advanced Analytical Fragment Analyzer. RNA samples that passed the quality check were used as input for RNA-Seq library preparation using Illumina TruSeq stranded mRNA, following manufacturer instruction. The resultant library was then quantified and pooled equal molar and was sequenced

with paired-end 100 bases format on an Illumina HiSeq 2500 using High Output V4 chemistry. Fastq files were generated from raw data using bcl2fastq (Illumina). The fastq files were mapped mouse mm10 reference genome with Tophat2. Normalized read counts were generated with Cufflinks2, and differential expression and hierarchical clustering analyses were performed with Cuffdiff2 and Qlucore Omics Explorer.

Statistical Analysis

All data are reported as the arithmetic mean ± standard error. Statistical analysis was done using Graphpad Prism 7 and the specific statistical test used are reported in the text and figure legends.

RESULTS

New β-cat cOE and APC/β-cat cKO Mouse Lines

We have generated two new mutant mouse lines with dysregulated β-cat during the early postnatal stage of major synaptic differentiation, a critical window of brain development relevant to ASD. We have utilized the CamKIIα Cre driver that is predominantly expressed in forebrain excitatory neurons and fully activated during the first three postnatal weeks in mice (Rios et al., 2001; Pirone et al., 2017) equivalent to the developmental age when glutamatergic neurons exhibit convergent expression of several ASD linked genes in both the human and mouse cortex (Parikshak et al., 2013; Willsey et al., 2013). We have used this CamKIIα-Cre driver to target the same cell types at the same developmental age in all of our mouse lines, including the APC cKO and β-cat cKO lines (Mohn et al., 2014; Wickham et al., 2019).

To upregulate β-cat in the presence of APC, we conditionally overexpressed (cOE), stabilized, N-terminal truncated β-cat by deleting the degradation domain. We crossed CamKIIα-Cre mice with mice expressing loxP sites flanking exon 3 of the *ctnnb1* (β-cat) gene (Harada et al., 1999; **Figure 1A**). Exon 3 of *ctnnb1* encodes a domain in the β-cat protein that contains the phosphorylation sites necessary for degradation by the APC/Axin/GSK3B destruction complex.

In our β-cat cOE mice, heterozygous expression of this degradation resistant isoform led to β-cat increases, with total β-cat levels comparable to that of APC cKOs (One-way ANOVA $F_{(3, 8)} = 87.39$, $p < 0.001$; **Figure 1B**), allowing us to assess the effects of similarly increased β-cat, in the presence vs. absence of APC, in causing autism relevant behavioral phenotypes. Although we observed what appeared to be an increase in APC in the β-cat cOE cortex by immunoblotting (One-way ANOVA $F_{(3, 8)} = 58.61$, $p < 0.0001$; **Figure 1C**), the APC signal has a widespread, and treatment with λ-phosphatase demonstrates that there is no significant difference in the levels of APC between β-cat cOE mice and controls (Student's t-test, $p = 0.616$; **Figure 1C**).

Additionally, we generated the double mutant APC/β-cat cKO mouse line to prevent the increase in β-cat in the absence of APC, to test whether the social and repetitive behavioral phenotypes that we observed in APC cKOs is caused by elevated β-cat or APC loss. We crossed the CamKIIα Cre mice with mice expressing loxP sites flanking exon 2 and exon 6 of the *ctnnb1* gene and flanking exon 11 and exon 12 of the *APC* gene (Brault et al., 2001; Gounari et al., 2005; **Figure 1A**). Cre-mediated recombination results in severely truncated β-cat and APC protein products that are unstable and rapidly degraded. The APC/β-cat cKO mice show large reductions in β-cat, compared to littermate controls, with the slight residual levels most likely due to other cell types that do not express CamKIIα (β-cat: One-way ANOVA $F_{(3, 8)} = 87.39$, $p < 0.001$; **Figure 1B**). Similarly, we observe comparable reductions in APC levels between this new line and APC cKO mice relative to controls (APC: One-way ANOVA $F_{(2, 6)} = 182.7$, $p < 0.0001$; APC cKO: 0.2273 ± 0.0162, $p < 0.0001$ Bonferroni-corrected Student's t-test; APC/β-cat cKO: 0.1048 ± 0.0303, $p < 0.0001$ Bonferroni-corrected Student's *t*-test; **Figure 1B**). We used these new mouse lines to test directly whether excessive β-cat can cause aberrant social and repetitive behavioral phenotypes.

β-cat cOEs Exhibit Phenotypes Relevant to ASD, But APC/β-cat cKOs Do Not

Using the classic three-chamber assay (Crawley, 2007), we tested for altered social interactions in the β-cat cOEs (elevated β-cat, normal APC levels) and APC/β-cat cKOs (reduced β-cat, reduced APC), compared to their control littermates and to APC cKOs (elevated β-cat, reduced APC). Relative to control littermates, β-cat cOEs displayed reduced social interest, measured as the ratio of time spent interacting with the novel mouse cage vs. the empty cage (One-way ANOVA, $F_{(3, 38)} = 13.17$, $p < 0.001$; **Figures 2A,B**). Distance traveled and velocity was normal (calculated during the habituation phase), eliminating motor deficits as a potential confound (One-way ANOVA $F_{(3, 38)} = 0.4467$, $p = 0.7211$, data not shown). The reduced social interactions of β-cat cOEs resembles that seen in APC cKOs (**Figures 2A,B**). In contrast, APC/β-cat cKOs demonstrated normal social interest (**Figures 2A,B**) suggesting that the aberrant social behavior of APC cKOs is averted by preventing elevated β-cat in neurons predisposed to excessive β-cat by APC loss. Similarly, β-cat cKOs (low β-cat, normal APC levels) show that β-cat down-regulation in the excitatory neurons, using the same CamKIIα-Cre driver did not affect their social behavior, relative to control littermates (Wickham et al., 2019).

Next, we tested for deficits in social memory using a novel vs. familiar mouse in the three-chamber paradigm. β-cat cOEs spent a significantly reduced ratio of time interacting with the novel mouse cage, relative to the familiar mouse cage, suggesting reduced social memory (One-way ANOVA $F_{(5, 50)} = 4.015$, $p = 0.0039$; **Figures 2A,C**). This resembles the deficiencies in the social memory of APC cKOs (**Figures 2A,C**). In contrast, APC/β-cat cKOs displayed increased interactions with the novel mouse cage, similar to control littermates, averting the reduced social interest phenotype of APC cKOs alone (**Figures 2A,C**).

We also tested for repetitive behaviors, using marble burying, a repetitive digging task (Thomas et al., 2009). Whereas

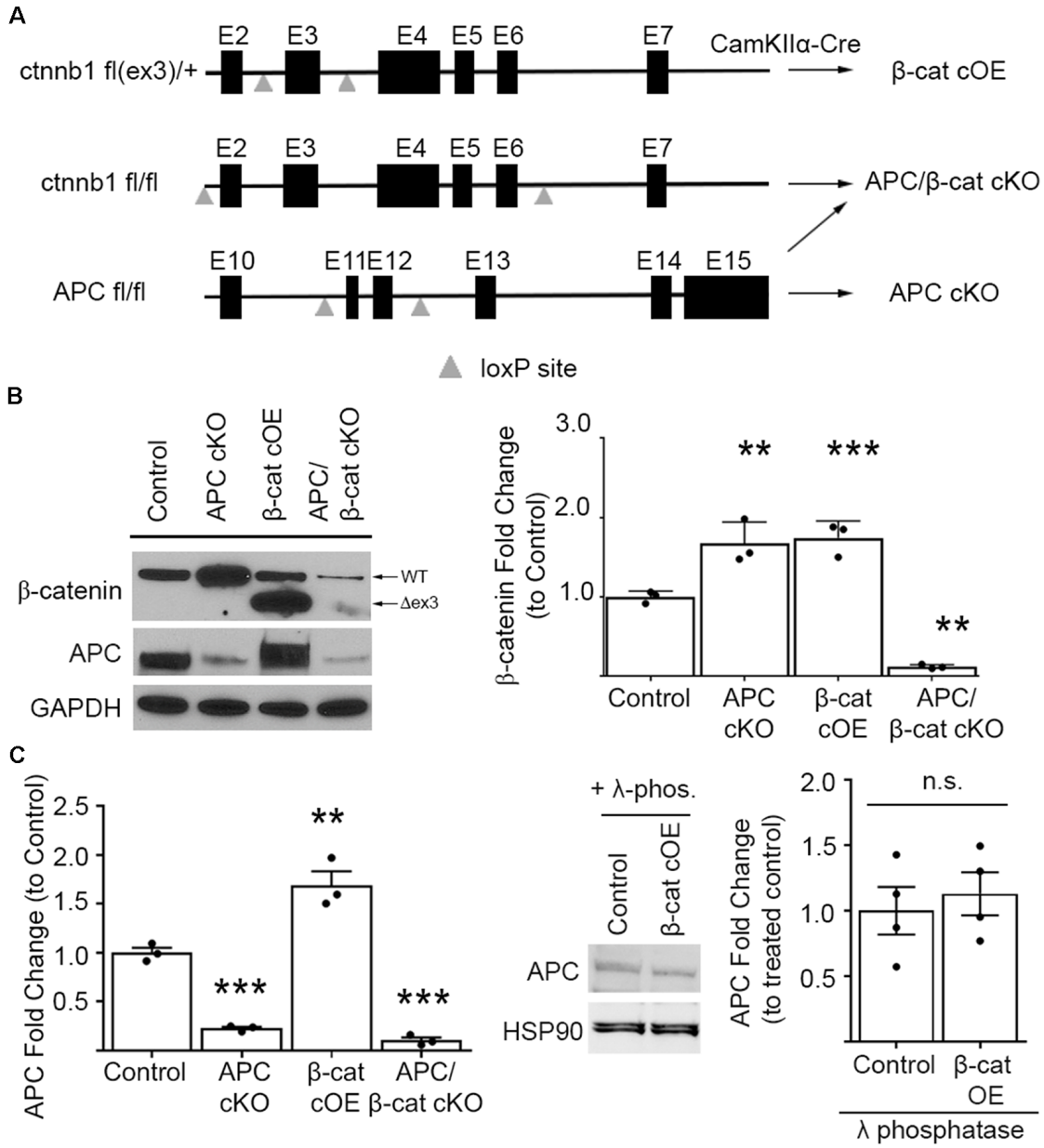

FIGURE 1 | Mouse lines comparing β-cat up- or down-dysregulation. **(A)** Schematic showing the floxed *ctnnb1* and *adenomatous polyposis coli (APC)* genes used to alter β-catenin levels in mice carrying CamKIIα-Cre recombinase. For excessive levels: β-cat cOE-overexpression of stable N-terminally truncated β-cat by deleting the degradation domain, and APC conditional knockout (cKO; Mohn et al., 2014)—deletion of the major negative regulator of β-cat; for reduced levels: APC/β-cat cKO with unstable, rapidly degraded protein products from both genes, and β-cat cKO (Wickham et al., 2019). **(B)** Immunoblot and quantification of β-cat prefrontal cortex (PFC) levels. β-cat increase in β-cat cOEs is comparable to that of APC cKOs, relative to control littermates. APC/β-cat cKOs show drastically reduced β-cat, with residual levels likely from non-CamKIIα expressing cell types ($n = 3$ per genotype. $^{**}p < 0.01$, $^{***}p < 0.001$ to control, *post hoc* Bonferroni corrected t-test). As expected, APC levels in APC cKO and APC/β-cat cKO mice are reduced ($n = 3$ per genotype, $^{**}p < 0.01$, $^{***}p < 0.001$ to control, *post hoc* Bonferroni corrected *t*-test) and, although we observe a mobility shift on the blot consistent with phosphorylation in β-cat cOEs, we observe no change in total APC levels **(C)** compared to control littermates after λ-phosphatase treatment ($n = 4$ per genotype), n.s., non-significant.

APC cKOs buried significantly more marbles than control littermates (**Figure 2D**), the β-cat cOEs buried fewer marbles than their littermate controls (One-way ANOVA $F_{(3, 34)} = 32.43$, $p < 0.0001$; **Figure 2D**). Observing their behavior showed that β-cat cOEs spent much of the time unidirectionally circling in the marble-containing novel environment, suggesting repetitive stereotypy behavior (Chi-squared 14.02, $df = 3$, $p = 0.029$; **Figure 2E**). The APC/β-cat cKOs buried a comparable number of marbles to control littermates and did not circle, suggesting that lowering β-cat prevents the autism relevant repetitive behavior

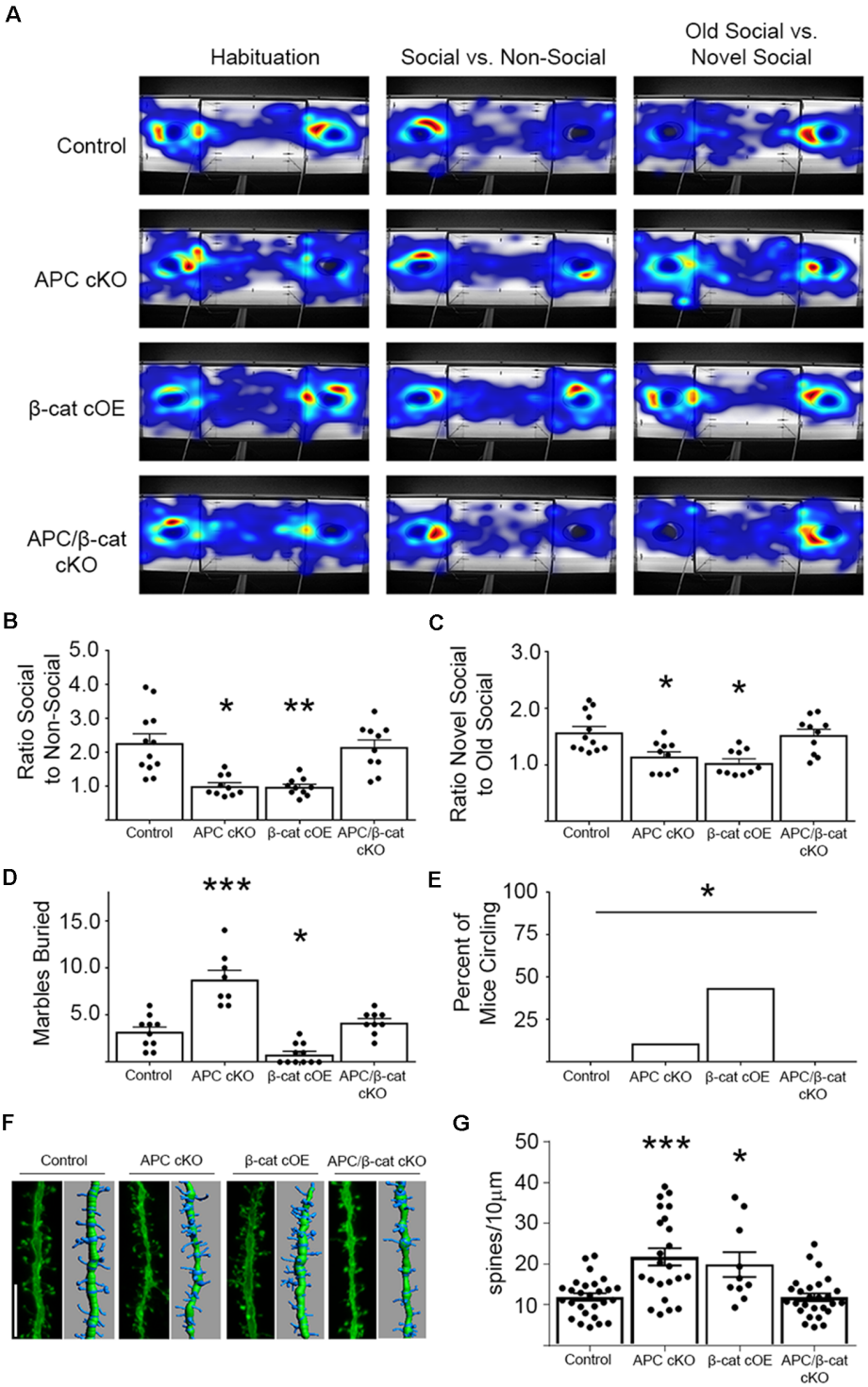

FIGURE 2 | β-cat increases, but not decreases in excitatory neurons, cause behavioral phenotypes relevant to autism spectrum disorders (ASD). **(A)** Representative heat-maps of the mouse models during the habituation, social interaction, and social memory phases of the three-chambered test. **(B)** Both β-cat cOEs and APC cKOs spend a significantly reduced ratio of time interacting with the social cage vs. the empty cage, compared to controls. APC/β-cat cKOs show normal sociability (n = 10–12 per genotype; $^{*}p < 0.05$, $^{**}p < 0.01$ to control, post-hoc Bonferroni corrected t-test). **(C)** Both β-cat cOEs and APC cKOs spend a reduced percent of time interacting with the novel mouse vs. the familiar mouse, whereas APC/β-cat cKOs interact with the novel mouse more, similar to controls ($^{*}p < 0.05$ to control, *post hoc* Bonferroni corrected t-test). **(D)** APC cKOs bury significantly more marbles than controls in the marble burying assay. This repetitive behavior is prevented in APC/β-cat cKOs (n = 8–11 per genotype; $^{*}p < 0.05$, $^{***}p < 0.001$, post-hoc Bonferroni corrected t-test). β-cat cOEs bury significantly fewer marbles than controls,

(*Continued*)

FIGURE 2 | Continued
and exhibit **(E)** repetitive circling behavior (n = 11–18 per genotype; $^*p < 0.05$, Chi-squared test). **(F)** Representative images and Imaris reconstructions of the proximal apical dendrite of layer V cortical neurons from the various mouse models. **(G)** Mice with elevated levels of β-cat (APC cKO, β-cat cOE) show increased dendritic spine density (n = 3–5 animals per genotype, 3–8 neurons per animal; $^*p < 0.05$, $^{***}p < 0.001$, *post hoc* Bonferroni corrected t-test) that is corrected in APC/β-cat cKO mice with low levels of β-cat.

phenotype seen in APC cKOs. Similarly, mice with β-cat cKO alone displayed normal behavior in the marble-burying assay (Wickham et al., 2019).

Studies of post-mortem brains from autistic patients show that dendritic complexity and spine density are commonly altered in the disease (Hutsler and Zhang, 2010; Tang et al., 2014; Weir et al., 2018). Our previous studies in APC cKO mice showed increases in cortical spine density concurrent with the ASD relevant behavioral phenotypes (Mohn et al., 2014). To assess whether spine density is similarly altered in the new β-cat cOE mouse line with high β-cat in the presence of APC, we employed gene-gun labeling of individual neurons in brain slices from the different mutant mouse lines followed by confocal microscopy and Imaris reconstruction analysis (**Figure 2F**). Similar to APC cKOs, β-cat cOEs showed an increase in dendritic spine density, measured on the 1st branch of the apical dendrite of layer V cortical neurons (One-way ANOVA $F_{(3, 83)} = 11.48$, $p < 0.0001$; **Figure 2G**). In contrast, APC/β-cat cKO mice show no significant difference in spine density, relative to control mice. These data suggest that high-levels of β-cat in glutamatergic neurons of the forebrain *in vivo* result in increased spine density, similar to what has been observed in primary cultures of hippocampal neurons (Murase et al., 2002).

Elevated β-cat Causes Altered Expression of Several Genes Linked to Human ASD

To begin to identify the molecular etiology of aberrant social and repetitive behaviors caused by increased β-cat in our mice, we employed unbiased next-generation sequencing of RNA from the prefrontal cortex (PFC)—a brain region associated with social behavior and implicated in ASD in human studies (Hashemi et al., 2017; Selimbeyoglu et al., 2017; Brumback et al., 2018; Carvalho Pereira et al., 2018; Lazaro et al., 2019). We compared mice with elevated β-cat and altered social and repetitive behaviors (β-cat cOEs, APC cKOs), mice with reduced β-cat that do not display the phenotypes (APC/β-cat cKOs) and control littermates. We found 87 dysregulated genes (70 increased, 17 decreased) that are shared between the elevated β-cat mouse lines, but not the reduced β-cat line (**Figure 3A**; primary component analysis ANOVA $p = 0.001$, $q = 0.298$). Nine of the dysregulated genes are canonical Wnt targets (Hödar et al., 2010; Wisniewska et al., 2012; **Figure 3**). Gene Ontology analysis for the up- and down-regulated gene sets show enrichment for several GO terms relevant to circuit malformations: *neuron projection development* ($q = 0.0033$) and *neuron differentiation* ($q = 0.0015$).

Importantly, 10 of the 87 dysregulated genes are annotated in the SFARI AutDB database (*crhr2, scn5a, pax6, c4b, dcx, kirrel3, fam19a2, nrp2, camk4, pvalb*), displaying a significant overrepresentation of gene changes in our models potentially linked to ASD (One-sided Fisher's exact test, $p = 0.001$). These genes function in neuron migration, cytoskeleton dynamics, cell adhesion, axon guidance, and neural activity. Our findings suggest that β-cat networks, dysregulated by excessive β-cat in excitatory neurons, leads to aberrant expression levels of multiple genes implicated in human autism.

From these 10 ASD-linked genes, we have focused initially on the downregulated gene, *pvalb*, encoding the calcium-binding protein, parvalbumin, in fast-spiking interneurons. Excitatory/inhibitory imbalance in the PFC has been shown to alter social behaviors (Yizhar et al., 2011), and our previous study of the APC cKO mouse shows a reduced number of parvalbumin-positive cells in the medial PFC, increased c-fos in excitatory neurons in the infralimbic subregion in response to a novel social stimulus and increased mEPSC frequency (Pirone et al., 2018). qPCR and immunoblots show reductions in *pvalb* mRNA (One-way ANOVA $F_{(3, 12)} = 11.07$, $p = 0.0009$; **Figure 3B**) and protein levels (One-way ANOVA $F_{(3, 12)} = 4.1742$, $p = 0.0306$; **Figure 3C**) in the PFC of both mouse lines with elevated β-cat. In contrast, PFC parvalbumin protein and mRNA levels are normal in APC/β-cat cKOs that do not exhibit the aberrant social and repetitive behaviors (**Figures 3B,C**). Consistent with our results, reduced parvalbumin levels in the PFC have been associated with altered social behaviors in both human and mouse studies (Wöhr et al., 2015; Filice et al., 2016; Hashemi et al., 2017).

DISCUSSION

Our major findings are that excessive β-cat leads to decreased social interest and increased repetitive behaviors and aberrant expression of multiple genes that have been implicated in human ASD and play roles in synaptic function and circuit connections in the brain. Decreasing β-cat in neurons predisposed by gene mutations to express excessive β-cat averts these phenotypes. Our data are elucidating how autism-linked human genes that converge on the β-cat network may incline neurons to disease.

Our APC and β-cat mutant mouse lines are experimentally amenable models of the mammalian brain. Although these conditional mutants are not direct models of disease-linked human gene mutations, they are valuable tools to elucidate the pathophysiological consequences of aberrant β-cat levels in neurons *in vivo*. Importantly, our β-cat genetic manipulations target glutamatergic neurons, at a relevant developmental age, as it coincides with the stage when cortical glutamatergic neurons of both the human and mouse brain display convergent expression of several ASD and ID linked genes (Parikshak et al., 2013; Willsey et al., 2013). Thus the time-frame of our β-cat genetic manipulations may target a critical developmental window. Conditional manipulation of β-cat and APC gene expression during synaptic differentiation, rather than earlier or later, is necessary to define behavioral and cognitive phenotypes. Global nulls lead to embryonic lethality (Haegel et al., 1995;

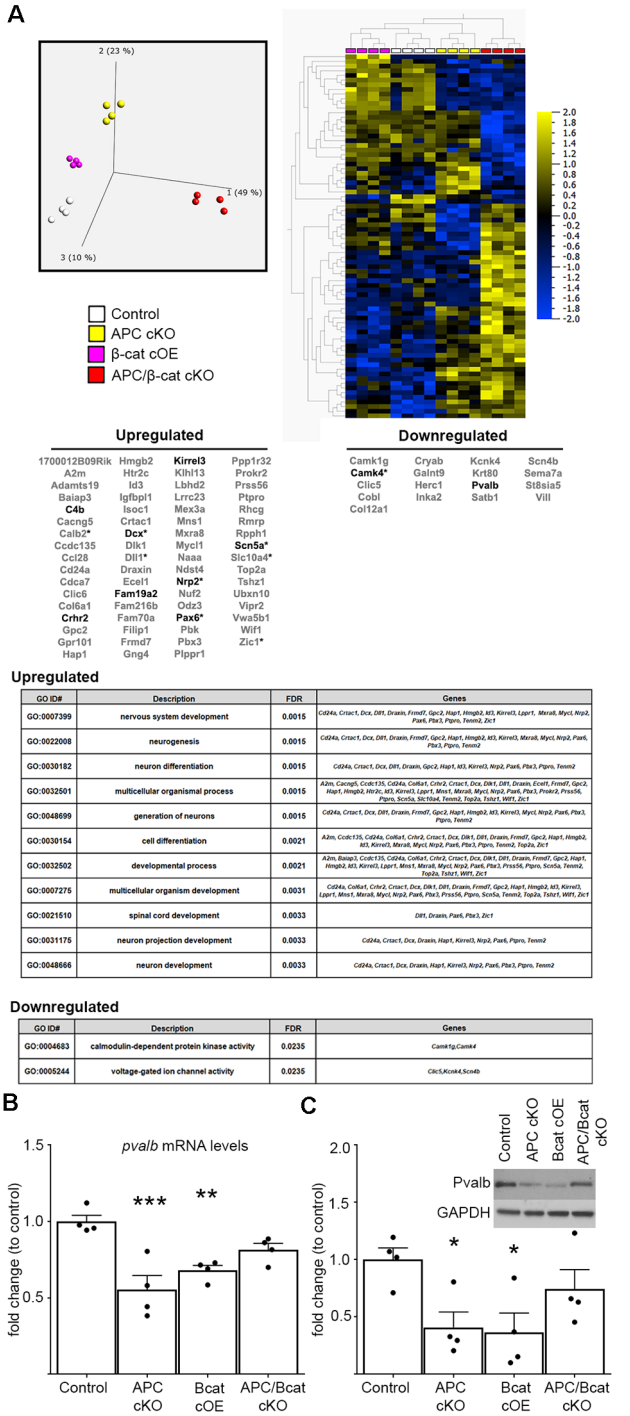

FIGURE 3 | Elevated β-cat causes altered expression of multiple autism-linked genes. **(A)** Next-generation data sets (n = 4 per genotype) were subject to primary component analysis and hierarchical clustering. The PFC shows 87 dysregulated genes (70 upregulated, 17 downregulated) shared between the two elevated β-cat models that exhibit altered social and repetitive behaviors, but not the reduced β-cat model that does not. Nine of the dysregulated genes are canonical Wnt target genes (asterisks). Ten are associated with human ASD (SFARI AutDB, bolded), and gene ontology analysis shows altered functions relevant to ASD pathology. Decreases in one

(*Continued*)

FIGURE 3 | Continued
of the identified ASD-linked genes, *pvalb*, at both **(B)** mRNA (qPCR) and **(C)** protein (immunoblot) levels in PFC of β-cat cOEs and APC cKOs, but normal levels in APC/β-cat cKOs (n = 4 per genotype, $^{*}p < 0.05$, $^{**}p < 0.01$, $^{***}p < 0.0001$, Sidak-Bonferroni corrected Student's t-test).

Moser et al., 1995; Huelsken et al., 2000). Conditional deletion and overexpression in progenitor cells causes severe brain malformation (Haegel et al., 1995; Moser et al., 1995; Brault et al., 2001; Chenn and Walsh, 2002, 2003; Gao et al., 2007; Grigoryan et al., 2008; Maguschak and Ressler, 2008; Ivaniutsin et al., 2009).

Our findings provide the first direct *in vivo* evidence, to our knowledge, that excessive levels of β-cat can lead to social deficits and increased repetitive behaviors. While most mutations in human *ctnnb1* (β-cat) gene result in loss of function of the protein (Krumm et al., 2014; Krupp et al., 2017), work by us and others suggests that maintenance of the proper levels of β-cat is critical for normal behavior and may have cell type-specific repercussions. This is highlighted by the fact we do not observe these behavioral deficits in our mice with low levels of β-cat in excitatory neurons, but social deficits have been observed in mice with deletion of β-cat in parvalbumin interneurons (Dong et al., 2016). Further, mutations in several other ASD-linked human genes are predicted to cause up- or down-regulation of β-cat functions.

Intriguingly, although the β-cat cOE and APC cKO mice show similar increases in β-cat protein levels, we note some differences in their behavioral phenotypes. While social interest is reduced to a similar extent, β-cat cOEs exhibit increased circling and a reduction in marble-burying activity relative to APC cKOs. Further, β-cat cOEs show hyperphosphorylation of APC, which may play a role in the behavioral differences. As APC is a large protein with 180 putative phosphorylation sites, further studies will be needed to test whether APC function is altered and its potential contribution to the divergent phenotypes. Additionally, APC loss in the APC cKOs may also impact the behavioral phenotypes compared to the β-cat cOEs.

The ability of this one dysregulated protein to cause a cascade of molecular changes that impact behavior likely derives from its role in two core pathways- the cadherin synaptic adhesion complex and canonical Wnt signal transduction. β-cat links the synaptic adhesion complex to the submembranous actin cytoskeleton, thereby stabilizing the synapse (Knudsen et al., 1995; Uchida et al., 1996; Yu and Malenka, 2004; Brigidi and Bamji, 2011). Additionally, β-cat binds directly to key postsynaptic scaffolds, the synaptic scaffolding cell adhesion molecule (S-SCAM/Magi2) and APC, that bring together other adhesion proteins, glutamate receptors and signaling molecules that impact synapse maturation and function (Nishimura et al., 2002; Rosenberg et al., 2010; Mohn et al., 2014). In the canonical Wnt signaling pathway, β-cat functions as a transcription co-activator with TCF/LEF to mediate Wnt responsive gene expression (Clevers and Nusse, 2012). Several studies show that manipulating cadherin and Wnt signaling in the brain alters axon

guidance cues, synapse maturation, density and plasticity, and network connectivity (Uchida et al., 1996; Mysore et al., 2007; Brigidi and Bamji, 2011; Park and Shen, 2012; Salinas, 2012; Rosso and Inestrosa, 2013).

Studies of cultured hippocampal neurons show that excessive β-cat increases dendritic branching, spine density and synaptic function (mEPSC frequency), suggesting the potential for excitability imbalance (Murase et al., 2002; Yu and Malenka, 2003, 2004; Okuda et al., 2007). Increased neural activity by optogenetic activation of glutamatergic pyramidal neurons in the PFC of wild-type mice is sufficient to cause reduced social interest (Yizhar et al., 2011). Both of our mouse lines with elevated β-cat, β-cat cOEs, and APC cKOs, display increased dendritic spine density and reductions in parvalbumin mRNA and protein levels. Further, APC cKOs exhibit increased excitation of pyramidal neurons in the medial PFC when presented with a novel social stimulus (Pirone et al., 2018). Preventing the increase in β-cat in APC cKOs (APC/β-cat cKOs) averts the reductions in parvalbumin and corrects the social and repetitive behavioral phenotypes. The decreases in parvalbumin in β-cat cOEs and APC cKOs are likely caused by non-cell autonomous changes in the cellular microenvironment as reporter studies of CamKIIα Cre mice show that it is not expressed in these interneurons (Rios et al., 2001; Pirone et al., 2017). Parvalbumin interneuron specification, including migration, localization, maturation and synaptogenesis, are known to be regulated by both intrinsic and cellular microenvironment signaling (Wamsley and Fishell, 2017; Loo et al., 2019). Future studies are needed to identify the signaling factors responsible for the reductions in parvalbumin. It is also important to assess the other molecular changes found in the β-cat cOEs and APC cKOs to elucidate their impact on excitatory and inhibitory synaptic and circuit functions that are critical for normal behavior.

Our findings define a novel role for β-cat by showing that its dysregulation leads to altered expression of several genes linked to autism in humans. We provide new insights into molecular changes caused by malfunction of β-cat, one of a small number of convergent targets identified in human ASD. Elucidating the molecular etiologies of ASD is essential for identifying shared pathological changes that may be root causes and potential targets for effective therapeutic intervention.

DATA AVAILABILITY STATEMENT

The datasets analyzed in this study can be found on the GEO Database at https://www.ncbi.nlm.nih.gov/geo/query/acc.cgi, under accession no: GSE147034.

ETHICS STATEMENT

All procedures involving animals were approved by the Tufts University Institutional Animal Care and Use Committee under the National Institutes of Health guidelines.

AUTHOR CONTRIBUTIONS

JA and MJ designed the research studies. JA performed behavioral and biochemical research and analyzed data. AP performed spine analysis studies. JA and MJ wrote the manuscript.

FUNDING

This work was funded by NIH National Institute of Mental Health (NIMH) R01MH106623 (to MJ), National Institute of Neurological Disorders and Stroke (NINDS) T32 NS061764 (to JA), and the Tufts Center for Neuroscience Research P30 NS047243 (Jackson).

ACKNOWLEDGMENTS

We would like to thank Dr. Yanmei Huang and Dr. Albert Tai for their assistance with the next-generation sequencing preparation and analysis.

REFERENCES

Akiyama, T., and Kawasaki, Y. (2006). Wnt signalling and the actin cytoskeleton. *Oncogene* 25, 7538–7544. doi: 10.1038/sj.onc.1210063

Brault, V., Moore, R., Kutsch, S., Ishibashi, M., Rowitch, D. H., McMahon, A. P., et al. (2001). Inactivation of the β-catenin gene by Wnt1-Cre-mediated deletion results in dramatic brain malformation and failure of craniofacial development. *Development* 128, 1253–1264.

Brigidi, G. S., and Bamji, S. X. (2011). Cadherin-catenin adhesion complexes at the synapse. *Curr. Opin. Neurobiol.* 21, 208–214. doi: 10.1016/j.conb.2010.12.004

Brumback, A. C., Ellwood, I. T., Kjaerby, C., Iafrati, J., Robinson, S., Lee, A. T., et al. (2018). Identifying specific prefrontal neurons that contribute to autism-associated abnormalities in physiology and social behavior. *Mol. Psychiatry* 23, 2078–2089. doi: 10.1038/mp.2017.213

Carvalho Pereira, A., Violante, I. R., Mouga, S., Oliveira, G., and Castelo-Branco, M. (2018). Medial frontal lobe neurochemistry in autism spectrum disorder is marked by reduced N-acetylaspartate and unchanged γ-aminobutyric acid and glutamate + glutamine levels. *J. Autism Dev. Disord.* 48, 1467–1482. doi: 10.1007/s10803-017-3406-8

Chenn, A., and Walsh, C. A. (2002). Regulation of cerebral cortical size by control of cell cycle exit in neural precursors. *Science* 297, 365–369. doi: 10.1126/science.1074192

Chenn, A., and Walsh, C. A. (2003). Increased neuronal production, enlarged forebrains and cytoarchitectural distortions in β-catenin overexpressing transgenic mice. *Cereb. Cortex* 13, 599–606. doi: 10.1093/cercor/13.6.599

Cho, I. T., Lim, Y., Golden, J. A., and Cho, G. (2017). Aristaless related homeobox (ARX) interacts with β-catenin, BCL9, and P300 to regulate canonical Wnt signaling. *PLoS One* 12:e0170282. doi: 10.1371/journal.pone.0170282

Clevers, H., and Nusse, R. (2012). Wnt/β-catenin signaling and disease. *Cell* 149, 1192–1205. doi: 10.1016/j.cell.2012.05.012

Crawley, J. N. (2007). Mouse behavioral assays relevant to the symptoms of autism. *Brain Pathol.* 17, 448–459. doi: 10.1111/j.1750-3639.2007.00096.x

de la Torre-Ubieta, L., Won, H., Stein, J. L., and Geschwind, D. H. (2016). Advancing the understanding of autism disease mechanisms through genetics. *Nat. Med.* 22, 345–361. doi: 10.1038/nm.4071

Dong, F., Jiang, J., McSweeney, C., Zou, D., Liu, L., and Mao, Y. (2016). Deletion of CTNNB1 in inhibitory circuitry contributes to autism-associated behavioral defects. *Hum. Mol. Genet.* 25, 2738–2751. doi: 10.1093/hmg/ddw131

Durak, O., Gao, F., Kaeser-Woo, Y. J., Rueda, R., Martorell, A. J., Nott, A., et al. (2016). Chd8 mediates cortical neurogenesis *via* transcriptional regulation

of cell cycle and Wnt signaling. *Nat. Neurosci.* 19, 1477–1488. doi: 10.1038/nn.4400

Filice, F., Vörckel, K. J., Sungur, A. Ö., Wöhr, M., and Schwaller, B. (2016). Reduction in parvalbumin expression not loss of the parvalbumin-expressing GABA interneuron subpopulation in genetic parvalbumin and shank mouse models of autism. *Mol. Brain* 9:10. doi: 10.1186/s13041-016-0192-8

Gao, X., Arlotta, P., Macklis, J. D., and Chen, J. (2007). Conditional knock-out of β-catenin in postnatal-born dentate gyrus granule neurons results in dendritic malformation. *J. Neurosci.* 27, 14317–14325. doi: 10.1523/JNEUROSCI.3206-07.2007

Gilman, S. R., Iossifov, I., Levy, D., Ronemus, M., Wigler, M., and Vitkup, D. (2011). Rare de novo variants associated with autism implicate a large functional network of genes involved in formation and function of synapses. *Neuron* 70, 898–907. doi: 10.1016/j.neuron.2011.05.021

Gounari, F., Chang, R., Cowan, J., Guo, Z., Dose, M., Gounaris, E., et al. (2005). Loss of adenomatous polyposis coli gene function disrupts thymic development. *Nat. Immunol.* 6, 800–809. doi: 10.1038/ni1228

Grigoryan, T., Wend, P., Klaus, A., and Birchmeier, W. (2008). Deciphering the function of canonical Wnt signals in development and disease: conditional loss- and gain-of-function mutations of β-catenin in mice. *Genes Dev.* 22, 2308–2341. doi: 10.1101/gad.1686208

Haegel, H., Larue, L., Ohsugi, M., Fedorov, L., Herrenknecht, K., and Kemler, R. (1995). Lack of β-catenin affects mouse development at gastrulation. *Development* 121, 3529–3537.

Harada, N., Tamai, Y., Ishikawa, T., Sauer, B., Takaku, K., Oshima, M., et al. (1999). Intestinal polyposis in mice with a dominant stable mutation of the β-catenin gene. *EMBO J.* 18, 5931–5942. doi: 10.1093/emboj/18.21.5931

Hashemi, E., Ariza, J., Rogers, H., Noctor, S. C., and Martínez-Cerdeño, V. (2017). The number of parvalbumin-expressing interneurons is decreased in the medial prefrontal cortex in autism. *Cereb. Cortex* 27, 1931–1943. doi: 10.1093/cercor/bhw021

Hödar, C., Assar, R., Colombres, M., Aravena, A., Pavez, L., González, M., et al. (2010). Genome-wide identification of new Wnt/β-catenin target genes in the human genome using CART method. *BMC Genomics* 11:348. doi: 10.1186/1471-2164-11-348

Huelsken, J., Vogel, R., Brinkmann, V., Erdmann, B., Birchmeier, C., and Birchmeier, W. (2000). Requirement for β-catenin in anterior-posterior axis formation in mice. *J. Cell Biol.* 148, 567–578. doi: 10.1083/jcb.148.3.567

Humrich, J., Bermel, C., Grubel, T., Quitterer, U., and Lohse, M. J. (2003). Regulation of phosducin-like protein by casein kinase 2 and N-terminal splicing. *J. Biol. Chem.* 278, 4474–4481. doi: 10.1074/jbc.m206347200

Hutsler, J. J., and Zhang, H. (2010). Increased dendritic spine densities on cortical projection neurons in autism spectrum disorders. *Brain Res.* 1309, 83–94. doi: 10.1016/j.brainres.2009.09.120

Iossifov, I., Ronemus, M., Levy, D., Wang, Z., Hakker, I., Rosenbaum, J., et al. (2012). De novo gene disruptions in children on the autistic spectrum. *Neuron* 74, 285–299. doi: 10.1016/j.neuron.2012.04.009

Ivaniutsin, U., Chen, Y., Mason, J. O., Price, D. J., and Pratt, T. (2009). Adenomatous polyposis coli is required for early events in the normal growth and differentiation of the developing cerebral cortex. *Neural Dev.* 4:3. doi: 10.1186/1749-8104-4-3

Kloth, K., Denecke, J., Hempel, M., Johannsen, J., Strom, T. M., Kubisch, C., et al. (2017). First de novo ANK3 nonsense mutation in a boy with intellectual disability, speech impairment and autistic features. *Eur. J. Med. Genet.* 60, 494–498. doi: 10.1016/j.ejmg.2017.07.001

Knudsen, K. A., Soler, A. P., Johnson, K. R., and Wheelock, M. J. (1995). Interaction of α-actinin with the cadherin/catenin cell-cell adhesion complex *via* α-catenin. *J. Cell Biol.* 130, 67–77. doi: 10.1083/jcb.130.1.67

Krumm, N., O'Roak, B. J., Shendure, J., and Eichler, E. E. (2014). A de novo convergence of autism genetics and molecular neuroscience. *Trends Neurosci.* 37, 95–105. doi: 10.1016/j.tins.2013.11.005

Krupp, D. R., Barnard, R. A., Duffourd, Y., Evans, S. A., Mulqueen, R. M., Bernier, R., et al. (2017). Exonic mosaic mutations contribute risk for autism spectrum disorder. *Am. J. Hum. Genet.* 101, 369–390. doi: 10.1016/j.ajhg.2017.07.016

Lazaro, M. T., Taxidis, J., Shuman, T., Bachmutsky, I., Ikrar, T., Santos, R., et al. (2019). Reduced prefrontal synaptic connectivity and disturbed oscillatory population dynamics in the CNTNAP2 model of autism. *Cell Rep.* 27, 2567.e6–2578.e6. doi: 10.1016/j.celrep.2019.05.006

Loo, L., Simon, J. M., Xing, L., McCoy, E. S., Niehaus, J. K., Guo, J., et al. (2019). Single-cell transcriptomic analysis of mouse neocortical development. *Nat. Commun.* 10:134. doi: 10.1038/s41467-018-08079-9

Maguschak, K. A., and Ressler, K. J. (2008). β-catenin is required for memory consolidation. *Nat. Neurosci.* 11, 1319–1326. doi: 10.1038/nn.2198

Martin, P. M., Yang, X., Robin, N., Lam, E., Rabinowitz, J. S., Erdman, C. A., et al. (2013). A rare WNT1 missense variant overrepresented in ASD leads to increased Wnt signal pathway activation. *Transl. Psychiatry* 3:e301. doi: 10.1038/tp.2013.75

Mohn, J. L., Alexander, J., Pirone, A., Palka, C. D., Lee, S. Y., Mebane, L., et al. (2014). Adenomatous polyposis coli protein deletion leads to cognitive and autism-like disabilities. *Mol. Psychiatry* 19, 1133–1142. doi: 10.1038/mp.2014.61

Moser, A. R., Shoemaker, A. R., Connelly, C. S., Clipson, L., Gould, K. A., Luongo, C., et al. (1995). Homozygosity for the Min allele of Apc results in disruption of mouse development prior to gastrulation. *Dev. Dyn.* 203, 422–433. doi: 10.1002/aja.1002030405

Murase, S., Mosser, E., and Schuman, E. M. (2002). Depolarization drives β-Catenin into neuronal spines promoting changes in synaptic structure and function. *Neuron* 35, 91–105. doi: 10.1016/s0896-6273(02)00764-x

Mysore, S. P., Tai, C. Y., and Schuman, E. M. (2007). Effects of N-cadherin disruption on spine morphological dynamics. *Front. Cell. Neurosci.* 1:1. doi: 10.3389/neuro.03.001.2007

Neale, B. M., Kou, Y., Liu, L., Ma'ayan, A., Samocha, K. E., Sabo, A., et al. (2012). Patterns and rates of exonic de novo mutations in autism spectrum disorders. *Nature* 485, 242–245. doi: 10.1038/nature11011

Nishimura, W., Yao, I., Iida, J., Tanaka, N., and Hata, Y. (2002). Interaction of synaptic scaffolding molecule and β -catenin. *J. Neurosci.* 22, 757–765. doi: 10.1523/JNEUROSCI.22-03-00757.2002

Okuda, T., Yu, L. M., Cingolani, L. A., Kemler, R., and Goda, Y. (2007). β-Catenin regulates excitatory postsynaptic strength at hippocampal synapses. *Proc. Natl. Acad. Sci. U S A* 104, 13479–13484. doi: 10.1073/pnas.0702334104

O'Roak, B. J., Vives, L., Fu, W., Egertson, J. D., Stanaway, I. B., Phelps, I. G., et al. (2012). Multiplex targeted sequencing identifies recurrently mutated genes in autism spectrum disorders. *Science* 338, 1619–1622. doi: 10.1126/science.1227764

Parikshak, N. N., Luo, R., Zhang, A., Won, H., Lowe, J. K., Chandran, V., et al. (2013). Integrative functional genomic analyses implicate specific molecular pathways and circuits in autism. *Cell* 155, 1008–1021. doi: 10.1016/j.cell.2013.10.031

Park, M., and Shen, K. (2012). WNTs in synapse formation and neuronal circuitry. *EMBO J.* 31, 2697–2704. doi: 10.1038/emboj.2012.145

Pirone, A., Alexander, J., Lau, L. A., Hampton, D., Zayachkivsky, A., Yee, A., et al. (2017). APC conditional knock-out mouse is a model of infantile spasms with elevated neuronal β-catenin levels, neonatal spasms, and chronic seizures. *Neurobiol. Dis.* 98, 149–157. doi: 10.1016/j.nbd.2016.11.002

Pirone, A., Alexander, J. M., Koenig, J. B., Cook-Snyder, D. R., Palnati, M., Wickham, R. J., et al. (2018). Social stimulus causes aberrant activation of the medial prefrontal cortex in a mouse model with autism-like behaviors. *Front. Synaptic Neurosci.* 10:35. doi: 10.3389/fnsyn.2018.00035

Preitner, N., Quan, J., Nowakowski, D. W., Hancock, M. L., Shi, J., Tcherkezian, J., et al. (2014). APC is an RNA-binding protein, and its interactome provides a link to neural development and microtubule assembly. *Cell* 158, 368–382. doi: 10.1016/j.cell.2014.05.042

Rios, M., Fan, G., Fekete, C., Kelly, J., Bates, B., Kuehn, R., et al. (2001). Conditional deletion of brain-derived neurotrophic factor in the postnatal brain leads to obesity and hyperactivity. *Mol. Endocrinol.* 15, 1748–1757. doi: 10.1210/mend.15.10.0706

Rosenberg, M. M., Yang, F., Mohn, J. L., Storer, E. K., and Jacob, M. H. (2010). The postsynaptic adenomatous polyposis coli (APC) multiprotein complex is required for localizing neuroligin and neurexin to neuronal nicotinic synapses *in vivo*. *J. Neurosci.* 30, 11073–11085. doi: 10.1523/JNEUROSCI.0983-10.2010

Rosso, S. B., and Inestrosa, N. C. (2013). WNT signaling in neuronal maturation and synaptogenesis. *Front. Cell. Neurosci.* 7:103. doi: 10.3389/fncel.2013.00103

Salinas, P. C. (2012). Wnt signaling in the vertebrate central nervous system: from axon guidance to synaptic function. *Cold Spring Harb. Perspect. Biol.* 4:a008003. doi: 10.1101/cshperspect.a008003

Sanders, S. J., He, X., Willsey, A. J., Ercan-Sencicek, A. G., Samocha, K. E., Cicek, A. E., et al. (2015). Insights into autism spectrum disorder genomic architecture and biology from 71 risk loci. *Neuron* 87, 1215–1233. doi: 10.1016/j.neuron.2015.09.016

Selimbeyoglu, A., Kim, C. K., Inoue, M., Lee, S. Y., Hong, A. S. O., Kauvar, I., et al. (2017). Modulation of prefrontal cortex excitation/inhibition balance rescues social behavior in CNTNAP2-deficient mice. *Sci. Transl. Med.* 9:eaah6733. doi: 10.1126/scitranslmed.aah6733

Staffend, N. A., and Meisel, R. L. (2011). DiOlistic labeling in fixed brain slices: phenotype, morphology, and dendritic spines. *Curr. Protoc. Neurosci.* Chapter 2:Unit 2.13. doi: 10.1002/0471142301.ns0213s55

Tang, G., Gudsnuk, K., Kuo, S. H., Cotrina, M. L., Rosoklija, G., Sosunov, A., et al. (2014). Loss of mTOR-dependent macroautophagy causes autistic-like synaptic pruning deficits. *Neuron* 83, 1131–1143. doi: 10.1016/j.neuron.2014.07.040

Thomas, A., Burant, A., Bui, N., Graham, D., Yuva-Paylor, L. A., and Paylor, R. (2009). Marble burying reflects a repetitive and perseverative behavior more than novelty-induced anxiety. *Psychopharmacology* 204, 361–373. doi: 10.1007/s00213-009-1466-y

Todd, B. P., and Bassuk, A. G. (2018). A de novo mutation in PRICKLE1 associated with myoclonic epilepsy and autism spectrum disorder. *J. Neurogenet.* 32, 313–315. doi: 10.1080/01677063.2018.1473862

Tucci, V., Kleefstra, T., Hardy, A., Heise, I., Maggi, S., Willemsen, M. H., et al. (2014). Dominant β-catenin mutations cause intellectual disability with recognizable syndromic features. *J. Clin. Invest.* 124, 1468–1482. doi: 10.1172/JCI70372

Uchida, N., Honjo, Y., Johnson, K. R., Wheelock, M. J., and Takeichi, M. (1996). The catenin/cadherin adhesion system is localized in synaptic junctions bordering transmitter release zones. *J. Cell Biol.* 135, 767–779. doi: 10.1083/jcb.135.3.767

Wamsley, B., and Fishell, G. (2017). Genetic and activity-dependent mechanisms underlying interneuron diversity. *Nat. Rev. Neurosci.* 18, 299–309. doi: 10.1038/nrn.2017.30

Weir, R. K., Bauman, M. D., Jacobs, B., and Schumann, C. M. (2018). Protracted dendritic growth in the typically developing human amygdala and increased spine density in young ASD brains. *J. Comp. Neurol.* 526, 262–274. doi: 10.1002/cne.24332

Wickham, R. J., Alexander, J. M., Eden, L. W., Valencia-Yang, M., Llamas, J., Aubrey, J. R., et al. (2019). Learning impairments and molecular changes in the brain caused by β-catenin loss. *Hum. Mol. Genet.* 28, 2965–2975. doi: 10.1093/hmg/ddz115

Willsey, A. J., Sanders, S. J., Li, M., Dong, S., Tebbenkamp, A. T., Muhle, R. A., et al. (2013). Coexpression networks implicate human midfetal deep cortical projection neurons in the pathogenesis of autism. *Cell* 155, 997–1007. doi: 10.1016/j.cell.2013.10.020

Wisniewska, M. B., Nagalski, A., Dabrowski, M., Misztal, K., and Kuznicki, J. (2012). Novel β-catenin target genes identified in thalamic neurons encode modulators of neuronal excitability. *BMC Genomics* 13:635. doi: 10.1186/1471-2164-13-635

Wöhr, M., Orduz, D., Gregory, P., Moreno, H., Khan, U., Vörckel, K. J., et al. (2015). Lack of parvalbumin in mice leads to behavioral deficits relevant to all human autism core symptoms and related neural morphofunctional abnormalities. *Transl. Psychiatry* 5:e525. doi: 10.1038/tp.2015.19

Yi, J. J., Paranjape, S. R., Walker, M. P., Choudhury, R., Wolter, J. M., Fragola, G., et al. (2017). The autism-linked UBE3A T485A mutant E3 ubiquitin ligase activates the Wnt/β-catenin pathway by inhibiting the proteasome. *J. Biol. Chem.* 292, 12503–12515. doi: 10.1074/jbc.m117.788448

Yizhar, O., Fenno, L. E., Prigge, M., Schneider, F., Davidson, T. J., O'Shea, D. J., et al. (2011). Neocortical excitation/inhibition balance in information processing and social dysfunction. *Nature* 477, 171–178. doi: 10.1038/nature10360

Yu, X., and Malenka, R. C. (2003). β-catenin is critical for dendritic morphogenesis. *Nat. Neurosci.* 6, 1169–1177. doi: 10.1038/nn1132

Yu, X., and Malenka, R. C. (2004). Multiple functions for the cadherin/catenin complex during neuronal development. *Neuropharmacology* 47, 779–786. doi: 10.1016/j.neuropharm.2004.07.031

Zhou, X. L., Giacobini, M., Anderlid, B. M., Anckarsater, H., Omrani, D., Gillberg, C., et al. (2007). Association of adenomatous polyposis coli (APC) gene polymorphisms with autism spectrum disorder (ASD). *Am. J. Med. Genet. B Neuropsychiatr. Genet.* 144B, 351–354. doi: 10.1002/ajmg.b.30415

Zoghbi, H. Y., and Bear, M. F. (2012). Synaptic dysfunction in neurodevelopmental disorders associated with autism and intellectual disabilities. *Cold Spring Harb. Perspect. Biol.* 4:a009886. doi: 10.1101/cshperspect.a009886

Zumbrunn, J., Kinoshita, K., Hyman, A. A., and Näthke, I. S. (2001). Binding of the adenomatous polyposis coli protein to microtubules increases microtubule stability and is regulated by GSK3 β phosphorylation. *Curr. Biol.* 11, 44–49. doi: 10.1016/s0960-9822(01)00002-1

Conflict of Interest: The authors declare that the research was conducted in the absence of any commercial or financial relationships that could be construed as a potential conflict of interest.

frontiers in Synaptic Neuroscience

ORIGINAL RESEARCH
published: 24 April 2020
doi: 10.3389/fnsyn.2020.00016

Chronic Presence of Oligomeric Aβ Differentially Modulates Spine Parameters in the Hippocampus and Cortex of Mice With Low APP Transgene Expression

Mariya V. Hrynchak[1†], Marina Rierola[1†], Nataliya Golovyashkina[1], Lorène Penazzi[1], Wiebke C. Pump[1], Bastian David[1], Frederik Sündermann[1], Roland Brandt[1,2,3] and Lidia Bakota[1]*

[1]Department of Neurobiology, School of Biology/Chemistry, University of Osnabrück, Osnabrück, Germany, [2]Center for Cellular Nanoanalytics, University of Osnabrück, Osnabrück, Germany, [3]Institute of Cognitive Science, University of Osnabrück, Osnabrück, Germany

OPEN ACCESS

Edited by:
Clive R. Bramham,
University of Bergen, Norway

Reviewed by:
Volkmar Lessmann,
University Hospital Magdeburg, Germany
Susanne Frykman,
Karolinska Institutet (KI), Sweden

***Correspondence:**
Lidia Bakota
lbakota@uni-osnabrueck.de

[†]These authors have contributed equally to this work

Received: 09 December 2019
Accepted: 25 March 2020
Published: 24 April 2020

Citation:
Hrynchak MV, Rierola M, Golovyashkina N, Penazzi L, Pump WC, David B, Sündermann F, Brandt R and Bakota L (2020) Chronic Presence of Oligomeric Aβ Differentially Modulates Spine Parameters in the Hippocampus and Cortex of Mice With Low APP Transgene Expression. Front. Synaptic Neurosci. 12:16. doi: 10.3389/fnsyn.2020.00016

Alzheimer's disease is regarded as a synaptopathy with a long presymptomatic phase. Soluble, oligomeric amyloid-β (Aβ) is thought to play a causative role in this disease, which eventually leads to cognitive decline. However, most animal studies have employed mice expressing high levels of the Aβ precursor protein (APP) transgene to drive pathology. Here, to understand how the principal neurons in different brain regions cope with moderate, chronically present levels of Aβ, we employed transgenic mice expressing equal levels of mouse and human APP carrying a combination of three familial AD (FAD)-linked mutations (Swedish, Dutch, and London), that develop plaques only in old age. We analyzed dendritic spine parameters in hippocampal and cortical brain regions after targeted expression of EGFP to allow high-resolution imaging, followed by algorithm-based evaluation of mice of both sexes from adolescence to old age. We report that Aβ species gradually accumulated throughout the life of APP_{SDL} mice, but not the oligomeric forms, and that the amount of membrane-associated oligomers decreased at the onset of plaque formation. We observed an age-dependent loss of thin spines under most conditions as an indicator of a loss of synaptic plasticity in older mice. We further found that hippocampal pyramidal neurons respond to increased Aβ levels by lowering spine density and shifting spine morphology, which reached significance in the CA1 subfield. In contrast, the spine density in cortical pyramidal neurons of APP_{SDL} mice was unchanged. We also observed an increase in the protein levels of PSD-95 and Arc in the hippocampus and cortex, respectively. Our data demonstrated that increased concentrations of Aβ have diverse effects on dendritic spines in the brain and suggest that hippocampal and cortical neurons have different adaptive and compensatory capacity during their lifetime. Our data also indicated that spine morphology differs between sexes in a region-specific manner.

Keywords: Aβ, Alzheimer's disease, cortex, dendritic spine, hippocampus

INTRODUCTION

Alzheimer's disease (AD) is the most common form of dementia in the elderly. The key histopathological features of AD are the formation of plaques consisting of extracellular deposits of β-amyloid (Aβ) peptides and intraneuronal neurofibrillary tangles (NFTs) composed of a hyperphosphorylated form of the microtubule-associated protein tau.

According to the amyloid hypothesis, Aβ deposits are thought to play a causative role in AD (Hardy and Selkoe, 2002), suggesting that Aβ accumulation initiates a cascade of events that result in synaptic changes, tau pathology, and neuron loss that eventually leads to cognitive decline (Bakota and Brandt, 2016). Although the amyloid hypothesis was initially based on the fact that insoluble Aβ aggregates could be observed in the brains of AD patients, it has changed to reflect the growing evidence that soluble, oligomeric forms of Aβ may represent the major neurotoxic species (Lacor et al., 2007; Shankar et al., 2008; Tu et al., 2014). Missense mutations in the genes coding for amyloid beta precursor protein (APP) or APP processing enzymes such as presenilin (PSEN) in familial forms of AD (FAD) have been found to result in increased amounts of Aβ. This has led to the generation of several mouse models transgenic for human *APP* or other disease-relevant genes harboring FAD-related mutations (Games et al., 1995; Moechars et al., 1999; Richardson and Burns, 2002; Jankowsky and Zheng, 2017). Recently, spontaneous cases of AD have also been identified where patients contained more DNA and increased *APP* copy number (Bushman et al., 2015), likely due to somatic gene recombination (Lee et al., 2018). This confirmed an important role in the long-term increase in Aβ production in the development of the disease. AD is considered a disease of synaptic failure (Selkoe, 2002; Arendt, 2009), which occurs substantially earlier than intense neuronal degeneration and plaque formation. The existence of a long presymptomatic/preclinical phase of AD indicates that the chronic exposure to low or moderate amounts of soluble Aβ might induce subtle changes in synaptic connectivity long before the emergence of cognitive impairment. It is also conceivable that AD could be treated before cognitive deficits and massive neurodegeneration occur to delay the onset of clinical symptoms. Consequently, it has recently become apparent that models of aging are needed to investigate age-related neurodegeneration (Johnson, 2015). Moreover, several studies have proposed the use of knock-in mice or mice with low overexpression of the transgene to better mimic the long-term progression of the disease (Saito et al., 2016). In such a context, transgenic mice that express moderate concentrations of soluble Aβ in a sustained manner and develop plaques only late in life could be instrumental for analyzing presymptomatic and chronic Aβ effects during aging. Mice transgenic for human APP695 with the combination of Swedish (KM595/596NL), Dutch (E618Q), and London (V642I) mutations under the control of the platelet-derived growth factor beta (*PDGFB*) promoter (APP_{SDL} mice) produce moderate levels of Aβ and develop plaques only in old age (Blanchard et al., 2003). These mice have proven to also be useful for the generation of *ex vivo* models since they already express Aβ40 and Aβ42 at early postnatal stages (Tackenberg and Brandt, 2009; Golovyashkina et al., 2015; Penazzi et al., 2016). It has been shown that male APP_{SDL} mice have a reduced olfactory habituation and a higher level of anxiety compared to control mice, but have no significant deficits in hippocampus-related spatial memory at 17–18 months when plaque formation starts to emerge (Penazzi et al., 2017). A deficit of olfactory function or anxiety-like behavior has been associated with amyloidosis-related pathologies and can be an informative biomarker for diagnosing the earliest stage of neuropathologies such as AD (Lee et al., 2004; Alvarado-Martínez et al., 2013).

The loss of synapses and dendritic spines, which represent the major excitatory input, is one of the common defects found in human AD brains (for a review see Tackenberg et al., 2009). Spine loss in specific brain regions appears to be an early event during disease development as individuals with mild AD already have fewer synapses (55%) in the *stratum radiatum* of the CA1 subfield (Scheff et al., 2007). A recent detailed 3D ultrastructural analysis performed on the transentorhinal cortex of AD patients showed that a reduction in the percentage of synapses affects the subset of asymmetric synapse types targeting spine heads (Dominguez-Álvaro et al., 2019). Results from human studies also indicate that spines become deformed during AD compared with those in normal aged brains (Baloyannis et al., 2007). This could be functionally relevant because spines with larger heads (mushroom spines) are thought to have stronger synapses (Matsuzaki et al., 2001) and provide higher compartmentalization (Brandt and Paululat, 2013). Aβ induces acute alterations in dendritic spines, as demonstrated in hippocampal cell and tissue culture experiments (Lacor et al., 2007; Shankar et al., 2008; Ortiz-Sanz et al., 2020), and spine loss is also seen in the brains of APP or PSEN transgenic mice (Smith et al., 2009; Merino-Serrais et al., 2011; Zago et al., 2012; Liang et al., 2019). Interestingly, several studies have also shown that short exposure to picomolar concentrations of Aβ positively modulates synaptic plasticity, while prolonged exposure or high (nanomolar) levels of Aβ impair synaptic transmission and induce neuronal loss (Puzzo et al., 2008; Koppensteiner et al., 2016). Therefore, the concentration, type, and duration of Aβ exposure, and likely also the type of receiving neuron, may determine the effect of Aβ on synaptic connectivity.

We hypothesized that the directionality or magnitude of the alterations may differ in various brain regions, depending on the adaptive/compensatory capacity of the respective region. However, to date, relatively few studies have examined early changes in synaptic connectivity before plaque formation, and no study has evaluated the effect of long-term, chronically present soluble Aβ species on changes in spine density and morphology. Furthermore, there are no reliable studies that would provide comparative knowledge of timeline trajectories regarding spine alteration in different brain regions during the long presymptomatic phase characterized by increasing Aβ levels. Finally, to the best of our knowledge, the evolution of dendritic spine parameters in the presence of elevated Aβ levels has not been studied in parallel in both sexes in AD mouse models.

Our motivation was to fill this knowledge gap by analyzing the brain of mice exposed to gradually increasing amounts of soluble Aβ species. We employed a mouse model (APP_{SDL} mice) that produces moderate levels of Aβ peptides throughout life and develops plaques only at an advanced age. To obtain a global understanding of how principal neurons in different brain regions cope with the chronic presence of Aβ from adolescence to old age, we analyzed two hippocampal and two cortical brain regions by algorithm-based evaluation of high-resolution cLSM image stacks. The structures could be analyzed due to the expression of EGFP in subsets of neurons (Feng et al., 2000). Moreover, owing to the emerging awareness of gender bias in AD development (May, 2016), we applied our spine parameter analysis to animals of both sexes.

MATERIALS AND METHODS

Animals

Heterozygous APP_{SDL} transgenic mice expressing human APP_{695} with three FAD-related mutations (Swedish [KM595/596NL], Dutch [E618Q], and London [V642I]) were used (Aventis Pharma; Strasbourg, France). The transgene in these mice is under the control of the *PDGFB* promoter (Blanchard et al., 2003). Age-matched C57BL/6 mice (Charles River Laboratories and Harlan Winkelmann) were employed as control. Genotyping of APP_{SDL} transgenic mice was performed from mouse tail DNA by PCR using the following primers: APP-forward, 5′-GTAGCAGAGGAGGAAGAAGTG-3′ and APP-reverse, 5′-CATGACCTGGGACATTCTC-3′. For analysis of synaptic connectivity and morphology, APP_{SDL} mice were crossed with homozygous EGFP-expressing mice (Thy1-GFP line M; obtained with the permission of Josh Sanes, Harvard University, Cambridge, MA, USA). In these mice, EGFP expression is governed by a neuron-specific *Thy1* promoter element (Feng et al., 2000). Littermates expressing EGFP and non-transgenic for human *APP* served as control. All animals were maintained and euthanized according to the National Institutes of Health guidelines and German animal care regulations.

Antibodies

The following antibodies were used: monoclonal anti-Aβ antibodies (mouse 4G8; Covance, Munich, Germany), monoclonal anti-neuronal nuclei antibody NeuN (mouse; Chemicon, Temecula, CA, USA), monoclonal anti-actin antibody (mouse; Calbiochem; Darmstadt, Germany), monoclonal anti-APP antibody (22C11; Millipore GmbH Schwalbach/Ts., Germany), monoclonal anti-synaptophysin antibody (mouse; Millipore), PSD-95 (7E3-1B8; mouse; Thermo Fisher Scientific, Rockford, IL, USA), monoclonal anti-Arc antibody (C-7; mouse; Santa Cruz Biotechnology, Dallas, TX, USA) and GAPDH (#AB2302; chicken; Millipore). The following anti-Tau antibodies were used: monoclonal phosphorylation independent Tau-5 (mouse; Labvision, Westinghouse, CA, USA), monoclonal AT8 (mouse; Thermo Fisher Scientific, Rockford, IL, USA), polyclonal pS199 (rabbit; Invitrogen, Carlsbad, CA, USA), and monoclonal PHF1 (mouse; a generous gift from Peter Davies, Albert Einstein College of Medicine, Bronx, NY, USA). As secondary antibodies, cyanine 3 (Cy3)-coupled anti-mouse (Dianova, Hamburg, Germany) and peroxidase-conjugated anti-mouse and anti-rabbit antibodies (Jackson Immuno Research, West Grove, PA, USA) were employed.

Analyses of Aβ Levels

Animals were euthanized by cervical dislocation. The brains were quickly removed, snap-frozen in liquid nitrogen, and stored at −80°C. Sequential extraction was performed essentially as previously described (Shankar et al., 2009). Briefly, frozen right hemibrains without cerebellum were homogenized in 1.1 ml of ice-cold Tris-buffered saline (TBS) containing a cocktail of protease and phosphates inhibitors (1 mM PMSF, 10 mg/ml each of leupeptin and pepstatin, 1 mM EGTA, 1 mM sodium orthovanadate, 20 mM sodium fluoride, and 1 mM sodium pyrophosphate) with 30 strokes using a mechanical Dounce homogenizer. Homogenates were centrifuged at 175,000× *g* and 4°C for 30 min. The supernatant (designated as TBS extract) was aliquoted and stored at −80°C. To solubilize the membrane-bound Aβ, the TBS-insoluble pellet was homogenized in 1.1 ml of TBS containing 1% Triton X-100 plus inhibitors (TBS-TX) with 30 strokes using a Dounce homogenizer, centrifuged at 175,000× *g* and 4°C for 30 min and the resultant supernatant (designated as TBS-TX extract) was aliquoted and stored at −80°C. TBS and TBS-TX extracts were subjected to an ELISA test using commercially available kits (EZHS40, EZHS42; Millipore GmbH Schwalbach/Ts., Germany; oligomeric Aβ ELISA Kit; Biosensis, Thebarton, Australia). The ELISA for the oligomeric Aβ utilizes the MOAB-2 antibody developed by LaDu and coworkers (Youmans et al., 2012). The authors showed that the MOAB-2 antibody specifically detects Aβ and not the precursor molecule APP. In ELISAs, the oligomeric form of the Aβ peptide (o-Aβ) can be assayed independently of the other forms of the molecule when the MOAB-2 monoclonal antibody is used. Cortices and hippocampi were isolated separately from another set of mice and processed as described above in 5× weight/volume extraction solutions. The samples were tested with ELISA Kit KHB3544 (Thermo Scientific, Schwerte, Germany).

Fixation and Staining

Mice were anesthetized and perfused transcardially with saline followed by fixation in 4% paraformaldehyde (PFA) in phosphate-buffered saline (PBS). Brains were removed, postfixed overnight at 4°C in 4% PFA/PBS, and stored in PBS at 4°C.

For thioflavin S staining, coronal vibratome sections (50 μm) were mounted on positively charged slides (SuperFrost Plus, Menzel). The sections were stained with 1% thioflavin S for 8 min and then differentiated in two changes of 85% ethanol for 3 min each and two changes of 95% ethanol for 3 min each followed by three washes with ddH_2O. The sections were mounted with Confocal-Matrix® (Micro-Tech-Lab, Graz, Austria) and a coverslip was applied.

For immunohistochemical staining, free-floating coronal sections (50 μm) were used. The slices were treated with 70%

formic acid for 30 min at room temperature and washed with PBS. Then, the slices were permeabilized with 0.4% (v/v) Triton X-100 in PBS for 30 min and washed with 1% (w/v) BSA and 0.1% (v/v) Tween 20 in PBS. The slices were incubated overnight at 4°C with primary antibodies. After washing with PBS, the slices were incubated with a Cy3-conjugated secondary antibody and DAPI for 3 h at RT, washed in PBS, and mounted in Confocal-Matrix® under a coverslip.

Microscopy

High-resolution microscopy images were obtained on a Nikon Eclipse TE2000-U fluorescence microscope (Tokyo, Japan) equipped with a digital camera (Vosskühler COOL-1300), Lucia G or NIS Elements AR software, and a C1 confocal laser scanning unit with Helium/Neon (He/Ne; 543 nm) and Argon (488 nm) laser, governed by EZ-C1 or NIS-Elements AR software. The objectives (Nikon) used were a dry 4 × (NA, 0.13), dry 10 × (NA, 0.3), dry 20 × (NA, 0.5), dry 40 × (NA, 0.75), 40× oil-immersion (NA, 1.0), and 60× oil-immersion (NA, 1.4). For imaging of whole neurons, a Zeiss 510 META confocal laser scanning microscope was employed using an Argon laser (488) and 40× oil-immersion (NA, 1.3) objective.

Algorithm-Based Spine Morphology Analysis

Secondary and tertiary segments (≥25 μm) of the apical (middle-third) dendritic subregions of pyramidal cells from hippocampal CA1 and CA3 (Bregma level from −1.58 to −2.03 mm) and two cortical areas, the parietal association cortex (ACTX; Bregma level from −1.46 to −2.06 mm) and the primary somatosensory cortex (SCTX; Bregma level from −1.34 to −2.06 mm) were imaged with a voxel size of 0.05 × 0.05 × 0.20 μm in x-y-z directions. Image stacks were processed using 3D blind deconvolution (Autodeblur Software) to improve signal-to-noise ratio and spatial resolution. Analysis of spine density, length, and shape was performed by algorithm-based, semi-automated evaluation of spine morphology using 3DMA-Neuron software as previously detailed (Sundermann et al., 2012). Spine morphology was classified into three groups: "stubby," "mushroom" and "thin" based on the ratio of head to neck diameter and the ratio of spine length to neck diameter as described in Koh et al. (2002). The software developers based their criteria on a thorough EM study by Harris et al. (1992). Data are represented using nonlinear curve fitting with allometric 1 function: $y = a*x^b$ (y = dependent variable; x = independent variable; a = coefficient; b = power).

For the 3D reconstruction of hippocampal neurons, pyramidal cells were imaged in 6–10 individual but overlapping stacks with a voxel size of 0.30 × 0.30 × 0.44 μm in x-y-z directions. Image stacks were converted into 8-bit grayscale .tif files using ImageJ software and then stitched to generate a single stack using VIAS software (Computational Neurobiology and Imaging Center, Mt. Sinai School of Medicine, New York, NY, USA). Three-dimensional reconstruction of whole neurons was performed using Neuromantic software (University of Reading, Reading, UK), which allows analysis of neuronal morphology after semi-automated tracing of dendritic processes, as previously described (Golovyashkina et al., 2014). Target neurons for all assessments were identified by anatomical location and cell morphology.

Determination of Neuron Density

For the determination of neuron numbers in cortical slices, a machine learning-based approach for fast and unbiased analysis was used (Penazzi et al., 2014). Images from coronal sections between Bregma −0.94 mm and −2.06 mm (Paxinos and Franklin, 2004) were acquired by epifluorescence microscopy and processed through a series of macros programmed for Fiji (Schindelin et al., 2012) consisting of the following plug-ins: Hybrid Median Filter 2D (Christopher Philip Mauer, Vytas Bindokas), Anisotropic Diffusion (Vladimir Pilny, Jiri Janacek), and enhance local contrast (CLAHE; Stephan Saalfeld). For machine learning, several classifiers were trained and applied with the Advanced Weka Segmentation Plug-in (Ignacio Arganda-Carreras, Albert Cardona, and Verena Kaynig).

Determination of Cortical Thickness, and Thickness of the Dentate Gyrus Granule Layer

The thickness of the neocortex was determined on the coronal sections of the same Bregma levels as those used for the determination of neuronal density. The thickness of the dentate gyrus (DG) was determined using coronal sections between Bregma −1.58 mm and −1.94 mm (Paxinos and Franklin, 2004) obtained from EGFP-expressing mice. The thickness was measured at the same position of the supra- and infra-pyramidal blade using the Fiji image processing package (Schindelin et al., 2012).

Western Blot Analyses

Brain tissue was homogenized in 4 ml of RIPA buffer (50 mM Tris-HCl, 150 mM NaCl, 1 mM EDTA, 1% NP-40, 0.5% sodium deoxycholate, and 0.1% SDS, pH 8.0) per gram brain in the presence of protease and phosphatase inhibitors (1 mM PMSF, 10 mg/ml each of leupeptin and pepstatin, 1 mM EGTA, 1 mM sodium orthovanadate, 20 mM sodium fluoride, and 1 mM sodium pyrophosphate), sonicated (10–15 pulses), and centrifuged for 10 min at 13,000× *g* at 4°C. The supernatant was frozen and stored at −80°C. Protein concentration was determined using a bicinchoninic acid (BCA) protein assay kit (Thermo Fisher Scientific, Waltham, MA, USA). The samples were subjected to SDS–PAGE and transferred to Immobilon-P membranes (Millipore) followed by immunoblotting. Protein bands were detected using enhanced chemiluminescence with SuperSignal West Dura extended duration substrate (Thermo Fisher Scientific, Waltham, MA, USA) according to the manufacturer's protocol. Quantification of the blots was performed with Gel-Pro Analyzer 4.0 (Media Cybernetics L.P., Baltimore, MD, USA) or by FusionCapt Advance (Vilber Lourmat, France).

Statistical Analyses

For dendritic spine analysis, a generalized linear model was used, which is a flexible generalization of ordinary linear regression

that allows for other than a normal distribution of the dependent variable and does not assume a linear relationship between the response variable and the model parameter. We have validated our generalized linear model (GZLM) with a finite sample corrected AIC (AICC). The normality of the data set was assessed by the Shapiro–Wilk test. All other measurements were statistically evaluated using the Student's *t*-test or ANOVA, as depicted in the figure legends.

Statistical analyses were performed using Origin 7.0 (Microcal Software, Northampton, MA, USA) and SPSS Statistics 23 and 24 (Armonk, NY, USA: IBM Corp).

RESULTS

APP_{SDL} Mice Accumulate Aβ40 and Aβ42 During Their Lifetime

To analyze the chronic effects of Aβ during aging, we used transgenic mice that produce moderate levels of Aβ and develop plaques only at old age (Blanchard et al., 2003). APP_{SDL} mice express a human *APP* splice variant with a combination of three FAD-linked mutations (Swedish, Dutch, and London). Transgene expression is governed by the *PDGFB* promoter that confers neuron-specific expression (Sasahara et al., 1991) from as early as embryonic day 15 (E15; Hutchins and Jefferson, 1992). Embryonic cortical cultures from these mice produce equimolar amounts of Aβ40 and Aβ42 in the picomolar range (Leschik et al., 2007). Mice were maintained on a C57BL/6J background and compared with nontransgenic littermates (designated as B6). We first confirmed brain parenchymal plaque formation on coronal sections stained by thioflavin S and further validated by 4G8 antibody staining. The Aβ deposits appeared sparsely first at 18 months, as previously described (Blanchard et al., 2003). The hippocampal DG was the most affected region; however, with the increasing age of the mice, plaques also appeared in the CA1 and CA3 regions and spread partially within the cortex (**Figure 1A**).

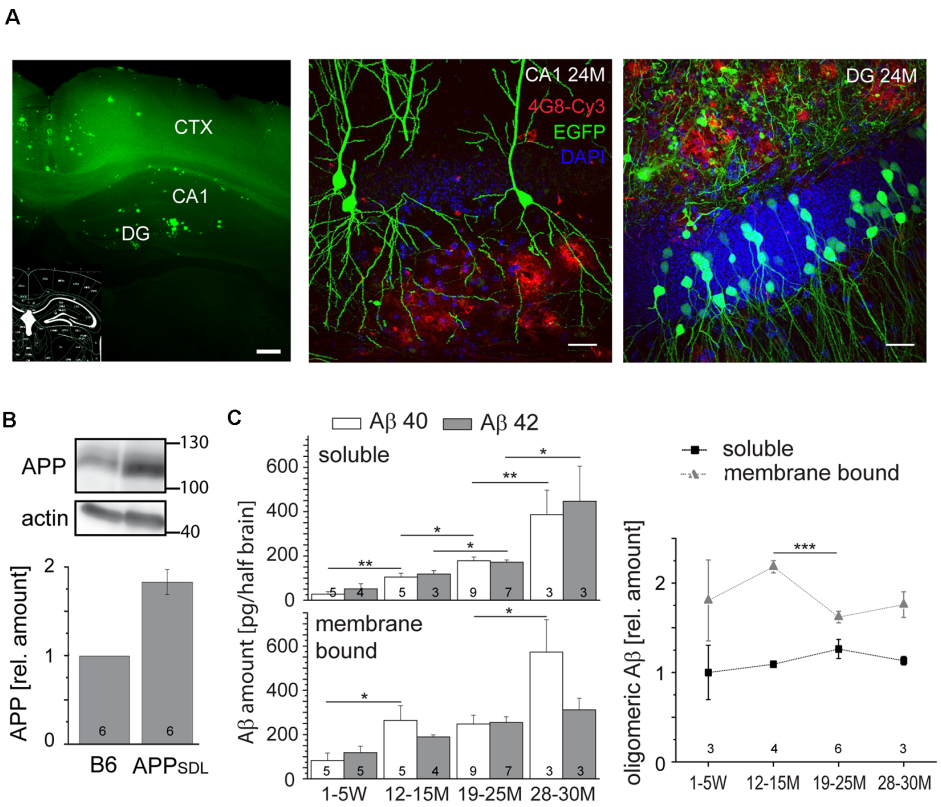

FIGURE 1 | Amyloid beta (Aβ) precursor protein (APP_{SDL}) mice accumulate Aβ40/Aβ42 during life with relatively stable amounts of the oligomeric forms. **(A)** Thioflavin S staining of a coronal vibratome section from a 24-month-old APP_{SDL} mouse, left. Confocal laser scanning micrographs showing Aβ deposits (4G8 staining, red) in the hippocampus from coronal sections of APP_{SDL} mice expressing EGFP in a population of hippocampal pyramidal neurons within the CA1 subfield, middle, and granule cells within the dentate gyrus (DG), right. Cell nuclei were visualized using DAPI. **(B)** The expression level of APP in B6 and APP_{SDL} animals. Immunoblot (top) of forebrain lysates from 24 months old mice detected with an anti-APP antibody that recognizes both human and mouse APP. Staining against actin is shown as loading control. Quantitation (bottom) of the APP signal was performed relative to actin and the value for B6 animals was set as 1.0. **(C)** Amount of soluble and membrane-bound human Aβ40 and Aβ42 (left), and the relative amount of oligomeric Aβ (right) from APP_{SDL} animals of different ages. Quantitation was performed by ELISA after the sequential extraction of brain lysates. The number of mice for each condition is indicated in bars (left) or right above the x-axis (right). Data represent mean ± SEM; the number of mice per genotype is shown at the graphs. Data were analyzed using Student's *t*-tests to address potential alterations between adjacent time points within the same condition and considered to be significantly different at $^{*}p < 0.05$, $^{**}p < 0.01$ and $^{***}p < 0.001$. Scale bar, 200 μm **(A)** left, 20 μm **(A)** middle, right.

Next, we analyzed the level to which APP_{SDL} mice expressed the human APP695 transgene. We observed a doubling of the total APP amount by semi-quantitative western blotting using a monoclonal antibody that detects both endogenous mouse and transgenic human APP (**Figure 1B**); there was an about equal expression of mouse and human APP. The expression of APP did not change throughout the life of the mice (data not shown). To determine the potential accumulation of Aβ species during aging, we quantified Aβ levels by ELISA. Because interaction with membranes may modulate amyloid aggregation and cytotoxicity (Evangelisti et al., 2016), we performed a sequential extraction of soluble and membrane-bound Aβ40 and Aβ42 before quantitation. We observed that the amount of aqueous soluble and membrane-bound (detergent-soluble) Aβ40 and Aβ42 gradually increased with age (**Figure 1C**, left). To test for the presence of oligomeric forms of Aβ and determine whether they accumulate in the same gradual manner, we employed an additional ELISA that is highly specific for the oligomeric form of the Aβ peptide. We observed that the levels of oligomeric Aβ were slightly higher in the membrane-bound fraction, consistent with the role of membrane components in promoting Aβ oligomerization (Wakabayashi and Matsuzaki, 2009; **Figure 1C**, right). The portion of oligomeric Aβ did not show an obvious age-dependent increase. Indeed, the amount of oligomeric membrane-bound fraction of Aβ even exhibited a significant drop at the time of plaque formation. Please note that Aβ peptides, the main components of senile plaques, predominantly form regular fibrils within the plaques, which are highly insoluble (Chen et al., 2017). Thus, they are not in the extracted fractions (both soluble and membrane-bound) that were used for the ELISAs.

These data indicate that APP_{SDL} mice accumulate predominantly monomeric Aβ during their lifetime, while the portion of the potentially most cytotoxic species (i.e., o-Aβ) remained constant.

APP_{SDL} Mice Do Not Show Evidence of Neuron Loss or Increased Tau Phosphorylation

AD is characterized by a neurodegenerative triad of synaptic changes, dendritic simplification, and neuron loss (Wu et al., 2010; Bakota and Brandt, 2016), where the death of neurons is thought to occur last during disease and in a tau-dependent manner. To analyze whether the chronic presence of Aβ causes loss of neurons in the neocortex, we used a machine-learning approach for unbiased analysis and determined the density of neuronal cell bodies in aged APP_{SDL} and age-matched B6 mice (**Figure 2A** and **Supplementary Figure S1**). As neurons in different cortical areas may differ concerning their susceptibility to age-related changes, four spatially and functionally distinct regions were subjected to analysis. To avoid bias due to tissue shrinkage, we also measured the thickness of the tissue of the same cortical regions. We did not observe a significant difference between the two genotypes, either in cell density or in the thickness of the cortex, indicating that APP_{SDL} mice do not exhibit neuron loss (**Figure 2A**). We also tested for neuron loss

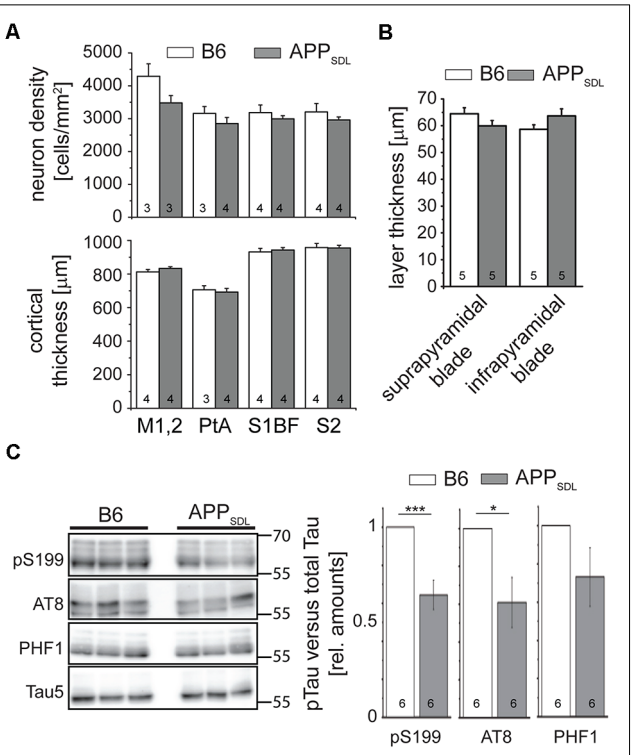

FIGURE 2 | APP_{SDL} mice do not show signs of neuron loss or tau pathology. **(A)** Neuron cell body density (top) and cortical thickness (bottom) in different cortical regions of APP_{SDL} and B6 mice at 21 months of age. Quantitation of neuronal density was performed using a machine learning approach (see **Supplementary Figure S1**). Sections were sampled through the complete volume of the respective brain regions: M1, 2 = primary motor cortex (n = 11 B6, 11 APP_{SDL}); PtA = parietal association cortex (n = 14 B6, 20 APP_{SDL}); S1BF = primary somatosensory cortex, barrel field (n = 32 B6, 41 APP_{SDL}); S2 = secondary somatosensory cortex (n = 20 B6, 43 APP_{SDL}). **(B)** Thickness of the suprapyramidal and infrapyramidal blades of the DG. Five averaged measurements from 10 mice/genotype were performed on epifluorescent images of coronal sections of EGFP expressing mice. **(C)** Phosphorylation profile of tau at disease-relevant sites in APP_{SDL} and B6 mice at 20–25 months of age. Quantitation of signals was performed relative to total tau (Tau5 staining) and values for B6 animals were set as 1.0. Representative western blots are shown left. Data represent mean ± SEM; the number of mice per genotype is shown in the bars. Data were analyzed using Student's t-test, and considered to be significantly different at $^*p < 0.05$ and $^{***}p < 0.001$.

in the DG since plaque formation in these mice affects this hippocampal subfield earliest. We determined the thickness of the granule cell layer of the supra- and infrapyramidal blade as an indicator of neuronal degeneration. This area also did not show reduced thickness in APP transgenic mice. In both genotypes, the thickness of the layer was approximately 60 µm, which agrees with published results (**Figure 2B**; Amaral et al., 2007).

To determine whether the mice develop early signs of tau pathology, we undertook a semi-quantitative western blot approach to identify a potential increase in tau phosphorylation at sites previously been shown to have increased levels of tau phosphorylation in AD patients (Buée et al., 2000). We observed that tau phosphorylation decreased at S199 and the AT8 epitope in old APP_{SDL} mice compared with age-matched, nontransgenic

littermates, indicating that the chronic presence of Aβ alone does not induce increased phosphorylation of endogenous mouse tau at AD-relevant sites (**Figure 2C**). While it is generally believed that high concentrations of Aβ induce hyperphosphorylation of tau during disease (Hanger et al., 2007), we have previously shown in a cell culture system that nanomolar concentrations of secreted Aβ can induce a decrease in tau phosphorylation at selected sites (Golovyashkina et al., 2015). In support, it was also shown that Aβ can activate phosphatases *via* NMDA glutamate receptors (Shankar et al., 2007), which can act on certain tau phosphoepitopes (Wei et al., 2002; Rahman et al., 2006).

Hippocampal Pyramidal Neurons Respond to Elevated Aβ by Decreasing Spine Density, Whereas Cortical Neurons Are More Resilient

Dendritic spines are considered to be the major loci of excitatory synaptic plasticity and function. They can respond to developmental challenges, novel experiences, and noxious stimuli. Higher than physiological Aβ levels pose great demands on dendritic spines (Terry et al., 1991; Shankar et al., 2008). Therefore, it is important to determine how chronic Aβ levels affect pyramidal cells within different brain regions during a lifetime and if the gradually increased amounts of Aβ exert a progressive burden on dendritic spines. To evaluate spine changes in age- and brain region-dependent manner, we employed algorithm-based image analyses of fluorescent neurons from 3D image stacks. To visualize neurons of interest, we crossed APP_{SDL} mice with those of the GFP M line (Feng et al., 2000) in which EGFP labels a small population of neurons in various brain regions, including the hippocampus and cortex. In these mice, EGFP expression is governed by the *Thy1* promoter, which drives expression during early postnatal life (Morris, 1985) and sufficiently labels some neurons already in 5-week-old mice. EGFP expression did not affect plaque formation as double-transgenic EGFP/APP_{SDL} mice showed a similar temporal and regional distribution of Aβ plaques as that previously described (**Figure 1A**, middle, right).

For the analysis, we chose four age groups to cover a broad spectrum of developmental stages representing adolescence (5 weeks of age), young adult (3 months of age), middle-age (15 months of age; shortly before plaque formation), and old (24 months of age; presenting with Aβ plaques). We sampled from two hippocampal (CA1 and CA3) and two cortical (parietal association cortex: ACTX, and primary sensory cortex; SCTX) brain areas to obtain information about developmental and coping strategies of different brain regions and subregions. Finally, we extended our analysis to both sexes to determine whether either sex has a potentially higher susceptibility to Aβ-mediated synaptic changes. It has been reported that there is pronounced instability in pre- and postsynaptic structures within the vicinity of amyloid plaques (Liebscher et al., 2014), which can markedly influence spine parameters. However, in our mouse model, only moderate amounts of plaques are present, and only in the old mice. Consequently, our analysis excluded possible changes in the spine parameters in the vicinity of plaques.

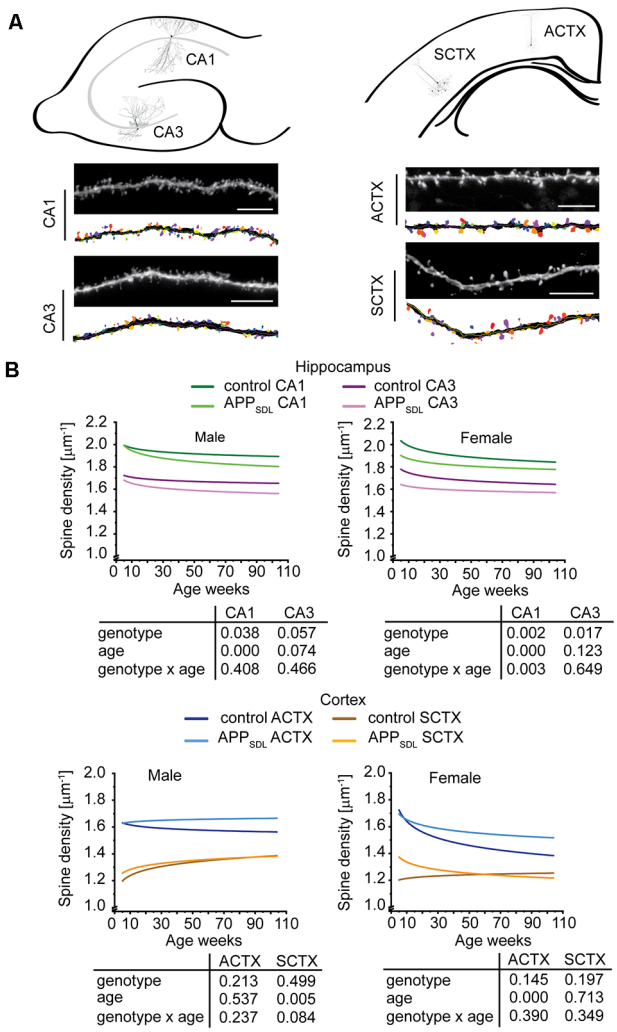

FIGURE 3 | Spine density trajectories of hippocampal and cortical pyramidal neurons. **(A)** Schematic representation of the hippocampus (top, left) and cortex (top, right) with the respective exemplary pyramidal neurons that were analyzed. Representative high-resolution images of dendritic segments from the respective neurons after blind deconvolution and 3DMA analysis (bottom) are shown. **(B)** Spine density trajectories of hippocampal CA1 and CA3 neurons and cortical parietal association (ACTX) and primary sensory (SCTX) neurons from EGFP and APP_{SDL} transgenic mice of different age. Please note that the age of mice had been displayed in weeks to represent it as scaled time intervals. Statistical data were assessed using a generalized linear model from six to seven mice per condition (see the total number of dendritic segments used for each condition in **Supplementary Table S1**). The *p*-value of the genotype, age effects, and their interaction are shown below the graphs. Scale bar, 10 µm. The distribution of individual data points are presented in **Supplementary Figure S2**.

We first quantified dendritic spine densities under different conditions because they could serve as indicators of the extent of alterations in synaptic connectivity in different brain regions (Segal, 2005; Harms and Dunaevsky, 2007; **Figure 3A**). To determine changes occurring over time, we analyzed our data using a generalized linear model (GZLM). As an extension to a traditional general linear model like a multivariate ANOVA, it allows for other than a normal distribution of the

dependent variable (Choi et al., 2018) and does not assume a linear relationship between the response variable and the model parameter, i.e., in this case the spine parameters and the age of mice (Faraway, 2010). The results were plotted as fitted spine density trajectories (Schumann et al., 2010; **Figure 3B**, **Supplementary Figure S2**). In the hippocampus, GZLM analysis revealed a significant genotype effect at most conditions (**Figure 3B**, top), where spine density trajectories representing data form CA1 and CA3 pyramidal neurons of APP_{SDL} mice ran below the trajectories of the respective data from control mice. This confirmed the negative effect, i.e., the spine loss initiated by Aβ on hippocampal principal neurons. In the CA1 subfield, the genotype effect was observed in both male and female mice, indicating that the hippocampus in both sexes is sensitive to elevated Aβ levels. Spine density trajectories also revealed a decrease during the lifetime of the mice, resulting in a significant age effect. The interaction between genotype and age could only be observed for the CA1 pyramidal neurons of female mice, implying that age and spine reduction by Aβ are generally not interdependent in the hippocampus.

Interestingly, the results were different for cortical regions. In most cases, the spine density trajectory depicting data from APP_{SDL} mice ran higher than the trajectory for the respective data from control mice; however, the difference did not result in a significant genotype effect in the two regions analyzed (**Figure 3B**, bottom).

Taken together, the data indicate that, although increased amounts of Aβ present a challenge for the dendritic spines throughout aging, under our conditions no extensive alterations occurred at the spine level. Moreover, hippocampal principal neurons responded to elevated Aβ levels in the brain with a loss of spines, whereas cortical neurons were less responsive, perhaps even showing an inverse reaction. Our data provide evidence that these changes are present in both sexes. Furthermore, they do not progress with age. The different effects of Aβ on the spine density trajectories in the hippocampus and the cortex may suggest a potential compensatory adaptation of pyramidal cells in the cortex.

Elevated Amounts of Aβ Induce Region-Specific Changes in Spine Morphology, Including a Shift From Mushroom Spines to Stubby Spines in the CA1 Subfield

Individual spines also develop morphological adaptations during maturation and exhibit changes during learning or noxious insult (Berry and Nedivi, 2017). Thus, the question arises as to whether elevated Aβ levels influence spine morphology in the brain areas analyzed.

To approach this question, we classified spines into three morphological categories, namely, "mushroom," "stubby," and "thin" (Harris et al., 1992), which are thought to represent functionally distinct entities. The analysis was performed by an algorithm-based method using cLSM image stacks as previously described (Sundermann et al., 2012).

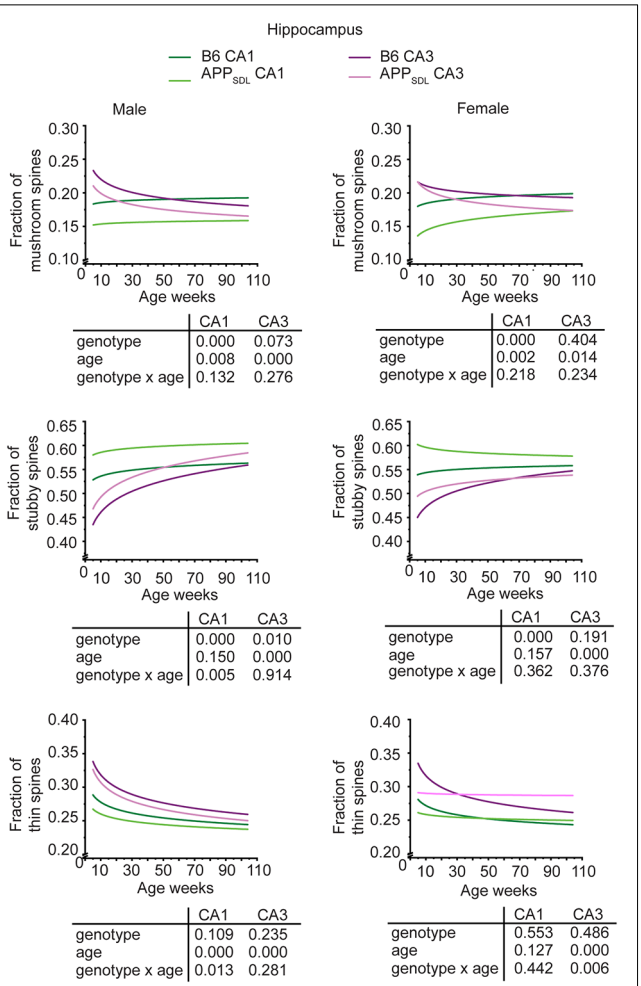

FIGURE 4 | Spine morphing in APP_{SDL} mice is differentially affected in hippocampal subfields of the two sexes. Trajectories representing the fractions of different spine classes from CA1 and CA3 pyramidal neurons in APP_{SDL} transgenic and control B6 mice of different ages as determined by algorithm-based classification. Please note that the age of mice had been displayed in weeks to represent it as scaled time intervals. Statistical data were assessed using a generalized linear model from six to seven mice per condition (see the total number of dendritic segments used for each condition in **Supplementary Table S1**). The *p*-value of the genotype, age effects, and their interaction are shown below the graphs. Distribution of individual data points are presented in **Supplementary Figures S3, S4**.

Region-specific differences developed with respect to the mushroom and stubby spine types. In the hippocampus, we observed a genotype effect with both mushroom and stubby spines in the CA1 subfield of both sexes (**Figure 4**, **Supplementary Figure S3**). In this subfield, the respective trajectories depicting spine fractions exhibited a shift between the ratios of the two spine classes. Specifically, mice with elevated amounts of Aβ showed an increase in the stubby fraction of spines compared with the mushroom fraction. A significant increase in the fraction of stubby spines was also observed for male mice in the CA3 subfield, while female mice did not exhibit a significant difference (**Figure 4**, **Supplementary Figure S4**). A decreased fraction of mushroom

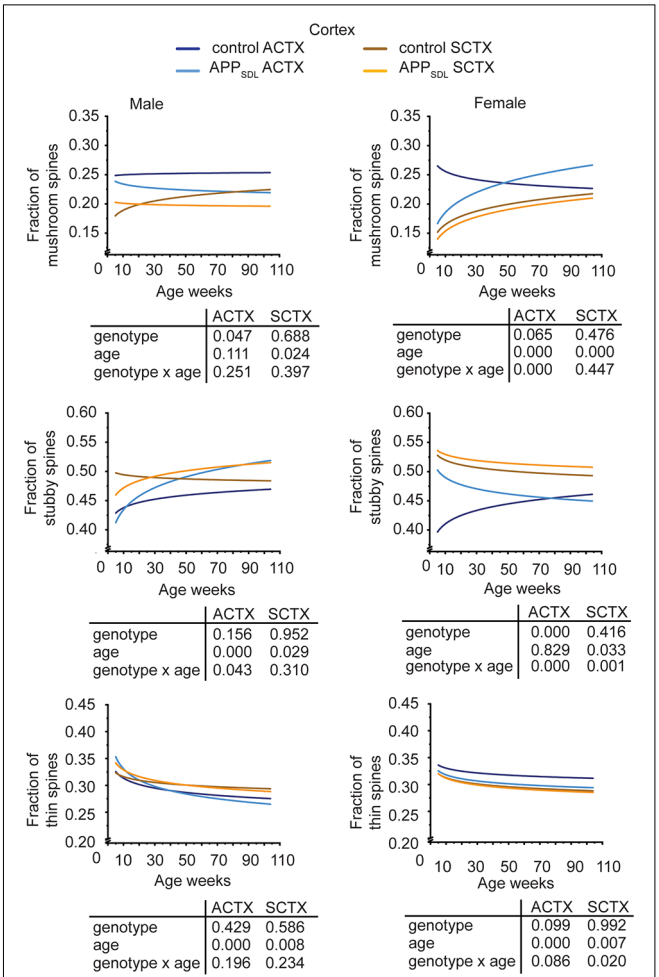

FIGURE 5 | Spine morphing in APP$_{SDL}$ mice is differentially affected in cortical brain regions of the two sexes. Trajectories representing the fractions of different spine classes from parietal association (ACTX) and primary sensory (SCTX) pyramidal neurons in APP$_{SDL}$ transgenic mice and control B6 mice of different ages as determined by algorithm-based classification. Please note that the age of mice had been displayed in weeks to represent it as scaled time intervals. Statistical data were assessed using a generalized linear model from six to seven mice per condition (see the total number of dendritic segments used for each condition in **Supplementary Table S1**). The *p*-value of the genotype, age effects, and their interaction are shown below the graphs. Distribution of individual data points are presented in **Supplementary Figures S5, S6**.

spine was observed in the ACTX of male mice, as evidenced by the genotype effect after a GZLM analysis. In contrast, the SCTX was completely unresponsive to the presence of increased levels of Aβ in both sexes (**Figure 5**, **Supplementary Figures S5, S6**).

A surprising observation was the change in the association cortex of female mice, where the proportion of mushroom spines started low in adolescent APP$_{SDL}$ mice, as also observed in the other brain areas. However, during aging, this spine type fraction showed an upward trajectory, overtaking the proportion of the mushroom spine fraction in control animals at later stages (**Figure 5**, **Supplementary Figure S5**).

In most brain regions analyzed, and for both genotypes and sexes, the trajectories of the fraction of thin spines showed a decrease with age. This decline during the lifetime of the mice is significant as the GZLM analysis showed a significant age effect (**Figures 4**, **5**). These results confirmed that there is an age-related loss of synaptic plasticity in older mice as previously described (Xu et al., 2018). However, we did not observe a significant genotype effect for the thin spines, further corroborating that the decrease in thin spines throughout the lifetime of mice is due to age-related, rather than Aβ-related, alterations in cell function (**Figures 4**, **5**).

Taken together, the data indicate that Aβ induces a clear shift in spine morphing from mushroom to stubby in the hippocampal CA1 region, whereas the SCTX was completely unresponsive. These data suggest that elevated levels of Aβ direct spine morphology towards lower compartmentalization in the affected brain areas. Furthermore, some of these morphological changes differ between sexes in a region-specific manner.

Transgenic APP Expression Does Not Differ Between the Hippocampus and Cortex

To address if the diverse effects on dendritic spines are due to different expression levels of the transgene between the cortex and hippocampus of APP$_{SDL}$ mice, we performed APP-targeted western blot analysis separately on both brain regions. We again observed a one-fold higher expression of the transgene, which was similar in both brain regions (**Figure 6A**). As APP processing or Aβ clearance can differ within the brain, we also determined the level of Aβ42, which is considered to be the main synaptotoxic species (Walsh and Selkoe, 2007). We did not see a significant difference either in the soluble or in the membrane-bound form of Aβ42 (**Figure 6B**), indicating that the differential spine alterations in the analyzed brain regions were not due to differences in the levels of APP or Aβ42.

Basal Dendrites of CA1 Pyramidal Neurons Exhibit Dendritic Simplification in Old APP$_{SDL}$ Mice

Dendritic simplification, an aspect of the neurodegenerative triad during AD, has been investigated substantially less than spine changes and neuronal death. However, changes in dendritic arborization have the potential to markedly influence synaptic connectivity.

We determined changes in the gross morphology of neurons from young (3 months) and old (24 months) EGFP/APP$_{SDL}$ mice and compared them to age-matched EGFP-expressing controls. We focused our investigation on the hippocampus, which we found to be the most susceptible to increases in Aβ levels, as indicated by changes in spine parameters. CA1 and CA3 pyramidal neurons were imaged in high-resolution tile z-stacks and reconstructed in 3D (**Figure 7A**). The morphological parameters total path length and the number of branching points were determined. We did not observe a statistically significant difference between neurons from APP$_{SDL}$ mice and those from control animals; however, there was a

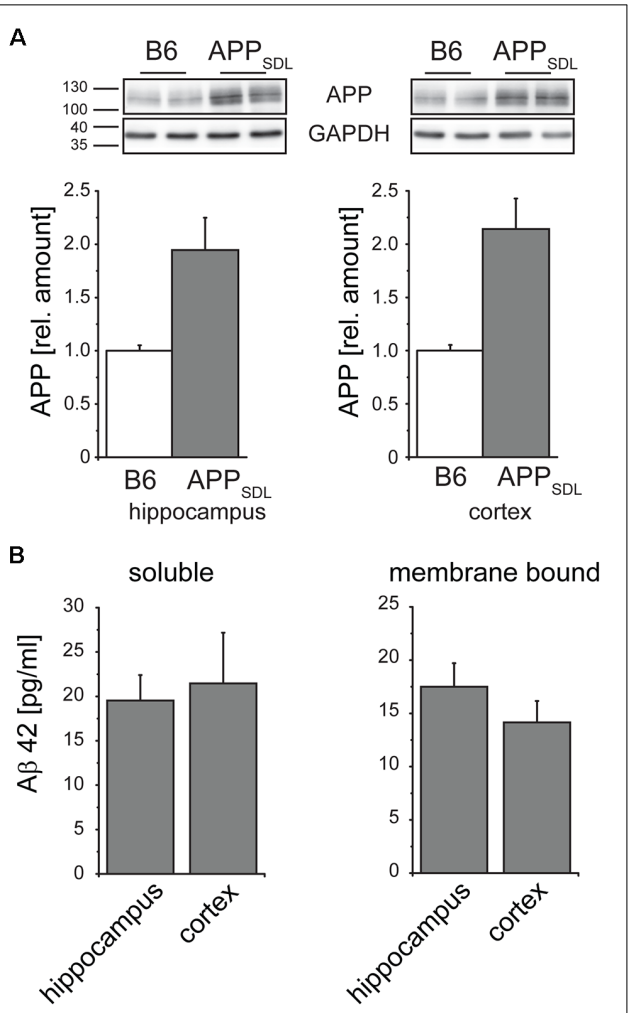

FIGURE 6 | Relative amounts of APP in the hippocampus and cortex do not differ in APP_{SDL} mice. **(A)** Representative immunoblots from cortical and hippocampal brain lysates (top). Graphs showing the relative amounts of APP expression in B6 and APP_{SDL} animals at 20–28 months of age between the two genotypes. Quantitation of signals was performed from 9 to 10 mice per genotype (bottom). Data were calculated relative to GAPDH and values for B6 animals were set as 1.0. **(B)** Quantification of the Aβ42 concentration within the soluble and membrane-bound fraction of hippocampal and cortical samples. Data originate from eight APP_{SDL} mice at 23–28 months of age. Data represent mean ± SEM.

general trend towards dendritic simplification in old APP_{SDL}-expressing mice (**Figure 7B**). To gather detailed information about potential region-specific morphological changes induced by Aβ, we employed Sholl analysis to measure dendritic field density and structure (Sholl, 1953). Compared with age-matched controls, we observed a reduced number of dendritic intersections in basal trees of the neurons, which reached significance at a distance of 60 μm from the cell body in CA1 neurons from old APP_{SDL} mice (**Figure 7C**). These data indicated that chronic Aβ levels induce dendritic simplification at old age in a regionally restricted manner and that dendritic simplification occurs before the loss of neurons.

PSD-95 and Arc Respond to Chronic Aβ Production in Old APP_{SDL} Mice

Synaptophysin (major synaptic vesicle protein p38) is an established general marker for the quantification of synapses and synaptic integrity (Li et al., 2010). To determine whether the differential effect of Aβ on spine density in hippocampal and cortical neurons is also reflected in changes in synaptophysin levels, we measured the relative levels of synaptophysin in both brain regions by semi-quantitative western blotting (**Figure 8A**). We did not observe any significant changes in the level of synaptophysin between the genotypes in either brain region (**Figure 8B**, left). To test for potential changes in the postsynapse, we measured the relative amounts of PSD-95, a pivotal postsynaptic scaffolding protein in excitatory neurons (Kaizuka and Takumi, 2018). Surprisingly, we found that the levels of PSD-95 in APP_{SDL} mice were increased when compared with those of B6 controls, and this increase reached significance in the hippocampus (**Figure 8B**, middle top). As a more functional molecular readout, we also determined the level of the activity-regulated cytoskeletal protein Arc, which is crucial for every form of neuronal plasticity and can affect synaptic strength (Guzowski et al., 2000; Messaoudi et al., 2007; Peebles et al., 2010). The Arc protein levels showed a pronounced increase in the cortex of APP_{SDL} transgenic mice compared with those of control mice (**Figure 8B**, right), but the level of increase was lower in the hippocampus. As Arc has a key role in the consolidation of explicit and implicit forms of memory (Bramham et al., 2010), our data suggest that Arc levels may be region-specifically increased to strengthen memory consolidation and maintenance in the cortex.

Combined, these data indicate that the differential effect of Aβ on spine density in the hippocampus and cortex is not reflected on a molecular level by a change in the level of synaptophysin, a marker for presynaptic structure. Changes in the concentrations of PSD-95 and Arc may point to the existence of a compensatory effect in respective brain regions under our experimental conditions.

DISCUSSION

Aβ deposits are thought to play a causative role in AD (Hardy and Selkoe, 2002). Disagreement with the classical amyloid hypothesis was driven by several studies reporting that a proportion of individuals at risk of AD show intact cognition regardless of extensive accumulation of the Aβ peptide in their brain (Bennett et al., 2006; Arendt, 2009; Villemagne et al., 2013). Furthermore, analysis of the distribution of the histopathological lesions in AD patients has shown that tau inclusions show a higher correlation with cognitive impairment than amyloid plaques (Nelson et al., 2012). This raises the question as to the nature of the difference that makes a population resilient towards cognitive decline, despite the accumulation of Aβ, and how different brain regions adjust to the chronic presence of increasing amounts of Aβ during the long prodromal phase of the disease. As an example, Boros et al. (2017) analyzed the brains of control subjects with AD pathology and AD brains

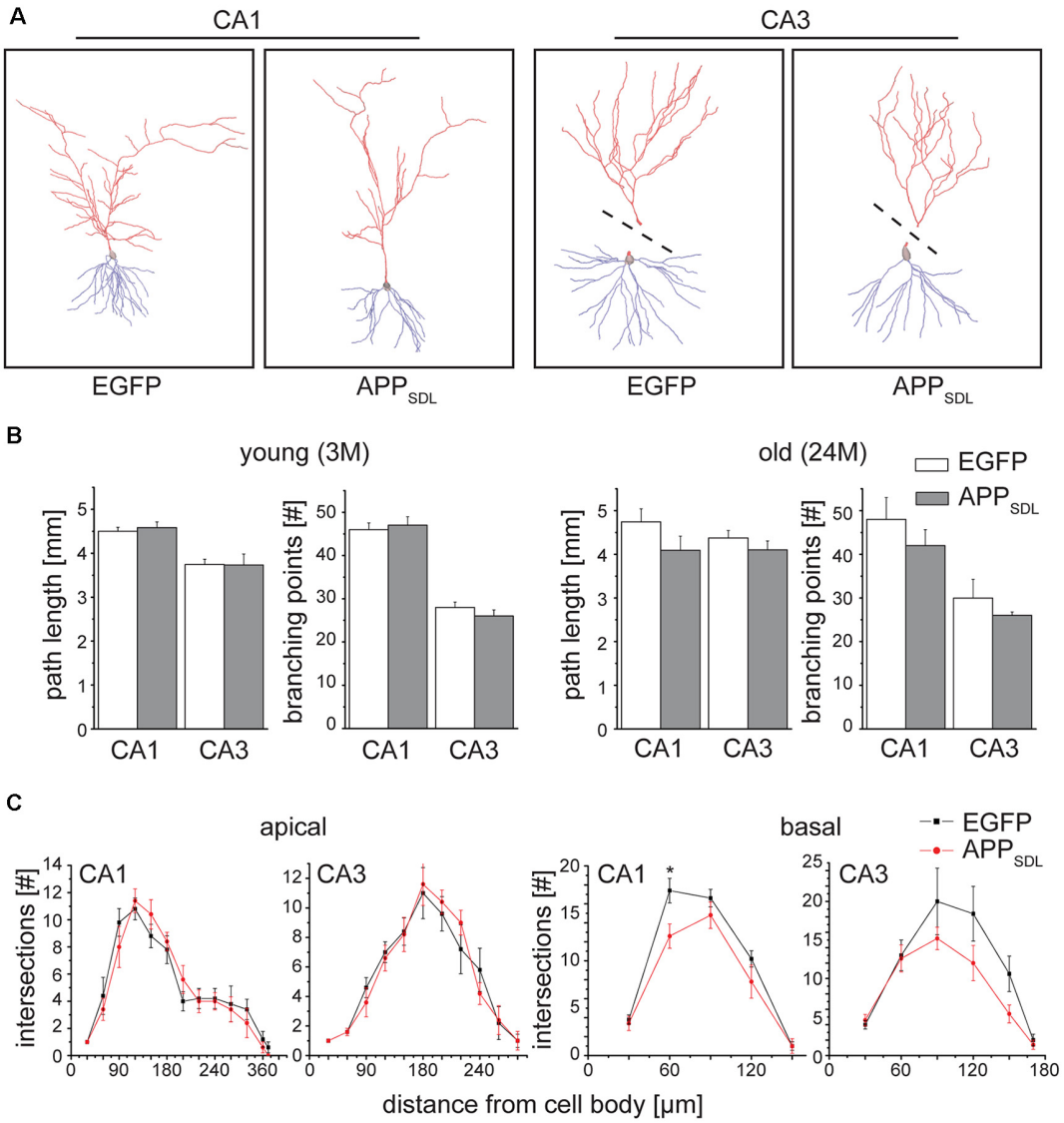

FIGURE 7 | Old APP_{SDL} mice exhibit dendritic simplification on basal dendrites in the hippocampus. **(A)** Representative reconstructed neurons from CA1 and CA3 regions of the hippocampus from 24 months old control and APP_{SDL} transgenic mice. Apical arbor is indicated in red, basal arbor in blue. Dashed lines indicate that apical and basal arbor were imaged and reconstructed separately due to the cutting angle during slicing. **(B)** Path length and the number of branching points of hippocampal pyramidal cells from young (3 months) and old (24 months) control and APP_{SDL} transgenic mice. **(C)** Sholl analysis of apical and basal arbors of hippocampal pyramidal cells from old (24 month) control and APP_{SDL} transgenic mice. CA1 pyramidal neurons from old APP_{SDL} transgenic mice show dendritic simplification on basal dendrites in comparison to control animals $F_{(1,4)} = 24.14$; $p = 0.0080$. Data represent mean ± SEM. Neurons were analyzed from five to six mice per genotype. Data were analyzed using repeated-measures ANOVA with Sidak *post hoc* test and considered to be significantly different at $^*p < 0.05$.

with dementia, and concluded that dendritic spines may provide cognitive resilience against AD. In light of this, we decided to analyze the effect of moderate concentrations of lifelong, chronic Aβ exposure, potential changes in oligomeric Aβ levels, and region-specific differences in spine parameters in a mouse model of amyloidosis.

Neurons and spines undergo structural adaptations throughout physiological aging that likely contribute to changes in their electrophysiological properties and cognition (Dickstein et al., 2013). However, AD already presents characteristics of a synaptopathology early during the disease process (Selkoe, 2002; Opazo et al., 2018), and synapse deficiencies may accelerate cognitive decline. In contrast, the magnitude of synaptic deficiencies appears not to be correlated with increasing Aβ levels, as otherwise the disease would be expected to turn symptomatic much earlier. Therefore, we aimed to analyze the extent to which established molecular and structural substrates of memory consolidation, i.e., the dendritic spines, develop alterations during the long prodromal stage of AD. For this, we used transgenic mice overexpressing low levels of the *APP* gene as a diagnostic tool for studying synaptic health. We reasoned that these mice might show a less pronounced, but

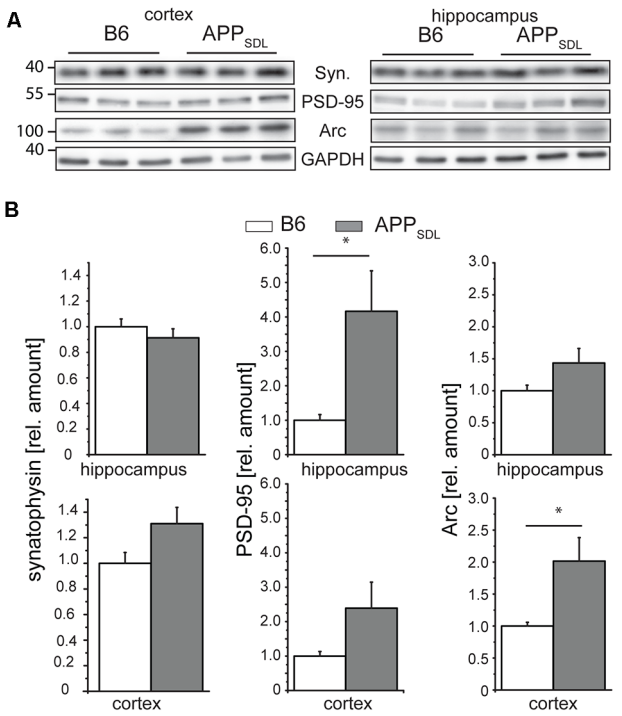

FIGURE 8 | Synaptophysin, PSD-95 and Arc expression in response to chronic Aβ in old APP_{SDL} mice. **(A)** Representative immunoblots from cortical and hippocampal brain lysates. **(B)** Expression of synaptophysin (left panel), PSD-95 (middle) and Arc (right panel) in cortex and hippocampus of B6 and APP_{SDL} mice at 20–28 months of age. Quantitation of signals was performed from 9 to 10 mice per genotype. Data were calculated relative to GAPDH and values for B6 animals were set as 1.0. Data represent mean ± SEM and were analyzed using Student's *t*-test. Data were considered to be significantly different at $^*p < 0.05$.

more realistic view, of the alterations and adaptive potential of synaptic plasticity in different brain regions long before the development of symptomatic AD. We selected this model owing to the increasing concern about potential artifacts connected to high overexpression of the APP protein in many mouse models (Saito et al., 2016). We hypothesized that the directionality or magnitude of the alterations may differ in various brain regions, depending on the adaptive/compensatory capacity of the respective region.

Our findings were as follows: (1) Aβ species show a gradual accumulation throughout the life of transgenic APP_{SDL} mice, which is not paralleled by an increase in the levels of the oligomeric form. (2) Hippocampal pyramidal neurons respond to increased Aβ concentrations by lowering spine density and undergoing a shift in spine morphology from mushroom towards stubby spines; both changes occur mainly in the CA1 subfield regardless of the sex. (3) In contrast, the spine density trajectories of cortical pyramidal neurons differ in that they do not show a difference in spine density in response to increased Aβ exposure. (4) Reduced spine compartmentalization also occurred in cortical neurons analyzed, specifically in the ACTX of male mice. (5) Increased concentrations of PSD-95 and Arc in the hippocampus and cortex, respectively, point towards a compensatory mechanism initiated during the prodromal stage of amyloidosis.

Soluble oligomeric Aβ has been shown to induce the loss of dendritic spines in culture (Lacor et al., 2007; Shankar et al., 2008; Tackenberg and Brandt, 2009) and a reduction in spine density in APP transgenic mice (Koffie et al., 2009; Jung and Herms, 2012). Spine loss could be reversed either by restoring the cAMP/PKA/CREB signaling pathway (Smith et al., 2009) or by antibody-mediated neutralization of soluble Aβ (Shankar et al., 2007; Zago et al., 2012), suggesting that local modulation of spine number could be a physiological and reversible action mediated by Aβ and may not necessarily be neurotoxic in itself. Indeed, picomolar levels of Aβ were shown to enhance synaptic plasticity (Puzzo et al., 2008), supporting the physiological role of Aβ. Our data show that gradually increasing Aβ levels do not lead to steadily intensified defects in postsynaptic structures. Under certain conditions, we even observed that the greatest differences occurred between the genotypes at a very young age, e.g., the spine density in the female hippocampus (see **Figure 3B**).

Potential changes in plasticity may result in some brain regions becoming more resilient to the Aβ present, or even initiate various mechanisms to compensate for impaired signaling in other brain regions. Accordingly, Elman et al. (2014), using PET imaging, showed that one possibility for a compensatory mechanism, potentially reflecting brain plasticity in response to Aβ deposition, is an increased activity associated with more detailed memories that occur in some brain regions. However, Aβ-dependent neuronal hyperactivity is believed to contribute to circuit dysfunction at the early stages of AD (Zott et al., 2019). We have previously shown that APP_{SDL} mice present hippocampal hyperactivity at 17–18 months of age (Penazzi et al., 2017). Our current data indicate that neurons can effectively adapt through a long period of advancing age, even to a several-fold increase in Aβ concentrations, if the oligomeric proportion does not substantially change.

The unequivocal observation of this study is that the hippocampal CA1 subfield is the most affected brain region in APP_{SDL} mice of both sexes. Nevertheless, male APP_{SDL} mice aged 17–18 months do not have spatial memory deficits when plaques occur (Penazzi et al., 2017), probably due to sufficient brain plasticity. This supports the observation that behavioral symptoms appear at the late stages of neurodegenerative diseases, although morphological changes can be detected much earlier. Although an expected decrease in spine density was observed in the hippocampus, the cortical regions showed no or even a tendency for an opposite effect. As the latter observation does not reflect the general expectations, such data are rarely published. However, increased spine density has also been recognized through *in vivo* imaging of the layer 5 cortical neurons in the most often examined mice with amyloid pathology, the Tg2567 mice, at 12 months of age, a time when these mice are already developing plaques (Jung and Herms, 2012). This may be due to a different regulation of the expression of synapse regulating proteins in the hippocampus compared to the cortex. Mice encoding mutant APP and mutant PSEN1 (APdE9) have been shown to increase BDNF protein levels significantly during aging in cortical

regions, but not in the hippocampus, compared to wild-type mice (Rantamäki et al., 2013).

We also showed that there were changes in synaptic connectivity by quantitative western blots for PSD-95 and the activity-regulated protein Arc at significant levels in a region-specific manner, whereas the level of the presynaptic protein, synaptophysin, showed no significant change. Accumulating evidence supports the functional importance of the early-expression *ARC* gene in regulating memory consolidation. Interestingly, AD patients express anomalous levels of the Arc protein (Rudinskiy et al., 2012). However, it is not clear what the effects are on the neurophysiology of AD-associated amyloidopathy. Arc interacts specifically with several effector proteins in different neuronal compartments such as dendritic spines and nuclear domains, and may bidirectionally regulate synaptic strength by distinct molecular mechanisms. This suggests that Arc may act as a master organizer of long-term synaptic plasticity, critical for information storage and cognition (Nikolaienko et al., 2018). In mice with high Aβ accumulation such as Tg2576 mice (Almeida et al., 2005), as well as in the postmortem brain (Proctor et al., 2010), the levels of PSD-95 were reported to be decreased and the degree of reduction correlated with the severity of dementia. However, Aβ pathology develops slowly in our mouse model and the presymptomatic phase is long. Therefore, increased PSD-95 levels, especially in the hippocampus where the spine alterations are more enhanced, could be indicative of potential compensatory mechanisms before the onset of severe symptoms.

Hippocampal and cortical neurons may differ in their sensitivity and adaptive response to increasing Aβ levels; moreover, cortical neurons might compensate for the loss of synaptic contacts in the hippocampus (or other brain regions that were not analyzed), thereby increasing memory consolidation and maintenance. Compared with those of AD patients with dementia, the levels of synaptic proteins such as synaptophysin and synaptopodin were also shown to be preserved in the brains of female subjects who presented with AD pathology but were resilient to cognitive decline (Arnold et al., 2013).

We showed that, in contrast to the distinct alterations in spine density within different brain regions, higher Aβ levels generally promote a lowering of the level of spine compartmentalization by inducing a decreased proportion of mushroom or increased proportion of stubby spine phenotype in the hippocampus and at specific conditions within the cortex. Using mathematical modeling, a recent study showed that shortening and widening of the necks should alter the electrical compartmentalization of the spines, leading to reduced postsynaptic potentials in spine heads, but not the soma, in APP×PS1-KI mice (Androuin et al., 2018). According to these observations, local EPSPs are likely to be lower at conditions where the stubby spine fraction in APP_{SDL} mice is increased compared to controls, which can affect the degree of potentiation of the postsynaptic cell. It would be interesting to address this experimentally in future studies. Taken together, our study highlights parallels and differences in spine plasticity mechanisms in cortical and hippocampal regions.

Females have a disproportionate occurrence of AD compared with males; however, the reason for this is not clear (Vina and Lloret, 2010). It is conceivable that changes in dendritic spines render females more susceptible to cognitive decline. Previous studies, performed mainly in rats, showed that gonadal hormones modulate dendritic spine densities (Chen et al., 2009). However, there is no consensus in the literature regarding the brain region affected or the stage of the estrus cycle that affects spine density (Shors et al., 2001; Peterson et al., 2015). To the best of our knowledge, no study to date has analyzed dendritic spine plasticity in both sexes throughout the life of mice. Our data do not support that certain brain regions or spine parameters in female mice are more markedly affected by increased Aβ levels than in male mice. Interestingly, in most cases where a genotype effect is observed in female mice, the largest differences in the trajectories of the two genotypes are found during adolescence and not in the aged brain. This suggests that the higher susceptibility of females to AD development is likely to be connected to other aspects of the disease rather than the sensitivity of dendritic spines to Aβ exposure.

The pathophysiology of AD is thought to develop over many years before the emergence of cognitive impairment and diagnosis of the disease. Recent disappointing clinical trial results raise the possibility that therapies may have a limited effect after neuronal degeneration has begun. This suggests that AD would be optimally treated in the presymptomatic stages of the disease. The possibility of analyzing changes in synaptic connectivity in a sensitive and temporospatially defined manner could provide a useful tool to guide the identification of potentially protective conditions or conditions that delay the onset of the disease. Our data provide evidence that, despite gradually increasing amounts of Aβ, some brain regions such as the primary somatosensory cortex, are more resilient to dendritic spine alterations than the hippocampus. The increased understanding of the mechanisms that drive this resilience could be of therapeutic relevance.

DATA AVAILABILITY STATEMENT

All datasets generated for this study are included in the article/**Supplementary Material**.

ETHICS STATEMENT

The animal study was reviewed and approved by Niedersächsische Landesamt für Verbraucherschutz und Lebensmittelsicherheit 26029 Oldenburg Germany.

AUTHOR CONTRIBUTIONS

RB and LB designed the research. MVH, MR, NG, LP, WCP, and BD performed the research. MVH, MR, NG, LP, WCP, BD FS, and LB analyzed the data. RB and LB wrote the article. All authors revised and approved the manuscript.

FUNDING

This work was supported by a Deutsche Forschungsgemeinschaft grant to RB (DFG BR1192/11-2) and an Incentive award of the Biology Faculty of the University of Osnabrück for LB.

ACKNOWLEDGMENTS

We thank Sarah Sandmann for help with ELISA and J. Sanes for advice regarding the use of the GFP M line. We thank Nataliya Trushina for creating violin plots in python.

SUPPLEMENTARY MATERIAL

The Supplementary Material for this article can be found online at: https://www.frontiersin.org/articles/10.3389/fnsyn.2020.00016/full#supplementary-material.

REFERENCES

Almeida, C. G., Tampellini, D., Takahashi, R. H., Greengard, P., Lin, M. T., Snyder, E. M., et al. (2005). β-amyloid accumulation in APP mutant neurons reduces PSD-95 and GluR1 in synapses. *Neurobiol. Dis.* 20, 187–198. doi: 10.1016/j.nbd.2005.02.008

Alvarado-Martínez, R., Salgado-Puga, K., and Peña-Ortega, F. (2013). Amyloid β inhibits olfactory bulb activity and the ability to smell. *PLoS One* 8:e75745. doi: 10.1371/journal.pone.0075745

Amaral, D. G., Scharfman, H. E., and Lavenex, P. (2007). The dentate gyrus: fundamental neuroanatomical organization (dentate gyrus for dummies). *Prog. Brain Res.* 163, 3–22. doi: 10.1016/s0079-6123(07)63001-5

Androuin, A., Potier, B., Nagerl, U. V., Cattaert, D., Danglot, L., Thierry, M., et al. (2018). Evidence for altered dendritic spine compartmentalization in Alzheimer's disease and functional effects in a mouse model. *Acta Neuropathol.* 135, 839–854. doi: 10.1007/s00401-018-1847-6

Arendt, T. (2009). Synaptic degeneration in Alzheimer's disease. *Acta Neuropathol.* 118, 167–179. doi: 10.1007/s00401-009-0536-x

Arnold, S. E., Louneva, N., Cao, K., Wang, L. S., Han, L. Y., Wolk, D. A., et al. (2013). Cellular, synaptic, and biochemical features of resilient cognition in Alzheimer's disease. *Neurobiol. Aging* 34, 157–168. doi: 10.1016/j.neurobiolaging.2012.03.004

Bakota, L., and Brandt, R. (2016). Tau biology and tau-directed therapies for Alzheimer's disease. *Drugs* 76, 301–313. doi: 10.1007/s40265-015-0529-0

Baloyannis, S. J., Costa, V., Mauroudis, I., Psaroulis, D., Manolides, S. L., and Manolides, L. S. (2007). Dendritic and spinal pathology in the acoustic cortex in Alzheimer's disease: morphological and morphometric estimation by Golgi technique and electron microscopy. *Acta Otolaryngol.* 127, 351–354. doi: 10.1080/00016480601126986

Bennett, D. A., Schneider, J. A., Arvanitakis, Z., Kelly, J. F., Aggarwal, N. T., Shah, R. C., et al. (2006). Neuropathology of older persons without cognitive impairment from two community-based studies. *Neurology* 66, 1837–1844. doi: 10.1212/01.wnl.0000219668.47116.e6

Berry, K. P., and Nedivi, E. (2017). Spine dynamics: are they all the same? *Neuron* 96, 43–55. doi: 10.1016/j.neuron.2017.08.008

Blanchard, V., Moussaoui, S., Czech, C., Touchet, N., Bonici, B., Planche, M., et al. (2003). Time sequence of maturation of dystrophic neurites associated with Aβ deposits in APP/PS1 transgenic mice. *Exp. Neurol.* 184, 247–263. doi: 10.1016/s0014-4886(03)00252-8

Boros, B. D., Greathouse, K. M., Gentry, E. G., Curtis, K. A., Birchall, E. L., Gearing, M., et al. (2017). Dendritic spines provide cognitive resilience against Alzheimer's disease. *Ann. Neurol.* 82, 602–614. doi: 10.1002/ana.25049

Bramham, C. R., Alme, M. N., Bittins, M., Kuipers, S. D., Nair, R. R., Pai, B., et al. (2010). The Arc of synaptic memory. *Exp. Brain Res.* 200, 125–140. doi: 10.1007/s00221-009-1959-2

Brandt, R., and Paululat, A. (2013). Microcompartments in the *Drosophila* heart and the mammalian brain: general features and common principles. *Biol. Chem.* 394, 217–230. doi: 10.1515/hsz-2012-0261

Buée, L., Bussière, T., Buée-Scherrer, V., Delacourte, A., and Hof, P. R. (2000). Tau protein isoforms, phosphorylation and role in neurodegenerative disorders. *Brain Res. Rev.* 33, 95–130. doi: 10.1016/s0165-0173(00)00019-9

Bushman, D. M., Kaeser, G. E., Siddoway, B., Westra, J. W., Rivera, R. R., Rehen, S. K., et al. (2015). Genomic mosaicism with increased amyloid precursor protein (APP) gene copy number in single neurons from sporadic Alzheimer's disease brains. *Elife* 4:e05116. doi: 10.7554/eLife.05116

Chen, J. R., Yan, Y. T., Wang, T. J., Chen, L. J., Wang, Y. J., and Tseng, G. F. (2009). Gonadal hormones modulate the dendritic spine densities of primary cortical pyramidal neurons in adult female rat. *Cereb. Cortex* 19, 2719–2727. doi: 10.1093/cercor/bhp048

Chen, G. F., Xu, T. H., Yan, Y., Zhou, Y. R., Jiang, Y., Melcher, K., et al. (2017). Amyloid beta: structure, biology and structure-based therapeutic development. *Acta Pharmacol. Sin.* 38, 1205–1235. doi: 10.1038/aps.2017.28

Choi, J. S., Ha, M. K., Trinh, T. X., Yoon, T. H., and Byun, H. G. (2018). Towards a generalized toxicity prediction model for oxide nanomaterials using integrated data from different sources. *Sci. Rep.* 8:6110. doi: 10.1038/s41598-018-24483-z

Dickstein, D. L., Weaver, C. M., Luebke, J. I., and Hof, P. R. (2013). Dendritic spine changes associated with normal aging. *Neuroscience* 251, 21–32. doi: 10.1016/j.neuroscience.2012.09.077

Dominguez-Álvaro, M., Montero-Crespo, M., Blazquez-Llorca, L., DeFelipe, J., and Alonso-Nanclares, L. (2019). 3D electron microscopy study of synaptic organization of the normal human transentorhinal cortex and its possible alterations in Alzheimer's disease. *eNeuro* 6:ENEURO.0140-19.2019. doi: 10.1523/eneuro.0140-19.2019

Elman, J. A., Oh, H., Madison, C. M., Baker, S. L., Vogel, J. W., Marks, S. M., et al. (2014). Neural compensation in older people with brain amyloid-β deposition. *Nat. Neurosci.* 17, 1316–1318. doi: 10.1038/nn.3806

Evangelisti, E., Cascella, R., Becatti, M., Marrazza, G., Dobson, C. M., Chiti, F., et al. (2016). Binding affinity of amyloid oligomers to cellular membranes is a generic indicator of cellular dysfunction in protein misfolding diseases. *Sci. Rep.* 6:32721. doi: 10.1038/srep32721

Faraway, J. J. (2010). "Generalized linear models," in *International Encyclopedia of Education*, eds P. Peterson, A. Baker and B. Mcgaw (Amsterdam: Elsevier Science).

Feng, G., Mellor, R. H., Bernstein, M., Keller-Peck, C., Nguyen, Q. T., Wallace, M., et al. (2000). Imaging neuronal subsets in transgenic mice expressing multiple spectral variants of GFP. *Neuron* 28, 41–51. doi: 10.1016/s0896-6273(00)00084-2

Games, D., Adams, D., Alessandrini, R., Barbour, R., Berthelette, P., Blackwell, C., et al. (1995). Alzheimer-type neuropathology in transgenic mice overexpressing V717F β-amyloid precursor protein. *Nature* 373, 523–527. doi: 10.1038/373523a0

Golovyashkina, N., Penazzi, L., Ballatore, C., Smith, A. B., Bakota, L., and Brandt, R. (2015). Region-specific dendritic simplification induced by Aβ, mediated by tau *via* dysregulation of microtubule dynamics: a mechanistic distinct event from other neurodegenerative processes. *Mol. Neurodegener.* 10:60. doi: 10.1186/s13024-015-0049-0

Golovyashkina, N., Sündermann, F., Brandt, R., and Bakota, L. (2014). "Reconstruction and morphometric analysis of hippocampal neurons from mice expressing fluorescent proteins," in *Neuromethods 87: Laser Scanning Microscopy and Quantitative Image Analysis of Neuronal Tissue*, eds L. Bakota and R. Brandt (New York, NY: Springer), 251–262.

Guzowski, J. F., Lyford, G. L., Stevenson, G. D., Houston, F. P., McGaugh, J. L., Worley, P. F., et al. (2000). Inhibition of activity-dependent arc protein expression in the rat hippocampus impairs the maintenance of long-term potentiation and the consolidation of long-term memory. *J. Neurosci.* 20, 3993–4001. doi: 10.1523/JNEUROSCI.20-11-03993.2000

Hanger, D. P., Byers, H. L., Wray, S., Leung, K. Y., Saxton, M. J., Seereeram, A., et al. (2007). Novel phosphorylation sites in tau from Alzheimer brain support a role for casein kinase 1 in disease pathogenesis. *J. Biol. Chem.* 282, 23645–23654. doi: 10.1074/jbc.m703269200

Hardy, J., and Selkoe, D. J. (2002). The amyloid hypothesis of Alzheimer's disease: progress and problems on the road to therapeutics. *Science* 297, 353–356. doi: 10.1126/science.1072994

Harms, K. J., and Dunaevsky, A. (2007). Dendritic spine plasticity: looking beyond development. *Brain Res.* 1184, 65–71. doi: 10.1016/j.brainres.2006.02.094

Harris, K. M., Jensen, F. E., and Tsao, B. (1992). Three-dimensional structure of dendritic spines and synapses in rat hippocampus (CA1) at postnatal day

15 and adult ages: implications for the maturation of synaptic physiology and long-term potentiation. *J. Neurosci.* 12, 2685–2705. doi: 10.1523/JNEUROSCI.12-07-02685.1992

Hutchins, J. B., and Jefferson, V. E. (1992). Developmental distribution of platelet-derived growth factor in the mouse central nervous system. *Dev. Brain Res.* 67, 121–135. doi: 10.1016/0165-3806(92)90213-g

Jankowsky, J. L., and Zheng, H. (2017). Practical considerations for choosing a mouse model of Alzheimer's disease. *Mol. Neurodegener.* 12:89. doi: 10.1186/s13024-017-0231-7

Johnson, I. P. (2015). Age-related neurodegenerative disease research needs aging models. *Front. Aging Neurosci.* 7:168. doi: 10.3389/fnagi.2015.00168

Jung, C. K., and Herms, J. (2012). Role of APP for dendritic spine formation and stability. *Exp. Brain Res.* 217, 463–470. doi: 10.1007/s00221-011-2939-x

Kaizuka, T., and Takumi, T. (2018). Postsynaptic density proteins and their involvement in neurodevelopmental disorders. *J. Biochem.* 163, 447–455. doi: 10.1093/jb/mvy022

Koffie, R. M., Meyer-Luehmann, M., Hashimoto, T., Adams, K. W., Mielke, M. L., Garcia-Alloza, M., et al. (2009). Oligomeric amyloid β associates with postsynaptic densities and correlates with excitatory synapse loss near senile plaques. *Proc. Natl. Acad. Sci. U S A* 106, 4012–4017. doi: 10.1073/pnas.0811698106

Koh, I. Y., Lindquist, W. B., Zito, K., Nimchinsky, E. A., and Svoboda, K. (2002). An image analysis algorithm for dendritic spines. *Neural Comput.* 14, 1283–1310. doi: 10.1162/089976602753712945

Koppensteiner, P., Trinchese, F., Fà, M., Puzzo, D., Gulisano, W., Yan, S., et al. (2016). Time-dependent reversal of synaptic plasticity induced by physiological concentrations of oligomeric Aβ42: an early index of Alzheimer's disease. *Sci. Rep.* 6:32553. doi: 10.1038/srep32553

Lacor, P. N., Buniel, M. C., Furlow, P. W., Clemente, A. S., Velasco, P. T., Wood, M., et al. (2007). Aβ oligomer-induced aberrations in synapse composition, shape and density provide a molecular basis for loss of connectivity in Alzheimer's disease. *J. Neurosci.* 27, 796–807. doi: 10.1523/JNEUROSCI.3501-06.2007

Lee, K. W., Lee, S. H., Kim, H., Song, J. S., Yang, S. D., Paik, S. G., et al. (2004). Progressive cognitive impairment and anxiety induction in the absence of plaque deposition in C57BL/6 inbred mice expressing transgenic amyloid precursor protein. *J. Neurosci. Res.* 76, 572–580. doi: 10.1002/jnr.20127

Lee, M. H., Siddoway, B., Kaeser, G. E., Segota, I., Rivera, R., Romanow, W. J., et al. (2018). Somatic APP gene recombination in Alzheimer's disease and normal neurons. *Nature* 563, 639–645. doi: 10.1038/s41586-018-0718-6

Leschik, J., Welzel, A., Weissmann, C., Eckert, A., and Brandt, R. (2007). Inverse and distinct modulation of tau-dependent neurodegeneration by presenilin 1 and amyloid-β in cultured cortical neurons: evidence that tau phosphorylation is the limiting factor in amyloid-β-induced cell death. *J. Neurochem.* 101, 1303–1315. doi: 10.1111/j.1471-4159.2006.04435.x

Li, L., Tasic, B., Micheva, K. D., Ivanov, V. M., Spletter, M. L., Smith, S. J., et al. (2010). Visualizing the distribution of synapses from individual neurons in the mouse brain. *PLoS One* 5:e11503. doi: 10.1371/journal.pone.0011503

Liang, F., Yang, S., Zhang, Y., and Hao, T. (2019). Social housing promotes cognitive function through enhancing synaptic plasticity in APP/PS1 mice. *Behav. Brain Res.* 368:111910. doi: 10.1016/j.bbr.2019.111910

Liebscher, S., Page, R. M., Käfer, K., Winkler, E., Quinn, K., Goldbach, E., et al. (2014). Chronic γ-secretase inhibition reduces amyloid plaque-associated instability of pre- and postsynaptic structures. *Mol. Psychiatry* 19, 937–946. doi: 10.1038/mp.2013.122

Matsuzaki, M., Ellis-Davies, G. C., Nemoto, T., Miyashita, Y., Iino, M., and Kasai, H. (2001). Dendritic spine geometry is critical for AMPA receptor expression in hippocampal CA1 pyramidal neurons. *Nat. Neurosci.* 4, 1086–1092. doi: 10.1038/nn736

May, M. (2016). Sex on the brain: unraveling the differences between women and men in neurodegenerative disease. *Nat. Med.* 22, 1370–1372. doi: 10.1038/nm1216-1370

Merino-Serrais, P., Knafo, S., Alonso-Nanclares, L., Fernaud-Espinosa, I., and Defelipe, J. (2011). Layer-specific alterations to CA1 dendritic spines in a mouse model of Alzheimer's disease. *Hippocampus* 21, 1037–1044. doi: 10.1002/hipo.20861

Messaoudi, E., Kanhema, T., Soulé, J., Tiron, A., Dagyte, G., da Silva, B., et al. (2007). Sustained Arc/Arg3.1 synthesis controls long-term potentiation consolidation through regulation of local actin polymerization in the dentate gyrus *in vivo*. *J. Neurosci.* 27, 10445–10455. doi: 10.1523/JNEUROSCI.2883-07.2007

Moechars, D., Dewachter, I., Lorent, K., Reversé, D., Baekelandt, V., Naidu, A., et al. (1999). Early phenotypic changes in transgenic mice that overexpress different mutants of amyloid precursor protein in brain. *J. Biol. Chem.* 274, 6483–6492. doi: 10.1074/jbc.274.10.6483

Morris, R. (1985). Thy-1 in developing nervous tissue. *Dev. Neurosci.* 7, 133–160. doi: 10.1159/000315714

Nelson, P. T., Alafuzoff, I., Bigio, E. H., Bouras, C., Braak, H., Cairns, N. J., et al. (2012). Correlation of Alzheimer disease neuropathologic changes with cognitive status: a review of the literature. *J. Neuropathol. Exp. Neurol.* 71, 362–381. doi: 10.1097/NEN.0b013e31825018f7

Nikolaienko, O., Patil, S., Eriksen, M. S., and Bramham, C. R. (2018). Arc protein: a flexible hub for synaptic plasticity and cognition. *Semin. Cell Dev. Biol.* 77, 33–42. doi: 10.1016/j.semcdb.2017.09.006

Opazo, P., Viana da Silva, S., Carta, M., Breillat, C., Coultrap, S. J., Grillo-Bosch, D., et al. (2018). CaMKII metaplasticity drives Aβ oligomer-mediated synaptotoxicity. *Cell Rep.* 23, 3137–3145. doi: 10.1016/j.celrep.2018.05.036

Ortiz-Sanz, C., Gaminde-Blasco, A., Valero, J., Bakota, L., Brandt, R., Zugaza, J. L., et al. (2020). Early effects of Aβ oligomers on dendritic spine dynamics and arborization in hippocampal neurons. *Front. Synaptic Neurosci.* 12:2. doi: 10.3389/fnsyn.2020.00002

Paxinos, G., and Franklin, K. B. J. (2004). *The Mouse Brain in Stereotaxic Coordinates*. San Diego, CA: Elsevier Science.

Peebles, C. L., Yoo, J., Thwin, M. T., Palop, J. J., Noebels, J. L., and Finkbeiner, S. (2010). Arc regulates spine morphology and maintains network stability *in vivo*. *Proc. Natl. Acad. Sci. U S A* 107, 18173–18178. doi: 10.1073/pnas.1006546107

Penazzi, L., Lorengel, J., Sündermann, F., Golovyashkina, N., Marre, S., Mathis, C. M. B., et al. (2017). DMSO modulates CNS function in a preclinical Alzheimer's disease model. *Neuropharmacology* 113, 434–444. doi: 10.1016/j.neuropharm.2016.10.020

Penazzi, L., Sündermann, F., Bakota, L., and Brandt, R. (2014). "Machine learning to evaluate neuron density in brain sections," in *Neuromethod 87: Laser Scanning Microscopy and Quantitative Image Analysis of Neuronal Tissue*, eds L. Bakota and R. Brandt (New York, NY: Springer), 263–291.

Penazzi, L., Tackenberg, C., Ghori, A., Golovyashkina, N., Niewidok, B., Selle, K., et al. (2016). Aβ-mediated spine changes in the hippocampus are microtubule-dependent and can be reversed by a subnanomolar concentration of the microtubule-stabilizing agent epothilone D. *Neuropharmacology* 105, 84–95. doi: 10.1016/j.neuropharm.2016.01.002

Peterson, B. M., Mermelstein, P. G., and Meisel, R. L. (2015). Estradiol mediates dendritic spine plasticity in the nucleus accumbens core through activation of mGluR5. *Brain Struct. Funct.* 220, 2415–2422. doi: 10.1007/s00429-014-0794-9

Proctor, D. T., Coulson, E. J., and Dodd, P. R. (2010). Reduction in post-synaptic scaffolding PSD-95 and SAP-102 protein levels in the Alzheimer inferior temporal cortex is correlated with disease pathology. *J. Alzheimers Dis.* 21, 795–811. doi: 10.3233/jad-2010-100090

Puzzo, D., Privitera, L., Leznik, E., Fa, M., Staniszewski, A., Palmeri, A., et al. (2008). Picomolar amyloid-β positively modulates synaptic plasticity and memory in hippocampus. *J. Neurosci.* 28, 14537–14545. doi: 10.1523/JNEUROSCI.2692-08.2008

Rahman, A., Grundke-Iqbal, I., and Iqbal, K. (2006). PP2B isolated from human brain preferentially dephosphorylates Ser-262 and Ser-396 of the Alzheimer disease abnormally hyperphosphorylated tau. *J. Neural Transm.* 113, 219–230. doi: 10.1007/s00702-005-0313-5

Rantamäki, T., Kemppainen, S., Autio, H., Stavén, S., Koivisto, H., Kojima, M., et al. (2013). The impact of Bdnf gene deficiency to the memory impairment and brain pathology of APPswe/PS1dE9 mouse model of Alzheimer's disease. *PLoS One* 8:e68722. doi: 10.1371/journal.pone.0068722

Richardson, J. A., and Burns, D. K. (2002). Mouse models of Alzheimer's disease: a quest for plaques and tangles. *ILAR J.* 43, 89–99. doi: 10.1093/ilar.43.2.89

Rudinskiy, N., Hawkes, J. M., Betensky, R. A., Eguchi, M., Yamaguchi, S., Spires-Jones, T. L., et al. (2012). Orchestrated experience-driven Arc responses are disrupted in a mouse model of Alzheimer's disease. *Nat. Neurosci.* 15, 1422–1429. doi: 10.1038/nn.3199

Saito, T., Matsuba, Y., Yamazaki, N., Hashimoto, S., and Saido, T. C. (2016). Calpain activation in Alzheimer's model mice is an artifact of app and presenilin overexpression. *J. Neurosci.* 36, 9933–9936. doi: 10.1523/JNEUROSCI.1907-16.2016

Sasahara, M., Fries, J. W., Raines, E. W., Gown, A. M., Westrum, L. E., Frosch, M. P., et al. (1991). PDGF B-chain in neurons of the central nervous system, posterior pituitary, and in a transgenic model. *Cell* 64, 217–227. doi: 10.1016/0092-8674(91)90223-l

Scheff, S. W., Price, D. A., Schmitt, F. A., DeKosky, S. T., and Mufson, E. J. (2007). Synaptic alterations in CA1 in mild Alzheimer disease and mild cognitive impairment. *Neurology* 68, 1501–1508. doi: 10.1212/01.wnl.0000260698.46517.8f

Schindelin, J., Arganda-Carreras, I., Frise, E., Kaynig, V., Longair, M., Pietzsch, T., et al. (2012). Fiji: an open-source platform for biological-image analysis. *Nat. Methods* 9, 676–682. doi: 10.1038/nmeth.2019

Schumann, C. M., Bloss, C. S., Barnes, C. C., Wideman, G. M., Carper, R. A., Akshoomoff, N., et al. (2010). Longitudinal magnetic resonance imaging study of cortical development through early childhood in autism. *J. Neurosci.* 30, 4419–4427. doi: 10.1523/JNEUROSCI.5714-09.2010

Segal, M. (2005). Dendritic spines and long-term plasticity. *Nat. Rev. Neurosci.* 6, 277–284. doi: 10.1038/nrn1649

Selkoe, D. J. (2002). Alzheimer's disease is a synaptic failure. *Science* 298, 789–791. doi: 10.1126/science.1074069

Shankar, G. M., Bloodgood, B. L., Townsend, M., Walsh, D. M., Selkoe, D. J., and Sabatini, B. L. (2007). Natural oligomers of the Alzheimer amyloid-β protein induce reversible synapse loss by modulating an NMDA-type glutamate receptor-dependent signaling pathway. *J. Neurosci.* 27, 2866–2875. doi: 10.1523/JNEUROSCI.4970-06.2007

Shankar, G. M., Leissring, M. A., Adame, A., Sun, X., Spooner, E., Masliah, E., et al. (2009). Biochemical and immunohistochemical analysis of an Alzheimer's disease mouse model reveals the presence of multiple cerebral Aβ assembly forms throughout life. *Neurobiol. Dis.* 36, 293–302. doi: 10.1016/j.nbd.2009.07.021

Shankar, G. M., Li, S., Mehta, T. H., Garcia-Munoz, A., Shepardson, N. E., Smith, I., et al. (2008). Amyloid-β protein dimers isolated directly from Alzheimer's brains impair synaptic plasticity and memory. *Nat. Med.* 14, 837–842. doi: 10.1038/nm1782

Sholl, D. A. (1953). Dendritic organization in the neurons of the visual and motor cortices of the cat. *J. Anat.* 87, 387–406.

Shors, T. J., Chua, C., and Falduto, J. (2001). Sex differences and opposite effects of stress on dendritic spine density in the male versus female hippocampus. *J. Neurosci.* 21, 6292–6297. doi: 10.1523/JNEUROSCI.21-16-06292.2001

Smith, D. L., Pozueta, J., Gong, B., Arancio, O., and Shelanski, M. (2009). Reversal of long-term dendritic spine alterations in Alzheimer disease models. *Proc. Natl. Acad. Sci. U S A* 106, 16877–16882. doi: 10.1073/pnas.0908706106

Sündermann, F., Golovyashkina, N., Tackenberg, C., Brandt, R., and Bakota, L. (2012). High-resolution imaging and evaluation of spines in organotypic hippocampal slice cultures. *Methods Mol. Biol.* 846, 277–293. doi: 10.1007/978-1-61779-536-7_24

Tackenberg, C., and Brandt, R. (2009). Divergent pathways mediate spine alterations and cell death induced by amyloid-β, wild-type tau, and R406W tau. *J. Neurosci.* 29, 14439–14450. doi: 10.1523/JNEUROSCI.3590-09.2009

Tackenberg, C., Ghori, A., and Brandt, R. (2009). Thin, stubby or mushroom: spine pathology in Alzheimer's disease. *Front. Cell. Neurosci.* 6, 261–268. doi: 10.2174/156720509788486554

Terry, R. D., Masliah, E., Salmon, D. P., Butters, N., Deteresa, R., Hill, R., et al. (1991). Physical basis of cognitive alterations in Alzheimer's disease: synapse loss is the major correlate of cognitive impairment. *Ann. Neurol.* 30, 572–580. doi: 10.1002/ana.410300410

Tu, S., Okamoto, S., Lipton, S. A., and Xu, H. (2014). Oligomeric Aβ-induced synaptic dysfunction in Alzheimer's disease. *Mol. Neurodegener.* 9:48. doi: 10.1186/1750-1326-9-48

Villemagne, V. L., Burnham, S., Bourgeat, P., Brown, B., Ellis, K. A., Salvado, O., et al. (2013). Amyloid β deposition, neurodegeneration, and cognitive decline in sporadic Alzheimer's disease: a prospective cohort study. *Lancet Neurol.* 12, 357–367. doi: 10.1016/S1474-4422(13)70044-9

Vina, J., and Lloret, A. (2010). Why women have more Alzheimer's disease than men: gender and mitochondrial toxicity of amyloid-β peptide. *J. Alzheimers Dis.* 20, S527–S533. doi: 10.3233/jad-2010-100501

Wakabayashi, M., and Matsuzaki, K. (2009). Ganglioside-induced amyloid formation by human islet amyloid polypeptide in lipid rafts. *FEBS Lett.* 583, 2854–2858. doi: 10.1016/j.febslet.2009.07.044

Walsh, D. M., and Selkoe, D. J. (2007). A β oligomers—a decade of discovery. *J. Neurochem.* 101, 1172–1184. doi: 10.1111/j.1471-4159.2006.04426.x

Wei, Q., Holzer, M., Brueckner, M. K., Liu, Y., and Arendt, T. (2002). Dephosphorylation of tau protein by calcineurin triturated into neural living cells. *Cell. Mol. Neurobiol.* 22, 13–24. doi: 10.1023/a:1015385527187

Wu, H. Y., Hudry, E., Hashimoto, T., Kuchibhotla, K., Rozkalne, A., Fan, Z., et al. (2010). Amyloid β induces the morphological neurodegenerative triad of spine loss, dendritic simplification and neuritic dystrophies through calcineurin activation. *J. Neurosci.* 30, 2636–2649. doi: 10.1523/JNEUROSCI.4456-09.2010

Xu, B., Sun, A., He, Y., Qian, F., Xi, S., Long, D., et al. (2018). Loss of thin spines and small synapses contributes to defective hippocampal function in aged mice. *Neurobiol. Aging* 71, 91–104. doi: 10.1016/j.neurobiolaging.2018.07.010

Youmans, K. L., Tai, L. M., Kanekiyo, T., Stine, W. B. Jr., Michon, S. C., Nwabuisi-Heath, E., et al. (2012). Intraneuronal Aβ detection in 5xFAD mice by a new Aβ-specific antibody. *Mol. Neurodegener.* 7:8. doi: 10.1186/1750-1326-7-8

Zago, W., Buttini, M., Comery, T. A., Nishioka, C., Gardai, S. J., Seubert, P., et al. (2012). Neutralization of soluble, synaptotoxic amyloid β species by antibodies is epitope specific. *J. Neurosci.* 32, 2696–2702. doi: 10.1523/JNEUROSCI.1676-11.2012

Zott, B., Simon, M. M., Hong, W., Unger, F., Chen-Engerer, H. J., Frosch, M. P., et al. (2019). A vicious cycle of β amyloid-dependent neuronal hyperactivation. *Science* 365, 559–565. doi: 10.1126/science.aay0198

Conflict of Interest: The authors declare that the research was conducted in the absence of any commercial or financial relationships that could be construed as a potential conflict of interest.

frontiers in Synaptic Neuroscience

ORIGINAL RESEARCH
published: 22 July 2020
doi: 10.3389/fnsyn.2020.00029

Taurine Promotes Neurite Outgrowth and Synapse Development of Both Vertebrate and Invertebrate Central Neurons

Brittany Mersman[1,2], *Wali Zaidi*[3], *Naweed I. Syed*[3] *and Fenglian Xu*[1,2]*

[1]*Department of Biology, College of Arts and Sciences, Saint Louis University, St. Louis, MO, United States,* [2]*Henry and Amelia Nasrallah Center for Neuroscience, Saint Louis University, St. Louis, MO, United States,* [3]*Department of Cell Biology and Anatomy, Hotchkiss Brain Institute and Alberta Children's Hospital Research Institute, University of Calgary, Calgary, AB, Canada*

Taurine is a sulfur-containing amino acid that is widely expressed throughout the human brain, heart, retina, and muscle tissues. Taurine deficiency is associated with cardiomyopathy, renal dysfunction, abnormalities of the developing nervous system, and epilepsy which suggests a role specific to excitable tissues. Like vertebrates, invertebrates maintain high levels of taurine during embryonic and larval development, which decline during aging, indicating a potential developmental role. Notwithstanding its extensive presence throughout, taurine's precise role/s during early brain development, function, and repair remains largely unknown in both vertebrate and invertebrate. Here, we investigated whether taurine affects neurite outgrowth, synapse formation, and synaptic transmission between postnatal day 0 rat cortical neurons *in vitro*, whereas its synaptogenic role was tested more directly using the *Lymnaea* soma-soma synapse model. We provide direct evidence that when applied at physiological concentrations, taurine exerts a significant neurotrophic effect on neuritic outgrowth and thickness of neurites as well as the expression of synaptic puncta as revealed by immunostaining of presynaptic synaptophysin and postsynaptic PSD95 proteins in rat cortical neurons, indicating direct involvement in synapse development. To demonstrate taurine's direct effects on neurons in the absence of glia and other confounding factors, we next exploited individually identified pre- and postsynaptic neurons from the mollusk *Lymnaea stagnalis*. We found that taurine increased both the incidence of synapse formation (percent of cells that form synapses) and the efficacy of synaptic transmission between the paired neurons. This effect was comparable, but not additive, to *Lymnaea* trophic factor-induced synaptogenesis. This study thus provides direct morphological and functional evidence that taurine plays an important role in neurite outgrowth, synaptogenesis, and synaptic transmission during the early stages of brain development and that this role is conserved across both vertebrate and invertebrate species.

Keywords: taurine, neural development, synapse, vertebrate, invertebrate, molluska, synaptic transmission and plasticity

OPEN ACCESS

Edited by:
Wayne S. Sossin,
McGill University, Canada

Reviewed by:
Jaewon Ko,
Daegu Gyeongbuk Institute of Science and Technology (DGIST), South Korea
Werner Kilb,
Johannes Gutenberg University Mainz, Germany

***Correspondence:**
Fenglian Xu
fenglian.xu@slu.edu

Received: *01 April 2020*
Accepted: *24 June 2020*
Published: *22 July 2020*

Citation:
Mersman B, Zaidi W, Syed NI and Xu F (2020) Taurine Promotes Neurite Outgrowth and Synapse Development of Both Vertebrate and Invertebrate Central Neurons. Front. Synaptic Neurosci. 12:29. doi: 10.3389/fnsyn.2020.00029

INTRODUCTION

Taurine, 2-aminoethanesulfonic acid, is an abundant, free amino acid in human and most animal brains (Huxtable, 1989) and is also present in the heart, retina, and muscle tissues (Ripps and Shen, 2012). Humans obtain taurine either from the diet or from biochemical synthesis (Jacobsen and Smith, 1968). Its biosynthesis is derived from cysteine in which cysteine dioxygenase and cysteinesulfinic acid decarboxylase form hypotaurine. Hypotaurine is then converted by hypotaurine dehydrogenase to form taurine (Vitvitsky et al., 2011). As a structural analog of the inhibitory neurotransmitter γ-aminobutyric acid (GABA), taurine mimics GABA action by activating $GABA_A$ receptors (El Idrissi and Trenkner, 2004; Jia et al., 2008), and transport of taurine into neurons occurs *via* Slc6a6/TauT, the same family of proteins that contribute to GABA transport (Smith et al., 1992; Uchida et al., 1992; Tomi et al., 2008). Taurine has been shown to play a role in many physiological processes including osmoregulation (Solis et al., 1988), membrane excitability changes (Galarreta et al., 1996), and neuronal development where it acts as a putative neurotrophic factor (Chen et al., 1998; Rak et al., 2014). Taurine is also neuroprotective, as it regulates calcium homeostasis (Chen et al., 2001), acts as an antioxidant (Martincigh et al., 1998), and functions as a modulator of inflammation (Marcinkiewicz and Kontny, 2014). Some of the neuroprotective pathways by which taurine acts have also been identified. For example, taurine activates the PI3-K/Akt pathway to increase cell survival during oxidative stress (Das et al., 2011) and downregulates Bax (pro-apoptotic Bcl-2-associated protein) and caspase-3 in traumatic brain injury (Niu et al., 2018).

As one of the most abundant organic molecules in the central nervous system (CNS), taurine has been deemed a key regulator of neurodevelopment for decades. As Sturman et al. (1985) showed in their seminal article, taurine-deficient kittens displayed developmental abnormalities, indicating its vital role in proper CNS development. In the developing nervous system, taurine acts as a trophic factor (Sturman, 1993; Chen et al., 1998; Rak et al., 2014) and is present at a concentration three times higher in the immature brain than the adult nervous system; some studies suggest a concentration up to the 1–9 mM range (Benitez-Diaz et al., 2003; Albrecht and Schousboe, 2005; Furukawa et al., 2014). The addition of taurine increases stem cell proliferation in the developing mouse hippocampus as well as expression of synaptic proteins in rat hippocampal primary culture, presumably contributing to the overall connectome of the mouse brain (Shivaraj et al., 2012). These studies, in addition to the fact that taurine concentration in the brain decreases with age, suggest that taurine plays a major role in the proper development of neurons and networks (Banay-Schwartz et al., 1989). However, it remains unknown if taurine acts to regulate multiple developing steps including neural morphogenesis, synaptogenesis, synaptic transmission, and plasticity and if taurine's effects in developing brains are species-specific (e.g., mouse vs. rat or vertebrate vs. invertebrate) or brain region-specific (e.g., hippocampus vs. cortex).

Like vertebrates, taurine is present in the nervous system of many invertebrates (Allen and Garrett, 1971; McCaman and Stetzler, 1977). Specifically, in marine invertebrates, taurine's robust role in osmoregulation is well characterized (Lange, 1963; Allen and Garrett, 1971; Gilles, 1972; Smith and Pierce, 1987; Miles et al., 2018). Other potential roles of taurine in invertebrates have been suggested such as an H_2S scavenger in hydrothermal vent invertebrates (Koito et al., 2018), a source of energy for marine prokaryotes (Clifford et al., 2019), and a regulator of temperature tolerance in the fish Preccottus glehnii (Karanova, 2009). Similar to vertebrates, taurine has been found in high concentrations in some invertebrate larvae species during development and metamorphosis (Welborn and Manahan, 1995). However, little research is carried to explore taurine's developmental and physiological roles in the nervous system of invertebrates.

Considering the above evidence, we first asked the question: Does taurine morphologically affect the development of molecular components such as the cytoskeletal and synaptic proteins in vertebrate neurons? To answer this question, we studied the effects of taurine on primary neurons derived from postnatal rat cortex, a brain region and species severely understudied in this context. Our results indicate that taurine increases the number of neuritic branches and the thickness of neurites. Taurine also significantly regulates the expression and/or puncta localization of presynaptic/postsynaptic markers in developing neurons, with a more robust effect on the presynaptic markers. We next asked the questions: Does taurine affect synapse formation, synaptic transmission, and plasticity between central neurons? Does it affect the pre- or postsynaptic machinery? Because direct cell-cell interactions between defined sets of pre- and postsynaptic neurons cannot be studied in vertebrates in the absence of glial and other confounding factors such as GABA and their receptors, we exploited the invertebrate *Lymnaea stagnalis* model where this could easily be achieved using soma-soma synapse culture and electrophysiological methods. Using this model, we, for the first time, demonstrate that taurine promotes synapse formation and synaptic transmission in invertebrate neurons of *Lymnaea stagnalis* brains, and taurine's actions do not involve the modulation of postsynaptic machinery, indicating a presynaptic origin. This study, together with previous knowledge about taurine's effects on hippocampal neurons, clearly demonstrates that taurine is a critical neuro-morphogenic and synaptogenic factor in different brain regions across both vertebrate and invertebrate species, and taurine-mediated effects are cell- or synaptic site-specific.

MATERIALS AND METHODS

Animals and Cell Culture

All animal procedures followed the standards established by the National Institute of Health Animal Use Guidelines in Canada and the US and have been approved by the Institutional Animal Care and Use Policy at the University of Calgary and Saint Louis University.

Rat Cortical Neuronal Cell Culture

The culture of cortical neurons was made using Sprague-Dawley rat pups on the day they were born (postnatal day 0, P0). Rat frontal cortices were removed and enzymatically dissociated with papain (50 μg/ml). To create a single-cell suspension, glass pipettes of decreasing size were used to triturate. Dissociated cortical neurons were then diluted in culture media and plated at an appropriate density onto culture dishes with glass coverslips coated with poly-D-lysine (30 μg/ml) and laminin (2μg/ml). After cells settled for 30 mins, 2 ml of culture medium was added to each culture dish. The culture medium included neurobasal medium, 2% B27, L-Glutamine (200 mM), 4% FBS, and penicillin-streptomycin (Invitrogen). Cortical neurons were kept in culture medium and maintained at 37°C in an airtight modular incubator chamber (Billups-Rothenberg) circulated with medical air and 5% carbon dioxide. Fifty percent of the culture medium was removed and replaced every 3–4 days. Control cells for each experiment were incubated in the same environment (37°C, 5% CO_2) as treatment cells.

Lymnaea Ganglion Dissection and Cell Culture

L. stagnalis were kept at room temperature in a well-aerated aquarium filled with filtered pond water at 20–22°C on a 12-h light/dark regimen and were fed romaine lettuce. For cell culture experiments, ∼2–3-month-old *L. stagnalis* were used while ∼4–6-month-old animals were used to make brain-conditioned medium (CM, containing trophic factors). Details of *Lymnaea* cell culture procedures and CM preparations are described in previous publications (Syed et al., 1990; Ridgway et al., 1991; Xu et al., 2009). In brief, deshelled snails were anesthetized for 10 mins in Listerine solution (ethanol, 21.9%; and methanol, 0.042%) diluted to 10% in normal saline (NaCl 51.3 mM, KCl 1.7 mM, $CaCl_2$ 4.0 mM, $MgCl_2$ 1.5 mM, and HEPES 10 mM), adjusted to pH 7.9. To make trophic factor-containing CM, the central ring ganglia (**Figure 5A**) were incubated in defined medium (DM; L-15; Invitrogen; special order) containing NaCl 40 mM, KCl 1.7 mM, $CaCl_2$ 4.1 mM, $MgCl_2$ 1.5 mM, and HEPES 10.0 mM (12 ganglia/6.5 ml DM) for at least 3 days before removing ganglia and collecting CM. To culture *L. stagnalis* neurons, the central ring ganglia were first treated for 21 mins with the proteolytic enzyme trypsin (2 mg/ml) dissolved in DM. The central ring ganglia were then incubated for 15 mins in a DM solution containing trypsin inhibitor (2 mg/ml) and subsequently pinned on a dissection dish containing high osmolarity DM (D-glucose, 20 mM). A dissection microscope was used to visualize *L. stagnalis* brains, and fine forceps were used to remove a thin layer of the sheath surrounding the ganglia. With gentle suction through a Sigmacote-treated, fire-polished pipette attached to a microsyringe filled with high osmolarity DM, individual cells were removed from the ganglia. Once isolated, well-defined pre- and postsynaptic cells were juxtaposed in a soma-soma configuration and plated on poly-$_L$-lysine coated culture dishes containing medium as described previously (Meems et al., 2003). In brief, somas of isolated cells were manually severed from their axons *via* a conventional intracellular electrode attached to a micromanipulator. Two isolated somata were then juxtaposed and cultured overnight in the absence or presence of taurine or CM, depending on the experiment. The cells used in this study are the visceral dorsal 4 (VD4, presynaptic) and the left pedal dorsal 1 (LPeD1, postsynaptic) neurons (**Figure 5B**). VD4 neurons contain neurotransmitter acetylcholine (ACh), and LPeD1 neurons express nicotinic ACh receptors (nAChR). VD4 and LPeD1 neurons *in vivo* form cholinergic synapses that control cardiorespiratory behavior in *L. stagnalis* (Buckett et al., 1990).

Immunocytochemistry and Confocal Microscopy

Immunostaining was performed to examine morphological changes in the neuronal cytoskeletal and synaptic proteins of cortical neurons cultured for 3 days and 10 days, respectively. Neurons were fixed with 4% paraformaldehyde and 15% picric acid for 1 h at room temperature. Permeabilization of fixed cultures was performed by incubation for 1 h in incubation media containing 5% goat serum and 0.1% Triton X. Cells were then incubated with primary antibodies rabbit anti-synaptophysin (1:500, Abcam) and mouse anti-PSD95 (1:2,000; NeuroMab) to study the development of synaptic proteins. Primary antibodies were applied at 4°C overnight. Following 3× wash with 1× PBS, secondary antibodies AlexaFluor 488 goat anti-rabbit IgG (1:200; Invitrogen) and AlexaFluor 546 goat anti-mouse IgG (1:200; Invitrogen) were applied for 1 h at room temperature. Mouse anti-β-tubulin (1:500; Invitrogen) was used to study the development of cytoskeletal proteins. Preparations were washed 3× in 1× PBS and mounted with MOWIOL mounting media. A Zeiss confocal microscope (LSM 510 Meta, Zeiss, Germany) was used to take fluorescence images. Image acquisition parameters such as exposure times, gain settings, laser intensity, pinhole size, etc., remained the same between control and treated cultures.

ImageJ Neurite Tracing and Synaptic Puncta Analysis

ImageJ was used to analyze phase contrast and immunofluorescent images of cortical cells. The ImageJ plugin NeuronJ was employed to measure neurite growth in phase-contrast images of cortical neurons 3 days in culture as previously described (Meijering et al., 2004; Pemberton et al., 2018). NeuronJ was programmed to output total neurite outgrowth (μm) and the number of neurites per phase-contrast image. Therefore, after counting the total number of cell bodies per image, the average neurite length was calculated by dividing the total neurite outgrowth by the total number of cell bodies. Using β-tubulin fluorescently stained day three cortical neurons, ImageJ was used to determine total β-tubulin intensity (IntDen output; the product of area and mean gray value) per image. From the same β-tubulin fluorescently stained neuronal images, primary neurites extending from pyramidal neurons were identified. The thickest part of each neurite was measured to compare the average neurite thickness. Using this method, 30–40 primary neurites were measured for thickness in each treatment.

Cortical neurons were cultured taurine-free or with 50 μM or 1 mM taurine, fluorescently labeled with the presynaptic marker synaptophysin and the postsynaptic marker

PSD95 after 10 days in culture, and imaged. Synaptophysin and PSD95 fluorescent intensity were measured in ImageJ as described for β-tubulin above. The ImageJ plugin SynapCountJ was used to measure the number of synapses (colocalization of synaptophysin and PSD95) per area of traced neurite as previously described (Mata et al., 2016). Synaptic puncta parameters were measured with the ImageJ plugin SynQuant (Wang et al., 2020). To look at synaptophysin (presynaptic) and PSD95 (postsynaptic) puncta measurements in entire fields of view (many neuronal networks taken together), uncropped fluorescent images were analyzed by SynQuant, and the number of synaptophysin and PSD95 puncta was outputted. To focus on neurites directly, primary neurites extending from pyramidal neurons were identified. A 50 μm × 20 μm square was placed on the start of primary pyramidal neurites (directly extending from the cell body) and cropped to create a 1,000 μm^2 area of a zoomed-in neurite. With this method, 13–22 neurites were measured per treatment. These neurite images were analyzed by SynQuant to measure number, intensity, and area of synaptophysin and PSD95 puncta.

Electrophysiology

Intracellular recording techniques were used to investigate neuronal excitability and synaptic physiology between the paired *Lymnaea* neurons. Glass microelectrodes (1.5 mm internal diameter; World Precision Instruments) were pulled using a vertical pipette puller (Model 700C, David Kopf Instruments). The electrodes were backfilled with a saturated solution of K_2SO_4 to yield a tip resistance ranging from 30 to 60 megaohms. Neurons were viewed under an inverted microscope (Axiovert 200 M; Zeiss) and impaled by Narishige micromanipulators (MO-202, Narishige). Electrical signals were amplified with a Neuro data amplifier (Neuron Data Instrument Corp) and recorded with the Axoscope program (Axon Instruments).

Using the *Lymnaea* synapse model in combination with intracellular recording techniques, we asked the following questions: Does taurine affect synapse formation (synaptogenesis), synaptic transmission, and synaptic plasticity between *Lymnaea* neurons? Does taurine exhibit synergistic actions with trophic factors to affect synaptic properties in invertebrate neurons? Does taurine act on the presynaptic or postsynaptic site?

Synaptogenesis Experiments

To evaluate the effects of taurine on synapse formation, presynaptic visceral dorsal 4 (VD4) and postsynaptic left pedal dorsal 1 (LPeD1) cells in *L. stagnalis* were paired and cultured in the absence or presence of 1 mM taurine (Sigma-Aldrich) in DM (no trophic factors) or CM (with trophic factors) overnight. Intracellular recordings were made the next day to monitor the development of synapses by recording postsynaptic potentials (PSPs) in the LPeD1 cell following the presynaptic stimulus. Current injection-induced action potentials in the presynaptic VD4 neuron triggered 1:1 PSPs in the postsynaptic LPeD1 neuron, indicating the formation of functional synapses. The current injection was made using a built-in current injector (Dual Channel Intracellular Recording Amplifier IR-283; Cygnus Technology, Delaware Water Gap, PA, USA). Averages of four successive PSPs measured from treated and untreated control groups were compared to determine the effects of taurine on the incidence and strength of synapse formation. The percentage of synapse formation was determined as the number of pairs that exhibited quantifiable transmission of stimuli between cells out of the total number of pairs that were treated.

Synaptic Transmission Experiments

To evaluate the effects of taurine on synaptic transmission at established synapses, VD4-LPeD1 neurons were cultured in the absence or presence of taurine (1 mM) in DM or CM overnight. Electrophysiological recordings were collected as described above to determine baseline synapse strength. Average amplitudes of PSPs were measured from control or treatments and compared to determine the effects of taurine, CM, or their combination on the strength of the synaptic transmission. The membrane potential of the LPeD1 neuron was maintained at −100 mV by current injection to enable a comparative evaluation of synapse strength.

Synaptic Plasticity (Post-tetanic Potentiation) Experiments

VD4-LPeD1 neurons were soma-soma juxtaposed and cultured in the absence (control) or presence of treatment overnight. Induced action potentials in the VD4 neuron triggered 1:1 PSPs in the postsynaptic LPeD1 neuron. Following a tetanic stimulation (a tetanic burst at 10 Hz), the PSP amplitude post-tetanus (pPSP) was substantially potentiated. The increase in the pPSP/PSP ratio is defined as (PTP; as shown in **Figures 6**, **7**), which underlies short-term synaptic plasticity. The pPSP/PSP values were recorded in neurons cultured in the absence (control) or presence of taurine (1 mM) in DM or CM. The tetanic stimulation was generated by injecting a square depolarizing current pulse in a duration of about 2 s into the presynaptic cell to elicit 12–16 action potentials, a well-defined stimulation paradigm for inducing consistent PTP as described in previous studies (Luk et al., 2011).

ACh Puffing Experiments

To further elucidate if taurine's action on synapse development and synaptic transmission involves the regulation of postsynaptic nAChRs, the transmitter ACh (1 μM) was pressure-applied (15 Psi, 100 ms duration) onto LPeD1 neurons to mimic transmitter release through a glass pipette (∼2 μm tip in diameter) which was connected to a PV800 Pneumatic Picopump (World Precision Instruments). Intracellular recordings were made on LPeD1 cells (held at −100 mV) to monitor the membrane potential change in response to the puffed ACh. The pipette containing ACh was placed at a distance of about two soma-lengths from LPeD1 to avoid mechanical disturbance.

ACh (A-2661), taurine (T8691), and all other chemicals were purchased from Sigma Aldrich (Saint Louis, MO, USA).

Statistical Analysis

ImageJ was used to analyze morphological structures of neurites and synapses in cortical neurons with phase-contrast images and immunofluorescent-labeled β-tubulin, synaptophysin, and PSD95. Mini Analysis software (Synaptosoft) was used to measure the amplitudes of PSPs. RStudio was used to run statistical significance tests. Data were statistically analyzed using Fisher's exact test, student *t*-tests, one-way analysis of variance (ANOVAs), and Tukey's HSD *Post hoc* tests as appropriate. Values were considered statistically significant at the level of $p < 0.05$. The data are presented as mean ± S.E.M. Each experiment was replicated a minimum of three times; the actual number of replicates for each experiment is described in the text or listed in the corresponding figure legend. All graphs/figures were made using GraphPad Prism 8.4.2 and Adobe Photoshop 2020.

RESULTS

Taurine Promotes Neuritic Growth in Rat Cortical Neurons

Taurine has been shown in previous studies to promote neurogenesis and neural progenitor cell (NPC) proliferation in both developing and adult mouse brains (Hernandez-Benitez et al., 2012). However, less is known about the effect of taurine on the development of neural processes such as dendrites and axons. Also, no studies have examined taurine's effects on neuritic development in brain regions such as the vertebrate cortex. To fill this knowledge gap, we first investigated whether taurine affects neuronal growth of developing rat cortical neurons. To this end, rat cortical cells from day 0 pups were cultured either in the absence or presence of taurine at physiological concentrations of 50 μM and 1 mM for 3 days. Phase-contrast images (**Figure 1**) were taken on day 3 to evaluate the effect of taurine on cells and the development of neuritic processes. We found that neurons cultured in taurine at concentrations of 50 μM and 1 mM exhibited healthy cell bodies with neuritic processes that formed complex networks. **Figure 1A** provides representative phase-contrast images of cultures treated without (control) and with taurine at 50 μM and 1 mM. To further define the effects of taurine on neuritic morphogenesis, we conducted neurite tracing and counting analyses using ImageJ neurite tracing methods (Meijering et al., 2004; Imaninezhad et al., 2018; Pemberton et al., 2018). Specifically, we counted and measured the number of neurites and the total neurite outgrowth (the neuritic lengths measured in each image). The total number of cell bodies was also counted and used to calculate the average length of a neurite per cell. **Figures 1B–E** show quantitative data and statistical analyses. Overall, our ANOVA statistical data revealed that compared to controls, taurine treatment at both concentrations significantly increased the total neurite outgrowth ($p < 0.001$) per image (but not per cell), the total number of cells ($p < 0.05$), and the total number of neurites ($p < 0.01$) in cultures.

To further confirm and define the positive effects of taurine on the morphogenesis observed in our phase-contrast study, we next performed an immunocytochemical study on fluorescently labeled neurites with an antibody against cytoskeletal protein β-tubulin, a microtubule protein component that exists in all neurites and plays essential roles for neuritic formation, growth, and network function. **Figure 2A** shows representative images of β-tubulin-stained day 3 cortical neurons. These cultures revealed robust expression of the cytoskeletal protein in both control and taurine (50 μM and 1 mM)—treated neurons. Consistent with our phase-contrast images, these fluorescent images revealed extensive neuritic processes (indicated by arrows) and interconnections (asterisks; **Figure 2A**). Next, we used ImageJ to analyze β-tubulin immunofluorescent images and conducted statistical analyses to determine if taurine treatments affect cytoskeletal expression (measured by the fluorescent intensity) and subtle changes of neurite thickness. Our data showed that taurine treatment at both concentrations significantly increased the thickness of neurites ($p < 0.001$) but did not affect the intensity of β-tubulin protein expression in neurons cultured for 3 days in treatment (**Figures 2B,C**). Intriguingly, though, neurons cultured in 1 mM taurine demonstrated significantly increased β-tubulin intensity compared to controls after 6 days in culture, suggesting that taurine may increase β-tubulin protein expression over developmental time (data not shown).

Neuritogenesis and cytoskeletal development are essential steps toward the functional development of cell-cell contacts (synapses), synaptic transmission, and plasticity. Next, we asked the question: Does taurine play a role in enhancing the synaptic properties of neurons?

Taurine Regulates the Expression and Punctualization of Synaptic Machinery Proteins in Cortical Neurons

To directly examine the role of taurine in synapse development, we asked whether taurine affects the development of molecular machinery at the synaptic sites of rat cortical neurons. To test this, neurons treated with taurine at the above-mentioned concentrations were maintained in culture for 10 days to allow the establishment of synaptic networks. Neurons were then fixed and stained with synaptic markers synaptophysin (presynaptic vesicle membrane-associated protein) and postsynaptic density protein 95 (PSD95, postsynaptic membrane-associated scaffolding protein). **Figure 3A** shows representative images of neurons treated with and without 50 μM or 1 mM taurine. Both synaptophysin and PSD95 exhibited puncta expression and distribution in neurites. To quantify taurine's effect on these synaptic proteins, we measured synaptic parameters including fluorescent intensity, number of individual puncta, and number of overlapped puncta (synapses) of synaptophysin and PSD95 in the entire image area. Our results revealed that taurine at 1 mM, but not 50 μM, significantly increased the expression of presynaptic synaptophysin protein compared to control (**Figure 3B**). Taurine at 1 mM also caused an increase in PSD95 expression, but this increase was not statistically significant (**Figure 3C**). Consistently, our data showed that the number of synaptophysin puncta, but not PSD95 puncta were increased significantly by taurine at 1 mM, but not 50 μM (**Figures 3D,E**). However, our data did not reveal a significant

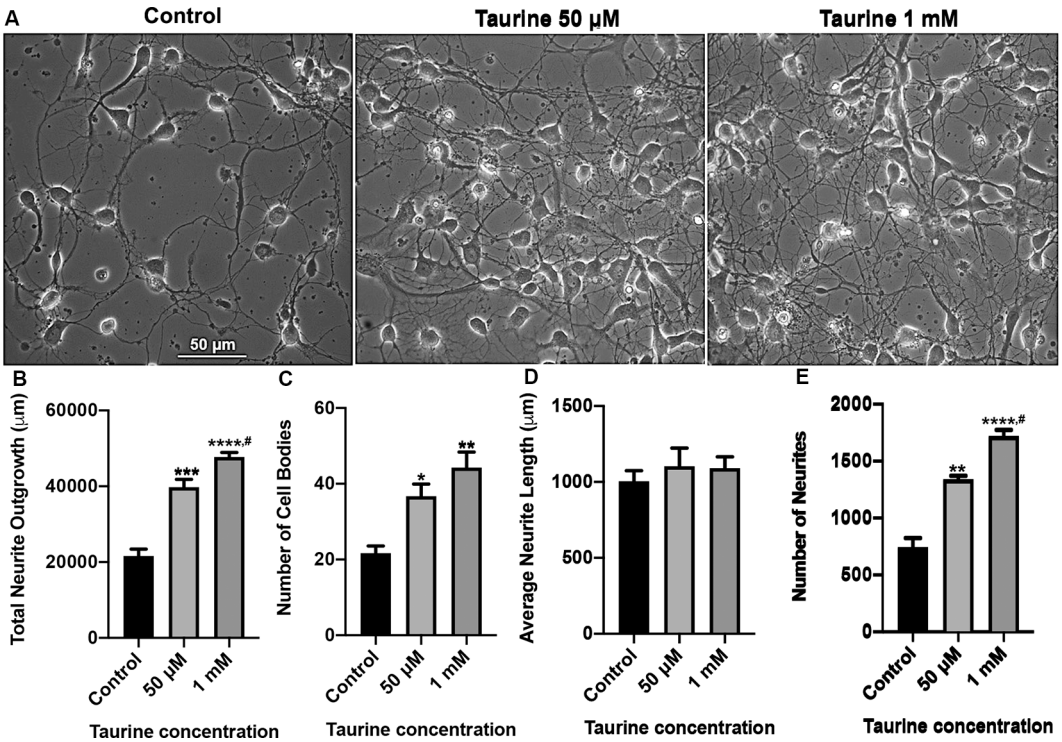

FIGURE 1 | Taurine exposure promotes rat cortical neuronal growth and increases the number of neurites and cells in culture. Rat cortical neurons were cultured either in the absence (control) or presence of taurine at different concentrations. **(A)** Phase-contrast images were taken on day 3 in culture. **(B)** Taurine treatment significantly increased the total neurite outgrowth in phase-contrast images. The total neurite outgrowth for control was 21,634.2 ± 1788.7 μm, for 50 μM taurine was 39,775.7 ± 2,056.3 μm, and for 1 mM taurine was 47,714.8 ± 1,222.5 μm ($p = 0.0007$ for control vs. 50 μM taurine, $p = 0.00009$ for control vs. 1 mM taurine, and $p = 0.04$ for 50 μM vs. 1 mM taurine). **(C)** Taurine treatment also significantly increased the number of cell bodies per image compared to controls. The cell body count was 21.7 ± 1.9 for control, 36.7 ± 3.2 for 50 μM taurine, and 44.3 ± 4.1 for 1 mM taurine ($p = 0.03$ for control vs. 50 μM taurine, and $p = 0.005$ for control vs. 1 mM taurine). **(D)** However, calculating the average neurite length revealed a nonsignificant difference between control and taurine treatments. Average neurite length for control was 1,004.7 ± 69.3 μm, for 50 μM taurine was 1,102.7 ± 120.1 μm, and for 1 mM taurine was 1,090 ± 76.1 μm ($p = 0.724$). **(E)** The number of neurites was significantly increased when cortical neurons were cultured with taurine at both concentrations. Number of neurites in control was 740 ± 84.9, 50 μM taurine was 1,337 ± 34, and 1 mM taurine was 1,718.3 ± 55.6 ($p = 0.001$ for control vs. 50 μM taurine, $p = 0.00007$ for control vs. 1 mM taurine, and $p = 0.01$ for 50 μM vs. 1 mM taurine; $n = 3$ images per treatment; the statistical test was one-way ANOVA in all cases). *Indicates a significance level of $p < 0.05$ vs. control; **$p < 0.01$, ***$p < 0.001$, ****$p < 0.0001$, and #indicates a significance level of $p < 0.05$ vs. 50 μM taurine.

difference in the number of overlapped puncta of synaptophysin and PSD95 (number of synapses; **Figure 3F**). Thus, our data analyses indicate that taurine at a higher concentration of 1 mM selectively enhances the expression of presynaptic synaptophysin protein and the number of synaptophysin puncta.

To gain further insight into the effect of taurine on synaptic machinery, we next focused on analyzing neurites (cropped 50 μm × 20 μm section of neurites extending from pyramidal neurons; see "Materials and Methods" section for detailed description) using the SynQuant plugin in ImageJ (Wang et al., 2020). This method allows for the identification of puncta and the detailed quantification of the puncta intensity and area (**Figure 4A**). Our data showed that although the average number of synaptophysin and PSD95 puncta per neuritic area was not significantly different between taurine treatments and controls (**Figures 4D,E**), the intensity (**Figure 4B**) and area (**Figure 4F**) of synaptophysin puncta were significantly increased by taurine at 1 mM compared to controls. Again, taurine at 50 μM did not affect synaptophysin puncta as compared to controls. Interestingly, taurine at 50 μM decreased the intensity (**Figure 4C**) and area (**Figure 4G**) of PSD95 puncta, while 1 mM taurine increased PSD95 puncta intensity and area compared to controls, though not to a significant degree. These data indicate that taurine increased the expression and probably the size (reflected by the area) of individual presynaptic puncta, but not the postsynaptic puncta. Taken together, our data indicated that taurine plays an important role in promoting synaptic machinery development by selectively acting on synaptic proteins to enhance protein expression and puncta development in cortical neurons.

While these data provide the first direct morphological evidence that taurine promotes growth and development of synaptic structures in cortical neurons, direct measurements of neural activity and synaptic properties at the level of single pre-and postsynaptic neurons in vertebrates are not feasible here; we thus opted to use an invertebrate model where this could

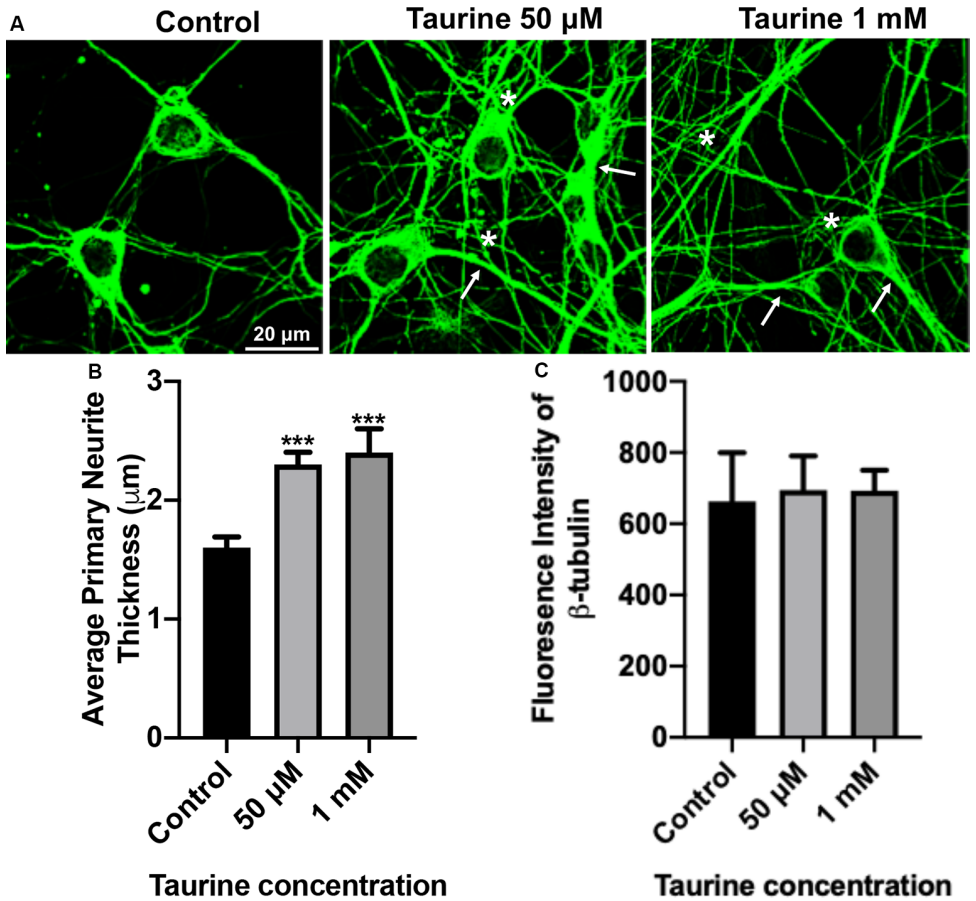

FIGURE 2 | β-tubulin-labeled cortical neurons reveal an increase in the thickness of neurites after taurine treatment. After 3 days in taurine-rich (50 μM or 1 mM) or -free media, cortical neurons were stained with the cytoskeletal marker β-tubulin and imaged. **(A)** Representative images demonstrate the extensive outgrowth of cultures in all treatments and control. Arrows indicate examples of extensive neuritic processes while asterisks show robust interconnections. **(B)** Taurine at both 50 μM and 1 mM concentrations significantly increased the average thickness of primary neurites compared to control. The average neurite thickness for control was 1.6 ± 0.09 μm, for 50 μM taurine was 2.3 ± 0.1 μm, and for 1 mM taurine was 2.4 ± 0.2 μm ($p = 0.0004$ for control vs. 50 μM taurine, and $p = 0.0002$ for control vs. 1 mM taurine). **(C)** The intensity of β-tubulin was not significantly changed by any concentration of taurine. Specifically, the β-tubulin intensity of control was 663.3 ± 136.2, for 50 μM taurine was 694.3 ± 96.3, and for 1 mM taurine was 692.5 ± 58.3 ($p = 0.971$; $n = 4$ images per treatment and number of neurites analyzed was 40, 39, and 30 for control, 50 μM taurine, and 1 mM taurine, respectively; the statistical test was one-way ANOVA in all cases). ***Indicates a significance level of $p < 0.001$ vs. control.

be done in functionally defined, individual large neurons in the absence of glia and confounding factors including taurine's analogous transmitters GABA and glycine.

Taurine Regulates Neural Excitability and Synaptic Activity Between Two *Lymnaea* Neurons That Form Functional Synapses *in vitro*

To accurately monitor the effects of taurine on the functional development of synapses between identified individual neurons, we first determined if taurine indeed has a functional impact on neuronal excitability and transmission in *Lymnaea* neurons whose synapses have been established. To test this, *L. stagnalis* visceral dorsal 4 (VD4, presynaptic, acetylcholine-containing neuron) and left pedal dorsal 1 (LPeD1, postsynaptic) cells were paired in the soma-soma configuration (**Figure 5B**) and were first allowed to develop proper excitatory cholinergic synapses overnight in CM (contains *Lymnaea* brain secreted neurotrophic factors, but devoid of taurine). The next day, intracellular recordings were made from both neurons. In one experimental paradigm, we tested if taurine could regulate neuronal action potential firing and synaptic transmission between VD4 and LPeD1. In another experimental paradigm, we examined if taurine affects the resting membrane potentials of VD4 and LPeD1 cells. To elicit neuronal activity, we selectively injected depolarizing currents into the presynaptic VD4 neuron to induce action potentials in VD4. Current injection into the postsynaptic LPeD1 neuron brought its membrane potential close to threshold potentials to increase the likelihood of action potential firing in LPeD1 in response to presynaptic excitatory neurotransmitter (ACh in this case).

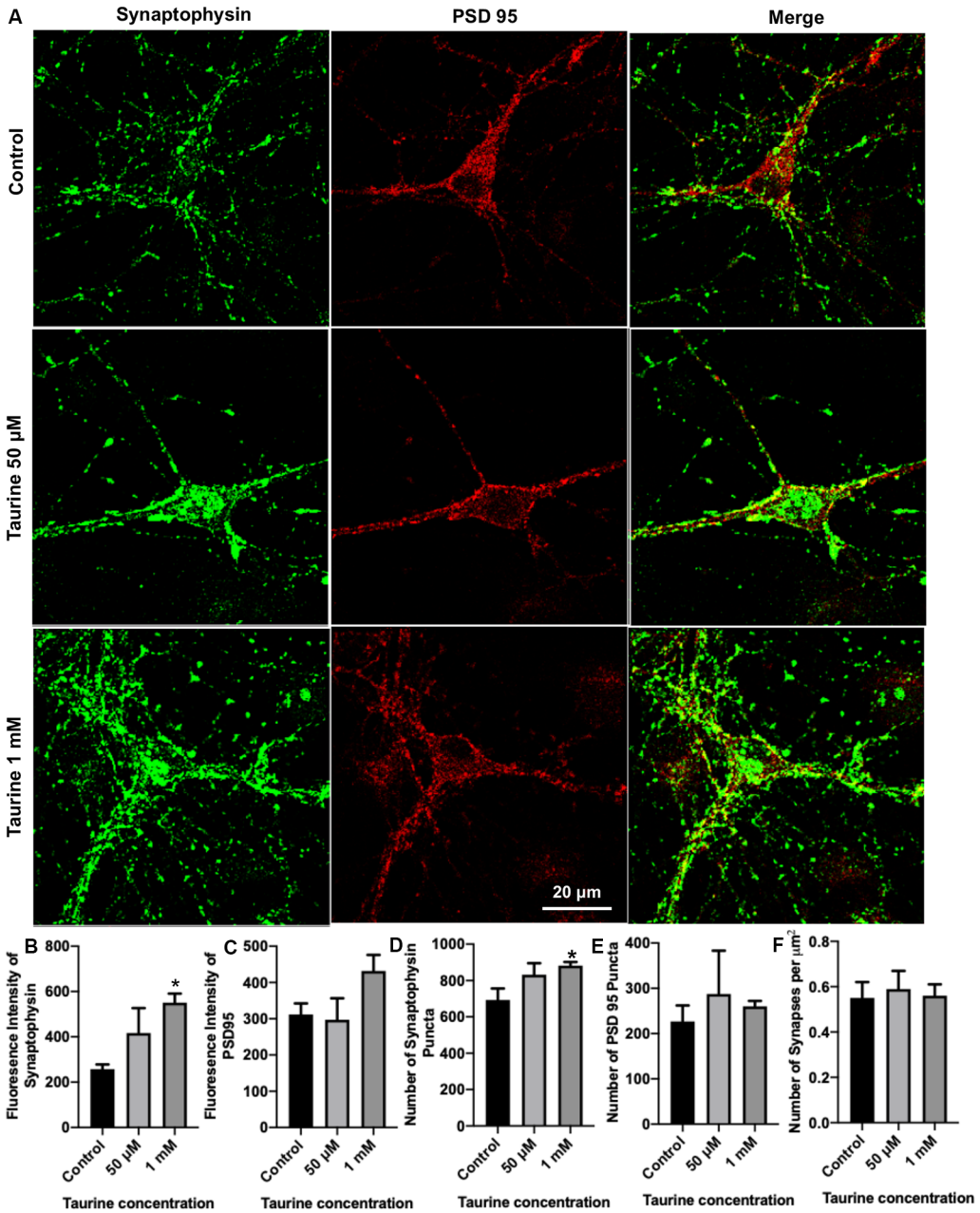

FIGURE 3 | Taurine enhances the expression of presynaptic protein and presynaptic puncta in rat cortical neurons. Cortical neurons were cultured with 50 μM taurine, 1 mM taurine, or without taurine (control) for 10 days to allow for the development of mature networks. On day 10, cells were fixed and stained with antibodies against the presynaptic vesicle protein synaptophysin and the postsynaptic receptor density protein PSD95. Images were acquired using confocal microscopy and whole networks (entire fluorescent images) were analyzed for synaptic protein intensity, puncta, and colocalization. **(A)** Representative immunofluorescent images show the staining of synaptic proteins of control, 50 μM, 1 mM taurine-treated cortical neurons. **(B,C)** The addition of 1 mM taurine to culture media significantly increased the intensity of synaptophysin expression while not significantly altering PSD95 intensity. Specifically, the fluorescent intensity of synaptophysin in control was 257.6 ± 20.7, in taurine at 50 μM was 417.3 ± 110, and in taurine at 1 mM was 551.1 ± 39.6 ($p = 0.02$ for control vs. 1 mM taurine). The fluorescence intensity of PSD95 in control was 311.9 ± 30.5, in taurine at 50 μM was 297.1 ± 59.5, and in taurine at 1 mM was 431.9 ± 44.3 ($p = 0.108$). **(D,E)** The number of presynaptic synaptophysin and postsynaptic PSD95 puncta in a fluorescent image was measured by the ImageJ plugin SynQuant. The only significant change in puncta number occurred after 1 mM taurine treatment for synaptophysin puncta. Specifically, the number of synaptophysin puncta in control was 692.8 ± 63.3, in taurine at 50 μM was 832.3 ± 63.3, and in taurine at 1 mM was 881.7 ± 20.7 ($p = 0.03$ for control vs. 1 mM taurine). The number of PSD95 puncta in control was 226.8 ± 35.3, in taurine at 50 uM was 287.5 ± 95.6, and in taurine at 1 mM was 260.2 ± 11.8 ($p = 0.743$). **(F)** SynapCountJ, an ImageJ plugin, was utilized to determine synapses (per μm^2) *via* colocalization of synaptophysin and PSD95 in traced neurites. There was no significant difference in the number of synapses between any treatments. Control cell number of synapses (per μm^2) was 0.55 ± 0.07, 50 μM taurine was 0.59 ± 0.08, and 1 mM taurine was 0.56 ± 0.05 ($p = 0.904$; $n = 4$ images for control and 50 μM taurine-treated neurons; $n = 6$ images for 1 mM taurine-treated neurons; the statistical test was one-way ANOVA in all cases). *Indicates a significance level of $p < 0.05$ vs. control.

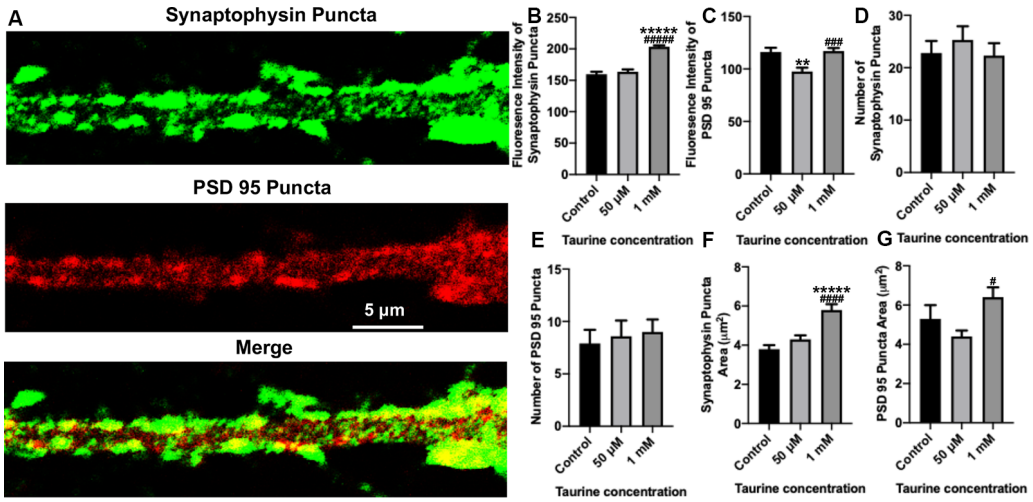

FIGURE 4 | In neurites, a higher concentration of taurine (1 mM) increases presynaptic puncta intensity and area while keeping postsynaptic puncta unaffected. Puncta parameters in neurites were examined by zooming in on a 1,000 μm^2 primary neurite extending from a pyramidal neuron and using the ImageJ plugin SynQuant. **(A)** Representative fluorescent images show an example of the 1,000 μm^2, zoomed-in neurite from a 50 μM taurine-treated neuron. **(B)** The intensity of synaptophysin puncta in the cropped, neurite image was measured and showed a significant increase in 1 mM taurine-treated neurons. The intensities of synaptophysin puncta in control was 159.7 ± 4.0, 50 μM taurine was 163.6 ± 3.7, and 1 mM taurine was 203.4 ± 2.4 ($p < 0.00001$ for control vs. 50 μM taurine, and $p < 0.00001$ for 50 μM taurine vs. 1 mM taurine). **(C)** The intensity of PSD95 puncta was significantly decreased in neurites cultured in 50 μM taurine. The intensities of PSD95 puncta in control was 116.2 ± 4.0, in 50 μM taurine was 97.6 ± 3.6, and in 1 mM taurine was 117 ± 2.9 ($p = 0.002$ for control vs. 50 μM taurine, and $p = 0.0001$ for 50 μM taurine vs. 1 mM taurine). **(D,E)** The number of presynaptic synaptophysin and postsynaptic PSD95 puncta did not differ significantly between any treatments. Specifically, the number of synaptophysin puncta was 22.8 ± 2.3 for control, 25.3 ± 2.6 for 50 μM taurine, and 22.3 ± 2.4 for 1 mM taurine ($p = 0.684$). The number of PSD95 puncta was 7.9 ± 1.3 for control, 8.6 ± 1.5 for 50 μM taurine, and 9 ± 1.2 for 1 mM taurine ($p = 0.852$). **(F)** The area of synaptophysin puncta was measured and resulted in a significant increase for 1 mM taurine-treated neurons. The area of synaptophysin puncta for control was 3.8 ± 0.2 μm^2, for 50 μM taurine was 4.3 ± 0.2 μm^2, and for 1 mM taurine was 5.8 ± 0.3 μm^2 ($p < 0.00001$ for control vs. 1 mM taurine, and $p = 0.00002$ for 50 μM taurine vs. 1 mM taurine). **(G)** Taurine treatment at 50 μM decreased the PSD95 puncta area, leading to a significant increase in puncta area of 1 mM taurine-treated neurites compared to 50 μM treatment. The area of PSD95 puncta was 5.3 ± 0.7 μm^2 for control, 4.4 ± 0.3 μm^2 for 50 μM taurine, and 6.4 ± 0.5 μm^2 for 1 mM taurine ($p = 0.01$ for 50 μM taurine vs. 1 mM taurine; $n = 13$, 15, and 22 cropped, neurite images analyzed The area of PSD95 puncta for control was 50 μM taurine, and 1 mM taurine, respectively; the statistical test was one-way ANOVA in all cases). **Indicates a significance level of $p < 0.01$ vs. control, *****$p < 0.00001$, and #indicates a significance level of $p < 0.05$ vs. 50 μM taurine, ###$p < 0.001$, ####$p < 0.0001$, and #####$p < 0.00001$.

Figure 5C shows that current injection-induced, presynaptic action potentials triggered the firing of action potentials on the postsynaptic cells (see inserts, synchronizing the firing). Next, we added taurine to test if it could affect the firing activity in either or both neurons. Our results showed that upon application of taurine at 2.5 mM, spontaneous firing activities in the postsynaptic LPeD1 cells were quickly prevented in all cells examined ($n = 4$), while firings in the presynaptic VD4 neurons remained active in three out of four cells with one cell eventually stopping firing after taurine application. Interestingly, while the spontaneous firing of the postsynaptic neurons stopped after taurine addition, it still exhibited 1:1 postsynaptic potential (synaptic transmission) in response to presynaptic action potentials for as long as VD4 action potentials remained (see **Figure 5C**). Furthermore, our data showed that when cells were held at resting membrane potential (no current injection applied in either cell), taurine only caused a small membrane hyperpolarization in VD4 cells and significantly larger membrane hyperpolarization in LPeD1 cells (student t-test, $p < 0.05$; **Figure 5D**), regardless if LPeD1 was quiescent or actively firing at rest (**Figure 5E**). Overall, these results indicate that taurine can induce an inhibitory or hyperpolarizing change in membrane excitability; also, these results indicate that taurine-induced effects are cell-specific, with there being more pronounced effects on the postsynaptic LPeD1 cell than that of presynaptic VD4 cell. Our data further indicate that taurine's effects on membrane excitability do not exclude the normal synaptic transmission and plasticity between two synaptic neurons. Together, these studies strongly suggest that taurine does indeed regulate neuronal excitability and synaptic activity in *Lymnaea* neurons.

Taurine Increases the Incidence of Synaptogenesis and Enhances Synaptic Strength Between Cultured Pre- and Postsynaptic Neurons From Invertebrate *Lymnaea*

We next examined if taurine could functionally regulate the formation of synapses (synaptogenesis), synaptic transmission, and plasticity using *L. stagnalis* central neurons. Such information is important for our understanding of taurine's roles in the development and function of invertebrate nervous systems, an area that remains under-explored. Also, results from *L. stagnalis* synapse studies help answer the question

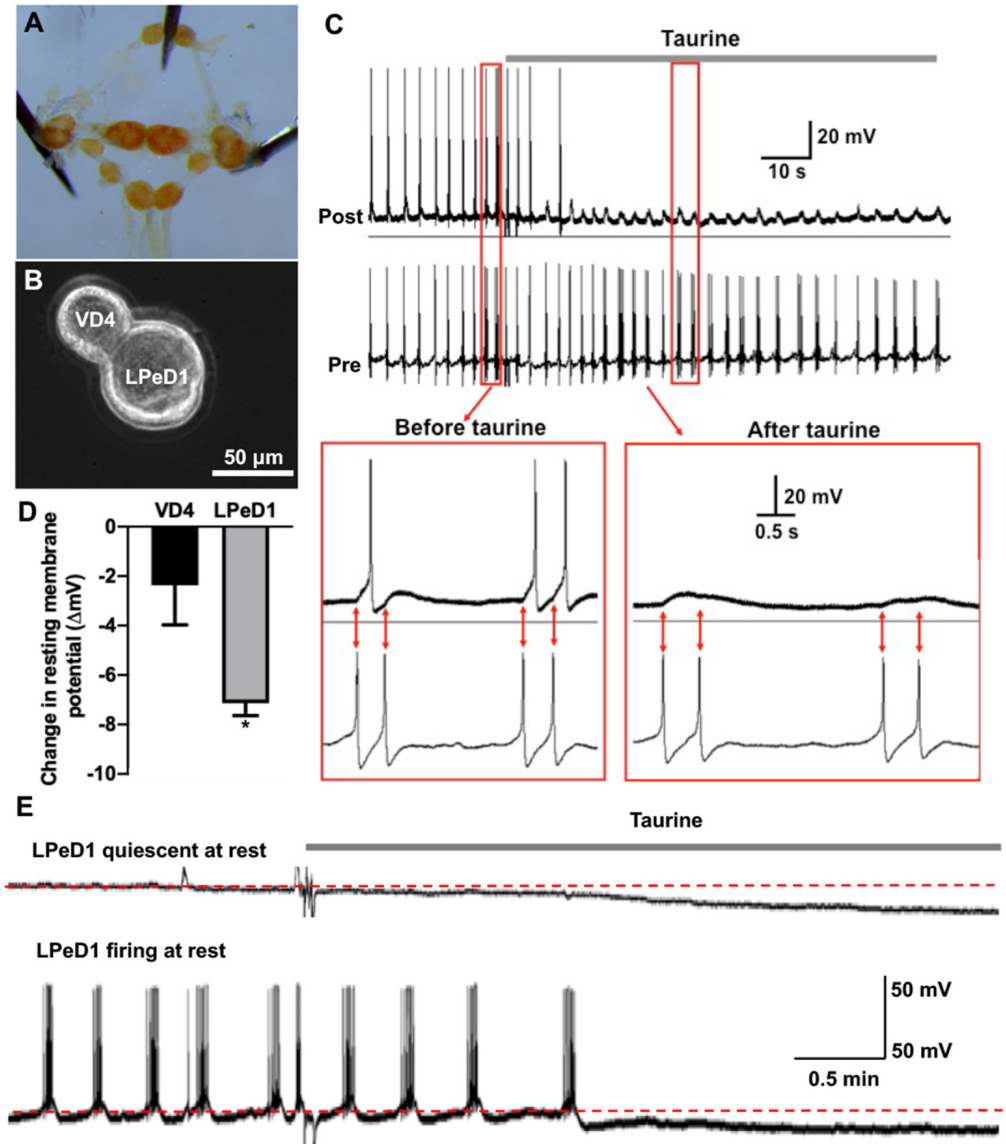

FIGURE 5 | Acute exposure of *Lymnaea* central neurons to taurine alters the excitability of two synapse-forming neurons. **(A)** *L. stagnalis* central ring ganglion was dissected. **(B)** To examine whether acute exposure to a high concentration of taurine affects neuronal excitability and/or synaptic transmission, well defined *L. stagnalis* pre- and postsynaptic VD4-LPeD1 neuronal pairs were cultured and allowed to form synapses ($n = 4$). **(C)** Intracellular recordings revealed that presynaptic action potentials elicited electrical activities in postsynaptic neurons, and these were quieted after exposure to taurine at 2.5 mM. Interestingly, the postsynaptic potentials (PSPs) remained throughout the presence of taurine, indicating that taurine can selectively modulate neural excitability change while allowing the synaptic transmission to occur between two synaptic neurons. **(D)** At rest, taurine caused a significantly larger hyperpolarizing membrane potential change (ΔmV) in LPeD1 neurons (7.14 ± 0.5 mV) than that in VD4 neurons (2.37 ± 1.6 mV; student *t*-test, $p = 0.049$; $n = 3$). Negative direction and Y-axis values indicate a hyperpolarizing action of taurine on the resting membrane potentials of VD4 and LPeD1. **(E)** The hyperpolarization in LPeD1 neurons occurred in either quiescent or actively firing LPeD1 cells. The dotted lines indicate basal membrane potential levels. *Indicates a significance level of $p < 0.05$.

of whether the role of taurine is evolutionally conserved between vertebrate and invertebrate nervous systems. With our above and previous evidence that taurine promotes the development of synaptic machinery in mammalian neurons (Shivaraj et al., 2012), we hypothesized that taurine would promote the functional development of synapses between *L. stagnalis* neurons, and its effect may be pre- or postsynaptic site-specific.

To test the above postulate, *Lymnaea* VD4 and LPeD1 cells were paired in the soma-soma configuration (**Figure 5B**) in the absence or presence of taurine overnight at 1 mM, a concentration that consistently promoted the development of rat cortical neurites and synaptic structures in the above experiments. The next day, intracellular recordings from both cells were made to determine synapse formation and synaptic transmission (representative recordings are shown

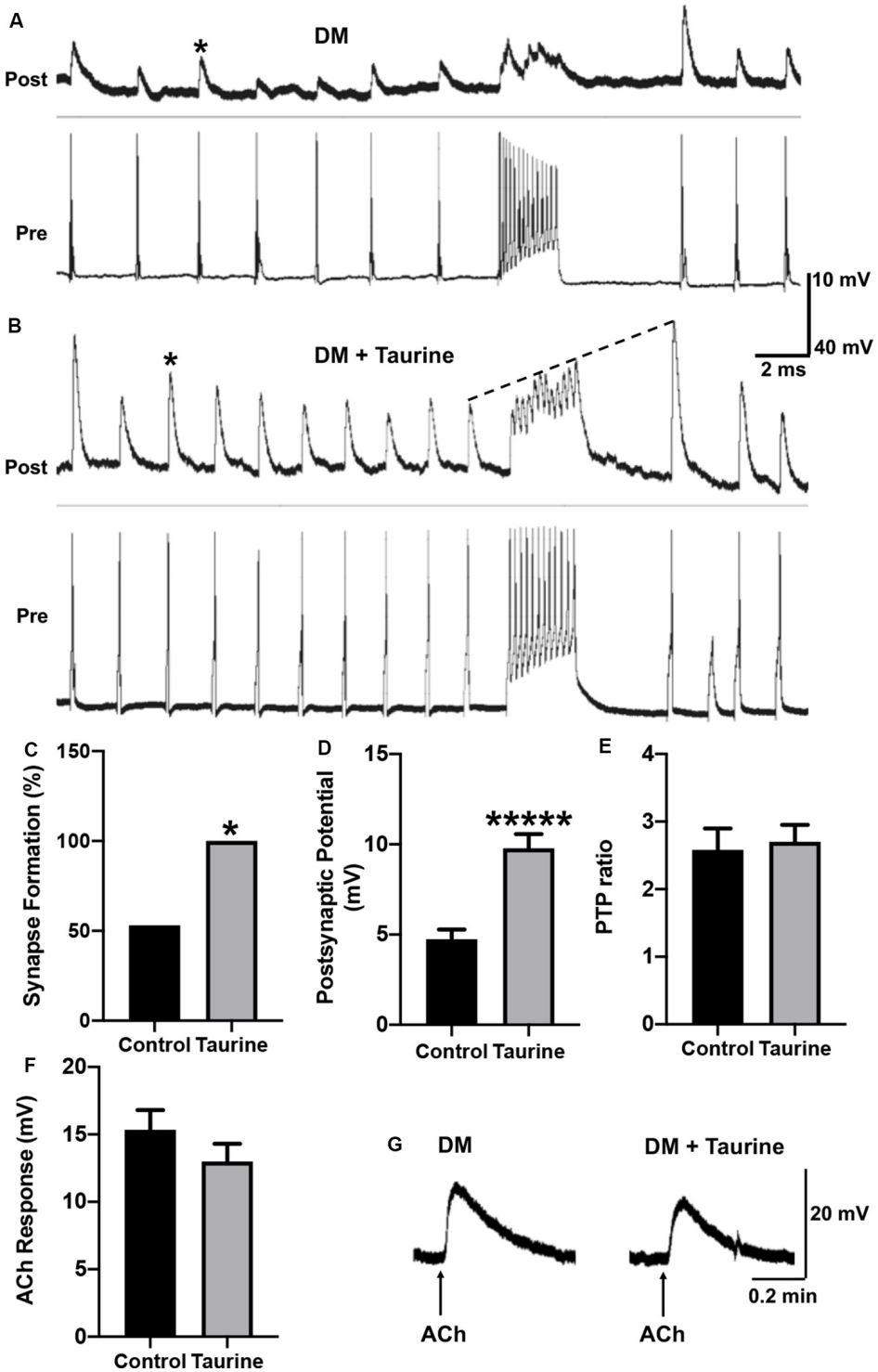

FIGURE 6 | Taurine enhances the development and strength of functional synapses between *L. stagnalis* central neurons but does not affect the postsynaptic response of exogenously applied transmitter. **(A,B)** Representative recordings show the responses of cell pairs cultured without taurine (control) and with 1 mM taurine. Asterisks denote peaks of PSPs. **(C)** Quantification of the incidence of synapse formation (reflected by the percent of cell pairs exhibiting 1:1 ratio of presynaptic action potential: postsynaptic cell PSPs) demonstrated that taurine enhances synaptic incidence. Specifically, 53% of control pairs formed synapses while 100% of 1 mM taurine-treated pairs formed synapses (n = 15 for control and n = 10 for 1 mM taurine; Fisher's exact test, p = 0.02019). **(D)** Statistical analyses of the efficacy of synaptic transmission (the mean amplitudes of PSPs) showed taurine significantly enhances synaptic transmission strength. The control PSP was 4.74 ± 0.54 mV and 1 mM taurine was 9.78 ± 0.79 mV (n = 8 for control and n = 10 for 1 mM taurine; student t-test, $p < 0.00001$). **(E)** Post-tetanic potentiation

(*Continued*)

FIGURE 6 | Continued
(PTP) ratio of postsynaptic potential before and after tetanic stimulation (PSP to pPSP ratio) was not significantly different between control neurons and neurons treated with taurine. The control PTP ratio was 2.58 ± 0.32 and 1 mM taurine was 2.7 ± 0.25 (n = 8 for control and n = 10 for 1 mM taurine; student t-test, p = 0.7684). The dotted line in B indicates an example of PTP in which the pPSP after high-frequency stimulation is higher than PSP before high-frequency stimulation. **(F)** To determine if taurine-induced increases in *Lymnaea* synaptogenesis and transmission involves the promotion of expression or function of postsynaptic transmitter receptors, LPeD1 cells were cultured in the absence or presence of taurine overnight. Intracellular recordings were made the next day and ACh (1 μM) was pressure-injected onto the cell bodies of LPeD1 while neurons were held at −100 mV. There was no significant difference between membrane potential responses in taurine-free (15.34 ± 1.46 mV; n = 17) and taurine-treated (12.99 ± 1.32 mV; n = 10) neurons (student t-test, p = 0.2393). **(G)** Examples of raw traces of postsynaptic membrane potential response to exogenously applied ACh in a neuron cultured in the absence or presence of taurine (1 mM). *Indicates a significance level of $p < 0.05$, and *****$p < 0.00001$.

in **Figures 6A,B**). Calculating the percentage of cell pairs forming functional synapses demonstrated that taurine significantly increased the incidence of synapse formation between cultured neurons (**Figure 6C**). The efficacy of synaptic transmission measured by the mean amplitudes of peak PSPs in response to presynaptic current injection-induced action potentials was also significantly increased in neurons cultured in taurine compared to neurons without taurine exposure (**Figure 6D**). Specifically, our data showed that neurons cultured in the absence of taurine (control) could form synapses in 53% (eight out of 15) of neurons, while all (100%, 10 out of 10) pairs of neurons cultured in 1 mM taurine formed synapses that exhibited robust PSPs (Fisher's exact test, p = 0.02). In cell pairs that formed synapses in the absence of taurine, the mean PSP amplitude was significantly smaller than those detected in taurine-treated neurons ($p < 0.00001$). These data indicate that taurine exerts synaptogenic effects by promoting not only the incidence of synaptogenesis (the increased percent of neuronal pairs that could form synapses) but also the efficacy of synaptic transmission (a single action potential induced a larger postsynaptic response) between individual pre- and postsynaptic neurons.

To further determine the possible role of taurine in synaptic plasticity, we also compared the amplitude of PSP to single presynaptic action potentials before and after a train of high-frequency action potential activity (tetanic stimulation, 10 Hz) in neural pairs cultured with or without taurine. A larger amplitude of action potential-triggered PSP after high-frequency stimulation (pPSP) than PSP before high-frequency stimulation (**Figure 6B**, indicated by the dotted line) is defined as PTP, a form of short-term synaptic plasticity. Our data showed that taurine did not affect the synaptic plasticity between single neurons (**Figure 6E**; p = 0.7684).

Now the question remains: Does taurine affect synaptic transmission by acting on the presynaptic transmitter release (ACh in this case) or postsynaptic nicotinic ACh receptor (nAChR) expression/response in *Lymnaea* neurons? To help answer this question, we conducted a functional analysis of postsynaptic nAChR response to exogenously applied ACh to mimic transmitter-receptor response *in vitro* (see "Materials and Methods" section). To this end, LPeD1 neurons were cultured either in the absence or presence of taurine at 1 mM overnight to allow for the expression of nAChRs. The next day, neurons were impaled with intracellular sharp electrodes, and ACh (1 μM) was pressure-injected onto LPeD1 cell bodies to monitor the change in membrane potentials (see "Materials and Methods" section and **Figures 6F,G**). Our results showed that neurons cultured in the presence of taurine did not exhibit a significant membrane potential change in response to ACh application compared to control neurons. Specifically, the mean amplitude of ACh-induced membrane potential in cells cultured in the absence of taurine was 15.33 ± 1.46 mV (n = 17) and in the presence of taurine was 12.99 ± 1.32 mV (n = 10), which was not statistically different (p = 0.2393). These data indicate that taurine-mediated increases in synaptogenesis and synaptic transmission does not involve the promotion of postsynaptic receptor expression/function and most likely involves action on the presynaptic site. However, this experiment cannot rule out the possibility that taurine may also regulate the clustering of postsynaptic receptors to the synaptic sites.

Taurine Effects on Synaptic Formation, Transmission, and Plasticity Are Comparable to Trophic Factors in Neurons From Invertebrate *Lymnaea*

Because taurine is considered a trophic factor during neuronal development (Sturman, 1993; Chen et al., 1998), we chose to study synaptic properties of *L. stagnalis* neurons that underwent taurine treatment in the presence of trophic factors to deduce if synergistic or additive effects exist. *L. stagnalis* cells were paired in the soma-soma configuration in the presence of medium containing *L. stagnalis* derived neurotrophic factors from *Lymnaea* brain CM, with (CM + taurine; 1 mM) or without taurine overnight. As described above, intercellular recordings (**Figures 7A,B**) were made from pre- and postsynaptic cells to determine synapse formation, synaptic transmission, and synaptic plasticity. While all (100%, five out of five) pairs of *L. stagnalis* cells formed functional synapses in the presence of CM + taurine, only 87.5% (7 out of 8) paired cells formed functional synapses when cultured in CM alone (**Figure 7C**; Fisher's exact test, p = 1). The mean PSP amplitude was not significantly different between cell pairs that formed synapses in CM alone or CM + taurine (**Figure 7D**; student t-test, p = 0.4107), while the PTP ratio of PSP before and after tetanic stimulation was increased in cell pairs cultured in CM + taurine as compared to cell pairs in CM alone (**Figure 7E**; student t-test, p = 0.4069). Synapse formation, synapse transmission, and synaptic plasticity were increased in the presence of taurine, though not to a statistically significant degree, indicating that taurine may act *via* the same or additional pathways as *L. stagnalis* derived neurotrophic factors present in CM.

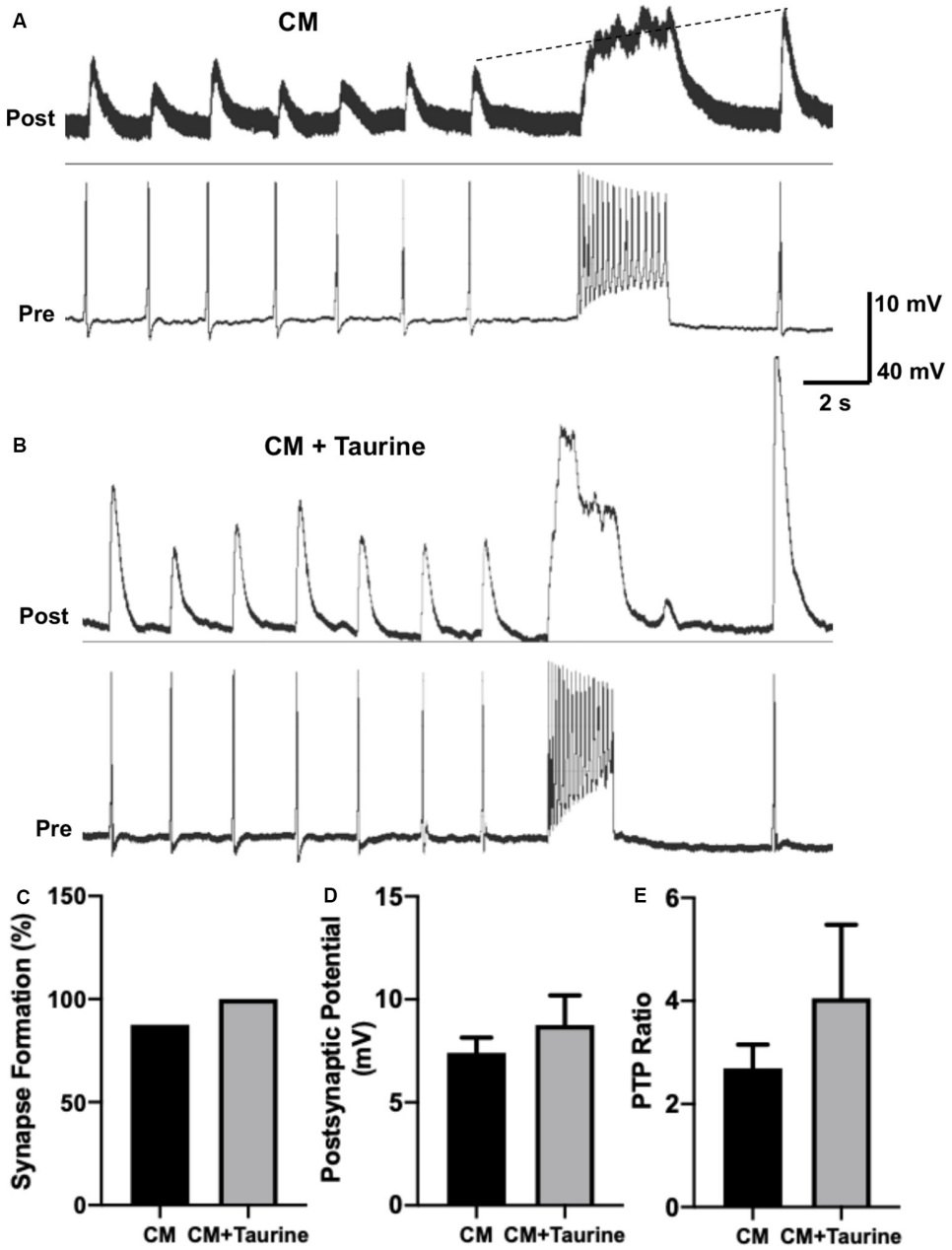

FIGURE 7 | Taurine nonsignificantly increases *L. stagnalis* neuron synapse formation, transmission, and plasticity in medium rich with trophic factors. *L. stagnalis* neurons were paired in a soma-soma configuration and cultured in medium containing *L. stagnalis* derived neurotrophic factors in *Lymnaea* brain conditioned medium (CM) alone or CM plus 1 mM taurine (CM + taurine). Intracellular recordings were made from the cell pairs. **(A,B)** Representative recordings show the responses of *L. stagnalis* cell pairs cultured in CM alone or CM + taurine. **(C)** Incidence of synapse formation was calculated as the percentage of cell pairs forming a 1:1 ratio of presynaptic action potential to postsynaptic PSP; cells cultured in CM + taurine formed strong synapses in all the pairs (100%) examined, while 87.5% of the pairs formed synapses in CM alone ($n = 5$ for CM and $n = 8$ for CM + taurine; Fisher's exact test, $p = 1$). **(D)** Average peak amplitudes of PSPs of cells cultured in CM + taurine was increased compared to cells cultured in CM alone. PSP in CM cultured cells was 7.40 ± 0.74 mV while PSP in CM + taurine cultured cells was 8.75 ± 1.44 mV ($n = 7$ for CM and $n = 5$ for CM + taurine; student *t*-test, $p = 0.4107$). **(E)** The ratio of postsynaptic potential before and after tetanic stimulation (PTP ratio) was larger in pairs cultured in CM + taurine than those cultured in CM alone, although this was not significant. PTP ratio for CM was 2.69 ± 0.46, and PTP ratio for CM + taurine was 4.05 ± 1.43 ($n = 7$ for CM, and $n = 5$ for CM + taurine; student *t*-test, $p = 0.4069$). The dotted line in **(A)** shows the increase in pPSP after high-frequency stimulation.

In summary, our *L. stagnalis* synapse study is supportive of our hypothesis that taurine plays an evolutionarily conserved role vis-à-vis synaptogenesis and synaptic transmission in both invertebrate and vertebrate neurons. Besides, our *Lymnaea* data also indicate that the effects of taurine were comparable to, but not significantly different from trophic factor effects on

synaptogenesis, synaptic transmission, and synaptic plasticity between individual *L. stagnalis* neurons.

DISCUSSION

Early neuronal development relies on many specific events, namely proliferation, migration, differentiation, and synaptogenesis, to achieve proper development of the nervous system. These steps rely on cellular cues such as neurotransmitter release, electrical activity, and binding of molecular ligands (Nguyen et al., 2001; Owens and Kriegstein, 2002; Munno and Syed, 2003; Spitzer, 2006; Batool et al., 2019). As one of the most abundant amino acids in the human body, it is no surprise that taurine has been linked to a variety of physiological functions including neuronal development (Huxtable, 1989; Kilb and Fukuda, 2017). Therefore, we sought to investigate the role of taurine in developing neurons of vertebrate and invertebrate brains. Our data provide the first direct evidence that taurine is a neuroactive substance that specifically impacts neuritic development and synaptic machinery expression and/or assembly, especially the presynaptic machinery. Using an invertebrate model, we demonstrated that acute exposure to taurine regulates neuronal excitability changes between two cultured *Lymnaea* neurons that form mature synapses. With more potent action on the postsynaptic neuron. Chronic (overnight) exposure to taurine at physiological concentrations enhances both the incidence and efficacy of synaptic transmission between two *Lymnaea* neurons, indicating taurine's *bona fide* synaptogenic function in neurons. Consistent with the cortical neuron synapse data, the chronic action of taurine in *Lymnaea* synapse development is of presynaptic origin. Together, these data demonstrate that taurine's morphogenic and synaptogenic functions are conserved in both invertebrate and vertebrate species, and taurine's effects are cell- and synaptic site-specific.

Taurine has been previously shown to promote neurogenesis and NPC proliferation in both developing and adult mouse brains. However, less is known about the effect of taurine on the development of neural processes. In embryonic day 18 (E18) rats, the addition of taurine on day 2 in the culture at 20 μM and 100 μM increased both the neurite length and the number of neurites in day 3 primary hippocampal cells, but not to a significant degree (Shivaraj et al., 2012). In our study, we added taurine at physiological concentrations of 50 μM and 1 mM on day 0 in culture, used postnatal rats (P0), and examined the effects on another brain region, cortical neurons *in vitro* after 3 days in culture. We found a significant enhancement in overall neuritic growth and the number of neurites. The difference in the observed taurine effects on neurites may be attributed to the following factors: difference in brain regions, age of rats during dissection, or taurine treatment protocol (day 0 vs. day 2 exposure). It is interesting that our data also revealed a significant increase in the thickness of primary neurites that were labeled by fluorescent staining of β-tubulin, which has not been reported previously. This increase in the thickness of primary neurites will lead to an increase in neuronal surface area for housing ionic channels/receptors and an increase in the efficiency of neural conductivity and synaptic transmission. Furthermore, our study found that taurine increased the number of cells in culture. This finding is consistent with a previous study showing that taurine treatment caused a significant increase in the number of cells and the length of neurites in primary cultured cochlear spiral ganglion cells (Rak et al., 2014). The increase in spiral ganglion cells was attributed to taurine-mediated neurotrophic effects of higher rates of cell survival of both neurons and glial cells (Rak et al., 2014). In our study, the overall number and length of neurites were increased by taurine, yet the length of neurites per cell was unaffected, further implying that the main function of taurine is enhancing neuronal survival in dissociated cell cultures. While these results suggest a neurotrophic role for taurine in cell survival, it is not known if the increase in cell density we observed is also due to other factors such as a higher rate of adhesion or glial cell proliferation. However, a study by Shivaraj et al. (2012) found that taurine did not affect the number of differentiated glial cells in their hippocampal culture using a specific fluorescent marker of glial fibrillary acidic protein. Nevertheless, it would be interesting to study these possibilities in our future cortical cell culture experiments.

Our data are in fact in agreement with the study by Shivaraj et al. (2012) showing that 100 μM taurine increased synapsin 1, a presynaptic marker, and PSD95 expression in primary mouse hippocampal neurons. Unfortunately, their study only provided evidence of protein level increases using western blotting methods. It, therefore, remains unknown whether taurine affects the level of clustering of synaptic proteins at the single neuron-, neurite-, or network-levels. We took advantage of well-established methods such as SynQuant (Wang et al., 2020) and SynapCountJ (Mata et al., 2016) to analyze different synaptic parameters in entire images (networks) and primary neurites. We found that taurine not only regulated synaptic protein expression in networks but also their intensity in synaptic puncta along neurites. Intriguingly, taurine was more effective at promoting the expression of presynaptic synaptophysin protein than the postsynaptic PSD95 protein. More intriguingly, our exogenous transmitter ACh puff experiments strongly implicate a presynaptic working mechanism in *Lymnaea* synapse development. Our findings are thus consistent with a previous study revealing that taurine selectively acts on the presynaptic NMDA receptors (*via* glycine-binding sites) to potentiate NMDR-induced facilitation of axon excitability and field EPSP in rat hippocampal slices (Suarez and Solis, 2006). It is important to note here that synaptophysin is a ubiquitous, presynaptic marker of all types of synapses, while PSD95 is restricted mainly to glutamatergic synapses. Therefore, a possibility exists that taurine's presynaptic effects are not restricted solely to a single type of synapse, as it may affect both inhibitory and excitatory. Together, these data indicate that taurine has neurotrophic and synaptogenic effects on developing vertebrate neurons, and taurine effects are more selective on the presynaptic sites.

Our data also revealed that taurine's effects are more robust and consistent at a higher concentration of 1 mM. It is important to note that concentrations of taurine have been revealed to vary widely between different brain regions and even between

pre- and postnatal animals (Palkovits et al., 1986; Miller et al., 2000). Therefore, the differences in the efficacy of taurine at various physiological concentrations seen in the data presented here and previous studies, particularly the E18 hippocampal culture by Shivaraj et al. (2012), is not entirely surprising. While our experiments focused on the effects of physiological levels of taurine on neurons, a recent study demonstrated that chronic exposure to extremely high concentrations of taurine (50 mM) induced cell apoptosis (Serdar et al., 2019), indicating that physiological levels and length of exposure are important factors in taurine's effects during early neural development. Also, the concentration effects of taurine have been found in taurine's actions on the regulation of neuronal excitability. For example, taurine has been reported to induce dose-dependent effects on immature hippocampal neurons in both excitatory and inhibitory directions (Chen et al., 2014; Winkler et al., 2019); it enhances neuronal excitability in the immature neocortex (Sava et al., 2014), while it exhibits a dominant, inhibitory effect on neuronal activity in the mature CNS (Kilb and Fukuda, 2017). Also, taurine at mM concentrations inhibits neuronal activity during anoxia in turtle central neurons *via* both glycine and $GABA_A$ receptors (Miles et al., 2018). Consistently, our data indicate that taurine at mM concentrations could also negatively regulate neuronal firing activity in *Lymnaea* neurons (**Figure 5C**) in a cell-specific manner.

In *Lymnaea*, a previous study focusing on taurine's effect on electrically regulated ionic currents revealed that taurine at mM concentrations decreased Na^+ currents (hence may reduce firing), yet at low concentrations (100 nM to 100 μM) increased Na^+ currents (Vislobokov et al., 1991). It is not known if the concentration-dependent effects of taurine on *L. stagnalis* neurons contributed to our observed synapse formation and neuronal activity regulation. For example, the increase of Na^+ current by lower concentrations of taurine may increase cell excitability and subsequently cause intracellular calcium transients, which is the causal factor of neurotrophic factor-induced synaptogenesis between *Lymnaea* neurons (Xu et al., 2009), while high concentrations of taurine may inhibit Na^+ currents and reduce neural excitability as seen in our acute exposure experiments (**Figure 5C**). It is, however, important to note that taurine immediately and completely abolished action potential firing in the postsynaptic but not presynaptic neurons (**Figure 5C**), suggesting that inhibition of sodium currents alone may not be sufficient to explain the selective action of taurine on the postsynaptic neurons. It is well known that taurine is an agonist of $GABA_A$ and glycine receptors, activation of which can counterbalance the neuronal excitability (Herbison and Moenter, 2011; Komm et al., 2014; Kilb and Fukuda, 2017; Ochoa-de la Paz et al., 2019). Thus, taurine may reduce cell excitability potentially *via* $GABA_A$ receptors that are expressed in *L. stagnalis* central neurons (Harvey et al., 1991; Darlison et al., 1993). Despite the unknown mechanism, our studies, together with others, clearly indicate that taurine acts as an active neuromodulator that is involved in regulating neuronal membrane excitability. The selective inhibition of postsynaptic excitability leads to a less likelihood of synchronized firing of action potentials between pre- and postsynaptic neurons that form excitatory synapses (such as the cholinergic synapses in our study, **Figure 5C**). More importantly, our data indicate that the hyperpolarization of postsynaptic neurons did not exclude the ability for presynaptic neurons to release transmitter and communicate with the postsynaptic neurons. These reveal novel insights into the role of taurine as a neuromodulator and neuroprotector to aid the interplay between membrane excitability and synaptic transmission, achieving optimal homeostasis of network activity in the nervous system.

Our data show that there is a conserved role of taurine between vertebrates and invertebrates to increase synapse development. Specifically, our data, for the first time, revealed the positive effect of taurine on the percentage of neurons that could form functional synapses and the robustness of synaptic transmission between individual partner neurons. While taurine's effect on the formation of functional synapses in invertebrate neurons is novel, increases in synaptic transmission have been reported in rat hippocampal slices after treatment with taurine (Galarreta et al., 1996). The effect of taurine on synapses is conserved between vertebrates and invertebrates, further providing evidence that *L. stagnalis* is a good model for studying the roles and cellular mechanisms of taurine on synapses that prove challenging in the mammalian brain.

Taurine has previously been linked to synaptic plasticity, particularly long-term potentiation (LTP), with conflicting results. The addition of taurine mitigated synaptic plasticity impairment in one study (Yu et al., 2007) but failed to alter late-LTP induction in another (Suarez et al., 2016). As a compound with structural similarities to GABA and a partial agonist of $GABA_A$ receptors, taurine begs the question of whether it can act on GABA receptors to induce synaptic LTP, as LTP is a previously established characteristic of GABAergic synapses (Gaiarsa et al., 2002; Ochoa-de la Paz et al., 2019). Interestingly, one study reported the ability of taurine to induce LTP in rat hippocampal slices, and the action was independent of $GABA_A$ and glutamate receptor activation but relied on the presence of calcium (del Olmo N. et al., 2000; del Olmo N. D. et al., 2000). While taurine's effects have been linked to LTP, we sought to determine if taurine affects short-term PTP in *L. stagnalis* central neurons. The addition of taurine alone did not alter synaptic plasticity PTP in *L. stagnalis* neurons. However, when taurine was added in combination with trophic factor-rich *Lymnaea* brain CM, synaptic plasticity increased more than *Lymnaea* trophic factors alone, although it did not reach a significant level. These findings might be the result of taurine's ability to reduce neuronal excitability in concentration-dependent manners as mentioned above. Nevertheless, it is important to note that although synaptic plasticity did not increase significantly between the two individual central neurons we recorded from, this does not mean that synapses among many neurons together cannot exhibit synaptic plasticity after addition of taurine. We found that synaptic puncta and synaptic strength were increased after the addition of taurine, and a possibility still exists that the effect of many neurons within a network increasing synaptic

abilities can exhibit a combined effect of synaptic plasticity within the network.

Taken together, our results demonstrate taurine as a stimulator of neuritogenesis and a regulator of synapses in vertebrates and invertebrates, and these effects are cell-specific. The discovery of the conserved developmental and synaptogenic actions of taurine in the *L. stagnalis* nervous system will open research avenues exploring the cellular, molecular, and synaptic mechanisms of taurine's actions using *L. stagnalis* and other invertebrate models. Particularly, these models accelerate our ability to study molecular mechanisms underlying taurine effects on growth and synapse development between single neurons *in vitro* in the absence of confounding factors including glia and taurine's analogous transmitters GABA and glycine. Such knowledge is fundamental for future efforts in targeting taurine as a therapeutic agent.

DATA AVAILABILITY STATEMENT

The raw data supporting the conclusions of this article will be made available by the authors, without undue reservation, to any qualified researcher.

ETHICS STATEMENT

The animal study was reviewed and approved by Institutional Animal Care and Use Policy at the University of Calgary and the Institutional Animal Care and Use Policy at Saint Louis University.

AUTHOR CONTRIBUTIONS

BM, FX, and NS designed the study. BM, WZ, and FX performed all experiments. BM and FX performed data analysis, created the figures and wrote the manuscript. BM, WZ, NS, and FX revised and edited the manuscript.

FUNDING

This work was supported by the National Science Foundation (1916563) and the Saint Louis University Start-up Fund to Dr. FX, the Sigma Xi Grants-In-Aid of Research (G2017031593402535) to Ms. BM, and the Canadian Institute of Health Research (CIHR, 64030-60-28350-10015088-00000) to Dr. NS.

REFERENCES

Albrecht, J., and Schousboe, A. (2005). Taurine interaction with neurotransmitter receptors in the CNS: an update. *Neurochem. Res.* 30, 1615–1621. doi: 10.1007/s11064-005-8986-6

Allen, J. A., and Garrett, M. R. (1971). Taurine in marine invertebrates. *Adv. Marine Biol.* 9, 205–253. doi: 10.1016/s0065-2881(08)60343-0

Banay-Schwartz, M., Lajtha, A., and Palkovits, M. (1989). Changes with aging in the levels of amino acids in rat CNS structural elements. II. Taurine and small neutral amino acids. *Neurochem. Res.* 14, 563–570. doi: 10.1007/bf00964919

Batool, S., Raza, H., Zaidi, J., Riaz, S., Hasan, S., and Syed, N. I. (2019). Synapse formation: from cellular and molecular mechanisms to neurodevelopmental and neurodegenerative disorders. *J. Neurophysiol.* 121, 1381–1397. doi: 10.1152/jn.00833.2018

Benitez-Diaz, P., Miranda-Contreras, L., Mendoza-Briceno, R. V., Pena-Contreras, Z., and Palacios-Pru, E. (2003). Prenatal and postnatal contents of amino acid neurotransmitters in mouse parietal cortex. *Dev. Neurosci.* 25, 366–374. doi: 10.1159/000073514

Buckett, K. J., Peters, M., and Benjamin, P. R. (1990). Excitation and inhibition of the heart of the snail, Lymnaea, by non-FMRFamidergic motoneurons. *J. Neurophysiol.* 63, 1436–1447. doi: 10.1152/jn.1990.63.6.1436

Chen, W. Q., Jin, H., Nguyen, M., Carr, J., Lee, Y. J., Hsu, C. C., et al. (2001). Role of taurine in regulation of intracellular calcium level and neuroprotective function in cultured neurons. *J. Neurosci. Res.* 66, 612–619. doi: 10.1002/jnr.10027

Chen, R., Okabe, A., Sun, H., Sharopov, S., Hanganu-Opatz, I. L., Kolbaev, S. N., et al. (2014). Activation of glycine receptors modulates spontaneous epileptiform activity in the immature rat hippocampus. *J. Physiol.* 592, 2153–2168. doi: 10.1113/jphysiol.2014.271700

Chen, X. C., Pan, Z. L., Liu, D. S., and Han, X. (1998). Effect of taurine on human fetal neuron cells: proliferation and differentiation. *Adv. Exp. Med. Biol.* 442, 397–403. doi: 10.1007/978-1-4899-0117-0_49

Clifford, E. L., Varela, M. M., De Corte, D., Bode, A., Ortiz, V., Herndl, G. J., et al. (2019). Taurine is a major carbon and energy source for marine prokaryotes in the north atlantic ocean off the iberian peninsula. *Microb. Ecol.* 78, 299–312. doi: 10.1007/s00248-019-01320-y

Darlison, M. G., Hutton, M. L., and Harvey, R. J. (1993). Molluscan ligand-gated ion-channel receptors. *EXS* 63, 48–64. doi: 10.1007/978-3-0348-7265-2_3

Das, J., Ghosh, J., Manna, P., and Sil, P. C. (2011). Taurine suppresses doxorubicin-triggered oxidative stress and cardiac apoptosis in rat *via* up-regulation of PI3-K/Akt and inhibition of p53, p38-JNK. *Biochem. Pharmacol.* 81, 891–909. doi: 10.1016/j.bcp.2011.01.008

del Olmo, N., Galarreta, M., Bustamante, J., Martin del Rio, R., and Solis, J. M. (2000). Taurine-induced synaptic potentiation: role of calcium and interaction with LTP. *Neuropharmacology* 39, 40–54. doi: 10.1016/s0028-3908(99)00078-7

del Olmo, N. D., Galarreta, M., Bustamante, J., Martin del Rio, R., and Solis, J. M. (2000). Taurine-induced synaptic potentiation: dependence on extra- and intracellular calcium sources. *Adv. Exp. Med. Biol.* 483, 283–292. doi: 10.1007/0-306-46838-7_31

El Idrissi, A., and Trenkner, E. (2004). Taurine as a modulator of excitatory and inhibitory neurotransmission. *Neurochem. Res.* 29, 189–197. doi: 10.1023/b:nere.0000010448.17740.6e

Furukawa, T., Yamada, J., Akita, T., Matsushima, Y., Yanagawa, Y., and Fukuda, A. (2014). Roles of taurine-mediated tonic GABAA receptor activation in the radial migration of neurons in the fetal mouse cerebral cortex. *Front. Cell. Neurosci.* 8:88. doi: 10.3389/fncel.2014.00088

Gaiarsa, J. L., Caillard, O., and Ben-Ari, Y. (2002). Long-term plasticity at GABAergic and glycinergic synapses: mechanisms and functional significance. *Trends Neurosci.* 25, 564–570. doi: 10.1016/s0166-2236(02)02269-5

Galarreta, M., Bustamante, J., Martin del Rio, R., and Solis, J. M. (1996). Taurine induces a long-lasting increase of synaptic efficacy and axon excitability in the hippocampus. *J. Neurosci.* 16, 92–102. doi: 10.1523/jneurosci.16-01-00092.1996

Gilles, R. (1972). Osmoregulation in three molluscs: *acanthochitona discrepans* (Brown), *glycymeris* (L.) and *Mytilus edulis* (L). *Biol. Bull.* 142, 25–35. doi: 10.2307/1540243

Harvey, R. J., Vreugdenhil, E., Zaman, S. H., Bhandal, N. S., Usherwood, P. N., Barnard, E. A., et al. (1991). Sequence of a functional invertebrate GABAA receptor subunit which can form a chimeric receptor with a vertebrate α subunit. *EMBO J.* 10, 3239–3245. doi: 10.1002/j.1460-2075.1991.tb04887.x

Herbison, A. E., and Moenter, S. M. (2011). Depolarising and hyperpolarising actions of GABA(A) receptor activation on gonadotrophin-releasing hormone neurones: towards an emerging consensus. *J. Neuroendocrinol.* 23, 557–569. doi: 10.1111/j.1365-2826.2011.02145.x

Hernandez-Benitez, R., Ramos-Mandujano, G., and Pasantes-Morales, H. (2012). Taurine stimulates proliferation and promotes neurogenesis of mouse adult

cultured neural stem/progenitor cells. *Stem Cell Res.* 9, 24–34. doi: 10.1016/j.scr.2012.02.004

Huxtable, R. J. (1989). Taurine in the central nervous system and the mammalian actions of taurine. *Prog. Neurobiol.* 32, 471–533. doi: 10.1016/0301-0082(89)90019-1

Imaninezhad, M., Pemberton, K., Xu, F., Kalinowski, K., Bera, R., and Zustiak, S. P. (2018). Directed and enhanced neurite outgrowth following exogenous electrical stimulation on carbon nanotube-hydrogel composites. *J. Neural Eng.* 15:056034. doi: 10.1088/1741-2552/aad65b

Jacobsen, J. G., and Smith, L. H. (1968). Biochemistry and physiology of taurine and taurine derivatives. *Physiol. Rev.* 48, 424–511. doi: 10.1152/physrev.1968.48.2.424

Jia, F., Yue, M., Chandra, D., Keramidas, A., Goldstein, P. A., Homanics, G. E., et al. (2008). Taurine is a potent activator of extrasynaptic GABA(A) receptors in the thalamus. *J. Neurosci.* 28, 106–115. doi: 10.3410/f.1099073.555272

Karanova, M. V. (2009). [Composition of free amino acids in blood and muscle of gobi Perccottus glehni at the period of preparation and completion of hibernation]. *Zh Evol Biokhim Fiziol* 45, 59–67. doi: 10.1134/S0022093009010062

Kilb, W., and Fukuda, A. (2017). Taurine as an essential neuromodulator during perinatal cortical development. *Front. Cell. Neurosci.* 11:328. doi: 10.3389/fncel.2017.00328

Koito, T., Saitou, S., Nagasaki, T., Yamagami, S., Yamanaka, T., Okamura, K., et al. (2018). Taurine-related compounds and other free amino acids in deep-sea hydrothermal vent and non-vent invertebrates. *Marine Biol.* 165:183. doi: 10.1007/s00227-018-3442-8

Komm, B., Beyreis, M., Kittl, M., Jakab, M., Ritter, M., and Kerschbaum, H. H. (2014). Glycine modulates membrane potential, cell volume and phagocytosis in murine microglia. *Amino Acids* 46, 1907–1917. doi: 10.1007/s00726-014-1745-8

Lange, R. (1963). The osmotic function of amino acids and taurine in the mussel, mytilus edulis. *Comp. Biochem. Physiol.* 10, 173–179. doi: 10.1016/0010-406x(63)90239-1

Luk, C. C., Naruo, H., Prince, D., Hassan, A., Doran, S. A., Goldberg, J. I., et al. (2011). A novel form of presynaptic CaMKII-dependent short-term potentiation between *Lymnaea* neurons. *Eur. J. Neurosci.* 34, 569–577. doi: 10.1111/j.1460-9568.2011.07784.x

Marcinkiewicz, J., and Kontny, E. (2014). Taurine and inflammatory diseases. *Amino Acids* 46, 7–20. doi: 10.1007/s00726-012-1361-4

Martincigh, B. S., Mundoma, C., and Simoyi, R. H. (1998). Antioxidant chemistry: hypotaurine-taurine oxidation by chlorite. *J. Phys. Chems. A* 102, 9838–9846. doi: 10.1021/jp982575c

Mata, G., Heras, J., Morales, M., Romero, A., and Rubio, J. (2016). "SynapCountJ: A tool for analyzing synaptic densities in neurons," in *Proceedings of the 9th International Joint Conference on Biomedical Engineering Systems and Technologies (BIOSTEC 2016)* (Rome: BIOSTEC), 41–55. doi: 10.1007/978-3-319-54717-6_3

McCaman, R., and Stetzler, J. (1977). Determination of taurine in individual neurones of *Aplysia californica*. *J. Neurochem.* 29, 739–741. doi: 10.1111/j.1471-4159.1977.tb07793.x

Meems, R., Munno, D., van Minnen, J., and Syed, N. I. (2003). Synapse formation between isolated axons requires presynaptic soma and redistribution of postsynaptic AChRs. *J. Neurophysiol.* 89, 2611–2619. doi: 10.1152/jn.00898.2002

Meijering, E., Jacob, M., Sarria, J. C., Steiner, P., Hirling, H., and Unser, M. (2004). Design and validation of a tool for neurite tracing and analysis in fluorescence microscopy images. *Cytometry A* 58, 167–176. doi: 10.1002/cyto.a.20022

Miles, A. R., Hawrysh, P. J., Hossein-Javaheri, N., and Buck, L. T. (2018). Taurine activates glycine and GABAA receptor currents in anoxia-tolerant painted turtle pyramidal neurons. *J. Exp. Biol.* 221:jeb181529. doi: 10.1242/jeb.181529

Miller, T. J., Hanson, R. D., and Yancey, P. H. (2000). Developmental changes in organic osmolytes in prenatal and postnatal rat tissues. *Comp. Biochem. Physiol. A Mol. Integr. Physiol.* 125, 45–56. doi: 10.1016/s1095-6433(99)00160-9

Munno, D. W., and Syed, N. I. (2003). Synaptogenesis in the CNS: an odyssey from wiring together to firing together. *J. Physiol.* 552, 1–11. doi: 10.1113/jphysiol.2003.045062

Nguyen, L., Rigo, J. M., Rocher, V., Belachew, S., Malgrange, B., Rogister, B., et al. (2001). Neurotransmitters as early signals for central nervous system development. *Cell Tissue Res.* 305, 187–202. doi: 10.1007/s004410000343

Niu, X., Zheng, S., Liu, H., and Li, S. (2018). Protective effects of taurine against inflammation, apoptosis, and oxidative stress in brain injury. *Mol. Med. Rep.* 18, 4516–4522. doi: 10.3892/mmr.2018.9465

Ochoa-de la Paz, L., Zenteno, E., Gulias-Canizo, R., and Quiroz-Mercado, H. (2019). Taurine and GABA neurotransmitter receptors, a relationship with therapeutic potential? *Expert Rev. Neurother.* 19, 289–291. doi: 10.1080/14737175.2019.1593827

Owens, D. F., and Kriegstein, A. R. (2002). Developmental neurotransmitters? *Neuron* 36, 989–991. doi: 10.1016/s0896-6273(02)01136-4

Palkovits, M., Elekes, I., Lang, T., and Patthy, A. (1986). Taurine levels in discrete brain nuclei of rats. *J. Neurochem.* 47, 1333–1335. doi: 10.1111/j.1471-4159.1986.tb00761.x

Pemberton, K., Mersman, B., and Xu, F. (2018). Using ImageJ to assess neurite outgrowth in mammalian cell cultures: research data quantification exercises in undergraduate neuroscience lab. *J. Undergrad. Neurosci. Educ.* 16, A186–A194.

Rak, K., Volker, J., Jurgens, L., Scherzad, A., Schendzielorz, P., Radeloff, A., et al. (2014). Neurotrophic effects of taurine on spiral ganglion neurons *in vitro*. *Neuroreport* 25, 1250–1254. doi: 10.1097/wnr.0000000000000254

Ridgway, R. L., Syed, N. I., Lukowiak, K., and Bulloch, A. G. (1991). Nerve growth factor (NGF) induces sprouting of specific neurons of the snail, *Lymnaea stagnalis*. *J. Neurobiol.* 22, 377–390. doi: 10.1002/neu.480220406

Ripps, H., and Shen, W. (2012). Review: taurine: a "very essential" amino acid. *Mol. Vis.* 18, 2673–2686.

Sava, B. A., Chen, R., Sun, H., Luhmann, H. J., and Kilb, W. (2014). Taurine activates GABAergic networks in the neocortex of immature mice. *Front. Cell. Neurosci.* 8:26. doi: 10.3389/fncel.2014.00026

Serdar, M., Mordelt, A., Muser, K., Kempe, K., Felderhoff-Muser, U., Herz, J., et al. (2019). Detrimental impact of energy drink compounds on developing oligodendrocytes and neurons. *Cells* 8:1381. doi: 10.3390/cells8111381

Shivaraj, M. C., Marcy, G., Low, G., Ryu, J. R., Zhao, X., Rosales, F. J., et al. (2012). Taurine induces proliferation of neural stem cells and synapse development in the developing mouse brain. *PLoS One* 7:e42935. doi: 10.1371/journal.pone.0042935

Smith, K. E., Borden, L. A., Wang, C. H., Hartig, P. R., Branchek, T. A., and Weinshank, R. L. (1992). Cloning and expression of a high affinity taurine transporter from rat brain. *Mol. Pharmacol.* 42, 563–569.

Smith, L. H., and Pierce, S. K. (1987). Cell volume regulation by molluscan erythrocytes during hypoosmotic stress: Ca^{2+} effects on ionic and organic osmolyte effluxes. *Biol. Bull.* 172, 407–418. doi: 10.2307/1541553

Solis, J. M., Herranz, A. S., Herreras, O., Lerma, J., and Martin del Rio, R. (1988). Does taurine act as an osmoregulatory substance in the rat brain? *Neurosci. Lett.* 91, 53–58. doi: 10.1016/0304-3940(88)90248-0

Spitzer, N. C. (2006). Electrical activity in early neuronal development. *Nature* 444, 707–712. doi: 10.1038/nature05300

Sturman, J. A. (1993). Taurine in development. *Physiol. Rev.* 73, 119–147. doi: 10.1152/physrev.1993.73.1.119

Sturman, J. A., Moretz, R. C., French, J. H., and Wisniewski, H. M. (1985). Taurine deficiency in the developing cat: persistence of the cerebellar external granule cell layer. *J. Neurosci. Res.* 13, 405–416. doi: 10.1002/jnr.490130307

Suarez, L. M., Munoz, M. D., Martin Del Rio, R., and Solis, J. M. (2016). Taurine content in different brain structures during ageing: effect on hippocampal synaptic plasticity. *Amino Acids* 48, 1199–1208. doi: 10.1007/s00726-015-2155-2

Suarez, L. M., and Solis, J. M. (2006). Taurine potentiates presynaptic NMDA receptors in hippocampal Schaffer collateral axons. *Eur. J. Neurosci.* 24, 405–418. doi: 10.1111/j.1460-9568.2006.04911.x

Syed, N. I., Bulloch, A. G., and Lukowiak, K. (1990). *In vitro* reconstruction of the respiratory central pattern generator of the mollusk Lymnaea. *Science* 250, 282–285. doi: 10.1126/science.2218532

Tomi, M., Tajima, A., Tachikawa, M., and Hosoya, K. (2008). Function of taurine transporter (Slc6a6/TauT) as a GABA transporting protein and its relevance to

GABA transport in rat retinal capillary endothelial cells. *Biochim. Biophys. Acta* 1778, 2138–2142. doi: 10.1016/j.bbamem.2008.04.012

Uchida, S., Kwon, H. M., Yamauchi, A., Preston, A. S., Marumo, F., and Handler, J. S. (1992). Molecular cloning of the cDNA for an MDCK cell Na(+)- and Cl(-)-dependent taurine transporter that is regulated by hypertonicity. *Proc. Natl. Acad. Sci. U S A* 89, 8230–8234. doi: 10.1073/pnas.89.17.8230

Vislobokov, A. I., Mantsev, V. V., Kopylov, A. G., and Gurevich, V. S. (1991). [The effect of taurine on the electrically controlled ion channels of the somatic membrane of pond snail neurons]. *Fiziol Zh SSSR Im I M Sechenova* 77, 37–42.

Vitvitsky, V., Garg, S. K., and Banerjee, R. (2011). Taurine biosynthesis by neurons and astrocytes. *J. Biol. Chem.* 286, 32002–32010. doi: 10.1074/jbc.m111.253344

Wang, Y., Wang, C., Ranefall, P., Broussard, G. J., Wang, Y., Shi, G., et al. (2020). SynQuant: an automatic tool to quantify synapses from microscopy images. *Bioinformatics* 36, 1599–1606. doi: 10.1093/bioinformatics/btz760

Welborn, J., and Manahan, D. (1995). Taurine metabolism in larvae of marine invertebrate molluscs (Bilvalvia, Gastropoda). *J. Exp. Biol.* 198, 1791–1799.

Winkler, P., Luhmann, H. J., and Kilb, W. (2019). Taurine potentiates the anticonvulsive effect of the GABAA agonist muscimol and pentobarbital in the immature mouse hippocampus. *Epilepsia* 60, 464–474. doi: 10.1111/epi.14651

Xu, F., Hennessy, D. A., Lee, T. K., and Syed, N. I. (2009). Trophic factor-induced intracellular calcium oscillations are required for the expression of postsynaptic acetylcholine receptors during synapse formation between *Lymnaea* neurons. *J. Neurosci.* 29, 2167–2176. doi: 10.1523/jneurosci.4682-08.2009

Yu, S. S., Wang, M., Li, X. M., Chen, W. H., Chen, J. T., Wang, H. L., et al. (2007). Influences of different developmental periods of taurine supplements on synaptic plasticity in hippocampal CA1 area of rats following prenatal and perinatal lead exposure. *BMC Dev. Biol.* 7:51. doi: 10.1186/1471-213x-7-51

Conflict of Interest: The authors declare that the research was conducted in the absence of any commercial or financial relationships that could be construed as a potential conflict of interest.

frontiers in Synaptic Neuroscience

MINI REVIEW
published: 21 August 2020
doi: 10.3389/fnsyn.2020.00034

Psychedelics as a Treatment for Alzheimer's Disease Dementia

Simon Andrew Vann Jones and Allison O'Kelly*

Cornwall Partnership NHS Foundation Trust, Liskeard, United Kingdom

Currently, there are no disease-modifying treatments for Alzheimer's disease (AD) or any other dementia subtype. The renaissance in psychedelic research in recent years, in particular studies involving psilocybin and lysergic acid diethylamide (LSD), coupled with anecdotal reports of cognitive benefits from micro-dosing, suggests that they may have a therapeutic role in a range of psychiatric and neurological conditions due to their potential to stimulate neurogenesis, provoke neuroplastic changes and reduce neuroinflammation. This inevitably makes them interesting candidates for therapeutics in dementia. This mini-review will look at the basic science and current clinical evidence for the role of psychedelics in treating dementia, especially early AD, with a particular focus on micro-dosing of the classical psychedelics LSD and psilocybin.

Keywords: psychedelic, Alzheimer's disease, dementia, plasticicity, microdosing

OPEN ACCESS

Edited by:
Christian Gonzalez-Billault, University of Chile, Chile

Reviewed by:
Yasmin Schmid, University Hospital of Basel, Switzerland
Charles D. Nichols, Louisiana State University, United States
Jaime Eduardo Hallak, University of São Paulo, Brazil

****Correspondence:***
Simon Andrew Vann Jones
s.vannjones@nhs.net

Received: *07 May 2020*
Accepted: *28 July 2020*
Published: *21 August 2020*

Citation:
Vann Jones SA and O'Kelly A (2020) Psychedelics as a Treatment for Alzheimer's Disease Dementia. Front. Synaptic Neurosci. 12:34. doi: 10.3389/fnsyn.2020.00034

INTRODUCTION

Globally an estimated 50 million people have a diagnosis of dementia and population prevalence continues to increase (Alzheimer's Society, 2019; UK Government Web Archive, 2020). Alzheimer's disease (AD) accounts for approximately 50–70% of cases (Draper, 2013).

AD is a progressive neurological disorder characterized by extracellular amyloid protein deposition and intracellular tau protein aggregates (tangles) that, in accumulation, are associated with a variety of pathological processes including microtubular damage, axonal transport disruption and, ultimately, cell death. The hippocampus, a key structure in the ability to learn and retain information and a site for neurogenesis, is particularly vulnerable to AD pathology and one of the earliest parts of the brain to be affected by the disease (Mu and Gage, 2011; Pilly and Grossberg, 2012; Setti et al., 2017).

Currently, there is a renaissance of research using psychedelics, potent 5HT2A receptor (5HT2A-R) agonists, in psychiatric and neurological disorders (Nichols, 2004; Halberstadt, 2015; Aday et al., 2020). The 5HT2A-R is found in high concentrations in regions of the brain vulnerable to dementia such as the prefrontal cortex and aforementioned hippocampus (Wood et al., 2012; Catlow et al., 2013; Bryson et al., 2017). Psychedelics induce brain plasticity and modify connectivity between brain regions and there is considerable anecdotal evidence of cognitive benefits from micro-dosing—a dose that does not cause perceptual change or impair functioning (Carhart-Harris et al., 2012; Wood et al., 2012; Catlow et al., 2013; Muthukumaraswamy et al., 2013; Zhang and Stackman, 2015; Griffiths et al., 2016; Carhart-Harris and Goodwin, 2017a; Carhart-Harris and Nutt, 2017; Johnstad, 2018; Fadiman and Korb, 2019; Kuypers et al., 2019; Lea et al., 2020a).

This mini-review will explore the role of classical psychedelics psilocybin and Lysergic acid diethylamide (LSD) in treating AD with a focus on sub-perceptual- or "micro"- dosing. Promoting neuroplasticity and neurogenesis *via* the 5HT2A-R in regions such as the hippocampus could theoretically help protect this and other brain structures and may, therefore, hold potential for treating AD.

COGNITIVE EFFECTS

High dose psilocybin reduces attention to both clinical and electrophysiological parameters. However, this may be due to an increased awareness of sensory stimuli that are usually filtered out (cost of attention) rather than reduced attentional ability *per se* (Carter et al., 2005; Bravermanová et al., 2018).

In younger adults, the only controlled studies of micro-dosing LSD to date (n = 20 and n = 24, respectively), both using a within-subjects design, found no effects either positive or negative on the cognitive function of healthy volunteers at different sub-perceptual doses (Bershad et al., 2019; Hutten et al., 2020). Participants had all previously experienced psychedelics. The former study used a placebo, 6.5, 13, and 26 μg, and the latter study placebo, 5, 10, or 20 μg. In the latter study, subjects had objective increases in psychomotor vigilance (and subjective happiness and mood scores) coupled with a paradoxical reduction in concentration and reduced set-shifting ability at the highest microdose (20 μg) hours after ingestion. Participants also reported subjectively greater productivity at 10 micrograms and no discernible subjective or objective differences at five micrograms compared to placebo (Hutten et al., 2020). Importantly, subjects were aware that they were on the active drug at the two higher doses and had the experience of recreational drug use.

A 2018 uncontrolled, open-label naturalistic trial found increased cognitive fluency, flexibility, and originality amongst the 33 participants at various micro-doses of psilocybin (Prochazkova et al., 2018). However, results should be interpreted with a degree of caution due to the risk of selection bias (the study was organized by the Dutch Psychedelic Society), a lack of a placebo control arm, risk of practice effect bias, and no intention-to-treat analysis.

In older adults, a recent double-blind placebo-controlled study in older adults (n = 48) who had not taken LSD for at least the past 5 years found no difference in the number of adverse events (including cognitive impairment) between those taking placebo, 5, 10, or 20 μg doses every 5 days for 28 days (Family et al., 2020). Headaches were reported more often in those taking LSD however the small number of participants and non-linear dose-response makes this difficult to interpret. In general, the medication was well tolerated with no serious adverse events or drop-outs.

LONGER-TERM EFFECTS

In rat models, 5HT2A-R activation with mid-dose psilocybin (0.13 mg/kg) enhances both prospective and retrospective learning with lesser effects at low-dose (0.06 mg/kg; Buchborn et al., 2014; Cini et al., 2019). Consecutive daily dosing diminished benefits, and older rodents learning was enhanced by an enriched environment (Buchborn et al., 2014).

An observational study of 89 recreational users micro-dosing psychedelics found self-reported improvement across multiple psychological domains, including creativity and attention, with a sustained improvement over 6 weeks (Polito and Stevenson, 2019). Studies of recreational micro-dosing, highly vulnerable to bias but arguably self-selecting for longer-term users, report improvement in cognitive focus and attention (14–61% of users; Anderson et al., 2019; Hutten et al., 2019; Lea et al., 2020b). However only one of these studies reported figures for the duration of use, with 60.5% of respondents using for 3 months of more (Lea et al., 2020b).

There have been no properly controlled studies of micro-dosing in cognitively impaired humans or effects on cognition or mood beyond the acute phase. However, studies of high dose LSD and psilocybin have shown long-term benefits on mood. A study of 16 healthy subjects showed subjective benefits of a single dose of 200 μg LSD 12 months later, with 10 participants rating the experience as one of the top 10 most meaningful of their lives (Schmid and Liechti, 2018). In 10 patients with a life-threatening disease, LSD-assisted psychotherapy reduced anxiety significantly, an effect that persisted 12-months after therapy in 77.7%. Two-thirds of the respondents also reported that the experience has improved their quality of life (Gasser et al., 2015).

Similar results have been observed following high dose psilocybin both in patients with anxiety related to life-threatening cancer, and cancer-related depression and anxiety (n = 51 and 29 respectively, both cross-over design; Griffiths et al., 2016; Ross et al., 2016). Both studies reported that approximately 60–80% of participants had a clinically significant response that was sustained some 6 months later. The latter study also followed up 4.5 years later and found that these results were sustained, with 71–100% of participants reporting the experience being one of the most meaningful of their lives (Agin-Liebes et al., 2020).

In treatment-resistant depression, 10 mg and 25 mg of psilocybin given 1 week apart (n = 20), led to clinical response or remission in 14 participants sustained at assessment 5 weeks later. This effect persisted at 6 months follow up despite no further treatment (Carhart-Harris et al., 2018).

These encouraging results have led, in part, to approval for a trial of high-dose psilocybin specifically targeting depression in early AD (Clinicaltrials.gov, 2020).

NEUROBIOLOGICAL EFFECTS

Specific 5HT2A-R polymorphisms impair verbal memory recall and object recognition and reduced 5HT2A-R density in areas of the brain responsible for key memory processes are associated with worse cognitive performance (Schott et al., 2011). Pre-task 5HT2A-R activation in mice enhances post-task hippocampal long-term potentiation and enables the re-consolidation of fear conditioning in the amygdala supporting a critical role in neuroplasticity (Catlow et al., 2013; Zhang et al., 2013). This effect can be reproduced in rats and rabbits by very low dose

psychedelics but is abolished by higher doses (Romano et al., 2010; Cameron et al., 2019).

In rats, 5HT2A-R activation stimulates neurogenesis and brain-derived neurotrophic factor (BDNF) expression in the neocortex but appears to consistently inhibit the same process in the hippocampus (Vaidya et al., 1997). This may be dose-dependent, with higher doses suppressing neurogenesis beyond a certain threshold. In cultured rat neurons, activation also stimulates dendritic spine proliferation and growth (Jones et al., 2009; Yoshida et al., 2011). In a mouse model of fear conditioning, both low and high dose psilocybin led to complete resolution of a cued fear response in animals that had been primed for a shock by an auditory tone (Catlow et al., 2013). This process was more rapid at lower doses where hippocampal neurogenesis was unimpaired. In rat cortical neuron cultures and drosophila larvae, LSD promotes neurogenesis and synaptogenesis in a dose-dependent manner suggesting both an important cross-species evolutionary pathway for this effect and that there may be an optimal dose to which it may be therapeutic for this purpose (Ly et al., 2018).

There is also likely to be an optimal dose spacing. Repeated administration of LSD and/or psilocybin leads to rapid tolerance, or tachyphylaxis, of mental effects from 24 h which peaks after just four consecutive daily doses, cannot be overcome even with substantial dose increases or switching to the other substance (cross-tolerance) and is completely reversed by 5 days of abstinence (Buchborn et al., 2016). In rats, high doses of LSD (0.16 mg/kg) given every 2 days for 90 days resulted in hyperactive and asocial symptoms (Martin et al., 2014). The aforementioned double-blind placebo-controlled safety study in older adults using a schedule of a dose every fourth day (Family et al., 2020). This may be optimal as tachyphylaxis is unlikely at this infrequency and, importantly, side effects were minimal and not significantly different to those on placebo.

NEUROPHYSIOLOGICAL EFFECTS

Human gamma frequency oscillations (30–100 Hz) within neuronal networks are important for communication between brain regions, particularly those involving attention and memory (Jensen et al., 2007; Verret et al., 2012; Mably and Colgin, 2018). These networks become disrupted decades before the onset of symptoms in AD, possibly linked to dysfunctional inhibitory interneurons leading to the disruption of the gamma-mediated temporal structure for cortical processing which allows for the coherent packaging of sensory information (Weber and Andrade, 2010; Palop and Mucke, 2016).

Studies in mild cognitive impairment and AD show contradictory results on levels of gamma activity with some showing an increase and others a decrease in vulnerable brain regions and networks (König et al., 2005; Van Deursen et al., 2008; Basar et al., 2017; Wang et al., 2017). However, a recent study found that gamma frequency response is slowed in response to stimulus in Alzheimer patients suggesting that the increase in gamma power seen in some studies with AD patients may the greater use of brain resources to maintain resting state (Basar et al., 2016). The same researchers found that long-distance gamma-related connectivity was heightened in AD patients compared to controls (Basar et al., 2017). It is possible that this increase in gamma activity is an initial response to brain failure but that this process is fatigable.

In recent studies, enhancing gamma frequency oscillations *via* external stimuli reduced amyloid burden, possibly *via* increased microglia activity, and improved cognitive function in rodents (Laccarino et al., 2016; Martorell et al., 2019). 5HT2A-R agonists enhance the power of gamma-frequency recordings suggesting a role for the 5HT2A-R both in mediating long-range projections and reducing focal Alzheimer's pathology (Puig et al., 2010; Athilingam et al., 2017).

NEUROIMAGING

In AD there is a reduction in global brain glucose metabolism which is marked in frontal and temporal-parietal areas (Garibotto et al., 2017; Rice and Bisdas, 2017). In the only psilocybin FDG-PET study to date, in healthy volunteers, acute ingestion of a 15 mg or 20 mg dose increased global brain glucose metabolism by approximately 25%, particularly in the frontal and medial temporal cortex (Vollenweider et al., 1997).

A 2019 fMRI study showed lasting benefits 4 months after a single dose of 315 μg/kg psilocybin in a group of 38 meditators (Smigielski et al., 2019). Acute MRI changes—reduced connectivity between self-perceiving medial prefrontal and ventral cingulate areas—were associated with positive changes at 4 months. A 2020 fMRI study involving 16 patients with depression who took a single dose of 10 mg of psilocybin and 25 mg a week later, found increased functional connectivity between the ventromedial prefrontal cortex and the default mode network in responders the day following treatment completion, with changes sustained 5 weeks post-dosing (Carhart-Harris et al., 2017b). Functional connectivity was increased between regions with high 5HT2A-R density suggesting that reorganizing of dysfunctional neural circuitry is an important component of the neuroplastic effects of 5HT2A-R agonists (Tagliazucchi et al., 2016; Deco et al., 2018).

Studies suggest that at least some of the antidepressant effect from psilocybin may be mediated *via* improved top-down control of the limbic system, which holds significant promise for impulse control and well-being in dementia where this control has diminished. In healthy adults, high-dose psilocybin (16 mg/kg and) has been shown to attenuate amygdala reactivity to emotional stimuli (Kraehenmann et al., 2015). In 19 adults with treatment-resistant depression, 10 mg and 25 mg psilocybin given a week apart, improved functional connectivity between the cortex and amygdala a day after the higher dose (Mertens et al., 2020). In another study, also in healthy adults, sub-perceptual doses of LSD (13 μg) was shown to significantly influence functional connectivity between the amygdala and other key regions within the limbic system suggesting 5HT2A-R mediated reorganization of more primitive networks is possible without profound acute perceptual changes, although whether these changes were lasting is unclear (Bershad et al., 2020).

These imaging studies reveal the potent reorganization of dysfunctional brain networks in affective and anxiety states.

Such changes may also yield improvements in cognition, mood, and behavior by ameliorating dysfunctional circuits in cognitive impairment and dementia.

ANTI-INFLAMMATORY MECHANISMS

All known genetic and environmental risk factors for AD are associated with increased inflammation, suggesting that reducing inflammation could be a target for preventing AD (Jones and Kounatidis, 2017). Psychedelics have been shown to have potent anti-inflammatory properties and, given their affinity for the 5HT2A-R, may represent a unique anti-inflammatory overwhelmingly targeted to brain tissue (Flanagan and Nichols, 2018).

In a rodent model of AD induced by chronic intracerebral inoculation of streptozotocin, 5HT1A- and 5HT2A-R agonists had a significant independent and synergistic neuroprotective effect in hippocampal neurons at 35 days *via* anti-apoptotic pathways (Shahidi et al., 2019). This neuroprotection infers activation of anti-inflammatory pathways, the corollary to this being that activation of 5HT2A-R in rodent neurons protects against reactive oxygen species (ROS) *via* the upregulation of neuroprotective Sirtuin 1 expression (Fanibunda et al., 2019). This pathway simultaneously stimulates mitochondrial biogenesis leading to greater availability of adenosine triphosphate and suggesting the potential for psychedelics to address impaired energy metabolism, another key pathological pathway to cognitive dysfunction in AD (Kapogiannis and Mattson, 2011).

DISCUSSION

After decades of repeated failure of treatments for dementia, there is an urgent need to develop new treatments for AD. The potential for psychedelic compounds to influence and enhance functional neuronal connectivity, stimulate neurogenesis, restore brain plasticity, reduce inflammation and enhance cognition provides a new therapeutic target and compelling argument for further investigation of the potential for psychedelics as a disease-modifying compound in conditions where currently none exists.

Animal models testing the neurobiological effects of psychedelic compounds have demonstrated hippocampal neurogenesis at lower doses and suppression at higher doses and potent neuroprotective properties. Studies in people suffering from depression and anxiety disorders have demonstrated lasting neuroplastic changes following just one or two large doses. This suggests a potential role for both sub-perceptual "micro"- and psychedelic-doses as a strategy for neuroprotection and cognitive enhancement in prodromal AD. For cognitive enhancement, the ideal dose and frequency have yet to be determined however the rapid desensitization of 5HT2A receptors by both psilocybin and LSD suggests that daily dosing is unlikely to be the optimal strategy.

Despite anecdotal evidence of widespread recreational use of micro-dosing for cognitive enhancement, robust scientific studies of the cognitive effects of micro-dosing in humans have so far been limited to acute changes in very small studies in cognitively normal individuals with no reports of persistent cognitive changes, either positive or negative, at psychedelic doses. Studies looking at both micro-dosing and psychedelic doses, longer-term, in cognitively impaired individuals are lacking and urgently needed.

AUTHOR CONTRIBUTIONS

SV came up with the idea for the review. Both SV and AO'K were involved in a review of the literature and writing and editing the final manuscript.

REFERENCES

Aday, J. S., Bloesch, E. K., and Davoli, C. C. (2020). Can psychedelic drugs attenuate age-related changes in cognition and affect? *J. Cogn. Enhan.* 4, 219–227. doi: 10.1007/s41465-019-00151-6

Agin-Liebes, G. I., Malone, T., Yalch, M. M., Mennenga, S. E., Ponté, K. L., Guss, J., et al. (2020). Long-term follow-up of psilocybin-assisted psychotherapy for psychiatric and existential distress in patients with life-threatening cancer. *J. Psychopharmacol.* 34, 155–166. doi: 10.1177/0269881119897615

Alzheimer's Society. (2019). *Demography*. Available online at: http://www.alzheimers.org.uk/site/scripts/documents_info.php?documentID=412. Accessed May 20, 2019.

Anderson, T., Petranker, R., Christopher, A., Rosenbaum, D., Weissman, C., Dinh-Williams, L. A., et al. (2019). Psychedelic microdosing benefits and challenges: an empirical codebook. *Harm Reduct. J.* 16:43. doi: 10.1186/s12954-019-0308-4

Athilingam, J. C., Ben-Shalom, R., Keeshen, C. M., Sohal, V. S., and Bender, K. J. (2017). Serotonin enhances excitability and γ frequency temporal integration in mouse prefrontal fast-spiking interneurons. *eLife* 6:e31991. doi: 10.7554/elife.31991.022

Basar, E., Emek-Savas, D. D., Güntekin, B., and Yener, G. G. (2016). Delay of cognitive γ responses in Alzheimer's disease. *Neuroimage Clin.* 11, 106–115. doi: 10.1016/j.nicl.2016.01.015

Basar, E., Femir, B., Emek-Savas, D. D., Güntekin, B., and Yener, G. G. (2017). Increased long distance event-related γ band connectivity in Alzheimer's disease. *Neuroimage Clin.* 14, 580–590. doi: 10.1016/j.nicl.2017.02.021

Bershad, A. K., Preller, K. H., Lee, R., Keedy, S., Wren-Jarvis, J., Bremmer, M. P., et al. (2020). Preliminary report on the effects of a low dose of LSD on resting state amygdalar functional connectivity. *Biol. Psychiatry Cogn. Neurosci. Neuroimaging* 5, 461–467. doi: 10.1016/j.bpsc.2019.12.007

Bershad, A. K., Schepers, S. T., Bremmer, M. P., Lee, R., and de Wit, H. (2019). Acute subjective and behavioral effects of microdoses of LSD in healthy human volunteers. *Biol. Psychiatry* 86, 792–800. doi: 10.1016/j.biopsych.2019.05.019

Bravermanová, A., Viktorinová, M., Tylš, F., Novák, T., Androvičová, R., Korčák, J., et al. (2018). Psilocybin disrupts sensory and higher order cognitive processing but not pre-attentive cognitive processing—study on P300 and mismatch negativity in healthy volunteers. *Psychopharmacology* 235, 491–503. doi: 10.1007/s00213-017-4807-2

Bryson, A., Carter, O., Norman, T., and Kanaan, R. (2017). 5-HT2A agonists: a novel therapy for functional neurological disorders? *Int. J. Neuropsychopharmacol.* 20, 422–427. doi: 10.1093/ijnp/pyx011

Buchborn, T., Grecksch, G., Dieterich, D. C., and Höllt, V. (2016). "Tolerance to lysergic acid diethylamide: overview, correlates, and clinical implications," in *Neuropathology of Drug Addictions and Substance Misuse*, ed. V. R. Preedy (San Diego, CA: Academic Press), 846–858.

Buchborn, T., Schröder, H., Höllt, V., and Grecksch, G. (2014). Repeated lysergic acid diethylamide in an animal model of depression: normalisation of learning behaviour and hippocampal serotonin 5-HT2 signalling. *J. Psychopharmacol.* 28, 545–552. doi: 10.1177/0269881114531666

Cameron, L. P., Benson, C. J., DeFelice, B. C., Fiehn, O., and Olson, D. E. (2019). Chronic, intermittent microdoses of the psychedelic *N*, *N*-Dimethyltryptamine (DMT) produce positive effects on mood and anxiety in rodents. *ACS Chem. Neurosci.* 10, 3261–3270. doi: 10.1021/acschemneuro.8b00692

Carhart-Harris, R. L., Bolstridge, M., Day, C. M., Rucker, J., Watts, R., Erritzoe, D. E., et al. (2018). Psilocybin with psychological support for treatment-resistant depression: six-month follow-up. *Psychopharmacology* 235, 399–408. doi: 10.1007/s00213-017-4771-x

Carhart-Harris, R. L., Erritzoe, D., Williams, T., Stone, J. M., Reed, L. J., Colasanti, A., et al. (2012). Neural correlates of the psychedelic state as determined by fMRI studies with psilocybin. *Proc. Natl. Acad. Sci. U S A* 109, 2138–2143. doi: 10.1073/pnas.1119598109

Carhart-Harris, R. L., and Goodwin, G. M. (2017a). The therapeutic potential of psychedelic drugs: past present and future. *Neuropsychopharmacology* 42, 2105–2113. doi: 10.1038/npp.2017.84

Carhart-Harris, R. L., Roseman, L., Bolstridge, M., Demetriou, L., Pannekoek, J. N., Wall, M. B., et al. (2017b). Psilocybin for treatment-resistant depression: fMRI-measured brain mechanisms. *Sci. Rep.* 7:13187. doi: 10.1038/s41598-017-13282-7

Carhart-Harris, R. L., and Nutt, D. J. (2017). Serotonin and brain function: a tale of two receptors. *J. Psychopharmacol.* 31, 1091–1120. doi: 10.1177/0269881117725915

Carter, O. L., Burr, D. C., Pettigrew, J. D., Wallis, G. M., Hasler, F., and Vollenweider, F. X. (2005). Using psilocybin to investigate the relationship between attention, working memory and the serotonin 1A and 2A receptors. *J. Cogn. Neurosci.* 17, 1497–1508. doi: 10.1162/089892905774597191

Catlow, B. J., Song, S., Paredes, D. A., Kirstein, C. L., and Sanchez-Ramos, J. (2013). Effects of psilocybin on hippocampal neurogenesis and extinction of trace fear conditioning. *Exp. Brain Res.* 228, 481–491. doi: 10.1007/s00221-013-3579-0

Cini, F. A., Ornelas, I., Marcos, E., Goto-Silva, L., Nascimento, J., Ruschi, S., et al. (2019). d-Lysergic acid diethylamide has major potential as a cognitive enhancer. *bioRxiv* [Preprint].doi: 10.1101/866814

Clinicaltrials.gov. (2020). *Psilocybin for Depression in People With Mild Cognitive Impairment or Early Alzheimer's Disease.* Available online at: https://clinicaltrials.gov/ct2/show/NCT04123314?term=psilocybinandcond=Alzheimer+Disease&draw=2&rank=1. Accessed June 24, 2020.

Deco, G., Cruzat, J., Cabral, J., Knudsen, G. M., Carhart-Harris, R. L., Whybrow, P. C., et al. (2018). Whole-brain multimodal neuroimaging model using serotonin receptor maps explains non-linear functional effects of LSD. *Curr. Biol.* 28, 3065.e6–3074.e6. doi: 10.1016/j.cub.2018.07.083

Draper, B. (2013). *Understanding Alzheimer's Disease and Other Dementias.* London: Jessica Kingsley.

Fadiman, J., and Korb, S. (2019). Might microdosing psychedelics be safe and beneficial? An initial exploration. *J. Psychoactive Drugs* 51, 118–122. doi: 10.1080/02791072.2019.1593561

Family, N., Maillet, E. L., Williams, L. T., Krediet, E., Carhart-Harris, R. L., Williams, T. M., et al. (2020). Safety, tolerability, pharmacokinetics, and pharmacodynamics of low dose lysergic acid diethylamide (LSD) in healthy older volunteers. *Psychopharmacology* 237, 841–853. doi: 10.1007/s00213-019-05417-7

Fanibunda, S. E., Deb, S., Maniyadath, B., Tiwari, P., Ghai, U., Gupta, S., et al. (2019). Serotonin regulates mitochondrial biogenesis and function in rodent cortical neurons via the 5-HT2A receptor and SIRT1-PGC-1α axis. *Proc. Natl. Acad. Sci. U S A* 116, 11028–11037.doi: 10.1073/pnas.1821332116

Flanagan, T. W., and Nichols, C. D. (2018). Psychedelics as anti-inflammatory agents. *Int. Rev. Psychiatry* 30, 363–375. doi: 10.1080/09540261.2018.1481827

Garibotto, V., Herholz, K., Boccardi, M., Picco, A., Varrone, A., Nordberg, A., et al. (2017). Clinical validity of brain fluorodeoxyglucose positron emission tomography as a biomarker for Alzheimer's disease in the context of a structured 5-phase development framework. *Neurobiol. Aging* 52, 183–195. doi: 10.1016/j.neurobiolaging.2016.03.033

Gasser, P., Kirchner, K., and Passie, T. (2015). LSD-assisted psychotherapy for anxiety associated with a life-threatening disease: a qualitative study of acute and sustained subjective effects. *J. Psychopharmacol.* 29, 57–68. doi: 10.1177/0269881114555249

Griffiths, R. R., Johnson, M. W., Carducci, M. A., Umbricht, A., Richards, W. A., Richards, B. D., et al. (2016). Psilocybin produces substantial and sustained decreases in depression and anxiety in patients with life-threatening cancer: a randomized double-blind trial. *J. Psychopharmacol.* 30, 1181–1197. doi: 10.1177/0269881116675513

Halberstadt, A. L. (2015). Recent advances in the neuropsychopharmacology of serotonergic hallucinogens. *Behav. Brain Res.* 277, 99–120. doi: 10.1016/j.bbr.2014.07.016

Hutten, N. R., Mason, N. L., Dolder, P. C., and Kuypers, K. P. (2019). Motives and side-effects of microdosing with psychedelics among users. *Int. J. Neuropsychopharmacol.* 22, 426–434. doi: 10.1093/ijnp/pyz029

Hutten, N., Mason, N., Dolder, P., Theunissen, E., Liechti, M., Feilding, A., et al. (2020). Cognitive and subjective effects of different low 'micro' doses of LSD in a placebo-controlled study. *Eur. Neuropsychopharmacol.* 31, S63–S64. doi: 10.1016/j.euroneuro.2019.12.086

Jensen, O., Kaiser, J., and Lachaux, J.-P. (2007). Human γ-frequency oscillations associated with attention and memory. *Trends Neurosci.* 30, 317–324. doi: 10.1016/j.tins.2007.05.001

Johnstad, P. G. (2018). Powerful substances in tiny amounts: an interview study of psychedelic microdosing. *Nordic Stud. Alcohol Drugs* 35, 39–51. doi: 10.1177/1455072517753339

Jones, S. V., and Kounatidis, I. (2017). Nuclear factor-κ B and Alzheimer disease, unifying genetic and environmental risk factors from cell to humans. *Front. Immunol.* 8:1805. doi: 10.3389/fimmu.2017.01805

Jones, K. A., Srivastava, D. P., Allen, J. A., Strachan, R. T., Roth, B. L., and Penzes, P. (2009). Rapid modulation of spine morphology by the 5-HT2A serotonin receptor through kalirin-7 signaling. *Proc. Natl. Acad. Sci. U S A* 106, 19575–19580. doi: 10.1073/pnas.0905884106

König, T., Prichep, L., Dierks, T., Hubl, D., Wahlund, L. O., John, E. R., et al. (2005). Decreased EEG synchronization in Alzheimer's disease and mild cognitive impairment. *Neurobiol. Aging* 26, 165–171. doi: 10.1016/j.neurobiolaging.2004.03.008

Kapogiannis, D., and Mattson, M. P. (2011). Disrupted energy metabolism and neuronal circuit dysfunction in cognitive impairment and Alzheimer's disease. *Lancet Neurol.* 10, 187–198. doi: 10.1016/S1474-4422(10)70277-5

Kraehenmann, R., Preller, K. H., Scheidegger, M., Pokorny, T., Bosch, O. G., Seifritz, E., et al. (2015). Psilocybin-induced decrease in amygdala reactivity correlates with enhanced positive mood in healthy volunteers. *Biol. Psychiatry* 78, 572–581. doi: 10.1016/j.biopsych.2014.04.010

Kuypers, K. P., Ng, L., Erritzoe, D., Knudsen, G. M., Nichols, C. D., Nichols, D. E., et al. (2019). Microdosing psychedelics: more questions than answers? An overview and suggestions for future research. *J. Psychopharmacol.* 33, 1039–1057. doi: 10.1177/0269881119857204

Laccarino, H. F., Singer, A. C., Martorell, A. J., Rudenko, A., Gao, F., Gillingham, T. Z., et al. (2016). γ frequency entrainment attenuates amyloid load and modifies microglia. *Nature* 540, 230–235. doi: 10.1038/nature20587

Lea, T., Amada, N., and Jungaberle, H. (2020a). Psychedelic microdosing: a subreddit analysis. *J. Psychoactive Drugs* 52, 101–112. doi: 10.1080/02791072.2019.1683260

Lea, T., Amada, N., Jungaberle, H., Schecke, H., and Klein, M. (2020b). Microdosing psychedelics: motivations, subjective effects and harm reduction. *Int. J. Drug Policy* 75:102600. doi: 10.1016/j.drugpo.2019.11.008

Ly, C., Greb, A. C., Cameron, L. P., Wong, J. M., Barragan, E. V., Wilson, P. C., et al. (2018). Psychedelics promote structural and functional neural plasticity. *Cell Rep.* 23, 3170–3182. doi: 10.1016/j.celrep.2018.05.022

Mably, A. J., and Colgin, L. L. (2018). γ oscillations in cognitive disorders. *Curr. Opin. Neurobiol.* 52, 182–187. doi: 10.1016/j.conb.2018.07.009

Martin, D. A., Marona-Lewicka, D., Nichols, D. E., and Nichols, C. D. (2014). Chronic LSD alters gene expression profiles in the mPFC relevant to schizophrenia. *Neuropharmacology* 83, 1–8. doi: 10.1016/j.neuropharm.2014.03.013

Martorell, A. J., Paulson, A. L., Suk, H. J., Abdurrob, F., Drummond, G. T., Guan, W., et al. (2019). Multi-sensory γ stimulation ameliorates Alzheimer's-associated pathology and improves cognition. *Cell* 177, 256–271. doi: 10.1016/j.cell.2019.02.014

Mertens, L. J., Wall, M. B., Roseman, L., Demetriou, L., Nutt, D. J., and Carhart-Harris, R. L. (2020). Therapeutic mechanisms of psilocybin: changes in amygdala and prefrontal functional connectivity during emotional processing

after psilocybin for treatment-resistant depression. *J. Psychopharmacol.* 34, 167–180. doi: 10.1177/0269881119895520

Mu, Y., and Gage, F. H. (2011). Adult hippocampal neurogenesis and its role in Alzheimer's disease. *Mol. Neurodegener.* 6:85. doi: 10.1186/1750-1326-6-85

Muthukumaraswamy, S. D., Carhart-Harris, R. L., Moran, R. J., Brookes, M. J., Williams, T. M., Errtizoe, D., et al. (2013). Broadband cortical desynchronization underlies the human psychedelic state. *J. Neurosci.* 33, 15171–15183. doi: 10.1523/JNEUROSCI.2063-13.2013

Nichols, D. E. (2004). Hallucinogens. *Pharmacol. Ther.* 101, 131–181. doi: 10.1016/j.pharmthera.2003.11.002

Palop, J. J., and Mucke, L. (2016). Network abnormalities and interneuron dysfunction in Alzheimer disease. *Nat. Rev. Neurosci.* 17, 777–792. doi: 10.1038/nrn.2016.141

Pilly, P. K., and Grossberg, S. (2012). How do spatial learning and memory occur in the brain? Coordinated learning of entorhinal grid cells and hippocampal place cells. *J. Cogn. Neurosci.* 24, 1031–1054. doi: 10.1162/jocn_a_00200

Polito, V., and Stevenson, R. J. (2019). A systematic study of microdosing psychedelics. *PLoS One* 14:e0211023. doi: 10.1371/journal.pone.0211023

Prochazkova, L., Lippelt, D. P., Colzato, L. S., Kuchar, M., Sjoerds, Z., and Hommel, B. (2018). Exploring the effect of microdosing psychedelics on creativity in an open-label natural setting. *Psychopharmacology* 235, 3401–3413. doi: 10.1007/s00213-018-5049-7

Puig, M. V., Watakabe, A., Ushimaru, M., Yamamori, T., and Kawaguchi, Y. (2010). Serotonin modulates fast-spiking interneuron and synchronous activity in the rat prefrontal cortex through 5-HT1A and 5-HT2A receptors. *J. Neurosci.* 30, 2211–2222. doi: 10.1523/JNEUROSCI.3335-09.2010

Rice, L., and Bisdas, S. (2017). The diagnostic value of FDG and amyloid PET in Alzheimer's disease—A systematic review. *Eur. J. Radiol.* 94, 16–24. doi: 10.1016/j.ejrad.2017.07.014

Romano, A. G., Quinn, J. L., Li, L., Dave, K. D., Schindler, E. A., Aloyo, V. J., et al. (2010). Intrahippocampal LSD accelerates learning and desensitizes the 5-HT 2A receptor in the rabbit. *Psychopharmacology* 212, 441–448. doi: 10.1007/s00213-010-2004-7

Ross, S., Bossis, A., Guss, J., Agin-Liebes, G., Malone, T., Cohen, B., et al. (2016). Rapid and sustained symptom reduction following psilocybin treatment for anxiety and depression in patients with life-threatening cancer: a randomized controlled trial. *J. Psychopharmacol.* 30, 1165–1180. doi: 10.1177/0269881116675512

Schmid, Y., and Liechti, M. E. (2018). Long-lasting subjective effects of LSD in normal subjects. *Psychopharmacology* 235, 535–545. doi: 10.1007/s00213-017-4733-3

Schott, B. H., Seidenbecher, C. I., Richter, S., Wüstenberg, T., Debska-Vielhaber, G., Schubert, H., et al. (2011). Genetic variation of the serotonin 2a receptor affects hippocampal novelty processing in humans. *PLoS One* 6:e15984. doi: 10.1371/journal.pone.0015984

Setti, S. E., Hunsberger, H. C., and Reed, M. N. (2017). Alterations in hippocampal activity and Alzheimer's disease. *Transl. Issues Psychol. Sci.* 3, 348–356. doi: 10.1037/tps0000124

Shahidi, S., Hashemi-Firouzi, N., Afshar, S., Asl, S. S., and Komaki, A. (2019). Protective effects of 5-ht1a receptor inhibition and 5-ht2a receptor stimulation against streptozotocin-induced apoptosis in the hippocampus. *Malays. J. Med. Sci.* 26, 40–51. doi: 10.21315/mjms2019.26.2.5

Smigielski, L., Scheidegger, M., Kometer, M., and Vollenweider, F. X. (2019). Psilocybin-assisted mindfulness training modulates self-consciousness and brain default mode network connectivity with lasting effects. *NeuroImage* 196, 207–215. doi: 10.1016/j.neuroimage.2019.04.009

Tagliazucchi, E., Roseman, L., Kaelen, M., Orban, C., Muthukumaraswamy, S. D., Murphy, K., et al. (2016). Increased global functional connectivity correlates with LSD-induced ego dissolution. *Curr. Biol.* 26, 1043–1050. doi: 10.1016/j.cub.2016.02.010

UK Government Web Archive. (2020). *The National Archives. Life Tables.* Available online at: http://www.ons.gov.uk/ons/rel/lifetables/historic-and-projected-data-from-the-period-and-cohort-life-tables/2012-based/stb-2012-based.html. Accessed January 2, 2020.

Vaidya, V. A., Marek, G. J., Aghajanian, G. K., and Duman, R. S. (1997). 5-HT2A receptor-mediated regulation of brain-derived neurotrophic factor mRNA in the hippocampus and the neocortex. *J. Neurosci.* 17, 2785–2795. doi: 10.1523/JNEUROSCI.17-08-02785.1997

Van Deursen, J. A., Vuurman, E. F., Verhey, F. R., van Kranen-Mastenbroek, V. H., and Riedel, W. J. (2008). Increased EEG γ band activity in Alzheimer's disease and mild cognitive impairment. *J. Neural Transm.* 115, 1301–1311. doi: 10.1007/s00702-008-0083-y

Verret, L., Mann, E. O., Hang, G. B., Barth, A. M., Cobos, I., Ho, K., et al. (2012). Inhibitory interneuron deficit links altered network activity and cognitive dysfunction in Alzheimer model. *Cell* 149, 708–721. doi: 10.1016/j.cell.2012.02.046

Vollenweider, F. X., Leenders, K. L., Scharfetter, C., Maguire, P., Stadelmann, O., and Angst, J. (1997). Positron emission tomography and fluorodeoxyglucose studies of metabolic hyperfrontality and psychopathology in the psilocybin model of psychosis. *Neuropsychopharmacology* 16, 357–372. doi: 10.1016/s0893-133x(96)00246-1

Wang, J., Fang, Y., Wang, X., Yang, H., Yu, X., and Wang, H. (2017). Enhanced γ activity and cross-frequency interaction of resting-state electroencephalographic oscillations in patients with Alzheimer's disease. *Front. Aging Neurosci.* 9:243. doi: 10.3389/fnagi.2017.00243

Weber, E. T., and Andrade, R. (2010). *Htr2a* gene and 5-HT^{2A} receptor expression in the cerebral cortex studied using genetically modified mice. *Front. Neurosci.* 4:36. doi: 10.3389/fnins.2010.00036

Wood, J., Kim, Y., and Moghaddam, B. (2012). Disruption of prefrontal cortex large scale neuronal activity by different classes of psychotomimetic drugs. *J. Neurosci.* 32, 3022–3031. doi: 10.1523/JNEUROSCI.6377-11.2012

Yoshida, H., Kanamaru, C., Ohtani, A., Li, F., Senzaki, K., and Shiga, T. (2011). Subtype specific roles of serotonin receptors in the spine formation of cortical neurons *in vitro*. *Neurosci. Res.* 71, 311–314. doi: 10.1016/j.neures.2011.07.1824

Zhang, G., Ásgeirsdóttir, H. N., Cohen, S. J., Munchow, A. H., Barrera, M. P., and Stackman, R. W. Jr. (2013). Stimulation of serotonin 2A receptors facilitates consolidation and extinction of fear memory in C57BL/6J mice. *Neuropharmacology* 64, 403–413. doi: 10.1016/j.neuropharm.2012.06.007

Zhang, G., and Stackman, R. W. Jr. (2015). The role of serotonin 5-HT2A receptors in memory and cognition. *Front. Pharmacol.* 6:225. doi: 10.3389/fphar.2015.00225

Conflict of Interest: The authors declare that the research was conducted in the absence of any commercial or financial relationships that could be construed as a potential conflict of interest.

frontiers in Synaptic Neuroscience

CORRECTION
published: 26 October 2020
doi: 10.3389/fnsyn.2020.607194

Corrigendum: Psychedelics as a Treatment for Alzheimer's Disease Dementia

Simon Andrew Vann Jones and Allison O'Kelly*

Cornwall Partnership NHS Foundation Trust, Liskeard, United Kingdom

Keywords: psychedelic, Alzheimer's disease, dementia, plasticicity, microdosing

OPEN ACCESS

Approved by:
Frontiers Editorial Office, Frontiers Media SA, Switzerland

***Correspondence:**
Simon Andrew Vann Jones
s.vannjones@nhs.net

Received: *16 September 2020*
Accepted: *17 September 2020*
Published: *26 October 2020*

Citation:
Vann Jones SA and O'Kelly A (2020) Corrigendum: Psychedelics as a Treatment for Alzheimer's Disease Dementia. Front. Synaptic Neurosci. 12:607194. doi: 10.3389/fnsyn.2020.607194

A Corrigendum on

Psychedelics as a Treatment for Alzheimer's Disease Dementia
by Vann Jones, S. A., and O'Kelly, A. (2020) Front. Synaptic Neurosci. 12:34. doi: 10.3389/fnsyn.2020.00034

In the original article, there was an error. In the "Neurophysiological effects" section, second paragraph, there was an error message in between two of the references: "Error! Bookmark not defined". All the references are present and correct.

A correction has been made to the "Neurophysiological effects" section, second paragraph. The sentence "Error! Bookmark not defined" has been removed.

The authors apologize for this error and state that this does not change the scientific conclusions of the article in any way. The original article has been updated.

frontiers in Synaptic Neuroscience

ORIGINAL RESEARCH
published: 30 October 2020
doi: 10.3389/fnsyn.2020.588785

The Requirement of the C-Terminal Domain of GluA1 in Different Forms of Long-Term Potentiation in the Hippocampus Is Age-Dependent

An Liu[1], Hong Ji[1], Qiaoyun Ren[1], Yanghong Meng[2], Haiwang Zhang[2,3], Graham Collingride[2], Wei Xie[1] and Zhengping Jia[2,3]**

[1]*The Key Laboratory of Developmental Genes and Human Disease, Ministry of Education, School of Life Science and Technology, Jiangsu Co-Innovation Center of Neuroregeneration, Southeast University, Nanjing, China,* [2]*Department of Physiology, Faculty of Medicine, University of Toronto, Toronto, ON, Canada,* [3]*Neurosciences and Mental Health, The Hospital for Sick Children, Toronto, ON, Canada*

Long-term potentiation (LTP) at glutamatergic synapses is an extensively studied form of long-lasting synaptic plasticity widely regarded as the cellular basis for learning and memory. At the CA1 synapse, there are multiple forms of LTP with distinct properties. Although AMPA glutamate receptors (AMPARs) are a key target of LTP expression, whether they are required in all forms of LTP remains unclear. To address this question, we have used our recently developed mouse line, GluA1^{C2KI}, where the c-terminal domain (CTD) of the endogenous GluA1 is replaced by that of GluA2. Unlike traditional GluA1 global or conditional KO mice, GluA1^{C2KI} mice have no changes in basal AMPAR properties or synaptic transmission allowing a better assessment of GluA1 in synaptic plasticity. We previously showed that these mice are impaired in LTP induced by high-frequency stimulation (HFS-LTP), but whether other forms of LTP are also affected in these mice is unknown. In this study, we compared various forms of LTP at CA1 synapses between GluA1^{C2KI} and wild-type littermates by using several induction protocols. We show that HFS-LTP is impaired in both juvenile and adult GluA1^{C2KI} mice. The LTP induced by theta-burst stimulation (TBS-LTP) is also abolished in juvenile GluA1^{C2KI} mice. Interestingly, TBS-LTP can still be induced in adult GluA1^{C2KI} mice, but its mechanisms are altered becoming more sensitive to protein synthesis and the extracellular signal-regulated kinase (ERK) inhibitors compared to wild type (WT) control. The GluA1^{C2KI} mice are also differentially altered in several forms of LTP induced under whole-cell recording paradigms. These results indicate that the CTD of GluA1 is differentially involved in different forms of LTP at CA1 synapse highlighting the complexity and adaptative potential of LTP expression mechanisms in the hippocampus.

Keywords: long-term potentiation, AMPA receptor, GluA1, C-terminal domain, high frequency stimulation, theta-burst stimulation, protein synthesis, ERK

Abbreviations: AMPARs, AMPA receptors; CaMKII, calcium/calmodulin-dependent protein kinase II; CTD, c-terminal domain; ERK, the extracellular signal-regulated kinase; fEPSP, field excitatory postsynaptic potential; EPSC, excitatory postsynaptic current; GluA1^{C2KI}, GluA1 CTD replaced by GluA2 CTD; KO, knock out; LTP, long-term potentiation; HFS, high-frequency stimulation; NMDARs, NMDA receptors; TBS, theta-burst stimulation; WT, wild type.

OPEN ACCESS

Edited by:
Fereshteh S. Nugent, Uniformed Services University, United States

Reviewed by:
Kari A. Johnson, Uniformed Services University of the Health Sciences, United States
Jung Hoon Shin, National Institute on Alcohol Abuse and Alcoholism (NIAAA), United States

****Correspondence:***
Wei Xie
wei.xie@seu.edu.cn
Zhengping Jia
zhengping.jia@sickkids.ca

Received: *29 July 2020*
Accepted: *25 September 2020*
Published: *30 October 2020*

Citation:
Liu A, Ji H, Ren Q, Meng Y, Zhang H, Collingride G, Xie W and Jia Z (2020) The Requirement of the C-Terminal Domain of GluA1 in Different Forms of Long-Term Potentiation in the Hippocampus Is Age-Dependent. Front. Synaptic Neurosci. 12:588785. doi: 10.3389/fnsyn.2020.588785

INTRODUCTION

Long-term potentiation (LTP) at glutamatergic synapses is an extensively studied form of synaptic plasticity widely regarded as key mechanisms for learning and memory (Bliss and Collingridge, 1993; Malenka and Bear, 2004; Kandel et al., 2014). LTP has been most intensively investigated at the Schaffer collateral-commissural projection between CA3 and CA1 pyramidal neurons of the hippocampus. At these synapses, NMDA receptor-dependent LTP (NMDAR-LTP) is triggered by the activation of NMDARs and subsequent Ca^{2+} influx into the postsynaptic spine (Collingridge et al., 1983; Bliss and Collingridge, 1993). However, how the activation of NMDARs leads to long-lasting enhancement in synaptic efficiency remains unclear. Many studies have shown that the trafficking of AMPA receptors (AMPARs) represents a key mechanism in the expression of LTP (Davies et al., 1989; Malinow and Malenka, 2002; Bredt and Nicoll, 2003; Collingridge et al., 2004; Malenka and Bear, 2004; Shepherd and Huganir, 2007; Kessels and Malinow, 2009; Anggono and Huganir, 2012; Henley and Wilkinson, 2016; Diering and Huganir, 2018). Also, *in vitro* studies using recombinant receptors and peptides have shown that the C-TERMINAL DOMAIN (CTD) of GluA1, but not of GluA2, is required for activity-dependent synaptic delivery of AMPARs and expression of LTP (Hayashi et al., 2000; Shi et al., 1999, 2001; Boehm et al., 2006; Kessels and Malinow, 2009).

Genetic manipulations of endogenous AMPARs in mice have provided a powerful approach to address the specific role of individual endogenous receptor subunits in synaptic regulation and behavior. In earlier studies, it was found that LTP was impaired in GluA1 KO mice (Zamanillo et al., 1999), but could be induced in GluA2 and GluA3 KO mice (Jia et al., 1996; Meng et al., 2003; Toyoda et al., 2007), supporting the unique contribution of GluA1 in LTP expression. A recent study using floxed GluA mice combined with the use of recombinant receptors demonstrated that LTP can be established in the absence of all major AMPAR subunits, suggesting that AMPARs may not be a primary site for LTP expression (Granger et al., 2013; Huganir and Nicoll, 2013; Henley and Wilkinson, 2016). However, it is difficult to conclusively interpret the data from these KO studies because they were altered in baseline AMPAR complex (e.g., formation aberrant homomeric receptors), channel properties, and synaptic transmission (Jia et al., 1996; Andrásfalvy et al., 2003; Meng et al., 2003; Sans et al., 2003; Biou et al., 2008; Asrar et al., 2009; Lu et al., 2009; Zhou et al., 2011; Granger et al., 2013; Cao et al., 2018). Therefore, the extent to which endogenous AMPARs are involved in LTP expression remains unclear, especially under normal physiological conditions where these receptors are present.

We have recently generated a knock-in (KI) mouse line, called GluA1^{C2KI}, where the CTD of endogenous GluA1 is replaced by that of GluA2 (Zhou et al., 2018). Unlike traditional GluA1 global or conditional KO mice, these mice have the expression of the GluA1 subunit, therefore avoiding the formation of the homomeric aberrant receptor complex. We have shown that GluA1^{C2KI} mice showed no impairments in AMPAR properties or long-term depression (LTD), but impairments in NMDAR-LTP induced by high-frequency stimulation (HFS, 100 Hz) in the hippocampal CA1 synapses. Because there are multiple forms of NMDAR-LTP at the CA1 synapse (Park et al., 2013), it is important to know whether the CTD of GluA1 equally contributes to these forms of LTP. Also, LTP mechanisms are subjected to developmental regulation (Yasuda et al., 2003; Palmer et al., 2004; Cao and Harris, 2012), therefore whether the involvement of GluA1 CTD also depends on the age of the animals is yet to be investigated. In this study, we compared hippocampal LTP induced by various protocols between GluA1^{C2KI} and their wild type (WT) littermates in both juvenile and young adult mice. We show that GluA1^{C2KI} mice are impaired in some, but not all forms of LTP, suggesting that the CTD of GluA1 differentially contributes to different forms of LTP.

MATERIALS AND METHODS

Housing, Maintenance, and Use of the Mice

The GluA1^{C2KI} mouse model, where the CTD of GluA1 is replaced by the CTD of GluA2, was generated by using standard homologous recombination techniques in embryonic stem cells as described previously (Zhou et al., 2018). The GluA1^{C2KI} homozygous and WT littermates used for the present study were obtained from GluA1^{C2KI} heterozygous breeders. Both male and female mice (sex-balanced) were used in the present study. They were housed (2–5 mice per cage) on a 12 h/12 h light/dark cycle with food and water *ad libitum*. All experimental procedures were conducted during the light cycle following the guidelines of the Canadian Council on Animal Care (CCAC) and approved by the Animal Care Committee at the Hospital for Sick Children, Canada, and Southeast University, China. All experiments were performed blind to the genotype of the mice, that is, the mice were coded by an independent investigator before the experimentation and decoded after the completion of the experiments for data grouping and analyses.

Slice Electrophysiology

All the electrophysiological recordings were done at the Schaffer collateral—commissural pathway in the hippocampus as previously described (Zhou et al., 2018). In brief, the mouse brains were removed and 360–400 μm brain slices prepared in ice-cold artificial cerebrospinal fluid (ACSF) saturated with 95% O_2/5% CO_2. ACSF contained (in mM): 120.0 NaCl, 3.0 KCl, 1.2 $MgSO_4$, 1.0 NaH_2PO_4, 26.0 $NaHCO_3$, 2.0 $CaCl_2$, and 11.0 D-glucose. The slices were recovered at 28°C for at least 2 h before a single slice was transferred to a submersion chamber constantly perfused with 95% O_2/5% CO_2 saturated ACSF. The perfusion flow rate was maintained constant at 2 ml/min. In whole-cell recordings, ACSF also contained 100 μM picrotoxin and the recorded CA1 neurons were identified using an infrared differential interference contrast microscope (Zeiss Axioscope or

Olympus X51). Synaptic response was elicited at 0.067 Hz for field potential recordings and 0.1 Hz for whole-cell currents, and recorded with glass pipettes (3–4 MΩ) filled with either ACSF (for field) or the intracellular solution (for whole-cell) containing (in mM) 130.0 $CsMeSO_4$, 5.0 NaCl, 1 $MgCl_2$, 0.05 EGTA, 10.0 HEPES, 3.0 Mg-ATP, 0.3 Na_3GTP, and 5.0 QX-314 (pH 7.5; 280–300 mOsm). For field recordings, HFS-LTP was induced by four trains of HFS (100 Hz, 1 s) with an inter-train interval of 10 s, and TBS-LTP was induced by four trains of theta burst stimulations (five pulses at 100 Hz every 200 ms) with an inter-train interval of 10 s. For whole-cell experiments, cells were clamped at −65 mV throughout the recording except during LTP induction stimuli. Whole-cell LTP was induced either by two trains of HFS (100 Hz, 1 s, with an inter-train interval of 10 s, delivered under a current-clamp mode; referred to as HFS-CC-LTP) or by a pairing protocol (2 Hz, 90 s, delivered under a holding potential of 0 mV; referred to as paired-LTP). The age of mice was 13–15 postnatal days for juvenile mice and 5–6 postnatal weeks for young adult mice. LTP was calculated and statistically evaluated by comparing the mean values of the last 10 min of the recording and the mean values of the entire baseline. The drugs used included: Picrotoxin (Sigma–Aldrich, #R284556), D-AP5 (Tocris, #0106), AG-126 (APExBIO, #C4338), KN62 (APExBIO, #A8180), Anisomycin (APExBIO, #B6674) and Cycloheximide (APExBIO, #A8244). The use of these drugs is indicated in specific figure legends and was added to ACSF during the entire period of recording.

Western Blot Analysis

Protein lysates were prepared from a hippocampal slice as previously described (Liu et al., 2016). Briefly, acute hippocampal slices were prepared, recovered, and treated with HFS or TBS in the same fashion as for electrophysiological recordings described above. Following the treatment, the slices were dissolved in ice-cold lysis buffer containing (in mM): 20 Tris-HCl (pH 7.5), 150 NaCl, 1 EDTA, 1 EGTA, 1% Triton X-100, 2.5 sodium pyrophosphate, 1 β-glycerophosphate, 1 Na_3VO_4, 20 NaF, and 1% protease inhibitor cocktail and phosphatase inhibitor (Roach) and kept at 4°C for 40 min and debris was removed by centrifugation at 14,000 *g* for 10 min. The protein samples were mixed with a 25% volume of 5× SDS loading buffer (250 mM Tris-HCl, 10% SDS, 0.5% bromophenol blue, 50% glycerol, 5% beta-mercaptoethanol, pH 7.4) for electrophoresis on an SDS–PAGE polyacrylamide gel and electrotransferred to a PVDF filter. The filter was then blocked with 5% dry milk in TBST (20 mM Tris-HCl, 9% NaCl, 1% Tween-20, pH 7.6) and incubated overnight at 4°C with suitable primary antibodies in TBST. Following washing and incubation with appropriate secondary antibodies, the filter was washed and developed using an enhanced chemiluminescence (Thermo Fisher Scientific, #34579) method of detection and analyzed using the AlphaEaseFC software according to manufacturer's instruction. The amount of total protein loaded was controlled by normalizing each tested protein with anti-GAPDH immunoreactivity on the same blot. The antibodies used included: anti-p-ERK (Cell Signaling Technology, rabbit, #4370), anti-ERK (Cell Signaling Technology, rabbit, #4695), anti-GAPDH (Proteintech, mouse, 60008-1-lg), anti-GluA1-NTD (Cell Signaling Technology, rabbit, #8850), anti-GluA2-NTD (Millipore, rabbit, #MAB397), goat anti-rabbit (Genscript, #A00098), goat anti-mouse (Genscript, #A00160).

Statistical Methods

All the averaged data in the graphs were stated as mean ± SEM and statistically evaluated by Student's two-sided *t*-test for comparisons of two groups or one-way ANOVA for three groups followed by *post hoc* Holm-Sidak multiple comparison test. $p < 0.05$ was considered as significant ($^*p < 0.05$, $^{**}p < 0.01$, $^{***}p < 0.001$). Key mean ± SEM values, statistical parameters, and sample size are included in respective figure legends.

RESULTS

The CTD of GluA1 Is Required for Both HFS- and TBS-LTP in Juvenile Mice

At the CA1 synapse, NMDAR-LTP can be induced either by HFS or theta-burst stimulation (TBS). Although the induction of both forms of LTP requires the activation of NMDARs, their expression mechanisms appear to be complex and partially distinct (Zhu et al., 2015). We previously showed LTP induced by either one train or multiple trains of 100 Hz HFS (referred to as HFS-LTP) is abolished in 3–4-week-old GluA1^{C2KI} mice (Zhou et al., 2018). However, whether LTP induced by TBS (referred to as TBS-LTP) is also affected in these mice is unknown. Also, although HFS-LTP is impaired in GluA1^{C2KI} mice, whether this effect is age-dependent remains to be determined. First, we examined LTP in juvenile mice (13–15 days old). As shown in **Figure 1A**, although HFS induced a persistent increase in field excitatory postsynaptic potential (fEPSP) in WT animals, this potentiation was not observed in GluA1^{C2KI} mice. Similarly, TBS induced LTP in WT mice, but not in GluA1^{C2KI} mice (**Figure 1B**). These results indicate that in juvenile mice the CTD of GluA1 is indispensable for both HFS- and TBS-LTP.

The CTD of GluA1 Is Required for HFS-LTP, but Not TBS-LTP, in Adult Mice

Next, we examined LTP in adult mice (5–6 weeks old). As shown in **Figure 2A**, HFS induced a persistent increase in fEPSP in WT animals, but this potentiation was not observed in GluA1^{C2KI} mice, indicating that the CTD of GluA1 is also indispensable for HFS-LTP in adult mice. However, TBS induced LTP with a similar magnitude in both WT and GluA1^{C2KI} mice (**Figure 2B**), suggesting that the CTD of GluA1 is not essential for TBS-LTP in adult mice. Therefore, although the requirement for the CTD of GluA1 for HFS-LTP persists in both juvenile and adult mice, its role in TBS-LTP is age-dependent.

Mechanisms of TBS-LTP Are Altered in Adult GluA1^{C2KI} Mice

Although TBS-LTP can be induced in adult GluA1^{C2KI} mice, its mechanisms may be different from those of WT animals. To test this possibility, we first examined the effect of the NMDAR antagonist AP5. As shown in **Figure 3A**, TBS-LTP was sensitive to AP5 in both WT and GluA1^{C2KI} mice, indicating that

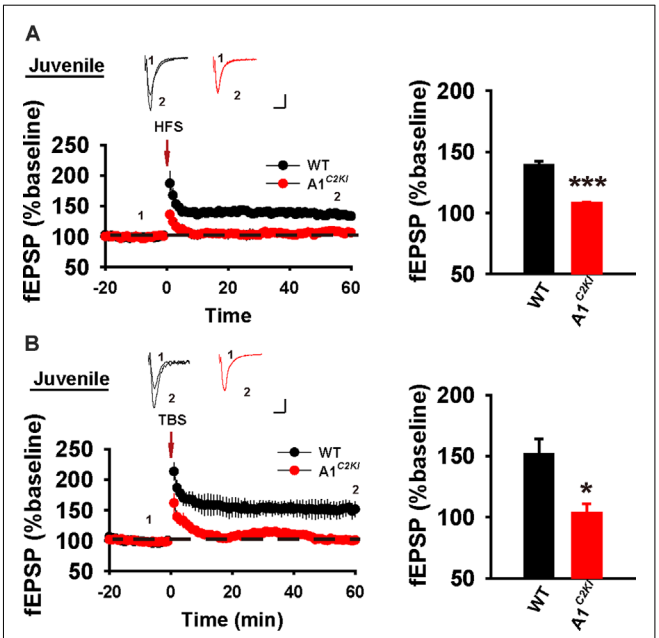

FIGURE 1 | Absence of both high-frequency stimulation (HFS)- and theta-burst stimulation (TBS)–long-term potentiation (LTP) in juvenile GluA1^{C2KI} mice. **(A)** Absence of HFS-LTP in juvenile GluA1^{C2KI} mice (WT 139.30 ± 3.18%, n = 5 slices from three mice; GluA1^{C2KI} 107.86 ± 1.31%, n = 5 slices from three mice; $t_{(8)}$ = 9.152, ***p < 0.001). **(B)** Absence of TBS-LTP in juvenile GluA1^{C2KI} mice (WT 151.52 ± 12.63%, n = 5 slices from three mice; GluA1^{C2KI} 103.54 ± 7.52%, n = 5 slices from three mice; $t_{(8)}$ = 3.263, *p = 0.011). Scale bars: 0.15 mV/10 ms.

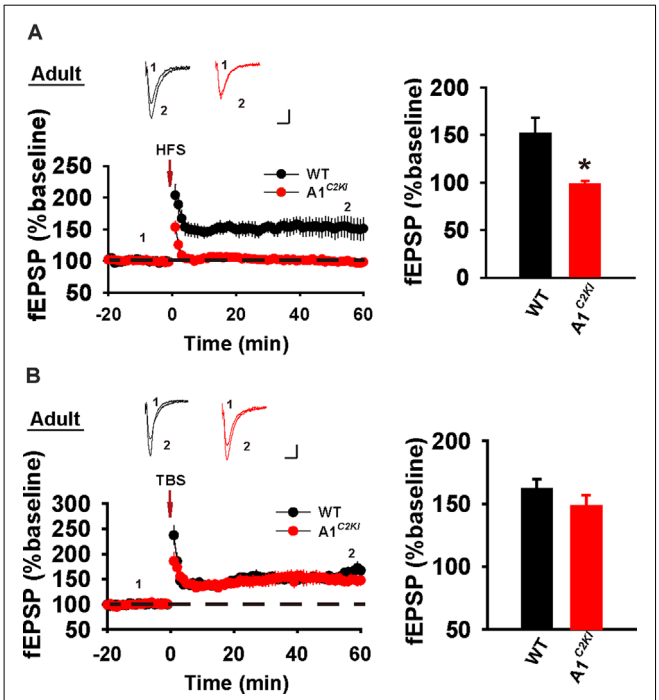

FIGURE 2 | Abolished HFS-, but not TBS-LTP in adult GluA1^{C2KI} mice. **(A)** Absence of HFS-LTP in adult GluA1^{C2KI} mice (WT 151.74 ± 16.52%, n = 6 slices from three mice; GluA1^{C2KI} 92.21 ± 2.47%, n = 5 slices from three mice; $t_{(9)}$ = 2.885, *p = 0.018). **(B)** Presence of TBS-LTP in adult GluA1^{C2KI} mice (wild type, WT 161.45 ± 8.06%, n = 5 slices from three mice; GluA1^{C2KI} 148.18 ± 8.95%, n = 5 slices from three mice; $t_{(8)}$ = 1.102, p = 0.302). Scale bars: 0.15 mV/10 ms.

the LTP is NMDAR-dependent in both genotypes. Therefore, the induction mechanism remains intact in the mutant mice. We then tested the effect of KN62, a general inhibitor for the calcium/calmodulin-dependent protein kinase II (CaMKII), and showed that the inhibitor inhibited TBS-LTP in both WT and GluA1^{C2KI} mice, indicating that TBS-LTP requires activation of CaMKII in both genotypes (**Figure 3B**). We also tested the effect of tyrphostin AG-126, an inhibitor for extracellular signal-regulated kinase 1/2 (ERK1/2), a key signaling pathway implicated in several forms of LTP, particularly in the protein synthesis-dependent late-phase LTP (English and Sweatt, 1996; Winder et al., 1999; Kelleher et al., 2004a,b; Sweatt, 2004; Shalin et al., 2006; Costa-Mattioli et al., 2009; Kandel et al., 2014; Zhu et al., 2015; Vithayathil et al., 2017). As shown in **Figure 4A**, TBS-LTP was induced in WT mice in the presence of AG-126, suggesting that TBS-LTP induced in the present study is largely protein synthesis-independent (also referred to early-phase LTP). However, in GluA1^{C2KI} mice, TBS-LTP was significantly lower in the presence of AG-126 (**Figure 4A**). To test whether the effect of AG-126 was on the induction or maintenance of LTP, we perfused the drug either during the induction (10 min before and 10 after TBS) or after the induction of LTP (after TBS). As shown in **Figure 4B**, TBS-LTP was reduced by AG-126 application during, but not after, the delivery of TBS. To directly test the involvement of protein synthesis, we used two inhibitors for protein synthesis, anisomycin, and cycloheximide. In WT mice, neither anisomycin (**Figure 5A**) nor cycloheximide (**Figure 5B**) affected the magnitude of LTP (compare **Figure 5** to **Figure 2B** without any inhibitors), confirming that TBS-LTP in WT mice does not require protein synthesis. In contrast, both anisomycin (**Figure 5A**) and cycloheximide (**Figure 5B**) significantly diminished TBS-LTP in GluA1^{C2KI} mice. These results suggest that TBS-LTP mechanisms in GluA1^{C2KI} mice have been modified to rely on ERK1/2 signaling and protein synthesis. Therefore, although TBS-LTP can be induced without the CTD of GluA1, its expression mechanisms are different from those of WT mice. Thus, the CTD of GluA1 appears to be particularly important for protein synthesis-independent, early-phase LTP.

The CTD of GluA1 is Required for Whole-Cell LTP in Juvenile Mice

In whole-cell recordings, LTP can be induced by the delivery of HFS under a current-clamp mode (referred to as HFS-CC-LTP, **Figure 6A**), which we used in our previous study (Zhou et al., 2018), or the delivery of moderate frequency stimulation paired with postsynaptic depolarization (referred to as paired-LTP, **Figure 6B**). In WT juvenile mice, both induction protocols induced a significant increase of the amplitude of excitatory postsynaptic currents (EPSCs) that persisted for at least 30 min and both forms of LTP were abolished in GluA1^{C2KI} mice (**Figure 6**). Therefore, similar to field potential recordings

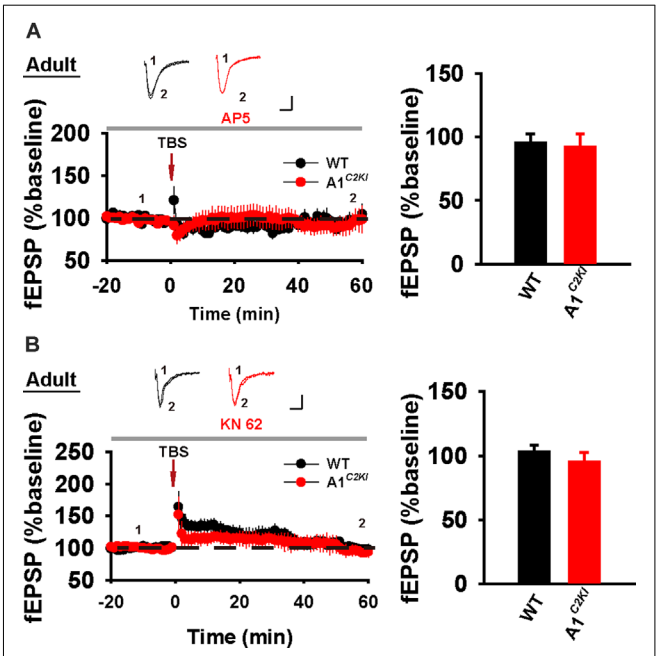

FIGURE 3 | The requirement of NMDAR and CaMKII for TBS-LTP in adult GluA1^{C2KI} mice. **(A)** TBS-LTP in the presence of NMDAR inhibitor D-AP5 (50 μM) in adult WT and GluA1^{C2KI} mice (WT 95.47 ± 6.86%, n = 5 slices from three mice; GluA1^{C2KI} 91.84 ± 10.63%, n = 5 slices from three mice; $t_{(8)}$ = 0.287, p = 0.782). **(B)** TBS-LTP in the presence of CaMKII inhibitor KN-62 (6 μM) in adult WT and GluA1C2KI mice (WT 103.11 ± 4.99%, n = 7 slices from four mice; GluA1^{C2KI} 95.20 ± 7.39%, n = 5 slices from three mice; $t_{(10)}$ = 0.925, p = 0.377). Scale bars: 0.15 mV/10 ms.

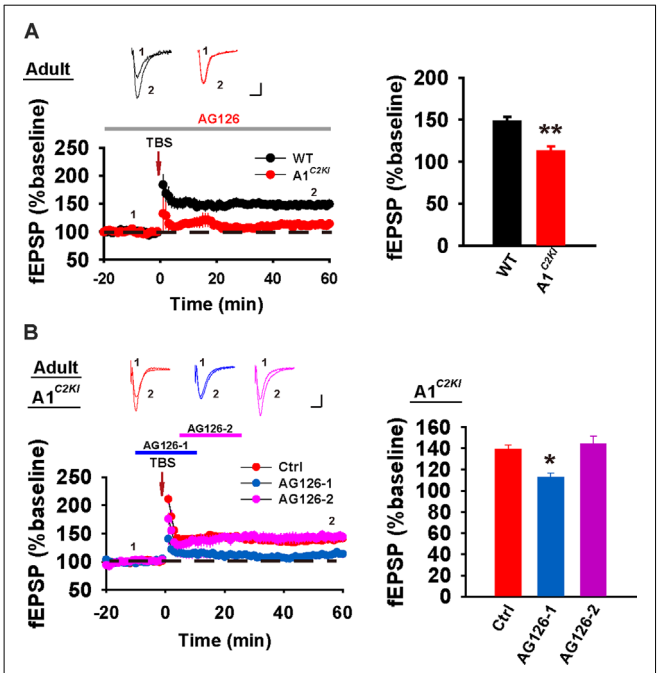

FIGURE 4 | The requirement for ERK1/2 for TBS-LTP in adult GluA1^{C2KI} mice. **(A)** TBS-LTP in the presence of EKR1/2 inhibitor AG126 (50 μM) in adult WT and GluA1^{C2KI} mice (WT 148.00 ± 5.23%, n = 5 slices from three mice; GluA1^{C2KI} 112.29 ± 6.28%, n = 5 slices from three mice; $t_{(8)}$ = 4.369, $^{**}p$ = 0.002). **(B)** Perfusion of AG126 during, but not after, the delivery of TBS impaired TBS-LTP in adult GluA1C2KI mice ($F_{(2,12)}$ = 9.449, $^{**}p$ = 0.003; Ctrl 139.04 ± 4.21%, n = 5 slices from three mice; AG126-1 112.79 ± 4.10%, n = 5 slices from three mice, $^{*}p$ = 0.011 compared to Ctrl with *post hoc* Holm-Sidak multiple comparison tests; AG126-2 144.05 ± 7.41%, n = 5 slices from three mice, p = 0.529 compared to Ctrl with *post hoc* Holm-Sidak multiple comparison tests). Scale bars: 0.15 mV/10 ms.

(**Figure 1**), whole-cell HFS-CC-LTP and paired-LTP in juvenile mice both require the CTD of GluA1.

The CTD of GluA1 Is Required for Whole-Cell HFS-CC-LTP, but Not Paired-LTP in Adult Mice

We next examined whole-cell LTP in adult mice using these two induction protocols. As shown in **Figure 7A**, HFS-CC-LTP was induced in WT, but not in GluA1^{C2KI} mice, indicating that the CTD of GluA1 is also required for whole-cell HFS-CC-LTP in adult mice. However, paired- LTP was induced in both WT and GluA1^{C2KI} mice (**Figure 7B**). Also, this form of LTP in both WT and GluA1^{C2KI} mice was NMDAR-dependent (**Figure 8A**) and showed no differences in the presence of the protein synthesis inhibitor anisomycin (**Figure 8B**). These results suggest that the CTD of GluA1 is dispensable for whole-cell paired-LTP in adult mice.

Enhanced ERK Activation and Increased GluA1 Protein Level Following TBS in Adult GluA1^{C2KI} Mice

To explore the biochemical basis for the observation that TBS-LTP in GluA1^{C2KI} requires ERK activation and protein synthesis, we analyzed protein lysates from dissected CA1 regions with or without HSF/TBS stimulation. As shown in **Figures 9A,B**, TBS, but not HFS, induced a significant increase in phosphorylated (active) forms of ERK1/2 (p-ERK). This TBS-induced increase in p-ERK was significantly higher in GluA1^{C2KI} compared to WT mice (**Figure 9B**). The total ERK1/2 protein level was not altered by either HFS or TBS in WT or GluA1^{C2KI} mice. We also analyzed the protein level of GluA1 and GluA2 with or without TBS and found that GluA1 protein level was significantly increased in GluA1^{C2KI}, but not in WT mice, following TBS treatment (**Figures 9C,D**). These results are consistent with the electrophysiological results that TBS-LTP in GluA1^{C2KI} is ERK- and protein synthesis-dependent (**Figures 4**, **5**).

DISCUSSION

There is huge interest in understanding how AMPARs are involved in LTP because of its direct relevance to learning and memory (Bliss and Collingridge, 1993; Malenka and Bear, 2004; Kandel et al., 2014). Although it is generally agreed that trafficking of AMPARs into and out of the synapse is a key mechanism involved in LTP, the exact subunits and domains involved are not clear (Malinow and Malenka, 2002; Bredt and Nicoll, 2003; Collingridge et al., 2004; Malenka

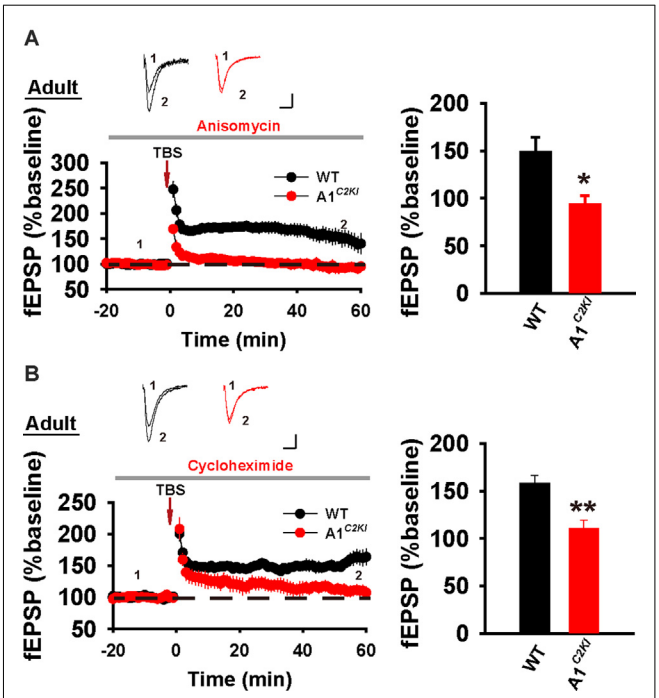

FIGURE 5 | The requirement for protein synthesis for TBS-LTP in adult GluA1^{C2KI} mice. **(A)** TBS-LTP in the presence of protein synthesis inhibitor anisomycin (10 μM) in adult WT and GluA1^{C2KI} mice (WT 148.47 ± 15.55%, n = 6 slices from three mice; GluA1^{C2KI} 93.26 ± 9.44%, n = 5 slices from three mice; $t_{(9)}$ = 2.877, $^{*}p$ = 0.018). **(B)** TBS-LTP in the presence of protein synthesis inhibitor cycloheximide (5 μM) in adult WT and GluA1^{C2KI} mice (WT 157.94 ± 8.47%, n = 6 slices from three mice; GluA1^{C2KI} 110.75 ± 8.30%, n = 5 slices from three mice; $t_{(9)}$ = 3.935, $^{**}p$ = 0.003). Scale bars: 0.15 mV/10 ms.

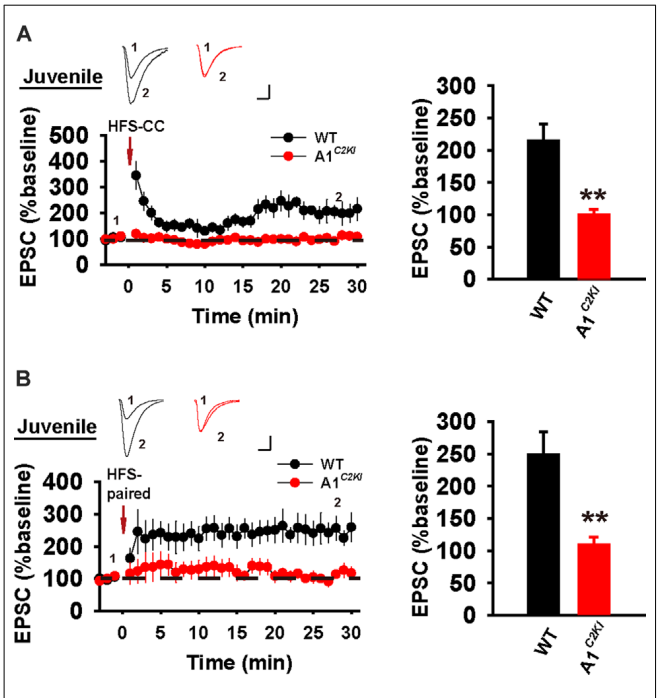

FIGURE 6 | Absence of whole-cell HFS-CC-LTP and paired-LTP in juvenile GluA1^{C2KI} mice. **(A)** HFS-CC-LTP was induced in juvenile WT, but not in GluA1^{C2KI} mice (WT 214.41 ± 25.87%, n = 5 slices from three mice; GluA1^{C2KI} 99.98 ± 8.54%, n = 5 slices from three mice; $t_{(8)}$ = 4.200, $^{**}p$ = 0.003). **(B)** Paired-LTP was induced LTP in WT, but not in juvenile GluA1^{C2KI} mice (WT 248.78 ± 35.70%, n = 5 slices from three mice; GluA1^{C2KI} 109.10 ± 11.95%, n = 5 slices from three mice; $t_{(8)}$ = 3.710, $^{**}p$ = 0.006). Scale bars: 20 pA/10 ms.

and Bear, 2004; Shepherd and Huganir, 2007; Kessels and Malinow, 2009; Anggono and Huganir, 2012; Huganir and Nicoll, 2013; Henley and Wilkinson, 2016). One limitation that is associated with the use of global or conditional GluA KO mice is that they are profoundly altered in AMPA receptor properties and basal synaptic transmission (Jia et al., 1996; Andrásfalvy et al., 2003; Meng et al., 2003; Lu et al., 2009; Granger et al., 2013; Cao et al., 2018), which greatly complicate the interpretation of the findings. In this study, we employed a recently generated mouse model where the CTD of the endogenous GluA1 is specifically replaced by that of GluA2. We previously demonstrated that these mice are impaired in hippocampal LTP induced by HFS (Zhou et al., 2018). In this study, we have extended LTP analysis with additional protocols in both juvenile and adult mice and shown that the involvement of the CTD of GluA1 in LTP is age- and induction protocol-dependent.

First, we showed that HFS-LTP is abolished in GluA1^{C2KI} mice consistent with previous results (Zhou et al., 2018). Also, this abolition of LTP applies to both juvenile and young adult mice. Furthermore, HFS-LTP is absent in both field and whole-cell recording conditions. These results indicate that the CTD of GluA1 is essential for HFS-LTP under various physiological conditions and developmental stages. These results are also consistent with the data obtained from GluA1 KO mice where LTP induced by tetanic stimulation (100 Hz, 1 s), an induction protocol similar to the HFS protocols used in the present study, is impaired (Zamanillo et al., 1999).

Second, we showed that TBS-LTP in GluA1^{C2KI} mice is age-dependent. In juvenile animals, TBS-LTP is abolished in GluA1^{C2KI} mice, whereas in adult mice, TBS-LTP is still present in GluA1^{C2KI} mice. These results suggest that the requirement for the CTD of GluA1 in TBS-LTP is developmentally regulated, being essential in early development, but maybe compensated by additional mechanisms in adult mice. These results are as per the results obtained from GluA1 KO mice where some forms of LTP can still be established in these mice (Hoffman et al., 2002; Jensen et al., 2003; Shimshek et al., 2017).

It is important to emphasize that although TBS-LTP can be induced in GluA1^{C2KI} adult mice, its mechanisms are altered. In both WT and GluA1^{C2KI} adult mice, TBS-LTP is sensitive to AP5 indicating that it is NMDAR-dependent. Also, TBS-LTP in both genotypes is affected by KN-62, and therefore requires activation of CaMKII. However, while the TBS-LTP in WT mice is insensitive to anisomycin or cycloheximide, TBS-LTP in GluA1^{C2KI} adult mice is inhibited by these drugs, and therefore it is dependent on new protein synthesis. The dependence of TBS-LTP on protein synthesis in GluA1^{C2KI} adult mice is also supported by the results that the inhibition

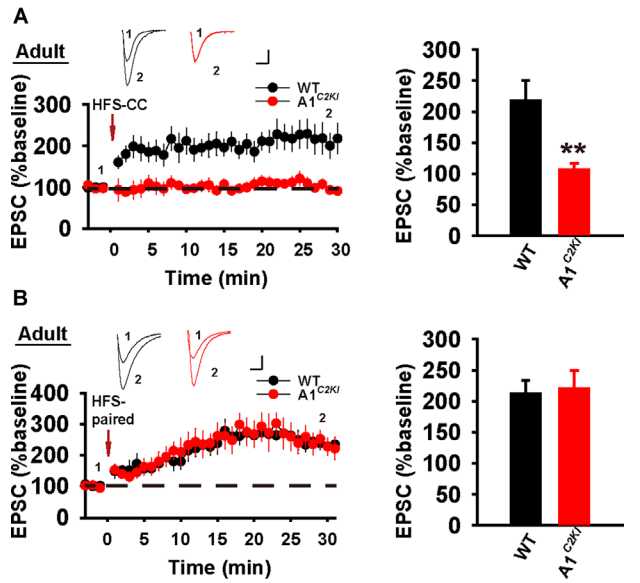

FIGURE 7 | Absence of whole-cell HFS-CC-LTP, but the presence of paired-LTP in adult GluA1^{C2KI} mice. **(A)** HFS-CC-LTP was induced in adult WT, but not in GluA1^{C2KI} mice (WT 217.54 ± 32.50%, n = 6 slices from three mice; GluA1^{C2KI} 106.68 ± 10.24%, n = 6 slices from three mice; $t_{(8)}$ = 3.254, $^{**}p$ = 0.009). **(B)** Paired-LTP was induced in both adult WT and GluA1^{C2KI} mice (WT 211.86 ± 21.31%, n = 5 slices from three mice; GluA1^{C2KI} 220.17 ± 29.25%, n = 5 slices from three mice; $t_{(8)}$ = −0.230, p = 0.824). Scale bars: 20 pA/10 ms.

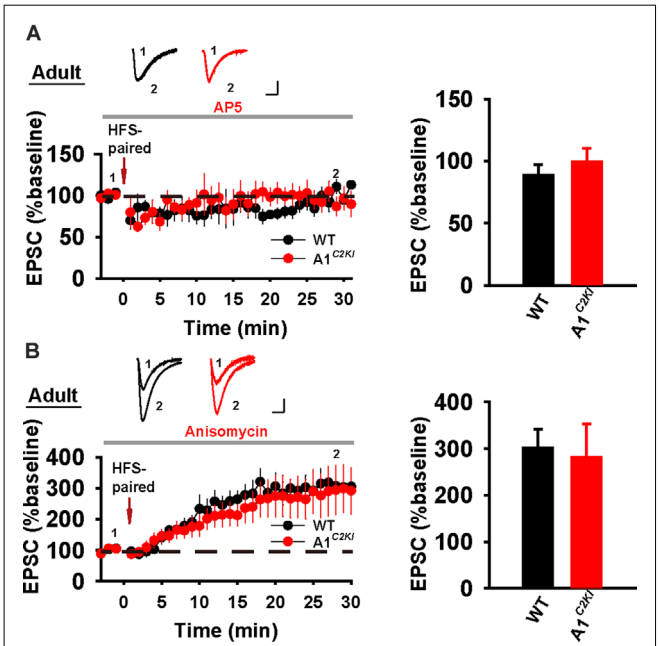

FIGURE 8 | Whole-cell paired-LTP is depending on NMDARs, but not protein synthesis in adult GluA1^{C2KI} mice. **(A)** Paired-LTP was sensitive to D-AP5 (50 μM) in both adult WT and GluA1^{C2KI} mice (WT 88.86 ± 8.18%, n = 4 slices from three mice; GluA1^{C2KI} 99.41 ± 11.12%, n = 5 slices from three mice; $t_{(7)}$ = −0.727, p = 0.491). **(B)** Paired-LTP in the presence of protein synthesis inhibitor anisomycin (10 μM) in adult WT and GluA1^{C2KI} mice (WT 302.15 ± 38.97%, n = 5 slices from three mice; GluA1^{C2KI} 281.81 ± 70.77%, n = 5 slices from three mice; $t_{(8)}$ = 0.252, p = 0.808). Scale bars: 20 pA/10 ms.

of ERK1/2, a key protein kinase involved in protein synthesis and late-phase LTP (Kelleher et al., 2004b; Costa-Mattioli et al., 2009), impairs TBS-LTP in GluA1^{C2KI}, but not in WT adult mice. Consistent with these recording data, TBS, but not HFS, induces activation of ERK1/2, and this TBS-induced ERK1/2 activation is significantly enhanced in GluA1^{C2KI}, compared to WT adult mice. It is possible that TBS used in the present study induces both protein synthesis-dependent and -independent pathways, but under normal physiological conditions, the protein-independent pathways such as protein phosphorylation and trafficking of existing AMPARs, is the predominant mechanism underlying LTP expression and this mechanism requires the CTD of GluA1 and CaMKII, but not ERK1/2. However, in GluA1^{C2KI} mice, TBS induces a higher level of ERK1/2 activation compared to WT, and this activates ERK1/2 downstream signaling pathways, which in turn initiate new protein synthesis and overcome the defect in protein delivery by overproducing GluA1 and/or other LTP related proteins. The fact that the application of AG-126 during, but not after TBS, blocks TBS-LTP suggests that ERK1/2 is transiently activated during the induction period and that its sustained activation may not be necessary for LTP maintenance. How the ERK1/2 activation leads to new protein synthesis in GluA1^{C2KI} mice is unknown, but it is well established that ERK1/2 is an upstream regulator of protein synthesis signaling molecules and regulatory factors, including the mTOR pathway and the translational initiation factors, that are involved in protein synthesis-dependent synaptic plasticity (Kelleher et al., 2004b; Costa-Mattioli et al., 2009). It would be interesting to examine whether these signaling proteins are altered following TBS, which would allow new protein synthesis more easily in GluA1^{C2KI} mice.

Finally, it is important to note that the results from whole-cell recordings are largely consistent with those of field potential recordings. In juvenile GluA1^{C2KI} mice, whole-cell HFS-CC-LTP and paired-LTP are both impaired, underscoring the significance of the CTD of GluA1 in LTP expression at this developmental stage. In adult GluA1^{C2KI} mice, whole-cell HFS-CC-LTP is also impaired in GluA1^{C2KI} mice, supporting the essential role of GluA1 CTD in the expression of HFS-CC-LTP throughout the lifetime of the mice. However, in adult GluA1^{C2KI} mice, whole-cell paired-LTP is still present. A pairing protocol may elicit multiple signaling processes, as a TBS protocol in the field potential recordings, that overcomes the requirement for the GluA1 CTD and allows the expression of LTP. Although this form of LTP is NMDAR-dependent and protein synthesis-independent, as in WT mice, further studies are needed to investigate whether it is mechanistically distinct.

A recent study by Díaz-Alonso et al. (2020) also tested the involvement of the GluA CTD in hippocampal CA1 LTP by using a gene replacement in a KO background and generating KI mice lacking the CTD of GluA1 *via* a CRISPR approach and found that LTP can be induced using a pairing protocol in whole-cell recordings in these mice. This result seems consistent

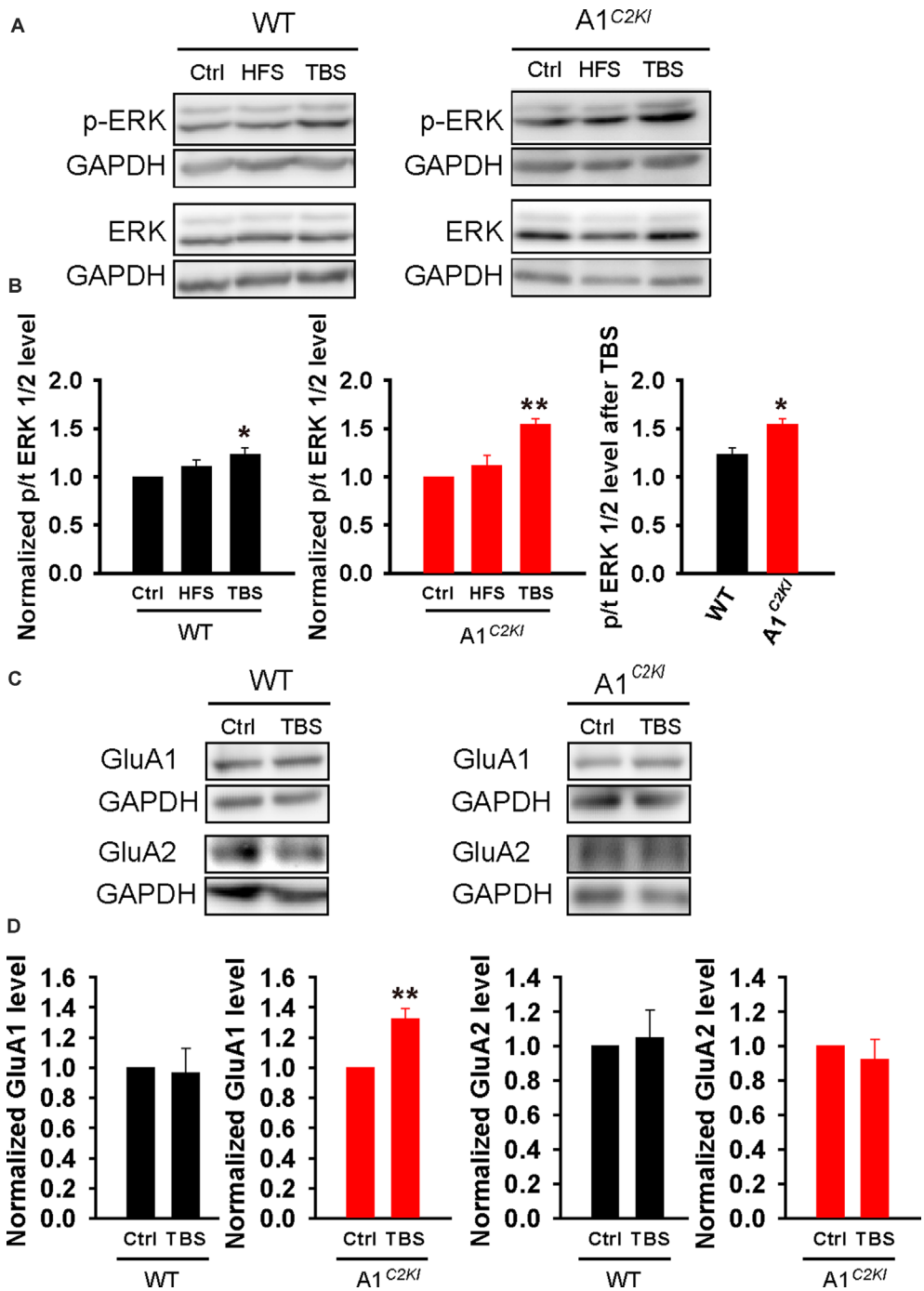

FIGURE 9 | Enhanced extracellular signal-regulated kinase (ERK) activation and increased GluA1 protein level following TBS in adult GluA1^{C2KI} mice. **(A,B)** Sample western blots **(A)** and summary graphs **(B)** showing TBS, but not HFS, increased ERK1/2 phosphorylation in adult WT ($F_{(2,9)}$ = 4.347, *p = 0.048; Ctrl 1.00 ± 0.00; HFS 1.11 ± 0.07, p = 0.204 compared to Ctrl with *post hoc* Holm-Sidak multiple comparison tests; TBS 1.23 ± 0.07, *p = 0.048 compared to Ctrl, and p = 0.276 compared to HFS with *post hoc* Holm-Sidak multiple comparison tests; n = 4 independent animals/experiments) and this increase was enhanced in adult GluA1^{C2KI} mice ($F_{(2,9)}$ = 14.239, **p = 0.002; Ctrl 1.00 ± 0.00; HFS 1.11 ± 0.12, p = 0.334 compared to Ctrl with *post hoc* Holm-Sidak multiple comparison test; TBS 1.54 ± 0.06, **p = 0.002 compared to Ctrl with *post hoc* Holm-Sidak multiple comparison tests; $t_{(6)}$ = 3.424, *p = 0.014 when comparing WT and GluA1^{C2KI} TBS; four independent animals/experiments). **(C,D)** Sample western blots **(C)** and summary graphs **(D)** showing increased GluA1 total protein level following TBS in adult GluA1^{C2KI}, but not in WT mice (WT: Ctrl 1.00 ± 0.00; TBS 0.97 ± 0.16, n = four independent animals/experiments, $t_{(6)}$ = 0.21, p = 0.841; GluA1^{C2KI}: Ctrl 1.00 ± 0.00; TBS 1.32 ± 0.07, n = 5 independent animals/experiments, $t_{(8)}$ = 4.486, **p = 0.002). The GluA2 protein level was not affected by TBS (WT: Ctrl 1.00 ± 0.00; TBS 1.05 ± 0.16, n = four independent animals/experiments, $t_{(6)}$ = −0.298, p = 0.841; GluA1^{C2KI}: Ctrl 1.00 ± 0.00; TBS 0.92 ± 0.12, n = 3 independent animals/experiments, $t_{(4)}$ = 0.657, p = 0.547).

with our data that paired-LTP can be induced in GluA1^{C2KI} mice as shown in this study. Since Díaz-Alonso et al study did not report data on field LTP or whole-cell HFS-CC-LTP, which show most significant impairments in GluA1^{C2KI} mice and GluA1 global KO mice (Zamanillo et al., 1999; Zhou et al., 2018; including the current study), no direct comparison between our and Díaz-Alonso et al study can be made under these conditions. Besides, the methodologies used in our and Díaz-Alonso et al study were also different that could contribute to the discrepancy (e.g., in spatial learning and memory). First, the gene replacement strategy in Díaz-Alonso et al study involves overexpression of exogenous receptors in a KO background and therefore may not represent the behavior of the endogenous receptors. Second, instead of the CTD replacement in our GluA1^{C2KI} mice which produce a full-length receptor, the GluA1 mutant mice in Díaz-Alonso et al study deleted the entire CTD of GluA1 plus the insertion of a HA tag, which resulted in a truncated form of GluA1. This truncation/insertion could potentially alter the confirmation/structure of the receptor thus confounding the analysis of LTP and behavior.

In summary, by using our recently created mouse strain where the CTD of the endogenous GluA1 is replaced by that of GluA2, we show that the CTD of GluA1 is differentially required for different forms of LTP and this effect is regulated by developmental stages. Our results are consistent with previous genetic studies using GluA1 global KO and phosphorylation site KI mice showing that GluA1 is indispensable for some, but not all, forms of hippocampal LTP (Zamanillo et al., 1999; Hoffman et al., 2002; Jensen et al., 2003; Lee et al., 2003; Shimshek et al., 2017). These results highlight the complexity of LTP expression mechanisms at the AMPAR level. This is not surprising given the diverse posttranslational modifications existing at the CTD of AMPARs (Diering and Huganir, 2018). It would be interesting to elucidate how the CTD of GluA1 differentially regulates these forms of LTP and how they might be altered in various brain disorders.

DATA AVAILABILITY STATEMENT

The raw data supporting the conclusions of this article will be made available by the authors, without undue reservation.

ETHICS STATEMENT

The animal study was reviewed and approved and all experimental procedures were conducted in accordance with the guidelines of the Canadian Council on Animal Care (CCAC) and approved by the Animal Care Committee at the Hospital for Sick Children, Canada and Southeast University, China.

AUTHOR CONTRIBUTIONS

ZJ, AL, and WX designed the experiments. AL, HJ, QR, YM, and HZ performed the experiments and analyzed the data. ZJ, AL, and GC wrote the article. All authors contributed to the article and approved the submitted version.

FUNDING

This work was supported by grants from the Natural Science Foundation of China (NSFC 91632201 WX, NSFC 31700906, AL), Natural Science Foundation of Jiangsu Province (BK20170702, AL), the Canadian Institutes of Health Research (CIHR PJT155959, CIHR PJT168922, ZJ), Canadian Natural Science and Engineering Research Council (NSERC RGPIN341498, RGPIN06295, ZJ), and the Hospital for Sick Children Foundation (ZJ).

ACKNOWLEDGMENTS

We are grateful to all members of the Jia lab for their technical assistance and comments on the manuscript.

REFERENCES

Andrásfalvy, B. K., Smith, M. A., Borchardt, T., Sprengel, R., and Magee, J. C. (2003). Impaired regulation of synaptic strength in hippocampal neurons from GluR1-deficient mice. *J. Physiol.* 552, 35–45. doi: 10.1113/jphysiol.2003.045575

Anggono, V., and Huganir, R. L. (2012). Regulation of AMPA receptor trafficking and synaptic plasticity. *Curr. Opin. Neurobiol.* 3, 461–469. doi: 10.1016/j.conb.2011.12.006

Asrar, S., Zhou, Z., Ren, W., and Jia, Z. (2009). Ca^{2+}-permeable AMPA receptor induced long-term potentiation requires PI3/MAP kinases but not Ca/CaM-dependent kinase II. *PLoS One* 4:e4339. doi: 10.1371/journal.pone.0004339

Biou, V., Bhattacharyya, S., and Malenka, R. C. (2008). Endocytosis and recycling of AMPA receptors lacking GluR2/3. *Proc. Natl. Acad. Sci. U SA* 105, 1038–1043. doi: 10.1073/pnas.0711412105

Bliss, T. V., and Collingridge, G. L. (1993). A synaptic model of memory: long-term potentiation in the hippocampus. *Nature* 361, 31–39. doi: 10.1038/361031a0

Boehm, J., Kang, M. G., Johnson, R. C., Esteban, J., Huganir, R. L., and Malinow, R. (2006). Synaptic incorporation of AMPA receptors during LTP is controlled by a PKC phosphorylation site on GluR1. *Neuron* 51, 213–225. doi: 10.1016/j.neuron.2006.06.013

Bredt, D. S., and Nicoll, R. A. (2003). AMPA receptor trafficking at excitatory synapses. *Neuron* 40, 361–379. doi: 10.1016/s0896-6273(03)00640-8

Cao, F., Zhou, Z., Cai, S., Xie, W., and Jia, Z. (2018). Hippocampal long-term depression in the presence of calcium-permeable AMPA receptors. *Front. Synaptic. Neurosci.* 10:41. doi: 10.3389/fnsyn.2018.00041

Cao, G., and Harris, K. M. (2012). Developmental regulation of the late phase of long-term potentiation (L-LTP) and metaplasticity in hippocampal area CA1 of the rat. *J. Neurophysiol.* 107, 902–912. doi: 10.1152/jn.00780.2011

Collingridge, G. L., Isaac, J. T., and Wang, Y. T. (2004). Receptor trafficking and synaptic plasticity. *Nat. Rev. Neurosci.* 5, 952–962. doi: 10.1038/nrn1556

Collingridge, G. L., Kehl, S. J., and McLennan, H. (1983). The antagonism of amino acid-induced excitations of rat hippocampal CA 1 neurones *in vitro*. *J. Physiol.* 334, 19–31. doi: 10.1113/jphysiol.1983.sp014477

Costa-Mattioli, M., Sossin, W. S., Klann, E., and Sonenberg, N. (2009). Translational control of long-lasting synaptic plasticity and memory. *Neuron* 61, 10–26. doi: 10.1016/j.neuron.2008.10.055

Davies, S. N., Lester, R. A., Reymann, K. G., and Collingridge, G. L. (1989). Temporally distinct pre- and post-synaptic mechanisms maintain long-term potentiation. *Nature* 338, 500–503doi: 10.1038/338500a0

Díaz-Alonso, J., Morishita, W., Incontro, S., Simms, J., Holtzman, J., Gill, M., et al. (2020). Long-term potentiation is independent of the C-tail of the GluA1 AMPA receptor subunit. *eLife* 9:e58042. doi: 10.7554/eLife.58042

Diering, G. H., and Huganir, R. L. (2018). The AMPA receptor code of synaptic plasticity. *Neuron* 100, 314–329. doi: 10.1016/j.neuron.2018.10.018

English, J. D., and Sweatt, J. D. (1996). Activation of p42 mitogen-activated protein kinase in hippocampal long term potentiation. *J. Biol. Chem.* 271, 24329–24332. doi: 10.1074/jbc.271.40.24329

Granger, A. J., Shi, Y., Lu, W., Cerpas, M., and Nicoll, R. A. (2013). LTP requires a reserve pool of glutamate receptors independent of subunit type. *Nature* 493, 495–500. doi: 10.1038/nature11775

Hayashi, Y., Shi, S. H., Esteban, J. A., Piccini, A., Poncer, J. C., and Malinow, R. (2000). Driving AMPA receptors into synapses by LTP and CaMKII: requirement for GluR1 and PDZ domain interaction. *Science* 287, 2262–2267. doi: 10.1126/science.287.5461.2262

Henley, J. M., and Wilkinson, K. A. (2016). Synaptic AMPA receptor composition in development, plasticity and disease. *Nat. Rev. Neurosci.* 17, 337–350. doi: 10.1038/nrn.2016.37

Hoffman, D. A., Sprengel, R., and Sakmann, B. (2002). Molecular dissection of hippocampal theta-burst pairing potentiation. *Proc. Natl. Acad. Sci. U S A* 99, 7740–7745. doi: 10.1073/pnas.092157999

Huganir, R. L., and Nicoll, R. A. (2013). AMPARs and synaptic plasticity: the last 25 years. *Neuron* 80, 704–717. doi: 10.1016/j.neuron.2013.10.025

Jensen, V., Kaiser, K. M., Borchardt, T., Adelmann, G., Rozov, A., Burnashev, N., et al. (2003). A juvenile form of postsynaptic hippocampal long-term potentiation in mice deficient for the AMPA receptor subunit GluR-A. *J. Physiol.* 553, 843–856. doi: 10.1113/jphysiol.2003.053637

Jia, Z., Agopyan, N., Miu, P., Xiong, Z., Henderson, J., Gerlai, R., et al. (1996). Enhanced LTP in mice deficient in the AMPA receptor GluR2. *Neuron* 17, 945–956. doi: 10.1016/s0896-6273(00)80225-1

Kandel, E. R., Dudai, Y., and Mayford, M. R. (2014). The molecular and systems biology of memory. *Cell* 157, 163–186. doi: 10.1016/j.cell.2014.03.001

Kelleher, R. J., Govindarajan, A., Jung, H. Y., Kang, H., and Tonegawa, S. (2004a). Translational control by MAPK signaling in long-term synaptic plasticity and memory. *Cell* 116, 467–479. doi: 10.1016/s0092-8674(04)00115-1

Kelleher, R. J., Govindarajan, A., and Tonegawa, S. (2004b). Translational regulatory mechanisms in persistent forms of synaptic plasticity. *Neuron* 44, 59–73. doi: 10.1016/j.neuron.2004.09.013

Kessels, H. W., and Malinow, R. (2009). Synaptic AMPA receptor plasticity and behavior. *Neuron* 61, 340–350. doi: 10.1016/j.neuron.2009.01.015

Lee, H. K., Takamiya, K., Han, J. S., Man, H., Kim, C. H., Rumbaugh, G., et al. (2003). Phosphorylation of the AMPA receptor GluR1 subunit is required for synaptic plasticity and retention of spatial memory. *Cell* 112, 631–643. doi: 10.1016/s0092-8674(03)00122-3

Liu, A., Zhou, Z., Dang, R., Zhu, Y., Qi, J., He, G., et al. (2016). Neuroligin 1 regulates spines and synaptic plasticity *via* LIMK1/cofilin-mediated actin reorganization. *J. Cell Biol.* 212, 449–463doi: 10.1083/jcb.201509023

Lu, W., Shi, Y., Jackson, A. C., Bjorgan, K., During, M. J., Sprengel, R., et al. (2009). Subunit composition of synaptic AMPA receptors revealed by a single-cell genetic approach. *Neuron* 62, 254–268. doi: 10.1016/j.neuron.2009.02.027

Malenka, R. C., and Bear, M. F. (2004). LTP and LTD: an embarrassment of riches. *Neuron* 44, 5–21. doi: 10.1016/j.neuron.2004.09.012

Malinow, R., and Malenka, R. C. (2002). AMPA receptor trafficking and synaptic plasticity. *Annu. Rev. Neurosci.* 25, 103–126. doi: 10.1146/annurev.neuro.25.112701.142758

Meng, Y., Zhang, Y., and Jia, Z. (2003). Synaptic transmission and plasticity in the absence of AMPA glutamate receptor GluR2 and GluR3. *Neuron* 39, 163–176. doi: 10.1016/s0896-6273(03)00368-4

Palmer, M. J., Isaac, J. T., and Collingridge, G. L. (2004). Multiple, developmentally regulated expression mechanisms of long-term potentiation at CA1 synapses. *J. Neurosci.* 24, 4903–4911. doi: 10.1523/JNEUROSCI.0170-04.2004

Park, P., Volianskis, A., Sanderson, T. M., Bortolotto, Z. A., Jane, D. E., Zhuo, M., et al. (2013). NMDA receptor-dependent long-term potentiation comprises a family of temporally overlapping forms of synaptic plasticity that are induced by different patterns of stimulation. *Philos. Trans. R. Soc. Lond. B Biol. Sci.* 369:20130131. doi: 10.1098/rstb.2013.0131

Sans, N., Vissel, B., Petralia, R. S., Wang, Y. X., Chang, K., Royle, G. A., et al. (2003). Aberrant formation of glutamate receptor complexes in hippocampal neurons of mice lacking the GluR2 AMPA receptor subunit. *J. Neurosci.* 23, 9367–9373. doi: 10.1523/JNEUROSCI.23-28-09367.2003

Shalin, S. C., Hernandez, C. M., Dougherty, M. K., Morrison, D. K., and Sweatt, J. D. (2006). Kinase suppressor of Ras1 compartmentalizes hippocampal signal transduction and subserves synaptic plasticity and memory formation. *Neuron* 50, 765–779. doi: 10.1016/j.neuron.2006.04.029

Shepherd, J. D., and Huganir, R. L. (2007). The cell biology of synaptic plasticity: AMPA receptor trafficking. *Annu. Rev. Cell Dev. Biol.* 23, 613–643. doi: 10.1146/annurev.cellbio.23.090506.123516

Shi, S., Hayashi, Y., Esteban, J. A., and Malinow, R. (2001). Subunit-specific rules governing AMPA receptor trafficking to synapses in hippocampal pyramidal neurons. *Cell* 105, 331–343. doi: 10.1016/s0092-8674(01)00321-x

Shi, S. H., Hayashi, Y., Petralia, R. S., Zaman, S. H., Wenthold, R. J., Svoboda, K., et al. (1999). Rapid spine delivery and redistribution of AMPA receptors after synaptic NMDA receptor activation. *Science* 284, 1811–1816. doi: 10.1126/science.284.5421.1811

Shimshek, D. R., Bus, T., Schupp, B., Jensen, V., Marx, V., Layer, L. E., et al. (2017). Different forms of AMPA receptor mediated LTP and their correlation to the spatial working memory formation. *Front. Mol. Neurosci.* 10:214. doi: 10.3389/fnmol.2017.00214

Sweatt, J. D. (2004). Mitogen-activated protein kinases in synaptic plasticity and memory. *Curr. Opin. Neurobiol.* 14, 311–317. doi: 10.1016/j.conb.2004.04.001

Toyoda, H., Wu, L. J., Zhao, M. G., Xu, H., Jia, Z., and Zhuo, M. (2007). Long-term depression requires postsynaptic AMPA GluR2 receptor in adult mouse cingulate cortex. *J. Cell Physiol.* 211, 336–343doi: 10.1002/jcp.20940

Vithayathil, J., Pucilowska, J., Friel, D., and Landreth, G. E. (2017). Chronic impairment of ERK signaling in glutamatergic neurons of the forebrain does not affect spatial memory retention and LTP in the same manner as acute blockade of the ERK pathway. *Hippocampus* 27, 1239–1249doi: 10.1002/hipo.22769

Winder, D. G., Martin, K. C., Muzzio, I. A., Rohrer, D., Chruscinski, A., Kobilka, B., et al. (1999). ERK plays a regulatory role in induction of LTP by θ frequency stimulation and its modulation by beta-adrenergic receptors. *Neuron* 24, 715–726. doi: 10.1016/s0896-6273(00)81124-1

Yasuda, H., Barth, A. L., Stellwagen, D., and Malenka, R. C. (2003). A developmental switch in the signaling cascades for LTP induction. *Nat. Neurosci.* 6, 15–16. doi: 10.1038/nn985

Zamanillo, D., Sprengel, R., Hvalby, O., Jensen, V., Burnashev, N., Rozov, A., et al. (1999). Importance of AMPA receptors for hippocampal synaptic plasticity but not for spatial learning. *Science* 284, 1805–1811. doi: 10.1126/science.284.5421.1805

Zhou, Z., Hu, J., Passafaro, M., Xie, W., and Jia, Z. (2011). GluA2 (GluR2) regulates metabotropic glutamate receptor-dependent long-term depression through N-cadherin-dependent and cofilin-mediated actin reorganization. *J. Neurosci.* 31, 819–833. doi: 10.1523/JNEUROSCI.3869-10.2011

Zhou, Z., Liu, A., Xia, S., Leung, C., Qi, J., Meng, Y., et al. (2018). The C-terminal tails of endogenous GluA1 and GluA2 differentially contribute to hippocampal synaptic plasticity and learning. *Nat. Neurosci.* 21, 50–62doi: 10.1038/s41593-017-0030-z

Zhu, G., Liu, Y., Wang, Y., Bi, X., and Baudry, M. (2015). Different patterns of electrical activity lead to long-term potentiation by activating different intracellular pathways. *J. Neurosci.* 35, 621–633. doi: 10.1523/JNEUROSCI.2193-14.2015

Conflict of Interest: The authors declare that the research was conducted in the absence of any commercial or financial relationships that could be construed as a potential conflict of interest.

frontiers in Synaptic Neuroscience

ORIGINAL RESEARCH
published: 03 December 2020
doi: 10.3389/fnsyn.2020.588295

Transient Enhanced GluA2 Expression in Young Hippocampal Neurons of a Fragile X Mouse Model

Tue G. Banke[*†] *and Andres Barria*

Department of Physiology and Biophysics, University of Washington, Seattle, WA, United States

AMPA-type glutamate receptors (AMPARs) are tetrameric ligand-gated channels made up of combinations of GluA1-4 subunits and play important roles in synaptic transmission and plasticity. Here, we have investigated the development of AMPAR-mediated synaptic transmission in the hippocampus of the Fmr1 knock-out (KO) mouse, a widely used model of Fragile X syndrome (FXS). FXS is the leading monogenic cause of intellectual disability and autism spectrum disorders (ASD) and it is considered a neurodevelopmental disorder. For that reason, we investigated synaptic properties and dendritic development in animals from an early stage when synapses are starting to form up to adulthood. We found that hippocampal CA1 pyramidal neurons in the Fmr1-KO mouse exhibit a higher AMPAR-NMDAR ratio early in development but reverses to normal values after P13. This increase was accompanied by a larger presence of the GluA2-subunit in synaptic AMPARs that will lead to altered Ca^{2+} permeability of AMPARs that could have a profound impact upon neural circuits, learning, and diseases. Following this, we found that young KO animals lack Long-term potentiation (LTP), a well-understood model of synaptic plasticity necessary for proper development of circuits, and exhibit an increased frequency of spontaneous miniature excitatory postsynaptic currents, a measure of synaptic density. Furthermore, *post hoc* morphological analysis of recorded neurons revealed altered dendritic branching in the KO group. Interestingly, all these anomalies are transitory and revert to normal values in older animals. Our data suggest that loss of FMRP during early development leads to temporary upregulation of the GluA2 subunit and this impacts synaptic plasticity and altering morphological dendritic branching.

Keywords: fragile X mental retardation protein, glutamate receptor (AMPAR), LTP (long term potentiation), dendritic spines and memory, FMR 1 gene, NMDAR (NMDA receptor), circuit, synapses

OPEN ACCESS

Edited by:
Carlos B. Duarte,
University of Coimbra, Portugal

Reviewed by:
Richard Lewis Huganir,
Johns Hopkins University,
United States
Maija Liisa Castrén,
University of Helsinki, Finland

****Correspondence:***
Tue G. Banke
tbanke@gmail.com

†Present address:
Tue G. Banke,
Department of Pharmacology and Chemical Biology, Emory University,
Atlanta, GA,
United States

Received: *28 July 2020*
Accepted: *10 November 2020*
Published: *03 December 2020*

Citation:
Banke TG and Barria A (2020) Transient Enhanced GluA2 Expression in Young Hippocampal Neurons of a Fragile X Mouse Model. Front. Synaptic Neurosci. 12:588295. doi: 10.3389/fnsyn.2020.588295

INTRODUCTION

Loss of the fragile X mental retardation protein (FMRP) in the brain causes the fragile X syndrome (FXS), a leading monogenic cause of often severe intellectual disability which is characterized by moderate-to-severe mental retardation. FXS is the most common inherited intellectual disability syndrome (Santoro et al., 2012) and is considered as the most common single-gene condition

associated with autism spectrum disorder (ASD; Hernandez et al., 2009). FMRP is highly expressed throughout the brain, including at synapses, where it may play critical roles regulating dendritic properties, synaptogenesis, and synaptic function. FMRP is encoded by the *Fmr1* gene that contains a CGG trinucleotide repeat, that, when expanded can results in abnormal DNA hypermethylation and transcriptional silencing of FMRP (Penagarikano et al., 2007; Garber et al., 2008). FMRP is involved in mRNA regulation of multiple downstream targets including members of the glutamate receptor family, thereby impacting the normal development of neurons, synapses, and brain circuits (Contractor et al., 2015). Furthermore, recent studies suggest that FMRP can directly regulate the intrinsic properties of neurons *via* direct interactions with potassium (Kv) and HCN channels in a cell-type-specific manner (Kalmbach et al., 2015).

Loss of FMRP results in abnormal neuronal structure and function in a brain-region and cell-type-specific manner, producing complex effects on circuit function in different sensory systems (Comery et al., 1997) and varied, sometimes contradictory, effects on synaptic properties and developmental plasticity (McBain and Fisahn, 2001; Yang et al., 2014).

The release of the neurotransmitter glutamate from presynaptic vesicles activates postsynaptic glutamate-gated ion channels including α-amino-3-hydroxy-5-methyl-4-isoxazolepropionic acid receptors (AMPARs). AMPA receptors play critical roles in synaptic signaling and plasticity, and AMPAR dysfunction is implicated in a variety of nervous system disorders (Bowie, 2008; Salpietro et al., 2019). Long-term potentiation (LTP) and long-term depression (LTD) are two well accepted and understood cellular models of synaptic plasticity (Lüscher and Malenka, 2012) that increase or decrease synaptic strength respectively. Previous work indicates an enhanced LTD in adult FMRP knock-out (KO) mice (Huber et al., 2002; Toft et al., 2016), however, this seems to be an age-dependent phenomenon as younger animals (<p21) did not show a difference in the amount of LTD induced (Toft et al., 2016). Discrepancies on whether LTP is affected in FMRP KO animals also exist and while it has been reported to be impaired in FMRP KO animals (Hu et al., 2008), it seems to be increased in a different FXS animal model that uses a double genetic manipulation to completely knock out the protein (Pilpel et al., 2009). The reasons for this discrepancy could be differences in the knockout model, age of the animals used, and/or differences in the LTP induction protocols used.

The development of excitatory synapses happens in a very tightly orchestrated manner; they are built as a complex of scaffolding proteins that link signaling proteins, cell adhesion molecules, and members of the glutamate receptor family to the microfilament-based cytoskeleton in dendritic spines. FMRP has been found to associate with the mRNA of various synaptic proteins including ionotropic glutamate receptor (iGluRs; Schütt et al., 2009; Edbauer et al., 2010), which could indicate that altered expression of iGluRs is involved in the pathophysiology of FXS.

Little is known about the role of FMRP in the early development of synapses and neuronal properties. A better understanding of the developmental profile of glutamatergic synaptic properties in the absence of FMRP is necessary to better understand how synaptic plasticity and the normal development of synapses are affected in FXS. Here, we studied the development of glutamatergic synapses, their synaptic plasticity properties, and the development of dendritic branching in mice hippocampal CA1 pyramidal neurons at different developmental stages from postnatal 6–33.

MATERIALS AND METHODS

Animals

We used male *Fmr1* KO mice (FMRP KO, RRID:IMSR_JAX:003025, The Jackson Laboratory), and the C57BL/6J WT mice for this study. The *Fmr1* KO mouse was bred in the C57BL/6J background in a non-littermate fashion. All animals were kept on a 12:12 h light:dark cycle with a constant room temperature and provided with *ad libitum* food and water. The animal experiments were conducted following the animal care guidelines of the University of Washington under approved IACUC protocols.

Slice Preparation

The animals were decapitated and the brains were rapidly removed and placed in ice-cold "slicing solution" equilibrated (130 NaCl, 3.5 KCl, 1.25 NaH_2PO_4, 24 $NaHCO_3$, 10 D-Glucose, 0.5 $CaCl_2$, and 5 $MgCl_2$) with 95% O_2/5% CO_2 mixture, pH 7.4 and 300 μm coronal slices were prepared. In LTP experiments, CA3 was surgically removed immediately after sectioning. After cutting, the slices recovered at 32°C for 1 h before leaving at RT.

Stimulation/Recording

Individual slices were placed in a submerged tissue slice chamber, where the temperature was maintained at 28.0 ± 1°C. Slices were perfused with carbogenated artificial cerebrospinal fluid (ACSF) with a flow rate through the chamber of 2.5 ml/min. ACSF was exactly like slicing solution except Mg^{2+} was lowered to 1.5 mM and Ca^{2+} was raised to 2 mM. A stimulating electrode was placed on the surface of the Stratum radiatum of area CA1 to stimulate the Schaffer collateral/commissural fibers. For LTP experiments, a second stimulating electrode was placed in Stratum radiatum near the subiculum and used to evoke responses in a control pathway that did not receive pattern stimulation. LTP was induced by stimulating the axons at 3 Hz for 120 s while clamping the cell at 0 mV.

Whole-cell voltage-clamp experiments were recorded from CA1 pyramidal neurons using the following intracellular solution (in mM): 115 $CeMeSO_4$, 20 CsCl, 10 Hepes, 2.5 $MgCl_2$, 4 Na_2ATP, 0.4 Na3GTP, 10 NaPhosphatase, 0.6 EGTA, 100 μm spermidine, 5 μM QX314; pH was set at ∼7.4 with CsOH; osmolarity was set at ∼290. For all recordings except LTP recordings, cells were allowed to rest for ∼5 min after whole-cell

configuration was established. Uncompensated series resistance (Rs) was monitored continuously throughout recordings with −5 mV voltage steps before stimulus steps.

Also, either 100 μM picrotoxin or 20 μM bicuculine and 3 μM CGP55845 were routinely added to block $GABA_A$ receptors and $GABA_B$ receptors mediated transmission, respectively. For miniEPSCs, tetrodotoxin (TTX, 1 μM) and DL-2-Amino-5-phosphonopentanoic acid (APV; 100 μM) was added to block sodium channels and NMDARs, respectively.

Other antagonists and blockers used: 2,3-dihydroxy-6-nitro-7-sulfamoyl-benzo[f]quinoxaline [NBQX (10 μM)], and philanthotoxin-74 [PhTx (5 μM)]. All chemicals used were acquired from either Tocris or Sigma–Aldrich.

Post hoc Anatomical Reconstruction and Imaging

For morphological reconstruction, in a subset of whole-cell recordings, 0.1% neurobiotin (Vector labs) were added to the internal solution just before the experiment. Slices were fixed over-night in 3% glutaraldehyde at 4°C, permeabilized in 0.1% Triton X-100, and incubated with Alexa 488-conjugated avidin. Slices were mounted on gelatin-coated slides using Mowiol mounting medium (Sigma) and imaged using a Zeiss LSM 710 confocal microscope (LSM 710). A 20× dry or 63× oil immersion objective was used for acquiring images of neurons. Image size for dendrite analysis was set at 425 × 425 μm and image size for spine analysis was set at 135 × 135 μm, respectively. Images were scanned with an interval of 0.5 μm along the Z-axis.

The maximum projection of Z-stacks was obtained using ImageJ for the spine and dendritic analysis. ImageJ's "Simple Neurite Tracer" (NIH) was used for dendritic reconstruction and Sholl analysis. Secondary apical branches (each dendritic length of 50–200 μm) 50–120 μm from the soma were manually analyzed for spine density and morphology using NeuronStudio (Computational Neurobiology and Imaging Center at the Neuroscience Department of the Mount Sinai School of Medicine, New York, NY, USA). One dendritic section per neuron and 1–3 neurons per animal was analyzed. A total of 17-21KO and 23–27 WT neurons were analyzed for the spine and dendritic morphology in the P6–9 and P14–19 groups, respectively.

The length of the spines was calculated as the difference from the dendritic surface to the tip of the head.

All statistical analysis was performed using GraphPad Prism 6 (GraphPad Software Inc.) or Microsoft Excel. For imaging, dendritic and analysis, and mEPSC analysis, the investigator was blinded with regards to the genotype and age of the animals. Each mEPSC was manually selected offline (MiniAnalysis; Synaptosoft, Decatur, GA, USA).

Significant differences between groups were tested using unpaired Student's *t*-tests, Kolmogorov–Smirnov (K–S), or one-way ANOVA (Tukey's) when appropriate. Asterisk on figures indicates statistical significance ($^*p < 0.05$; $^{**}p < 0.01$; $^{***}p < 0.001$).

RESULTS

Altered synaptic structure and function is a well-known hallmark of FXS and thus, here we wanted to compare early synaptic development of glutamate receptors with a focus on AMPA receptors in FXS and WT hippocampal slices.

AMPA-NMDAR Ratio

First, to investigate glutamatergic neurotransmission in hippocampal synapses of FXS animals during postnatal development, we compared the amplitude of evoked postsynaptic currents (EPSCs) mediated by AMPARs and NMDARs in acute mice hippocampal slices at different developmental stages from early development (P6) to young adult (P33). In WT slices, an increase in the AMPAR to NMDAR ratio was observed from 0.53 ± 0.06 at P6–9 to 1.50 ± 0.21 at $P > 30$ (**Figure 1**), likely reflecting a shift from more silent synapses, i.e., synapses containing only NMDARs, to synapses with a larger content of AMPARs in the developing hippocampus (Liao et al., 1995). Overall, in KO slices the same picture emerged: a shift over time in the AMPAR/NMDAR ratio from 0.75 ± 0.07 at P6–9 to 1.63 ± 0.08 at $P > 30$.

Here, we report no significant difference in the AMPAR/NMDAR ratio between WT and KO in any group tested older than P14. However, in younger age groups (P6-9 and P11-13) a significant increase in the AMPAR/NMDAR ratio was observed in the KO ($p < 0.02$), suggesting a larger AMPAR component or a smaller NMDAR component in KO slices (**Figure 1A**). In the same recordings, in agreement with several other labs (Pfeiffer and Huber, 2007; Pilpel et al., 2009; Zhang et al., 2009; Deng et al., 2011; Eadie et al., 2012), no significant change in pair-pulse ratio was observed (**Figure 1B**) implying no changes in the probability of neurotransmitter release.

Due to changes in stimulation configuration across slices, it is not pertinent to compare absolute values of AMPAR or NMDAR responses between KO and WT slices. However, we noticed that in KO slices younger than P14 AMPAR responses were consistently larger than in their WT slices from P6–9 WT animals had AMPAR responses of −31 ± 3 pA ($n = 17$) while slices of the same age from KO animals have an average response of −55 ± 5 pA ($n = 41$; $p < 0.01$ Student's *t*-test; data not shown). Slices from P11–13 animals also showed a significant difference with average amplitudes of −40 ± 3 pA in the WT slices ($n = 42$) and −57 ± 7 pA in KO slices ($n = 16$; $p < 0.05$; data not shown). AMPAR responses in slices from animals older than P14 were not significantly different. This hinted that AMPAR mediated transmission in KO mice could be altered early in development. Next, we decided to focus on the development of AMPAR mediated transmission in FMRP KO slices to test whether an abnormal AMPAR-mediated transmission occurs early in development.

GluA2 Is Altered in the KO During a "Critical Maturation Period"

The AMPAR subunit GluA2 dictates important biophysical properties like Ca^{2+} permeability through the channel

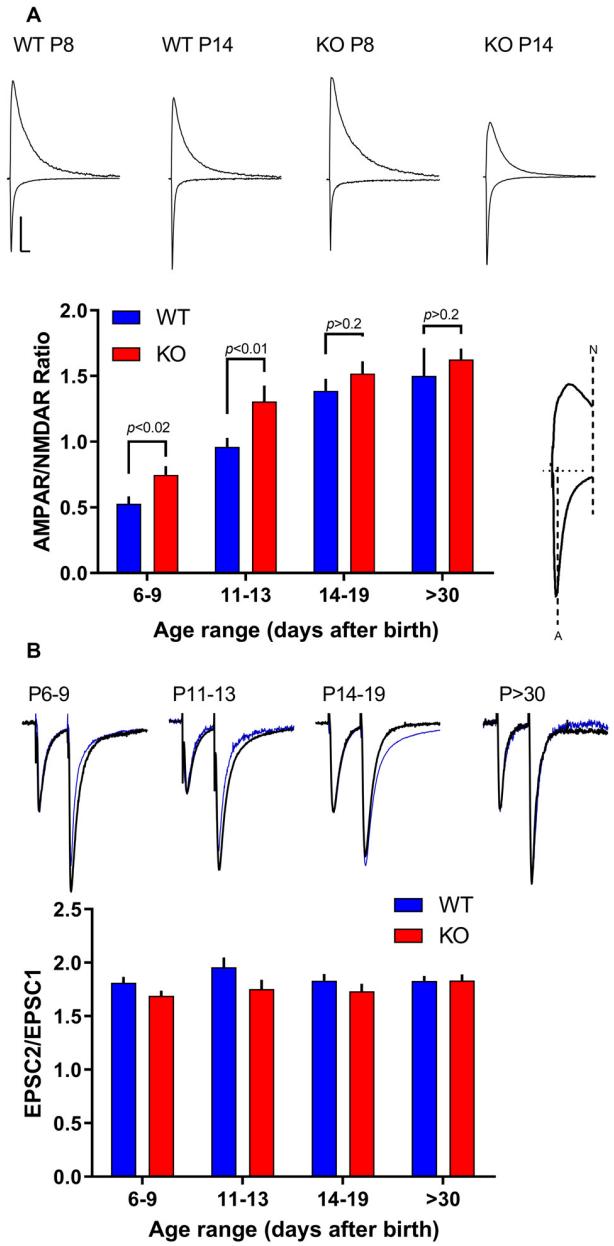

FIGURE 1 | Amplitude of AMPA-type glutamate receptor (AMPAR) and NMDAR-mediated evoked postsynaptic currents (EPSCs) during development. **(A)** Developmental profile of the AMPA Receptor to NMDA Receptor ratio. Top, sample traces of evoked responses from CA1 pyramidal cells recorded in voltage-clamp at −60 mV or +40 mV from wild type (WT) and fragile X mental retardation protein (FMRP) knock-out (KO) slices as indicated. Scale bar = 50 ms and 50 pA. Bottom, population data of AMPAR to NMDAR ratio from WT neurons (blue bars) from slices P6–9 (n = 17), P11–13 (n = 42), P14–19 (n = 47), and $P > 30$ (n = 23). Red bars are from FMRP KO neurons from slices at same age groups (P6–9: n = 36; P11–13: n = 16; P14–19: n = 37; $P > 30$: n = 24). The amplitude of the AMPAR-mediated response was measured at the pick of the response at −60 mV. The amplitude of the NMDAR response was measured at +40 mV 80 ms after the stimulus artifact as indicated in the example on the right. Student's t-test p-values are indicated in the figure. **(B)** Paired-pulse facilitation (PPR) in FMRP KO and WT CA1 neurons at different ages as

(*Continued*)

FIGURE 1 | Continued
indicated. Top, superimposed sample traces of evoked responses from CA1 pyramidal cells recorded in voltage-clamp at −60 mV from WT (thick line) and FMRP KO slices (blue line) as indicated. The traces were normalized to the first peak. PPR quantified as shown in the bar graph below, with the two stimuli delivered 50 ms apart (recorded at −60 mV). n values for WT neurons from P6–9 to $P > 30$ are: 10, 31, 36, 12. n-values for KO neurons from P6–9 to $P > 30$ are: 26, 10, 25, 14. No significant difference was found between WT and KO within age groups ($p > 0.05$).

pore allowing it to play important roles in many Ca^{2+}-dependent cell processes downstream of channel activation like synaptic plasticity. AMPARs lacking GluA2 subunits have high Ca^{2+} permeability, often called Ca^{2+}-permeable AMPARs (CP-AMPARs), and exhibit inward rectification caused by intracellular polyamine block. In contrast, AMPARs containing GluA2 have low calcium permeability, called calcium impermeable-AMPARs (CI-AMPARs), and exhibit a linear current-voltage (I–V) relationship. Thus, the shape of the AMPAR I–V curve reveals whether GluA2 is present or not in the AMPAR complex (Isaac et al., 2007). We define a rectification index (RI) calculated as the amplitude of AMPAR-mediated currents recorded in voltage-clamp while holding the cell at +40 mV over the amplitude of AMPAR-mediated currents recorded at a holding potential of −60 mV. The presence of GluA2 would mean a linear I/V curve, therefore an RI closer to 0.67 (=40/60).

WT slices exhibit an overall rectification value of 0.28 ± 0.12 (n = 59) that remains constant through the periods studied (**Figures 2A–C**), suggesting the presence at synapses of mostly GluA2 lacking AMPARs. However, in slices from KO animals, early in development (<P14), we found a higher RI index (0.39–0.59; **Figures 2A–C**) indicating an enhanced synaptic content of GluA2-containing AMPARs. Because GluA2-containing AMPARs are Ca^{2+} impermeable, this could have important consequences in the normal development of synapses, development of dendrites and spines, and other Ca^{2+}-dependent processes like synaptic plasticity.

This relatively enhanced synaptic GluA2-containing AMPARs seems to go back to normal in slices from KO animals older than P14, as indicated by an RI similar to WT slices. This data suggests that overexpression of GluA2 early in development is only temporary.

This enhanced GluA2 containing AMPARs could indicate the insertion of a completely "novel" AMPAR population, like those composed of the GluA4 and GluA2 subunits to synapses already containing GluA1/GluA2 receptors. The expression of GluA4 is known to be restricted to the first postnatal week in Hippocampus (Zhu et al., 2000) and thus is an interesting candidate. This could be detected in the kinetics of decay of the AMPAR-mediated EPSCS because of the fast kinetics of Glu4 subunits (Lomeli et al., 1994). However, we detect no difference in the decay times of EPSCs in young slices (P6-9; **Figure 2F**) arguing against such a scenario.

To study this phenomenon in more detail, we took advantage of philanthotoxins (PhTXs). AMPARs are blocked by PhTXs which are polyamine toxins isolated from the venom of wasps

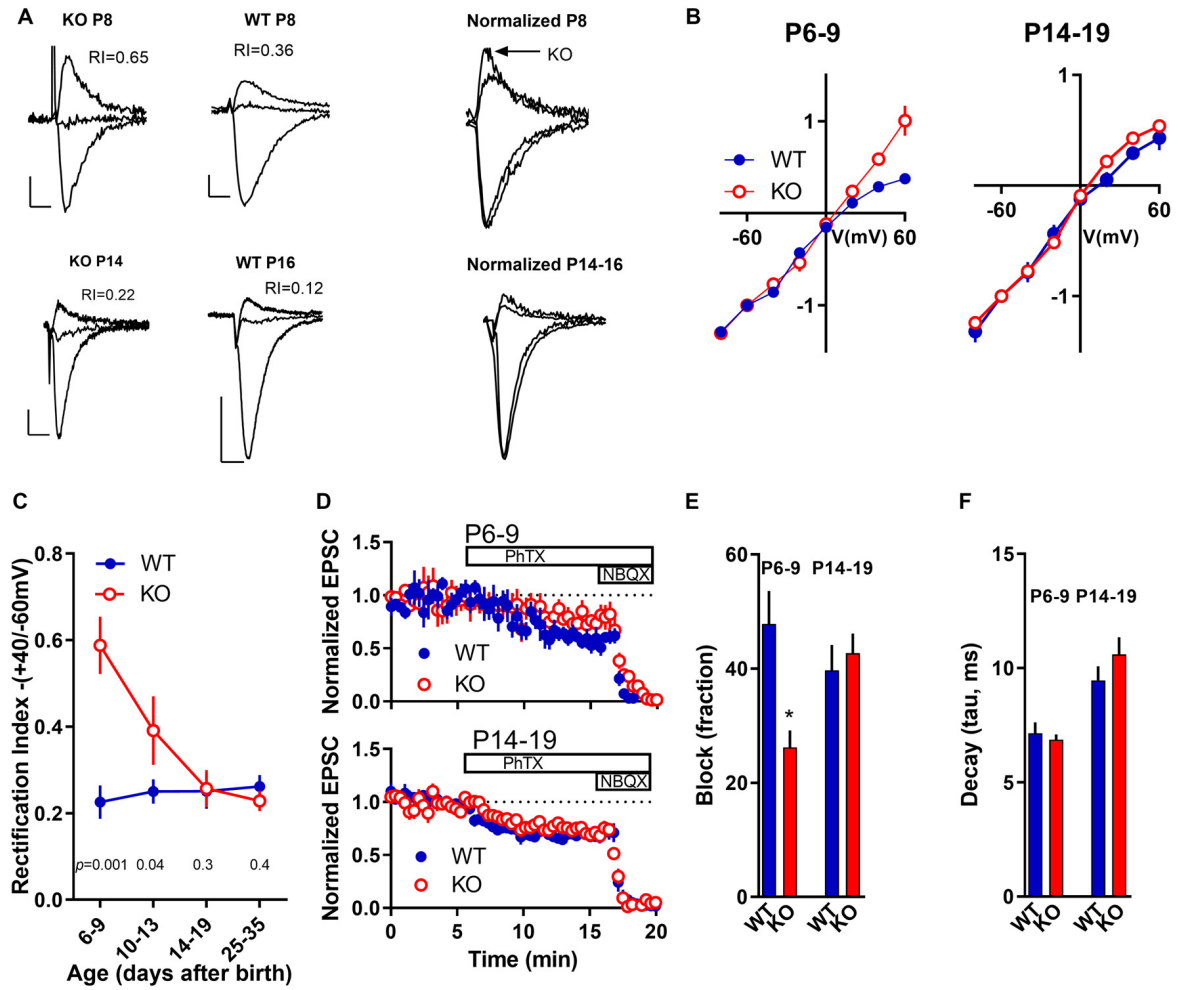

FIGURE 2 | Developmental subunit composition of synaptic AMPARs in the FMRP KO. **(A)** Sample traces of AMPAR EPSCs recorded at −60, 0, and +40 mV in the presence of 100 μM DL-2-Amino-5-phosphonopentanoic acid (APV) in CA1 neurons from FMRP KO or WT neurons as indicated. To the right are the same traces with amplitude normalized to −60 mV. Scale bar = 10 ms and 50 pA. **(B)** Normalized current-voltage plot from P6–9 and P14–19 neurons from KO (white dots; n = 13–22) and WT slices (black dots; n = 8–25). **(C)** Rectification Index (RI) was calculated as the ratio of responses at +40 mV and −60 mV for KO neurons (white dots) and WT neurons (black dots). n values for WT neurons from P6–9 to $P > 30$ are: 16, 17, 9, 5. n values for KO neurons from P6–9 to $P > 30$ are: 10, 11, 17, 10. Student's t-test p-value comparing KO vs. WT at each specific age is indicated in the figure. **(D)** Blockade of AMPAR-mediated currents with PhTx-74. After a 5 min baseline, PhTx was applied to the perfusion bath. Then, 20 μM of the general AMPAR blocker NBQX was added to the bath. Effect of PhTx in slices P6–9 (top) and in P14–19 (bottom) in WT neurons (black dots; n = 6–8) and KO neurons (white dots; n = 7–8). **(E)** The fraction of PhTx-74 blockade measured at the 15–18 min time window in slices as indicated. The asterisk indicates $p < 0.05$ significant difference between P6–9 WT and KO. **(F)** The decay phase of AMPAR-mediated responses was fitted with a single exponential curve and the time constant (tau) was estimated. No significant differences between WT and KO neurons at each age group were observed.

and spiders (Strømgaard et al., 2005). However, the degree of the block depends upon the AMPAR subunit composition. Thus, AMPARs lacking the GluA2 subunit have a higher affinity towards PhTXs that AMPAR containing GluA2 subunits. Thus, we tested the PhTX analog PhTX-74 (Poulsen et al., 2013) on young (P6-9) vs. older slices (P14-19). In slices from young animals (P6-9), after establishing a 5-min baseline, the application of PhTx-74 blocked a larger fraction of AMPAR-mediated EPSCs in WT slices than in KO slices ($p < 0.05$; **Figure 2D**). In slices from older animals (P14-19), no difference in the amount of blockade of AMPAR responses was observed between WT and KO slices ($p > 0.05$; **Figures 2D,E**). This experiment confirms that in the younger FXS Hippocampus, while both GluA2-containing and GluA2-lacking AMPARs exist, a larger proportion of the AMPARs contain the GluA2 subunit in KO than in WT.

Lack of LTP at Synapses in Young KO Animals

AMPARs play important roles in the initiation and maintenance of synaptic plasticity, including LTP (Malinow et al., 2000). Since we observed an increase in GluA2-containing AMPARs

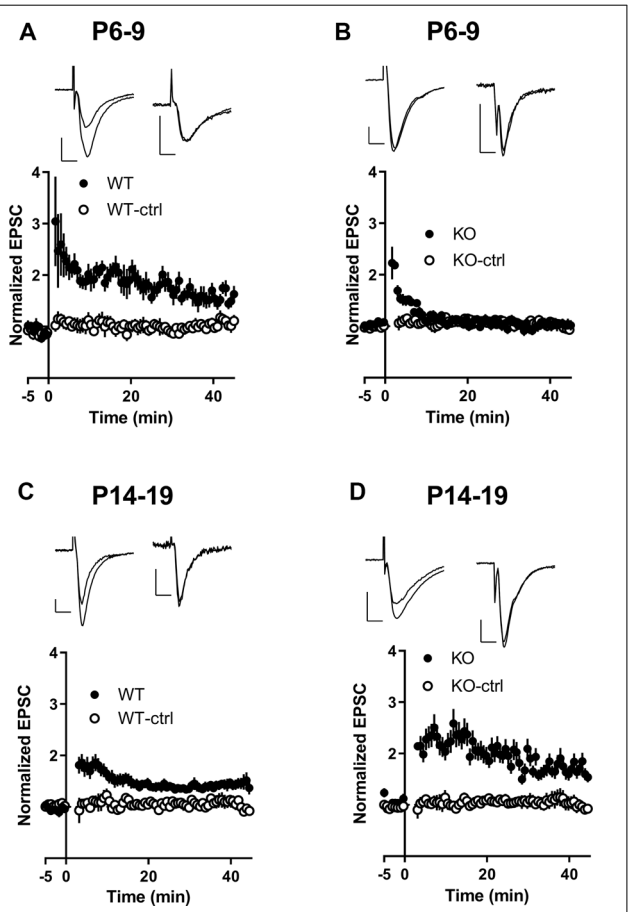

FIGURE 3 | Long-term potentiation (LTP) of Schaffer collateral-CA1 synapses in FMRP KO during early development. **(A–D)** In the presence of a GABAA inhibitor, after obtaining a 5-min baseline, LTP was induced in CA3-CA1 synapses by stimulation of Schaffer collaterals by stimulating the axons at 3 Hz for 2 min while clamping the cell at 0 mV (black dots). A second stimulation electrode was used as a control (white dots). This protocol readily induced LTP in WT P6–9 slices (**A**; $n = 8$) and P14–19 slices (**C**; $n = 13$). **(B,D)** LTP induction in KO slices P6–9 (**B**; $n = 12$) and KO slices P14–19 (**D**; $n = 7$). Insets are examples of evoked EPSCs from the baseline period and 40 min after LTP induction. The left pair of traces are from the test path and the right are from the control path. Scale bars 10 ms and 50 pA.

TABLE 1 | mEPSC statistics.

	IEI (ms)	Amp (pA)	Rise (ms)	Decay (ms)	*n*
P6–9					
p	0.03	<0.001	0.21	0.19	
Average WT	2.9 ± 0.1	10.5 ± 0.5	2.7 ± 0.2	3.8 ± 0.3	25
Average KO	1.1 ± 0.1	16.8 ± 1.6	2.3 ± 0.1	3.2 ± 0.2	26
P14–19					
p	0.79	0.32	0.054	0.6	
Average WT	3.6 ± 0.1	15.2 ± 1.1	2.3 ± 0.06	3.8 ± 0.2	21
Average KO	3.2 ± 0.1	13.5 ± 1.1	2.5 ± 0.1	4.0 ± 0.3	21

Recordings of miniature excitatory postsynaptic currents (mEPSCs) from P6–9 (top) or P14–19 (bottom) CA1 pyramidal neurons in the presence of tetrodotoxin (TTX) and DL-2-Amino-5-phosphonopentanoic acid (APV).. Data are presented as average ± SEM. Inter-event interval (IEI), amplitude (Amp), rise time, decay time, and number (n) of recordings are shown. p calculated from Student's t-test are shown at the top.

in KO animals in an age-depending manner we next attempted to induce LTP in pyramidal neurons using a standard paired stimulation protocol (see "Materials and Methods" section). Robust LTP was obtained in slices from young (P6-9) and older (P14–19) WT animals as described before (Yasuda et al., 2003; Palmer et al., 2004). In slices from KO animals, LTP was induced normally in slices from older animals (P14–19) but it failed to be induced in slices from the younger age group (P6–9; **Figure 3**).

Next, we analyzed the development of synaptic connections by recording miniature EPSCs (mEPSCs) in our slices. We used the mEPSC inter-event interval (IEI) as an indicator of functional synapse number (Gambrill and Barria, 2011), and mEPSC amplitude as a measurement of individual synaptic strength.

The mEPSCs were recorded in the presence of TTX and APV to block sodium channels and NMDARs, respectively. In the P14–19 age group, mEPSC IEI in KO was not significantly different from WT (**Table 1**), whereas the younger KO group (P6–9) exhibited increased mEPSC IEI compared to both the WT (P6–9) group and the P14–19 age groups (**Table 1**; **Figures 4A–D**).

The amplitude of mEPSCs was increased in slices from younger KO animals when compared to WT slices in the same age group. On average, the amplitude of mEPSCs in KO slices at the P6–9 age group was 17 ± 2 pA, significantly higher than their WT counterpart of 10 ± 1 pA (**Table 1**; $p < 0.01$; Student's *t*-test; **Figures 4A–D**). The amplitude in slices from older animals was not significantly different between KO animals and WT; 15 ± 1 pA in WT and 14 ± 1 pA in KO ($p > 0.05$; *t*-test). As shown in **Table 1** there was no significant difference in either rise time or decay time of mEPSCs among the groups.

This data suggests that in animals lacking FMRP, an early increase in synaptic connections exist as indicated by an increase in mEPSCs. Interestingly, this apparent increase in the number of synapses seems to go back to normal as the mEPSC frequency is not different later. More importantly, an increase in the amplitude of mEPSCs is observed in these early synapses, suggesting they may be already be potentiated, thus occluding induction of LTP as shown in **Figure 3**.

Dendritic Morphology

Synaptic plasticity, in particular LTP, it is an important mechanism to stabilize synapses and proper dendritic branching. Considering that early in development, FMRP KO animals show a deficit in LTP we decided to investigate whether this affected the normal dendritic branching of apical and basal dendrites in CA1 pyramidal neurons.

Recording pipettes were backfilled with neurobiotin for *post hoc* neuronal reconstruction. Each reconstructed neuron was built from a series of dendritic branch fragments, each attached to the primary dendrite at specific branch points (**Figure 5A**). Although we found no significant difference in the total number of dendritic fragments within each age group (data not shown), no significant change in overall apical or basal total dendritic length (**Figure 6A**), and no significant difference in the average branch points, we did find a significant difference in the first dendritic branch point between KO and WT. Thus, the first branch point was located further away from the soma in KO in

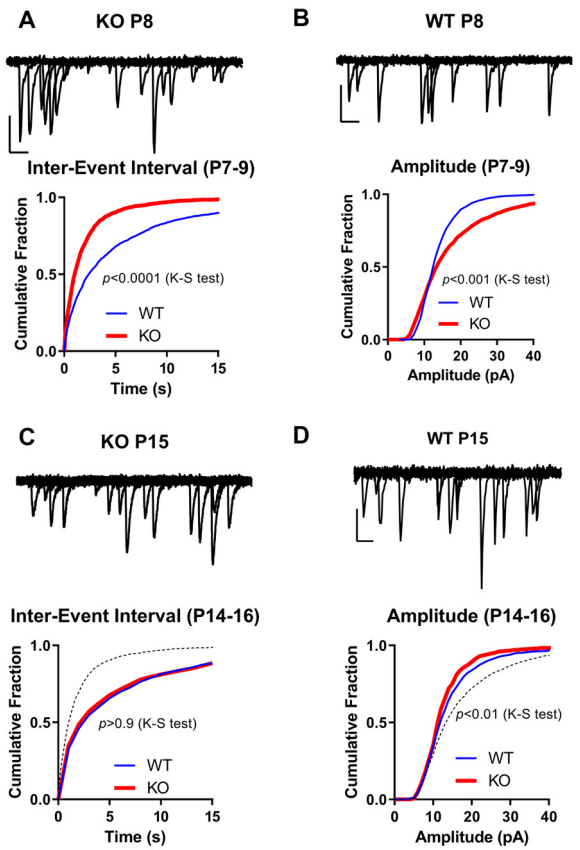

FIGURE 4 | Spontaneous miniature EPSCs in FMRP KO slices. **(A–D)** Cumulative distribution of Inter-Event Intervals **(A,C)** of spontaneous events in CA1 neurons recorded at −60 mV in the presence of TTX and the amplitude of those events **(B,D)** from WT (blue line; n = 19–29) or FMRP KO slices (n = 31–31). **(A,B)** P6–9. **(C,D)** P14–16. Kolmogorov-Smirnov (K-S) test p-value is shown in the figure. For comparison, superimposed on Figure C is WT P6-9 (dotted black line; from **A**). Note the large increase in frequency of mEPSCs (decrease in Inter-Event Intervals) and in the amplitude of those events in KO neurons from slices P6-9. On top of each graph are shown 10 superimposed 250 ms long mEPSC events of KO P8 **(A)**, WT P8 **(B)**, KO P15 **(C)**, and WT P15 **(D)**. Scale bars: X-axis: 20 ms; Y-axis: 20 pA.

both the basal and apical dendritic tree (**Figure 6B**). In support of this, Sholl analysis did reveal similar significant differences in the number of intersections between KO and WT neurons within the first ∼100 μm from the soma in both apical and basal dendritic tree (**Figure 5B**). Combined, these data suggest that WT neurons have, on average, a slightly denser dendritic tree structure near the soma than KO neurons.

Finally, a prominent neuronal phenotype described, and frequently cited, in the FMRP KO mouse as well as in FXS patients is an excessive proportion of thin immature-like tortuous spines. It is important to point out that this phenotype corresponds to cerebral cortex neurons of adult (16-week-old) mice (Comery et al., 1997). Given the age-dependent alterations in synaptic GluA2 expression, lack of hippocampal LTP in young animals, and a less dense dendritic tree in young FMRP KO animals, we next decided to test also dendritic morphology at this critical early stage of development. Secondary apical branches 50–120 μm from the soma of CA1 pyramidal neurons were selected and analyzed for spine density and morphology.

Spine density in WT neurons increased from 0.29 ± 0.03 to 0.49 ± 0.03 spines per micron ($p < 0.01$; **Figure 7**) similar to what has been previously reported in hippocampal pyramidal neurons (Gambrill and Barria, 2011). Similarly, spine density in KO neurons increased from 0.39 ± 0.02 to 0.53 ± 0.06 spines per micron ($p < 0.05$).

When spine density from P6–9 KO neurons is compared to P6–9 WT neurons, a slightly larger spine density in KO neurons is observed, consistent with the increase in mEPSCs frequency observed at this age ($p < 0.01$, t-test). Spine density between WT and KO neurons was no different at P14–19 ($p > 0.5$, t-test).

No significant difference was observed in the spine head diameter within the four groups (**Figure 7C**; $F_{(3,38)} = 0.6272$; $p > 0.5$, one-way ANOVA). Spine length in WT neurons decreased in a significant manner from P6–9 to P14–19 ($p < 0.05$; t-test) as expected as the spines are maturing. In contrast, spines in KO neurons remain at the same length ($p > 0.5$; t-test; **Figure 7D**), suggesting they are unable to properly mature perhaps due to the lack of LTP as observed earlier.

DISCUSSION

Both ASD and FXS are considered neurodevelopmental synaptopathies with an imbalance in excitatory and inhibitory neurotransmission (Spooren et al., 2012; Uzunova et al., 2014; Bagni and Zukin, 2019). The mechanisms that underlie learning and memory, cognitive, and social deficits associated with ASD and FXS are complex and depend on multiple factors including glutamate neurotransmission. ASD has a strong genetic component and genetic studies have implicated hundreds of genes associated with increased risk of ASD (Persico and Napolioni, 2013) where several members of the glutamate receptor family are included (Spooren et al., 2012).

Here, we have investigated the developmental profile of hippocampal CA1 principal neurons at two different developmental time windows; at P6–9 right when the first synaptic connection is being established in these cells, and P14–19, a period characterized by strong synaptogenesis and synaptic plasticity (Dailey and Smith, 1996; De Simoni et al., 2003; Gambrill and Barria, 2011).

Our electrophysiological recordings from FMRP KO slices focusing on ionotropic AMPA glutamate receptors have revealed a critical period by the end of the first 9 days after birth where the GluA2 subunit is upregulated. This confers synaptic AMPARs Ca^{2+} impermeability and a more linear I/V relationship at an age wherein WT slices AMPARs are more Ca^{2+} permeable and therefore could contribute to synaptic plasticity necessary for proper stabilization of nascent synapses (Park et al., 2018). We suggest that the improper brain development that takes place in KO mice is, at least in part, due to this abnormal expression of this important AMPAR subunit. Thus, it is well known that defects in GluA2 cause neurodevelopmental

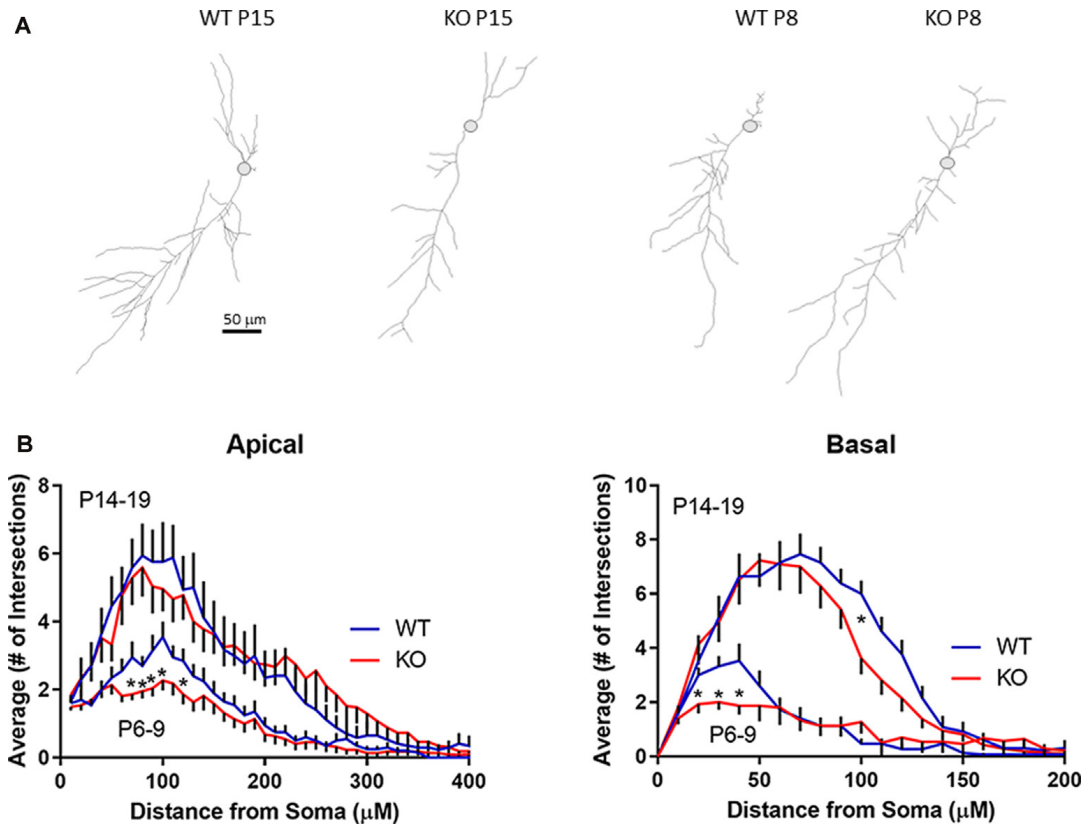

FIGURE 5 | Development of dendritic branching in FMRP KO CA1 neurons. **(A)** Examples of skeleton drawings of CA1 neurons from slices as indicated. Neurons were backfilled with biotin for *post hoc* morphological analysis. Scale bar = 50 μm. **(B)** Sholl analysis indicating the average number of intersections of apical dendrites (left) or basal dendrites (right) with concentric circles spaced 10 μm apart from P6–9 or P14–19 pyramidal neurons from either FMRP KO slices (red line; $n = 23$ and $n = 27$, respectively) or WT slices (blue line; $n = 21$ and $n = 17$, respectively). Asterisks indicate $p < 0.05$ *t*-test statistical significance when comparing WT and KO slices within a particular age group.

disorders. For example, Salpietro et al. (2019) found 28 *de novo* GluA2 mutations in unrelated patients with intellectual disability and neurodevelopmental abnormalities including ASD, Rett syndrome-like features, and seizures or developmental epileptic encephalopathy. Some of these mutations were found to be in the "Q/R" site affecting AMPAR calcium permeability, thus an alternative explanation could be dysregulation of ADAR2 (the Q/R editing enzyme) rather than a change in the expression of GluA2 protein itself.

The basis for the FXS phenotype is the lack of FMRP. The FMRP protein is highly localized to dendrites and spines (Pimentel, 1999; Bagni and Oostra, 2013) and has a wide variety of targets it is a selective RNA-binding protein that associates with polyribosomes and acts as a negative regulator of translation. FMRP has been shown to selectively bind approximately 4% of the mRNA in the mammalian brain (Ashley et al., 1993; Brown et al., 2001) and thereby affecting a wide variety of proteins, including many synaptic proteins and proteins involved in spine formation (Liu-Yesucevitz et al., 2011) and synaptic plasticity (Sidorov et al., 2013), including glutamate receptors (Sidorov et al., 2013). Expression and regulation of individual subunits that compose AMPARs, as well as the Ca^{2+} permeable NMDA-type glutamate receptors, happens in a very tightly orchestrated manner (Lohmann and Kessels, 2014). Any divergence from this can have serious consequences, including neurological conditions. Our results indicate a larger AMPAR to NMDAR ratio before postnatal 14 in slices from KO animals. This increase becomes normal after the beginning of the second postnatal week. This transient increase in AMPAR transmission could have developmental consequences in the formation of neuronal circuits, such that later, even though the ratio becomes normal, circuits have already been altered. The shift in the AMPAR/NMDAR ratio will also be influenced by impaired regulation of NMDARs known in the Fmr1 mouse. Disrupted NMDAR dependent synaptic plasticity has been reported mainly in the dentate gyrus (Yun and Trommer, 2011; Eadie et al., 2012; Franklin et al., 2014; Bostrom et al., 2015, 2016) but also in the CA1 area of the hippocampus (Toft et al., 2016; Lundbye et al., 2018). In contrast to our findings, Pilpel and colleagues reported a decreased AMPAR to the NMDAR ratio in the P14–16 age group in CA1 pyramidal neurons. The exact reason for this is

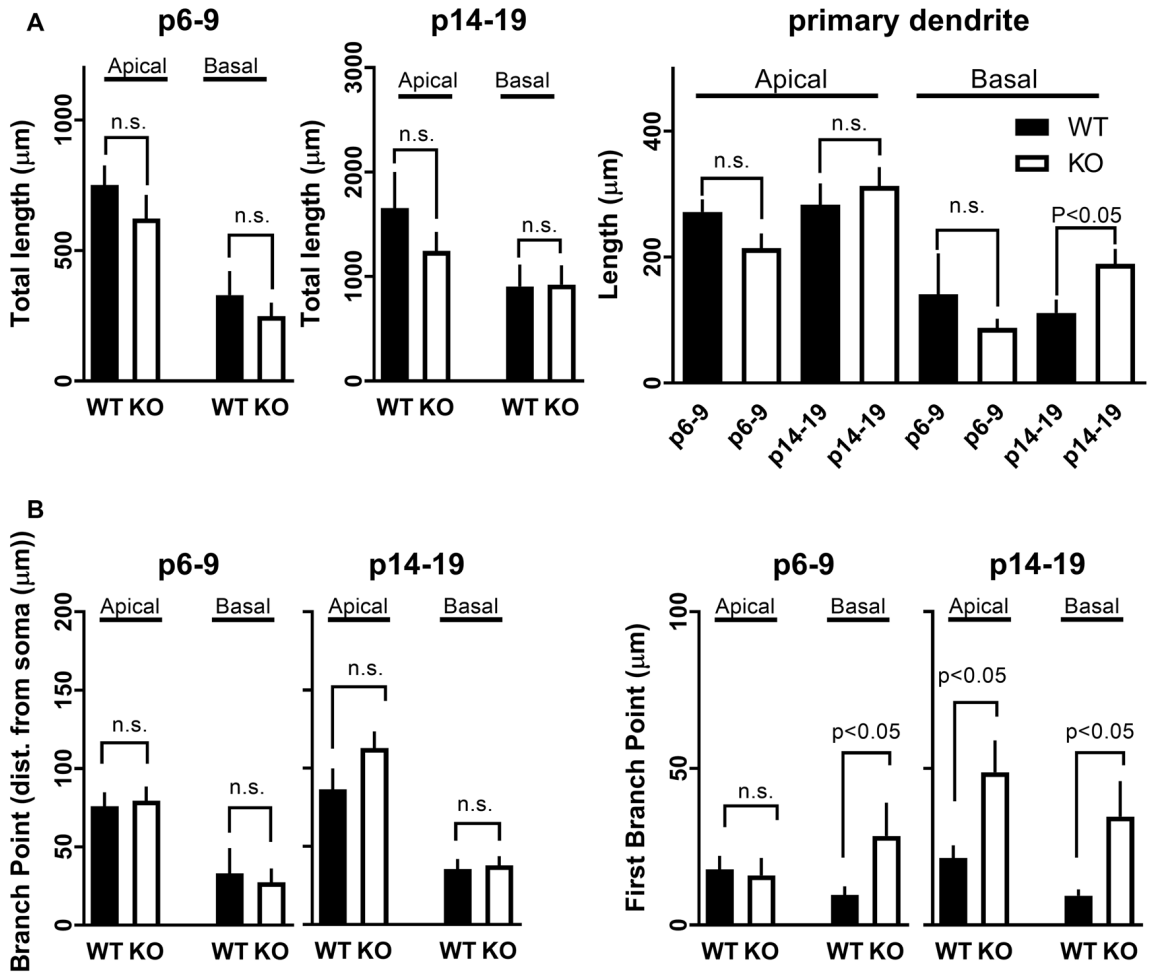

FIGURE 6 | Development of dendritic branches in CA1 pyramidal neurons in FMRP KO mice. **(A)** Total length of dendritic branches in CA1 neurons either WT (black bars) or FMRP KO (white bars). The length of apical or basal dendrites was measured in slices either P6–9 (left) or slice P14–19 (right). The Student's *t*-test shows no significance between WT and FMRP KO neurons within the different age groups or types of the dendrite. (Right) Length of dendritic branches broken down into primary dendrite from CA1 neurons as indicated. **(B)** Distance from soma to average all (left) or first (right) branching point in CA1 neurons from either WT (black bars) or FMRP KO (white bars) from slices P6–9 or slices P14–19 as indicated in Figure. The Student's *t*-test shows significance ($p < 0.05$) between WT and FMRP KO neurons within the different age groups for the first branch point. n.s.: not significant.

unknown but it is important to point out that (Pilpel et al., 2009) used a double KO (Fmr1 KO2) and perhaps that remaining Fmr1 mRNA in the "conventional" Fmr1KO mouse (used here) are involved in synaptic regulation.

Spine Morphogenesis

While the literature on dendritic spines in Fmr1 KO mice has been contradictory, there is a growing consensus that dendritic spine density is increased in Fmr1 KO hippocampus and cortex (Levenga et al., 2011; Pop et al., 2014; Jawaid et al., 2016; see also Bostrom et al., 2016 for review). Discrepancies in CA1 dendritic spine density and morphology in the KO are likely due to several variables including the age of the animals and the method of spine detection.

Interestingly, GluA2 has been reported to be directly involved in spine morphogenesis. Overexpression of GluA2 increases spine length, spine head width, and density in hippocampal cell cultures (Passafaro et al., 2003; Saglietti et al., 2007), all hallmarks of FXS spine abnormalities (He and Portera-Cailliau, 2013). Our data indicate that the upregulation of GluA2 happens during a critical developmental phase with intense synaptogenesis and synaptic pruning in the hippocampus and elsewhere in the brain. Interestingly, in the barrel cortex, a similar temporarily early development disruption of glutamate receptors was found as reported here (Harlow et al., 2010). Also in pluripotent stem cell lines generated from boys with FXS had altered GluA2 level compared to control (Achuta et al., 2018). Overall, our data combined with (Harlow et al., 2010), points toward a scenario where during early development, glutamate receptors are temporarily dysregulated. The temporary window might be short (just a few days) where after the receptors seems to settle down to normal. Thus, it is perhaps not surprising that

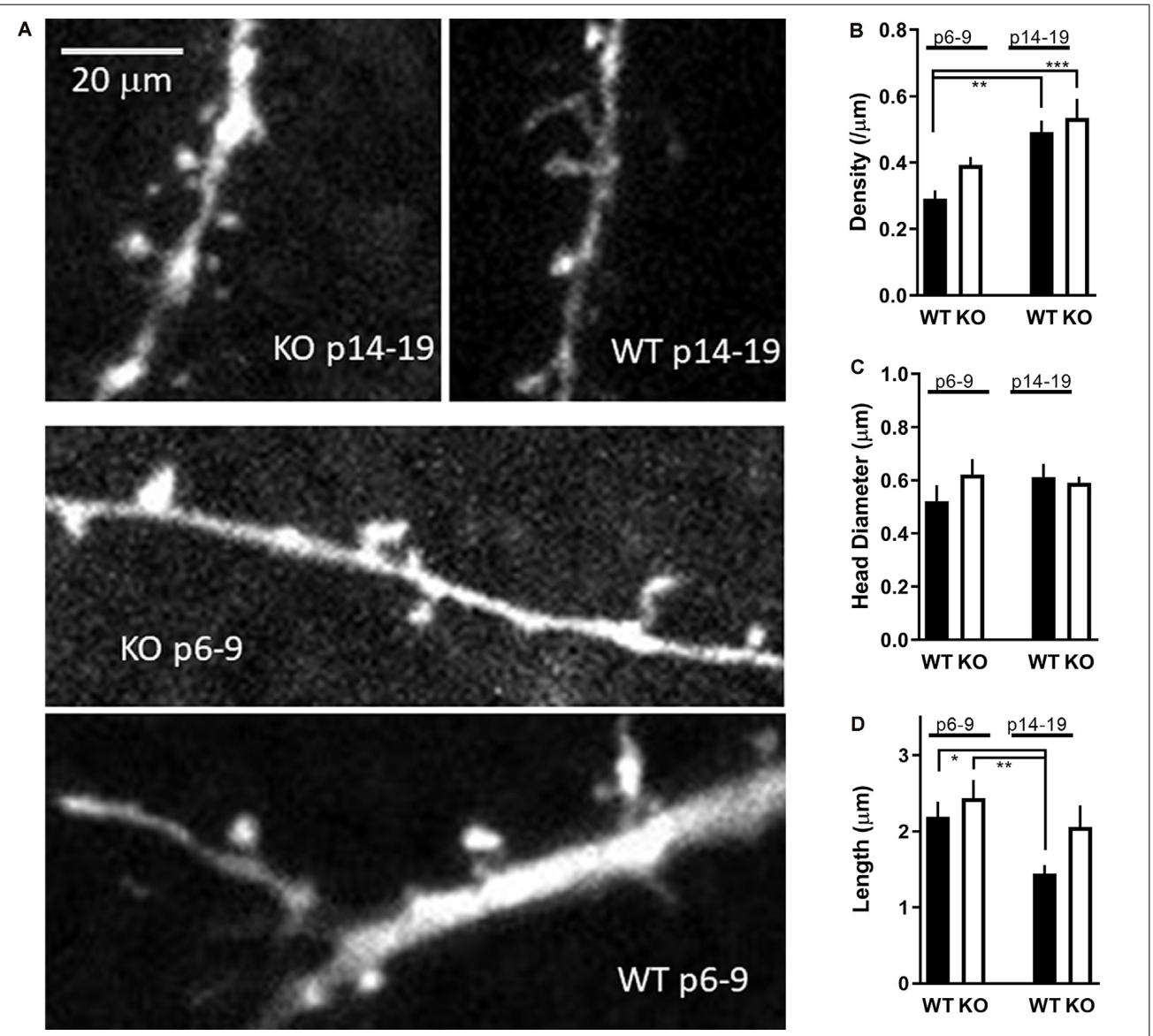

FIGURE 7 | Development of dendritic spines in FMR1 KO CA1 neurons. **(A)** Sample images of apical dendrites with spines from WT and FMRP KO neurons as indicated in the figure. A total of 17–21 KO and 23–27 WT neurons were analyzed for spine morphology in the P6–9 and P14–19 groups, respectively. The scale bar is shown in the upper left is 20 μm. **(B)** Spine density in WT CA1 neurons (black bars) or FMRP KO neurons (white bars) from slices P6–9 or P14–19 as indicated. The asterisk indicates significance using one-way ANOVA ($F_{(1.959,15.67)}$ = 8.663) with Tukey *post hoc* analysis. **(C)** Spine head diameter from CA1 neurons as in panel **(B)**. **(D)** Spine length from CA1 neurons as in panel **(B)**. Asterisk indicates statistical significance (one-way ANOVA $F_{(F1.872,14.35)}$ = 6.831).

the premature expression of this important synaptic protein influences the function and development of new synapses in the KO animal. Despite no clear difference in gross morphology in CA1 neurons from KO animals, we did found less branching for both apical and basal dendrites as determined by the number of dendritic crossing each concentric circle in Sholl analysis (**Figure 5**) as well as shifted first branch point in the KO (**Figure 6**). This is in agreement with previous reports that described similar findings in CA1 pyramidal neurons isolated from patients with autism (Raymond et al., 1996). Altered branching will ultimately lead to altered dendritic inputs and subsequent altered dendritic integration of inputs. On the other hand, dendritic spines density was upregulated in the immature KO age group to the same level as detected in the older age group. However, the only group where we could detect a maturing of spines was in the (P14–19) WT group where the average spine length shrunk over time suggesting more "mushroom" like spines than in the KO groups. In summary, at around the end of first postnatal week, an abnormal neuronal dendritic branching pattern is observed in CA1 pyramidal neurons from KO animals along with dendritic spines with a more immature morphology.

Altered synaptic glutamate receptors in the immature KO could interfere with the ability of the synapse to undergo plasticity. Early reports indicate that in mice lacking GluA2, LTP could still be induced (Jia et al., 1996). Since GluA2-lacking receptors are Ca^{2+} permeable (Burnashev et al., 1992), this suggested that CP-AMPARs may be alternative triggers for LTP at CA1 synapses. If the Ca^{2+} contribution of GluA2-lacking AMPARs is important for LTP early in development, it is reasonable to think that overexpression of GluA2 could diminish or eliminate LTP depending on the strength of the inducing protocol used. Here, we show that in the P6–9 KO group LTP was not observed suggesting that lack of Ca^{2+} permeable AMPARs limits the ability of synapses to undergo potentiation.

A wealth of information exists about LTP in the CA1 area in the KO with varying results from reduced (Lauterborn et al., 2007; Hu et al., 2008; Shang et al., 2009; Lundbye et al., 2018) to no difference (Godfraind et al., 1996; Li et al., 2002; Larson et al., 2005) in KO LTP. The vast majority of these LTP experiments are done in older mice than used here and thus the diversity of these results might be a result of recordings at different ages in addition to using different LTP-inducing protocols or other technical differences.

We observed a decrease in the frequency of AMPAR-mediated mEPSCs early in KO development as well as a decrease in their amplitude within the range of previous publications (Pfeiffer and Huber, 2007; Pilpel et al., 2009; Anggono et al., 2011; Luchkina et al., 2014; Lee et al., 2018). In addition to the lack of Ca^{2+} permeability, a larger fraction of synaptic AMPARs as indicated by larger mEPSCs amplitude could also contribute to occlude induction of LTP (Lledo et al., 1995).

The fact that synapses seem to be already potentiated with a larger ratio of AMPARs to NMDARs but morphological immature, suggests that synapses have not undergone regular plasticity. The increase in synapses observed, measured as an increase in spine density and increased mEPSC frequency with no changes in the pre-synaptic release, could be a compensatory cellular mechanism due to synapses that have not undergone required plasticity that stabilizes and selects some spines and synapses and allows removal of others.

What comes first: abnormal dendritic spine morphology, dysregulated synaptic proteins, or dysregulated synaptic plasticity? To solve the order of problems is challenging. What seems clear here, however, is that once the KO P6–9 reaches the P14 state, almost every parameter investigated here has gone back to normal and no differences with WT CA1 neurons are observed. In other words, the CA1 pyramidal neurons seem to have adapted to their changing environment. All the alterations observed early in development, increased AMPAR to NMDAR ratio, increased synaptic expression of GluA2, increased mEPSCs frequency and amplitude, immature spines, and lack of LTP, happen at a time when the brain is rapidly developing and any of these alterations will impact the developing neuronal circuits needed for proper brain function.

CONCLUSION

One puzzling hallmark of the FMRP KO mouse is that yet, despite lacking the Fmr1 protein, despite having spine morphology issues, despites having plasticity issues, the KO phenotype is still roughly identical to WT, i.e., it eats and breed normally, and are by large hard to distingue from WT. This suggests that the mouse during early development seems able to adapt to it inherited "errors." Here, we have established a critical period early in the Fmr1 KO mouse' life where an important synaptic protein is dysregulated. As also demonstrated here this receptor is heavily involved in different types of synaptic plasticity and is directly involved in dendritic spine morphology. We found that about 2 weeks postnatal (5 days after the critical period), most of the abnormalities have normalized. This critical adaption period might explain why the Fmr1 KO mouse behaves largely as its WT counterpart.

DATA AVAILABILITY STATEMENT

The original contributions presented in the study are included in the article, further inquiries can be directed to the corresponding author.

ETHICS STATEMENT

The animal study was reviewed and approved by Institutional Animal Care and Use Committee (IACUC) at the University of Washington.

AUTHOR CONTRIBUTIONS

TB and AB designed the experiments, analyzed the data, and wrote the article. All authors contributed to the article and approved the submitted version.

FUNDING

This work was supported by a FRAXA Research Foundation grant to TB and an National Science Foundation (NSF) grant (IOS-1755004) to AB.

REFERENCES

Achuta, V. S., Möykkynen, T., Peteri, U.-K., Turconi, G., Rivera, C., Keinänen, K., et al. (2018). Functional changes of AMPA responses in human induced pluripotent stem cell-derived neural progenitors in fragile x syndrome. *Sci. Signal.* 11:eaan8784. doi: 10.1126/scisignal.aan8784

Anggono, V., Clem, R. L., and Huganir, R. L. (2011). PICK1 loss of function occludes homeostatic synaptic scaling. *J. Neurosci.* 31, 2188–2196. doi: 10.1523/JNEUROSCI.5633-10.2011

Ashley, C. T. Jr., Wilkinson, K. D., Reines, D., and Warren, S. T. (1993). FMR1 protein: conserved RNP family domains and selective RNA binding author. *Science* 262, 563–566. doi: 10.1126/science.7692601

Bagni, C., and Oostra, B. A. (2013). Fragile X syndrome: from protein function to therapy. *Am. J. Med. Genet. A* 161, 2809–2821. doi: 10.1002/ajmg.a.36241

Bagni, C., and Zukin, R. S. (2019). A synaptic perspective of fragile X syndrome and autism spectrum disorders. *Neuron* 101, 1070–1088. doi: 10.1016/j.neuron.2019.02.041

Bostrom, C. A., Majaess, N.-M., Morch, K., White, E., Eadie, B. D., and Christie, B. R. (2015). Rescue of NMDAR-dependent synaptic plasticity in Fmr1 knock-out mice. *Cereb. Cortex* 25, 271–279. doi: 10.1093/cercor/bht237

Bostrom, C., Yau, S.-Y., Majaess, N., Vetrici, M., Gil-Mohapel, J., and Christie, B. R. (2016). Hippocampal dysfunction and cognitive impairment in Fragile-X Syndrome. *Neurosci. Biobehav. Rev.* 68, 563–574. doi: 10.1016/j.neubiorev.2016.06.033

Bowie, D. (2008). Ionotropic glutamate receptors and CNS disorders derek. *CNS Neurol. Disord. Drug Targets* 7, 129–143. doi: 10.2174/187152708784083821

Brown, V., Jin, P., Ceman, S., Darnell, J. C., O'Donnell, W. T., Tenenbaum, S. A., et al. (2001). Microarray identification of FMRP-associated brain mRNAs and altered mRNA translational profiles in fragile X syndrome. *Cell* 107, 477–487. doi: 10.1016/s0092-8674(01)00568-2

Burnashev, N., Monyer, H., Seeburg, P. H., and Sakmann, B. (1992). Divalent ion permeability of AMPA receptor channels is dominated by the edited form of a single subunit. *Neuron* 8, 189–198. doi: 10.1016/0896-6273(92)90120-3

Comery, T. A., Harris, J. B., Willems, P. J., Oostra, B. A., Irwin, S. A., Weiler, I. J., et al. (1997). Abnormal dendritic spines in fragile X knockout mice: maturation and pruning deficits. *Proc. Natl. Acad. Sci. U S A* 94, 5401–5404. doi: 10.1073/pnas.94.10.5401

Contractor, A., Klyachko, V. A., and Portera-Cailliau, C. (2015). Altered neuronal and circuit excitability in fragile X syndrome. *Neuron* 87, 699–715. doi: 10.1016/j.neuron.2015.06.017

Dailey, M. E., and Smith, S. J. (1996). The dynamics of dendritic hippocampal slices. *J. Neurosci.* 16, 2983–2994. doi: 10.1523/JNEUROSCI.16-09-02983.1996

De Simoni, A., Griesinger, C. B., and Edwards, F. A. (2003). Development of rat CA1 neurones in acute versus organotypic slices: role of experience in synaptic morphology and activity. *J. Physiol.* 550, 135–147. doi: 10.1113/jphysiol.2003.039099

Deng, P.-Y., Sojka, D., and Klyachko, V. A. (2011). Abnormal presynaptic short-term plasticity and information processing in a mouse model of fragile X syndrome. *J. Neurosci.* 31, 10971–10982. doi: 10.1523/JNEUROSCI.2021-11.2011

Eadie, B. D., Cushman, J., Kannangara, T. S., Fanselow, M. S., and Christie, B. R. (2012). NMDA receptor hypofunction in the dentate gyrus and impaired context discrimination in adult Fmr1 knockout mice. *Hippocampus* 22, 241–254. doi: 10.1002/hipo.20890

Edbauer, D., Neilson, J. R., Foster, K. A., Wang, C.-F., Seeburg, D. P., Batterton, M. N., et al. (2010). Regulation of synaptic structure and function by FMRP-associated microRNAs miR-125b and miR-132. *Neuron* 65, 373–384. doi: 10.1016/j.neuron.2010.01.005

Franklin, A. V., King, M. K., Palomo, V., Martinez, A., McMahon, L. L., and Jope, R. S. (2014). Glycogen synthase kinase-3 inhibitors reverse deficits in long-term potentiation and cognition in fragile X mice. *Biol. Psychiatry* 75, 198–206. doi: 10.1016/j.biopsych.2013.08.003

Gambrill, A. C., and Barria, A. (2011). NMDA receptor subunit composition controls synaptogenesis and synapse stabilization. *Proc. Natl. Acad. Sci. U S A* 108, 5855–5860. doi: 10.1073/pnas.1012676108

Garber, K. B., Visootsak, J., and Warren, S. T. (2008). Fragile X syndrome. *Eur. J. Hum. Genet.* 16, 666–672. doi: 10.1038/ejhg.2008.61

Godfraind, J.-M., Reyniers, E., De Boulle, K., D'Hooge, R., De Deyn, P. P., Bakker, C. E., et al. (1996). Long-term potentiation in the hippocampus of fragile X knockout mice. *Am. J. Med. Genet.* 64, 246–251. doi: 10.1002/(SICI)1096-8628(19960809)64:2<246::AID-AJMG2>3.0.CO;2-S

Harlow, E. G., Till, S. M., Russell, T. A., Wijetunge, L. S., Kind, P., and Contractor, A. (2010). Critical period plasticity is disrupted in the barrel cortex of Fmr1 knockout mice. *Neuron* 65, 385–398. doi: 10.1016/j.neuron.2010.01.024

He, C. X., and Portera-Cailliau, C. (2013). The trouble with spines in fragile X syndrome: density, maturity and plasticity. *Neuroscience* 251, 120–128. doi: 10.1016/j.neuroscience.2012.03.049

Hernandez, R. N., Feinberg, R. L., Vaurio, R., Passanante, N. M., Thompson, R. E., and Kaufmann, W. E. (2009). Autism spectrum disorder in fragile X syndrome: a longitudinal evaluation. *Am. J. Med. Genet.* 149A, 1125–1137. doi: 10.1002/ajmg.a.32848

Hu, H., Qin, Y., Bochorishvili, G., Zhu, Y., van Aelst, L., and Zhu, J. J. (2008). Ras signaling mechanisms underlying impaired GluR1-dependent plasticity associated with fragile X syndrome. *J. Neurosci.* 28, 7847–7862. doi: 10.1523/JNEUROSCI.1496-08.2008

Huber, K. M., Gallagher, S. M., Warren, S. T., and Bear, M. F. (2002). Altered synaptic plasticity in a mouse model of fragile X mental retardation. *Proc. Natl. Acad. Sci. U S A* 99, 7746–7750. doi: 10.1073/pnas.122205699

Isaac, J. T. R., Ashby, M. C., and McBain, C. J. (2007). The role of the GluR2 subunit in AMPA receptor function and synaptic plasticity. *Neuron* 54, 859–871. doi: 10.1016/j.neuron.2007.06.001

Jawaid, S., Kidd, G., Wang, J., Swetlik, C., Dutta, R., and Trapp, B. (2016). Alterations in CA1 hippocampal synapses in a mouse model of fragile X syndrome. *Glia* 118, 6072–6078. doi: 10.1002/glia.23284

Jia, Z., Agopyan, N., Miu, P., Xiong, Z., Henderson, J., Gerlai, R., et al. (1996). Enhanced LTP in mice deficient in the AMPA receptor GluR2. *Neuron* 17, 945–956. doi: 10.1016/s0896-6273(00)80225-1

Kalmbach, B. E., Johnston, D., and Brager, D. H. (2015). Cell-type specific channelopathies in the prefrontal cortex of the fmr1-/y mouse model of fragile X syndrome. *eNeuro* 2:ENEURO.0114-15.2015. doi: 10.1523/ENEURO.0114-15.2015

Larson, J., Jessen, R. E., Kim, D., Fine, A. K. S., and Du Hoffmann, J. (2005). Age-dependent and selective impairment of long-term potentiation in the anterior piriform cortex of mice lacking the fragile X mental retardation protein. *J. Neurosci.* 25, 9460–9469. doi: 10.1523/JNEUROSCI.2638-05.2005

Lauterborn, J. C., Rex, C. S., Kramár, E., Chen, L. Y., Pandyarajan, V., Lynch, G., et al. (2007). Brain-derived neurotrophic factor rescues synaptic Plasticity in a mouse model of Fragile X syndrome. *J. Neurosci.* 27, 10685–10694. doi: 10.1523/JNEUROSCI.2624-07.2007

Lee, K. Y., Jewett, K. A., Chung, H. J., and Tsai, N. P. (2018). Loss of fragile X protein FMRP impairs homeostatic synaptic downscaling through tumor suppressor p53 and ubiquitin E3 ligase Nedd4–2. *Hum. Mol. Genet.* 27, 2805–2816. doi: 10.1093/hmg/ddy189

Levenga, J., de Vrij, F. M. S., Buijsen, R. A. M., Li, T., Nieuwenhuizen, I. M., Pop, A., et al. (2011). Subregion-specific dendritic spine abnormalities in the hippocampus of Fmr1 KO mice. *Neurobiol. Learn. Mem.* 95, 467–472. doi: 10.1016/j.nlm.2011.02.009

Li, J., Pelletier, M. R., Perez Velazquez, J.-L., and Carlen, P. L. (2002). Reduced cortical synaptic plasticity and GluR1 expression associated with fragile X mental retardation protein deficiency. *Mol. Cell. Neurosci.* 19, 138–151. doi: 10.1006/mcne.2001.1085

Liao, D., Hessler, N. A., and Malinow, R. (1995). Activation of postsynaptically silent synapses during pairing-induced LTP in CA1 region of hippocampal slice. *Nature* 375, 400–404. doi: 10.1038/375400a0

Liu-Yesucevitz, L., Bassell, G. J., Gitler, A. D., Hart, A. C., Klann, E., Richter, J. D., et al. (2011). Local RNA translation at the synapse and in disease. *J. Neurosci.* 31, 16086–16093. doi: 10.1523/JNEUROSCI.4105-11.2011

Lledo, P. M., Hjelmstadt, G. O., Mukherjil, S., Soderlingt, T. R., Malenka, R. C., and Nicoll, R. A. (1995). Calcium/calmodulin-dependent kinase II and long-term potentiation enhance synaptic transmission by the same mechanism. *Proc. Natl. Acad. Sci. U S A* 92, 11175–11179. doi: 10.1073/pnas.92.24.11175

Lohmann, C., and Kessels, H. W. (2014). The developmental stages of synaptic plasticity. *J. Physiol.* 592, 13–31. doi: 10.1113/jphysiol.2012.235119

Lomeli, H., Mosbacher, J., Melcher, T., Höger, T., Jörg, R. P., Kuner, T., et al. (1994). Control of kinetic properties of AMPA receptor channels by nuclear RNA editing. *Science* 266, 1709–1713. doi: 10.1126/science.7992055

Luchkina, N. V., Huupponen, J., Clarke, V. R. J., Coleman, S. K., Keinanen, K., Taira, T., et al. (2014). Developmental switch in the kinase dependency of long-term potentiation depends on expression of GluA4 subunit-containing AMPA receptors. *Proc. Natl. Acad. Sci. U S A* 111, 4321–4326. doi: 10.1073/pnas.1315769111

Lundbye, C. J., Toft, A. K. H., and Banke, T. G. (2018). Inhibition of GluN2A NMDA receptors ameliorates synaptic plasticity deficits in the Fmr1−/y mouse model. *J. Physiol.* 596, 5017–5031. doi: 10.1113/JP276304

Lüscher, C., and Malenka, R. C. (2012). NMDA receptor-dependent long-term potentiation and long-term depression (LTP/LTD). *Cold Spring Harb. Perspect. Biol.* 4:a005710. doi: 10.1101/cshperspect.a005710

Malinow, R., Mainen, Z. F., and Hayashi, Y. (2000). LTP mechanisms: from silence to four-lane traffic. *Curr. Opin. Neurobiol.* 10, 352–357. doi: 10.1016/s0959-4388(00)00099-4

McBain, C. J., and Fisahn, A. (2001). Interneurons unbound. *Nat. Rev. Neurosci.* 2, 11–23. doi: 10.1038/35049047

Palmer, M. J., Isaac, J. T. R., and Collingridge, G. L. (2004). Multiple, developmentally regulated expression mechanisms of long-term potentiation at CA1 synapses. *J. Neurosci.* 24, 4903–4911. doi: 10.1523/JNEUROSCI.0170-04.2004

Park, P., Kang, H., Sanderson, T. M., Bortolotto, Z. A., Georgiou, J., Zhuo, M., et al. (2018). The role of calcium-permeable AMPARs in long-term potentiation at principal neurons in the rodent hippocampus. *Front. Synaptic Neurosci.* 10:42. doi: 10.3389/fnsyn.2018.00042

Passafaro, M., Nakagawa, T., Sala, C., and Sheng, M. (2003). Induction of dendritic spines by an extracellular domain of AMPA receptor subunit GluR2. *Nat. Neurosci.* 424, 677–681. doi: 10.1038/nature01781

Penagarikano, O., Mulle, J. G., and Warren, S. T. (2007). The pathophysiology of fragile x syndrome. *Annu. Rev. Genomics Hum. Genet.* 8, 109–129. doi: 10.1146/annurev.genom.8.080706.092249

Persico, A. M., and Napolioni, V. (2013). Autism genetics. *Behav. Brain Res.* 251, 95–112. doi: 10.1016/j.bbr.2013.06.012

Pfeiffer, B. E., and Huber, K. M. (2007). Fragile X mental retardation protein induces synapse loss through acute postsynaptic translational regulation. *J. Neurosci.* 27, 3120–3130. doi: 10.1523/JNEUROSCI.0054-07.2007

Pilpel, Y., Kolleker, A., Berberich, S., Ginger, M., Frick, A., Mientjes, E., et al. (2009). Synaptic ionotropic glutamate receptors and plasticity are developmentally altered in the CA1 field of Fmr1 knockout mice. *J. Physiol.* 587, 787–804. doi: 10.1113/jphysiol.2008.160929

Pimentel, M. M. G. (1999). Fragile X syndrome (review). *Int. J. Mol. Med.* 3, 639–645.

Pop, A. S., Levenga, J., De Esch, C. E. F., Buijsen, R. A. M., Nieuwenhuizen, I. M., Li, T., et al. (2014). Rescue of dendritic spine phenotype in Fmr1 KO mice with the mGluR5 antagonist AFQ056/Mavoglurant. *Psychopharmacology* 231, 1227–1235. doi: 10.1007/s00213-012-2947-y

Poulsen, M. H., Lucas, S., Stromgaard, K., and Kristensen, A. S. (2013). Evaluation of PhTX-74 as subtype-selective inhibitor of GluA2-containing AMPA receptors. *Mol. Pharmacol.* 85, 261–268. doi: 10.1124/mol.113.089961

Raymond, G., Bauman, M., and Kemper, T. (1996). Hippocampus in autism: a Golgi analysis. *Acta Neuropathol.* 91, 117–119. doi: 10.1007/s004010050401

Saglietti, L., Dequidt, C., Kamieniarz, K., Rousset, M. C., Valnegri, P., Thoumine, O., et al. (2007). Extracellular interactions between GluR2 and N-cadherin in spine regulation. *Neuron* 54, 461–477. doi: 10.1016/j.neuron.2007.04.012

Salpietro, V., Dixon, C. L., Guo, H., Bello, O. D., Vandrovcova, J., Efthymiou, S., et al. (2019). AMPA receptor GluA2 subunit defects are a cause of neurodevelopmental disorders. *Nat. Commun.* 10:3094. doi: 10.1038/s41467-019-10910-w

Santoro, M. R., Bray, S. M., and Warren, S. T. (2012). Molecular mechanisms of fragile X syndrome: a twenty-year perspective. *Annu. Rev. Pathol. Mech. Dis.* 7, 219–245. doi: 10.1146/annurev-pathol-011811-132457

Schütt, J., Falley, K., Richter, D., Kreienkamp, H.-J., and Kindler, S. (2009). Fragile X mental retardation protein regulates the levels of scaffold proteins and glutamate receptors in postsynaptic densities. *J. Biol. Chem.* 284, 25479–25487. doi: 10.1074/jbc.M109.042663

Shang, Y., Wang, H., Mercaldo, V., Li, X., Chen, T., and Zhuo, M. (2009). Fragile X mental retardation protein is required for chemically-induced long-term potentiation of the hippocampus in adult mice. *J. Neurochem.* 111, 635–646. doi: 10.1111/j.1471-4159.2009.06314.x

Sidorov, M. S., Auerbach, B. D., and Bear, M. F. (2013). Fragile X mental retardation protein and synaptic plasticity. *Mol. Brain* 6:15. doi: 10.1186/1756-6606-6-15

Spooren, W., Lindemann, L., Ghosh, A., and Santarelli, L. (2012). Synapse dysfunction in autism: a molecular medicine approach to drug discovery in neurodevelopmental disorders. *Trends Pharmacol. Sci.* 33, 669–684. doi: 10.1016/j.tips.2012.09.004

Strømgaard, K., Jensen, L. S., and Vogensen, S. B. (2005). Polyamine toxins: development of selective ligands for ionotropic receptors. *Toxicon* 45, 249–254. doi: 10.1016/j.toxicon.2004.11.013

Toft, A. K. H., Lundbye, C. J., and Banke, T. G. (2016). Dysregulated NMDA-receptor signaling inhibits long-term depression in a mouse model of Fragile X syndromee. *J. Neurosci.* 36, 9817–9827. doi: 10.1523/JNEUROSCI.3038-15.2016

Uzunova, G., Hollander, E., and Shepherd, J. (2014). The role of ionotropic glutamate receptors in childhood neurodevelopmental disorders: autism spectrum disorders and fragile x syndrome. *Curr. Neuropharmacol.* 12, 71–98. doi: 10.2174/1570159X113116660046

Yang, S., Yang, S., Park, J. S., Kirkwood, A., and Bao, S. (2014). Failed stabilization for long-term potentiation in the auditory cortex of Fmr1 knockout mice. *PLoS One* 9:e104691. doi: 10.1371/journal.pone.0104691

Yasuda, H., Barth, A. L., Stellwagen, D., and Malenka, R. C. (2003). A developmental switch in the signaling cascades for LTP induction. *Nat. Neurosci.* 6, 15–16. doi: 10.1038/nn985

Yun, S. H., and Trommer, B. L. (2011). Fragile X mice: reduced long-term potentiation and *N*-methyl-D-aspartate receptor-mediated neurotransmission in dentate gyrus. *J. Neurosci. Res.* 89, 176–182. doi: 10.1002/jnr.22546

Zhang, J., Hou, L., Klann, E., and Nelson, D. L. (2009). Altered hippocampal synaptic plasticity in the FMR1 gene family knockout mouse models. *J. Neurophysiol.* 101, 2572–2580. doi: 10.1152/jn.90558.2008

Zhu, J. J., Esteban, J. A., Hayashi, Y., and Malinow, R. (2000). Postnatal synaptic potentiation: delivery of GluR4-containing AMPA receptors by spontaneous activity. *Nat. Neurosci.* 3, 1098–1106. doi: 10.1038/80614

Conflict of Interest: The authors declare that the research was conducted in the absence of any commercial or financial relationships that could be construed as a potential conflict of interest.

frontiers in Synaptic Neuroscience

ORIGINAL RESEARCH
published: 21 December 2020
doi: 10.3389/fnsyn.2020.567075

Clmp Regulates AMPA and Kainate Receptor Responses in the Neonatal Hippocampal CA3 and Kainate Seizure Susceptibility in Mice

Seil Jang[1], *Esther Yang*[2], *Doyoun Kim*[3], *Hyun Kim*[2] *and Eunjoon Kim*[1,4]*

[1] Center for Synaptic Brain Dysfunctions, Institute for Basic Science, Daejeon, South Korea, [2] Department of Anatomy and Division of Brain Korea 21, Biomedical Science, College of Medicine, Korea University, Seoul, South Korea, [3] Center for Drug Discovery Platform Research, Korea Research Institute of Chemical Technology (KRICT), Daejeon, South Korea, [4] Department of Biological Sciences, Korea Advanced Institute of Science and Technology (KAIST), Daejeon, South Korea

Synaptic adhesion molecules regulate synapse development through trans-synaptic adhesion and assembly of diverse synaptic proteins. Many synaptic adhesion molecules positively regulate synapse development; some, however, exert negative regulation, although such cases are relatively rare. In addition, synaptic adhesion molecules regulate the amplitude of post-synaptic receptor responses, but whether adhesion molecules can regulate the kinetic properties of post-synaptic receptors remains unclear. Here we report that Clmp, a homophilic adhesion molecule of the Ig domain superfamily that is abundantly expressed in the brain, reaches peak expression at a neonatal stage (week 1) and associates with subunits of AMPA receptors (AMPARs) and kainate receptors (KARs). *Clmp* deletion in mice increased the frequency and amplitude of AMPAR-mediated miniature excitatory post-synaptic currents (mEPSCs) and the frequency, amplitude, and decay time constant of KAR-mediated mEPSCs in hippocampal CA3 neurons. *Clmp* deletion had minimal impacts on evoked excitatory synaptic currents at mossy fiber-CA3 synapses but increased extrasynaptic KAR, but not AMPAR, currents, suggesting that Clmp distinctly inhibits AMPAR and KAR responses. Behaviorally, *Clmp* deletion enhanced novel object recognition and susceptibility to kainate-induced seizures, without affecting contextual or auditory cued fear conditioning or pattern completion-based contextual fear conditioning. These results suggest that Clmp negatively regulates hippocampal excitatory synapse development and AMPAR and KAR responses in the neonatal hippocampal CA3 as well as object recognition and kainate seizure susceptibility in mice.

Keywords: synaptic adhesion molecule, synaptic transmission, AMPA receptors, kainate receptors, NMDA receptors, hippocampus, learning and memory, seizure

Edited by:
Alfredo Kirkwood, Johns Hopkins University, United States

Reviewed by:
Se-Young Choi, Seoul National University, South Korea
Pablo E. Castillo, Albert Einstein College of Medicine, United States

***Correspondence:**
Eunjoon Kim
kime@kaist.ac.kr

Received: *11 June 2020*
Accepted: *02 December 2020*
Published: *21 December 2020*

Citation:
Jang S, Yang E, Kim D, Kim H and Kim E (2020) Clmp Regulates AMPA and Kainate Receptor Responses in the Neonatal Hippocampal CA3 and Kainate Seizure Susceptibility in Mice. Front. Synaptic Neurosci. 12:567075. doi: 10.3389/fnsyn.2020.567075

INTRODUCTION

Synaptic adhesion molecules mediate and regulate diverse aspects of synapse development and function (Dalva et al., 2007; Shen and Scheiffele, 2010; Siddiqui and Craig, 2011; Takahashi and Craig, 2013; Um and Ko, 2013; Ko et al., 2015; de Wit and Ghosh, 2016; Jang et al., 2017; Krueger-Burg et al., 2017; Südhof, 2017; Sudhof, 2018; Yuzaki, 2018; Kurshan and Shen, 2019; Ribic and Biederer, 2019). Synaptic adhesion molecules localized to early axo-dendritic contacts

contribute to synapse maturation by promoting the recruitment and stabilization of various pre- and post-synaptic membrane and cytoplasmic proteins.

Among the important synaptic proteins that are recruited to early synapses by synaptic adhesion molecules are post-synaptic neurotransmitter receptors. Recent studies have reported several such interactions involving, for instance, NMDA (N-methyl-d-aspartate)- and AMPA (α-amino-3-hydroxy-5-methyl-4-isoxazolepropionic acid)-type glutamate receptors (NMDARs and AMPARs) (Nuriya and Huganir, 2006; Saglietti, 2007; Uemura et al., 2010; Zhang et al., 2010; Pozo et al., 2012; Sarto-Jackson et al., 2012; Budreck, 2013; Tomioka et al., 2014; Matsuda et al., 2016; Um et al., 2018). Although detailed mechanisms of these interactions still remain to be clarified, these results suggest that synaptic adhesion molecules and post-synaptic receptors form physical and functional complexes that modulate post-synaptic receptor responses.

AMPARs and kainate receptors (KARs) are members of the ionotropic glutamate receptor (iGluR) family that act as ligand-gated ion channels to mediate excitatory synaptic transmission and plasticity. Both receptor types are grouped together to form the non-NMDAR family (Mayer and Westbrook, 1987; Collingridge and Lester, 1989). Whereas AMPARs mediate fast excitatory synaptic transmission (Huganir and Nicoll, 2013), KARs mediate slow excitatory synaptic transmission (Castillo et al., 1997b). KARs, which are structurally similar to AMPARs (Chen et al., 2003; Nanao et al., 2005), are widely distributed in different brain regions and are highly enriched on the post-synaptic side of mossy fiber (MF)-pyramidal cell synapses in the CA3 region of the hippocampus (Bahn et al., 1994; Castillo et al., 1997b; Bannister et al., 2005; Zhuo, 2017). Exogenous kainate, the agonist of KARs, produces partial, but non-desensitizing, openings of AMPAR channels (Tomita et al., 2007). Importantly, both AMPARs and KARs have been implicated in seizure pathophysiology and have been suggested as potential therapeutic targets (Rawls et al., 2009; Hibi et al., 2012; Kato et al., 2016; Falcon-Moya et al., 2018).

Clmp (CXADR-like membrane protein), also known as ASAM or ACAM, was originally identified as a novel member of the CAR subgroup of the CTX family (Raschperger et al., 2004), and was termed ASAM or ACAM for its expression in adipocytes (Eguchi et al., 2005). Clmp is also expressed in the intestine and is required for intestinal development (van der Werf et al., 2013; Langhorst et al., 2018). Like other members of the CAR subgroup (CAR, ESAM, and IgSF11), Clmp mediates homophilic adhesion (Raschperger et al., 2004; Eguchi et al., 2005). In the human brain, expression of the *CLMP* gene was reported in the developing cerebral neocortex and other brain areas, including the hippocampus, striatum, amygdala, thalamus, and cerebellum (Kang et al., 2011; Pletikos et al., 2014). Recently, members of the CAR subgroup have been shown to regulate synaptic function in the brain. For example, IgSF11 is a synaptic cell-adhesion molecule that interacts with AMPARs and regulates AMPAR-mediated synaptic transmission and plasticity (Jang et al., 2016). CAR, detected in native AMPAR complexes as an AMPAR-interacting membrane protein using shotgun liquid chromatography-tandem mass spectrometry (LC-MS/MS) protein analysis (AP-MS/MS) (Shanks et al., 2012), was found to negatively regulate excitatory synaptic transmission through presynaptic exocytosis-related mechanisms (Wrackmeyer et al., 2019). These results suggest the possibility that Clmp might also regulate aspects of synapse development and function in the brain.

In the present study, we found that Clmp exhibits early post-natal expression and interacts with AMPAR and KAR subunits. Moreover, results from mice lacking Clmp suggest that Clmp negatively regulates synapse development and distinctly suppress AMPAR and KAR responses in the CA3 region of the hippocampus. Behaviorally, *Clmp* deletion also altered object recognition and kainate seizure susceptibility, but not contextual or cued fear conditioning or pattern completion.

MATERIALS AND METHODS

cDNA Constructs

Full-length human Clmp (NM_024769, aa 1–373, Origene RC203362) were amplified by PCR, and subcloned into pGW1-CMV (British Biotechnology). For HA-Clmp, the HA epitope was added to the N-terminus of human Clmp in pGW1. Deletion variants of Clmp were generated by PCR using HA-Clmp (human) as a template and deleting the following regions; aa 317–373 (Clmp ECD-TM), aa 231–373 (Clmp ECD-PDGFR TM), aa 1–316 (Clmp ICD-PDGFR TM). For Clmp ECD-PDGFR TM and Clmp ICD-PDGFR TM, the signal peptide and the transmembrane domain of Clmp were replaced with the N-terminal signal peptide and the C-terminal transmembrane anchoring domain of platelet-derived growth factor receptor (PDGFR) of pDisplay (Invitrogen). All Clmp expression constructs were generated by subcloning the inserts to pGW1 except Clmp ECD-PDGFR was subcloned into pDisplay. The following constructs have been described: pGW1-PSD-95 (Kim et al., 1995). pRK5-GluA1 and pRK5-GluA2 were kindly provided by Dr. Richard Huganir (Shen et al., 2000).

Antibodies

Peptides containing mouse Clmp (aa 345–373) were used to immunize guinea pigs (2090). The specificity of anti-Clmp antibodies (2090) was confirmed by immunoblot experiments using $Clmp^{-/-}$ whole-brain lysates. The following antibodies have been described: PSD-95 (1688) (Yang, 2011), GluA1 (1193) (Kim, 2009), GluA2 (1195) (Kim, 2009). The following antibodies were purchased: HA rabbit polyclonal (Santa Cruz sc-805), HA mouse monoclonal (Boehringer Mannheim 12CA5), PSD-95 (75-028) (NeuroMab), Synaptophysin (Santa Cruz sc-9116), GluA1 (Sigma-Aldrich MAB2263), GluA2 (Sigma-Aldrich MAB397), GluK2 (Sigma-Aldrich 04-921), GluK5 (Sigma-Aldrich 06-315), α-tubulin (Sigma T5168), β-actin (Sigma, A5316).

Radioisotope *in situ* Hybridization

Mouse brain sections (14 μm thick) at embryonic day (E18) and post-natal days (P1, P7, P14, P21, and P56) were prepared using a cryostat (Leica CM 1950). Hybridization probes specific for mouse Clmp mRNAs were prepared using the following regions:

nt 1351–1650 (C-term) of Clmp (NM_133733.4). Antisense riboprobes were generated using 35^S-uridine triphosphate (UTP) and the Riboprobe system (Promega).

Fluorescence *in situ* Hybridization

Frozen mouse brain sections (14 μm thick) at post-natal days (P7 and P56) were cut coronally through the hippocampal formation. The sections were fixed in 4% paraform aldehyde for 10 min, dehydrated in increasing concentrations of ethanol for 5 min, and finally air-dried. Tissues were then pre-treated for protease digestion for 10 min at room temperature. The probes used in this study were three synthetic oligonucleotides complementary to the nucleotide (nt) sequence 396–1462 of Mm-Clmp-C1, nt 464–1415 of MmSlc17a7/Vglut1-C2, nt 1986–2998 of Mm-Slc17a6/Vglut2-C3, nt 62–3113 of Mm-Gad1-C3, nt 552–1506 of Mm-Gad2-C2 (ACDBio, Newark, CA, United States). The labeled probes were conjugated to Atto 550 (C1), Alexa Fluor 488 (C2), and Atto 647 (C3). The sections were hybridized at 40°C with labeled probe mixtures (C1 + C2 + C3) per slide for 2 h. Amplification steps involved sequential incubations with Amplifier 1-FL for 30 min, Amplifier 2-FL for 15 min, Amplifier 3-FL for 30 min, and Amplifier 4 Alt B-FL at 40°C for 15 min. Fluorescent images were acquired using TCS SP8 Dichroic/CS (Leica), and the ImageJ program (NIH) was used to analyze the images.

Brain Lysates Preparation

Whole mouse or rat brain lysates [1-week-old (P7) or 6-week-old (P42)] were prepared as previously described (Jang et al., 2016). After the brain dissection, obtained brain tissues were briefly homogenized in 10 volumes of ice-cold homogenization buffer (0.32 M sucrose, 10 mM HEPES pH 7.4, 2 mM EDTA, protease inhibitors, phosphatase inhibitors). Protein concentrations were measured by the Bradford assay. The relative amount of α-tubulin or β-actin was used as a loading control.

Subcellular and PSD Fractions

Subcellular and PSD fractions of rat brains [1-week-old (P7)] were prepared as described previously (Jang et al., 2016). Triton X-100-soluble fractions enriched with perisynaptic, presynaptic and extrasynaptic proteins were collected as the non-post-synaptic density membrane fraction (non-PSD). The non-PSD enrichment was checked by PSD-95 and synaptophysin immunoblotting. Immunoblot analysis of these fractions was performed using Clmp (2090), PSD-95 (1688), synaptophysin, α-tubulin, and β-actin antibodies.

Cell-Surface Biotinylation Assay

Hippocampal slices were prepared as described for electrophysiology. After 1 h, slices were transferred into 24-well plates containing 0.5 mg/ml sulfo-NHS-LC-Biotin (21335; Pierce). Slices were biotinylated for 30 min on ice, followed by three 10-min washes in cold ACSF and then two 25-min washes in ACSF containing 100 mM glycine. The hippocampus was then dissected from each slice and solubilized in RIPA buffer containing 50 mM Tris-HCl, 150 mM NaCl, 1% NP-40, 1% sodium deoxycholate, 2 mM EDTA, supplemented with protease inhibitors for 1 h at 4 °C. Samples were then cleared by centrifugation at 20,000 × g for 30 min and then the supernatants were collected. The samples were then incubated with 40 μl of washed neutravidin agarose beads (29200; Pierce) overnight at 4°C. Beads were then washed three times with lysis buffer, and proteins were eluted by heating at 95°C for 5 min with Laemmli sample buffer containing β-mercaptoethanol. The surface protein enrichment was checked by β-actin immunoblotting.

Co-immunoprecipitation

HEK293T cells were harvested 36–48 h after transfection and were solubilized in Tris-buffered saline (pH 7.4) containing 50 mM Tris-HCl, 150 mM NaCl, 1% NP-40, 1% sodium deoxycholate, 2 mM EDTA, supplemented with protease inhibitors at 4°C. Following centrifugation at 20,000 × g for 30 min at 4°C, the clarified lysates were subjected to immunoprecipitation using HA monoclonal antibodies coupled to agarose beads (Pierce) for 2 h at 4°C. Following 4–6 washes with 1 ml of the solubilizing buffer, bound proteins were eluted with SDS sample buffer containing 5% β-mercaptoethanol and boiled for 5–10 min for SDS-PAGE analyses.

Molecular Modeling

The structure of mouse Clmp was generated by homology modeling using the I-TASSER server (Zhang, 2008; Yang and Zhang, 2015) and SWISS-MODEL server (Arnold et al., 2006; Waterhouse et al., 2018), using the crystal structure of the extracellular domain of CAR (a close relative of Clmp) as a template [PDB ID: 3JZ7; The Protein Data Bank (Berman et al., 2000)], which shows 32.84% sequence identity with mouse Clmp. Structural prediction of the C-terminal part of Clmp and IgSF11 proteins containing the last 10 amino acid sequences were further refined from the initial homology models using termini or loops modeling. Global optimization of an energy function composed of knowledge-based energy terms and physics-based energy terms was performed. The loop sampling efficiency was enhanced by generating proper closed-loop conformations with the triaxial loop closure (TLC) algorithm during global optimization (Ko et al., 2012; Park and Seok, 2012; Park et al., 2014). The surface electrostatic potential was calculated using PDB2PQR (v.2.1.1) (Dolinsky et al., 2004) and APBS (v.1.5) (Baker et al., 2001). All structural images were generated using PyMOL (The PyMOL Molecular Graphics System, Version 2.0 Schrödinger, LLC.) and UCSF Chimera (Pettersen et al., 2004).

Generation of *Clmp*$^{-/-}$ Mice

The *Clmp*$^{-/-}$ mice used in the present study were originally generated by Genentech, Inc. (Tang et al., 2010). Briefly, to generate *Clmp* knockouts by homologous recombination, coding exons 3 through 5 targeted embryonic stem cells (Lexicon cell line derived from 129S5/SvEvBrd) were implanted into C57BL/6 albino-type blastocysts using standard procedures. The chimeric mice are bred to C57BL/6-Tyr^{c-Brd} albino mice albino mice to generate F1 heterozygous animals. These progenies were intercrossed to generate F2 wild type, heterozygous, and homozygous mutant progenies, which were further crossed for more than 6 generations. These *Clmp*$^{-/-}$ mice were provided

to us by the Mutant Mouse Resource & Research Centers (MMRRC:031613-UCD). We then backcrossed the heterozygous mice (N1; *Clmp*$^{+/-}$) with C57BL/6J for at least 8 generations before being bred in the mixed background of C57BL/6J and 129S1/Sv (Jackson Labs) (50:50), as described previously (Zhou et al., 2016), to improve pre- and perinatal lethality. Littermates derived from heterozygous parents were used for all analysis. Genotyping of the *Clmp*$^{-/-}$ mice was performed using PCR and the following four primers; P1 (5′- CGT ATT CCA GCC GTC ATG TC−3′′, P2 (5′- GGC TGT CTC TTG CCT CAT AG−3′), P3 (5′- TCC ACC GTA AAA GGA AGA CAA CC−3′), P4 (5′- GCA GCG CAT CGC CTT CTA TC−3′). The size of the PCR products for WT (P1 and P2) and mutant (*Clmp*$^{-/-}$; P3 and P4) alleles were 514 and 209 bp, respectively. Both male and female mice were used for all measurements except behavioral experiments, which used only male mice. All mice were bred and maintained according to the KAIST Animal Research Requirements, and all procedures were approved by the Committees of Animal Research at KAIST (KA2016-32). Mice were fed *ad libitum* by standard rodent chow and tap water, and housed in specific pathogen-free condition under 12-h light/dark cycle (lights off at 19:00).

Electrophysiology-Patch Recordings

Electrophysiological recordings for whole-cell patches were performed as previously described (Kim, 2009; Chung et al., 2015; Jang et al., 2016). Briefly, WT and *Clmp*$^{-/-}$ mice at around week 1 (P7–11) were anesthetized by isoflurane inhalation. Acute sagittal dorsal hippocampal slices or acute horizontal middorsal hippocampal slices (300–400 μm thick for whole-cell recordings) were prepared using a vibratome (Leica VT1200s) in ice-cold high sucrose cutting solution containing (in mM) 212 sucrose, 25 $NaHCO_3$, 2.5 or 5 KCl, 1.25 NaH_2PO_4, 0.5 $CaCl_2$, 3.5 or 10 $MgCl_2$, 10 D-glucose, 1.25 L-ascorbic acid, 2 Na-pyruvate equilibrated with 95% O_2/5% CO_2. Brain slices were then allowed to recover at 32°C for 30 min in artificial cerebral spinal fluid (aCSF) containing (in mM): 125 NaCl, 25 $NaHCO_3$, 2.5 KCl, 1.25 NaH_2PO_4, 2.5 $CaCl_2$, 1.3 $MgCl_2$, 10 D-glucose) with pH 7.3–7.4 and osmolarity 296–300 mOsm and maintained at room temperature before recordings (0.5–1 h).

Whole-cell patch recordings were performed with recording pipettes pulled from borosilicate glass capillaries (Harvard Apparatus, 1.5 mm OD, GC150T-7.5) with a micropipette puller (Narishige PC-10). For whole-cell recordings, CA1 pyramidal cells, CA3 pyramidal cells, and DG granule cells were held at −70 mV with recording pipettes (4–5 MΩ) at 26°C (400 μm slice thickness) using Multiclamp 700B amplifier (Axon Instruments). For mEPSC recordings, Cs-based intracellular solution contained (in mM) 110 Cs-gluconate, 30 CsCl, 20 HEPES, 4 MgATP, 0.3 NaGTP, 4 NaVitC, 0.5 EGTA with pH 7.3 and osmolarity 295 mOsm. Picrotoxin (100 μM), D-AP5 (50 μM), and TTX (1 μM) were used to block inhibitory synaptic currents, N-methyl-D-aspartate receptor (NMDAR)-mediated synaptic currents and sodium channel-mediated action potentials, respectively. For consistent mEPSC measurements, the baseline was monitored for 5 min, and mEPSCs were began to be measured at the same time point (5–15 min) after whole-cell access was established to minimize time-dependent fluctuation. For DCG-IV CA3 mEPSCs, the group II mGluR agonist DCG-IV [(2S,2′R,3′R)-2-(2′,3′-Dicarboxycyclopropyl)glycine] (2 μM) was used in bath application. For LY354740 CA3 mEPSCs, the group II mGluR agonist LY354740 (0.5 μM) was used in bath application. For KAR mEPSCs, GYKI 53655 (30 μM) was used to block AMPAR receptor-mediated currents. Signals were filtered at 400 Hz to detect very small KAR mEPSCs ranging from 3 to 10 pA. For NMDAR mEPSCs, recordings were performed in 0 Mg^{2+} ACSF, the Mg^{2+} was replaced with additional glucose. NBQX (10 μM) was used to block AMPAR/KAR-mediated synaptic currents. Signals were filtered at 400 Hz to allow reliable detection of small NMDAR mEPSCs <10 pA. For mIPSC recordings, Cs-based intracellular solution contained (in mM) 120 CsCl, 10 TEA-Cl, 8 NaCl, 10 HEPES, 5 QX-314-Cl, 4 Mg-ATP, 0.3 Na-GTP, and 10 EGTA, with pH 7.35, 280 mOsm. TTX (1 μM), NBQX (10 μM), and D-AP5 (50 μM) was used to block spontaneous action potential-mediated synaptic currents, AMPAR/KAR-mediated synaptic currents and NMDAR-mediated synaptic currents, respectively. All miniature excitatory/inhibitory post-synaptic whole-cell recordings were performed in sagittal dorsal hippocampal slices. For mossy fiber (MF)-CA3 and recurrent associational/commissural (A/C)-CA3 EPSC recordings, acute horizontal middorsal hippocampal slices from WT and *Clmp*$^{-/-}$ mice of at around week 1 (P9–11) were used to record mossy fiber-CA3 evoked synaptic responses (Marchal and Mulle, 2004; Bischofberger et al., 2006). The recording electrode was placed in the CA3 pyramidal cell layer but ∼50 μm away from the stimulating electrode in the stratum lucidum of CA3. For pharmacological isolation of both AMPAR and KAR synaptic responses, picrotoxin (100 μM) and D-AP5 (50 μM) were used to block inhibitory synaptic currents and NMDAR-mediated synaptic currents, respectively. Cs-based intracellular solution containing (in mM) 110 Cs-gluconate, 30 CsCl, 20 HEPES, 4 MgATP, 0.3 NaGTP, 4 NaVitC, 0.5 EGTA with pH 7.3, and osmolarity 295 mOsm was used. For input-output experiments measuring MF-CA3 EPSCs and KAR EPSCs, input stimulus intensities ranged from 10 to 60 μA with 10 μA increments, and the output was the amplitude of the EPSCs averaged from five individual traces. AMPAR EPSCs were obtained by the subtraction of KAR EPSCs in the input-output experiments. To determine fast and slow decay kinetics of AMPAR- and KAR-mediated post-synaptic currents, respectively, the decay phase of MF-CA3 EPSCs was fitted to a double exponential function as previously described (Cossart et al., 2002; Pinheiro et al., 2013). Rise time values were assessed by measuring the time course from 20 to 80% of the total response amplitude. For slow rise kinetics of KAR-mediated post-synaptic currents, the fast rise kinetics of AMPAR-mediated post-synaptic currents were further pharmacologically blocked using GYKI 53655 (30 μM), a selective AMPAR antagonist (Paternain et al., 1995). For input-output experiments measuring NMDAR EPSCs, NBQX (10 μM) was used to block AMPA/KAR receptor-mediated currents and holding potential was changed to +40 mV to record NMDAR-mediated EPSCs. To determine NMDAR-mediated post-synaptic currents, the decay phase of NMDAR EPSCs was fitted to single exponential function. For

extrasynaptic AMPAR experiments, AMPAR-mediated whole-cell currents were obtained by bath application of 1 μM (S)-α-amino-3-hydroxy-5-methyl-4-isoxazolepropionic acid (S-AMPA) for 5 min in the presence of 1 μM TTX and 100 μM picrotoxin after stable 5 min baseline holding currents were established. For extrasynaptic KAR experiments, KAR-mediated whole-cell currents were obtained by bath application of 3 μM kainate for 5 min in the presence of 1 μM TTX, 30 μM GYKI 53655, and 100 μM picrotoxin after stable 5 min baseline holding currents were established. For extrasynaptic NMDAR experiments, NMDAR-mediated whole-cell currents were obtained by bath application of 10 μM NMDA for 5 min in the presence of 1 μM TTX, 10 μM NBQX and 100 μM picrotoxin after stable 5 min baseline holding currents were established. All agonist-induced excitatory post-synaptic whole-cell recordings were performed in acute horizontal middorsal hippocampal slices. Liquid junction potentials were not corrected. Series access resistance was 10–25 MΩ, and only the cells with a change in series access resistance <25% were included in the analysis.

Electrophysiology-Field Recordings

Electrophysiological recordings for extracellular field recordings were performed as previously described (Jang et al., 2016). Briefly, WT and *Clmp*$^{-/-}$ mice at P 9–11 and weeks 8–16 were anesthetized by isoflurane inhalation. Acute horizontal middorsal hippocampal slices (400–500 μm thick) were used for extracellular field recordings at 28–30°C (TC-324B, Warner Instruments) (Bischofberger et al., 2006). Field excitatory post-synaptic potentials (fEPSPs) were recorded with glass electrodes (1–2 MΩ tip resistance) filled with ACSF or 1 M NaCl, and evoked every 20 s using a stimulating glass electrode filled with ACSF. For mossy fiber-CA3 fEPSP recordings, the recording electrode was placed in the stratum lucidum of CA3 but ∼400 μm away from the stimulating electrode in the hilus of the DG region. To verify mossy fiber inputs, the strong paired-pulse facilitation of this input, a hallmark of MF-CA3 synapses, was measured by delivering paired pulses every 20 s. Paired pulse ratios were determined by evoking two fEPSPs (averages of three individual traces) that are 50 ms apart and dividing the initial slope of the second fEPSP by that of the first (fEPSP2/fEPSP1). For synaptic plasticity experiments, LTP at MF-CA3 synapses was induced by a single tetanus of 125 pulses at 25 Hz (Castillo et al., 1997a). At the end of the experiment, the degree of inhibition by the group II mGluR agonist DCG-IV [(2S,2′R,3′R)-2-(2′,3′-Dicarboxycyclopropyl)glycine] (2 μM) was used to verify that mossy fiber responses were recorded (Nicoll and Schmitz, 2005). For recurrent associational/commissural (A/C)-CA3 fEPSP recordings, the recording electrode was placed in the stratum radiatum of CA3 but 100–150 μm away from the stimulating electrode in the stratum radiatum of CA3 region. For perforant path (PP)-CA3 fEPSP recordings, the recording electrode was placed in the stratum lacunosum moleculare of CA3 but 100 μm away from the stimulating electrode in the stratum lacunosum moleculare of CA3 region.

Electrophysiology-Data Acquisition and Analysis

All the recording data were digitized at 10 kHz and filtered at 2 kHz (except for the recording of KAR mEPSCs and NMDAR mEPSCs at 400 Hz). Analog-to-digital conversion was performed using Digidata 1440A (Molecular Devices). Data were acquired using Clampex 10 (Molecular Devices), and analyzed using Clampfit 10 (Axon Instruments) except that KAR mEPSCs were manually analyzed using MiniAnalysis Program 6.0.3 (Synaptosoft, Fort Lee, NJ, United States) to reliably detect the amplitude and the decaying phase of very small KAR-mediated miniature excitatory post-synaptic currents ranging from 3 to 10 pA. The experimenters were blind to the genotypes of the mice.

Animal Behavioral Tests

All behavioral assays were performed using littermates or age-matched male animals during light-off periods. All behavioral tests were performed and analyzed in a blinded manner.

Contextual Fear Conditioning Test

All experiments were carried out in a fear conditioning system (Coulbourn Instruments). Training and testing were performed in a chamber with a stainless steel grid floor. On the training day, mice at 2–6 months of age were placed in the fear chamber and allowed to freely move around the chamber for 2 min before they received five foot shocks as an unconditioned stimulus (US) (2 s, 0.7 mA, 1 min apart). The 10-s period before each US was used to measure inter-US freezing. 24 h later, animals were tested for contextual fear retrieval in context A for 5 min. Freezing behavior was quantified using an automatic detection system (FreezeFrame 3, Coulbourn Instruments). The animals were considered to freezing behavior if no movement was detected for 2 s, and freezing levels were indicated as the percentage of time spent freezing.

Auditory-Cued Fear Conditioning and Contextual Fear Renewal Test

Mice at 2–6 months of age were submitted to an auditory fear conditioning paradigm. Two different contexts for conditioning (context A) and extinction (context B) were used. Context A and B were cleaned before and after each session with 70% ethanol or 1% acetic acid, respectively. During fear conditioning, the CS was paired to the US (2 s, 0.7 mA foot shock back to back with the last CS; 5 CS/US pairings; inter-trial interval: 60 s). Each behavior session consisted of a 10 min baseline prior to the presentation of the first conditioned stimulus (CS) (frequency: 8 kHz; sound pressure level: 75 dB), which gave the animal enough time to show normal locomotor activity after exposure to conditioning or extinction context. Two-min time prior to the first CS was used to measure baseline freezing. Each CS was 30-s long. CS inter-trial intervals were 60 s. After auditory fear conditioning in context A, animals were tested for cued retrieval in context B. Twenty-four hours later, mice were subjected to an extinction learning session composed of 20 identical tones (at intervals of 5 s) without shocks. Twenty-four hours later, animals were tested for extinction retrieval for 3 min in context B followed by

contextual retrieval test for context-dependent fear renewal for 5 min in context A 1 h later.

Pattern Completion-Based Contextual Fear Conditioning Test

Pre-exposure, pattern-completion version of contextual fear conditioning was previously described (Wagatsuma et al., 2018). Mice at 2–6 months of age were exposed to Context A for 10 min in the absence of shock on day 1. Immediate shock procedures were followed on day 2 in Context A, where a single 0.8 mA shock of 2 s duration was delivered at 8 s after being placed in the chamber, with all mice removed 30 s after the completion of the shock. On day 3, the mice were returned to the conditioning chamber for 5 min to recall contextual fear memory.

Novel Object Recognition Test

Mice at 2–4 months of age were habituated in an open-field box without objects for 60 min a day before training session under low-light (15 lux) conditions. Object recognition test was performed in the same open-field box. On the first day, mice were allowed to explore two identical objects for 20 min. Twenty-four hours later, mice were placed the same box where one of the objects was replaced with a new object. Object recognition was scored manually by the amount of time with the nose of the mouse pointed and located within 2 cm from the object for 10 min.

Kainate-Induced Seizure

Mice (2–6 months of age or post-natal day 10–12) were allowed to acclimate to a clean glass beaker containing bedding for 30 min under low-light (50 lux) conditions. After habituation to the testing room, mice received an intraperitoneal injection (20 mg/kg to adult male mice; 2 mg/kg to male and female neonatal mice) of kainic acid (Tocris 0222) in 1x phosphate-buffered saline (PBS; pH 7.4) (Vissel et al., 2001; Koh et al., 2004), and were monitored for 120 min following injection. Seizure levels were scored by an experimenter blinded to the genotype according to a modified Racine scale (Racine, 1972): stage 0, normal behavior; stage 1, behavioral arrest (absence-like immobility); stage 2, myoclonic seizure; stage 3, rearing with repetitive rhythmic bilateral forelimb clonus (2–3 Hz); stage 4, continuous rearing and falling; stage 5, generalized tonic-clonic seizure, jumping continues, and wild rushing; stage 6, death.

Experimental Design

Experiments, data collection, and analyses were performed by researchers blinded to the experimental conditions. The following a priori criteria were established for appropriate exclusion of data points: cells that were morphologically unhealthy were excluded; in whole-cell experiments, cells that did not fulfill the standard criteria of electrophysiological properties, including cell capacitance, input resistance, series resistance, resting membrane potential, and baseline holding current, were excluded.

Statistics

No statistical methods were used to predetermine sample sizes, but our sample sizes were similar to those generally employed in the field. All data were randomly collected. Normally distributed data were analyzed using the Student's *t*-test, whereas the data that did not conform to a normal distribution were analyzed using the non-parametric Mann-Whitney test. Outliers were determined using ROUT test and removed from the analysis. Statistical tests and data point plotting were performed using GraphPad Prism 7. All details of statistical analyses are described in **Supplementary Table 1**.

RESULTS

Widespread Expression of Clmp mRNAs in the Mouse Brain

Clmp, a member of the immunoglobulin superfamily, is a type I transmembrane protein that is conserved among various vertebrate species (**Supplementary Figure 1**). Clmp, which is ∼373 amino acid (aa)-long in humans and mice, contains an extracellular region with two immunoglobulin-like (Ig) domains (one V-type and one C2-type), a single transmembrane domain, and an intracellular region (**Figure 1A**).

To determine the expression patterns of the *Clmp* gene in the mouse brain, we first characterized the distribution patterns of Clmp mRNA in the mouse brain by *in situ* hybridization. Radioisotope probes revealed a widespread distribution pattern of Clmp mRNA in the mouse brain at various developmental stages [embryonic day 18 and post-natal (P) days 1, 7, 14, 21, and 56], including the olfactory bulb, cortex, striatum, hippocampus, thalamus, and cerebellum (**Figure 1B**). A separate fluorescence *in situ* hybridization (FISH) analyses revealed a similar widespread distribution of Clmp mRNA in mouse brain regions, including the cortex, hippocampus and thalamus, at two different post-natal stages: week 1 (P7) and week 8 (P56) (**Figure 1C**; **Supplementary Figure 2**).

Notably, Clmp mRNA was abundant in the CA1, CA2, and CA3 regions of the hippocampus, but not in dentate gyrus (DG) regions, at week 1 (**Figure 1D**). In contrast, at week 8, Clmp mRNA was also detected in the DG area, in addition to other hippocampal regions (**Figure 1E**). This indicates an age-dependent change in Clmp expression in the hippocampal DG area.

We also tested whether Clmp mRNA is differentially expressed in glutamatergic and GABAergic neurons using the FISH technique. These experiments revealed the presence of Clmp mRNA in both types of neurons in brain regions that included the cortex and hippocampus at two different post-natal stages (week 1 and 8) (**Figure 1C**; **Supplementary Figure 2**).

Clmp Protein Is Enriched in Synaptic, but Not PSD, Fractions, and Fails to Interact With PSD-95

Clmp protein (∼48 kDa) was detected at relatively high levels in the hippocampus compared with other brain regions (**Figure 2A**). Levels of Clmp protein rapidly increased after birth,

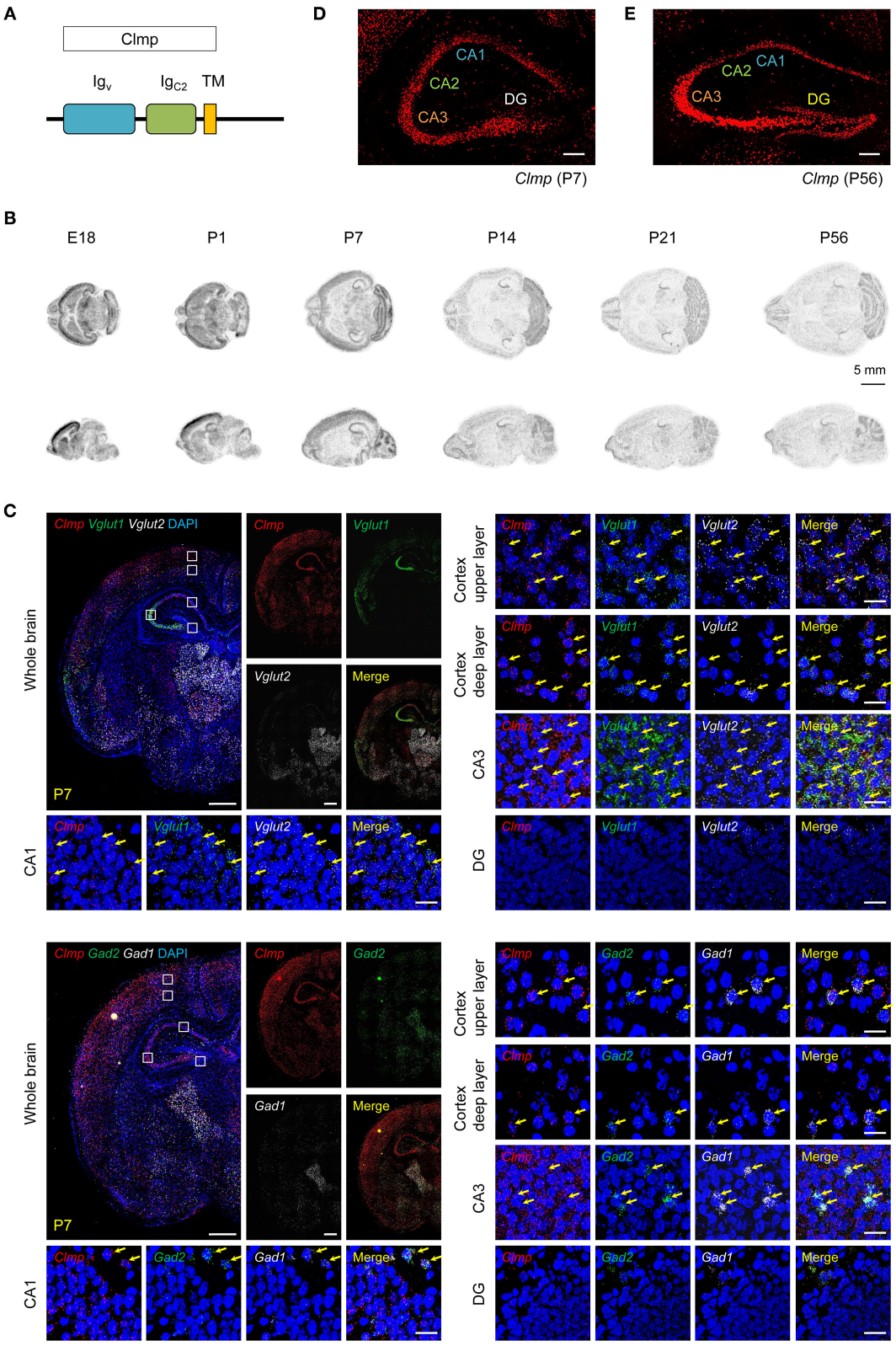

FIGURE 1 | Distribution patterns of Clmp mRNAs. **(A)** Domain structure of Clmp. Ig$_{v/C2}$, immunoglobulin V/C2-like; TM, transmembrane. **(B)** Distribution patterns of Clmp mRNA in the mouse brain at E18 and P1, P7, P14, P21, and P56, as revealed by isotopic *in situ* hybridization. **(C)** Expression of Clmp mRNA

(Continued)

FIGURE 1 | in Vglut1/2-positive glutamatergic neurons (upper panels) and Gad1/2-positive GABAergic neurons (lower panels) in the neocortex and hippocampus in the mouse brain [week 1 (P7)], as revealed by fluorescence *in situ* hybridization (FISH). Coronal brain sections were doubly stained for Clmp and Vglut1/2 or Gad1/2, and counterstained with DAPI (nuclear stain; blue). Images at right show enlarged views of white boxes in the images at left. The yellow arrows indicate neurons that express both Clmp and neuronal markers. Note that the DG area shows faint signals for Clmp mRNA. Scale bar, 300 μm (left) and 20 μm (right). **(D,E)** Age-dependent changes in the distribution patterns of Clmp mRNA in the hippocampus of the mouse brain at weeks 1 and 8, revealed by FISH. Note that the DG area shows strong Clmp mRNA signals at week 8, but not at week 1. Scale bar, 200 μm.

reaching a peak at approximately week 1 and decreasing to adult levels around week 3, an expression pattern that contrasted with that of PSD-95, a major excitatory post-synaptic protein (Sheng and Sala, 2001), which steadily increased until reaching a peak at about week 3 (**Figure 2B**).

Biochemical fractionation experiments on whole mouse brain samples at week 1 indicated that Clmp protein is enriched in synaptic fractions, including crude synaptosomes (P2), the synaptic vesicle fraction (P3), the synaptosomal membrane fraction (LP1), and the synaptosomal vesicle fraction (LP2) (**Figure 2C**). Subcellular distribution patterns at week 6 were similar to those at week 1, although levels of Clmp protein in the LP2 fraction were decreased at week 6 (**Figure 2D**). Intriguingly, Clmp protein was not enriched in post-synaptic density (PSD) fractions at week 1 or 6 (**Figures 2E,F**). These results contrast sharply with the abovementioned enrichment of Clmp protein in synaptic membrane and synaptic vesicle fractions, suggesting that Clmp protein is present at synaptic sites but is not tightly associated with the PSD.

IgSF11, a relative of Clmp, binds to the PDZ domains (PDZ1 + PDZ2) of PSD-95 through its C-terminal PDZ-binding motif (Jang et al., 2016). The C-terminal tail of the Clmp protein containing the last four residues, FQTV, partly resembles the Class I PDZ domain-binding motif (X-S/T-X-V) (Sheng and Sala, 2001). We thus tested whether Clmp could directly bind to and form a complex with PSD-95 in heterologous cells. Clmp failed to bind PSD-95, whereas IgSF11 did form a complex with PSD-95 in a manner that required the last four amino acid (aa) residues (**Figure 2G**). Molecular modeling indicated steric hindrance between the F residue in the FQTV sequence of the Clmp tail and the tail-binding pocket of the PDZ1 domain of PSD-95 (**Figure 2H**), which is predicted to suppress the interaction. These results indicate that Clmp is unable to bind PSD-95, a major component of the PSD, in line with the limited enrichment of Clmp in PSD fractions.

Increased AMPAR and KAR mEPSCs and Decreased NMDAR mEPSCs in Clmp$^{-/-}$ Hippocampal CA3 Neurons

Clmp protein is detected at synaptic sites, despite not being enriched in PSD fractions, and previous studies indicate that the Clmp relatives, IgSF11, and CAR, regulate excitatory synaptic transmission in the hippocampus (Jang et al., 2016; Wrackmeyer et al., 2019). We thus tested if *Clmp* deletion in mice alters synaptic transmission in the hippocampus, where Clmp is most strongly expressed (**Figure 2A**). To this end, we generated mice carrying a homozygous deletion of exons 3–5 of the *Clmp* gene ($Clmp^{-/-}$) (**Supplementary Figures 3A,B**). Complete loss of Clmp protein was confirmed by immunoblot analyses using whole-brain lysates of the $Clmp^{-/-}$ brain and an antibody directed against the last 29 aa residues of the protein generated as part of the present study (**Supplementary Figure 3C**). At P7, $Clmp^{-/-}$ mice showed a Mendelian ratio of 0.30:0.50:0.20 (WT, $Clmp^{+/-}$, and $Clmp^{-/-}$), indicative of a reduction in the proportion of $Clmp^{-/-}$ mice compared with the expected ratio of 0.25:0.50:0.25 and similar to a previous report (Langhorst et al., 2018). In line with this, $Clmp^{-/-}$ mice displayed decreased (∼50%) survival rate during post-natal stages (**Supplementary Figure 3D**).

We next examined miniature post-synaptic currents in $Clmp^{-/-}$ hippocampal regions, including CA1, CA3 and the DG, at week 1 (**Figure 3A**), the developmental stage at which *Clmp* expression peaks. $Clmp^{-/-}$ pyramidal neurons in the CA3 region showed increases in both the frequency and amplitude of miniature excitatory post-synaptic currents (mEPSCs) (**Figure 3B**). In contrast, $Clmp^{-/-}$ pyramidal neurons in the CA1 and DG region showed unaltered mEPSCs (**Figures 3C,D**). Inhibitory synaptic transmission, determined by measuring miniature inhibitory post-synaptic currents (mIPSCs), was unaltered in CA3 neurons (**Figure 3E**), indicative of a selective increase in excitatory transmission. Importantly, DCG-IV, a selective agonist of group II metabotropic glutamate receptors (mGluR2/3) that is known to reduce synaptic transmission at mossy fiber inputs but not at associational inputs in the CA3 region (Yoshino et al., 1996), fully reversed the increased mEPSC frequency and amplitude in $Clmp^{-/-}$ CA3 pyramidal neurons (**Figure 3F**), by more strongly decreasing mEPSCs in $Clmp^{-/-}$ than in WT CA3 neurons (82% vs. 65% in mEPSC frequency) (**Figures 3B,F**). In addition, another mGluR2/3 agonist, LY354740, eliminated the genotype differences in the frequency and amplitude of mEPSCs between WT and $Clmp^{-/-}$ CA3 neurons (**Figure 3G**), by less strongly decreasing $Clmp^{-/-}$ mEPSCs (69 vs. 34% in mEPSC frequency) (**Figures 3B,G**).

The abovementioned mEPSCs in different hippocampal regions, including CA3, are mainly mediated by AMPARs. We thus tried to isolate mEPSCs mediated by KARs or NMDARs. KAR-mEPSCs, isolated by the selective AMPAR antagonist GYKI 53655 and the NMDAR blocker AP5, showed increases in the frequency and amplitude as well as in the decay time constant but not in the rise time (**Figure 3H**). In addition, NMDAR-mEPSCs, isolated by the AMPAR/KAR antagonist NBQX, revealed a decrease in the frequency but not amplitude (**Figure 3I**). Together, these results collectively suggest that *Clmp* deletion leads to changes in AMPAR, KAR, and NMDAR mEPSCs in $Clmp^{-/-}$ CA3 neurons; increased frequency and amplitude of AMPAR mEPSCs, increased frequency, amplitude, and decay time constant of KAR mEPSCs, and decreased frequency of NMDAR mEPSCs.

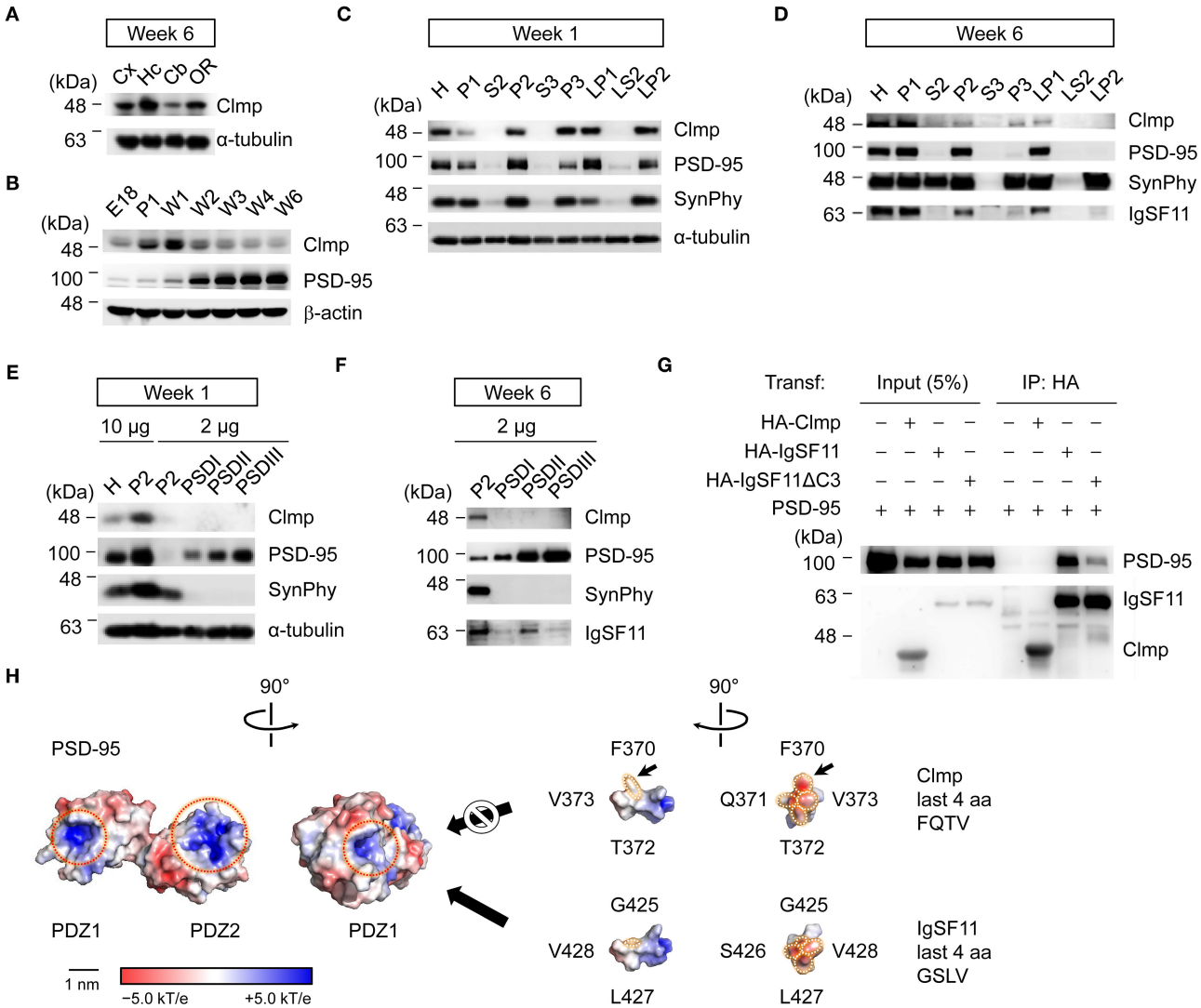

FIGURE 2 | Clmp protein is enriched in synaptic, but not PSD, fractions and fails to interact with PSD-95. **(A)** Levels of Clmp proteins in different brain regions (6 weeks, rat), revealed by immunoblot analysis. Cx, cortex; Hc, hippocampus; Cb, cerebellum; OR, other brain regions. **(B)** Changes in Clmp protein levels during stages of post-natal brain developmental (rat), revealed by immunoblot analysis. PSD-95, a control post-synaptic protein; β-actin, a loading control. **(C,D)** Subcellular fractionation patterns of Clmp protein in the rat brain (weeks 1 and 6), revealed by immunoblot analysis. Note that Clmp protein is more abundant in synaptic membrane and vesicle fractions (P2, P3, LP1, and LP2) at week 1 and also at week 6, although at this latter stage, LP2 levels are strongly reduced. H, homogenates; P1, cells and nuclei-enriched pellet; P2, crude synaptosomes; S2, supernatant after P2 precipitation; S3, cytosol; P3, light membranes; LP1, synaptosomal membranes; LS2, synaptosomal cytosol; LP2, synaptic vesicle-enriched fraction. **(E,F)** Minimal enrichment of Clmp proteins in PSD fractions in the rat brain (weeks 1 and 6). PSD I, Triton X-100 once; PSD II, Triton X-100 twice; PSD III, Triton X-100 and sarcosyl. **(G)** Clmp does not form a complex with PSD-95 in HEK293T cells. IgSF11, a positive control for PSD-95 association; IgSF11 ΔC3, a mutant IgSF11 that lacks PSD-95 binding; Transf, Transfection; IP, immunoprecipitation; HA, HA-tag. **(H)** Molecular modeling indicates steric hindrance between the F residue in the Clmp C-terminus and the tail-binding pocket in the PDZ1 domain of PSD-95, predicted using the structures of the PDZ1 and PDZ2 domains of PSD-95 (PDB 3GSL) and the last 10 aa residues of Clmp and IgSF11. Dotted red circles, tail-binding pockets in the PDZ domain; dotted white circles, last four aa residues of Clmp and IgSF11. The surface is color-coded based on electrostatic potential, contoured from −5.0 kT/e (red: acidic) to +5.0 kT/e (blue: basic). Hydrophobic surface patches are shown in white. Scale bar, 1 nm.

Moderately Changed Kinetics of Evoked Excitatory Synaptic Transmission at Clmp$^{-/-}$ MF-CA3 Synapses

Because the abovementioned results suggest that Clmp negatively regulates miniature excitatory post-synaptic currents at CA3 synapses, we tested whether Clmp also negatively regulates evoked excitatory transmission in MF-CA3 pathway, one of the principal inputs to the CA3 neurons. The amount of evoked excitatory post-synaptic current (eEPSCs), measured in the presence of the NMDAR antagonist AP5, was normal at *Clmp*$^{-/-}$ MF-CA3 synapses, as indicated by the input-output curve of EPSC amplitudes plotted against stimulus intensities

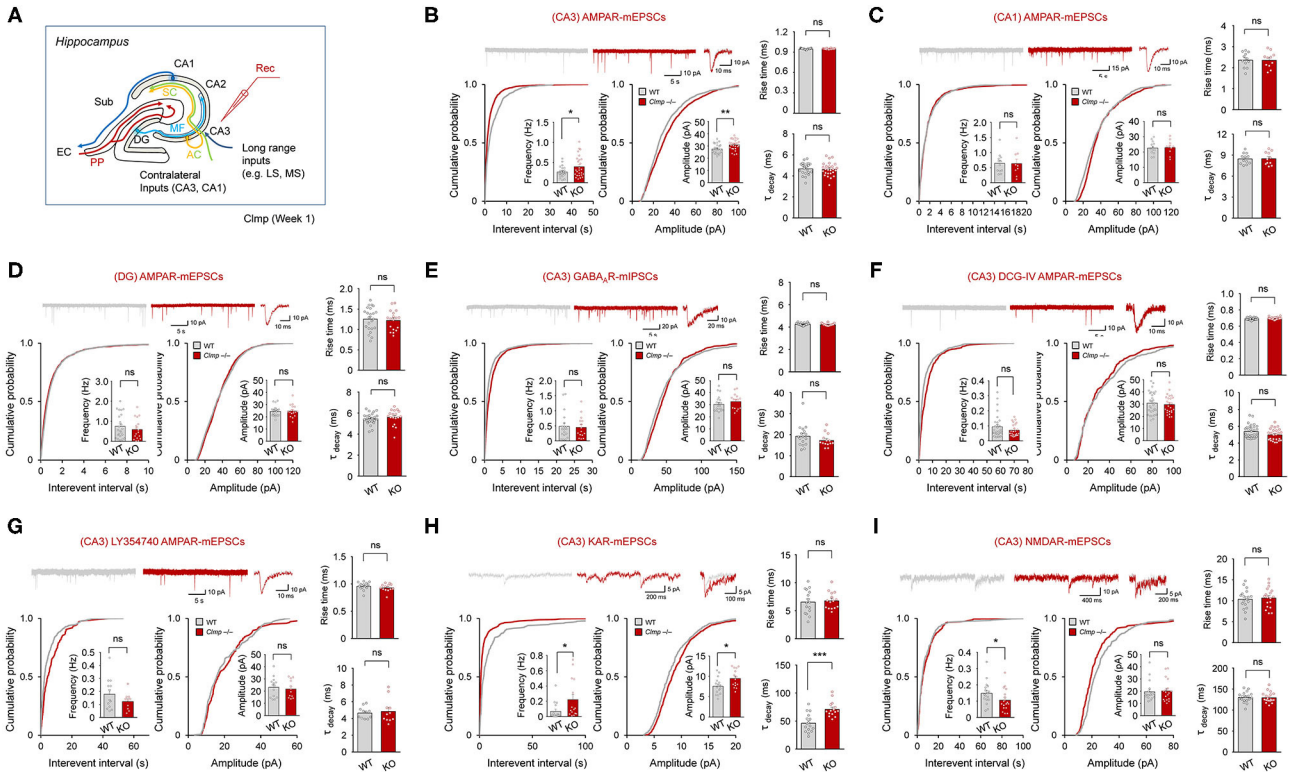

FIGURE 3 | Increased AMPAR and KAR mEPSCs and decreased NMDAR mEPSCs in *Clmp*$^{-/-}$ hippocampal CA3 neurons. **(A)** Schematic diagram showing synaptic pathways in the hippocampus. PP, performant pathways; MF, mossy fiber pathway; AC, associational commissural pathway; SC, Schaffer collateral pathway; LS/MS, lateral/medial septum; EC, entorhinal cortex; DG, dentate gyrus; CA1/2/3, Cornu Ammonis area 1/2/3; Sub, subiculum. **(B)** Increased frequency and amplitude but unaltered rise time and decay time constant in AMPAR mEPSCs in CA3 pyramidal neurons in *Clmp*$^{-/-}$ mice (week 1). Data are presented as means ± SEM. [n = 23 neurons from 7 mice (WT) and 26, 7 (KO), $^{*}P < 0.05$, $^{**}P < 0.01$, Student's t-test (frequency and amplitude)]. **(C)** Normal AMPAR mEPSC frequency, amplitude, rise time, and decay time constant in CA1 pyramidal neurons in *Clmp*$^{-/-}$ mice (week 1). [n = 13, 4 mice (WT), and 10, 4 (KO), ns, not significant, Student's t-test (frequency and amplitude)]. **(D)** Normal AMPAR mEPSC frequency, amplitude, rise time, and decay time constant in DG cells in *Clmp*$^{-/-}$ mice (week 1). [n = 23, 5 mice (WT), and 17, 5 (KO), ns, not significant, Student's t-test (frequency and amplitude)]. **(E)** Normal AMPAR mIPSC frequency, amplitude, rise time, and decay time constant in CA3 pyramidal neurons in *Clmp*$^{-/-}$ mice (week 1). [n = 20, 4 (WT), and 15, 4 (KO), ns, not significant, Student's t-test (frequency and amplitude)]. **(F)** No genotype difference between WT and *Clmp*$^{-/-}$ CA3 pyramidal neurons (week 1) in the frequency and amplitude of AMPAR mEPSCs measured in the presence of with DCG-IV treatment (2 μM) throughout recordings. [n = 30, 8 (WT), and 25, 8 (KO), ns, not significant, Student's t-test (frequency and amplitude)]. **(G)** No genotype difference between WT and *Clmp*$^{-/-}$ CA3 pyramidal neurons (week 1) in the frequency and amplitude of AMPAR mEPSCs measured in the presence of with LY354740 treatment (0.5 μM) throughout recordings. [n = 14, 4 (WT), and 13, 4 (KO), ns, not significant, Student's t-test]. **(H)** Increases in the frequency, amplitude, and decay time constant, but unaltered rise time, in KAR mEPSCs in CA3 pyramidal neurons in *Clmp*$^{-/-}$ mice (week 1). Data are presented as means ± SEM. [n = 16 neurons from 8 mice (WT) and 15, 8 (KO), $^{*}P < 0.05$, $^{***}P < 0.001$, Student's t-test]. **(I)** Decreased frequency but normal amplitude, rise time, and decay time constant in NMDAR mEPSCs in CA3 pyramidal neurons in *Clmp*$^{-/-}$ mice (week 1). Data are presented as means ± SEM. [n = 18 neurons from 4 mice (WT) and 18, 4 (KO), $^{*}P < 0.05$, Student's t-test].

(**Figures 4A,B**). Notably, however, *Clmp*$^{-/-}$ eEPSCs displayed increased fast-rise and slow-decay (but not fast-decay) time constants (**Figures 4C–F**) characteristic of the kinetic properties of AMPAR- and KAR-mediated eEPSCs, respectively.

Isolation of KAR-mediated evoked EPSCs using the AMPAR antagonist GYKI 53655, which were sensitive to NBQX (AMPAR and KAR antagonist) (**Supplementary Figure 4**), revealed that the peak amplitude of KAR eEPSCs was unaltered at *Clmp*$^{-/-}$ MF-CA3 synapses (**Figures 4G,H**); kinetics of KAR eEPSCs were not analyzed because of the apparent presence of multiple components. Consistent with this, the ratio of KAR eEPSCs to total eEPSCs was unaltered at *Clmp*$^{-/-}$ MF-CA3 synapses (**Figures 4I,J**). In addition, AMPAR eEPSCs, obtained by subtracting KAR eEPSCs from total eEPSCs, and the ratio of KAR to AMPAR eEPSCs were unchanged at MF-CA3 synapses (**Figures 4K,L**). NMDAR-mediated EPSCs at *Clmp*$^{-/-}$ MF-CA3 synapses, isolated by NBQX treatment, showed unaltered peak amplitude and kinetic parameters (rise time and decay constant) (**Figures 4M–P**).

In the A/C-CA3 pathway, AMPAR/KAR eEPSCs were unaltered in *Clmp*$^{-/-}$ mice (**Figures 4Q–S**). AMPAR/KAR eEPSCs in the PP-CA3 pathway were not analyzed because of the small sizes of eEPSCs. These results collectively suggest that *Clmp* deletion induces a moderate change in the kinetics of AMPAR/KAR eEPSCs without affecting the peak amplitudes of AMPAR, KAR, or NMDAR eEPSCs at MF-CA3 synapses.

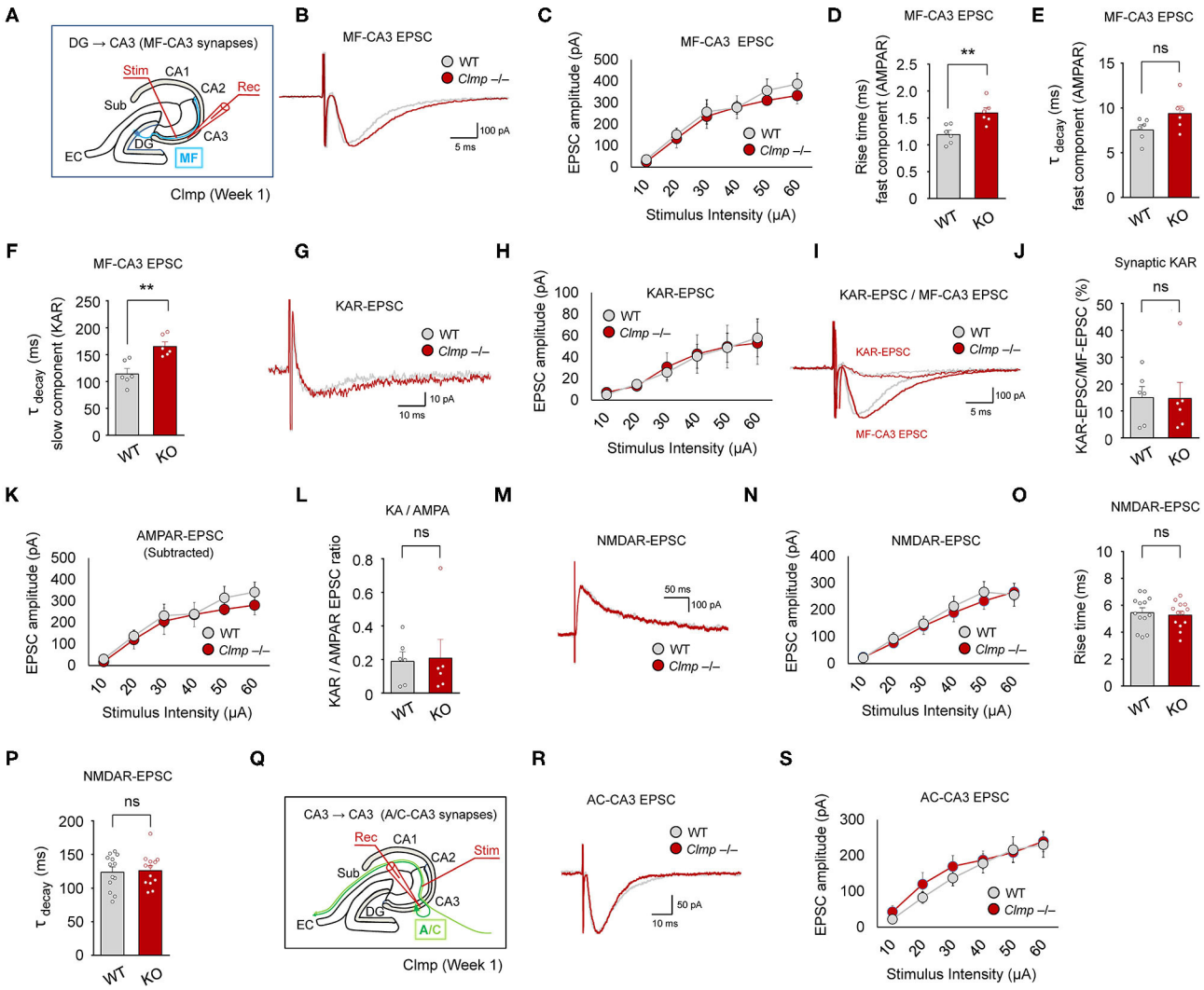

FIGURE 4 | Moderately changed kinetics of evoked excitatory synaptic transmission at *Clmp*$^{-/-}$ MF-CA3 synapses. **(A)** Schematic diagram showing the MF-CA3 pathway and sites of electrical stimulation and evoked EPSC (eEPSC) measurements. **(B,C)** Normal amounts of eEPSCs at MF-CA3 synapses of *Clmp*$^{-/-}$ mice (week 1), as indicated by the input-output relationship between eEPSC amplitudes plotted against stimulus intensities. Data are presented as means ± SEM. [$n = 6$ neurons from 6 mice (WT and KO), ns, not significant, two-way ANOVA with Sidak's multiple comparison test]. **(D–F)** Increased fast-rise time constant (involving AMPARs), unaltered fast-decay time constant (involving AMPARs), and increased slow-decay time constant (involving KARs) of eEPSCs at MF-CA3 synapses of *Clmp*$^{-/-}$ mice (week 1). [$n = 6$, 6 (WT and KO), ns, not significant, $^{**}P < 0.01$, ns, not significant, Student's *t*-test]. **(G,H)** Normal amounts of KAR eEPSCs at MF-CA3 synapses of *Clmp*$^{-/-}$ mice (week 1), as indicated by the input-output relationship between KAR eEPSC amplitudes plotted against stimulus intensities. [$n = 6$, 6 (WT and KO), ns, not significant, two-way ANOVA with Sidak's test]. **(I,J)** Normal ratios of KAR eEPSCs and total eEPSCs at MF-CA3 synapses of *Clmp*$^{-/-}$ mice (week 1). [$n = 6$, 6 (WT and KO), ns, not significant, Student's *t*-test]. **(K)** Normal amounts of AMPAR eEPSCs, obtained by subtracting KAR eEPSCs from total eEPSCs, at MF-CA3 synapses of *Clmp*$^{-/-}$ mice (week 1), as indicated by the input-output relationship between AMPAR eEPSC amplitudes plotted against stimulus intensities. [$n = 6$, 6 (WT and KO), ns, not significant, two-way ANOVA with Sidak's test]. **(L)** Normal ratios of KAR- and AMPAR-mediated eEPSCs (KA/AMPA ratio) at MF-CA3 synapses of *Clmp*$^{-/-}$ mice (week 1). [$n = 6$, 6 (WT and KO), ns, not significant, Student's *t*-test]. **(M,N)** Normal amounts of NMDAR eEPSCs at MF-CA3 synapses of *Clmp*$^{-/-}$ mice (week 1). [$n = 13$, 6 (WT and KO), ns, not significant, two-way ANOVA with Sidak's multiple comparison test]. **(O,P)** Normal rise and decay time constants in NMDAR eEPSCs at MF-CA3 synapses of *Clmp*$^{-/-}$ mice (week 1). [$n = 13$, 6 (WT and KO), ns, not significant, Student's *t*-test]. **(Q–S)** Normal amounts of eEPSCs at A/C-CA3 synapses of *Clmp*$^{-/-}$ mice (week 1), as indicated by the input-output relationship between eEPSC amplitudes plotted against stimulus intensities. [$n = 16$, 14 (WT), and 15, 13 (KO), ns, not significant, two-way ANOVA with Sidak's multiple comparison test].

Extracellular and Cytoplasmic Regions of Clmp Interact With AMPARs and KARs

How does Clmp affect the kinetics of AMPAR- and KAR-mediated EPSCs? One possibility involves the interaction of Clmp with AMPARs and KARs. To address this possibility, we tested whether Clmp formed a complex with AMPAR or KAR subunits in heterologous cells. Notably, we found that Clmp indeed formed a complex with GluA1 and GluA2 subunits of AMPARs in HEK293T cells (**Figures 5A,B**).

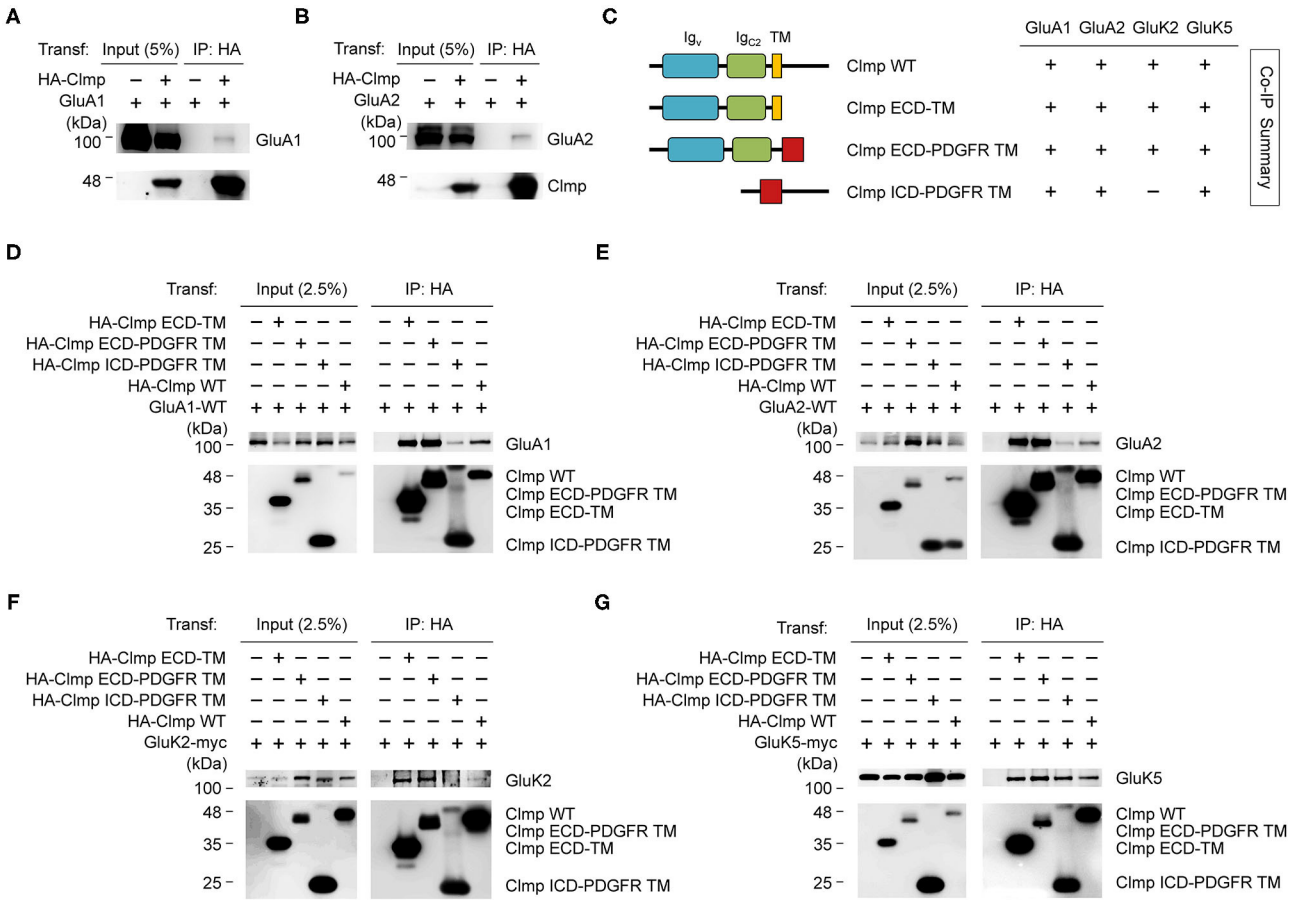

FIGURE 5 | Extracellular and cytoplasmic regions of Clmp interact with AMPARs and KARs. **(A,B)** Clmp forms a complex with GluA1 and GluA2 subunits of AMPARs. HEK293T cells transfected with HA-Clmp and GluA1/2, or GluA1/2 alone, were subjected to immunoprecipitation (IP) with HA antibodies and immunoblotting with the indicated antibodies. HA-IgSF11, N-terminally HA-tagged Clmp. **(C)** Schematic diagram of Clmp deletion variants, and summary of coimmunoprecipitation experiments using these variants to test binding to GluA and GluK. ECD-TM, extracellular domains of Clmp + transmembrane domain of Clmp; ECD-PDGFR TM, extracellular domains of Clmp + transmembrane domain from unrelated PDGF receptor; ICD-PDGFR TM, intracellular/cytoplasmic domain of Clmp + transmembrane domain from unrelated PDGF receptor. **(D,E)** All Clmp deletion variants form a complex with AMPAR subunits (GluA1 and GluA2). HEK293T cells transfected with the HA-tagged deletion variants of Clmp and GluA1/2, or GluA1/2 alone, were subjected to immunoprecipitation with HA antibodies and immunoblotting. **(F,G)** All Clmp deletion variants form a complex with GluK2 and GluK5, with the exception of Clmp-ICD (cytoplasmic domain), which showed no binding to GluK2. HEK293T cells transfected with the HA-tagged deletion variants of Clmp and GluK2/5, or GluK2/5 alone, were subjected to immunoprecipitation with HA antibodies and immunoblotting.

We next used deletion variants of Clmp to identify the domains involved in AMPAR/KAR interactions (**Figure 5C**). Deletion mutants of Clmp containing only the extracellular Ig domains, Ig domains + transmembrane domain, or cytoplasmic domain were able to associate with GluA1 or GluA2, although the extracellular Ig domains seemed to contribute more strongly (**Figures 5C–E**). These results suggest that both extracellular and cytoplasmic regions of Clmp contribute to GluA1/2 binding.

In the case of KAR subunits, all deletion variants of Clmp could associate with GluK5, similar to the results from GluA1/2, although GluK2 failed to associate with a Clmp variant containing only the cytoplasmic domain (**Figures 5F,G**). These results suggest that the extracellular domains of Clmp are more important than the cytoplasmic domain for interacting with GluK2, but not GluK5. Together, these results suggest that, with the exception of GluK2, Clmp associates with AMPARs and KARs through both extracellular and cytoplasmic domains.

A Clmp Deficiency Does Not Alter Presynaptic Function or Synaptic Plasticity at MF-CA3 Synapses

We next examined whether *Clmp* deletion affects presynaptic function at MF-CA3 synapses, associational commissural (AC)-CA3 synapses, or perforant path (PP)-CA3 synapses. We found that paired-pulse ratios were not changed in any of these CA3 synapse types in the *Clmp*$^{-/-}$ hippocampus at week 1 (**Figures 6A–F**).

KARs represent one of the major glutamate receptor subtypes that have been implicated in the regulation of long-term

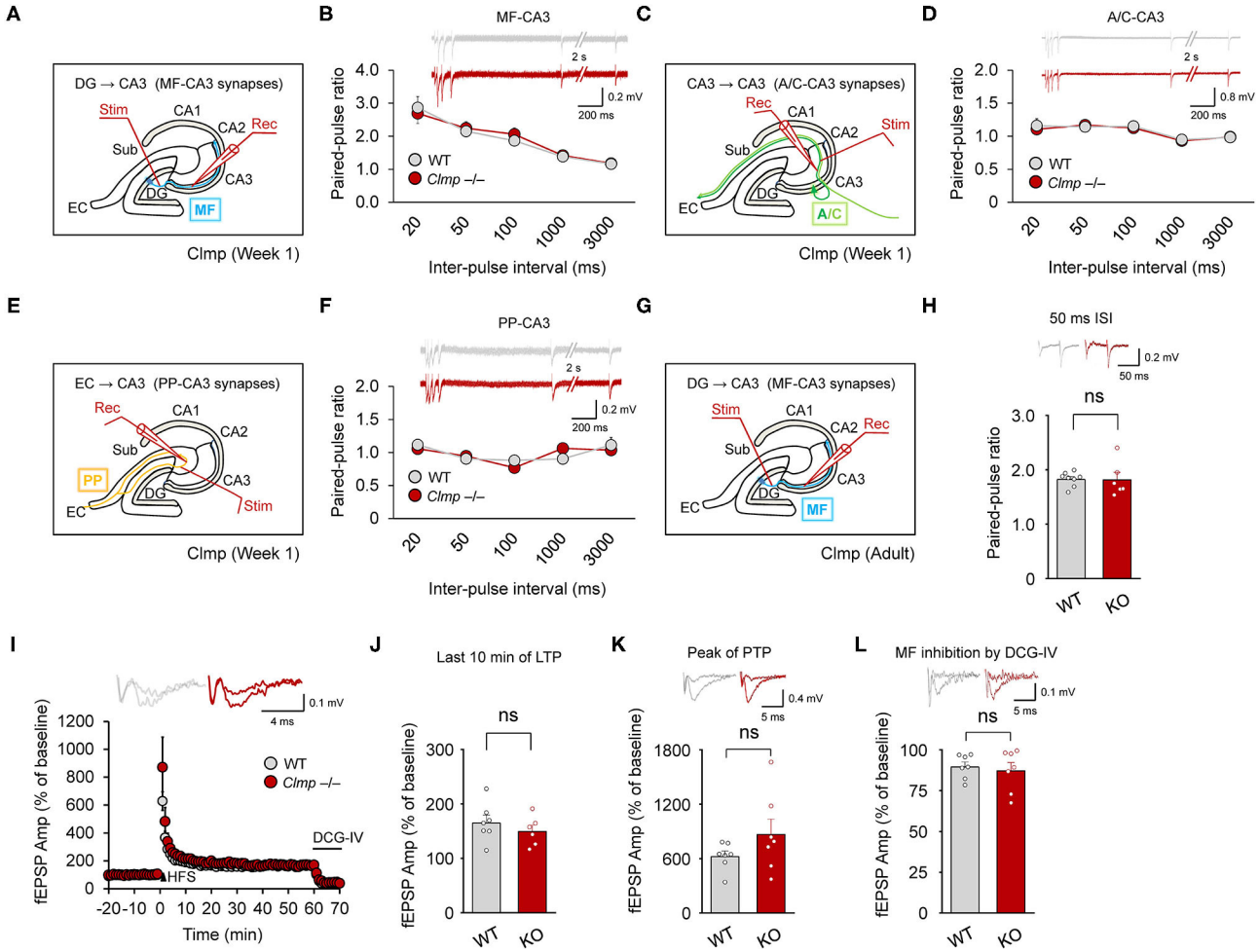

FIGURE 6 | Normal presynaptic function and synaptic plasticity at *Clmp*$^{-/-}$ CA3 synapses. **(A,B)** Normal paired-pulse ratios at MF-CA3 synapses of *Clmp*$^{-/-}$ mice (week 1). [$n = 7$ slices from 7 mice (WT and KO), ns, not significant, two-way ANOVA with Sidak's multiple comparison test]. **(C,D)** Normal paired-pulse ratios at AC (associational commissural)-CA3 synapses of *Clmp*$^{-/-}$ mice (week 1). [$n = 7, 7$ (WT and KO), ns, not significant, two-way ANOVA with Sidak's multiple comparison test]. **(E,F)** Normal paired-pulse ratios at PP (performant path)-CA3 synapses of *Clmp*$^{-/-}$ mice (week 1). [$n = 6, 6$ (WT and KO), ns, not significant, two-way ANOVA with Sidak's multiple comparison test]. **(G–L)** Normal LTP and PTP at MF-CA3 synapses of *Clmp*$^{-/-}$ mice (8–16 weeks). LTP was induced by a single train of high-frequency stimuli (125 pulses at 25 Hz). Synaptic transmission at MF-CA3 synapses was validated by inhibition with the group II mGluR agonist DCG-IV **(I,L)** and by the observed high paired-pulse ratios **(H).** [$n = 7, 7$ (WT), and 7, 6 (KO), ns, not significant, Student's *t*-test (last 10 min)].

potentiation (LTP) at MF-CA3 synapses (Nicoll and Schmitz, 2005), and our data indicate changes in the kinetic properties of KARs at these synapses in *Clmp*$^{-/-}$ mice (**Figure 3**). Thus, we asked whether Clmp affects synaptic plasticity at MF-CA3 synapses (**Figure 6G**). To this end, we measured MF-CA3 LTP at weeks 8–16, a time chosen because Clmp mRNA is detectable in presynaptic neurons (DG granule cells) of the MF-CA3 pathway at week 8 but not at week 1, and LTP at MF-CA3 synapses mainly involves presynaptic mechanisms (Rebola et al., 2017).

However, we detected no genotype difference in LTP at MF-CA3 synapses (**Figures 6H,I**) or post-tetanic potentiation (PTP) (**Figure 6J**) of excitatory synaptic transmission at MF-CA3 synapses, as validated by the inhibition of synaptic transmission by the group II mGluR agonist DCG-IV (**Figure 6K**) and high paired-pulse ratios (**Figure 6L**). Together, these results suggest that Clmp does not affect presynaptic function or synaptic plasticity at MF-CA3 synapses.

Increased Extrasynaptic KAR Currents and Decreased NMDAR Currents in *Clmp*$^{-/-}$ Hippocampal CA3 Neurons

The abovementioned alterations in AMPAR- and KAR-mediated synaptic currents may involve changes in extrasynaptic pools of these receptors. To this end, we measured extrasynaptic AMPAR-, KAR- and NMDAR-mediated currents in *Clmp*$^{-/-}$ CA3 neurons by applying AMPA, kainate, or NMDA to CA3 neurons in slices and measuring the ligand-induced currents (mainly extrasynaptic).

Intriguingly, while AMPAR currents were unaltered, KAR currents were increased, and NMDAR currents were decreased

(**Figures 7A–F**). These changes, however, did not accompany detectable changes in the levels of AMPAR or KAR subunits at the surface membrane of the hippocampus or in PSD fractions of whole brains (**Figures 7G,H**). These results suggest that Clmp deficiency alters the extrasynaptic functions of AMPARs and KARs in CA3 pyramidal neurons without affecting the surface or synaptic expression levels of these receptors.

Enhanced Susceptibility to Kainate-Induced Seizures and Increased Novel Object-Recognition Memory

Clmp protein is abundant in the hippocampus (**Figure 2A**), and *Clmp* deletion alters miniature and evoked excitatory post-synaptic currents in the hippocampal CA3 region (**Figures 3**, **4**). We thus tested whether *Clmp* deletion affects hippocampus-dependent learning and memory or AMPA and kainate receptor-dependent seizure responses in mice.

Clmp$^{-/-}$ mice showed normal levels of contextual fear memory acquisition and 24-h retrieval (**Figures 8A,B**). In the auditory-cued fear test, *Clmp*$^{-/-}$ mice showed normal fear memory acquisition, 24-h retrieval, and contextual fear renewal after auditory-cued fear memory extinction (**Figures 8C–E**). *Clmp*$^{-/-}$ mice also showed normal levels of pattern completion-based contextual fear memory (**Figures 8F,G**), which is known to require intact CA3 function (Nakazawa et al., 2004; Neunuebel and Knierim, 2014).

Intriguingly, however, *Clmp*$^{-/-}$ mice performed better in the novel object-recognition test, in which the subject mouse is exposed to two identical objects on day 1, followed by replacement of one of the two objects with a new one on day 2 (**Figures 8H,I**). The total object-sniffing time for *Clmp*$^{-/-}$ mice was normal, indicating unaltered motivation for object exploration (**Figure 8J**). These results show that *Clmp* deletion does not affect contextual or auditory cued fear memory or pattern completion-based contextual fear memory, but does improve object-recognition memory.

Lastly, because *Clmp* deletion leads to increased miniature excitatory post-synaptic currents in CA3 pyramidal cells and alters the kinetics of AMPAR- and KAR-mediated evoked excitatory synaptic transmission, we tested whether *Clmp*$^{-/-}$ mice display altered susceptibility to seizures induced by kainate (a KAR agonist and a partial AMPAR agonist at MF-CA3 synapses), modeling temporal lobe epilepsy (Nadler, 1981; Engel, 1996; Ben-Ari and Cossart, 2000). Notably, *Clmp*$^{-/-}$ mice at both adult and neonatal stages displayed increased susceptibility to kainate-induced seizure (**Figures 8K–M**). Together, these results suggest that *Clmp* deletion leads to enhanced object recognition memory and increased susceptibility to kainate-induced seizures in mice.

DISCUSSION

The present study investigated the spatiotemporal expression patterns of Clmp, protein interactions of Clmp, and Clmp-dependent regulation of synaptic transmission and behaviors. Our results reveal several properties of Clmp that are unique relative to other members of the CAR subgroup of Ig superfamily proteins (IgSF11, CAR, and ESAM). First, Clmp expression reached a peak at around post-natal week 1 (**Figure 2B**), whereas IgSF11 expression steadily increases during post-natal brain development (Jang et al., 2016), and CAR expression reaches a peak around birth (Honda et al., 2000). Second, Clmp does not have a functional PDZ-binding motif, as supported by protein-interaction experiments and molecular modeling (**Figures 2G,H**), whereas IgSF11, CAR, and ESAM have canonical PDZ-binding motifs that interact with PDZ domain-containing proteins. Third, Clmp regulates synaptic transmission in the hippocampal CA3 region, whereas IgSF11 and CAR regulate synaptic transmission in DG (Jang et al., 2016) and CA1 (Wrackmeyer et al., 2019) regions, respectively. Fourth, Clmp interacts with AMPAR subunits (GluA1 and GluA2) and KAR subunits (GluK2 and GluK5) (**Figure 5**), whereas IgSF11 interacts with AMPAR subunits (GluA1 and GluA2) but not with NMDAR subunits (GluN1); IgSF11 was not tested for KAR subunit interactions (Jang et al., 2016). CAR was not tested for the interactions with AMPAR, KAR, or NMDAR subunits (Wrackmeyer et al., 2019). These results indicate that CAR subgroup members have distinct spatiotemporal expression patterns, synapse-regulatory functions, and molecular interactions with ionotropic glutamate receptors.

Our results indicate that *Clmp* deletion leads to altered AMPAR responses in *Clmp*$^{-/-}$ CA3 neurons. The increased frequency and amplitude of AMPAR mEPSCs (**Figure 3B**) could be explained by increased excitatory synapse number/maturation or increased presynaptic release. The latter, however, is an unlikely possibility because paired pulse facilitations at three different pathways (MF-CA3, A/C-CA3, and PP-CA3) onto CA3 neurons were not altered in *Clmp*$^{-/-}$ mice (**Figures 5A–H**). Therefore, the former (enhanced excitatory synapse development) is the likely possibility. These changes at the individual synapse level, however, does not seem to be reflected at evoked synaptic AMPAR/KAR currents measured at *Clmp*$^{-/-}$ MF-CA3 or A/C-CA3 synapses (**Figures 4A–C,Q–S**) or extrasynaptic AMPAR currents in *Clmp*$^{-/-}$ CA3 neurons (**Figures 7A,B**). It is possible that other synaptic pathways onto CA3 pyramidal neurons such as PP-CA3 may be enhanced, although evoked PP-CA3 currents were not analyzed for their small sizes. Notably, eEPSCs at *Clmp*$^{-/-}$ MF-CA3 synapses showed increased rise time (**Figure 4D**), suggesting that Clmp might regulate the kinetics of AMPAR eEPSCs, although AMPAR mEPSCs did not show altered kinetic properties (**Figure 3B**). These results collectively suggest that Clmp may negatively regulate the development of AMPAR-containing excitatory synapses in CA3 neurons.

Clmp deletion also leads to altered KAR responses in *Clmp*$^{-/-}$ CA3 neurons. Similar to the changes in AMPAR mEPSCs, *Clmp*$^{-/-}$ KAR mEPSCs show increases in the frequency, amplitude, and decay time constant (**Figure 3H**). Peak amplitudes of KAR eEPSCs were also unchanged in the *Clmp*$^{-/-}$ MF-CA3 pathway (**Figures 4G,H**), again similar to the results of AMPAR eEPSC measurements. Distinctly, however, extrasynaptic KAR currents were strongly increased in *Clmp*$^{-/-}$ CA3 neurons, contrary to the unaltered extrasynaptic

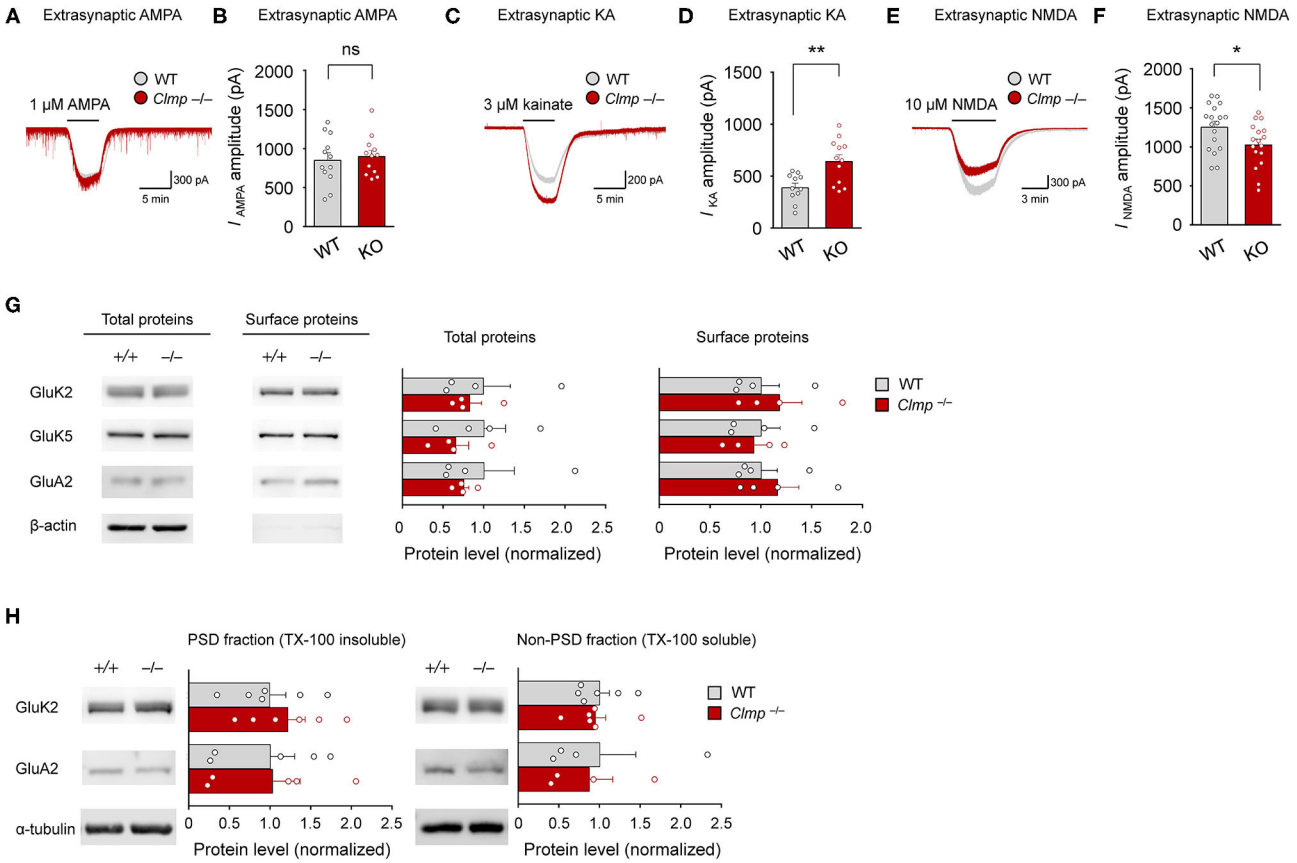

FIGURE 7 | Increased extrasynaptic KAR currents and decreased extrasynaptic NMDAR currents in *Clmp*$^{-/-}$ hippocampal CA3 neurons. **(A,B)** Normal extrasynaptic AMPAR currents in *Clmp*$^{-/-}$ CA3 neurons (1 week), as determined peak currents induced AMPA treatment. [$n = 12$ neurons from 12 mice (WT and KO), ns, not significant, Student's *t*-test]. **(C,D)** Increased extrasynaptic KAR currents in *Clmp*$^{-/-}$ CA3 neurons (1 week), as determined peak currents induced kainate treatment. [$n = 11$ neurons from 9 mice (WT) and 12, 8 (KO), $^{**}P < 0.01$, Student's *t*-test]. **(E,F)** Decreased extrasynaptic NMDAR currents in *Clmp*$^{-/-}$ CA3 neurons (1 week), as determined peak currents induced NMDA treatment. [$n = 18$ neurons from 3 mice (WT) and 17, 3 (KO), $^{*}P < 0.05$, Student's *t*-test]. **(G)** Comparable levels of total and surface AMPAR and KAR receptor subunit proteins in the *Clmp*$^{-/-}$ hippocampus (P10–11), as determined by immunoblot analyses of total lysates and avidin/biotin precipitates of surface proteins from the hippocampus. Note that the minimal levels of β-catenin in the surface samples support the authenticity of the samples. [$n = 4$ mice (WT and KO), ns, not significant, Student's *t*-test]. **(H)** Comparable levels of PSD-enriched AMPAR and KAR receptor subunit proteins in *Clmp*$^{-/-}$ whole brains (P10–11), as determined by immunoblot analyses of PSD fractions. [$n = 6$ mice (WT and KO) except for GluA2 ($n = 5$ for PSD and 4 for non-PSD), ns, not significant, Student's *t*-test].

AMPAR currents (**Figures 7A–D**), suggesting the possibility that Clmp may suppress the response properties of KARs such as kainate binding. Therefore, Clmp seems to similarly suppress the development of AMPAR- and KAR-containing excitatory synapses but distinctly suppress response properties of extrasynaptic KARs not AMPARs. Whether these changes would involve the interactions of Clmp with AMPARs/KARs, which employee slightly different domains of Clmp (**Figure 5**), remains to be determined.

Clmp deletion does not affect LTP at MF-CA3 synapses in the *Clmp*$^{-/-}$ hippocampus (**Figures 6I,J**). This is line with the lack of changes in hippocampus-dependent memory, including contextual fear memory, auditory cued fear memory, contextual fear renewal, and pattern completion-based contextual fear conditioning (**Figures 8A–G**). Intriguingly, however, *Clmp*$^{-/-}$ mice showed increased novel-object recognition (**Figures 8H–J**). Increasing evidence suggests that the dorsal hippocampus is important for novel object recognition memory (Broadbent et al., 2010; Antunes and Biala, 2012; Patten et al., 2015; Liu et al., 2016), although one study reported that the hippocampal CA3 region is less important for object recognition memory in mice (Stupien et al., 2003). Notably, a recent study has reported a novel object-dependent increase in c-fos activity in the DG hilar region (Bernstein et al., 2019), a brain region where Clmp is expressed in the adult, but not neonatal, stage (**Figure 1E**; **Supplementary Figures 2A,B**). However, previous studies have associated novel-object recognition memory with brain regions other than the DG, including the lateral entorhinal cortex, perirhinal cortex, and hippocampal CA1 region (Barker and Warburton, 2011; Wilson et al., 2013; Warburton and Brown, 2015; Furini et al., 2020). Therefore, the brain regions accounting for the enhanced novel object recognition in *Clmp*$^{-/-}$ mice

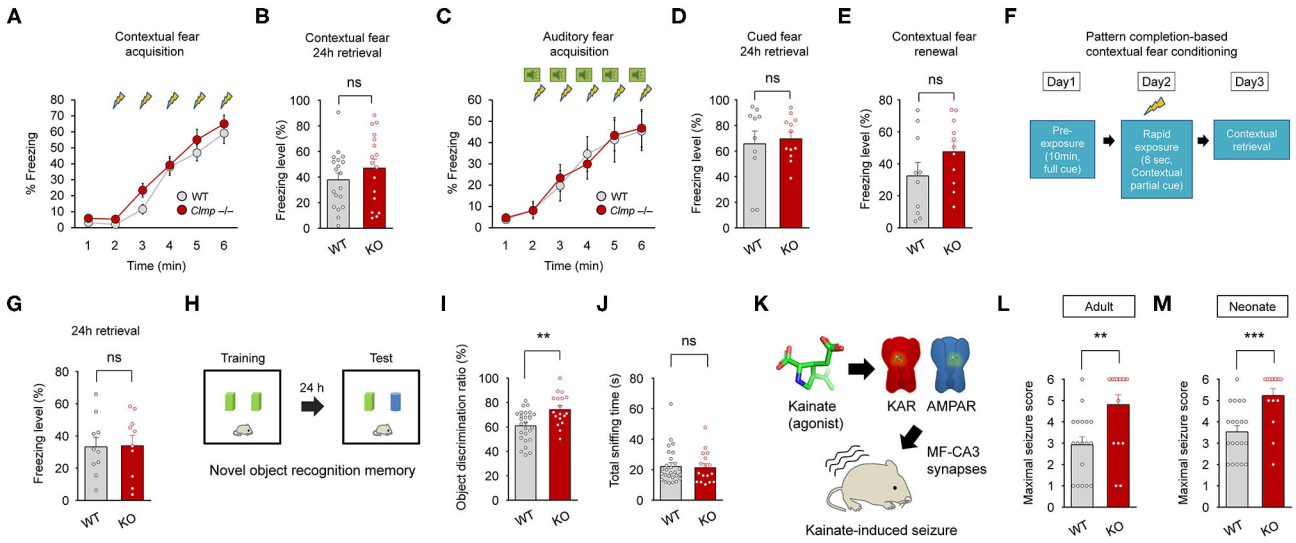

FIGURE 8 | Enhanced object recognition memory and increased susceptibility to kainate-induced seizures in *Clmp*$^{-/-}$ mice. **(A,B)** Normal contextual fear memory acquisition and 24-h retrieval in *Clmp*$^{-/-}$ mice (2–6 months). [$n = 19$ mice (WT) and 17 (KO), ns, not significant, two-way ANOVA with Sidak's test (acquisition) and Student's *t*-test (24-h retrieval)]. **(C–E)** Normal cued fear memory acquisition, 24-h retrieval, and contextual fear renewal in *Clmp*$^{-/-}$ mice (2–4 months). [$n = 10$ (WT) and 12 (KO), ns, not significant, two-way ANOVA with Sidak's test (acquisition) and Student's *t*-test (24-h retrieval and renewal)]. **(F,G)** Normal pattern completion-based contextual fear conditioning in *Clmp*$^{-/-}$ mice (2–4 months). A subject mouse fully exposed to context A on day 1 was briefly (8 s) exposed to the same context on day 2, followed by measurements of context- and pattern completion-dependent freezing on day 3. [$n = 10$ (WT and KO), ns, not significant, Student's *t*-test]. **(H–J)** Normal novel object recognition memory in *Clmp*$^{-/-}$ mice (2–4 months), as shown by the discrimination ratio for old and new objects. Total sniffing time was determined as a measure of general motivation for object exploration. [$n = 28$ (WT) and 18 (KO), $^{**}P < 0.01$, ns, not significant, Student's *t*-test]. **(K–M)** Increased susceptibility to kainate-induced seizures in adult and neonatal *Clmp*$^{-/-}$ mice (2–6 months and P10–12). [$n = 18$ (WT) and 17 (KO) for 2–6 months, 20 (WT), and 16 (KO) for P10–12, $^{**}P < 0.01$, $^{***}P < 0.001$, Student's *t*-test].

might involve both hippocampal and non-hippocampal brain regions expressing Clmp. In addition, the synaptic changes induced by Clmp deletion in neonatal CA3 neurons may represent compensatory changes and thus not be causally linked to the enhanced novel object recognition observed in adult *Clmp*$^{-/-}$ mice.

Clmp$^{-/-}$ mice also displayed increased susceptibility to kainate-induced seizures in both neonates and adults (**Figures 8K–M**). Our electrophysiological results are mainly obtained from neonates but not from adults because peak expression of *Clmp* was observed at ∼P7. However, the similar kainate-induced seizures in *Clmp*$^{-/-}$ neonates and adults suggest that the CA3 region may also be excitable in *Clmp*$^{-/-}$ adults. The hippocampal CA3 region has been closely linked to susceptibility to kainate-induced seizures. For instance, mice lacking the NMDAR subunit GluN1 in the CA3 region show increased susceptibility to kainate-induced seizures (Fukushima et al., 2009; Jinde et al., 2009). Because synaptic transmission in CA3 pyramidal cells is required for kainate-induced seizure activity (Yu et al., 2016), the enhanced synaptic transmission in the *Clmp*$^{-/-}$ CA3 region may contribute to the increased susceptibility to kainate-induced seizures. Notably, Clmp has not been linked to epilepsy. However, the *CLMP* gene is expressed in the developing human cerebral neocortex in regions including the hippocampus, striatum, amygdala, thalamus, and cerebellum (Kang et al., 2011; Pletikos et al., 2014). In addition, synaptic adhesion molecules have been increasingly associated with epilepsy (Gorlewicz and Kaczmarek, 2018), suggesting the possible association of CLMP with epilepsy as well.

In conclusion, our study identifies Clmp as a novel synaptic cell adhesion molecule involved in the negative regulation of AMPAR/KAR-mediated synaptic transmission in the CA3 region of the neonatal hippocampus. In addition, our results implicate Clmp in the regulation of object recognition and seizure susceptibility. Further studies on Clmp will help elucidate the mechanisms underlying synaptic and AMPAR/KAR regulation and behavioral and brain abnormalities.

DATA AVAILABILITY STATEMENT

The original contributions presented in the study are included in the article/**Supplementary Materials**, further inquiries can be directed to the corresponding author/s.

ETHICS STATEMENT

The animal study was reviewed and approved by all animals were bred and maintained according to the Requirements of Animal Research at KAIST, and all procedures were approved by the Committees of Animal Research at KAIST (KA2016-32).

AUTHOR CONTRIBUTIONS

SJ performed the biochemical experiments, structural prediction analyses, electrophysiological experiments, mouse breeding and behavioral experiments, and generated *Clmp*$^{-/-}$ mice. SJ and DK performed designed constructs. DK made *in situ* probe. EY performed *in situ* hybridization experiments. SJ and EK designed the experiments and wrote the manuscript. All authors contributed to the article and approved the submitted version.

FUNDING

This work was supported by the National Research Foundation of Korea (NRF), funded by the Ministry of Science, ICT and Future Planning (2017M3C7A1079692 to HK), the Korea Research Institute of Chemical Technology (KRICT) (KK2031-10 to DK), and the Institute for Basic Science (IBSR002-D1 to EK).

SUPPLEMENTARY MATERIAL

The Supplementary Material for this article can be found online at: https://www.frontiersin.org/articles/10.3389/fnsyn.2020.567075/full#supplementary-material

Supplementary Figure 1 | Amino acid sequence alignment of Clmp proteins from various vertebrate species. **(A)** Amino acid residues in black and gray backgrounds indicate fully and partially conserved residues, respectively. The following aa sequences were used for comparison; human (NP_079045.1), chimpanzee (JAA42653.1), macaque monkey (XP_001108111.1), marmoset (JAB43212.1), rat (NP_775177.1), mouse (NP_598494.2), finch (ENSTGUT00000022861.1), turtle (XP_006116688.1), lizard (ENSACAT00000004856.3), and zebrafish (XP_695564.4). TM, transmembrane domain.

Supplementary Figure 2 | Expression of Clmp mRNA in both glutamatergic and GABAergic neurons in the mouse brain at week 8. **(A,B)** Expression of Clmp mRNA in Vglut1/2-positive glutamatergic neurons **(A)** and Gad1/2-positive GABAergic neurons **(B)** in the neocortex and hippocampus in the mouse brain [week 8 (P56)], as detected by FISH. Coronal brain sections were triply stained for Clmp, Vglut1/2 or Gad1/2, and DAPI. Note that the DG area show strong signals for *Clmp* mRNAs. Scale bar, 300 μm (left) and 20 μm (right).

Supplementary Figure 3 | Generation and characterization of *Clmp*$^{-/-}$ mice. **(A)** Schematic diagram showing the strategy for generating *Clmp*$^{-/-}$ mice lacking exons 3–5 of the *Clmp* gene. P1, P2, P3, and P4, primers for PCR genotyping. **(B)** Genotyping of wild-type (*Clmp*$^{+/+}$; WT), *Clmp*$^{+/-}$, and *Clmp*$^{-/-}$ mice by PCR. **(C)** *Clmp*$^{-/-}$ mice show no detectable levels of Clmp proteins in the whole brain (week 8). β-actin blot was used as a control. **(D)** Survival curve of *Clmp*$^{-/-}$ mice during post-natal stages [$n = 28$ mice (+/+; WT), 76 (+/–; hetero), and 31 (-/-; KO)].

Supplementary Figure 4 | Elimination of KAR eEPSCs by NBQX at MF-CA3 synapses. **(A)** KAR eEPSCs isolated by the treatment of the slices with GYKI 53655 (AMPAR antagonist), AP5 (NMDAR antagonist), and picrotoxin (GABA receptor antagonist) were eliminated by the treatment of NBQX (AMPAR and KAR antagonist), as shown by two examples of KAR eEPSCs recorded at WT MF-CA3 synapses (week 1).

Supplementary Table 1 | Statistical Details.

REFERENCES

Antunes, M., and Biala, G. (2012). The novel object recognition memory: neurobiology, test procedure, and its modifications. *Cogn. Process* 13, 93–110. doi: 10.1007/s10339-011-0430-z

Arnold, K., Bordoli, L., Kopp, J., and Schwede, T. (2006). The SWISS-MODEL workspace: a web-based environment for protein structure homology modelling. *Bioinformatics* 22, 195–201. doi: 10.1093/bioinformatics/bti770

Bahn, S., Volk, B., and Wisden, W. (1994). Kainate receptor gene expression in the developing rat brain. *J. Neurosci.* 14, 5525–5547. doi: 10.1523/JNEUROSCI.14-09-05525.1994

Baker, N. A., Sept, D., Joseph, S., Holst, M. J., and Mccammon, J. A. (2001). Electrostatics of nanosystems: application to microtubules and the ribosome. *Proc. Natl. Acad. Sci. U.S.A.* 98, 10037–10041. doi: 10.1073/pnas.181342398

Bannister, N. J., Benke, T. A., Mellor, J., Scott, H., Gurdal, E., Crabtree, J. W., et al. (2005). Developmental changes in AMPA and kainate receptor-mediated quantal transmission at thalamocortical synapses in the barrel cortex. *J. Neurosci.* 25, 5259–5271. doi: 10.1523/JNEUROSCI.0827-05.2005

Barker, G. R., and Warburton, E. C. (2011). When is the hippocampus involved in recognition memory? *J. Neurosci.* 31, 10721–10731. doi: 10.1523/JNEUROSCI.6413-10.2011

Ben-Ari, Y., and Cossart, R. (2000). Kainate, a double agent that generates seizures: two decades of progress. *Trends Neurosci.* 23, 580–587. doi: 10.1016/S0166-2236(00)01659-3

Berman, H. M., Westbrook, J., Feng, Z., Gilliland, G., Bhat, T. N., Weissig, H., et al. (2000). The protein data bank. *Nucleic Acids Res.* 28, 235–242. doi: 10.1093/nar/28.1.235

Bernstein, H. L., Lu, Y. L., Botterill, J. J., and Scharfman, H. E. (2019). Novelty and novel objects increase c-Fos immunoreactivity in mossy cells in the mouse dentate gyrus. *Neural Plast.* 2019:1815371. doi: 10.1155/2019/1815371

Bischofberger, J., Engel, D., Li, L., Geiger, J. R., and Jonas, P. (2006). Patch-clamp recording from mossy fiber terminals in hippocampal slices. *Nat. Protoc.* 1, 2075–2081. doi: 10.1038/nprot.2006.312

Broadbent, N. J., Gaskin, S., Squire, L. R., and Clark, R. E. (2010). Object recognition memory and the rodent hippocampus. *Learn. Mem.* 17, 5–11. doi: 10.1101/lm.1650110

Budreck, E. C. (2013). Neuroligin-1 controls synaptic abundance of NMDA-type glutamate receptors through extracellular coupling. *Proc. Natl. Acad. Sci. U.S.A.* 110, 750–730. doi: 10.1073/pnas.1214718110

Castillo, P. E., Janz, R., Sudhof, T. C., Tzounopoulos, T., Malenka, R. C., and Nicoll, R. A. (1997a). Rab3A is essential for mossy fibre long-term potentiation in the hippocampus. *Nature* 388, 590–593. doi: 10.1038/41574

Castillo, P. E., Malenka, R. C., and Nicoll, R. A. (1997b). Kainate receptors mediate a slow postsynaptic current in hippocampal CA3 neurons. *Nature* 388, 182–186. doi: 10.1038/40645

Chen, L., El-Husseini, A., Tomita, S., Bredt, D. S., and Nicoll, R. A. (2003). Stargazin differentially controls the trafficking of alpha-amino-3-hydroxyl-5-methyl-4-isoxazolepropionate and kainate receptors. *Mol. Pharmacol.* 64, 703–706. doi: 10.1124/mol.64.3.703

Chung, W., Choi, S. Y., Lee, E., Park, H., Kang, J., Park, H., et al. (2015). Social deficits in IRSp53 mutant mice improved by NMDAR and mGluR5 suppression. *Nat. Neurosci.* 18, 435–443. doi: 10.1038/nn.3927

Collingridge, G. L., and Lester, R. A. (1989). Excitatory amino acid receptors in the vertebrate central nervous system. *Pharmacol. Rev.* 41, 143–210.

Cossart, R., Epsztein, J., Tyzio, R., Becq, H., Hirsch, J., Ben-Ari, Y., et al. (2002). Quantal release of glutamate generates pure kainate and mixed AMPA/kainate EPSCs in hippocampal neurons. *Neuron* 35, 147–159. doi: 10.1016/S0896-6273(02)00753-5

Dalva, M. B., Mcclelland, A. C., and Kayser, M. S. (2007). Cell adhesion molecules: signalling functions at the synapse. *Nat. Rev. Neurosci.* 8, 206–220. doi: 10.1038/nrn2075

de Wit, J., and Ghosh, A. (2016). Specification of synaptic connectivity by cell surface interactions. *Nat. Rev. Neurosci.* 17, 22–35. doi: 10.1038/nrn.2015.3

Dolinsky, T. J., Nielsen, J. E., Mccammon, J. A., and Baker, N. A. (2004). PDB2PQR: an automated pipeline for the setup of Poisson-Boltzmann electrostatics calculations. *Nucleic Acids Res.* 32, W665–667. doi: 10.1093/nar/gkh381

Eguchi, J., Wada, J., Hida, K., Zhang, H., Matsuoka, T., Baba, M., et al. (2005). Identification of adipocyte adhesion molecule (ACAM), a novel CTX gene family, implicated in adipocyte maturation and development of obesity. *Biochem. J.* 387, 343–353. doi: 10.1042/BJ20041709

Engel, J. Jr. (1996). Introduction to temporal lobe epilepsy. *Epilepsy Res.* 26, 141–150. doi: 10.1016/S0920-1211(96)00043-5

Falcon-Moya, R., Sihra, T. S., and Rodriguez-Moreno, A. (2018). Kainate receptors: role in epilepsy. *Front. Mol. Neurosci.* 11:217. doi: 10.3389/fnmol.2018.00217

Fukushima, F., Nakao, K., Shinoe, T., Fukaya, M., Muramatsu, S., Sakimura, K., et al. (2009). Ablation of NMDA receptors enhances the excitability of hippocampal CA3 neurons. *PLoS ONE* 4:e3993. doi: 10.1371/journal.pone.0003993

Furini, C. R. G., Nachtigall, E. G., Behling, J. A. K., Assis Brasil, E. S., Saenger, B. F., Narvaes, R. F., et al. (2020). Molecular mechanisms in hippocampus involved on object recognition memory consolidation and reconsolidation. *Neuroscience* 435, 112–123. doi: 10.1016/j.neuroscience.2020.03.047

Gorlewicz, A., and Kaczmarek, L. (2018). Pathophysiology of trans-synaptic adhesion molecules: implications for epilepsy. *Front. Cell Dev. Biol.* 6:119. doi: 10.3389/fcell.2018.00119

Hibi, S., Ueno, K., Nagato, S., Kawano, K., Ito, K., Norimine, Y., et al. (2012). Discovery of 2-(2-oxo-1-phenyl-5-pyridin-2-yl-1,2-dihydropyridin-3-yl)benzonitrile (perampanel): a novel, noncompetitive alpha-amino-3-hydroxy-5-methyl-4-isoxazolepropanoic acid (AMPA) receptor antagonist. *J. Med. Chem.* 55, 10584–10600. doi: 10.1021/jm301268u

Honda, T., Saitoh, H., Masuko, M., Katagiri-Abe, T., Tominaga, K., Kozakai, I., et al. (2000). The coxsackievirus-adenovirus receptor protein as a cell adhesion molecule in the developing mouse brain. *Brain Res. Mol. Brain Res.* 77, 19–28. doi: 10.1016/S0169-328X(00)00036-X

Huganir, R. L., and Nicoll, R. A. (2013). AMPARs and synaptic plasticity: the last 25 years. *Neuron* 80, 704–717. doi: 10.1016/j.neuron.2013.10.025

Jang, S., Lee, H., and Kim, E. (2017). Synaptic adhesion molecules and excitatory synaptic transmission. *Curr. Opin. Neurobiol.* 45, 45–50. doi: 10.1016/j.conb.2017.03.005

Jang, S., Oh, D., Lee, Y., Hosy, E., Shin, H., Van Riesen, C., et al. (2016). Synaptic adhesion molecule IgSF11 regulates synaptic transmission and plasticity. *Nat. Neurosci.* 19, 84–93. doi: 10.1038/nn.4176

Jinde, S., Belforte, J. E., Yamamoto, J., Wilson, M. A., Tonegawa, S., and Nakazawa, K. (2009). Lack of kainic acid-induced gamma oscillations predicts subsequent CA1 excitotoxic cell death. *Eur. J. Neurosci.* 30, 1036–1055. doi: 10.1111/j.1460-9568.2009.06896.x

Kang, H. J., Kawasawa, Y. I., Cheng, F., Zhu, Y., Xu, X., Li, M., et al. (2011). Spatio-temporal transcriptome of the human brain. *Nature* 478, 483–489. doi: 10.1038/nature10523

Kato, A. S., Burris, K. D., Gardinier, K. M., Gernert, D. L., Porter, W. J., Reel, J., et al. (2016). Forebrain-selective AMPA-receptor antagonism guided by TARP gamma-8 as an antiepileptic mechanism. *Nat. Med.* 22, 1496–1501. doi: 10.1038/nm.4221

Kim, E., Niethammer, M., Rothschild, A., Jan, Y. N., and Sheng, M. (1995). Clustering of Shaker-type K+ channels by interaction with a family of membrane-associated guanylate kinases. *Nature* 378, 85–88. doi: 10.1038/378085a0

Kim, M. H. (2009). Enhanced NMDA receptor-mediated synaptic transmission, enhanced long-term potentiation, and impaired learning and memory in mice lacking IRSp53. *J. Neurosci.* 29, 1586–1595. doi: 10.1523/JNEUROSCI.4306-08.2009

Ko, J., Choii, G., and Um, J. W. (2015). The balancing act of GABAergic synapse organizers. *Trends Mol. Med.* 21, 256–68.doi: 10.1016/j.molmed.2015.01.004

Ko, J., Park, H., Heo, L., and Seok, C. (2012). GalaxyWEB server for protein structure prediction and refinement. *Nucleic Acids Res.* 40, W294–W297. doi: 10.1093/nar/gks493

Koh, S., Tibayan, F. D., Simpson, J. N., and Jensen, F. E. (2004). NBQX or topiramate treatment after perinatal hypoxia-induced seizures prevents later increases in seizure-induced neuronal injury. *Epilepsia* 45, 569–575. doi: 10.1111/j.0013-9580.2004.69103.x

Krueger-Burg, D., Papadopoulos, T., and Brose, N. (2017). Organizers of inhibitory synapses come of age. *Curr. Opin. Neurobiol.* 45, 66–77. doi: 10.1016/j.conb.2017.04.003

Kurshan, P. T., and Shen, K. (2019). Synaptogenic pathways. *Curr. Opin. Neurobiol.* 57, 156–162. doi: 10.1016/j.conb.2019.03.005

Langhorst, H., Juttner, R., Groneberg, D., Mohtashamdolatshahi, A., Pelz, L., Purfurst, B., et al. (2018). The IgCAM CLMP regulates expression of Connexin43 and Connexin45 in intestinal and ureteral smooth muscle contraction in mice. *Dis. Model. Mech.* 11:dmm032128. doi: 10.1242/dmm.032128

Liu, Y., Du, S., Lv, L., Lei, B., Shi, W., Tang, Y., et al. (2016). Hippocampal activation of Rac1 regulates the forgetting of object recognition memory. *Curr. Biol.* 26, 2351–2357. doi: 10.1016/j.cub.2016.06.056

Marchal, C., and Mulle, C. (2004). Postnatal maturation of mossy fibre excitatory transmission in mouse CA3 pyramidal cells: a potential role for kainate receptors. *J. Physiol.* 561, 27–37. doi: 10.1113/jphysiol.2004.069922

Matsuda, K., Budisantoso, T., Mitakidis, N., Sugaya, Y., Miura, E., Kakegawa, W., et al. (2016). Transsynaptic modulation of kainate receptor functions by C1q-like proteins. *Neuron* 90, 752–767. doi: 10.1016/j.neuron.2016.04.001

Mayer, M. L., and Westbrook, G. L. (1987). The physiology of excitatory amino acids in the vertebrate central nervous system. *Prog. Neurobiol.* 28, 197–276. doi: 10.1016/0301-0082(87)90011-6

Nadler, J. V. (1981). Minireview. Kainic acid as a tool for the study of temporal lobe epilepsy. *Life Sci.* 29, 2031–2042. doi: 10.1016/0024-3205(81)90659-7

Nakazawa, K., Mchugh, T. J., Wilson, M. A., and Tonegawa, S. (2004). NMDA receptors, place cells and hippocampal spatial memory. *Nat. Rev. Neurosci.* 5, 361–372. doi: 10.1038/nrn1385

Nanao, M. H., Green, T., Stern-Bach, Y., Heinemann, S. F., and Choe, S. (2005). Structure of the kainate receptor subunit GluR6 agonist-binding domain complexed with domoic acid. *Proc. Natl. Acad. Sci. U.S.A.* 102, 1708–1713. doi: 10.1073/pnas.0409573102

Neunuebel, J. P., and Knierim, J. J. (2014). CA3 retrieves coherent representations from degraded input: direct evidence for CA3 pattern completion and dentate gyrus pattern separation. *Neuron* 81, 416–427. doi: 10.1016/j.neuron.2013.11.017

Nicoll, R. A., and Schmitz, D. (2005). Synaptic plasticity at hippocampal mossy fibre synapses. *Nat. Rev. Neurosci.* 6, 863–876. doi: 10.1038/nrn1786

Nuriya, M., and Huganir, R. L. (2006). Regulation of AMPA receptor trafficking by N-cadherin. *J. Neurochem.* 97, 652–661. doi: 10.1111/j.1471-4159.2006.03740.x

Park, H., Lee, G. R., Heo, L., and Seok, C. (2014). Protein loop modeling using a new hybrid energy function and its application to modeling in inaccurate structural environments. *PLoS ONE* 9:e113811. doi: 10.1371/journal.pone.0113811

Park, H., and Seok, C. (2012). Refinement of unreliable local regions in template-based protein models. *Proteins* 80, 1974–1986. doi: 10.1002/prot.24086

Paternain, A. V., Morales, M., and Lerma, J. (1995). Selective antagonism of AMPA receptors unmasks kainate receptor-mediated responses in hippocampal neurons. *Neuron* 14, 185–189. doi: 10.1016/0896-6273(95)90253-8

Patten, A. R., Yau, S. Y., Fontaine, C. J., Meconi, A., Wortman, R. C., and Christie, B. R. (2015). The benefits of exercise on structural and functional plasticity in the rodent hippocampus of different disease models. *Brain Plast.* 1, 97–127. doi: 10.3233/BPL-150016

Pettersen, E. F., Goddard, T. D., Huang, C. C., Couch, G. S., Greenblatt, D. M., Meng, E. C., et al. (2004). UCSF Chimera–a visualization system for exploratory research and analysis. *J. Comput. Chem.* 25, 1605–1612. doi: 10.1002/jcc.20084

Pinheiro, P. S., Lanore, F., Veran, J., Artinian, J., Blanchet, C., Crepel, V., et al. (2013). Selective block of postsynaptic kainate receptors reveals their function at hippocampal mossy fiber synapses. *Cereb. Cortex* 23, 323–331. doi: 10.1093/cercor/bhs022

Pletikos, M., Sousa, A. M., Sedmak, G., Meyer, K. A., Zhu, Y., Cheng, F., et al. (2014). Temporal specification and bilaterality of human neocortical topographic gene expression. *Neuron* 81, 321–332. doi: 10.1016/j.neuron.2013.11.018

Pozo, K., Cingolani, L. A., Bassani, S., Laurent, F., Passafaro, M., and Goda, Y. (2012). beta3 integrin interacts directly with GluA2 AMPA receptor subunit and regulates AMPA receptor expression in hippocampal neurons. *Proc. Natl. Acad. Sci. U.S.A.* 109, 1323–1328. doi: 10.1073/pnas.1113736109

Racine, R. J. (1972). Modification of seizure activity by electrical stimulation. II. Motor seizure. *Electroencephalogr. Clin. Neurophysiol.* 32, 281–294. doi: 10.1016/0013-4694(72)90177-0

Raschperger, E., Engstrom, U., Pettersson, R. F., and Fuxe, J. (2004). CLMP, a novel member of the CTX family and a new component of epithelial tight junctions. *J. Biol. Chem.* 279, 796–804. doi: 10.1074/jbc.M308249200

Rawls, S. M., Thomas, T., Adeola, M., Patil, T., Raymondi, N., Poles, A., et al. (2009). Topiramate antagonizes NMDA- and AMPA-induced seizure-like activity in planarians. *Pharmacol. Biochem. Behav.* 93, 363–367. doi: 10.1016/j.pbb.2009.05.005

Rebola, N., Carta, M., and Mulle, C. (2017). Operation and plasticity of hippocampal CA3 circuits: implications for memory encoding. *Nat. Rev. Neurosci.* 18, 208–220. doi: 10.1038/nrn.2017.10

Ribic, A., and Biederer, T. (2019). Emerging roles of synapse organizers in the regulation of critical periods. *Neural Plast.* 2019:1538137. doi: 10.1155/2019/1538137

Saglietti, L. (2007). Extracellular interactions between GluR2 and N-cadherin in spine regulation. *Neuron* 54, 461–477. doi: 10.1016/j.neuron.2007.04.012

Sarto-Jackson, I., Milenkovic, I., Smalla, K. H., Gundelfinger, E. D., Kaehne, T., Herrera-Molina, R., et al. (2012). The cell adhesion molecule neuroplastin-65 is a novel interaction partner of gamma-aminobutyric acid type A receptors. *J. Biol. Chem.* 287, 14201–14214. doi: 10.1074/jbc.M111.293175

Shanks, N. F., Savas, J. N., Maruo, T., Cais, O., Hirao, A., Oe, S., et al. (2012). Differences in AMPA and kainate receptor interactomes facilitate identification of AMPA receptor auxiliary subunit GSG1L. *Cell Rep.* 1, 590–598. doi: 10.1016/j.celrep.2012.05.004

Shen, K., and Scheiffele, P. (2010). Genetics and cell biology of building specific synapse connectivity. *Annu. Rev. Neurosci.* 33, 473–507.doi: 10.1146/annurev.neuro.051508.135302

Shen, L., Liang, F., Walensky, L. D., and Huganir, R. L. (2000). Regulation of AMPA receptor GluR1 subunit surface expression by a 4. 1N-linked actin cytoskeletal association. *J. Neurosci.* 20, 7932–7940. doi: 10.1523/JNEUROSCI.20-21-07932.2000

Sheng, M., and Sala, C. (2001). PDZ domains and the organization of supramolecular complexes. *Annu. Rev. Neurosci.* 24, 1–29. doi: 10.1146/annurev.neuro.24.1.1

Siddiqui, T. J., and Craig, A. M. (2011). Synaptic organizing complexes. *Curr. Opin. Neurobiol.* 21, 132–143. doi: 10.1016/j.conb.2010.08.016

Stupien, G., Florian, C., and Roullet, P. (2003). Involvement of the hippocampal CA3-region in acquisition and in memory consolidation of spatial but not in object information in mice. *Neurobiol. Learn. Mem.* 80, 32–41. doi: 10.1016/S1074-7427(03)00022-4

Südhof, T. C. (2017). Synaptic neurexin complexes: a molecular code for the logic of neural circuits. *Cell* 171, 745–769. doi: 10.1016/j.cell.2017.10.024

Sudhof, T. C. (2018). Towards an understanding of synapse formation. *Neuron* 100, 276–293. doi: 10.1016/j.neuron.2018.09.040

Takahashi, H., and Craig, A. (2013). Protein tyrosine phosphatases PTPδ, PTPσ, and LAR: presynaptic hubs for synapse organization. *Trends Neurosci.* 36, 522–534. doi: 10.1016/j.tins.2013.06.002

Tang, T., Li, L., Tang, J., Li, Y., Lin, W. Y., Martin, F., et al. (2010). A mouse knockout library for secreted and transmembrane proteins. *Nat. Biotechnol.* 28, 749–755. doi: 10.1038/nbt.1644

Tomioka, N. H., Yasuda, H., Miyamoto, H., Hatayama, M., Morimura, N., Matsumoto, Y., et al. (2014). Elfn1 recruits presynaptic mGluR7 in trans and its loss results in seizures. *Nat. Commun.* 5:4501. doi: 10.1038/ncomms5501

Tomita, S., Byrd, R. K., Rouach, N., Bellone, C., Venegas, A., O'brien, J. L., et al. (2007). AMPA receptors and stargazin-like transmembrane AMPA receptor-regulatory proteins mediate hippocampal kainate neurotoxicity. *Proc. Natl. Acad. Sci. U.S.A.* 104, 18784–18788. doi: 10.1073/pnas.0708970104

Uemura, T., Lee, S. J., Yasumura, M., Takeuchi, T., Yoshida, T., Ra, M., et al. (2010). Trans-synaptic interaction of GluRdelta2 and Neurexin through Cbln1 mediates synapse formation in the cerebellum. *Cell* 141, 1068–1079. doi: 10.1016/j.cell.2010.04.035

Um, J. W., and Ko, J. (2013). LAR-RPTPs: synaptic adhesion molecules that shape synapse development. *Trends Cell Biol.* 23, 465–475. doi: 10.1016/j.tcb.2013.07.004

Um, S. M., Ha, S., Lee, H., Kim, J., Kim, K., Shin, W., et al. (2018). NGL-2 deletion leads to autistic-like behaviors responsive to NMDAR modulation. *Cell Rep.* 23, 3839–3851. doi: 10.1016/j.celrep.2018.05.087

van der Werf, C. S., Hsiao, N. H., Conroy, S., Paredes, J., Ribeiro, A. S., Sribudiani, Y., et al. (2013). CLMP is essential for intestinal development, but does not play a key role in cellular processes involved in intestinal epithelial development. *PLoS ONE* 8:e54649. doi: 10.1371/journal.pone.0054649

Vissel, B., Royle, G. A., Christie, B. R., Schiffer, H. H., Ghetti, A., Tritto, T., et al. (2001). The role of RNA editing of kainate receptors in synaptic plasticity and seizures. *Neuron* 29, 217–227. doi: 10.1016/S0896-6273(01)00192-1

Wagatsuma, A., Okuyama, T., Sun, C., Smith, L. M., Abe, K., and Tonegawa, S. (2018). Locus coeruleus input to hippocampal CA3 drives single-trial learning of a novel context. *Proc. Natl. Acad. Sci. U.S.A.* 115, E310–E316. doi: 10.1073/pnas.1714082115

Warburton, E. C., and Brown, M. W. (2015). Neural circuitry for rat recognition memory. *Behav. Brain Res.* 285, 131–139. doi: 10.1016/j.bbr.2014.09.050

Waterhouse, A., Bertoni, M., Bienert, S., Studer, G., Tauriello, G., Gumienny, R., et al. (2018). SWISS-MODEL: homology modelling of protein structures and complexes. *Nucleic Acids Res.* 46, W296–W303. doi: 10.1093/nar/gky427

Wilson, D. I., Langston, R. F., Schlesiger, M. I., Wagner, M., Watanabe, S., and Ainge, J. A. (2013). Lateral entorhinal cortex is critical for novel object-context recognition. *Hippocampus* 23, 352–366. doi: 10.1002/hipo.22095

Wrackmeyer, U., Kaldrack, J., Juttner, R., Pannasch, U., Gimber, N., Freiberg, F., et al. (2019). The cell adhesion protein CAR is a negative regulator of synaptic transmission. *Sci. Rep.* 9:6768. doi: 10.1038/s41598-019-43150-5

Yang, J. (2011). DGKiota regulates presynaptic release during mGluR-dependent LTD. *EMBO J.* 30, 165–180. doi: 10.1038/emboj.2010.286

Yang, J., and Zhang, Y. (2015). I-TASSER server: new development for protein structure and function predictions. *Nucleic Acids Res.* 43, W174–181. doi: 10.1093/nar/gkv342

Yoshino, M., Sawada, S., Yamamoto, C., and Kamiya, H. (1996). A metabotropic glutamate receptor agonist DCG-IV suppresses synaptic transmission at mossy fiber pathway of the guinea pig hippocampus. *Neurosci. Lett.* 207, 70–72. doi: 10.1016/0304-3940(96)12486-1

Yu, L. M., Polygalov, D., Wintzer, M. E., Chiang, M. C., and Mchugh, T. J. (2016). CA3 synaptic silencing attenuates kainic acid-induced seizures and hippocampal network oscillations. *eNeuro* 3:ENEURO.0003-16.2016. doi: 10.1523/ENEURO.0003-16.2016

Yuzaki, M. (2018). Two classes of secreted synaptic organizers in the central nervous system. *Annu. Rev. Physiol.* 80, 243–262. doi: 10.1146/annurev-physiol-021317-121322

Zhang, C., Atasoy, D., Arac, D., Yang, X., Fucillo, M. V., Robison, A. J., et al. (2010). Neurexins physically and functionally interact with GABA(A) receptors. *Neuron* 66, 403–416. doi: 10.1016/j.neuron.2010.04.008

Zhang, Y. (2008). I-TASSER server for protein 3D structure prediction. *BMC Bioinformatics* 9:40. doi: 10.1186/1471-2105-9-40

Zhou, Y., Kaiser, T., Monteiro, P., Zhang, X., van Der Goes, M. S., Wang, D., et al. (2016). Mice with Shank3 mutations associated with ASD and schizophrenia display both shared and distinct defects. *Neuron* 89, 147–162. doi: 10.1016/j.neuron.2015.11.023

Zhuo, M. (2017). Cortical kainate receptors and behavioral anxiety. *Mol. Brain* 10:16. doi: 10.1186/s13041-017-0297-8

Conflict of Interest: The authors declare that the research was conducted in the absence of any commercial or financial relationships that could be construed as a potential conflict of interest.

frontiers in Synaptic Neuroscience

ORIGINAL RESEARCH
published: 05 February 2021
doi: 10.3389/fnsyn.2020.581714

Cyfip1 Regulates SynGAP1 at Hippocampal Synapses

*Abhishek Sahasrabudhe[1], Fatema Begum[1], Christopher A. Guevara[1,2], Chenel Morrison[1], Kuangfu Hsiao[1†], Nebojsa Kezunovic[1], Ozlem Bozdagi-Gunal[3] and Deanna L. Benson[1]**

[1] Icahn School of Medicine at Mount Sinai, Nash Family Department of Neuroscience, Friedman Brain Institute, New York, NY, United States, [2] Graduate School of Biomedical Sciences, New York, NY, United States, [3] Department of Psychiatry, Rutgers New Jersey Medical School, Newark, NJ, United States

In humans, copy number variations in *CYFIP1* appear to have sweeping physiological and structural consequences in the brain, either producing or altering the severity of intellectual disability, autism, and schizophrenia. Independently, *SynGAP1* haploinsufficiency produces intellectual disability and, frequently, autism. Cyfip1 inhibits protein translation and promotes actin polymerization, and SynGAP1 is a synaptically localized Ras/Rap GAP. While these proteins are clearly distinct, studies investigating their functions in mice have shown that each regulates the maturation of synapses in the hippocampus and haploinsufficiency for either produces an exaggerated form of mGluR-dependent long-term depression, suggesting that some signaling pathways converge. In this study, we examined how *Cyfip1* haploinsufficiency impacts SynGAP1 levels and localization, as well as potential sites for mechanistic interaction in mouse hippocampus. The data show that synaptic, but not total, levels of SynGAP1 in *Cyfip1*$^{+/-}$ mice were abnormally low during early postnatal development and in adults. This may be in response to a shift in the balance of kinases that activate SynGAP1 as levels of Cdk5 were reduced and those of activated CaMKII were maintained in *Cyfip1*$^{+/-}$ mice compared to wild-type mice. Alternatively, this could reflect altered actin dynamics as Rac1 activity in *Cyfip1*$^{+/-}$ hippocampus was boosted significantly compared to wild-type mice, and levels of synaptic F-actin were generally enhanced due in part to an increase in the activity of the WAVE regulatory complex. Decreased synaptic SynGAP1 coupled with a CaMKII-mediated bias toward Rap1 inactivation at synapses is also consistent with increased levels of synaptic GluA2, increased AMPA receptor-mediated responses to stimulation, and increased levels of synaptic mGluR1/5 compared to wild-type mice. Collectively, our data suggest that Cyfip1 regulates SynGAP1 and the two proteins work coordinately at synapses to appropriately direct actin polymerization and GAP activity.

Keywords: CYFIP1, SynGAP, AMPA receptors, mGluR, PP2A, Rac

OPEN ACCESS

Edited by:
Lucas Pozzo-Miller, University of Alabama at Birmingham, United States

Reviewed by:
Christine Gall, University of California, Irvine, United States
Cecilia Beatriz Conde, Medical Research Institute Mercedes and Martín Ferreyra (INIMEC), Argentina
Zhengping Jia, Hospital for Sick Children, Canada

***Correspondence:**
Deanna L. Benson
deanna.benson@mssm.edu

†Present address:
Kuangfu Hsiao, Rockefeller University, New York, NY, United States

Received: *09 July 2020*
Accepted: *23 December 2020*
Published: *05 February 2021*

Citation:
Sahasrabudhe A, Begum F, Guevara CA, Morrison C, Hsiao K, Kezunovic N, Bozdagi-Gunal O and Benson DL (2021) Cyfip1 Regulates SynGAP1 at Hippocampal Synapses. Front. Synaptic Neurosci. 12:581714. doi: 10.3389/fnsyn.2020.581714

INTRODUCTION

Appropriate levels and regulation of Cyfip1 are important for brain development and function. In humans, either increases or decreases in *CYFIP1* gene dosage are risk factors for intellectual disability, autism, and schizophrenia (Chai et al., 2003; Kirov et al., 2009; van der Zwaag et al., 2010; Leblond et al., 2012; De Rubeis et al., 2014; Kushima et al., 2018), and deletions in chromosome 15

that include *CYFIP1* are associated with increased symptom severity in Prader–Willi and Angelman syndromes (Chai et al., 2003; Butler et al., 2004; Bittel et al., 2006; Sahoo et al., 2006). In rodents, *Cyfip1* manipulation has strong anatomical, cellular, and physiological consequences that overlap mechanistically with cell signaling pathways employed by other genes relevant to intellectual disability, autism, and schizophrenia (Bozdagi et al., 2012; Dominguez-Iturza et al., 2019; Fricano-Kugler et al., 2019; Silva et al., 2019). Such studies suggest that Cyfip1-regulated pathways are part of a nexus of vulnerable developmental events.

An example of this is that mice haploinsufficient for *Cyfip1* show greatly enhanced mGluR1/5-dependent long-term depression (LTD) in the hippocampus that is independent of the usual requirement for protein synthesis (Bozdagi et al., 2012). This phenomenon is strikingly similar to what is observed in mice lacking fragile X mental retardation protein (FMRP; Huber et al., 2002), and the shared dysregulated protein synthesis is consistent with data showing that Cyfip1 and FMRP can bind to one another and act together to repress protein translation (Schenck et al., 2001; Napoli et al., 2008). Interestingly, reduced levels of SynGAP1, a synaptic Ras/Rap GTPase activating protein (Chen et al., 1998; Kim et al., 1998) in humans, can cause a syndromic form of intellectual disability (Holder et al., 1993; Chen et al., 1998; Kim et al., 1998) and also produce enhanced mGluR-dependent, protein synthesis independent LTD in mouse hippocampus (Barnes et al., 2015). The mechanisms by which Cyfip1, FMRP, or SynGAP modifies mGluR signaling are not fully understood, but emerging themes of dysregulated protein synthesis and ERK signaling support the general idea that there are shared, vulnerable pathways (Schenck et al., 2003; Rumbaugh et al., 2006; Carlisle et al., 2008; De Rubeis et al., 2013; Zhao et al., 2013; Pathania et al., 2014; Barnes et al., 2015; Hsiao et al., 2016; Paul et al., 2019). Whether or how SynGAP and Cyfip1 regulatory pathways are related has not been investigated.

In addition to pathways regulating protein synthesis and signaling, SynGAP1 and Cyfip1 may also share pathways regulating F-actin polymerization. Actin cytoskeleton gives dendritic spines their characteristic shape and in excitatory neurons plays a critical role anchoring AMPA receptors (AMPARs) at synapses (Allison et al., 1998; Zhang and Benson, 2000). When Cyfip1 levels are reduced in neurons during development, presynaptic vesicle release probability and terminal size are increased, inhibitory synaptic activity is increased, and postsynaptic dendritic spines fail to develop properly, remaining thin and immature in appearance (De Rubeis et al., 2013; Pathania et al., 2014; Hsiao et al., 2016; Davenport et al., 2019). These actions at synapses are mediated largely by Cyfip1's participation in the WAVE regulatory complex (WRC), which promotes the generation of branched actin filaments in response to Rac activation and binding (Kunda et al., 2003; Schenck et al., 2003; Steffen et al., 2004; Abekhoukh et al., 2017). Significantly, reduced levels of SynGAP1 enhance Rac activation and have been associated with an increase in dendritic spine size (Vazquez et al., 2004; Carlisle et al., 2008; Clement et al., 2012).

Based on the idea that the actions of Cyfip1 would have mechanistic overlap with those of SynGAP1, we examined how reduced levels of Cyfip1 impacted key measures of synapse function and regulation that are also relevant to SynGAP1. The data show that Cyfip1 regulates the localization and anchoring of SynGAP1, shifting the balance of signaling pathways in a manner that alters baseline levels of AMPAR subunits and mGluR1s in the hippocampus. These data illustrate how modest changes in the level of a single protein can be amplified at synapses.

RESULTS

SynGAP Levels Are Abnormally Low in Synaptosome Fractions From *Cyfip1*$^{+/-}$ Mice

In hippocampal glutamatergic terminals of Cyfip1 haploinsufficient (*Cyfip1*$^{+/-}$) mice, presynaptic vesicle size and release probability are increased during development, but the effect is transient and recovers by postnatal day 21 (P21). At P21 and later, amplitudes of excitatory currents appear normal, but there is an increased density of thin dendritic spines, and activity-dependent AMPAR recycling is disrupted (De Rubeis et al., 2013; Pathania et al., 2014; Hsiao et al., 2016). These data suggest that there may be abnormalities in the protein scaffold supporting the structure of synapses in *Cyfip1*$^{+/-}$ mice. To examine this, we compared the distribution and levels of canonical pre- and post-synaptic proteins (synaptophysin and PSD95, respectively) and SynGAP1, which is enriched postsynaptically, in total homogenates and synaptosome fractions prepared from *Wt* and *Cyfip1*$^{+/-}$ mice at two ages, P10 and P60. At P10, most synapses are nascent, there are few dendritic spines, and synaptosome fractions contain growth cones, as well as synapses. The data from P10 mice show that the accumulation of all three proteins in synaptosomal fractions is reduced in *Cyfip1*$^{+/-}$ fractions compared with *Wt* (**Figures 1A,B**), whereas levels in total homogenates are similar between genotypes. On its surface, these findings suggest that there may be fewer synapses in *Cyfip1*$^{+/-}$ hippocampus, but this is unlikely based on previous experiments, which showed that at this age, the density of immunolabeled presynaptic terminal puncta in tissue sections from hippocampal CA1 was similar in *Cyfip1*$^{+/-}$ and *Wt*, and that miniature excitatory postsynaptic current (mEPSC) frequency in CA1 stratum radiatum was actually increased in *Cyfip1*$^{+/-}$ mice at P10 compared with *Wt* (Hsiao et al., 2016). Thus, reduced levels of pre- and post-synaptic proteins in synaptic fractions from *Cyfip1*$^{+/-}$ mice probably reflect differences in protein–protein or protein–cytoskeletal interactions that impact how proteins separate into particular biochemical fractions.

At P60, the distribution of synaptophysin and PSD95 in both total homogenates and synaptosome fractions is similar between *Cyfip1*$^{+/-}$ and *Wt* mice. Levels of SynGAP1 in total homogenates are also similar between *Cyfip1*$^{+/-}$ and *Wt*, but SynGAP1 levels in *Cyfip1*$^{+/-}$ synaptosome fractions remain abnormally low and are similar to what is observed at P10 (**Figures 1C,D**).

Because Cyfip1 can regulate local protein synthesis as part of a complex with FMRP (Napoli et al., 2008), we used translating ribosome affinity purification (TRAP) to address whether SynGAP1 translation was suppressed in *Cyfip1*$^{+/-}$

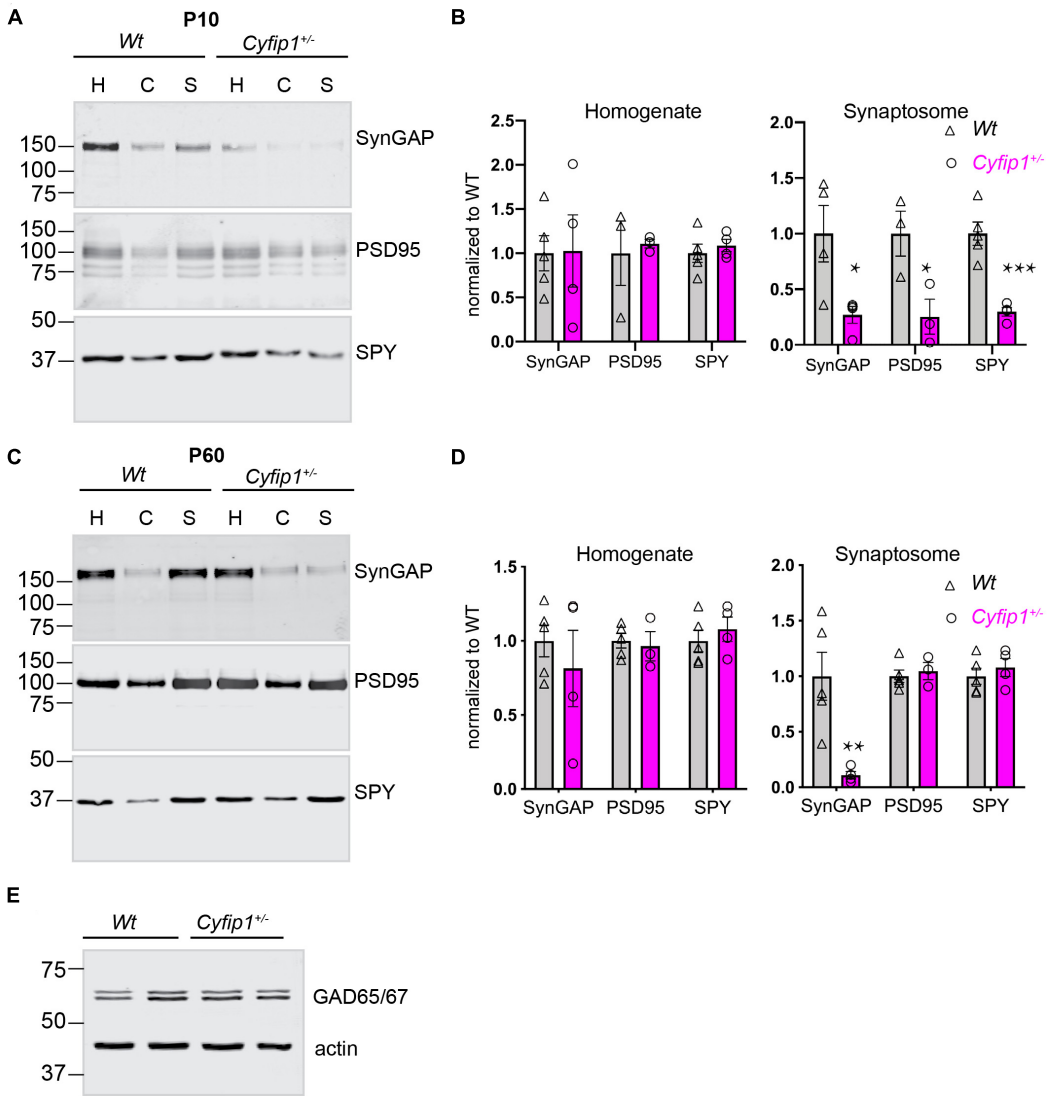

FIGURE 1 | Compositional differences in developing and mature synaptic fractions from *Cyfip1*$^{+/-}$ mice. P10 **(A)** and P60 **(C)** hippocampi fractionated on 10% gels, 25 μg per lane and blotted for the antibodies indicated. H, homogenate; C, cytoplasmic fraction; S, synaptosome fraction. Mean intensities are shown at the right in **(B)** (P10) and **(D)** (P60). *$p \leq 0.05$; **$p = 0.014$; ***$p = 0.008$; unpaired *t*-tests with Welch's correction ($n = 5$ *Wt* and 4 Cyfip1 except for P60 PSD95 where $n = 3$ Cyfip1). Levels of GAD65/67 in hippocampal total lysates (statistics in the text) **(E)**.

mice. However, on ribosomes purified from CA1, there was no significant decrease in levels of SynGAP1 transcripts in *Cyfip1*$^{+/-}$ compared with *Wt* mice (log fold change = −0.067, $p = 0.78$, $n = 3$ *Wt* and 4 *Cyfip1*$^{+/-}$ mice). As these data are consistent with the absence of SynGAP1 regulation in CA1 from *Fmr1*$^{-/y}$ mice, assessed either by TRAP (log fold change = −0.075, $p = 0.61$, $n = 3$ *Wt* and 3 *Fmr1*$^{-/y}$) (Thomson et al., 2017) or by RiboTag (log fold change = −0.15, $p = 0.45$, $n = 6$ *Wt* and 6 *Fmr1*$^{-/y}$) (Ceolin et al., 2017), it is unlikely that Cyfip1 and FMRP repress SynGAP1 translation.

The maturation of GABAergic synapses has been shown to be altered in the neurons expressing increased levels of Cyfip1 (Davenport et al., 2019). Based on this, we compared levels of GAD65/67 by Western blot in *Cyfip1*$^{+/-}$ and *Wt* mice, but we observed no differences in levels (**Figure 1E**; GAD/actin; Mann–Whitney test, $p = 0.8$), similar to what has been reported for Gephyrin in mice having a conditional deletion of Cyfip1 (Davenport et al., 2019).

SynGAP Puncta Are Reduced at PSDs *in situ*

Biochemical data support that levels of SynGAP1 associated with postsynaptic densities (PSDs)s are tightly regulated (Gamache et al., 2020; Zhang et al., 2020). To confirm that the decreased synaptosomal levels of SynGAP1 reflect decreased association with PSDs, we determined the percentage of immunolabeled SynGAP1 puncta that were associated with putative postsynaptic

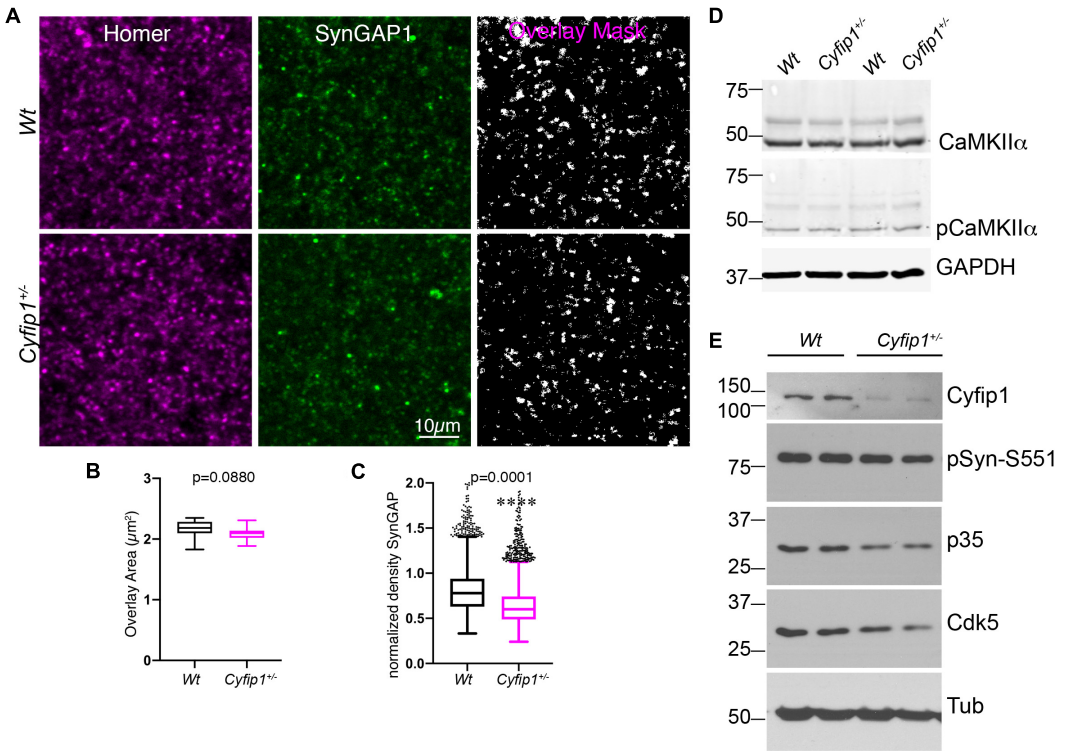

FIGURE 2 | Reduced synaptic SynGAP and Cdk5 activity. Area CA1 in *Wt* and *Cyfip1*$^{+/-}$ mice was imaged at high magnification in sections immunolabeled for SynGAP1 [green; **(A)**] and Homer1b/c [red; **(A)**], analyzed using ImageJ [overlay mask in panel **(A)**]. Box plots show the mean area of overlap **(B)** and the integrated intensity of SynGAP puncta **(C)** in *Wt* and *Cyfip1*$^{+/-}$ CA1. Data were compared using unpaired *t*-test, $p = 0.0880$ **(B)** and $p = 0.0001$ **(C)**. **(D)** Western blot for total and phosphorylated CaMKIIα (comparison values are in the text). **(E)** Western blots for Cdk5, its activator, p35, and a substrate, p-Synapsin-Ser 551 in *Wt* and *Cyfip1*$^{+/-}$ mutant mouse hippocampi (comparison values are in the text).

sites identified by Homer (a pan-glutamatergic PSD marker) in tissue sections from CA1 stratum radiatum. In high magnification confocal images acquired from the hippocampus of *Wt* or *Cyfip1*$^{+/-}$ mice, we applied a multiplication-based analysis strategy in ImageJ to compare Homer/SynGAP1 overlapping puncta (**Figure 2A**). For sites having both labels, the extent of overlap was similar between the two genotypes (**Figure 2B**), but consistent with the Western blot data, SynGAP1 intensity at sites delineated by Homer was reduced significantly in *Cyfip1*$^{+/-}$ mutants compared with *Wt* (**Figure 2C**). *Cyfip1*$^{+/-}$ and *Wt* hippocampi had similar densities of Homer clusters, supporting equal densities of postsynaptic structures, as expected (*t*-test, $p = 0.9257$, $n = 3$). The overall density of SynGAP1 puncta did not differ between genotypes either (*t*-test, $p = 0.2634$, $n = 3$). These data support reduced SynGAP1 anchoring at synapses in *Cyfip1*$^{+/-}$ mice.

Cyfip1 Haploinsufficiency Decreases Cdk5 Activity

Mechanisms supporting SynGAP1 recruitment and retention are differentially modulated downstream of CaMKII- or Cdk5-mediated phosphorylation (Walkup et al., 2015). Based on this, we asked whether either kinase showed altered activation in *Cyfip1*$^{+/-}$ mice. In Western blots, the data show no differences between genotypes in levels of total and phosphorylated (activated) CaMKIIα (**Figure 2D**; pCKIIα/totCKIIα; *t*-test, $p = 0.2186$). In contrast, total levels of Cdk5, its activator p35, and Synapsin I phosphorylation at S551, a Cdk5 site (Matsubara et al., 1996), were consistently reduced in *Cyfip1*$^{+/-}$ mice compared with *Wt* (**Figure 2E**; Cdk5; *t*-tests, $p = 0.04$; p35, $p = 0.008$; pSyn, $p = 0.03$; Cyfip1, $p = 0.0003$). Based on previous work assessing the impact of SynGAP1 phosphorylation on its GAP activity (Walkup et al., 2015), these data suggest that with decreased levels of Cyfip1, SynGAP1 activity would be biased toward Rap.

Glutamatergic Activity and GluA2 Levels Are Increased in *Cyfip1*$^{+/-}$ Mice

Our data and those of others support that spontaneous EPSC frequency and amplitude are similar in adult *Cyfip1*$^{+/-}$ and *Wt* mice (Hsiao et al., 2016; Davenport et al., 2019). However, decreased levels of SynGAP or reduced Cdk5 activity would be expected to enhance AMPA responses (Kim et al., 2003; Walkup et al., 2015; Jeyabalan and Clement, 2016). Whole cell recordings of CA1 neurons in hippocampal slices were used to assess AMPAR-mediated currents in response to a range of stimulation intensities. The data show that amplitudes of AMPAR-mediated responses were consistently greater in *Cyfip1*$^{+/-}$ relative to *Wt* neurons over a range of depolarizing

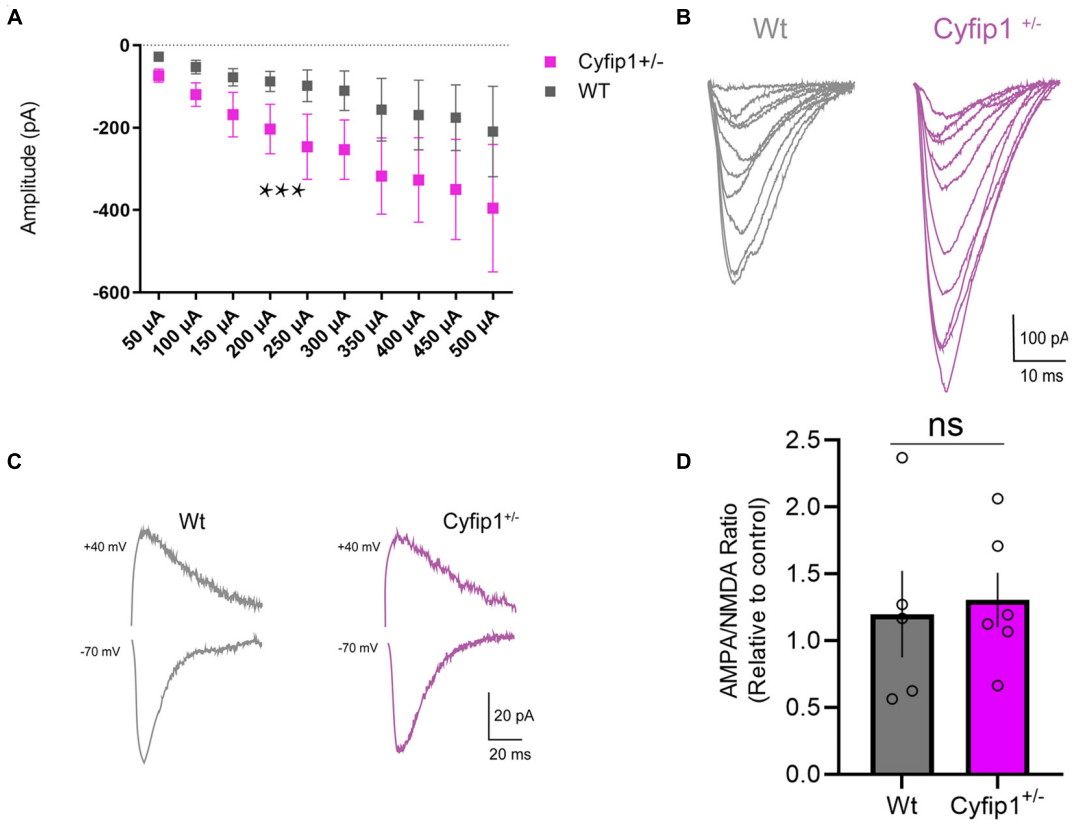

FIGURE 3 | AMPA receptor regulation in *Cyfip1*$^{+/-}$ mice. Whole cell recordings **(A)** show increased AMPA receptor responses in CA1 in response to Schaeffer collateral stimulation (slope *Wt* = 0.327; slope *Cyfip1*$^{+/-}$ = 0.683; p = 0.0003, mixed effects analysis, n = 4 each). Individual traces **(B)** from the data shown in **(A)**. Representative traces of AMPA and NMDA currents **(C)** from *Wt* and *Cyfip1*$^{+/-}$ mice. Quantification of AMPA:NMDA ratios **(D)** shows no significant differences between the two genotypes. Groups were compared using unpaired *t*-test, p = 0.7832.

current steps (**Figures 3A,B**). However, the increase in AMPAR responses did not translate into increased AMPA:NMDA ratios. When we recorded evoked currents at −70 and +40 mV (**Figure 3C**), there was no difference between *Cyfip1*$^{+/-}$ and *Wt* mice in AMPA:NMDA ratios (**Figure 3D**).

We next asked whether the change in AMPA responses reflected increased levels of particular AMPAR subunits. TRAP data showed no significant differences in levels of any of the mRNA transcripts encoding AMPAR (*Gria1-4*) in *Cyfip1*$^{+/-}$ compared with *Wt* mice (log fold change range, −0.017 to −0.24, p range, 0.17–0.92, n = 3 *Wt* and 4 *Cyfip1*$^{+/-}$ mice). Western blots of hippocampal tissue lysates also showed no obvious differences in GluA1 or GluA2 levels between *Wt* and *Cyfip1*$^{+/-}$ mutants (**Figure 4A**). However, changes in regional or synaptic distribution could be masked in whole hippocampal lysates. To address this possibility, hippocampal sections were labeled for Homer, GluA1 or GluA2, and phalloidin to label F-actin, and then using Homer1 puncta to identify synaptic regions, labeling intensity was assessed at high magnification in regions sampled from CA1 and CA3 stratum radiatum, dentate gyrus molecular layer, and stratum lucidum (**Figures 4B–D**). The data show that GluA1 levels were consistently lower in *Cyfip1*$^{+/-}$ than in *Wt* mice, and that conversely, GluA2 levels were increased (**Figures 4E,F**). F-actin levels were unchanged in CA3 and SLM, but were significantly elevated in CA1, CA2, and dentate gyrus (**Figure 4G**). The data suggest that levels of Cyfip1 regulate GluA subunit composition at synapses.

Synaptic Levels of mGluR1/5 Are Enriched in CA Fields

Since mGluR5-mediated function is dysregulated at Schaeffer collateral synapses in mice haploinsufficient for either *Cyfip1* or *SynGAP1* (Bozdagi et al., 2012; Barnes et al., 2015), we asked whether spatial relationships between immunolabeled mGluR1/5 and Homer, its PSD binding partner, were different in *Cyfip1*$^{+/-}$ mice. Using an approach similar to that for GluAs, Homer puncta were used to define synaptic regions of interest in which Homer and mGluR1/5 labeling intensity were assessed. The intensity of mGluR1/5 within Homer domains increased significantly in CA1, CA2, and CA3, but there were no changes observed in SLM (**Figure 5**). These data suggest that enhanced levels of synaptic mGluR1/5 may contribute to the exaggerated mGluR-dependent LTD observed in *Cyfip1*$^{+/-}$ mice.

There are a variety of potential sources for increasing synaptic actin polymerization. Based on previous work in the laboratory, we used an ELISA-based activity assay to measure Rac1 activity in

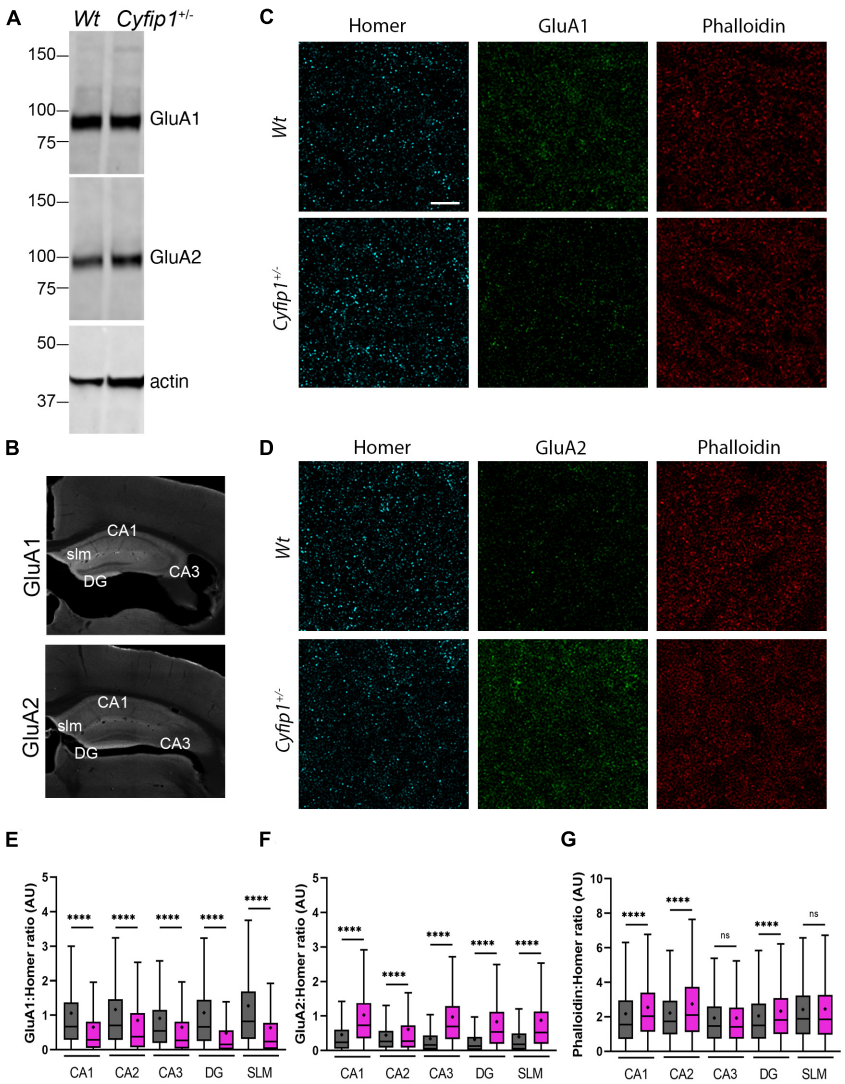

FIGURE 4 | AMPA receptor and F-actin regulation in *Cyfip1*$^{+/-}$ mice. Western blot **(A)** suggests that GluA1 and GluA2 levels are similar in *Wt* and *Cyfip1*$^{+/-}$ hippocampal lysates. Representative low magnification images **(B)** of GluA1 and GluA2 immunostained hippocampal sections highlighting the regions in which dendritic zones were evaluated quantitatively. Confocal images **(C,D)** of synaptic puncta immunostaining for Homer1 (cyan), GluA1, GluA2 (green), or Phalloidin (red). Homer puncta were used to identify the potential synapses and were used as masks to measure grayscale intensities for Homer, GluA1, GluA2, and Phalloidin. Homer intensities were used to normalize the corresponding GluA1, GluA2, and Phalloidin intensities **(E–G)**. Groups were compared using one-way ANOVA (Kruskal–Wallis test), followed by Dunn's multiple comparison, $^{****}p < 0.0001$ (scale bar = 10 μm).

synaptic fractions isolated from *Wt* and *Cyfip1*$^{+/-}$ hippocampi. The data show that Rac1 activity was increased significantly in the *Cyfip1*$^{+/-}$ fractions compared with *Wt* (**Figure 6A**). This occurred in the absence of any noticeable change in total levels of Rac1 in immunoblots (**Figure 6B**, *t*-test; $p = 56$; $n \geq 4$). Active Rac can promote actin assembly by a pathway that decreases cofilin activity, but we observed no significant differences in levels of cofilin phosphorylation (**Figure 6C**; Mann–Whitney test, pCof/totCof; $p = 0.19$; $n \geq 4$). Alternatively, active Rac also promotes WRC activity. As an essential subunit, decreased Cyfip1 levels serve to reduce levels of WRC, so we asked whether the remaining WRC is more active. Since WAVE1 activity is negatively regulated by phosphorylation (Kim et al., 2006), we first confirmed that we could detect phosphorylated WAVE1 by Western blot. A brief treatment with Cdk5 inhibitor, roscovitine, facilitated WAVE1 mobility and yielded a single, lower MW band. In contrast, treatment with calyculin A, a PP2A inhibitor, produced a super shift in WAVE1 bands (**Figure 6D**). In lysates from *Cyfip1*$^{+/-}$ hippocampus, high MW bands were reduced compared with *Wt*, consistent with decreased WAVE1 phosphorylation (**Figures 6E,F**). We did not detect an increase in PP2A isoforms in our TRAP data, but in previous work, the mRNA encoding the catalytic subunit of the Ser/Thr phosphatase 2A (PP2Acβ) was identified as a regulatory target of FMRP

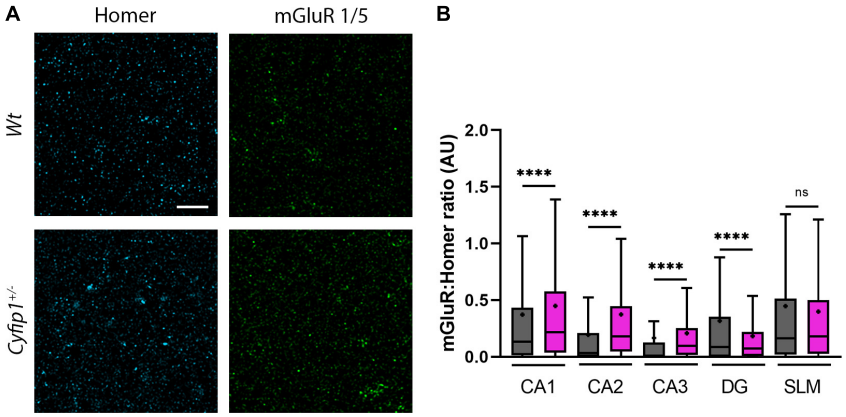

FIGURE 5 | mGluR and F-actin regulation in *Cyfip1*$^{+/-}$ mice. Confocal images **(A)** of synaptic puncta immunostaining for Homer1 (cyan) and mGluR1/5 (green). Homer puncta were used to identify the potential synapses and were used as masks to measure grayscale intensities for Homer and mGluR1/5. Homer intensities were used to normalize the corresponding mGluR intensities **(B)**. Groups were compared using one-way ANOVA (Kruskal–Wallis test), followed by Dunn's multiple comparison, ****$p < 0.0001$ (scale bar = 10 μm).

and Cyfip1 (Castets et al., 2005; Darnell et al., 2011). Based on this, we probed for PP2Acα/β subunits by Western blot. The data show a negative correlation between levels of PP2Ac and levels of WAVE1 phosphorylation (**Figures 6E,F**). We further examined this difference by assessing levels of phosphatase activity directly using a p-nitrophenylphosphate – a pan phosphatase chromogenic substrate. The data show increased phosphatase activity in *Cyfip1*$^{+/-}$ hippocampus compared with *Wt* (**Figures 6G,H**). Collectively, these data support that F-actin levels may be increased in part by the compensatory activation of WRC.

DISCUSSION

Recent research shows that SynGAP1 homo-trimers *in vitro* can bind multiple copies of PSD95 provoking a phase separation of the complex (Zeng et al., 2016). While implications of such interactions are not understood, the data suggest that PSDs lacking SynGAP1 would have an altered organization. To a similar end, but by a different mechanism, a separate study has shown data suggesting that decreased levels of synaptic SynGAP1 can open "slots" in PSD95, permitting interactions with alternate partners and promoting a change in PSD composition (Walkup et al., 2016; Lautz et al., 2018). The data presented here support the idea that synapse composition is altered in the hippocampus of *Cyfip1*$^{+/-}$ mice by having reduced levels of SynGAP1 and GluA1 at synapses and enhanced levels of mGluR1/5, GluA2, and F-actin compared with *Wt*. Collectively, the data suggest that changes in composition are driven in part by a shift in the balance of SynGAP1's location and its activity toward Ras and Rap at synaptic and non-synaptic sites (**Figure 7**).

Our data support a model in which Cyfip1 plays a role anchoring SynGAP1 to the PSD, since synaptic, but not total, levels of SynGAP1 were diminished in *Cyfip1*$^{+/-}$ mice. The loss of SynGAP1 from synaptosomal fractions is stark and nearly complete (**Figure 1**), and while this could be due to a deficiency in either the targeting or anchoring of SynGAP1, the more modestly, but still significantly, reduced overlap between SynGAP1 and Homer seen in intact immunolabeled preparations (**Figure 2**) better supports the idea that anchoring or short range interactions are altered. This difference in SynGAP1 localization is likely to be mediated by changes in the composition of actin cytoskeleton. Our data show increased levels of Homer-associated F-actin in CA1, CA2, and dentate gyrus (**Figure 4**), and that this may reflect a compensatory increase in WRC activity (**Figure 6**). Levels of active Rac, the upstream activator for WRC, were increased and are consistent with previous work showing that Rac inhibition rescued deficits in synapse function in *Cyfip1*$^{+/-}$ mice (Hsiao et al., 2016) and phosphorylation of WAVE1, which negatively regulates its activity (Kim et al., 2006), was decreased. At the same time, there was no change in cofilin phosphorylation (and inactivation), which downstream of Rac activation can enhance F-actin polymerization (Yang et al., 1998; Chen et al., 2010). No matter the pathway, however, any increase in F-actin appears to be insufficient to generate normal synapse structure as it fails to corral or support appropriate levels of SynGAP1 trafficking and anchoring (**Figure 1**), and previous work suggests that it also fails to support the generation of normal spine shape (De Rubeis et al., 2013; Pathania et al., 2014).

AMPA receptor levels typically scale with spine size (Kopec et al., 2007), but this coordinated regulation appears to be altered when Cyfip1 levels are reduced. Spine size is reduced in *Cyfip1*$^{+/-}$ neurons (De Rubeis et al., 2013; Pathania et al., 2014), and our data show that CA1 synapses have increased AMPAR responses. The increased AMPA current may reflect enhanced levels of GluA2, but GluA1 levels are reduced, and AMPA/NMDA ratios remain similar to *Wt* neurons (**Figures 3**, **4**). Changes in AMPAR levels and composition could lie downstream of decreased levels of Cdk5 activity (**Figure 6**). The decreased Cdk5 and p35 levels that we observe in *Cyfip1*$^{+/-}$

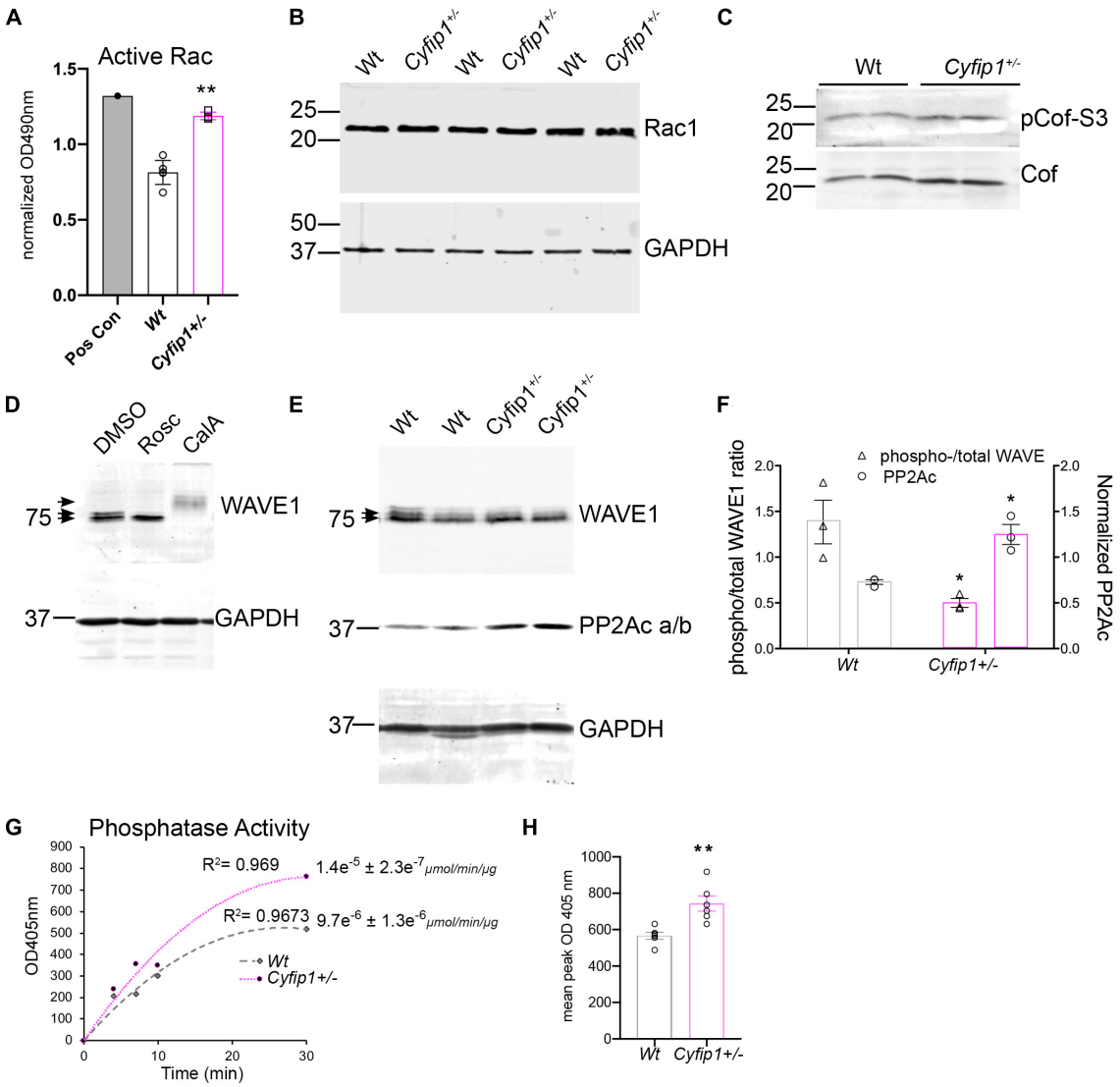

FIGURE 6 | Cyfip1 haploinsufficiency increases Rac1 activity. **(A)** Bar graph shows the results from ELISA for Rac activity (unpaired *t*-test, $^{**}p = 0.002$; $n = 4$ *Cyfip1*$^{+/-}$ and 6 *Wt*). **(B)** Western blot shows Rac1 levels in total hippocampal lysates from the same preparations used for the data in (**A**; statistics in the text). **(C)** Western blots for total and phosphorylated cofilin in lysates from the hippocampus (statistics in the text). **(D)** Western blots of WAVE1 from cell lysates in response to treatments indicated. **(E)** Blots of WAVE1 and PP2Ac a/b in hippocampal lysates from *Wt* and *Cyfip1*$^{+/-}$ mice. **(F)** Graph of data in **(E)** showing the ratio of upper "phospho" to total WAVE1 (left *y* axis) and PP2Ac intensity (right *y* axis) (unpaired *t*-tests; pWAVE/WAVE1; $^{*}p = 0.002$; PP2Ac, $^{*}p = 0.04$, $n = 3$ each). **(G)** Phosphatase activity assay and **(H)** mean comparison of max OD at 405 nm, $^{**}p = 0.003$, $n = 6$ each.

hippocampus (**Figure 2**) would be expected to bias any remaining SynGAP activity toward Rap inactivation (Walkup et al., 2015), an action that would be expected to favor GluA2 exocytosis (Huang et al., 2004; Fu et al., 2007). This effect could help to counter the impact of longer and thinner spines, since hippocampal LTD induced by any of a variety of protocols in *Cyfip1*$^{+/-}$ mice is similar to that evoked in *Wt* (Bozdagi et al., 2012). Enhanced GluA2 levels may also generate a favorable state for mGluR-dependent LTD (Waung et al., 2008; Pick et al., 2017).

mGluR-dependent LTD is exaggerated in *Cyfip1*$^{+/-}$ mice, independent of the normal requirement for protein synthesis (Bozdagi et al., 2012), and similar to what is observed in mice lacking FMRP (Huber et al., 2002) or having reduced levels of SynGAP1 (Barnes et al., 2015). This is thought to be in part due to dysregulated protein translation, which appears to be de-repressed in all three mouse models through partially overlapping mechanisms: Cyfip1 and FMRP are binding partners that work together to suppress a fraction of protein translation at mRNA start sites binding FMRP, FMRP additionally prevents mRNA translation by binding to other sites (Schenck et al., 2001; Napoli et al., 2008; Darnell et al., 2011), and FMRP levels are reduced in mice haploinsufficient for SynGAP1 (Darnell et al., 2011; Paul et al., 2019). It has been challenging, however, to draw straight lines between the mRNAs targeted by Cyfip1 and FMRP and

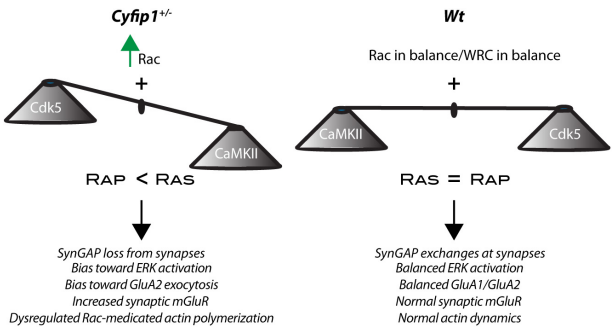

FIGURE 7 | Cyfip1 haploinsufficiency alters the balance of activity. Diagram places the results from this study into a larger framework outlined in the section "Discussion."

functional outcomes observed (Ceolin et al., 2017; Thomson et al., 2017; Das Sharma et al., 2019, this paper), and it is significant that enhanced Ras-ERK1/2 signaling has emerged as a target that is common to *SynGAP1*$^{+/-}$ and *Fmr1*$^{-/y}$ mutant mice (Rumbaugh et al., 2006; Osterweil et al., 2010; Barnes et al., 2015). Our data from *Cyfip1*$^{+/-}$ mice are consistent with this idea in that decreased levels of SynGAP1 at synapses and decreased Cdk5 signaling would be expected to generate a bias toward Ras signaling. This imbalance could also contribute to the increased levels of mGluR1/5 observed at Homer-labeled sites in CA fields, providing an additional source for enhanced mGluR-dependent signaling in *Cyfip1*$^{+/-}$ mice. Increased mGluR levels may also be related to what has been observed in mice lacking FMRP where mGluRs are triton-extractable (Giuffrida et al., 2005) and more mobile than *Wt* mice (Aloisi et al., 2017). Additionally, it is significant that enhanced mGluR5 levels were not observed in SLM in the *Cyfip1*$^{+/-}$ mice, a hippocampal region that does not express SynGAP1 (Porter et al., 2005) and fails to undergo mGluR-dependent LTD (Fitzjohn et al., 2016).

Together our data reveal that Cyfip1 regulates the synaptic expression of AMPARs, SynGAP1 and mGluRs. Reduced levels of Cyfip1 enhance Rac signaling, and downstream of SynGAP1, alter the balance between Ras and Rap signaling, ultimately shifting the range and flexibility of synapse responses (**Figure 7**).

MATERIALS AND METHODS

Mice

Cyfip1 haploinsufficient mice were bred as heterozygotes to generate *Cyfip1*$^{+/-}$ mice and *Wt* littermates. Unless otherwise noted, mice were ∼2 months old and included both males and females. Sex was noted and parsed for analyses, but no differences or even trends toward differences were observed, and males and females were grouped. For biochemical and electrophysiological experiments, mice were deeply anesthetized with isoflurane and then decapitated; brains were removed and dissected. For immunolabeling, mice were deeply anesthetized with ketamine and xylazine, and brains were fixed by transcardial perfusion with 4% paraformaldehyde (PFA) in phosphate buffered saline (PBS), pH 7.3. Brains were removed, postfixed overnight in the same fixative, and then placed in 4% sucrose in PBS. Tissue sections were acquired through the dorsal hippocampus using a freezing microtome at a setting of 30 μ m.

Antibodies

Primary antibodies included: mouse anti-GluA1 (NeuroMAB; 1:10 IHC), rabbit anti-GluA1 (Cell Signaling Technologies; 13185, 1:1,000), mouse anti-GluA2 (NeuroMAB; 1:10 IHC), mouse anti-GluA2 (MAB1189; 1:500), chicken anti-Homer (SySy; 160006, 1:500), mouse anti-SynGAP (Thermo Fisher Scientific; PA1-046, 1:500 IHC, 1:5,000 WB), mouse anti-PSD95 (Thermo Fisher; MA1-045, 1:1,000 WB), rabbit anti-Synaptophysin (PA1-1043, 1:5,000 WB), mouse anti-Cdk5 (Invitrogen; AHZ0492, 1:500), mouse anti-WAVE1 (mAb K91/361; NeuroMab), goat anti-PPA2c (Santa Cruz; sc-6110), rabbit anti-CaMKIIα (Abcam; EP1829Y, 1:1,000), rabbit-anti-p-Synapsin1-Ser 551 (Abcam; Ab32532), rabbit anti-p35 (Cell Signaling; 2680, 1:250), mouse anti-GAPDH (Millipore; MAB374, 1:4,000), and Phalloidin Alexa 647 (Thermo Fisher Scientific; A22287, 1:200). Secondary antibodies included: donkey anti-mouse Alexa 488 (Thermo Fisher Scientific; R37114, 1:200), donkey anti-mouse Dy 488 (Abcam; 96875, 1:500), donkey anti-chicken Alexa 488 (Jackson ImmunoResearch; 703-545-155), and LI-COR (anti-mouse, anti-goat, and anti-rabbit IRDye 680 and 800; 1:10,000).

Immunohistochemistry

Tissue sections were permeabilized with 0.50% Triton X-100 in PBS for 15 min, washed six times for 10 min in PBS, and blocked in 5% normal donkey serum (NDS) for 1 h and 30 min, shaking at room temperature (RT). After removing the NDS blocking buffer, tissue sections were incubated with primary antibodies at 4°C for three nights on a shaker (primary antibodies were diluted in 2% NDS and 0.1% Triton X-100 in PBS). After three nights of incubation, brain sections were washed in PBS, six times for 10 min at RT on a shaker. Secondary antibodies were diluted in 2% NDS and 0.1% Triton X-100 in PBS, and incubation of tissue sections included shaking for 1 h at RT, shielded from light. After incubation was completed, six 10-min washes at RT were performed. Next, tissue sections were mounted on Superfrost Plus slides using Vectashield that included approximately 5 ng/ml of DAPI for widefield and with Prolong Diamond (Molecular Probes) for confocal microscope preparations. Slides were sealed using nail polish and dried overnight in the dark.

Image Acquisition and Analysis

To compare receptor distribution and immunolabeling intensity in hippocampal fields, images were captured on a Leica DMi8 widefield microscope at 10× magnification, with an exposure time of 500 ms and no binning. Images were exported, stitched, and analyzed using ImageJ. Using the rectangle tool, five boxes, ∼48 μm^2, were overlaid in the CA1, CA2, CA3, SLM, and DG regions. Mean intensity levels were measured and recorded. To analyze the overall distribution and overlap of SynGAP1 and Homer-labeled puncta, images were captured on a Leica

780 LSM confocal microscope using a 63× 1.4 NA objective. In ImageJ, a mask of the Homer and SynGAP1 puncta was created and multiplied to assess overlap. To assess levels of GluA1, GluA2, mGluR1/5, and F-actin at Homer-labeled sites, labeled sections were imaged on a Leica SP8 STED using a 100× objective (1.5 NA) and deconvolved using Huygens (SVI), and intensity was measured within a region of interest (ROI) defined by Homer1b/c labeling using ImageJ. GluA1, GluA2, and Phalloidin signals were normalized to the respective Homer signals in individual images. Data were exported to Excel, and groups were compared and plotted using Prism (GraphPad).

Western Blot

The hippocampus, cortex, or cortical cells grown in culture were solubilized in ice cold RIPA or Syn-PER (Thermo Fisher Scientific) lysis buffer containing protease (Roche) and phosphatase (Life Technologies) inhibitors as detailed previously (Matikainen-Ankney et al., 2016). Then, 25–75 μg of each protein were loaded per lane on 8–10% SDS gels, blotted, labeled with antibodies indicated, and visualized using LI-COR Odyssey. Band intensities were measured using the Gel Analyzer tool in ImageJ. GluA1 and GluA2 Western blots were carried out with the assistance of Shakti BioResearch (Woodbridge, CT, United States).

Electrophysiology

Whole cell recordings were carried out in acute, coronal hippocampal slices (350 μm) from 4 Wt and 4 *Cyfip1*$^{+/-}$ adult (∼P70) male mice. Slices were cut on a Leica VT1000 vibratome in ice cold aCSF (in mM: 233.7 sucrose, 26 $NaHCO_3$, 3 KCl, 8 $MgCl_2$, 0.5 $CaCl_2$, 20 glucose, and 0.4 ascorbic acid) after which they were allowed to equilibrate in oxygenated recording aCSF (in mM: 117 NaCl, 4.7 KCl, 1.2 $MgSO_4$, 2.5 $CaCl_2$, 1.2 NaH_2PO_4, 24.9 $NaHCO_3$, and 11.5 glucose) for 1 h at RT. The neurons were visualized using an upright epifluorescence microscope (BX50WI; Olympus) with 40× water immersion lens and IR-1000 infrared CCD monochrome video camera (DAGE MTI). Whole cell recordings were performed with glass micropipettes filled with high potassium intracellular solution containing (in mM): 124 K-gluconate, 10 HEPES, 10 phosphocreatine di(tris), 0.2 EGTA, 4 Mg_2ATP, and 0.3 Na_2GTP. Recordings were made at 31°C in an immersion chamber containing gabazine (GBZ, 10 μM) and APV (40 μM). All AMPA responses were recorded in voltage-clamp mode using a MultiClamp 700B amplifier (Molecular Devices). Analog signals were low-pass filtered at 2 kHz and digitized at 5 kHz with the use of a Digidata 1440A. Gigaseal and further access to the intracellular neuronal compartment were achieved in voltage-clamp mode, with the holding potential set at −70 mV. Soon after rupturing the membrane, the intracellular neuronal fluid reached equilibrium with the pipette solution without significant changes in either series resistance or membrane capacitance values. Membrane voltage was kept at −70 mV though all our voltage-clamp experiments. The input–output (I–O) relationships were measured for AMPAR current amplitudes elicited by stimulating currents with increasing intensity (50–500 μA; 5 stimuli per step). Off-line analysis was performed and analyzed with pClamp10 software (Molecular Devices).

To capture AMPA/NMDA ratios, electrode internal solution consisted of (in mM): 120 Cs-methanesulfonate, 10 HEPES, 0.5 EGTA, 8 NaCl, 5 TEA-CL, 4 Mg-ATP, 0.4 NaGTP, and 10 phosphocreatine. All responses were evoked at 0.1 Hz. AMPA/NMDA ratio was calculated as the peak EPSC value at −70 mV, a timepoint where NMDA response is negligible, divided by the peak response at 40 mV 100 ms after current onset, which is the timepoint where the current response is predominantly NMDA current (Arruda-Carvalho and Clem, 2014). Final ratios were normalized relative to *Wt*.

Activity Assays

Rac1 activity was measured in dissected hippocampi (P21) from 6 *Wt* mice and 4 *Cyfip1*$^{+/-}$ mice using a Rac1 G-ELISA activation assay kit (Cytoskeleton) according to the manufacturer's protocol. Absorbance was read at 490 nm using a VICTOR X 4 plate reader (Perkin Elmer). Total levels of Rac1 were examined in samples separated using 15% SDS PAGE, blotted with mouse anti-Rac1 (Cytoskeleton) and rabbit anti-GAPDH (Cell Signaling), and visualized using LICOR. Para-nitrophenylphosphate (pNPP) A phosphatase assay kit (BioAssay Systems) was used to measure phosphatase activity in cortical brain lysates prepared from 2- to 3-weeks-old *Cyfip1*$^{+/-}$ or *Wt* mice (three each) in the absence of phosphatase inhibitors and then mixed with pNPP. Phosphatase activity in the lysates dephosphorylates pNPP and produces para-nitrophenol, which exhibits a strong absorption at 405 nm, which was measured on a plate reader. Activity was calculated according to Lambert–Beer's law as follows: $A = E_{405} \cdot V_{total} / t \cdot \varepsilon \cdot d \cdot m_{enzyme}$). As a control, phosphatases in the sample were neutralized by adding Ser/Thr phosphatase inhibitor cocktail 3 (Sigma; P0044) to the pNPP reaction. To detect WAVE1 phosphorylation, cultured, 4-week-old cortical neurons were treated for 45 min with either roscovitine (50 nM; Sigma), calyculin (25 nM; Calbiochem), or vehicle (DMSO).

TRAP

Three *Wt* and 4 *Cyfip1*$^{+/-}$ male mice were injected with pAAV-FLEX-EGFPL10a and pENN.AAV.CaMKII 0.4.Cre.SV40 in CA1. The site and extent of expression (through about 2/3 of the dorsal hippocampus) were confirmed in pilot studies. The hippocampus was dissected, and the GFP expression was used to pull down ribosomes as described (Heiman et al., 2008). Associated mRNAs were used to generate cDNA. Sequencing and analysis were conducted by GENEWIZ.

Analysis and Statistics

Genotypes were compared using unpaired *t*-test (unless otherwise mentioned) or for multiple comparisons, by using one-way or two-way ANOVA, or a mixed effects model when appropriate. For all multiple comparisons, *post-hoc* tests were used to identify the source/s of differences. Data were compared,

graphed, and plotted using Prism (GraphPad). Numbers and statistical values are provided in the graphs and figure legends, or in the text, when relevant.

DATA AVAILABILITY STATEMENT

The raw data supporting the conclusions of this article will be made available by the authors, without undue reservation.

ETHICS STATEMENT

The animal study was reviewed and approved by Institutional Animal Care and Use Committee, Icahn School of Medicine at Mount Sinai.

AUTHOR CONTRIBUTIONS

AS, KH, OB-G, and DB designed the study. AS, CG, KH, FB, CM, and NK conducted the experiments. AS, CG, KH, FB, CM, and DB analyzed the experiments. AS and DB wrote the manuscript, and all the other authors provided feedback and edits. All authors contributed to the article and approved the submitted version.

FUNDING

National Institute of Mental Health R01 MH103455, T32MH087004 and National Institute of Neurological Disease R01 NS115469.

ACKNOWLEDGMENTS

We would like to acknowledge the technical assistance provided by Frances Williams, Kristen Szabla, and Vivian Jackson. We would like to thank Dr. Anne Schaefer, Dr. Josefa Sullivan, and Dr. Ana Badimon for the TRAP assay and the Microscopy and Advanced Bioimaging Core at Icahn School of Medicine for access to widefield, confocal, and Leica TCS 3× STED microscopes (supported with funding from NIH Shared Instrumentation Grant, FAIN: S10OD021838). We also thank Dr. Kirstie Cummings for helpful advice on electrophysiological analyses.

REFERENCES

Abekhoukh, S., Sahin, H. B., Grossi, M., Zongaro, S., Maurin, T., Madrigal, I., et al. (2017). New insights into the regulatory function of CYFIP1 in the context of WAVE- and FMRP-containing complexes. *Dis. Model. Mech.* 10, 463–474. doi: 10.1242/dmm.025809

Allison, D. W., Gelfand, V. I., Spector, I., and Craig, A. M. (1998). Role of actin in anchoring postsynaptic receptors in cultured hippocampal neurons: differential attachment of NMDA versus AMPA receptors. *J. Neurosci.* 18, 2423–2436. doi: 10.1523/jneurosci.18-07-02423.1998

Aloisi, E., Le Corf, K., Dupuis, J., Zhang, P., Ginger, M., Labrousse, V., et al. (2017). Altered surface mGluR5 dynamics provoke synaptic NMDAR dysfunction and cognitive defects in Fmr1 knockout mice. *Nat. Commun.* 8:1103.

Arruda-Carvalho, M., and Clem, R. L. (2014). Pathway-selective adjustment of prefrontal-amygdala transmission during fear encoding. *J. Neurosci.* 34, 15601–15609. doi: 10.1523/jneurosci.2664-14.2014

Barnes, S. A., Wijetunge, L. S., Jackson, A. D., Katsanevaki, D., Osterweil, E. K., Komiyama, N. H., et al. (2015). Convergence of hippocampal pathophysiology in Syngap+/- and Fmr1-/y Mice. *J. Neurosci.* 35, 15073–15081. doi: 10.1523/jneurosci.1087-15.2015

Bittel, D. C., Kibiryeva, N., and Butler, M. G. (2006). Expression of 4 genes between chromosome 15 breakpoints 1 and 2 and behavioral outcomes in Prader-Willi syndrome. *Pediatrics* 118, e1276–e1283.

Bozdagi, O., Sakurai, T., Dorr, N., Pilorge, M., Takahashi, N., and Buxbaum, J. D. (2012). Haploinsufficiency of Cyfip1 produces fragile X-like phenotypes in mice. *PLoS One* 7:e42422. doi: 10.1371/journal.pone.0042422

Butler, M. G., Bittel, D. C., Kibiryeva, N., Talebizadeh, Z., and Thompson, T. (2004). Behavioral differences among subjects with Prader-Willi syndrome and type I or type II deletion and maternal disomy. *Pediatrics* 113, 565–573. doi: 10.1542/peds.113.3.565

Carlisle, H. J., Manzerra, P., Marcora, E., and Kennedy, M. B. (2008). SynGAP regulates steady-state and activity-dependent phosphorylation of cofilin. *J. Neurosci.* 28, 13673–13683. doi: 10.1523/jneurosci.4695-08.2008

Castets, M., Schaeffer, C., Bechara, E., Schenck, A., Khandjian, E. W., Luche, S., et al. (2005). FMRP interferes with the Rac1 pathway and controls actin cytoskeleton dynamics in murine fibroblasts. *Hum. Mol. Genet.* 14, 835–844. doi: 10.1093/hmg/ddi077

Ceolin, L., Bouquier, N., Vitre-Boubaker, J., Rialle, S., Severac, D., Valjent, E., et al. (2017). Cell type-specific mRNA dysregulation in hippocampal CA1 pyramidal neurons of the fragile X syndrome mouse model. *Front. Mol. Neurosci.* 10:340. doi: 10.3389/fnmol.2017.00340

Chai, J. H., Locke, D. P., Greally, J. M., Knoll, J. H., Ohta, T., Dunai, J., et al. (2003). Identification of four highly conserved genes between breakpoint hotspots BP1 and BP2 of the Prader-Willi/Angelman syndromes deletion region that have undergone evolutionary transposition mediated by flanking duplicons. *Am. J. Hum. Genet.* 73, 898–925. doi: 10.1086/378816

Chen, H. J., Rojas-Soto, M., Oguni, A., and Kennedy, M. B. (1998). A synaptic Ras-GTPase activating protein (p135 SynGAP) inhibited by CaM kinase II. *Neuron* 20, 895–904. doi: 10.1016/s0896-6273(00)80471-7

Chen, L. Y., Rex, C. S., Babayan, A. H., Kramar, E. A., Lynch, G., Gall, C. M., et al. (2010). Physiological activation of synaptic Rac>PAK (p-21 activated kinase) signaling is defective in a mouse model of fragile X syndrome. *J. Neurosci.* 30, 10977–10984. doi: 10.1523/jneurosci.1077-10.2010

Clement, J. P., Aceti, M., Creson, T. K., Ozkan, E. D., Shi, Y., Reish, N. J., et al. (2012). Pathogenic SYNGAP1 mutations impair cognitive development by disrupting maturation of dendritic spine synapses. *Cell* 151, 709–723. doi: 10.1016/j.cell.2012.08.045

Darnell, J. C., Van Driesche, S. J., Zhang, C., Hung, K. Y., Mele, A., Fraser, C. E., et al. (2011). FMRP stalls ribosomal translocation on mRNAs linked to synaptic function and autism. *Cell* 146, 247–261. doi: 10.1016/j.cell.2011.06.013

Das Sharma, S., Metz, J. B., Li, H., Hobson, B. D., Hornstein, N., Sulzer, D., et al. (2019). Widespread alterations in translation elongation in the brain of juvenile Fmr1 knockout mice. *Cell Rep.* 26, 3313.e15–3322.e15.

Davenport, E. C., Szulc, B. R., Drew, J., Taylor, J., Morgan, T., Higgs, N. F., et al. (2019). Autism and schizophrenia-associated CYFIP1 regulates the balance of synaptic excitation and inhibition. *Cell Rep.* 26, 2037.e6–2051.e6.

De Rubeis, S., He, X., Goldberg, A. P., Poultney, C. S., Samocha, K., Cicek, A. E., et al. (2014). Synaptic, transcriptional and chromatin genes disrupted in autism. *Nature* 515, 209–215.

De Rubeis, S., Pasciuto, E., Li, K. W., Fernandez, E., Di Marino, D., Buzzi, A., et al. (2013). CYFIP1 coordinates mRNA translation and cytoskeleton remodeling to ensure proper dendritic spine formation. *Neuron* 79, 1169–1182. doi: 10.1016/j.neuron.2013.06.039

Dominguez-Iturza, N., Lo, A. C., Shah, D., Armendariz, M., Vannelli, A., Mercaldo, V., et al. (2019). The autism- and schizophrenia-associated protein CYFIP1 regulates bilateral brain connectivity and behaviour. *Nat. Commun.* 10: 3454.

Fitzjohn, S., Bashir, Z., and Farrow, P. (2016). Group I mGluR induced LTD of NMDAR-synaptic transmission at the schaffer collateral but not temperoammonic input to CA1. *Curr. Neuropharmacol.* 14, 435–440. doi: 10.2174/1570159x13666150615221502

Fricano-Kugler, C., Gordon, A., Shin, G., Gao, K., Nguyen, J., Berg, J., et al. (2019). CYFIP1 overexpression increases fear response in mice but does not affect social or repetitive behavioral phenotypes. *Mol. Autism* 10:25.

Fu, Z., Lee, S. H., Simonetta, A., Hansen, J., Sheng, M., and Pak, D. T. (2007). Differential roles of Rap1 and Rap2 small GTPases in neurite retraction and synapse elimination in hippocampal spiny neurons. *J. Neurochem.* 100, 118–131. doi: 10.1111/j.1471-4159.2006.04195.x

Gamache, T. R., Araki, Y., and Huganir, R. L. (2020). Twenty years of SynGAP research: from synapses to cognition. *J. Neurosci.* 40, 1596–1605. doi: 10.1523/jneurosci.0420-19.2020

Giuffrida, R., Musumeci, S., D'antoni, S., Bonaccorso, C. M., Giuffrida-Stella, A. M., Oostra, B. A., et al. (2005). A reduced number of metabotropic glutamate subtype 5 receptors are associated with constitutive homer proteins in a mouse model of fragile X syndrome. *J. Neurosci.* 25, 8908–8916. doi: 10.1523/jneurosci.0932-05.2005

Heiman, M., Schaefer, A., Gong, S., Peterson, J. D., Day, M., Ramsey, K. E., et al. (2008). A translational profiling approach for the molecular characterization of CNS cell types. *Cell* 135, 738–748. doi: 10.1016/j.cell.2008.10.028

Holder, J. L. Jr., Hamdan, F. F., and Michaud, J. L. (1993). "SYNGAP1-related intellectual disability," in *GeneReviews((R))*, eds M. P. Adam, H. H. Ardinger, R. A. Pagon, S. E. Wallace, L. J. H. Bean, K. Stephens, et al. (Seattle,WA: University of Washington).

Hsiao, K., Harony-Nicolas, H., Buxbaum, J. D., Bozdagi-Gunal, O., and Benson, D. L. (2016). Cyfip1 regulates presynaptic activity during development. *J. Neurosci.* 36, 1564–1576. doi: 10.1523/jneurosci.0511-15.2016

Huang, C. C., You, J. L., Wu, M. Y., and Hsu, K. S. (2004). Rap1-induced p38 mitogen-activated protein kinase activation facilitates AMPA receptor trafficking via the GDI.R*ab*5 complex. Potential role in (S)-3,5-dihydroxyphenylglycene-induced long term depression. *J. Biol. Chem.* 279, 12286–12292. doi: 10.1074/jbc.m312868200

Huber, K. M., Gallagher, S. M., Warren, S. T., and Bear, M. F. (2002). Altered synaptic plasticity in a mouse model of fragile X mental retardation. *Proc. Natl. Acad. Sci. U.S.A.* 99, 7746–7750. doi: 10.1073/pnas.122205699

Jeyabalan, N., and Clement, J. P. (2016). SYNGAP1: mind the gap. *Front. Cell. Neurosci.* 10:32. doi: 10.3389/fncel.2016.00032

Kim, J. H., Lee, H. K., Takamiya, K., and Huganir, R. L. (2003). The role of synaptic GTPase-activating protein in neuronal development and synaptic plasticity. *J. Neurosci.* 23, 1119–1124. doi: 10.1523/jneurosci.23-04-01119.2003

Kim, J. H., Liao, D., Lau, L. F., and Huganir, R. L. (1998). SynGAP: a synaptic RasGAP that associates with the PSD-95/SAP90 protein family. *Neuron* 20, 683–691. doi: 10.1016/s0896-6273(00)81008-9

Kim, Y., Sung, J. Y., Ceglia, I., Lee, K. W., Ahn, J. H., Halford, J. M., et al. (2006). Phosphorylation of WAVE1 regulates actin polymerization and dendritic spine morphology. *Nature* 442, 814–817. doi: 10.1038/nature04976

Kirov, G., Grozeva, D., Norton, N., Ivanov, D., Mantripragada, K. K., Holmans, P., et al. (2009). Support for the involvement of large copy number variants in the pathogenesis of schizophrenia. *Hum. Mol. Genet.* 18, 1497–1503. doi: 10.1093/hmg/ddp043

Kopec, C. D., Real, E., Kessels, H. W., and Malinow, R. (2007). GluR1 links structural and functional plasticity at excitatory synapses. *J. Neurosci.* 27, 13706–13718. doi: 10.1523/jneurosci.3503-07.2007

Kunda, P., Craig, G., Dominguez, V., and Baum, B. (2003). Abi, Sra1, and Kette control the stability and localization of SCAR/WAVE to regulate the formation of actin-based protrusions. *Curr. Biol.* 13, 1867–1875. doi: 10.1016/j.cub.2003.10.005

Kushima, I., Aleksic, B., Nakatochi, M., Shimamura, T., Okada, T., Uno, Y., et al. (2018). Comparative analyses of copy-number variation in autism spectrum disorder and schizophrenia reveal etiological overlap and biological insights. *Cell Rep.* 24, 2838–2856.

Lautz, J. D., Brown, E. A., Williams Vanschoiack, A. A., and Smith, S. E. P. (2018). Synaptic activity induces input-specific rearrangements in a targeted synaptic protein interaction network. *J. Neurochem.* 146, 540–559. doi: 10.1111/jnc.14466

Leblond, C. S., Heinrich, J., Delorme, R., Proepper, C., Betancur, C., Huguet, G., et al. (2012). Genetic and functional analyses of SHANK2 mutations suggest a multiple hit model of autism spectrum disorders. *PLoS Genet.* 8:e1002521. doi: 10.1371/journal.pgen.1002521

Matikainen-Ankney, B. A., Kezunovic, N., Mesias, R. E., Tian, Y., Williams, F. M., Huntley, G. W., et al. (2016). Altered development of synapse structure and function in striatum caused by Parkinson's disease-linked LRRK2-G2019S mutation. *J. Neurosci.* 36, 7128–7141. doi: 10.1523/jneurosci.3314-15.2016

Matsubara, M., Kusubata, M., Ishiguro, K., Uchida, T., Titani, K., and Taniguchi, H. (1996). Site-specific phosphorylation of synapsin I by mitogen-activated protein kinase and Cdk5 and its effects on physiological functions. *J. Biol. Chem.* 271, 21108–21113. doi: 10.1074/jbc.271.35.21108

Napoli, I., Mercaldo, V., Boyl, P. P., Eleuteri, B., Zalfa, F., De Rubeis, S., et al. (2008). The fragile X syndrome protein represses activity-dependent translation through CYFIP1, a new 4E-BP. *Cell* 134, 1042–1054. doi: 10.1016/j.cell.2008.07.031

Osterweil, E. K., Krueger, D. D., Reinhold, K., and Bear, M. F. (2010). Hypersensitivity to mGluR5 and ERK1/2 leads to excessive protein synthesis in the hippocampus of a mouse model of fragile X syndrome. *J. Neurosci.* 30, 15616–15627. doi: 10.1523/jneurosci.3888-10.2010

Pathania, M., Davenport, E. C., Muir, J., Sheehan, D. F., Lopez-Domenech, G., and Kittler, J. T. (2014). The autism and schizophrenia associated gene CYFIP1 is critical for the maintenance of dendritic complexity and the stabilization of mature spines. *Transl. Psychiatry* 4:e374. doi: 10.1038/tp.2014.16

Paul, A., Nawalpuri, B., Shah, D., Sateesh, S., Muddashetty, R. S., and Clement, J. P. (2019). Differential regulation of Syngap1 translation by FMRP modulates eEF2 mediated response on NMDAR activity. *Front. Mol. Neurosci.* 12:97. doi: 10.3389/fnmol.2019.00097

Pick, J. E., Khatri, L., Sathler, M. F., and Ziff, E. B. (2017). mGluR long-term depression regulates GluA2 association with COPII vesicles and exit from the endoplasmic reticulum. *Embo J.* 36, 232–244. doi: 10.15252/embj.201694526

Porter, K., Komiyama, N. H., Vitalis, T., Kind, P. C., and Grant, S. G. (2005). Differential expression of two NMDA receptor interacting proteins, PSD-95 and SynGAP during mouse development. *Eur. J. Neurosci.* 21, 351–362. doi: 10.1111/j.1460-9568.2005.03874.x

Rumbaugh, G., Adams, J. P., Kim, J. H., and Huganir, R. L. (2006). SynGAP regulates synaptic strength and mitogen-activated protein kinases in cultured neurons. *Proc. Natl. Acad. Sci. U.S.A.* 103, 4344–4351. doi: 10.1073/pnas.0600084103

Sahoo, T., Peters, S. U., Madduri, N. S., Glaze, D. G., German, J. R., Bird, L. M., et al. (2006). Microarray based comparative genomic hybridization testing in deletion bearing patients with Angelman syndrome: genotype-phenotype correlations. *J. Med. Genet.* 43, 512–516. doi: 10.1136/jmg.2005.036913

Schenck, A., Bardoni, B., Langmann, C., Harden, N., Mandel, J. L., and Giangrande, A. (2003). CYFIP/Sra-1 controls neuronal connectivity in Drosophila and links the Rac1 GTPase pathway to the fragile X protein. *Neuron* 38, 887–898. doi: 10.1016/s0896-6273(03)00354-4

Schenck, A., Bardoni, B., Moro, A., Bagni, C., and Mandel, J. L. (2001). A highly conserved protein family interacting with the fragile X mental retardation protein (FMRP) and displaying selective interactions with FMRP-related proteins FXR1P and FXR2P. *Proc. Natl. Acad. Sci. U.S.A.* 98, 8844–8849. doi: 10.1073/pnas.151231598

Silva, A. I., Haddon, J. E., Ahmed Syed, Y., Trent, S., Lin, T. E., Patel, Y., et al. (2019). Cyfip1 haploinsufficient rats show white matter changes, myelin thinning, abnormal oligodendrocytes and behavioural inflexibility. *Nat. Commun.* 10:3455.

Steffen, A., Rottner, K., Ehinger, J., Innocenti, M., Scita, G., Wehland, J., et al. (2004). Sra-1 and Nap1 link Rac to actin assembly driving lamellipodia formation. *Embo J.* 23, 749–759. doi: 10.1038/sj.emboj.7600084

Thomson, S. R., Seo, S. S., Barnes, S. A., Louros, S. R., Muscas, M., Dando, O., et al. (2017). Cell-type-specific translation profiling reveals a novel strategy for treating Fragile X Syndrome. *Neuron* 95, 550.e5–563.e5.

van der Zwaag, B., Staal, W. G., Hochstenbach, R., Poot, M., Spierenburg, H. A., De Jonge, M. V., et al. (2010). A co-segregating microduplication of chromosome

15q11.2 pinpoints two risk genes for autism spectrum disorder. *Am. J. Med. Genet. B Neuropsychiatr. Genet.* 153B, 960–966.

Vazquez, L. E., Chen, H. J., Sokolova, I., Knuesel, I., and Kennedy, M. B. (2004). SynGAP regulates spine formation. *J. Neurosci.* 24, 8862–8872. doi: 10.1523/jneurosci.3213-04.2004

Walkup, W. G., Mastro, T. L., Schenker, L. T., Vielmetter, J., Hu, R., Iancu, A., et al. (2016). A model for regulation by SynGAP-alpha1 of binding of synaptic proteins to PDZ-domain 'Slots' in the postsynaptic density. *eLife* 5:e16813.

Walkup, W. G. T., Washburn, L., Sweredoski, M. J., Carlisle, H. J., Graham, R. L., Hess, S., et al. (2015). Phosphorylation of synaptic GTPase-activating protein (synGAP) by Ca2+/calmodulin-dependent protein kinase II (CaMKII) and cyclin-dependent kinase 5 (CDK5) alters the ratio of its GAP activity toward Ras and Rap GTPases. *J. Biol. Chem.* 290, 4908–4927. doi: 10.1074/jbc.m114.614420

Waung, M. W., Pfeiffer, B. E., Nosyreva, E. D., Ronesi, J. A., and Huber, K. M. (2008). Rapid translation of Arc/Arg3.1 selectively mediates mGluR-dependent LTD through persistent increases in AMPAR endocytosis rate. *Neuron* 59, 84–97. doi: 10.1016/j.neuron.2008.05.014

Yang, N., Higuchi, O., Ohashi, K., Nagata, K., Wada, A., Kangawa, K., et al. (1998). Cofilin phosphorylation by LIM-kinase 1 and its role in Rac-mediated actin reorganization. *Nature* 393, 809–812. doi: 10.1038/31735

Zeng, M., Shang, Y., Araki, Y., Guo, T., Huganir, R. L., and Zhang, M. (2016). Phase transition in postsynaptic densities underlies formation of synaptic complexes and synaptic plasticity. *Cell* 166, 1163.e12–1175.e12.

Zhang, Q., Yang, H., Gao, H., Liu, X., Li, Q., Rong, R., et al. (2020). PSD-93 interacts with SynGAP and promotes SynGAP ubiquitination and ischemic brain injury in mice. *Transl. Stroke Res.* 11, 1137–1147. doi: 10.1007/s12975-020-00795-z

Zhang, W., and Benson, D. L. (2000). Development and molecular organization of dendritic spines and their synapses. *Hippocampus* 10, 512–526. doi: 10.1002/1098-1063(2000)10:5<512::aid-hipo2>3.0.co;2-m

Zhao, L., Wang, D., Wang, Q., Rodal, A. A., and Zhang, Y. Q. (2013). Drosophila cyfip regulates synaptic development and endocytosis by suppressing filamentous actin assembly. *PLoS Genet.* 9:e1003450. doi: 10.1371/journal.pgen.1003450

Conflict of Interest: The authors declare that the research was conducted in the absence of any commercial or financial relationships that could be construed as a potential conflict of interest.

frontiers in Synaptic Neuroscience

ORIGINAL RESEARCH
published: 18 March 2021
doi: 10.3389/fnsyn.2021.618391

Disposition of Proteins and Lipids in Synaptic Membrane Compartments Is Altered in Q175/Q7 Huntington's Disease Mouse Striatum

*Maria Iuliano†, Connor Seeley†, Ellen Sapp, Erin L. Jones, Callie Martin, Xueyi Li, Marian DiFiglia and Kimberly B. Kegel-Gleason**

Department of Neurology, Massachusetts General Hospital, Boston, MA, United States

Dysfunction at synapses is thought to be an early change contributing to cognitive, psychiatric and motor disturbances in Huntington's disease (HD). In neurons, mutant Huntingtin collects in aggregates and distributes to the same sites as wild-type Huntingtin including on membranes and in synapses. In this study, we investigated the biochemical integrity of synapses in HD mouse striatum. We performed subcellular fractionation of striatal tissue from 2 and 6-month old knock-in Q175/Q7 HD and Q7/Q7 mice. Compared to striata of Q7/Q7 mice, proteins including GLUT3, Na^+/K^+ ATPase, NMDAR 2b, PSD95, and VGLUT1 had altered distribution in Q175/Q7 HD striata of 6-month old mice but not 2-month old mice. These proteins are found on plasma membranes and pre- and postsynaptic membranes supporting hypotheses that functional changes at synapses contribute to cognitive and behavioral symptoms of HD. Lipidomic analysis of mouse fractions indicated that compared to those of wild-type, fractions 1 and 2 of 6 months Q175/Q7 HD had altered levels of two species of PIP2, a phospholipid involved in synaptic signaling, increased levels of cholesterol ester and decreased cardiolipin species. At 2 months, increased levels of species of acylcarnitine, phosphatidic acid and sphingomyelin were measured. EM analysis showed that the contents of fractions 1 and 2 of Q7/Q7 and Q175/Q7 HD striata had a mix of isolated synaptic vesicles, vesicle filled axon terminals singly or in clusters, and ER and endosome-like membranes. However, those of Q175/Q7 striata contained significantly fewer and larger clumps of particles compared to those of Q7/Q7. Human HD postmortem putamen showed differences from control putamen in subcellular distribution of two proteins (Calnexin and GLUT3). Our biochemical, lipidomic and EM analysis show that the presence of the HD mutation conferred age dependent disruption of localization of synaptic proteins and lipids important for synaptic function. Our data demonstrate concrete biochemical changes suggesting altered integrity of synaptic compartments in HD mice that may mirror changes in HD patients and presage cognitive and psychiatric changes that occur in premanifest HD.

Keywords: cholesteryl ester, lipidomics, PIP2, synapse, neurotransmitter receptors, electron microscopy, Huntingtin, density gradient centrifugation

OPEN ACCESS

Edited by:
Carl R. Lupica, National Institute on Drug Abuse (NIDA), United States

Reviewed by:
Sandy Bajjalieh, University of Washington, United States
Amber L. Southwell, University of Central Florida, United States

***Correspondence:**
Kimberly B. Kegel-Gleason
kegel@helix.mgh.harvard.edu

† These authors have contributed equally to this work

Received: *16 October 2020*
Accepted: *24 February 2021*
Published: *18 March 2021*

Citation:
Iuliano M, Seeley C, Sapp E, Jones EL, Martin C, Li X, DiFiglia M and Kegel-Gleason KB (2021) Disposition of Proteins and Lipids in Synaptic Membrane Compartments Is Altered in Q175/Q7 Huntington's Disease Mouse Striatum. Front. Synaptic Neurosci. 13:618391. doi: 10.3389/fnsyn.2021.618391

INTRODUCTION

Patients with Huntington's disease (HD) develop cognitive and motor dysfunctions accompanied by neuronal loss in the striatum and cortex. Altered synaptic connectivity of the basal ganglia underlies these deficits and is associated with remodeling dendritic morphology and spine loss of medium spiny striatal neurons where most synaptic contacts in the striatum occur (Graveland et al., 1985; Ferrante et al., 1991; Sotrel et al., 1991). Imaging studies in prodromal or early symptomatic HD patients and controls support a role for early changes in connectivity in cortex and in cortico-striatal networks in causing depression and trouble with executive processing (Wolf et al., 2008; Unschuld et al., 2012a,b). A profound loss of white matter also occurs early in HD (Tabrizi et al., 2011) and loss of white matter in premanifest HD carriers correlated with transcriptional changes in synaptic proteins (McColgan et al., 2018).

Studies in different HD mouse models also support the idea that synaptic dysfunction occurs early in disease significantly affecting the striatum (Nithianantharajah and Hannan, 2013). Decreased spine number and changes in dendritic morphology preceded neuron loss in human HD postmortem brain and in different HD mouse models (Graveland et al., 1985; Guidetti et al., 2001; Klapstein et al., 2001; Spires et al., 2004; Lerner et al., 2012). Using two-photon microscopy and a cranial window, Murmu et al. (2013) showed that spines have an increased rate of turnover and a lower survival rate in R6/2 HD mice, which overexpress a small fragment of mutant Huntingtin. Loss of excitatory terminals projecting from cortex to striatum occurs prior to striatal volume or neuronal loss in knock-in Q140 heterozygous mice (Deng et al., 2013). Shifts in spine types at 21 days and reduced spine density by 5 weeks occur in dorsal striatum of the knock-in Q175 (zQ175) compared to wild-type (McKinstry et al., 2014). These morphological changes are likely to contribute to altered synaptic function in HD. Differences in synaptic organization at the EM level have been reported in HD mice. Wheeler and colleagues found altered synaptic density and synaptic morphology in the striatum of 18-month old Q111/Q7 HD mice (Kovalenko et al., 2018). Based on studies in human postmortem brain and Q140 HD mice there are stages of synaptic loss with reduced inputs from cortex and thalamus to the striatum occurring early and output pathways of the striatum affected later (Reiner and Deng, 2018). In neurons, mutant Huntingtin collects in aggregates including at synapses (Li et al., 2003; Sapp et al., 2020), and distributes to the same sites as wild-type Huntingtin including on membranes and in synapses (Aronin et al., 1995). Wild-type Huntingtin has been shown to be associated with the presynaptic cytomatrix (Yao et al., 2014) and mutant Huntingtin can sequester Bassoon, a polyglutamine containing structural protein, and Piccolo away from the cytoskeletal matrix of the active zone (CAZ) in R6/1 mice and human HD brain (Huang et al., 2020).

Changes at plasma membranes and endosomes may contribute to dysfunction in HD. Studies in HD models showed that the HD mutation affects the organization of cholesterol enriched lipid rafts at plasma membranes where most growth factor signaling occurs in neurons and alters distribution of the Na^+/K^+ ATPase from detergent resistant membranes (Valencia et al., 2010). Displacement of the NMDAR 2b receptor subunit away from the synapse with no changes in protein levels was shown in YAC72 HD mice and correlated with altered current (Fan et al., 2007). Redistribution of AMPA receptors affect memory in HD models (Zhang et al., 2018). Glucose transport across the plasma membrane is impaired in primary HD neurons (McClory et al., 2014) and glucose utilization is both impaired in HD patients (Ciarmiello et al., 2006) and mirrors progression in premanifest HD (Tang et al., 2013). There is no evidence for loss of glucose transporter 3 (GLUT3) protein in HD cell and mouse models (McClory et al., 2014) or in HD brain (Gamberino and BrennanJr., 1994). However, mutant Huntingtin alters the endocytic recycling of Rab11 dependent cargo including transferrin receptor and GLUT3 back to the plasma membrane in primary Q140/Q140 HD neurons compared to wild-type without changing its protein levels (Li et al., 2009; McClory et al., 2014). Changes in GLUT3 subcellular localization have thus far not been demonstrated in animal models.

Cellular fractionation is a useful method to enrich for subcellular compartments including plasma membranes, organelles and synaptic profiles and for the low abundant proteins they may contain. With these preparations it is possible to determine by biochemical or enzymatic assays the effects of genetic mutations or drug treatments on altered trafficking within subcellular compartments [examples in HD (Fan et al., 2007)]. Moreover, the subcellular compartments where mutant proteins reside or have effects can be determined (Aronin and DiFiglia, 1992; De Rooij et al., 1996; Velier et al., 1998; Kim et al., 1999; Kegel et al., 2002; Fan et al., 2007). Sucrose has been commonly used to create density gradients to separate organelles including synaptosomes which are enriched in pre- and postsynaptic structures. In a study of synaptosomes isolated in a 0.35-2M discontinuous sucrose gradient from striatum of 6-month-old Q140/Q140 HD mice, mutant Huntingtin was detected and there were altered levels of pre- and post synaptic proteins compared to Q7/Q7 mice (Valencia et al., 2013). Gradients made using Percoll (colloidal silica), Nycodenz (a derivative of benzoic acid with three aliphatic hydrophilic side chains), and iodixanol (a water-soluble contrast agent) have been used for preparation of synaptosomes (Ford and Rickwood, 1982; Dunkley et al., 1986). These preparations are useful for retaining organelle osmolarity and viscosity throughout the density gradient (Zhang et al., 1998; Graham, 2015). OptiPrep which is a 60% solution of iodixanol has been used in cellular fractionation to isolate cell compartments for the study of disease models (Mamada et al., 2017) including HD (Velier et al., 1998; Kim et al., 1999).

In this study, we used OptiPrep as a medium for subcellular fractionation to examine the distribution of proteins and lipids in striatal lysates from Q7/Q7 and Q175/Q7 HD mice. Results showed that in comparison to those of Q7/Q7 mice, "synaptic" fractions 1 and 2 of 6-month old Q175/Q7 HD mice had differences from Q7/Q7 in the size and number of particles separated from these fractions and an altered distribution of membrane associated proteins, and the levels of PIP2, cholesterol ester, and other lipids involved in synapse signaling

and maintenance. These changes may contribute to altered synaptic function in HD.

MATERIALS AND METHODS

Animals

Knock-in heterozygous Q175/Q7 HD and Q7/Q7 C57BL/6J mice were obtained from The Jackson Laboratory (Stock 370832, JAX number 4156350). Mice were genotyped twice, once by PCR at Jackson Laboratory, as well as by western blot for Huntingtin protein. The animal protocol was approved by the MGH Subcommittee on Research Animal Care (SRAC)-OLAW #2004N000248. All procedures conform to the USD Animal Welfare Act, the "ILAR Guide for the Care and Use of Laboratory Animals," and the PHS Policy on Humane Care and Use of Laboratory Animals. Animals were euthanized by CO_2 followed by cervical dislocation and decapitation. Brains were extracted and rapidly dissected on ice to isolate the striata, which were immediately processed for density gradient ultracentrifugation.

Human Brain

Unfixed, frozen human brain tissue was obtained from the Massachusetts General Hospital Neuropharmacology Laboratory Brain Bank and the Neuropathology Core of the Massachusetts Alzheimer Disease Research Center (P50 AG05134) and stored at −80°C. Post-mortem interval ranged from 4 to 48 h. Dorsal putamen was dissected from frozen blocks sectioned in the coronal plane.

Striatal Sample Preparation and Cell Fractionation by Density Gradient Ultracentrifugation

The entire mouse striatum (both hemispheres) or a ∼2 cubic mm specimen of human putamen were homogenized with a Dounce homogenizer (10–20 strokes per sample) in 0.75 ml homogenization buffer (HB), containing 10 mM HEPES, 1 mM EDTA, 0.25M sucrose, and protease inhibitors (pH 7.4). Each sample was analyzed microscopically to verify that the nuclei had sheared from cellular components but had not ruptured. Additional 5 stroke increments were completed until an acceptable level of shearing had been obtained. Crude homogenate was spun for 10 min at 2,000g. The supernatant (S1) was collected and 0.45 ml was mixed with 50% OptiPrep (Sigma, cat #D1556) for a final concentration of 35% OptiPrep, then underlaid beneath the continuous density gradient. Continuous density gradients were prepared the day before by pouring discontinuous gradients (2.5 mL of 30%, 24%, 17%, and 10% OptiPrep diluted in HB buffer) in 14 × 89 mm Ultra-Clear centrifuge tubes (Beckman Coulter, 344059) and allowing them to diffuse and equilibrate overnight at 4°C. The loaded gradients were overlaid with HB to completely fill tubes and balance the rotor. Samples were centrifuged using a SW41 rotor in a Beckman L8-80 M Ultracentrifuge at 4°C for 2.5 h at 37,000 rpm with acceleration and deceleration set at 7. After centrifugation, 0.75 ml fractions were manually collected from top to bottom using a glass Pasteur pipette. Samples were then processed for SDS-PAGE and western blot analysis and stored at −80°C.

SDS-PAGE and Western Blot

Fractions 1 through 15–16 were loaded by volume onto a 3–8% Tris-Acetate or 4–12% Bis-Tris gel using Tricine and MOPS running buffers, respectively, then transferred onto nitrocellulose via Trans-Blot Turbo transfer system (Bio-Rad). For some proteins, only $N = 3$ were investigated for all 1–16 fractions (including SNAP25). Fractions 1–3 were run on large format gels to compare samples from different animals on the same blot. $N = 9$ per group were examined in this manner for all reported probes. To prevent the aggregation of membrane proteins, samples were not boiled and gel electrophoresis chambers were run on ice. Blots were blocked in 5% milk in TBST (TBS + 0.1% Tween-20) then incubated overnight in blocking solution with diluted primary antibody. Blots were washed with TBST, incubated in blocking solution with diluted secondary antibody for 1 h, and then treated with SuperSignal West Pico Plus Chemiluminescent substrate (Pierce) for 5 min for band detection on film. We performed both film and digital readouts for many of the proteins detected. Examples of digital signals versus film signals are shown in **Supplementary Figure 2A**. For most proteins, film gave stronger, more consistent results compared to digital; the latter were in general agreement with film but for some proteins the digital signals were too low or absent to be useful. For film, we routinely used multiple exposure times (1, 10, or 30 s and 1, 3, and 30 min) and selected exposure times for quantification where the most intense signal among the fractions was not saturated. Signal for each fraction was standardized as a percentage of the total signal for all fractions and not based on absolute magnitude. For figures showing fractions 1–16, we used longer exposures so that the small amounts of protein in some fractions could be appreciated. Blots were stripped using ReBlot Strong Stripping Buffer (Millipore), and then blocked and re-probed for additional antibody detection. Antibody sources and dilutions can be found in the next section.

Antibodies

Actin (Sigma, A4700) 1:400, Alpha Actinin 2 (Abcam, ab68167) 1:2000, AMPA Receptor 1 GluR1a (Alomone, AGC-004) 1:500, BIII Tubulin (Sigma, T8660) 1:2000, Calnexin (StressGen, SPA-860) 1:2000, DARPP32 (Abcam, 40801) 1:10,000, GABA(A) a1 Receptor (Alomone, AGA-001) 1:500, Glucose Transporter GLUT3 (Abcam, ab41525) 1:500, Na+/K+ ATPase (Affinity Bioreagents, MA3-915) 1:5,000, NMDA Receptor 2B GluN2B (Alomone, AGC-003) 1:500, PDE10a (Abcam, 177933) 1:2000, PSD95 (Cell Signaling, 2507S) 1:1000, SCN4B (Abcam, ab80539) 1:200, SNAP25 (BD Transduction Labs, 610366) 1:10,000, Transferrin (Thermo Fisher, 13-6800) 1:1000, VGlut1 (Synaptic Systems, 135302) 1:10,000, VGlut2 (Synaptic Systems, 135402) 1:10,000, XK (Aviva Systems Bio, ARP33809_P050) 1:1000, Huntingtin [Ab1, aa1-17, (DiFiglia et al., 1995)] 1:2000, poly-Q (1C2, EMD Millipore MAB1574) 1:1000. Horseradish peroxidase secondary antibodies (Jackson Immunoresearch) were diluted 1:5000.

Pixel Intensity Quantification and Statistical Analysis

Signal intensity was measured using ImageJ software (NIH) and standardized to background signal. Signal from each fraction was standardized as a percentage of the sum of signal from all fractions. Wild-type and mutant Huntingtin were measured separately in the Q175/Q7 HD mice as detected with Ab1. In human post-mortem tissue, wild-type and mutant Huntingtin could not be distinguished using these assay conditions so the results are reported for total Huntingtin as detected with Ab1. Analyses of signal intensities were compared using a 2-tailed unpaired *t*-test. Fisher's exact test was also used to compare peak signals in fractions 1 and 2. Statistical analyses were performed using GraphPad Prism version 7.00 for Windows (GraphPad Software, La Jolla, CA, United States). For Tukey-style box plots, the lower and upper hinges correspond to the first and third quartiles (the 25th and 75th percentiles). The upper whisker extends from the hinge to the largest value no further than 1.5 times the inter-quartile range (distance between the first and third quartiles) from the hinge. The lower whisker extends from the hinge to the smallest value no further than 1.5 times the inter-quartile range from the hinge. Data beyond the end of the whiskers are called "outlying" points and are plotted individually. The outlying values are included in the statistical analyses. A power analysis to determine group size for 95% confidence was performed using signal intensities for GLUT3 with the initial $n = 3$ per group data using G*Power software which specified $n = 8$ per group. We fractionated $n = 9$ mice per group.

Electron Microscopy

Aliquots from continuous density fractionation (fractions 1 and 2) of Q7/7 and Q175/Q7 mice ($N = 9$ per group) were fixed for 1 h in 4% PFA, then 4 μl was dropped onto Formvar grids and allowed to air dry before staining with 6% uranyl acetate and 6% lead citrate in closed chambers. Stained grids were examined at the Philly Dake Electron Microscope Facility using a JEOL JEM-1011 transmission electron microscope with AMTv601 software (Advanced Microscopy Techniques, Woburn, MA, United States) at 30,000×. For quantification, images were taken at 500×, using two grids per animal. Micrographs were cropped to standardize size in Photoshop to (1971 × 1900) by a blinded operator to select areas of micrograph devoid of shadows or artifacts. Images were imported into FIJI software (NIH), and thresholds adjusted using Renyi entropy method, then analyzed for particle number and size. Particle analysis was completed on all images using particle size greater than 1 pixel up to infinity pixels, all other settings were left as default. Results were exported to Excel and average particle size, median particle size and number of particles standardized to the number of fields were calculated in 7–45 fields per mouse. The number of images per group per fraction were, Q7/Q7 fraction 1: 36, 20, 8, 13, 7, 14, 11, 16, 16; Q175/Q7 fraction 1: 13, 16, 35, 39, 15, 32, 30, 27; Q7/Q7 fraction 2: 21, 15, 17, 38, 27, 14, 8, 18, 21; Q175/Q7 fraction 2: 13, 14, 34, 21, 7, 33, 45, 27,22. The mean particle size and number of particles was determined for each field and the results are reported as mean particle size per mouse ($N = 9$).

Lipidomics

Samples were prepared and analyzed using ion switching mass spectrometry exactly as previously described (Breitkopf et al., 2017). Briefly, 100 μl of fractions 1 and 2 from each continuous iodixanol gradient were aliquoted into 10 ml glass scintillation vials. 750 μl methanol was added to each sample. Subsequently, 2.5 ml of Methyl tert-butyl ether (MTBE) was added to each sample, this mixture was incubated at room temperature on a platform shaker for 1 h. Following mixing, 625 μl of water was added to separate polar and non-polar phases. The upper phase was collected and placed into a HPLC vial with Teflon lids. The lower phase was re-extracted with 1 ml (MTBE/methanol/water, by volume 10/3/2.5). The upper MTBE phase of this re-extraction was collected and combined with initial upper phase. Pellets were dried and overlaid with N_2 gas and stored at -20°C. Samples were hand delivered to Beth Israel Deaconess Medical Center mass spectroscopy core.

Data Analysis of Lipids

For each fraction we calculated the ratio of the individual lipid intensity (area under the peak) to the intensity of total lipids per mouse and obtained the means of Q7/Q7 and Q175/Q7 HD mice ($N = 9$ per group) for each fraction and performed unpaired student's *t*-tests assuming unequal variance. Peak intensity was translated into a percentage of sample total intensity, class total intensity and class total expressed as a percentage of the sample total. These values were compared between Q7Q/7 and Q175/Q7 samples using students *t*-test in Excel. We also compared the ratio of the intensities of all lipids in one class to the total lipids in fractions 1 and 2 and obtained mean values for Q7/Q7 and Q175/Q7 mice ($N = 9$ mice per group) for the sum intensity/total intensity for each class. *T*-tests were performed and significance was accepted at the $p < 0.05$ level. Additionally, *P*-value adjustments were made using Benjamini Hochberg correction in Rstudio.

Amplex Red Quantification of Total Cholesterol in Sample

Small amounts of fractions 1 and 2 were analyzed using the Amplex red cholesterol kit (Invitrogen, 3–5 μl for 6-month samples and 10 μl for 2-month samples). The Tukey-style box plot shows the median and interquartile ranges for both Q175/Q7 and Q7/Q7 in fractions 1 and 2.

Annotation of Lipids

Phospholipids were annotated as Lipid Class (total fatty acid chain length: total number of unsaturated bonds). If acyl chains could be identified, carbon length of each fatty acyl chain and number of unsaturated bonds is listed in tables; however, assignment of the sn-1 and sn-2 positions is ambiguous (ex., PA 38:4 (18:0/20:4). Glycerophosphate or phosphatidic acid (PA), glycerophosphatidylcholine (PC), glycerophosphatidylethanolamine (PE), glycerophosphatidylglycerol (PG), glycerophosphatidylinositol (PI), glycerol-phosphatidylmethanol (PMe), glycerophosphatidylserine (PS), sphingomyelin (SM), and

cardiolipin (CL). Lyso-PA (LPA), lyso-PC (LPC), lyso-PE (LPE), lyso-PG (LPG), lyso-PI (LPI), ceramide (Cer), sphingosine (So), sphingosine phosphate (SoP), methyl-PC (MePC), PI bis phosphate (PIP2). Glycerolipids: diacylglycerol, (DG). monoacylglycerol (MG), and triacylglycerol (TG). Neutral lipids: Fatty acids (FA), acylcarnitine (Acca), sterol (ST), cholesteryl ester, (ChE), zymosteryl (ZyE), wax ester (WE), Coenzyme (Co). E, ether linkage; P, plasmalogen; Ox, oxidized lipid; P, phosphate; Ganglioside (GM, GD).

RESULTS

Analysis of OptiPrep Fractions of Q7/Q7 and Q175/Q7 HD Striatum for Presence of Standard Subcellular Markers and Huntingtin

We sought to determine if the HD mutation altered the subcellular distribution of Huntingtin and other proteins in the striata of HD Q175/Q7 mice. Continuous iodixanol gradients were used to fractionate the post nuclear supernatants of Q7/Q7 and Q175/Q7 HD striata (N = 3 mice per genotype) These supernatants contain numerous membrane-bound compartments such as synaptosomes, light endosomes, endoplasmic reticulum (ER), mitochondria, peroxisomes, plasma membrane (PM) and recycling compartments, as well as cytosol (**Figure 1A** and **Supplementary Figure 1**). After ultracentrifugation, 16 fractions from each gradient were collected and analyzed by SDS-PAGE and western blot to establish the distribution of proteins known to be found in different compartments including PM (Na^+/K^+ ATPase), ER (Calnexin), recycling compartment (Transferrin receptor), and mitochondria (cytochrome C). The boxes in the diagram in **Figure 1A** summarize the distribution of proteins in fractionations from Q7/Q7 striata. Na^+/K^+ ATPase distributed to the least dense fractions (#1–6). Transferrin receptor distributed to fractions 1–10, but also to dense fractions (14–16) as expected for a protein that is found both on the plasma membrane and in the perinuclear recycling compartment which distributes to the denser fractions. In contrast, cytochrome C distributed to fractions 1 and 2 peaking in fraction 2 and to the center of the gradient (middle fractions 7–9) showing good separation of organelles on the gradients. Signal for Calnexin was also found in the lighter fractions but had a wider distribution (fractions 1–10) than the PM marker Na^+/K^+ ATPase. The protein XK, which has been implicated in non-Huntington's chorea (Park and Neiman, 2020), distributes to light fractions 1–5 and to the center of the gradient (fractions 7–9). Syntaxin 6, a marker of trans-golgi network (TGN) and TGN-derived light vesicles distributes to fractions 1–4 and dense fractions 14–16 in Q7/Q7 mice. The lysosomal protease Cathepsin D fractionated to light fractions 1–9 with lower levels in fractions 3 and 4 and to heavy fractions 14–16. Wild-type Huntingtin signal occurred in fractions 1–6 and 14–16 with a distribution profile highly similar to Transferrin receptor, as previously described for human fibroblasts (Velier et al., 1998; **Figures 1B,C**). The location of synaptic components was identified by probing for the presynaptic marker SNAP25 which showed strong signal distributed to fractions 1 and 2 with lower levels in fractions 3–5 for Q7/Q7 striatum. Fractionations from Q175/Q7 HD striatum showed similar profiles for most proteins with no significant differences or trends in distribution for Calnexin, Transferrin receptor, and cytochrome C. The presynaptic marker SNAP25 appeared slightly shifted from its normal peak distribution in fraction 2 in Q7/Q7 to fraction 1 for Q175/Q7 in 2 of N = 3 mice (**Figure 1B** and **Supplementary Figure 1**).

In fractions from heterozygous Q175/Q7 striatum, wild-type Huntingtin distributed nearly identically to wild-type Huntingtin from Q7/Q7 striatum (**Figures 1B,C**). Mutant Huntingtin from Q175/Q7 striatum also distributed with a very similar profile, although a significant reduction of mutant Huntingtin occurred in fraction 4 (**Figure 1D**, $^*p$ = 0.027, unpaired t-test, N = 7). The distribution of Na^+/K^+ ATPase appeared to be changed in Q175/Q7 fractions compared to Q7/Q7 (**Supplementary Figure 1**). We also looked at the distribution of the neuronal specific protein GLUT3, presynaptic proteins such as VGLUT1 and VGLUT2, and post synaptic proteins. For PSD95 and VGLUT2 we have reported significant reductions in levels in synaptosomes of Q175/Q7 versus Q7/Q7 striatum; no change in protein levels was observed for Na^+/K^+ ATPase, SNAP25, and VGLUT1 (Sapp et al., 2020). We observed that several membrane-associated proteins that distribute to fractions 1–4 appeared altered from their normal distribution of peaking in fraction 2 in Q7/Q7 mice to peaking in fraction 1 in Q175/Q7 HD mice, (**Figure 1B**, shown for GLUT3 and **Supplementary Figure 1B**) similar to SNAP25. No changes were observed in fractions 3 and 4 between wild-type and Q175/Q7 mice. We chose to quantify changes in the peak signals, therefore one caveat to our results is that we may have missed changes that might occur in fractions where low levels of proteins distributed as they may be out of the linear range that we measured.

The Presence of the HD Mutation Alters Distribution of Membrane Associated Proteins in Synaptic Compartments of Q175/Q7 HD Mice

Results established that in HD mice there was a minor difference in the subcellular distribution of wild-type and mutant Huntingtin, but the presence of the HD mutation changed the subcellular distribution of some other proteins in the lighter fractions 1–2. To quantify the change in distribution of proteins in the light fractions, we ran fractions 1–3 from each mouse on large format gels (26 lanes) and increased the sample size to N = 9 mice based on a power analysis (G*Power). **Figure 2** shows graphical representations of pixel intensity quantification results from western blots for 16 proteins; representative images of western blots are shown in **Supplementary Figures 2A,B**. A shift in the peak for several proteins did occur. A significant reduction of signal was observed in fraction 2 in Q175/Q7 mice for GLUT3, Na^+/K^+ ATPase, NMDAR 2b, PSD95, and VGLUT1 (**Table 1**) compared to Q7/Q7 mice, with a contingent significant or near significant increase in signal in fraction 1. Although

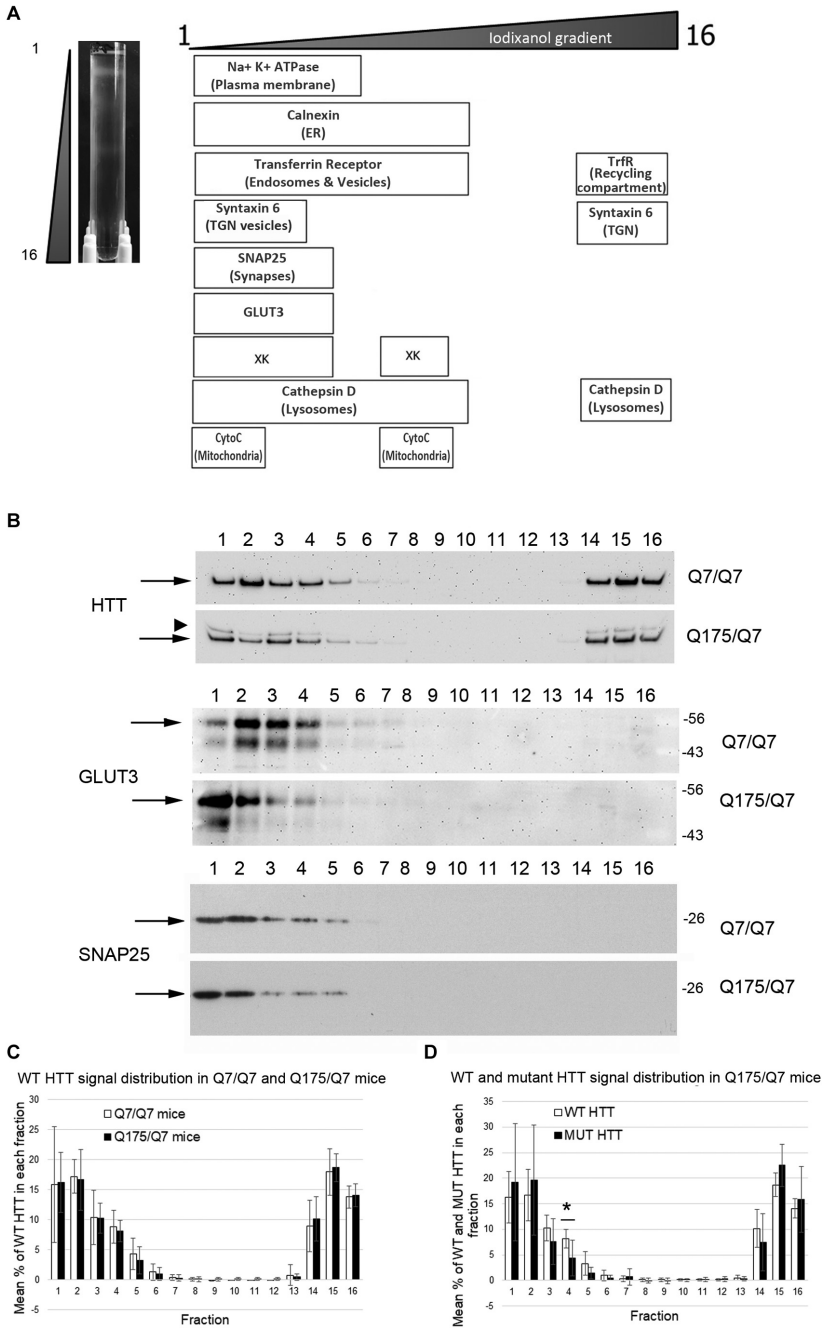

FIGURE 1 | Subcellular fractionation by continuous iodixanol density gradient ultracentrifugation of 6-month old Q7/Q7 and Q175/Q7 HD mouse striatum. **(A)** Striata were fractionated as described in section "Materials and Methods." Picture at left shows ultracentrifugation tube after equilibration of compartments by centrifugation; banding pattern indicates successful fractionation of cellular components. Fractions 1–16 were removed from top to bottom as indicated. Fractions were assessed by SDS-PAGE and western blot analysis using the cell compartment markers indicated at top right to ensure complete separation. Equal volumes of each fraction were loaded per lane. **(B)** Representative images of western blots detecting Huntingtin (HTT) (WT and mutant (arrowhead)), GLUT3, and SNAP25. HTT distributes to light fractions 1–5 and co-fractionates with a marker of pre-synaptic compartment, SNAP25 and to dense fractions 14–16. GLUT3 co-fractionates in fractions 1–4 and shows a marked shift in the peak signal intensity between Q7/Q7 and Q175/Q7 HD resulting in an increase in signal for GLUT3 in Q175/Q7 in fraction 1 and a reduction in fractions 2–4. **(C)** Pixel intensity analysis of western blots for WT HTT. Bar graph shows mean percent ± SD of WT HTT in each of 16 fractions as a percent of total WT HTT signal summed across all fractions (1–16). White bars show WT HTT in Q7/Q7 mice and black bars show WT HTT in Q175/Q7 striata. There was no significant difference in WT HTT signal as percent of total signal between Q7/Q7 and Q175/Q7 mice for any fraction. **(D)** Pixel intensity analysis of western blots for mutant HTT and WT HTT in fractions from Q175/Q7 striata. Bar graph shows percent ± SD of WT HTT (white bars) and mutant HTT (black bars) signal in each of 16 fractions as a percent of total WT and mutant HTT signal summed across all fractions (1–16) in Q175/Q7 6-month old mice. There is a significant difference between WT and mutant HTT signal as a percent of total signal in fraction 4 (*p = 0.0266, unpaired t-test, N = 7).

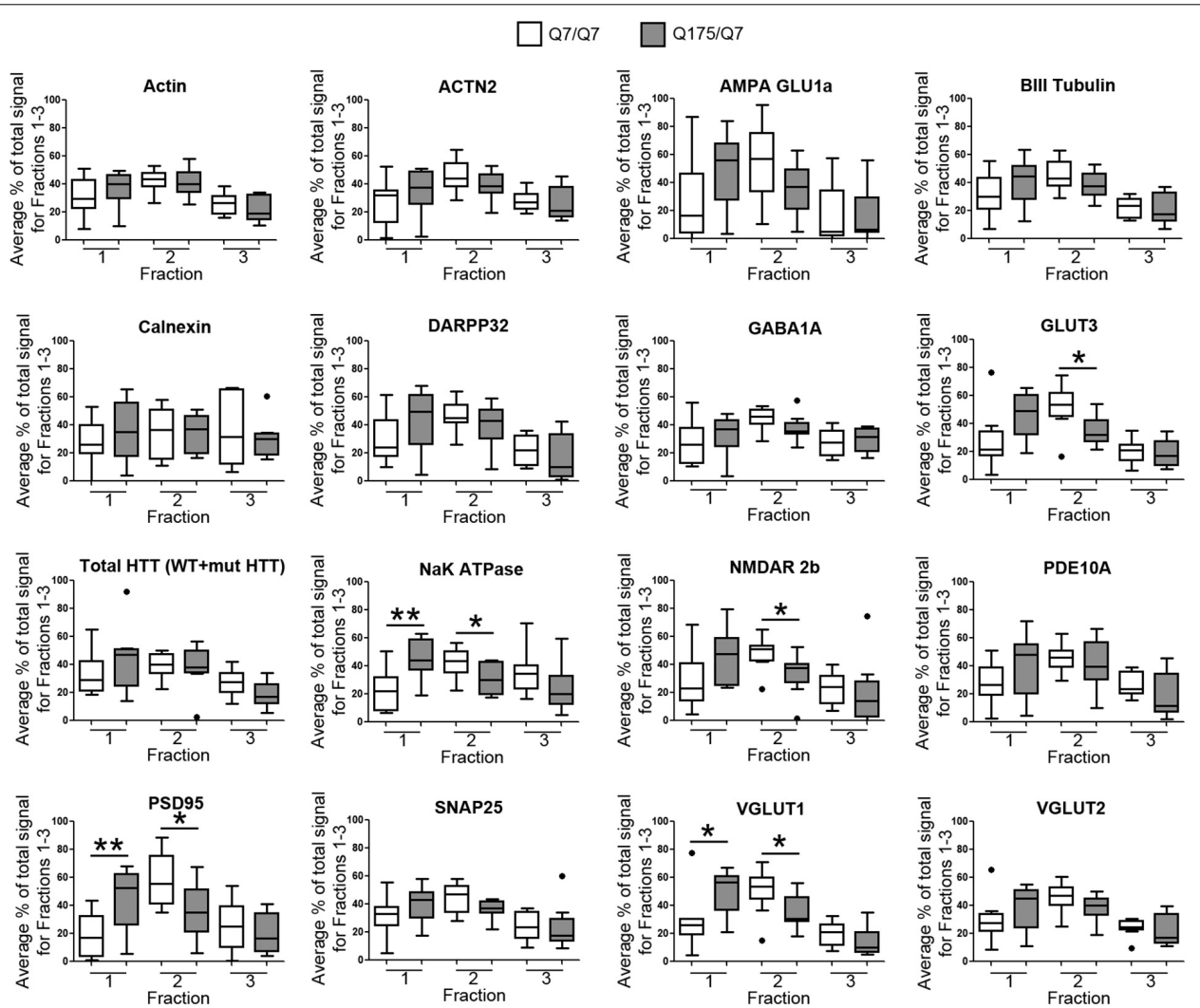

FIGURE 2 | GLUT3, VGLUT1, Na^+/K^+ ATPase, NMDAR 2b, and PSD95 from 6-month old Q175/Q7 striata show altered distribution after fractionation compared to that of Q7/Q7 mouse striata. Equal volumes of fractions 1–3 from **Figure 1** were run on large format SDS-PAGE gels and analyzed by western blot and ECL for proteins indicated. We performed both film and digital readouts for the many of proteins detected. We selected exposure times for quantification where the most intense signal among the fractions was not saturated. Signal for each fraction was standardized as a percentage of the total signal for all fractions and not based on absolute magnitude. Pixel intensity quantification was performed using ImageJ software (NIH) and graphed as percent of total signal summed for each protein in fractions 1–3 shown as a percentage of 100% Q7 or a percentage of Q175 100% ($N = 9$ mice per group, $^*p < 0.05$, $^{**}p < 0.01$, unpaired t-test). Graphs show Tukey-style box plots where the lower and upper hinges correspond to the first and third quartiles (the 25th and 75th percentiles) as described in section "Materials and Methods." Data beyond the end of the whiskers are called "outlying" points and are plotted individually. The outlying values are included in the statistical analyses. Proteins with altered subcellular distribution include GLUT3, Na^+/K^+ ATPase, NMDAR 2b, PSD95 and VGLUT1. See **Supplementary Figure 2B** for representative western blot images.

our previous results with $n = 3$ mice showed that SNAP25 had a trend to shift from fraction 2 in Q7/Q7 to fraction 1 in Q175/Q7 HD (see also **Figure 1B**), the change was not significant with a larger sample size (**Figure 2**; $p = 0.0527$, unpaired t-test, $N = 9$). We also analyzed distribution of proteins well-known to have reduced levels in HD mouse models including DARPP32, PDE10A, and SCN4B (Sapp et al., 2020). Although the levels of these proteins were all reduced in total signal on the western blots of fractions from Q175 compared to wild-type, their peak distribution was in lower fractions (3–7) and no shift in their percent distribution in the gradient occurred. We also looked at XK, a protein that when mutated produces chorea (Jung et al., 2003; Urata et al., 2019) and found no change in levels or distribution occurred in fractionations for XK for Q175/Q7 HD compared to Q7/Q7 striatum.

To determine if changes in the distribution of membrane associated proteins occurred earlier than 6 months in the Q175/Q7 HD mice, we prepared fractions from striatum of 2-month old mice. There was a similar distribution of Huntingtin and the cellular markers in Q175/Q7 HD compared to Q7/Q7 mice (**Supplementary Figure 3B**). There were also no shifts observed between fractions 1–4 in the proteins altered at

TABLE 1 | Statistical analysis for protein detection in fractions 1–3.

	Unpaired *t*-test			Fisher's exact test		Samples
	Fraction 1	Fraction 2	Fraction 3	1 to 2	2 to 3	*N*=
Huntingtin	0.2683	0.7130	0.0692	0.3147	1.0000	8
Actin	0.3828	0.6770	0.3598	0.3348	1.0000	9
ACTN2	0.2532	0.1982	0.6719	0.1312	0.3846	9
AMPA Glu1A	0.1193	0.0636	0.9497	0.1319	1.0000	9
BIII Tubulin	0.2153	0.1312	0.7261	0.1534	1.0000	9
Calnexin	0.4110	0.8667	0.5269	0.5758	0.5758	8
DARPP32	0.1342	0.2541	0.3200	0.1534	1.0000	9
GLUT3	0.0626	0.0209	0.8403	0.0152	1.0000	9
Na^+/K^+ ATPase	0.0032	0.0278	0.1641	0.1189	1.0000	9
NMDAR 2B	0.0869	0.0338	0.7863	0.0567	0.2727	9
PDE10A	0.1614	0.5048	0.1816	0.1534	0.3636	9
PSD95	0.0076	0.0339	0.4660	0.0070	0.4545	9
SNAP25	0.1492	0.0527	0.9096	0.1189	1.0000	9
VGlut1	0.0230	0.0324	0.2280	0.0152	1.0000	9
VGlut2	0.2121	0.0946	0.7437	0.0498	1.0000	9

Shown are p-values for unpaired t-test of pixel intensities comparing Q175/Q7 and Q7/Q7 for each fraction. Also reported are p-values for a Fisher exact (chi square) test comparing Q7/Q7 and Q175/Q7 fractions 1 to 2 or fractions 2 to 3. Gray shading indicates $p < 0.05$.

6 months (**Supplementary Figure 3A**). These results suggest that the alterations in membrane associated proteins in the striatal synaptic fractions seen at 6 months are age dependent and not due to altered development or an early degenerative event.

These results show an age dependent change in the intracellular distribution of select proteins in Q175/Q7 HD mouse striatum that occurs independent of protein levels. These changes might imply a change in the physical nature of the compartment/organelle or a change in trafficking of proteins from one organelle to another.

Mass Spectrometry of Lipids in Fractions 1 and 2 Reveals Marked Changes in Levels of Numerous Lipids Including Acyl Carnitine, Cardiolipin, Cholesterol Ester, Phosphatidic Acid, and PIP2 in Q175/Q7 HD Mice

In view of the changes described above in subcellular distribution of some membrane associated proteins in fractions 1 and 2 of the 6 months old HD mice, we addressed by mass spectrometry if lipid composition of these fractions was altered by the HD mutation. Lipidomic analysis of fractions 1 and 2 from 6 months old mice showed a consistent high yield of lipid species in all the samples examined. The number of individual lipids species identified in each Q175/Q7 HD mouse ranged from 544 to 816 in Q175/Q7 HD mice and from 613 to 815 in Q7/Q7 mice. The number of subclasses of lipids in the fractions from the Q175/Q7 HD mice varied from 26 to 34 and in the Q7/Q7 mice from 30 to 34. Bar graphs in **Supplementary Figure 2** show different subclasses of lipids grouped by their relative abundance and compared between Q7/Q7 and Q175/Q7 HD mice at 6 months (**Supplementary Figure 4A**, Glycerophospholipids and **Supplementary Figure 4B**, "Other Lipids"; $N = 9$ per genotype). The abundance of the major Glycerophospholipid subclasses which compose cell membranes did not differ by genotype in either fraction (PC, PE, SM, PS, PI, PA, PG; **Supplementary Figure 4A**). Only three changes were identified among all lipid subclasses detected (**Table 2**). In fraction 1, phosphatidylethanol (PEt) was significantly lower in Q175/Q7 mice versus Q7/Q7 ($p = 0.0469$, unpaired *t*-test, $N = 9$; **Table 2** and **Supplementary Figure 4A**, middle panel). In fraction 2, LPI was significantly decreased in Q175/Q7 mice compared to Q7/Q7 ($p = 0.0452$, unpaired *t*-test, $N = 9$; **Table 2** and **Supplementary 4A**, bottom panel); this change was due to only one species detected and although not significantly different in fraction 1, an inverse change occurred in fraction 1 with more LPI in Q175/Q7 than in Q7/Q7 (**Figure 3A**), showing a similar redistribution pattern to the proteins in **Figure 2**. Intriguingly, a significant increase (nearly 3.5 fold) in Sterol (ST) occurred in Q175/Q7 compared to Q7/Q7 in fraction 2 (**Table 2** and **Supplementary Figure 4B**). The only species measured in this subclass was cholesterol ester (ChE, also known as cholesteryl ester) (**Figure 3B**). In contrast to LPI, cholesterol ester increased in fraction 2 and trended to increase in fraction 1 in Q175/Q7 samples, suggesting an overall increase of cholesterol ester in the HD fractions instead of a shift from one fraction to another. To further validate the change in cholesterol ester levels we measured total cholesterol in fractions 1 and 2 using an Amplex colormetric assay which measures both cholesterol and cholesterol ester. Results showed a trend toward the same results as that found by LC MS (increased in both fractions 1 and 2 for Q175/Q7 versus Q7/Q7), but did not reach significance (**Supplementary Figure 5**).

Looking at individual lipid species at 6 months revealed numerous changes (**Supplementary Tables 1**, **2**) in addition to LPI and cholesterol ester. A species of cardiolipin (CL), which is a component of mitochondria, was significantly decreased

TABLE 2 | Altered lipid classes.

6 months F1							
Subclass	**Subclass names**	**# of species within subclass**	**Mean Q7/Q7 F1**	**SD Q7/Q7 F1**	**Mean Q175/Q7 F1**	**SD Q175/Q7 F1**	***T*-test**
PEt	Phosphatidylethanol	4	0.00037	0.00023	0.00018	0.00011	0.04686
6 months F2							
Subclass	**Subclass names**	**# of species within subclass**	**Mean Q7/Q7 F2**	**SD Q7/Q7 F2**	**Mean Q175/Q7 F2**	**SD Q175/Q7 F2**	***T*-test**
ChE	Sterol	1	0.00001	0.00002	0.00005	0.00003	0.01206
LPI	Lysophosphatidylinositol	1	0.00003	0.00002	0.00001	0.00001	0.04521
2 months F1							
Subclass	**Subclass names**	**# of species within subclass**	**Mean Q7/Q7 F1**	**SD Q7/Q7 F1**	**Mean Q175/Q7 F1**	**SD Q175/Q7 F1**	***T*-test**
Cer	Ceramides	101	0.00444	0.00100	0.00244	0.00087	0.00037
CerG2	Simple Glc series	1	0.00001	0.00001	0.00000	0.00000	0.04463
MGDG	Monogalactosyldiacylglycerol	14	0.00058	0.00058	0.00010	0.00010	0.03814
PA	Phosphatidic acid	18	0.00076	0.00057	0.00027	0.00028	0.04229
PIP2	Phosphatidylinositol 2	3	0.00004	0.00004	0.00000	0.00000	0.01366
SQDG	Sulfoquinovosyldiacylglycerol	3	0.00011	0.00010	0.00000	0.00001	0.01099
STd	Steroid	54	0.00116	0.00095	0.00335	0.00212	0.01636
phSM	Sphingomyelin (phytosphingosine)	6	0.00018	0.00010	0.00003	0.00007	0.00181
2 months F2							
Subclass	**Subclass names**	**# of species within subclass**	**Mean Q7/Q7 F2**	**SD Q7/Q7 F2**	**Mean Q175/Q7 F2**	**SD Q175/Q7 F2**	***T*-test**
AcCa	Acylcarnitine	44	0.60458	0.24917	0.32401	0.20944	0.02024
DG	Diglyceride	98	0.03664	0.03203	0.00601	0.00415	0.02095

Values in columns 4–7 represent total class intensities standardized to total intensity for each sample. Red, decreased in Q175/Q7; Green, increased in HD.

Q175/Q7 in fraction 1 compared to Q7/Q7 (**Figure 3C**). In fact, the cardiolipin subclass which includes numerous species also trended to be lower in fraction 1 but did not reach significance (**Supplementary Figure 4A**, bottom panel). Since no changes in fraction 2 were measured, this result suggests either a loss of this species of cardiolipin from mitochondria or possibly a loss of mitochondria themselves from fraction 1, possibly from the HD synapses. Another interesting change was for a species of phytosphingosine (phSM; **Figure 3D** and **Supplementary Tables 1**, **2**) which changed inversely in fractions 1 and 2 with an increase in fraction 1 and a decrease in fraction 2, similar to LPI.

A significant change in levels of one species of PIP2 occurred (**Figure 4** and **Supplementary Table 2**). PIPs are of interest because they are involved in important signal transduction pathways and wild-type and mutant Huntingtin bind them (Kegel et al., 2005, 2009). They can act as secondary messengers (as in PLC signaling) or to recruit protein complexes to membranes (as in PIK3 signaling). Using the MBTE extraction method, three species of the signaling glycerophospholipids PIP2 were detected (**Figure 4**). One PIP species (C44 H84 O18 N0 P3) was significantly lower in Q175/Q7 fraction 2 compared to Q7/Q7 (**Figure 4A**) and was much less abundant than a second species that was not significantly different (C46 H88 O18 N0 P3) (**Figure 4B**). Because the mass of the phospholipid head group is identical, using this method it is not possible to identify the exact PIP2 without further study using standards and methods designed to optimize PIP extraction and analysis (HPLC or GC methods). However, given the relative abundance of the second PIP2 species (C46 H88 O18 N0 P3) compared to the first (note *y*-axis in **Figure 4B** compared to A), we speculate that (C46 H88 O18 N0 P3) is PI (4,5)P2 which is known to be a fold more abundant than PI (3,4)P2 and PI(3,5)P2. Changes in individual species of PE, PC and PS reflected subtle changes in acyl chain usage rather than shifts between compartments at 6 months.

Next, we performed a lipidomic analysis in fractions from 2 months old mice to see if changes observed in HD mice at 6 months occur early or were degenerative or compensatory. Bar graphs in **Supplementary Figure 6** show different subclasses of lipids grouped by their relative abundance and compared between Q7/Q7 and Q175/Q7 HD mice at 2 months (Glycerophospholipids, **Supplementary Figures 6A,C**; "Other Lipids", **Supplementary Figures 6B,D**; $N = 9$ per genotype). Similar to results at 6 months the abundance of the many Glycerophospholipid subclasses did not differ by genotype in either fraction (PC, PE, SM, PS, PI, PG; **Supplementary Figures 6A,C**). However, several changes were identified among lipid subclasses of lower abundance (**Table 2**). In fraction 1, significant changes in 8 subclasses were found (Ceramides, neutral glycosphingolipids, MGDG, PA, PIP2, SQGQ, Sterols, and sphingolipid (phSM) (**Table 2** and **Supplementary Figure 6**). The reduction in subclass of phSM in fraction 1 mirrors the change that was observed in a species of phSM at 6 months.

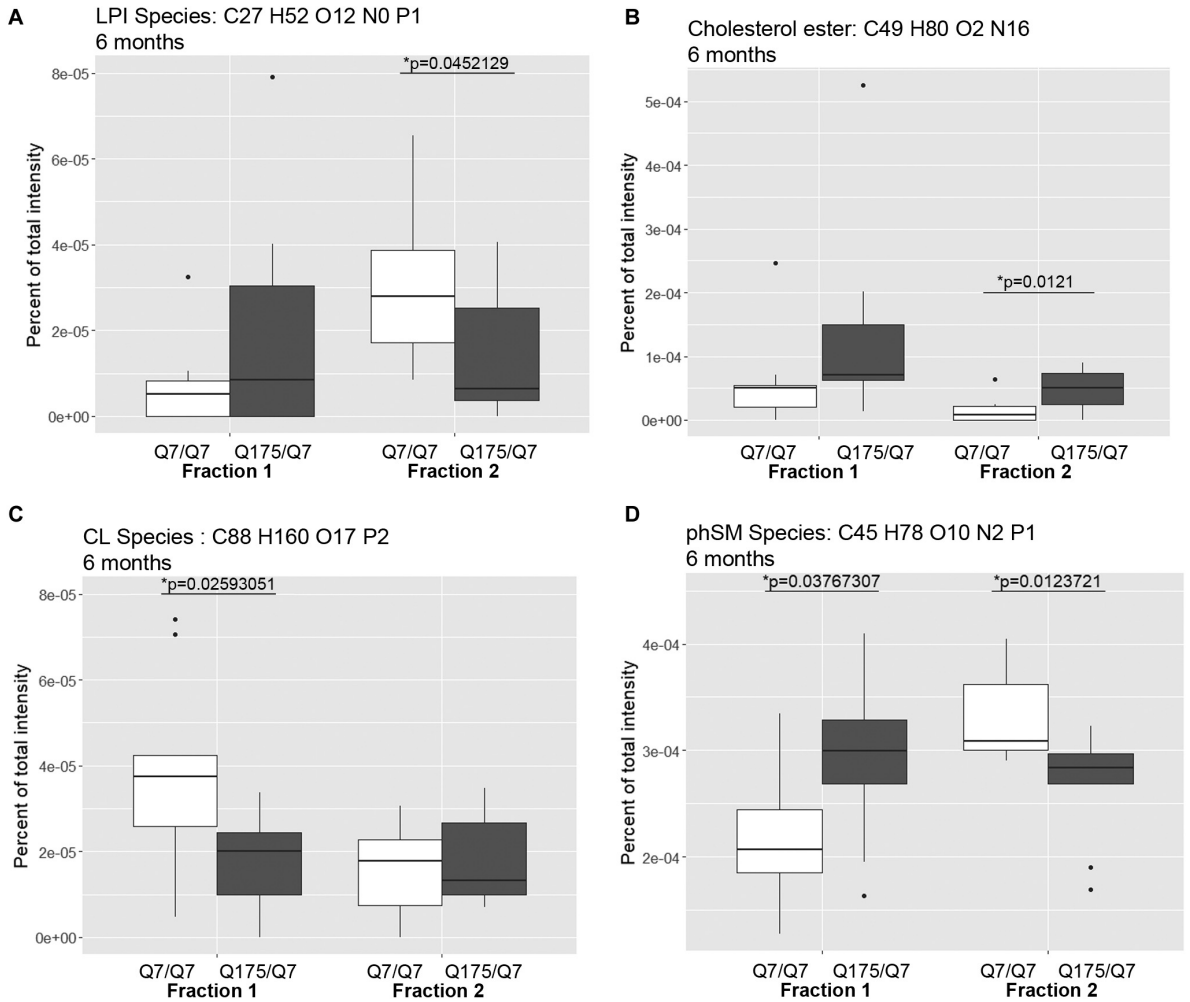

FIGURE 3 | Levels of selected individual species of lipids detected by LC-MS/MS in fractions 1 and 2 of continuous density gradients of fractionated 6 months old Q175/Q7 and Q7/Q7 striata. Graphs show Tukey-style box plots where the lower and upper hinges correspond to the first and third quartiles (the 25th and 75th percentiles) as described in section "Materials and Methods." Data beyond the end of the whiskers are called "outlying" points and are plotted individually. Outliers were not removed from statistical analysis. NOT DETECTED indicates species was not detected using the modified 80% rule (Yang et al., 2015). Changes at 6 months are shown for specific species of **(A)** lyso-phosphoinositol (LPI), **(B)** Cholesterol ester, **(C)** Cardiolipin (CL), and **(D)** Sphingomyelin, phytosphingosine (phSM). All significant changes are shown in **Supplementary Tables 1–8**. Comparisons were made between genotype for each fraction (*$p < 0.05$, unpaired *t*-test, $N = 9$ per group).

In fraction 2, acylcarnitine (Acca) and diacylglyceride (DG) content were significantly decreased in Q175/Q7 compared to Q7/Q7 (**Table 2** and **Supplementary Figure 6D**). Cholesterol ester was not detected at 2 months; Zymosterol ester was detected at 2 months but was not significantly changed (**Supplementary Figure 6B**).

Looking at individual lipid species at 2 months also revealed numerous changes among lipids that were detected in both genotypes (**Supplementary Table 3** for fraction 1 and **Supplementary Table 6** for fraction 2). Many species of lipids were detected in Q7/Q7 but not detected in Q175/Q7 (**Supplementary Table 4** for fraction 1 and **Supplementary Table 7** for fraction 2). The reverse was also true: some lipids were detectible in Q175/Q7 that were not detected in Q7/Q7 (**Supplementary Table 5** for fraction 1 and **Supplementary Table 8** for fraction 2). One of the changes at 2 months was in a species of Acylcarnitine (Acca C18 H30 O4 N1) (**Figure 5A**) which was significantly higher in Q175/Q7 compared to Q7/Q7 for both fractions. This increase contrasts with results for Acca as a subclass which was significantly reduced in Q175/Q7 compared to Q7/Q7 in fraction 2 (**Table 2**). One possibility is that the decrease of several species of Acca drives a compensatory increase of this species of Acca or vice versus. A species of PA was significantly increased in fraction 1 (PA C39 H74 O8 N0 P1) (**Figure 5B**) but was not detected in fraction 2. A species of sphingomyelin (SM C43 H80 O6 N2 P1) had a similar profile to with a significant increase in fraction 1 but not detected in fraction 2 (**Figure 5C**). These results suggest real increases in these glycerophospholipid species and not just a shift that occurred with cell membrane redistribution in the gradient.

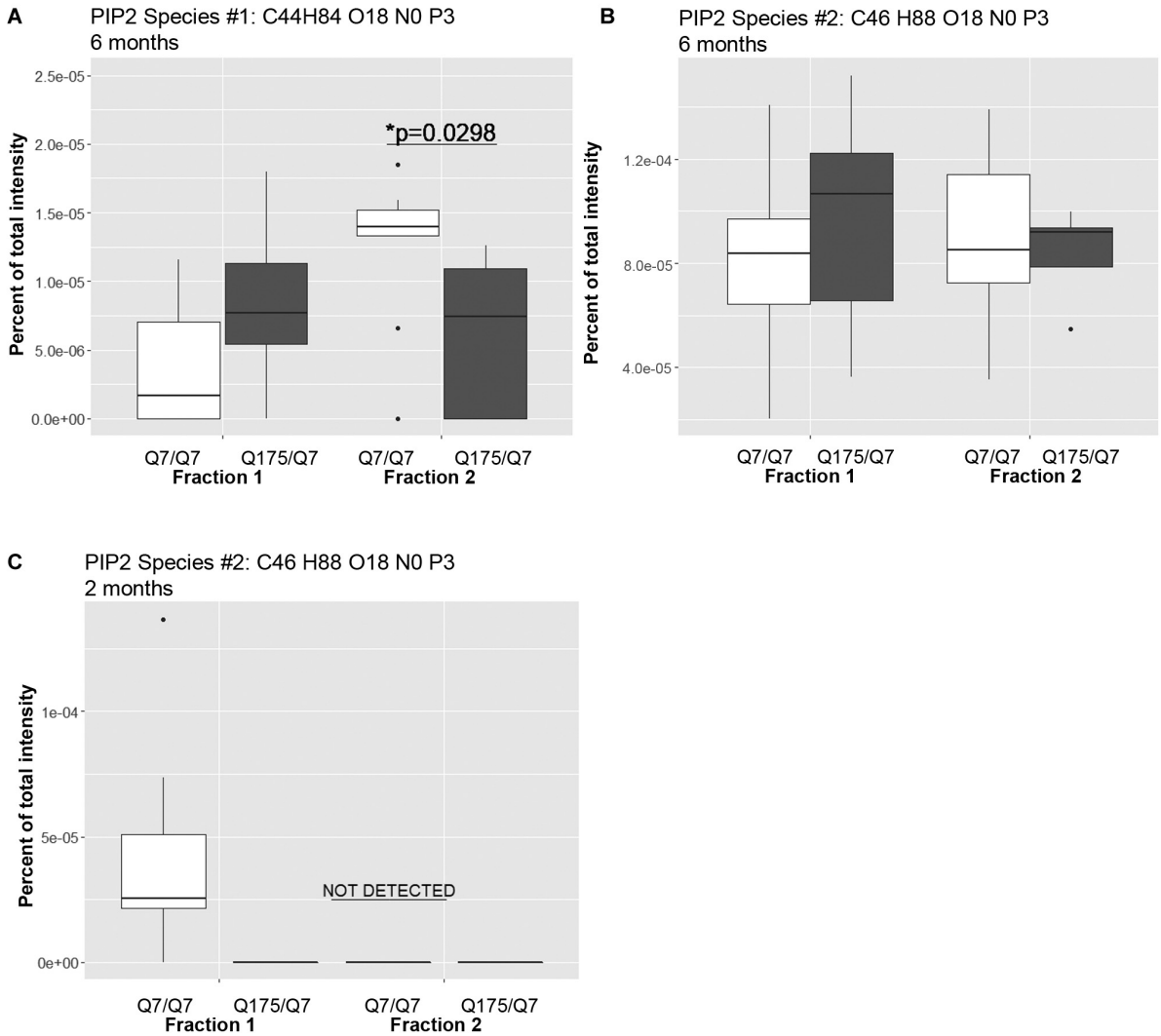

FIGURE 4 | Levels of PIP2 species detected by LC-MS/MS in fractions 1 and 2 of continuous density gradients of fractionated Q175/Q7 and Q7/Q7 striata. Graphs show Tukey-style box plots where the lower and upper hinges correspond to the first and third quartiles (the 25th and 75th percentiles) as described in section "Materials and Methods." Data beyond the end of the whiskers are called "outlying" points and are plotted individually. Outliers were not removed from statistical analysis. NOT DETECTED, indicates species was not detected using the modified 80% rule (Yang et al., 2015). **(A,B)** Levels of the two PIP2 species detected at 6 months in fractions 1 and 2. In **(A)**, there was a significant increase in PIP2 species #1 (C44 H84 O18 N0 P3) in fraction 2 between Q7/Q7 and Q175/Q7 (*$p <$ 0.05, unpaired *t*-test, $N = 9$ per group), whereas there was no significant difference in the second species in either fraction between genotypes **(B)**. **(C)** Levels of PIP2 species #2 (C46 H88 O18 N0 P3) detected in fractions 1 and 2 at 2 months. This was the sole species detected at 2 months and was only detected in fraction 1 from Q7/Q7 striata.

Within the PIP2 group, a third PIP2 species #2 (C46 H88 O18 N0 P3) was detected in Q7/Q7 in fraction 1 but "not detected" in other fractions (**Figure 4C**). This same species of PIP2 was not changed at 6 months (**Figure 4B**).

Together, these data showed no change in the overall levels of glycerophospholipids that constitute the bulk of membranes in HD mice. However, distinct changes in individual species of PIPs occurred that reveal altered PI3 kinase signaling. Reduced levels of cardiolipin in both fractions from Q175/Q7 striata may have implications for mitochondrial function. Finally, a time dependent increase in cholesterol ester at 6 months in both fractions is indicative of dysfunctional intracellular cholesterol flux which may in turn impact cholesterol levels in membranes there-by altering the behavior of organelles in gradients.

Electron Microscopy of Fractions 1 and 2 Reveals Differences in Subcellular Synaptic Components and Differences in Particle Size and Number Between 6-Month Old Q7/Q7 and Q175/Q7 HD Mice

The results above showed that the HD mutation affected the subcellular distribution of membrane associated proteins and

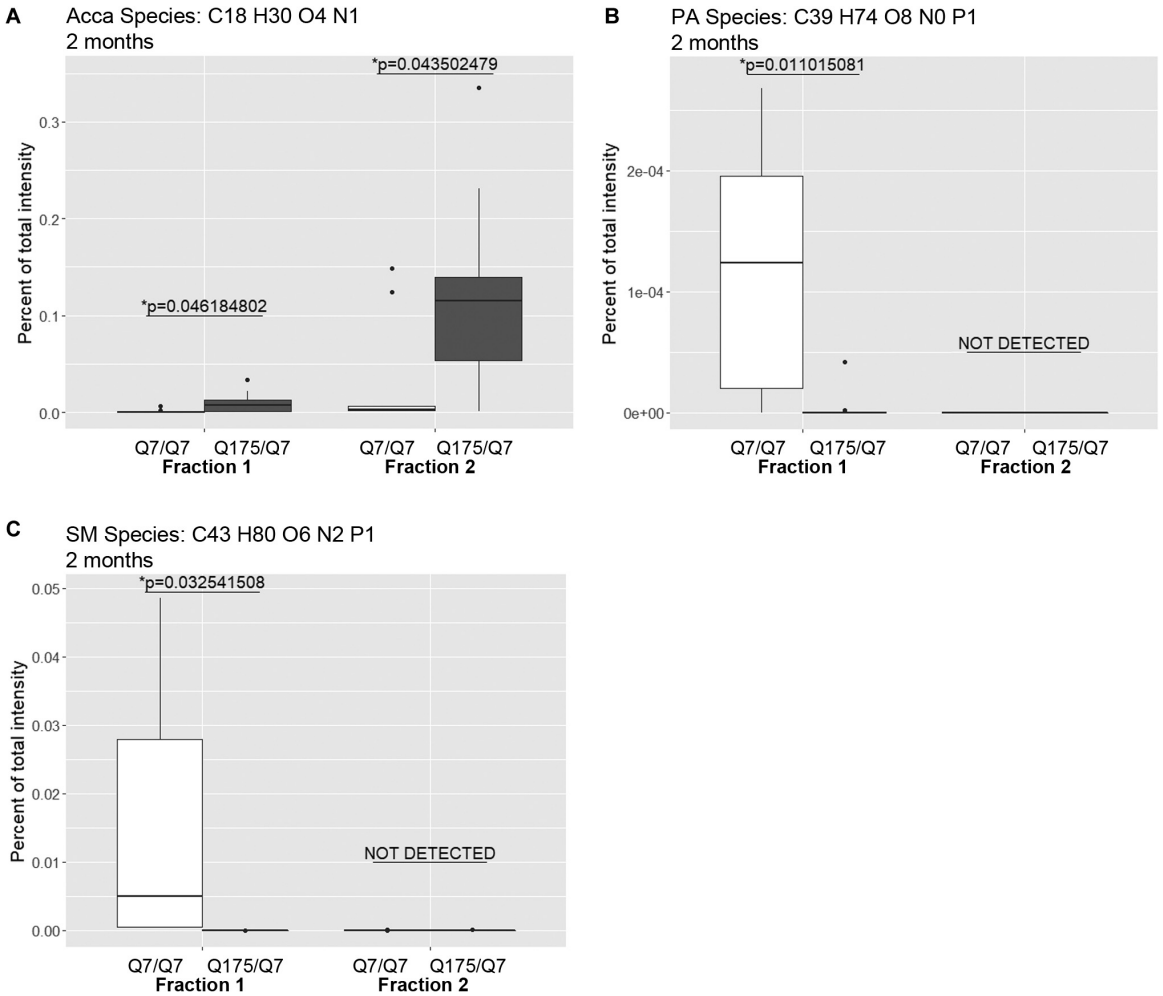

FIGURE 5 | Levels of selected individual species of lipids detected by LC-MS/MS in fractions 1 and 2 of continuous density gradients of fractionated 2 months old Q175/Q7 and Q7/Q7 striata. Graphs show Tukey-style box plots where the lower and upper hinges correspond to the first and third quartiles (the 25th and 75th percentiles) as described in section "Materials and Methods." Data beyond the end of the whiskers are called "outlying" points and are plotted individually. Outliers were not removed from statistical analysis. Changes at 2 months are shown for specific species of **(A)** Acyl Carnitine (Acca), **(B)** Phosphatidic acid (PA), and **(C)** Sphingomyelin (SM). Cholesteryl ester species was not detected by LC-MS/MS in the 2-month samples. All significant changes are shown in **Supplementary Tables 1–8**. Comparisons were made between genotype for each fraction (*$p < 0.05$, unpaired *t*-test, $N = 9$ per group).

lipids in light fractions 1 and 2. To verify the ultrastructural constituents of fractions 1 and 2, electron microscopic analysis was performed. Drops of each fraction were placed on formvar grids and stained with uranyl acetate and lead citrate. Analysis at 30,000 X revealed microscopic fields that were heterogeneous in the type and density of subcellular structures and included those characteristic of synaptic enrichment as previously described by Whittaker et al. (1964). Fractions 1 and 2 of Q7/Q7 and Q175/Q7 mice (**Figures 6A–H**) contained areas with scattered synaptic vesicles and axon terminals that were vesicle filled (**Figures 6A,G**) or partly devoid of vesicles (lower axon terminal in **Figure 6F**). The synaptic vesicles were 40–50 nm in diameter and mostly lucent. Some axon terminals had mitochondria (**Figure 6A**). The plasma membrane encircling the axon terminals was more electron dense than the vesicle membranes and appeared interrupted (best seen in upper axon terminal of **Figure 6A**). The axon terminals appeared singly or in clusters (**Figures 6 A,C,F,G**). The axon terminals were mainly round or ovoid shaped in Q7/Q7 fraction 1 and 2 and in Q175/Q7 fraction 1. In Q175 fraction 2, terminals had irregular shapes, electron dense cytoplasm, and some larger irregular shaped vesicles (**Figure 6G**). Some axon terminals that were seen in clusters appeared proximal to tubular shaped structures with short branches that we interpreted to be pre-terminal axons. These pre-terminal axons which were also seen separate from axon terminals, appeared mostly in fraction 2 of Q7/Q7 preparations and fraction 1 of Q175/Q7 samples (**Figures 6D,F**). Present but more scattered in both fractions were larger round clear vesicles (100–200 nm) consistent with the size of microsomes that are derived from ER or lipid droplets. Also present were electron lucent irregular-shaped tubulovesicular membranes (**Figures 6B,E,H**) that may belong to ER or endosomes.

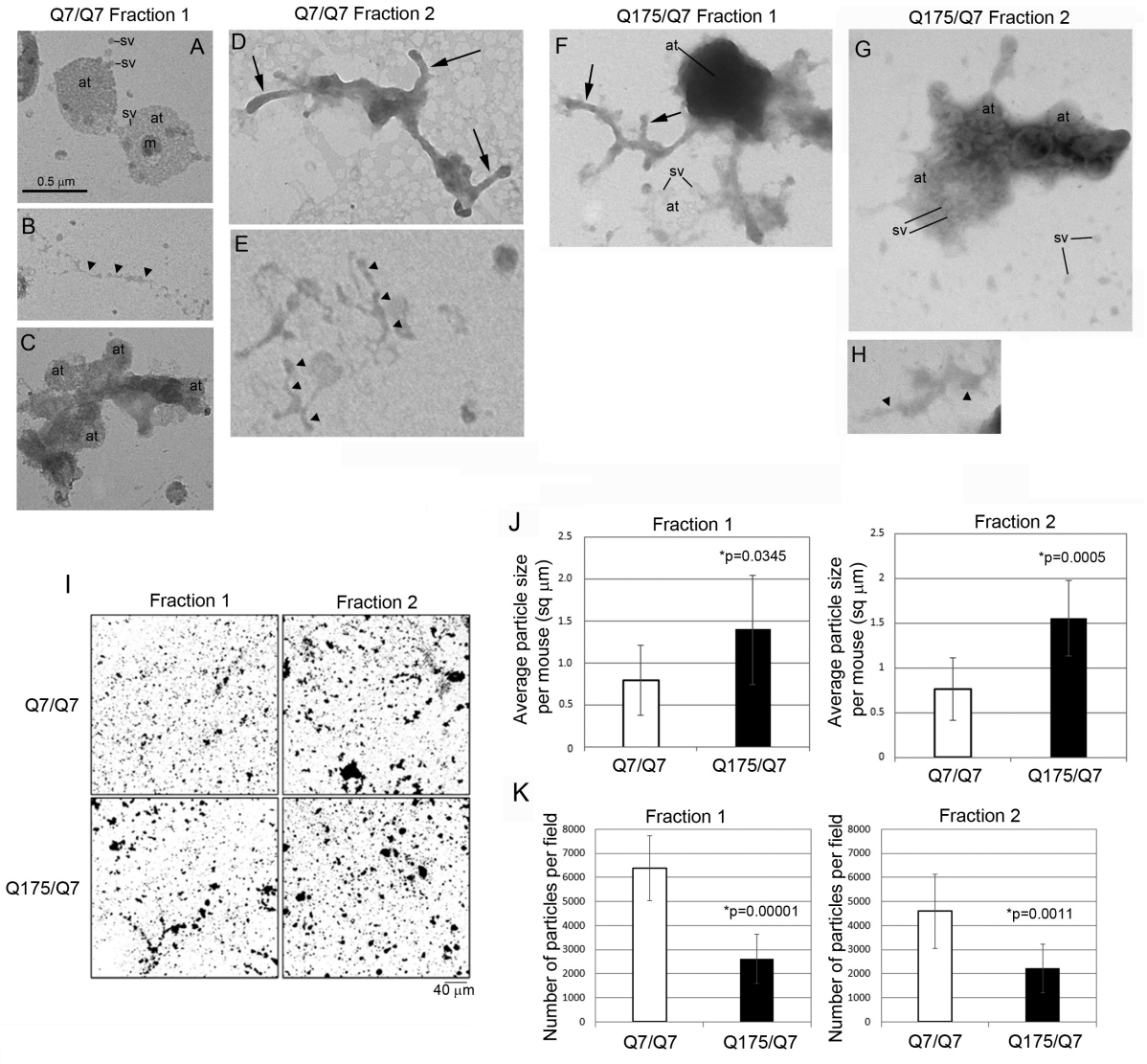

FIGURE 6 | Electron microscopic analysis of subcellular morphology and particle sizes and numbers in fractions 1 and 2. **(A–H)** EM images of fractions 1 and 2. Specimens for EM analysis were prepared and analyzed as described in section "Materials and Methods." Sv, synaptic vesicle; at, axon terminal; arrowheads, tubular-vesicular membranes that may be ER or endosomes **(B,E,H)**; arrows, preterminal axons and axon branches. Note that axon terminals (at) appear in groups in **(A,C,F)**, some are filled (axon terminals in **A**) or partly filled with vesicles (lower axon terminal in **F**) or overlap and appear electron dense (top axon terminal in **F**). Synaptic vesicles (sv) appear inside the axon terminals and scattered outside the terminals **(A,G)**. Note in **(G)** that axon terminals have irregular shapes, electron dense cytoplasm, and some larger irregular shaped vesicles. Scale bar in **A** = 0.5 μm and applies to all images. **(I–K)** Analysis of particle sizes and number in fractions 1 and 2. **(I)** shows representative electron microscope images of fractions 1 and 2 taken at 5,000× that were used for quantification. Scale bar = 40 μm and applies to all images. Data in **(J,K)** were obtained using ImageJ. Threshold was set for images on automatic settings using Renyi entropy method. Particles were excluded that were only 1 pixel. Students *t*-test was performed on *N* = 9 animals for each genotype. Bar graph in **(J)** shows mean particle size ± SD per mouse for Q7/Q7 and Q175/Q7 samples for fractions 1 and 2 (*$p < 0.05$, unpaired *t*-test, *N* = 9 mice, 7–45 images per mouse). There are significantly larger particles in Q175/Q7 samples compared to Q7/Q7 in fraction 1 and fraction 2. Bar graph in **(K)** shows number of particles ± SD per field for Q7/Q7 and Q175/Q7 samples for fractions 1 and 3 (*N* = 9 mice, 7–45 image per mouse). There are significantly fewer particles in Q175/Q7 samples compared to Q7/Q7 in fraction 1 and fraction 2.

Since there was heterogeneity across microscopic fields and some difference in organelle distribution in fractions 1 and 2 between Q7/Q7 and Q175/Q7 HD samples, we sought to determine whether the overall density and size distribution of subcellular structures was the same between Q7/Q7 and Q175/Q7 HD mice. EM analysis was performed on 500x images (**Figure 6I**) to examine particle size and number in fractions 1 and 2 of the 6-month-old Q7/Q7 and Q175/Q7 HD mice as described in Methods. Results showed a significant difference in particle size and number of particles in fractions 1 and 2 between Q7/Q7 and Q175/Q7 HD (**Figures 6J,K**). Particle size was significantly increased in both fractions 1 and 2 prepared from Q175/Q7 HD compared to Q7/Q7 mice (**Figure 6J**). Conversely, particle number was reduced in both fractions 1 and 2 prepared from Q175/Q7 HD compared to Q7/Q7 (**Figure 6K**).

Analysis of Human Putamen Shows Alterations in Subcellular Distribution of Some Synaptic Proteins

Previous study has shown successful isolation of synaptosome fractions from postmortem fresh brain tissue of different species using sucrose for separation (Shinagawa et al., 1963; Whittaker et al., 1964; Garey et al., 1974; Sapp et al., 2020). To determine whether frozen postmortem tissue could be assessed using iodixanol gradient fractionation and if HD mutation affected the subcellular distribution of proteins in the synaptic compartment, we examined samples of human putamen from 3 controls to 3 HD postmortem brains (**Supplementary Table 9**). Relative distribution of subcellular markers after fractionation is similar to that seen in mice although SNAP25 separated to higher fractions than in mice in human putamen (**Figures 7A,B**). Similar to the mouse western blot results, no difference in distribution of wild-type and mutant Huntingtin in the fractions between control and HD putamen was observed (**Figures 7C,D**). There was a significant difference between control and HD in fraction 3 for Calnexin ($p = 0.0052$, $N = 3$, unpaired t-test) and GLUT3 ($p = 0.047$, $N = 3$, unpaired t-test) (**Figures 7E,F**). There was no significant difference in subcellular distribution between control and HD for Na^+/K^+ ATPase, NMDAR 2b, SNAP25, VGLUT1, and PSD95 (**Supplementary Figure 7**). These results show that human postmortem tissue can be used for analysis of subcellular

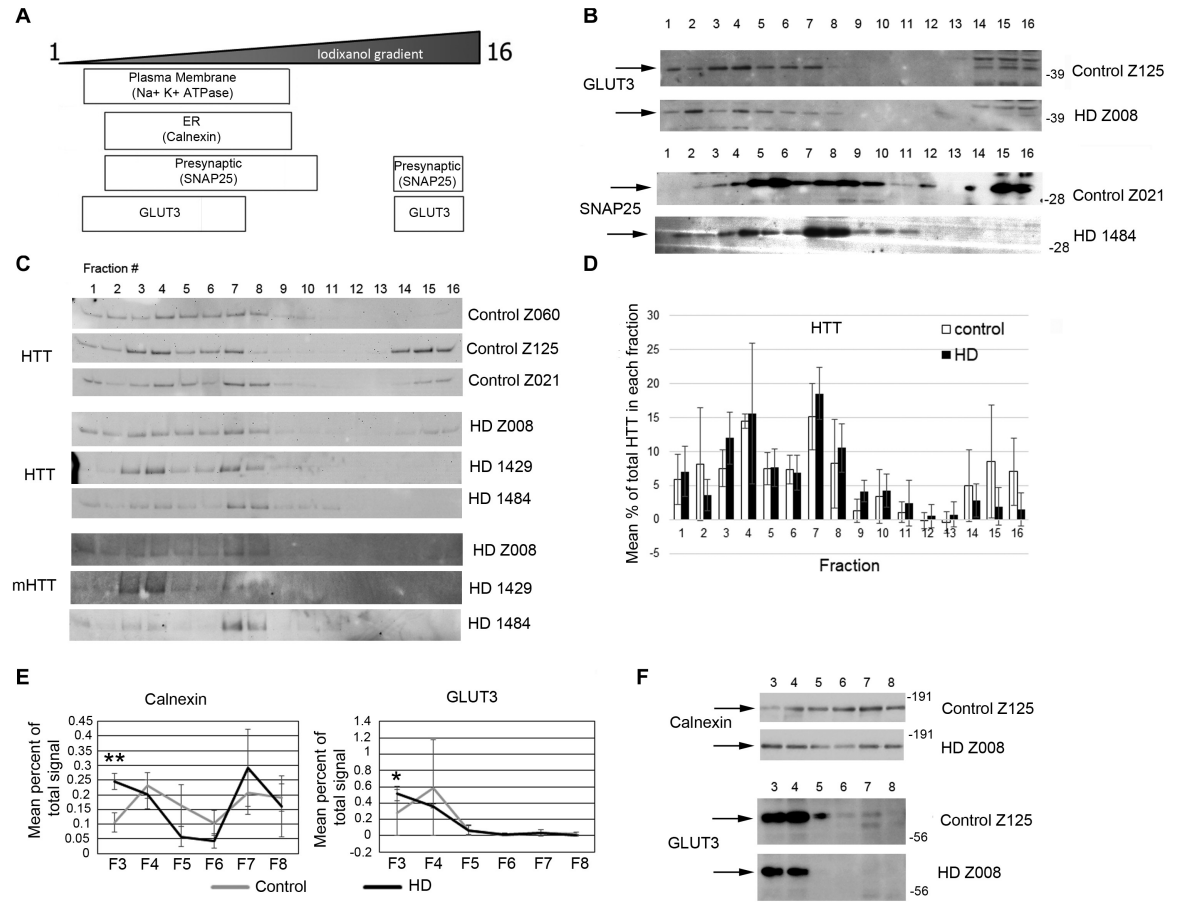

FIGURE 7 | Subcellular fractionation by density gradient ultracentrifugation of human putamen. Dorsal putamen was fractionated as described in section "Materials and Methods." Fractions were assessed by SDS-PAGE and western blot analysis using different cell compartment markers. Fractions 1–16 were removed from top to bottom. Equal volumes of each fraction were loaded per lane. **(A)** Diagram at left shows approximate distribution of proteins representative of different subcellular compartments in the control putamen. **(B)** Shown are representative images of western blots detecting GLUT3 and SNAP25 in control and HD putamen. **(C)** Shown are WB images of Huntingtin (HTT) and mutant HTT (mHTT) signals in 16 fractions from all human putamen samples. mHTT was detected with 1C2 which recognizes the expanded polyQ region in mutant HTT but not HTT in control samples. **(D)** Bar graph shows mean percent ± SD of HTT signal obtained with antibody Ab1 in control and HD human putamen in each of 16 fractions as a percent of total HTT signal summed across all fractions. There was no significant difference in HTT signal between control and HD in any of the fractions ($N = 3$). **(E)** Fractions 3–8 were analyzed in pairs and run on the same gel to eliminate variability due to different runs. These fractions were chosen because most proteins tested had peaks in this range. Seven probes were analyzed by western blot for each gel (Calnexin, GLUT3, Na+/K+ ATPase, NMDAR 2b, PSD95, SNAP25, and XK). Band intensity for each fraction was standardized to sum of intensities for bands in fractions 3–8. Line graphs show mean percent of total signal ± SD obtained in fractions 3–8 for each fraction ($N = 3$). There was a significant difference in percent of total signal in fractions 3–8 in fraction 3 for Calnexin (**$p = 0.0052$, $N = 3$, unpaired t-test for all analyses) and GLUT3 (*$p = 0.047$). **(F)** Representative images of western blots for Calnexin and GLUT3 in control and HD putamen related to the data shown. See **Supplementary Figure 5** for other line graphs.

fractions using iodixanol and that the HD mutation alters the distribution of some synaptic proteins.

DISCUSSION

Altered function of striatal neurons including synaptic interactions occurs early in HD pathogenesis. Here we used an HD mouse model (Q175/Q7) and human HD postmortem brain to address if there is a change in the subcellular distribution of membrane associated proteins and lipids in the HD striatum. We found a change in the relative distribution of wild-type and mutant Huntingtin in a single fraction (fraction 4) but a change in the distribution of five membrane proteins (intrinsic or membrane-associated) in synaptic fractions generated by iodixanol separation of Q175/Q7 HD mice versus Q7/Q7 mouse brain lysates providing evidence to support synaptic changes in the HD mice. Lipidomic analysis of these fractions identified changed distribution of cholesterol ester, cardiolipin, PIP2 and numerous other lipids. EM analysis confirmed the presence of synaptic profiles and revealed abnormal morphology of some axon terminals and vesicles in Q175/Q7 HD mice. Together, these data suggest a physical and/or structural change in membrane or organelle integrity or a redistribution of several proteins among membrane compartments which becomes evident after disruption by homogenization and fractionation.

Mounting evidence from studies using many different approaches have shown that changes in synaptic function are the basis for early cognitive and psychiatric symptoms in HD (Giralt et al., 2012) and account for deficits in motor control including initiation and execution of movement (Reiner and Deng, 2018) and involve changes in pre- and postsynaptic sites (Nithianantharajah and Hannan, 2013). Reduced glutamate release in HD has been ascribed to impaired synaptic release due to physical association of mutant Huntingtin with synaptic vesicles (Li et al., 2003). Impaired glutamate release has also been reported in YAC128 transgenic mice (Joshi et al., 2009) and in synaptosomes from Q140/Q140 knock-in mice (Valencia et al., 2013). Altered GABA transmission occurs in R6/2 mice (Cepeda et al., 2004). Mutant Huntingtin expression altered functions of Synapsin 1 when targeted to the synapse in transgenic mice (Xu et al., 2013), reduces transcription of Synaptic Vesicle Protein 2C in N171-82Q transgenic mice (Peng et al., 2018) and affected interactions with Syntaxin 1A (Kaltenbach et al., 2007). Differences were found in levels of pre- and postsynaptic proteins in Q50/Q7, Q140/Q7, Q175/Q7, and Q140/Q140 HD mouse brain synaptosomes compared to wild-type including SCN4B, GABAa1, calmodulin, VGlut1, VGlut2, SNAP25, and PSD95 (Valencia et al., 2013; Sapp et al., 2020). Significant loss of the postsynaptic signaling proteins, PDE10a and DARPP32 was reported by us and others (Beaumont et al., 2016; Hosp et al., 2017; Skotte et al., 2018; Sapp et al., 2020). Here using a biochemical analysis of subcellular fractions separated by iodixanol (OptiPrep) we found no overall change in Huntingtin distribution except in fraction 4 but an altered distribution of 5 proteins within synaptic fractions of Q175/Q7 HD mice. They include plasma membrane proteins (Na^+/K^+ ATPase and GLUT3), presynaptic (vGlut1) and postsynaptic proteins (PSD95 and NMDAR 2B). A shift in presynaptic SNAP25 was nearly significant ($p = 0.0527$) as was another post synaptic receptor protein, AMPA Glu1A ($p = 0.06$). The results further support the idea that both pre- and postsynaptic features are affected in HD.

Four of the five proteins with aberrant subcellular distribution in HD mice are trans membrane proteins bearing membrane spanning domains. This finding suggests that there is (1) a change in membrane architecture which transforms biochemical behavior or (2) modified targeting/distribution among cellular membranes. In HD mouse models, redistribution of NMDA 2b between postsynaptic and extra-synaptic sites on plasma membranes has been demonstrated using electrophysiology and immunofluorescent readouts (Fan et al., 2007; Milnerwood et al., 2012). The shift we observed in biochemical gradients for NMDA 2b from fraction 2 in Q7/Q7 mice to fraction 1 in Q175/Q7 preparations may reflect the shift from postsynaptic to extra-synaptic membranes described by Raymond and colleagues. The extra-synaptic shift they described for NMDA 2b is regulated by palmitoylation at cysteine cluster II (Kang et al., 2019). Palmitoylation occurs dynamically for many synaptic proteins (Kang et al., 2008) and can regulate their trafficking (Kang et al., 2004). Interestingly, PSD95 was shifted and SNAP25 was trending toward significance ($p = 0.0527$) and both are also palmitoylated. Thus, palmitoylation catalyzed by the Huntingtin interactor proteins HIP14 (zDHHC17) or HIP14L (zDHHC13) may account for the biochemical redistribution we observe. In fact, palmitoylation has been reported for vGlut1 (Zareba-Koziol et al., 2018), Na^+/K^+ ATPase (Plain et al., 2020), and GLUT3 (Stapel et al., 2019), AMPAR and GABAR (Zareba-Koziol et al., 2018).

Abnormal receptor mediated endocytosis and recycling could explain the redistributed proteins seen in our study in HD mice. Wild-type Huntingtin interacts with Rab11 (Li et al., 2008) and mutant Huntingtin disrupts Rab11 dependent recycling of transferrin, GLUT3, and EAAC1 receptors (Li et al., 2010). Huntingtin also interacts with proteins involved in endocytosis including AP2 (Faber et al., 1998), and dynamin (El-Daher et al., 2015). Depolarization-dependent endocytosis is a specific form of endocytosis at synapses and is used to retrieve membrane and proteins after synaptic vesicle release [reviewed by Lou (2018)] and utilizes proteins known to interact with and be affected by mutant Huntingtin such as Synapsin 1 (Valencia et al., 2013; Xu et al., 2013). One possibility is that depolarization dependent recycling is changed in HD creating altered distribution of membrane proteins between the plasma membrane and internal vesicles.

Remarkably, frozen samples of human postmortem brain of control and HD individuals could be separated by iodixanol (OptiPrep) to reveal a relative distribution of subcellular markers and of Huntingtin similar to that in mice, although the synaptic proteins PSD95 and SNAP 25 were separated to higher fractions (3–6) than in mice in both control and HD putamen. Since

membranous compartments may change with freezing and thawing, one would not expect the frozen postmortem human tissue to fractionate identically to freshly dissected mouse tissue. Only GLUT3 and calnexin were changed in human HD putamen with both proteins being increased compared to control in fraction 3. The small number of cases available for analysis ($N = 3$) may account for the limited number of proteins affected. The transmembrane protein GLUT3 which was also changed in Q175/Q7 HD mice striatum (decreased compared to wild-type in fraction 2) is noteworthy since as noted above this protein is the major glucose transporter in neurons and its recycling is impaired in HD due to reduced Rab11 activity (McClory et al., 2014).

Lipidomics of synaptic fractions 1 and 2 from wild-type and HD mice were compatible with the biochemical protein data in revealing significant lipid changes in these fractions. For example, there was increased cholesterol ester content in Q175/Q7 HD mice synaptic fractions. Cholesterol ester is a storage form of cholesterol created by modification with an acyl chain by esterification at the OH group of cholesterol (by Acat-1 and fatty acyl co-A). Cholesterol ester is moved within cells via lipid transfer proteins such as cholesterol ester transport protein (CETP) and is stored almost exclusively in lipid droplets (Wong et al., 2019). A change in the load of cholesterol ester may contribute to altered membrane stiffness by sequestering cholesterol away from plasma membranes. Cholesterol is an important component of plasma membranes and is required for synaptogenesis (Mauch et al., 2001), normal learning (Xu et al., 1998), and axon regeneration (de Chaves et al., 1997). Changes in cholesterol levels are reported to affect both presynaptic events (Thiele et al., 2000; Dason et al., 2010, 2014; Linetti et al., 2010), and postsynaptic architecture including localization of NMDAR (Frank et al., 2004, 2008) and AMPARs (Hering et al., 2003; Renner et al., 2009; Martin et al., 2014). Augmenting cholesterol in brain improved electrophysiology readouts in R6/2 HD mice which expresses mutant Huntingtin exon 1 including normalizing both membrane capacitance and inhibitory postsynaptic current (IPSC) frequencies in striatal medium spiny neurons (Valenza et al., 2015a). Although behavior deficits were not rescued, some cognitive dysfunction was improved in R6/2 mice treated with direct delivery of cholesterol to brain and levels of some synaptic proteins were preserved (Valenza et al., 2015a).

There is evidence that the HD mutation affects cholesterol levels. We and others have reported decreased levels of total cholesterol in Q140/Q140 HD mouse primary neurons (Ritch et al., 2012), synaptosomes (Valenza et al., 2010) and brain (Valenza et al., 2007). It is noteworthy that the distribution of cholesterol enriched lipid rafts which mediate signaling at plasma membranes is altered in HD (Valencia et al., 2010). In human plasma 24S-hydroxycholesterol (24S-OHC) a form of cholesterol modified to allow efflux across the blood brain barrier is reduced (Leoni et al., 2008, 2013). These findings have led to mechanistic studies supporting the hypothesis that cholesterol synthesis is reduced in HD (Valenza et al., 2005). However, cholesterol homeostasis is complex and increases in total cholesterol have also been reported using colorimetric assays (Trushina et al., 2006; Del Toro et al., 2010). Of note, knockout mice null for expression of CYP4A1, the enzyme which creates 24SOHC displays normal levels of cholesterol indicating tight feedback regulation: reduced efflux results in decreased production to maintain cholesterol homeostasis (Lund et al., 2003). Our data showing increased cholesterol ester in fractions containing synaptic elements suggest that in addition to reduced cholesterol production, altered redistribution within cells or flux may also play a role in changing membrane function. Indeed, changes in cholesterol flux affect membrane ordering and structure, ultimately impacting synaptic function including glutamate release (Petrov et al., 2020).

Other changes in lipid levels that we observed in HD mouse synaptic fractions may give insights into HD pathology. Cardiolipin was reduced in fraction 1 of Q175/Q7 HD mouse striatum at 6 months. We showed that wild-type and mutant Huntingtin have a strong association with cardiolipin *in vitro* (Kegel et al., 2009). Cardiolipin is enriched in mitochondrial membranes and its reduction in mitochondria of HD synapses could affect bioenergetics, a problem known to occur in HD. Cardiolipin is usually found on inner mitochondrial membranes (Chicco and Sparagna, 2007) but with apoptotic stimulation can also be located at the interface of inner and outer mitochondrial membranes (Gonzalvez et al., 2008). Mutant Huntingtin has been found on the outer mitochondrial membranes and can affect cytochrome c release and apoptosis (Choo et al., 2004; Orr et al., 2008). However, recently Huntingtin was detected in the intermembrane space of mitochondria and therefore could potentially be in contact with cardiolipin (Yablonska et al., 2019).

An increase in Acyl carnitine occurred in both fractions 1 and 2 of Q175/Q7 from striatum for one species and was higher as a subclass in fraction 2 at 2 months. DAG was also higher as a subclass in fraction 2 at 2 months. Acyl carnitine and DAG are precursor energy metabolites. Acyl carnitine is imported to mitochondria for conversion to ATP. The increased levels of Acyl carnitine could indicate reduced transport by lipid import/transport proteins into mitochondria or a loss of mitochondria both of which would result in reduced energy metabolism.

We found a change in a less abundant PIP2, most likely PI(3,4)P2 or PI(3,5)P2. Wild-type and mutant Huntingtin bind all PIP2s and mutant Huntingtin has altered binding to PIP3 (not detected here) and PIPs with lower affinity (Kegel et al., 2005, 2009). Mutant Huntingtin could affect the creation of PI(3,4)P2 and/or PI(3,5)P2 which is catalyzed by PI 3-kinase family members on cellular membranes including plasma membranes and autophagic vesicles. Alternatively, mutant Huntingtin could interfere with effector molecules that bind PIP2s. PIP2s are particularly important in synaptic compartments where PI(4,5)P2 controls endocytosis of synaptic vesicles in axon terminals [reviewed by Koch and Holt (2012)] and where PI(3,5)P2 has been shown to control localization of AMPA receptors post-synaptically (McCartney et al., 2014; Kim et al., 2017). Altered levels of these PIP lipid signaling molecules direct changes in membrane trafficking through Rab proteins (Tan et al., 2015) and changes in actin dynamics through Rac1. We have shown that a Rac1/PI 3-kinase/Huntingtin/alpha-actinin-2

protein complex forms incorrectly using lysate from wild-type and knock-in Q140/Q140 mouse striatum (Tousley et al., 2019b).

Consistent with our reported changes in PA in Q140/Q140 HD knock-in mice at 11 months (Vodicka et al., 2015), we saw changes in the subclass PA with decreased PA in Q175/Q7 fraction 1; some species of PA were undetectable in mutant cells compared to Q7/Q7. PA is a building block for other phospholipids but also a signaling molecule itself.

There was no change in the distribution pattern of wild-type and mutant Huntingtin in subcellular fractions, although a significant decrease in mutant Huntingtin compared to wild-type occurred in fraction 4 of Q175/Q7 mice compared to Q7/Q7 mice. These data showing normal targeting of mutant Huntingtin are consistent with earlier studies (Aronin et al., 1995; Sharp et al., 1995; Velier et al., 1998; Kim et al., 1999). The fact that mutant Huntingtin fractionates normally in fractions 1 and 2 but several other proteins do not implies a change in mutant Huntingtin function. Mutant Huntingtin may create problems by interacting as a soluble monomer or as an aggregate in the synapse (Li and Conforti, 2013; Sapp et al., 2020). As a soluble monomer, mutant Huntingtin may change the function of numerous interactor proteins [reviewed by Wanker et al. (2019)]. Mutant Huntingtin also changes the function of two interactor proteins, HIP14 and HIP14L, which are palmitoyl acyltransferases that can impact synaptic function (Kang et al., 2019). Conversely, aggregation has been shown to drastically alter the proteome of R6/2 mice which may have profound consequences for function (Hosp et al., 2017). In addition, mutant Huntingtin may also indirectly affect synaptic function by changing transcription of synaptic genes (Langfelder et al., 2016) or have pleiomorphic effects. For instance, alpha-actinin-2, which is an actin bundling protein, interacts with Huntingtin (Tousley et al., 2019a) and also interacts with NMDA 2b in spines (Wyszynski et al., 1997). Alpha-actinin-2 is also transcriptionally downregulated in HD models (Langfelder et al., 2016) which may create instability in spines and impact NMDA 2B receptors distribution. Mutant Huntingtin also alters transcription of fatty acid and cholesterol metabolism in neurons through direct effects on SREB in astrocytes (Valenza et al., 2015b).

Transmission electron microscopy confirmed our biochemical findings that fractions 1 and 2 were enriched in synaptic profiles. These observations which were made in fixed droplets (with no embedding or thin sectioning) of fractions 1 and 2 in Q7/Q7 and Q175/Q7 mice showed synaptic vesicles in isolation and vesicle filled axon terminals including some that contained intact mitochondria. The presence of presynaptic terminals agrees with detection of SNAP25 by western blot in fractions 1 and 2 of the Q7/Q7 and Q175/Q7 and mouse striatum. These features are among those also seen in synaptosome fractions separated in 0.32 sucrose buffer. Synaptosomes fractionated by sucrose gradient are enriched for presynaptic profiles with some profiles having attached postsynaptic densities as we and others have seen by EM analysis (De Robertis et al., 1961; Garey et al., 1974; Sapp et al., 2020). In contrast, it was difficult to find evidence of a post-synaptic density on the axon terminal membranes in the iodixanol separated fractions by EM despite detection of PSD95 in fractions 1–2 by western blot. These results suggest that these membranes and densities are still present but not recognizable. We did see interruptions in the continuity of the plasma membranes of some axon terminals which could relate to an altered distribution of lipids including cholesterol. The increased prevalence of preterminal axons in fraction 1 of Q175 compared to Q7 is unclear. The presence of multilamellar processes (myelinated axons) sometimes noted at the EM level in synaptosomes isolated by a sucrose gradient (Petrushka and Giuditta, 1959; Shinagawa et al., 1963) were not present in our iodixanol separated fractions 1 and 2. Marked heterogeneity and polymorphic profiles have been noted in synaptosome preparations obtained using sucrose (Petrushka and Giuditta, 1959; Shinagawa et al., 1963; Whittaker et al., 1964). Our method for preparing fractions for EM analysis and the ultrastructural appearance observed was most similar to the images and descriptions of Whittaker et al. who also applied fixed droplets of non-embedded fractions to a coated grid (Whittaker et al., 1964).

Ultrastructural analysis at low magnification revealed increased size and decreased particle number in Q175/Q7 fraction 1 and 2 compared to Q7/Q7 fractions. While the significance of these findings from isolated fractions is unclear, there is evidence that a depletion of synapses occurs in the intact striatum of Q140/Q7 HD mice (Deng et al., 2013). It is possible that during preparation of the fractions in our study homogenization weakened structural integrity to give rise to the altered axon terminal and vesicle morphology we observed. Huntingtin has been implicated in actin morphology directly through interactions with actin (Angeli et al., 2010) and interactions with actin binding proteins such as profilin, cofilin, alpha-actinins (Culver et al., 2012; Shirasaki et al., 2012; Tourette et al., 2014; Tousley et al., 2019a) and mutant Huntingtin can exert negative effects through ROCK (Shao et al., 2008), Rac1 (Tousley et al., 2019b) and potentially other interacting proteins such as HIP1 and GIT1 (Harjes and Wanker, 2003; Goehler et al., 2004). Alternatively, failure of vesicles to bud due to impaired Rab11 dependent trafficking in the presence of mutant Huntingtin (Li et al., 2009) may account for the change in distribution in size of measured particles.

In summary, the work presented here using subcellular fraction methods suggests that the HD mutation alters the physical distribution of proteins and the levels of specific lipids important to membrane functions at the synapse. Multiple membrane compartments may be impaired including the plasma membrane, endosomes, and mitochondrial membrane. The impairment of membrane functions fits with previously identified abnormal protein interactions by mutant Huntingtin that affect extra-synaptic redistribution of synaptic proteins, endosome recycling, the organization of lipid rafts, and mitochondria membrane functions.

DATA AVAILABILITY STATEMENT

The original contributions presented in the study are included in the article/**Supplementary Material**, further inquiries can be directed to the corresponding author/s.

ETHICS STATEMENT

The animal study was reviewed and approved by the MGH Subcommittee on Research Animal Care (SRAC)-OLAW #2004N000248.

AUTHOR CONTRIBUTIONS

MI and CS performed the experiments and data analysis, and wrote the manuscript. ES performed the experiments and edited the manuscript. EJ performed electron microscopy. CM performed the experiments. XL contributed to study design and preliminary experiments. MD and KK-G contributed to study design and oversight and wrote and edited manuscript. All authors contributed to the article and approved the submitted version.

FUNDING

This work was supported by the Cure Huntington's Disease Initiative (CHDI) foundation, Dake family fund to MD and KK-G, and NIH 1S10RR023594S10 to MD.

ACKNOWLEDGMENTS

The authors would like to acknowledge the Dake family for their support.

SUPPLEMENTARY MATERIAL

The Supplementary Material for this article can be found online at: https://www.frontiersin.org/articles/10.3389/fnsyn.2021.618391/full#supplementary-material

REFERENCES

Angeli, S., Shao, J., and Diamond, M. I. (2010). F-actin binding regions on the androgen receptor and huntingtin increase aggregation and alter aggregate characteristics. *PLoS One* 5:e9053. doi: 10.1371/journal.pone.0009053

Aronin, N., Chase, K., Young, C., Sapp, E., Schwarz, C., Matta, N., et al. (1995). CAG expansion affects the expression of mutant Huntingtin in the Huntington's disease brain. *Neuron* 15, 1193–1201. doi: 10.1016/0896-6273(95)90106-x

Aronin, N., and DiFiglia, M. (1992). The subcellular localization of the G-protein Gi alpha in the basal ganglia reveals its potential role in both signal transduction and vesicle trafficking. *J. Neurosci.* 12, 3435–3444. doi: 10.1523/jneurosci.12-09-03435.1992

Beaumont, V., Zhong, S., Lin, H., Xu, W., Bradaia, A., Steidl, E., et al. (2016). Phosphodiesterase 10A inhibition improves cortico-basal ganglia function in Huntington's disease models. *Neuron* 92, 1220–1237. doi: 10.1016/j.neuron.2016.10.064

Breitkopf, S. B., Ricoult, S. J. H., Yuan, M., Xu, Y., Peake, D. A., Manning, B. D., et al. (2017). A relative quantitative positive/negative ion switching method for untargeted lipidomics via high resolution LC-MS/MS from any biological source. *Metabolomics* 13:30.

Cepeda, C., Starling, A. J., Wu, N., Nguyen, O. K., Uzgil, B., Soda, T., et al. (2004). Increased GABAergic function in mouse models of Huntington's disease: reversal by BDNF. *J. Neurosci. Res.* 78, 855–867. doi: 10.1002/jnr.20344

Chicco, A. J., and Sparagna, G. C. (2007). Role of cardiolipin alterations in mitochondrial dysfunction and disease. *Am. J. Physiol. Cell Physiol.* 292, C33-C44.

Choo, Y. S., Johnson, G. V., Macdonald, M., Detloff, P. J., and Lesort, M. (2004). Mutant huntingtin directly increases susceptibility of mitochondria to the calcium-induced permeability transition and cytochrome c release. *Hum. Mol. Genet.* 13, 1407–1420. doi: 10.1093/hmg/ddh162

Ciarmiello, A., Cannella, M., Lastoria, S., Simonelli, M., Frati, L., Rubinsztein, D. C., et al. (2006). Brain white-matter volume loss and glucose hypometabolism precede the clinical symptoms of Huntington's disease. *J. Nucl. Med.* 47, 215–222.

Culver, B. P., Savas, J. N., Park, S. K., Choi, J. H., Zheng, S., Zeitlin, S. O., et al. (2012). Proteomic analysis of wild-type and mutant huntingtin-associated proteins in mouse brains identifies unique interactions and involvement in protein synthesis. *J. Biol. Chem.* 287, 21599–21614. doi: 10.1074/jbc.m112.359307

Dason, J. S., Smith, A. J., Marin, L., and Charlton, M. P. (2010). Vesicular sterols are essential for synaptic vesicle cycling. *J. Neurosci.* 30, 15856–15865. doi: 10.1523/jneurosci.4132-10.2010

Dason, J. S., Smith, A. J., Marin, L., and Charlton, M. P. (2014). Cholesterol and F-actin are required for clustering of recycling synaptic vesicle proteins in the presynaptic plasma membrane. *J. Physiol.* 592, 621–633. doi: 10.1113/jphysiol.2013.265447

de Chaves, E. I., Rusinol, A. E., Vance, D. E., Campenot, R. B., and Vance, J. E. (1997). Role of lipoproteins in the delivery of lipids to axons during axonal regeneration. *J. Biol. Chem.* 272, 30766–30773. doi: 10.1074/jbc.272.49.30766

De Robertis, E., Pellegrino De Iraldi, A., Rodriguez, G., and Gomez, C. J. (1961). On the isolation of nerve endings and synaptic vesicles. *J. Biophys. Biochem. Cytol.* 9, 229–235. doi: 10.1083/jcb.9.1.229

De Rooij, K. E., Dorsman, J. C., Smoor, M. A., Den Dunnen, J. T., and Van Ommen, G. J. (1996). Subcellular localization of the Huntington's disease gene product in cell lines by immunofluorescence and biochemical subcellular fractionation. *Hum. Mol. Genet.* 5, 1093–1099. doi: 10.1093/hmg/5.8.1093

Del Toro, D., Xifro, X., Pol, A., Humbert, S., Saudou, F., Canals, J. M., et al. (2010). Altered cholesterol homeostasis contributes to enhanced excitotoxicity in Huntington's disease. *J. Neurochem.* 115, 153–167. doi: 10.1111/j.1471-4159.2010.06912.x

Deng, Y. P., Wong, T., Bricker-Anthony, C., Deng, B., and Reiner, A. (2013). Loss of corticostriatal and thalamostriatal synaptic terminals precedes striatal projection neuron pathology in heterozygous Q140 Huntington's disease mice. *Neurobiol. Dis.* 60, 89–107. doi: 10.1016/j.nbd.2013.08.009

DiFiglia, M., Sapp, E., Chase, K., Schwarz, C., Meloni, A., Young, C., et al. (1995). Huntingtin is a cytoplasmic protein associated with vesicles in human and rat brain neurons. *Neuron* 14, 1075–1081. doi: 10.1016/0896-6273(95)90346-1

Dunkley, P. R., Jarvie, P. E., Heath, J. W., Kidd, G. J., and Rostas, J. A. (1986). A rapid method for isolation of synaptosomes on Percoll gradients. *Brain Res.* 372, 115–129. doi: 10.1016/0006-8993(86)91464-2

El-Daher, M. T., Hangen, E., Bruyere, J., Poizat, G., Al-Ramahi, I., Pardo, R., et al. (2015). Huntingtin proteolysis releases non-polyQ fragments that cause toxicity through dynamin 1 dysregulation. *EMBO J.* 34, 2255–2271. doi: 10.15252/embj.201490808

Faber, P. W., Barnes, G. T., Srinidhi, J., Chen, J., Gusella, J. F., and Macdonald, M. E. (1998). Huntingtin interacts with a family of WW domain proteins. *Hum. Mol. Genet.* 7, 1463–1474. doi: 10.1093/hmg/7.9.1463

Fan, M. M., Fernandes, H. B., Zhang, L. Y., Hayden, M. R., and Raymond, L. A. (2007). Altered NMDA receptor trafficking in a yeast artificial chromosome transgenic mouse model of Huntington's disease. *J. Neurosci.* 27, 3768–3779. doi: 10.1523/jneurosci.4356-06.2007

Ferrante, R. J., Kowall, N. W., and Richardson, E. P Jr. (1991). Proliferative and degenerative changes in striatal spiny neurons in Huntington's disease: a combined study using the section-Golgi method and calbindin D28k

immunocytochemistry. *J. Neurosci.* 11, 3877–3887. doi: 10.1523/jneurosci.11-12-03877.1991

Ford, T. C., and Rickwood, D. (1982). Formation of isotonic Nycodenz gradients for cell separations. *Anal. Biochem.* 124, 293–298. doi: 10.1016/0003-2697(82)90041-0

Frank, C., Giammarioli, A. M., Pepponi, R., Fiorentini, C., and Rufini, S. (2004). Cholesterol perturbing agents inhibit NMDA-dependent calcium influx in rat hippocampal primary culture. *FEBS Lett.* 566, 25–29. doi: 10.1016/j.febslet.2004.03.113

Frank, C., Rufini, S., Tancredi, V., Forcina, R., Grossi, D., and D'arcangelo, G. (2008). Cholesterol depletion inhibits synaptic transmission and synaptic plasticity in rat hippocampus. *Exp. Neurol.* 212, 407–414. doi: 10.1016/j.expneurol.2008.04.019

Gamberino, W. C., and Brennan, W. A. Jr. (1994). Glucose transporter isoform expression in Huntington's disease brain. *J. Neurochem.* 63, 1392–1397. doi: 10.1046/j.1471-4159.1994.63041392.x

Garey, R. E., Harper, J. W., and Heath, R. G. (1974). Postmortem isolation of synaptosomes from human brain. *Brain Res.* 82, 151–162. doi: 10.1016/0006-8993(74)90900-7

Giralt, A., Saavedra, A., Alberch, J., and Perez-Navarro, E. (2012). Cognitive dysfunction in huntington's disease: humans, mouse models and molecular mechanisms. *J. Huntingtons Dis.* 1, 155–173. doi: 10.3233/jhd-120023

Goehler, H., Lalowski, M., Stelzl, U., Waelter, S., Stroedicke, M., Worm, U., et al. (2004). A protein interaction network links GIT1, an enhancer of huntingtin aggregation, to Huntington's disease. *Mol. Cell* 15, 853–865. doi: 10.1016/j.molcel.2004.09.016

Gonzalvez, F., Schug, Z. T., Houtkooper, R. H., Mackenzie, E. D., Brooks, D. G., Wanders, R. J., et al. (2008). Cardiolipin provides an essential activating platform for caspase-8 on mitochondria. *J. Cell Biol.* 183, 681–696. doi: 10.1083/jcb.200803129

Graham, J. M. (2015). Fractionation of subcellular organelles. *Curr. Protoc. Cell Biol.* 69, 3.1.1–3.1.22.

Graveland, G. A., Williams, R. S., and Difiglia, M. (1985). Evidence for degenerative and regenerative changes in neostriatal spiny neurons in Huntington's disease. *Science* 227, 770–773. doi: 10.1126/science.3155875

Guidetti, P., Charles, V., Chen, E. Y., Reddy, P. H., Kordower, J. H., Whetsell, W. O., et al. (2001). Early degenerative changes in transgenic mice expressing mutant huntingtin involve dendritic abnormalities but no impairment of mitochondrial energy production. *Exp. Neurol.* 169, 340–350. doi: 10.1006/exnr.2000.7626

Harjes, P., and Wanker, E. E. (2003). The hunt for huntingtin function: interaction partners tell many different stories. *Trends Biochem. Sci.* 28, 425–433. doi: 10.1016/s0968-0004(03)00168-3

Hering, H., Lin, C. C., and Sheng, M. (2003). Lipid rafts in the maintenance of synapses, dendritic spines, and surface AMPA receptor stability. *J. Neurosci.* 23, 3262–3271. doi: 10.1523/jneurosci.23-08-03262.2003

Hosp, F., Gutierrez-Angel, S., Schaefer, M. H., Cox, J., Meissner, F., Hipp, M. S., et al. (2017). Spatiotemporal proteomic profiling of Huntington's disease inclusions reveals widespread loss of protein function. *Cell Rep.* 21, 2291–2303. doi: 10.1016/j.celrep.2017.10.097

Huang, T. T., Smith, R., Bacos, K., Song, D. Y., Faull, R. M., Waldvogel, H. J., et al. (2020). No symphony without bassoon and piccolo: changes in synaptic active zone proteins in Huntington's disease. *Acta Neuropathol. Commun.* 8:77.

Joshi, P. R., Wu, N. P., Andre, V. M., Cummings, D. M., Cepeda, C., Joyce, J. A., et al. (2009). Age-dependent alterations of corticostriatal activity in the YAC128 mouse model of Huntington disease. *J. Neurosci.* 29, 2414–2427. doi: 10.1523/jneurosci.5687-08.2009

Jung, H. H., Hergersberg, M., Vogt, M., Pahnke, J., Treyer, V., Rothlisberger, B., et al. (2003). McLeod phenotype associated with a XK missense mutation without hematologic, neuromuscular, or cerebral involvement. *Transfusion* 43, 928–938. doi: 10.1046/j.1537-2995.2003.t01-1-00434.x

Kaltenbach, L. S., Romero, E., Becklin, R. R., Chettier, R., Bell, R., Phansalkar, A., et al. (2007). Huntingtin interacting proteins are genetic modifiers of neurodegeneration. *PLoS Genet.* 3:e82. doi: 10.1371/journal.pgen.0030082

Kang, R., Swayze, R., Lise, M. F., Gerrow, K., Mullard, A., Honer, W. G., et al. (2004). Presynaptic trafficking of synaptotagmin I is regulated by protein palmitoylation. *J. Biol. Chem.* 279, 50524–50536. doi: 10.1074/jbc.m404981200

Kang, R., Wan, J., Arstikaitis, P., Takahashi, H., Huang, K., Bailey, A. O., et al. (2008). Neural palmitoyl-proteomics reveals dynamic synaptic palmitoylation. *Nature* 456, 904–909. doi: 10.1038/nature07605

Kang, R., Wang, L., Sanders, S. S., Zuo, K., Hayden, M. R., and Raymond, L. A. (2019). Altered regulation of striatal neuronal *N*-Methyl-D-aspartate receptor trafficking by palmitoylation in Huntington disease mouse model. *Front. Synaptic Neurosci.* 11:3. doi: 10.3389/fnsyn.2019.00003

Kegel, K. B., Meloni, A. R., Yi, Y., Kim, Y. J., Doyle, E., Cuiffo, B. G., et al. (2002). Huntingtin is present in the nucleus, interacts with the transcriptional corepressor C-terminal binding protein, and represses transcription. *J. Biol. Chem.* 277, 7466–7476. doi: 10.1074/jbc.m103946200

Kegel, K. B., Sapp, E., Alexander, J., Valencia, A., Reeves, P., Li, X., et al. (2009). Polyglutamine expansion in huntingtin alters its interaction with phospholipids. *J. Neurochem.* 110, 1585–1597. doi: 10.1111/j.1471-4159.2009.06255.x

Kegel, K. B., Sapp, E., Yoder, J., Cuiffo, B., Sobin, L., Kim, Y. J., et al. (2005). Huntingtin associates with acidic phospholipids at the plasma membrane. *J. Biol. Chem.* 280, 36464–36473. doi: 10.1074/jbc.m503672200

Kim, M., Velier, J., Chase, K., Laforet, G., Kalchman, M. A., Hayden, M. R., et al. (1999). Forskolin and dopamine D1 receptor activation increase huntingtin's association with endosomes in immortalized neuronal cells of striatal origin. *Neuroscience* 89, 1159–1167. doi: 10.1016/s0306-4522(98)00400-x

Kim, S. J., Jeong, M. J., Jo, H. J., Jung, J. H., Kaang, B. K., Choi, Y. B., et al. (2017). Identification of postsynaptic phosphatidylinositol-4,5-bisphosphate (PIP2) roles for synaptic plasticity using chemically induced dimerization. *Sci. Rep.* 7:3351.

Klapstein, G. J., Fisher, R. S., Zanjani, H., Cepeda, C., Jokel, E. S., Chesselet, M. F., et al. (2001). Electrophysiological and morphological changes in striatal spiny neurons in R6/2 Huntington's disease transgenic mice. *J. Neurophysiol.* 86, 2667–2677. doi: 10.1152/jn.2001.86.6.2667

Koch, M., and Holt, M. (2012). Coupling exo- and endocytosis: an essential role for PIP(2) at the synapse. *Biochim. Biophys. Acta* 1821, 1114–1132. doi: 10.1016/j.bbalip.2012.02.008

Kovalenko, M., Milnerwood, A., Giordano, J., St Claire, J., Guide, J. R., Stromberg, M., et al. (2018). HttQ111/+ Huntington's disease knock-in mice exhibit brain region-specific morphological changes and synaptic dysfunction. *J. Huntingtons Dis.* 7, 17–33. doi: 10.3233/jhd-170282

Langfelder, P., Cantle, J. P., Chatzopoulou, D., Wang, N., Gao, F., Al-Ramahi, I., et al. (2016). Integrated genomics and proteomics define huntingtin CAG length-dependent networks in mice. *Nat. Neurosci.* 19, 623–633. doi: 10.1038/nn.4256

Leoni, V., Long, J. D., Mills, J. A., Di Donato, S., Paulsen, J. S., and Group, P. -H. S. (2013). Plasma 24S-hydroxycholesterol correlation with markers of Huntington disease progression. *Neurobiol. Dis.* 55, 37–43. doi: 10.1016/j.nbd.2013.03.013

Leoni, V., Mariotti, C., Tabrizi, S. J., Valenza, M., Wild, E. J., Henley, S. M., et al. (2008). Plasma 24S-hydroxycholesterol and caudate MRI in pre-manifest and early Huntington's disease. *Brain* 131, 2851–2859. doi: 10.1093/brain/awn212

Lerner, R. P., Trejo Martinez Ldel, C., Zhu, C., Chesselet, M. F., and Hickey, M. A. (2012). Striatal atrophy and dendritic alterations in a knock-in mouse model of Huntington's disease. *Brain Res. Bull.* 87, 571–578. doi: 10.1016/j.brainresbull.2012.01.012

Li, H., Wyman, T., Yu, Z. X., Li, S. H., and Li, X. J. (2003). Abnormal association of mutant huntingtin with synaptic vesicles inhibits glutamate release. *Hum. Mol. Genet.* 12, 2021–2030. doi: 10.1093/hmg/ddg218

Li, J. Y., and Conforti, L. (2013). Axonopathy in Huntington's disease. *Exp. Neurol.* 246, 62–71. doi: 10.1016/j.expneurol.2012.08.010

Li, X., Sapp, E., Valencia, A., Kegel, K. B., Qin, Z. H., Alexander, J., et al. (2008). A function of huntingtin in guanine nucleotide exchange on Rab11. *Neuroreport* 19, 1643–1647. doi: 10.1097/wnr.0b013e328315cd4c

Li, X., Standley, C., Sapp, E., Valencia, A., Qin, Z. H., Kegel, K. B., et al. (2009). Mutant huntingtin impairs vesicle formation from recycling endosomes by interfering with Rab11 activity. *Mol. Cell. Biol.* 29, 6106–6116. doi: 10.1128/mcb.00420-09

Li, X., Valencia, A., Sapp, E., Masso, N., Alexander, J., Reeves, P., et al. (2010). Aberrant Rab11-dependent trafficking of the neuronal glutamate transporter EAAC1 causes oxidative stress and cell death in Huntington's disease. *J. Neurosci.* 30, 4552–4561. doi: 10.1523/jneurosci.5865-09.2010

Linetti, A., Fratangeli, A., Taverna, E., Valnegri, P., Francolini, M., Cappello, V., et al. (2010). Cholesterol reduction impairs exocytosis of synaptic vesicles. *J. Cell Sci.* 123, 595–605. doi: 10.1242/jcs.060681

Lou, X. (2018). Sensing exocytosis and triggering endocytosis at synapses: synaptic vesicle exocytosis-endocytosis coupling. *Front. Cell. Neurosci.* 12:66. doi: 10.3389/fncel.2018.00066

Lund, E. G., Xie, C., Kotti, T., Turley, S. D., Dietschy, J. M., and Russell, D. W. (2003). Knockout of the cholesterol 24-hydroxylase gene in mice reveals a brain-specific mechanism of cholesterol turnover. *J. Biol. Chem.* 278, 22980–22988. doi: 10.1074/jbc.m303415200

Mamada, N., Tanokashira, D., Ishii, K., Tamaoka, A., and Araki, W. (2017). Mitochondria are devoid of amyloid beta-protein (Abeta)-producing secretases: evidence for unlikely occurrence within mitochondria of Abeta generation from amyloid precursor protein. *Biochem. Biophys. Res. Commun.* 486, 321–328. doi: 10.1016/j.bbrc.2017.03.035

Martin, M. G., Ahmed, T., Korovaichuk, A., Venero, C., Menchon, S. A., Salas, I., et al. (2014). Constitutive hippocampal cholesterol loss underlies poor cognition in old rodents. *EMBO Mol. Med.* 6, 902–917. doi: 10.15252/emmm.201303711

Mauch, D. H., Nagler, K., Schumacher, S., Goritz, C., Muller, E. C., Otto, A., et al. (2001). CNS synaptogenesis promoted by glia-derived cholesterol. *Science* 294, 1354–1357. doi: 10.1126/science.294.5545.1354

McCartney, A. J., Zolov, S. N., Kauffman, E. J., Zhang, Y., Strunk, B. S., Weisman, L. S., et al. (2014). Activity-dependent PI(3,5)P2 synthesis controls AMPA receptor trafficking during synaptic depression. *Proc. Natl. Acad. Sci. U.S.A.* 111, E4896-E4905.

McClory, H., Williams, D., Sapp, E., Gatune, L. W., Wang, P., Difiglia, M., et al. (2014). Glucose transporter 3 is a rab11-dependent trafficking cargo and its transport to the cell surface is reduced in neurons of CAG140 Huntington's disease mice. *Acta Neuropathol. Commun.* 2:179.

McColgan, P., Gregory, S., Seunarine, K. K., Razi, A., Papoutsi, M., Johnson, E., et al. (2018). Brain regions showing white matter loss in Huntington's disease are enriched for synaptic and metabolic genes. *Biol. Psychiatry* 83, 456–465. doi: 10.1016/j.biopsych.2017.10.019

McKinstry, S. U., Karadeniz, Y. B., Worthington, A. K., Hayrapetyan, V. Y., Ozlu, M. I., Serafin-Molina, K., et al. (2014). Huntingtin is required for normal excitatory synapse development in cortical and striatal circuits. *J. Neurosci.* 34, 9455–9472. doi: 10.1523/jneurosci.4699-13.2014

Milnerwood, A. J., Kaufman, A. M., Sepers, M. D., Gladding, C. M., Zhang, L., Wang, L., et al. (2012). Mitigation of augmented extrasynaptic NMDAR signaling and apoptosis in cortico-striatal co-cultures from Huntington's disease mice. *Neurobiol. Dis.* 48, 40–51. doi: 10.1016/j.nbd.2012.05.013

Murmu, R. P., Li, W., Holtmaat, A., and Li, J. Y. (2013). Dendritic spine instability leads to progressive neocortical spine loss in a mouse model of Huntington's disease. *J. Neurosci.* 33, 12997–13009. doi: 10.1523/jneurosci.5284-12.2013

Nithianantharajah, J., and Hannan, A. J. (2013). Dysregulation of synaptic proteins, dendritic spine abnormalities and pathological plasticity of synapses as experience-dependent mediators of cognitive and psychiatric symptoms in Huntington's disease. *Neuroscience* 251, 66–74. doi: 10.1016/j.neuroscience.2012.05.043

Orr, A. L., Li, S., Wang, C. E., Li, H., Wang, J., Rong, J., et al. (2008). N-terminal mutant huntingtin associates with mitochondria and impairs mitochondrial trafficking. *J. Neurosci.* 28, 2783–2792. doi: 10.1523/jneurosci.0106-08.2008

Park, J. S., and Neiman, A. M. (2020). XK is a partner for VPS13A: a molecular link between Chorea-Acanthocytosis and McLeod Syndrome. *Mol. Biol. Cell* 31, 2425–2436. doi: 10.1091/mbc.e19-08-0439-t

Peng, C., Zhu, G., Liu, X., and Li, H. (2018). Mutant Huntingtin causes a selective decrease in the expression of synaptic vesicle protein 2C. *Neurosci. Bull.* 34, 747–758. doi: 10.1007/s12264-018-0230-x

Petrov, A. M., Mast, N., Li, Y., Denker, J., and Pikuleva, I. A. (2020). Brain sterol flux mediated by cytochrome P450 46A1 affects membrane properties and membrane-dependent processes. *Brain Commun.* 2:fcaa043.

Petrushka, E., and Giuditta, A. (1959). Electron microscopy of two subcellular fractions isolated from cerebral cortex homogenate. *J. Biophys. Biochem. Cytol.* 6, 129–132. doi: 10.1083/jcb.6.1.129

Plain, F., Howie, J., Kennedy, J., Brown, E., Shattock, M. J., Fraser, N. J., et al. (2020). Control of protein palmitoylation by regulating substrate recruitment to a zDHHC-protein acyltransferase. *Commun. Biol.* 3:411.

Reiner, A., and Deng, Y. P. (2018). Disrupted striatal neuron inputs and outputs in Huntington's disease. *CNS Neurosci. Ther.* 24, 250–280. doi: 10.1111/cns.12844

Renner, M., Choquet, D., and Triller, A. (2009). Control of the postsynaptic membrane viscosity. *J. Neurosci.* 29, 2926–2937. doi: 10.1523/jneurosci.4445-08.2009

Ritch, J. J., Valencia, A., Alexander, J., Sapp, E., Gatune, L., Sangrey, G. R., et al. (2012). Multiple phenotypes in Huntington disease mouse neural stem cells. *Mol. Cell. Neurosci.* 50, 70–81. doi: 10.1016/j.mcn.2012.03.011

Sapp, E., Seeley, C., Iuliano, M., Weisman, E., Vodicka, P., Difiglia, M., et al. (2020). Protein changes in synaptosomes of Huntington's disease knock-in mice are dependent on age and brain region. *Neurobiol. Dis.* 141:104950. doi: 10.1016/j.nbd.2020.104950

Shao, J., Welch, W. J., Diprospero, N. A., and Diamond, M. I. (2008). Phosphorylation of profilin by ROCK1 regulates polyglutamine aggregation. *Mol. Cell. Biol.* 28, 5196–5208. doi: 10.1128/mcb.00079-08

Sharp, A. H., Loev, S. J., Schilling, G., Li, S. H., Li, X. J., Bao, J., et al. (1995). Widespread expression of Huntington's disease gene (IT15) protein product. *Neuron* 14, 1065–1074. doi: 10.1016/0896-6273(95)90345-3

Shinagawa, Y., Date, Y., and Kataoka, K. (1963). Electronmicroscopical observations on the so-called "synaptic vesicle" fraction from rabbit's brain. *J. Electronmicrosc.* 12, 50–56.

Shirasaki, D. I., Greiner, E. R., Al-Ramahi, I., Gray, M., Boontheung, P., Geschwind, D. H., et al. (2012). Network organization of the huntingtin proteomic interactome in mammalian brain. *Neuron* 75, 41–57. doi: 10.1016/j.neuron.2012.05.024

Skotte, N. H., Andersen, J. V., Santos, A., Aldana, B. I., Willert, C. W., Norremolle, A., et al. (2018). Integrative characterization of the R6/2 mouse model of Huntington's disease reveals dysfunctional astrocyte metabolism. *Cell Rep.* 23, 2211–2224. doi: 10.1016/j.celrep.2018.04.052

Sotrel, A., Paskevich, P. A., Kiely, D. K., Bird, E. D., Williams, R. S., and Myers, R. H. (1991). Morphometric analysis of the prefrontal cortex in Huntington's disease. *Neurology* 41, 1117–1123. doi: 10.1212/wnl.41.7.1117

Spires, T. L., Grote, H. E., Garry, S., Cordery, P. M., Van Dellen, A., Blakemore, C., et al. (2004). Dendritic spine pathology and deficits in experience-dependent dendritic plasticity in R6/1 Huntington's disease transgenic mice. *Eur. J. Neurosci.* 19, 2799–2807. doi: 10.1111/j.0953-816x.2004.03374.x

Stapel, B., Gorinski, N., Gmahl, N., Rhein, M., Preuss, V., Hilfiker-Kleiner, D., et al. (2019). Fluoxetine induces glucose uptake and modifies glucose transporter palmitoylation in human peripheral blood mononuclear cells. *Expert Opin. Ther. Targets* 23, 883–891. doi: 10.1080/14728222.2019.1675639

Tabrizi, S. J., Scahill, R. I., Durr, A., Roos, R. A., Leavitt, B. R., Jones, R., et al. (2011). Biological and clinical changes in premanifest and early stage Huntington's disease in the TRACK-HD study: the 12-month longitudinal analysis. *Lancet Neurol.* 10, 31–42. doi: 10.1016/s1474-4422(10)70276-3

Tan, X., Thapa, N., Choi, S., and Anderson, R. A. (2015). Emerging roles of PtdIns(4,5)P2–beyond the plasma membrane. *J. Cell Sci.* 128, 4047–4056. doi: 10.1242/jcs.175208

Tang, C. C., Feigin, A., Ma, Y., Habeck, C., Paulsen, J. S., Leenders, K. L., et al. (2013). Metabolic network as a progression biomarker of premanifest Huntington's disease. *J. Clin. Invest.* 123, 4076–4088. doi: 10.1172/jci69411

Thiele, C., Hannah, M. J., Fahrenholz, F., and Huttner, W. B. (2000). Cholesterol binds to synaptophysin and is required for biogenesis of synaptic vesicles. *Nat. Cell Biol.* 2, 42–49. doi: 10.1038/71366

Tourette, C., Li, B., Bell, R., O'hare, S., Kaltenbach, L. S., Mooney, S. D., et al. (2014). A large scale Huntingtin protein interaction network implicates Rho GTPase signaling pathways in Huntington disease. *J. Biol. Chem.* 289, 6709–6726. doi: 10.1074/jbc.m113.523696

Tousley, A., Iuliano, M., Weisman, E., Sapp, E., Richardson, H., Vodicka, P., et al. (2019a). Huntingtin associates with the actin cytoskeleton and alpha-actinin isoforms to influence stimulus dependent morphology changes. *PLoS One* 14, e0212337. doi: 10.1371/journal.pone.0212337

Tousley, A., Iuliano, M., Weisman, E., Sapp, E., Zhang, N., Vodicka, P., et al. (2019b). Rac1 activity is modulated by Huntingtin and dysregulated in models of Huntington's disease. *J. Huntingtons Dis.* 8, 53–69. doi: 10.3233/jhd-180311

Trushina, E., Singh, R. D., Dyer, R. B., Cao, S., Shah, V. H., Parton, R. G., et al. (2006). Mutant huntingtin inhibits clathrin-independent endocytosis and causes accumulation of cholesterol *in vitro* and *in vivo*. *Hum. Mol. Genet.* 15, 3578–3591. doi: 10.1093/hmg/ddl434

Unschuld, P. G., Joel, S. E., Liu, X., Shanahan, M., Margolis, R. L., Biglan, K. M., et al. (2012a). Impaired cortico-striatal functional connectivity in prodromal Huntington's Disease. *Neurosci. Lett.* 514, 204–209. doi: 10.1016/j.neulet.2012.02.095

Unschuld, P. G., Joel, S. E., Pekar, J. J., Reading, S. A., Oishi, K., Mcentee, J., et al. (2012b). Depressive symptoms in prodromal Huntington's Disease correlate with Stroop-interference related functional connectivity in the ventromedial prefrontal cortex. *Psychiatry Res.* 203, 166–174. doi: 10.1016/j.pscychresns.2012.01.002

Urata, Y., Nakamura, M., Sasaki, N., Shiokawa, N., Nishida, Y., Arai, K., et al. (2019). Novel pathogenic XK mutations in McLeod syndrome and interaction between XK protein and chorein. *Neurol. Genet.* 5:e328. doi: 10.1212/nxg.0000000000000328

Valencia, A., Reeves, P. B., Sapp, E., Li, X., Alexander, J., Kegel, K. B., et al. (2010). Mutant huntingtin and glycogen synthase kinase 3-beta accumulate in neuronal lipid rafts of a presymptomatic knock-in mouse model of Huntington's disease. *J. Neurosci. Res.* 88, 179–190. doi: 10.1002/jnr.22184

Valencia, A., Sapp, E., Kimm, J. S., Mcclory, H., Ansong, K. A., Yohrling, G., et al. (2013). Striatal synaptosomes from Hdh140Q/140Q knock-in mice have altered protein levels, novel sites of methionine oxidation, and excess glutamate release after stimulation. *J. Huntingtons Dis.* 2, 459–475. doi: 10.3233/jhd-130080

Valenza, M., Carroll, J. B., Leoni, V., Bertram, L. N., Bjorkhem, I., Singaraja, R. R., et al. (2007). Cholesterol biosynthesis pathway is disturbed in YAC128 mice and is modulated by huntingtin mutation. *Hum. Mol. Genet.* 16, 2187–2198. doi: 10.1093/hmg/ddm170

Valenza, M., Chen, J. Y., Di Paolo, E., Ruozi, B., Belletti, D., Ferrari Bardile, C., et al. (2015a). Cholesterol-loaded nanoparticles ameliorate synaptic and cognitive function in Huntington's disease mice. *EMBO Mol. Med.* 7, 1547–1564. doi: 10.15252/emmm.201505413

Valenza, M., Marullo, M., Di Paolo, E., Cesana, E., Zuccato, C., Biella, G., et al. (2015b). Disruption of astrocyte-neuron cholesterol cross talk affects neuronal function in Huntington's disease. *Cell Death Differ.* 22, 690–702. doi: 10.1038/cdd.2014.162

Valenza, M., Leoni, V., Karasinska, J. M., Petricca, L., Fan, J., Carroll, J., et al. (2010). Cholesterol defect is marked across multiple rodent models of Huntington's disease and is manifest in astrocytes. *J. Neurosci.* 30, 10844–10850. doi: 10.1523/jneurosci.0917-10.2010

Valenza, M., Rigamonti, D., Goffredo, D., Zuccato, C., Fenu, S., Jamot, L., et al. (2005). Dysfunction of the cholesterol biosynthetic pathway in Huntington's disease. *J. Neurosci.* 25, 9932–9939. doi: 10.1523/jneurosci.3355-05.2005

Velier, J., Kim, M., Schwarz, C., Kim, T. W., Sapp, E., Chase, K., et al. (1998). Wild-type and mutant huntingtins function in vesicle trafficking in the secretory and endocytic pathways. *Exp. Neurol.* 152, 34–40. doi: 10.1006/exnr.1998.6832

Vodicka, P., Mo, S., Tousley, A., Green, K. M., Sapp, E., Iuliano, M., et al. (2015). Mass Spectrometry analysis of wild-type and knock-in Q140/Q140 Huntington's disease mouse brains reveals changes in glycerophospholipids including alterations in phosphatidic acid and lyso-phosphatidic acid. *J. Huntingtons Dis.* 4, 187–201. doi: 10.3233/jhd-150149

Wanker, E. E., Ast, A., Schindler, F., Trepte, P., and Schnoegl, S. (2019). The pathobiology of perturbed mutant huntingtin protein-protein interactions in Huntington's disease. *J. Neurochem.* 151, 507–519. doi: 10.1111/jnc.14853

Whittaker, V. P., Michaelson, I. A., and Kirkland, R. J. (1964). The separation of synaptic vesicles from nerve-ending particles ('synaptosomes'). *Biochem. J.* 90, 293–303. doi: 10.1042/bj0900293

Wolf, R. C., Sambataro, F., Vasic, N., Schonfeldt-Lecuona, C., Ecker, D., and Landwehrmeyer, B. (2008). Aberrant connectivity of lateral prefrontal networks in presymptomatic Huntington's disease. *Exp. Neurol.* 213, 137–144. doi: 10.1016/j.expneurol.2008.05.017

Wong, L. H., Gatta, A. T., and Levine, T. P. (2019). Lipid transfer proteins: the lipid commute via shuttles, bridges and tubes. *Nat. Rev. Mol. Cell Biol.* 20, 85–101. doi: 10.1038/s41580-018-0071-5

Wyszynski, M., Lin, J., Rao, A., Nigh, E., Beggs, A. H., Craig, A. M., et al. (1997). Competitive binding of alpha-actinin and calmodulin to the NMDA receptor. *Nature* 385, 439–442. doi: 10.1038/385439a0

Xu, G., Servatius, R. J., Shefer, S., Tint, G. S., O'brien, W. T., Batta, A. K., et al. (1998). Relationship between abnormal cholesterol synthesis and retarded learning in rats. *Metabolism* 47, 878–882. doi: 10.1016/s0026-0495(98)90130-5

Xu, Q., Huang, S., Song, M., Wang, C. E., Yan, S., Liu, X., et al. (2013). Synaptic mutant huntingtin inhibits synapsin-1 phosphorylation and causes neurological symptoms. *J. Cell Biol.* 202, 1123–1138. doi: 10.1083/jcb.201303146

Yablonska, S., Ganesan, V., Ferrando, L. M., Kim, J., Pyzel, A., Baranova, O. V., et al. (2019). Mutant huntingtin disrupts mitochondrial proteostasis by interacting with TIM23. *Proc. Natl. Acad. Sci. U.S.A.* 116, 16593–16602. doi: 10.1073/pnas.1904101116

Yang, J., Zhao, X., Lu, X., Lin, X., and Xu, G. (2015). A data preprocessing strategy for metabolomics to reduce the mask effect in data analysis. *Front. Mol. Biosci.* 2:4. doi: 10.3389/fmolb.2015.00004

Yao, J., Ong, S. E., and Bajjalieh, S. (2014). Huntingtin is associated with cytomatrix proteins at the presynaptic terminal. *Mol. Cell. Neurosci.* 63, 96–100. doi: 10.1016/j.mcn.2014.10.003

Zareba-Koziol, M., Figiel, I., Bartkowiak-Kaczmarek, A., and Wlodarczyk, J. (2018). Insights into protein S-palmitoylation in synaptic plasticity and neurological disorders: potential and limitations of methods for detection and analysis. *Front. Mol. Neurosci.* 11:175. doi: 10.3389/fnmol.2018.00175

Zhang, H., Zhang, C., Vincent, J., Zala, D., Benstaali, C., Sainlos, M., et al. (2018). Modulation of AMPA receptor surface diffusion restores hippocampal plasticity and memory in Huntington's disease models. *Nat. Commun.* 9:4272.

Zhang, J., Kang, D. E., Xia, W., Okochi, M., Mori, H., Selkoe, D. J., et al. (1998). Subcellular distribution and turnover of presenilins in transfected cells. *J. Biol. Chem.* 273, 12436–12442. doi: 10.1074/jbc.273.20.12436

Conflict of Interest: KK-G spouse owns less than 0.1% stock in the following companies: Bristol-Myers Squibb Company, Cisco Systems, Inc., GE Healthcare Life Sciences, Generex Biotechnology Corporation, GlaxoSmithKline, Metabolix Bioplastics, Nanogen, Inc., Nanometrics Inc., Repligen, and StemCells, Inc.

The remaining authors declare that the research was conducted in the absence of any commercial or financial relationships that could be construed as a potential conflict of interest.

frontiers in Synaptic Neuroscience

ORIGINAL RESEARCH
published: 03 June 2021
doi: 10.3389/fnsyn.2021.670467

Striatal Synapse Degeneration and Dysfunction Are Reversed by Reactivation of Wnt Signaling

*Soledad Galli[1], Stefka H. Stancheva[1], Tom Dufor[1], Alasdair J. Gibb[2] and Patricia C. Salinas[1]**

[1] Department of Cell and Developmental Biology, University College London, London, United Kingdom, [2] Department of Neuroscience, Physiology and Pharmacology, University College London, London, United Kingdom

Synapse degeneration in the striatum has been associated with the early stages of Parkinson's and Huntington's diseases (PD and HD). However, the molecular mechanisms that trigger synaptic dysfunction and loss are not fully understood. Increasing evidence suggests that deficiency in Wnt signaling triggers synapse degeneration in the adult brain and that this pathway is affected in neurodegenerative diseases. Here, we demonstrate that endogenous Wnt signaling is essential for the integrity of a subset of inhibitory synapses on striatal medium spiny neurons (MSNs). We found that inducible expression of the specific Wnt antagonist Dickkopf-1 (Dkk1) in the adult striatum leads to the loss of inhibitory synapses on MSNs and affects the synaptic transmission of D2-MSNs. We also discovered that re-activation of the Wnt pathway by turning off Dkk1 expression after substantial loss of synapses resulted in the complete recovery of GABAergic and dopamine synapse number. Our results also show that re-activation of the Wnt pathway leads to a recovery of amphetamine response and motor function. Our studies identify the Wnt signaling pathway as a potential therapeutic target for restoring neuronal circuits after synapse degeneration.

Keywords: synapse degeneration, Dkk1, neuronal circuit restoration, medium spiny neurons, neurodegenerative disease

OPEN ACCESS

Edited by:
Zhiping P. Pang, Rutgers, The State University of New Jersey, United States

Reviewed by:
Sandra M. Holley, David Geffen School of Medicine at UCLA, United States
Steven M. Graves, University of Minnesota, United States

****Correspondence:***
Patricia C. Salinas
p.salinas@ucl.ac.uk

Received: *21 February 2021*
Accepted: *19 April 2021*
Published: *03 June 2021*

Citation:
Galli S, Stancheva SH, Dufor T, Gibb AJ and Salinas PC (2021) Striatal Synapse Degeneration and Dysfunction Are Reversed by Reactivation of Wnt Signaling. Front. Synaptic Neurosci. 13:670467. doi: 10.3389/fnsyn.2021.670467

INTRODUCTION

Synapse degeneration is an early occurrence in several neurodegenerative diseases. In the striatum, patients with conditions such as Huntington's and Parkinson's diseases (HD and PD, respectively) exhibit synapse dysfunction and loss, which strongly correlate with early symptoms of these conditions (Cheng et al., 2010; Milnerwood and Raymond, 2010; Janezic et al., 2013). However, the mechanisms contributing to synapse degeneration are not fully characterized. Importantly, it is currently unclear whether synaptic function can be fully restored in different brain regions after substantial synapse loss. Understanding these processes is crucial for developing therapeutic strategies to restore function in these neurodegenerative diseases.

The integrity of neuronal circuits in the striatum is essential for motor coordination. GABAergic medium spiny neurons (MSNs) are the principal neurons of the striatum that receive dopaminergic

inputs from the substantia nigra and glutamatergic inputs from the cortex and thalamus (Gerfen, 1992; Surmeier et al., 2007; Kreitzer and Malenka, 2008). In addition, MSNs form synapses with each other and receive inhibitory inputs from local interneurons (Taverna et al., 2007, 2008; Gittis et al., 2010). There are two main populations of MSNs, D1-MSNs and D2-MSNs, that express D1 or D2 dopaminergic receptors and are part of the direct (motor facilitation) and indirect (motor suppression) pathway, respectively (Kreitzer and Malenka, 2008; Kravitz et al., 2010; Lee et al., 2016). In PD, early defects in dopaminergic inputs into the two population of MSNs are observed (Picconi et al., 2012; Schirinzi et al., 2016). In HD, synaptic dysfunction and synapse loss in MSNs appears early in the disease affecting first D2-expressing MSN pathway (Albin et al., 1992; Reiner et al., 1988). However, the molecular mechanisms that trigger these early synaptic defects are not fully understood. Understanding the mechanisms that lead to synapse damage even outside the context of PD and HD could unravel important insights into how synapses become dysfunctional.

Increasing evidence suggests that deficiency in Wnt signaling contributes to synapse dysfunction and degeneration in neurodegenerative diseases (Galli et al., 2014; Liu et al., 2014; Marzo et al., 2016; Elliott et al., 2018). For example, expression of an endogenous potent and specific secreted Wnt antagonist, Dickkopf-1 (Dkk1), is elevated in the human Alzheimer's disease (AD) brain and in mouse models of AD (Caricasole et al., 2004; Rosi et al., 2010). Notably, amyloid-β (Aβ) oligomers, the pathogenic molecule in AD, rapidly increase Dkk1 expression as synapses degenerate (Purro et al., 2012) and knockdown or blockade of Dkk1 protects synapses against Aβ (Purro et al., 2012; Sellers et al., 2018). Moreover, inhibition of Wnt signaling in the adult mouse hippocampus by inducible expression of Dkk1 results in the loss of 40% of excitatory synapses, defects in long-term plasticity such as long-term potentiation (LTP) and long-term depression (LTD) and long-term memory (Marzo et al., 2016). In addition, in mature neurons, conditional loss of function of LRP6, a co-receptor for canonical Wnt signaling, results in synapse degeneration as mice age and exacerbates AD pathology when these animals are crossed to an AD model (Liu et al., 2014). Thus, deficiency in Wnt signaling affects the structural and functional integrity of excitatory synapses in the adult hippocampus and is linked to AD pathology. However, the contribution of dysfunctional Wnt signaling to synapse degeneration in other brain areas is less understood.

In the adult striatum, induced neuronal expression of Dkk1 in transgenic mice (iDkk1) results in a significant decrease in the number of β-catenin puncta consistent with the view that canonical Wnt signaling is compromised in iDkk1 mice (Galli et al., 2014). Notably, Dkk1 expression in the striatum also results in the specific degeneration of glutamatergic synapses from cortical but not from thalamic inputs as well as the loss of dopaminergic synapses in the absence of increased cell death (Galli et al., 2014). Importantly, Dkk1 expression triggers motor defects characteristic of striatal dysfunction (Galli et al., 2014), demonstrating a critical role of endogenous Wnt signaling in the maintenance of corticostriatal excitatory and dopaminergic synapses onto MSNs. However, the effect of Wnt deficiency on inhibitory synapses and whether these synaptic defects are reversible remain unknown.

Here, we investigated the impact of deficient Wnt signaling on the stability of GABAergic synapses in the adult striatum and whether synaptic defects are reversible. We used the iDkk1 transgenic mouse model where Dkk1 is expressed in neurons of the adult brain under a tetracycline-inducible system (Galli et al., 2014; Marzo et al., 2016). We found that induced Dkk1 expression for 14 days led to the loss of 40% of inhibitory GABAergic synapses in the adult striatum accompanied by a decrease in the frequency of miniature inhibitory currents in D2-MSNs. Thus, Dkk1 affected GABAergic synapse function on a specific subset of MSNs. Importantly, reactivation of the Wnt pathway by cessation of Dkk1 expression after substantial synapse degeneration resulted in the full recovery of GABAergic and dopaminergic synapse number. Our previous studies showed that blockade of Wnt signaling by induced expression of Dkk1 in the adult results in motor deficits (Galli et al., 2014). In the current study, we demonstrate that cessation of Dkk1 results in normal motor coordination and the ability to respond to amphetamine. These findings reveal the requirement of Wnt signaling for the maintenance of synaptic connections in the striatum and that reactivation of the Wnt pathway promotes the reassembly of functional neuronal circuits in this brain region. Thus, modulation of Wnt signaling could provide a potential therapeutic strategy to restore synaptic connectivity in neurodegenerative diseases where synapses are affected.

MATERIALS AND METHODS

In vivo Induction of Dkk1 Expression in the Adult Brain

Experiments were performed according to the Animals Scientific Procedures Act United Kingdom (1986). Heterozygous tetO-Dkk1 transgenic mice (Chu et al., 2004) were crossed with heterozygous CaMKIIα-rtTA mice (Mansuy et al., 1998) to obtain the double transgenic iDkk1 (Galli et al., 2014), and their genotypes were confirmed by PCR. The triple transgenic mice iDkk1-D2R were obtained by crossing the double transgenic iDkk1 with D2R-EGFP mice (obtained from University of North Carolina MMRRC-UNC) (Gong et al., 2003). Primers used for genotyping were as follows: 5′ TGCCTTTCTCTCCACAGGTGTCC 3′ (forward) and 5′ GAGAGCACAGCGGAATGAC 3′ (reverse) for CaMKIIα-rtTA; 5′ GCGTCCTTCGGAGATGATGG 3′ (forward) and 5′ AAATGGCTGTGGTCAGAGGG 3′ (reverse) for tetO-Dkk1. In addition, we used 5′ GAGGAAGCATGCCTTGAAAA 3′ (forward) and 5′ TGGTGCAGATGAACTTCAGG 3′ (reverse) for D2R-GFP. The strain background was C57BL/6J. iDkk1 mice (or iDkk1-D2R mice) and control mice (3–6 months old) were fed with pellets supplemented with 6 mg/kg doxycycline (Dates and group) for 14 days unless otherwise indicated. Control mice were both wild-type and single transgenic animals fed with doxycycline. In some experiments, D2R-EGFP mice were used as controls. Similar numbers of male and female mice were used

for cellular biology and electrophysiology experiments, whereas only males were used for behavioral experiments.

Acute Brain Slices and Immunofluorescence Microscopy

Brains were rapidly dissected and placed into ice-cold artificial cerebrospinal fluid (ACSF) (in mM): 150 NaCl, 3 KCl, 1 $CaCl_2$, 1 $MgCl_2$, 1.25 NaH_2PO_4, 26 $NaHCO_3$, and 10 D-glucose, pH 7.4. Sagittal slices (200 μm) were cut at 4°C with a vibratome (Campden Instruments) and fixed in 4% PFA/4% sucrose (w/v) in PBS for 20–30 min at RT. Sections were subsequently washed with PBS and blocked in 10% donkey serum and 0.02% Triton X-100 in PBS for ∼4 h at RT. Primary antibodies against vesicular GABA transporter (vGAT) (Synaptic Systems, 1:1000), Gephyrin (Synaptic Systems, 1:500), GABAARα1 (Millipore, 1:500), GABABR2 (Millipore 1:250), vGlut1 (Millipore, 1:1000), PSD95 (Abcam, 1:500), D1R (Sigma, 1:200), D2R (Millipore, 1:500), Vesicular monoamine transporter 2 (VMAT2) (Acris, 1:1000), EGFP (Millipore, 1:1000), and Microtubule-associated protein 2 (MAP2) (Abcam, 1:500) were incubated overnight at 4°C. Secondary antibodies conjugated with Alexa 488, Alexa 568, and Alexa 647 from Invitrogen (dilution 1:800) were used. For the cell nucleus labeling, Hoechst (Sigma, 1:10,000) was used. Slices were washed in PBS and mounted in Fluoromount-G (SouthernBiotech). In some experiments, sagittal slices (300 μm) used for electrophysiology were stained after recordings for Neurobiotin and EGFP.

Confocal Microscopy

Confocal images were acquired using Olympus FV1000 or Leica DMRE confocal microscopes using a 60 × 1.35 NA oil objective or 63 × 1.40 NA oil objective, respectively. Image stacks of eight equidistant planes (∼200 nm) of 76 nm/pixel × 76 nm/pixel were taken for each field. Analyses were performed using Volocity software (Perkin Elmer). Images were acquired from four to six mice. Three to four brain slices were evaluated per mouse, and three images were taken per slice. Synaptic puncta volume and number as well as VMAT2 intensity were quantified in Volocity using custom protocols based on standard thresholding techniques. Number of pre- or postsynaptic puncta and number of synapses (determined by the co-localization of a pre- and postsynaptic marker) were normalized to control mice that were fed with doxycycline for 14 days and expressed as percentage of control. Data from different independent experiments were pooled and significance was tested by non-parametric Mann–Whitney or Kruskal–Wallis ANOVA depending on the number of comparisons.

Accelerating Rotarod

Mice fed for 14 days with doxycycline and subsequently fed with normal diet for additional 2–3 weeks were evaluated on an accelerating rotarod task. Mice were placed on a rotarod (Med Associates) accelerating from 4 to 40 rpm in 5 min and the latency to fall was recorded. Mice performed five consecutive trials per day (∼30 s rest between trials), for a total of four consecutive days. Maximum trial length was 5 min, after which the animals were returned to the cage. Data from eight control and eight iDkk1 mice was evaluated by repeated measures one-way ANOVA.

Amphetamine Induced Locomotion

Motor activity was recorded in eight identical activity monitor chambers (43 cm × 43 cm) equipped with 16 infrared light emitters and detectors (Med Associates), connected to a computer that counts the number of times the photo beams are broken (as the animal crosses between the emitter and the detector). The total number of horizontal beam breaks was used as a measure of locomotion. Mice fed with doxycycline for 14 days and subsequently returned to normal diet for an additional 2–3 weeks were placed individually in the activity chamber and habituated for 1 h prior to the experiment. After habituation, mice were intraperitoneally administered with amphetamine (D-amphetamine sulfate, Sigma, 2 mg/kg in saline) or saline as control. Locomotion was monitored for 1 h immediately after the injection by registering the infrared photo beam interruptions. Significance was evaluated by two-way ANOVA (four control mice injected with saline, five control mice injected with amphetamine, four iDkk1 injected with saline, and four with amphetamine).

Slice Preparation for Electrophysiology

Brains were rapidly removed and placed into ice-cold "slicing solution" containing (in mM): 75 sucrose, 87 NaCl, 25 $NaHCO_3$, 2.5 KCl, 1.25 NaH_2PO_4, 10 glucose, 0.5 $CaCl_2$, and 7 $MgCl_2$ bubbled with 95% O_2 and 5% CO_2. Sagittal slices (300 μm) containing the striatal region were prepared with a vibratome (Leica, Germany) and kept in an oxygenated holding chamber containing (in mM): 125 NaCl, 26 $NaHCO_3$, 2.5 KCl, 1.26 NaH_2PO_4, 25 glucose, 2 $CaCl_2$, and 1 $MgCl_2$ (Krebs solution) at RT and maintained at pH 7.4 by permanent bubbling with 95% O_2 and 5% CO_2.

Electrophysiological Recordings

After 1-h recovery period, slices were transferred to a recording chamber on an upright microscope with Normanski-differential interference contrast optics (Zeiss Axioskop, Germany) and continuously perfused with oxygenated Krebs solution at RT (22–24°C). Patch-clamp recording pipettes were made from thick-walled borosilicate glass (GC150F, Harvard Apparatus, Kent, United Kingdom) using a vertical pipette puller (Narashige) and filled with a Cs Gluconate-based pipette solution, containing (in mM): 139 D-gluconic acid lactone, 10 HEPES, 10 EGTA, 10 NaCl, 0.5 $CaCl_2$, 1 $MgCl_2$, 1 ATP, and 0.5 GTP adjusted to pH 7.2 with CsOH and 3 μg/ml Neurobiotin (Vector Labs) or 135 K-gluconate, 10 HEPES, 0.1 EGTA, 10 KCl, 0.5 $CaCl_2$, 2 $MgCl_2$, 5 phosphocreatine, 2 ATP, and 0.5 GTP. Individual MSNs from the dorsal part of the striatum were voltage-clamped at −80 mV following establishment of whole-cell mode. Membrane capacitance was estimated "online" using the Axopatch 200B amplifier capacitance cancelation circuit to cancel the current capacitance transients evoked in voltage-clamp mode in response to 5-mV, 20-ms duration depolarizing voltage steps evoked at −70 mV as previously described (Sherman-Gold, 1993).

Neurons were identified by morphological and electrophysiological criteria (cell size, membrane capacitance, and cell response to depolarizing current injection). In triple transgenic mice, iDkk1-D2R-GFP (which labels MSNs from the indirect pathway), neurons were identified by the expression of EGFP. Some large cholinergic interneurons express D2R; therefore, GFP-positive cells that had a morphology (cell body diameter of more than 20 μm) and a firing pattern (accommodating spike firing) typical of large cholinergic interneurons were excluded from the mEPSCs and the morphology analyses. In these experiments, Cs-gluconate-based internal solution was used. Currents were recorded using an Axopatch 200B Amplifier (Axon Instruments, United States), filtered at 1 kHz, and digitized in the computer at 10 kHz with a Micro 1401 interface (Cambridge Electronic Design, United Kingdom). The data were acquired with Win EDR and analyzed using Win EDR and Win WCP (Strathclyde Electrophysiology Software freely available at: http://spider.science.strath.ac.uk/sipbs/showPage.php?page=software_ses).

Whole-cell current-clamp recordings were made with patch pipettes containing K+-gluconate-based pipette solution. Once whole-cell configuration was stabilized, the holding current was adjusted to set a membrane potential of −70 mV and then 500-ms duration current steps were applied at 10-s intervals from 10 to 100 pA in amplitude in 10-pA increments, and the resulting membrane potential depolarizations and action potential firing were recorded at a bandwidth of 2 kHz and digitized at 10 kHz. To record the miniature postsynaptic currents, 0.5 μM Tetrodotoxin (TTX) was added to the Krebs solution. Recordings of mIPSCs were made at +10 mV. The mIPSC decay was best fit by two exponential components using the following equation where current (I) is measured in pA and time constant τ in ms: $I_{total} = I_{fast}\exp(-\text{time}/\tau_{fast}) + I_{slow}\exp(-\text{time}/\tau_{slow})$, where τ_{fast} and τ_{slow} are the deactivation time constants for the fast and slow components, respectively. To summarize, in the mIPSC deactivation kinetics, a weighted decay time constant was calculated using the following equation: $\tau_{weighted} = (\tau_{fast}I_{fast} + \tau_{slow}I_{slow})/(I_{fast} + I_{slow})$.

Data are presented as mean ± standard error (SE), with n indicating the number of cells, which also corresponds to the number of slices since, for each cell, excitability was first recorded without TTX and then TTX was added to the external solution to record mIPSCs. Statistical analyses were performed using SPSS 26. A log10 transformation of the mIPSC frequency values was applied to meet parametric test criteria. Two-way ANOVA (genotype and type of neuron) was performed and revealed a significant difference between different types of neurons (D1R and D2R MSN; $p = 0.0001$) and a significant interaction between the genotype and the type of neurons ($p = 0.006$). Student's t-test was then used to compare pairs of observations within each type of neuron patched in whole-cell patch-clamp configuration.

Filling, Staining, and Reconstruction of MSN Morphology

To track the dendritic arbor of the recorded neurons, 3 μg/ml Neurobiotin (Vector Labs) was added into the intracellular solution. The MSNs were patched in whole-cell clamp configuration for at least 15 min to allow the spread of the Neurobiotin. Consequently, the slices were fixed in 4% PFA for 24–48 h, washed in 0.1 M PBS, blocked in 10% donkey serum, permeabilized with 0.05% Triton X-100, and then incubated for 2 h with 2 mg/ml Alexa Fluor® 594 Streptavidin (Thermo Fisher Scientific). For the neuronal reconstruction, the open-source software ImageJ (Fiji) (Schindelin et al., 2012) was used.

Statistical Analyses

All data were explored for normality, outliers, and fulfillment of statistical test assumptions in SPSS 26 (IBM Corp., Armonk, NY, United States). When samples are normally distributed and their variance are homogeneous, parametric tests were used. Student's t-test to compare pairs of observations and one-way ANOVA or two-way ANOVA with Tukey's *post hoc* correction for multiple group comparisons were made. When data failed to meet those criteria, we used a non-parametric test such as Mann–Whitney U to compare two groups or Kruskal–Wallis non-parametric ANOVA. Generally, $^{*}p < 0.05$, $^{**}p < 0.01$, and $^{***}p < 0.005$.

RESULTS

Induced Dkk1 Expression Triggers GABAergic Synapse Degeneration in the Adult Striatum

Our previous studies showed that deficient Wnt signaling triggers the loss of excitatory and dopaminergic synapses in the adult mouse striatum (Galli et al., 2014). We therefore examined whether GABAergic synapses, which are the most abundant synapses in the striatum, were also affected by a deficiency in the Wnt pathway. We used the double transgenic iDkk1 mouse model in which Wnt signaling activation, in response to Wnts, is blocked by inducing the expression of the specific and potent Wnt antagonist Dkk1 (Galli et al., 2014; Marzo et al., 2016; **Figure 1A**). We used a transgenic mouse line expressing Dkk1 under the control of the tetracycline-inducible system and the Ca^{2+}/calmodulin-dependent protein kinase II (CaMKII) promoter resulting in the expression of the transgene in principal neurons of brain (Mansuy et al., 1998). Previous studies showed that expression of the LacZ gene under this promoter system is mainly expressed in large neurons in the striatum but not in small neurons, suggesting that the CamKII promoter probably drives expression in MSNs and in large cholinergic interneurons but not in small interneurons (Odeh et al., 2011). Our previous studies showed that Dkk1 is expressed in the striatum after adult mice were fed with doxycycline (Galli et al., 2014). Using this inducible system, Wnt signaling was unaffected during embryonic and postnatal development when this pathway is required for embryonic patterning, axon guidance, and synapse formation (Budnik and Salinas, 2011; Nusse and Clevers, 2017). In addition, our previous studies showed that induction of Dkk1 expression for 14 days does not affect cell death in the striatum (Galli et al., 2014). To determine the impact of Dkk1 on GABAergic synapses, we

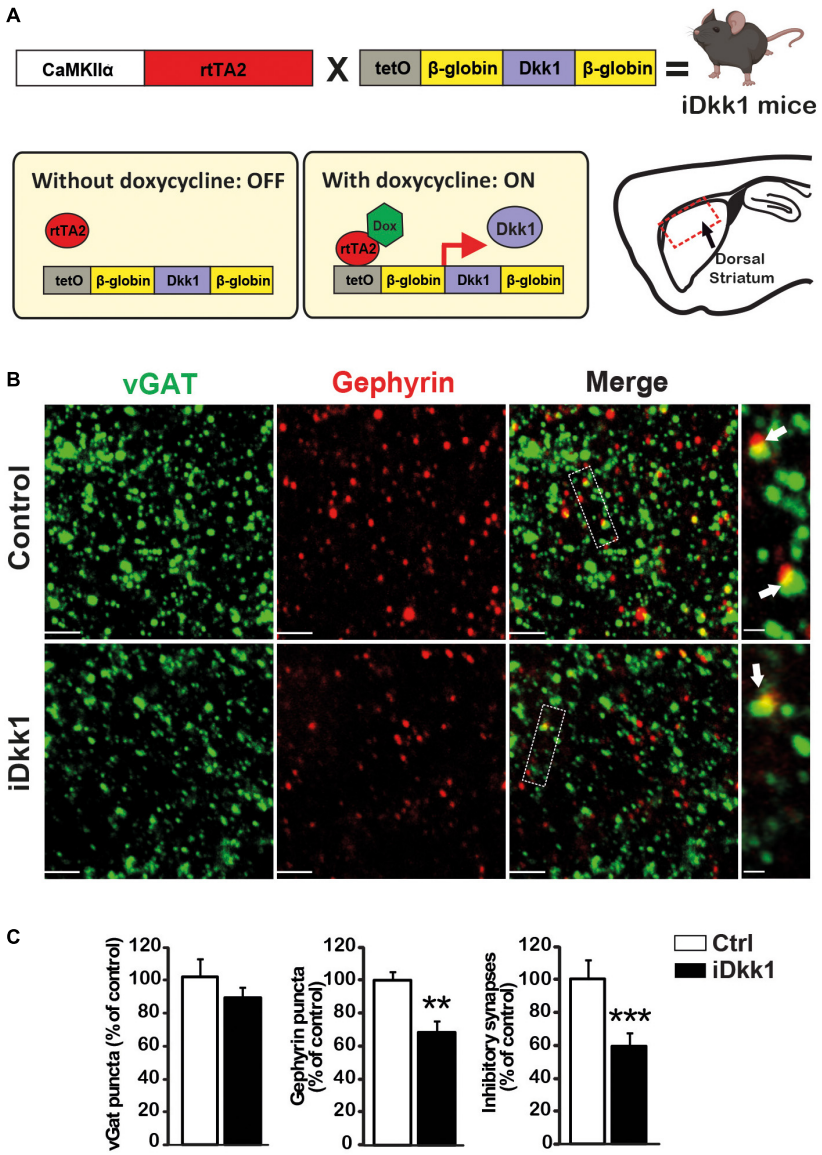

FIGURE 1 | Induction of Dkk1 induces 40% loss of inhibitory synapses in dorsal striatum. **(A)** Schematic representation of the generation of iDkk1 mice by the crossing of mice carrying the Dkk1 cDNA under the control of a doxycycline responsive promoter (tetO) with mice carrying the doxycycline-controlled transactivator 2 (rtTA2) downstream of the CaMKIIα promoter. In the absence of doxycycline (OFF), Dkk1 expression was not induced, whereas in animals fed with doxycycline (ON), Dkk1 is expressed, notably but not exclusively, in the dorsal striatum, the region under study here (red square on the sagittal brain scheme) in iDkk1 mice. **(B)** Confocal images from dorsal striatum show a dramatic reduction in inhibitory synapse number (white arrows) based on the co-localized pre- and postsynaptic markers; vGAT (green) and Gephyrin (red) puncta. The scale bars represent 2 μm; Dashed boxes correspond to enlarged areas depicted on the right-most panels, scale bar: 0.5 μm. **(C)** Forty percent of inhibitory synapses were lost in iDkk1 mice as shown on the quantification of pre- and postsynaptic markers and their co-localization. $N = 5$ mice per group; $^{**}p < 0.01$; $^{***}p < 0.005$, Mann–Whitney.

evaluated the co-localization of the inhibitory presynaptic marker vGAT and the postsynaptic marker Gephyrin in the dorsal striatum. Single transgenic mice that do not express Dkk1 were fed with doxycycline for 14 days and used as controls. In double transgenic mice, induction of Dkk1 expression did not affect the number or volume of presynaptic terminals labeled with vGAT (**Figures 1B,C** and **Supplementary Figure 1A**) but induced a significant decrease (30–35%) in the number of Gephyrin puncta. Importantly, Dkk1 induced a significant decrease (40%) in the number of inhibitory synapses based on the co-localization of vGAT and Gephyrin puncta (**Figures 1B,C**). However, Dkk1 did not affect the volume of the postsynaptic scaffolding protein Gephyrin (**Supplementary Figure 1B**). Next, we investigated whether the number of GABAA receptors (GABAAR α1 and GABABR2) was affected by Dkk1 induction. GABAAR α1 cluster number was unaffected by Dkk1 as assessed by immunostaining (**Supplementary Figure 1C**). In contrast, GABABR2 cluster number and co-localization with VAMP2, a

presynaptic marker, were significantly decreased in the striatum of iDkk1 mice (**Supplementary Figure 1D**). Thus, blockade of Wnt signaling in the adult striatum results in the loss of GABAergic synapses and a decrease in GABABR2 puncta, demonstrating a critical role for endogenous Wnts in the maintenance of inhibitory synapses.

Dkk1 Affects GABAergic Synapses of the Indirect Pathway in the Striatum

Inhibitory synaptic connections in the striatum come from reciprocal contacts between MSNs and local interneurons (Koos and Tepper, 1999; Koos et al., 2004; Taverna et al., 2008). As MSNs expressing D1R (D1-MSNs) or D2R (D2-MSNs) are characteristic of the direct and indirect basal ganglia pathways, respectively, we decided to determine whether Dkk1 specifically affects a subpopulation of MSNs. We therefore crossed iDkk1 mice with D2R-BAC EGFP mice, which specifically express EGFP in D2-MSNs (Gong et al., 2003; Wang et al., 2006). We verified that EGFP-labeled neurons were D2-MSNs by examining their action potential firing profile (**Figure 2A**) coupled to *post hoc* EGFP immunolabeling. Our electrophysiological recordings revealed a clear difference in the pattern of firing between D1-MSNs (low excitability) and other types of neurons (D2-MSNs and interneurons). For example, D2R-EGFP cells exhibited sustained and high excitability when compared to EGFP-negative neurons possibly representing D1-MSNs (**Figure 2A** and **Supplementary Figure 2**) as described previously (Gertler et al., 2008; Cazorla et al., 2012). Dkk1 expression was induced in the adult brain by feeding D2-iDkk1 mice with doxycycline for 14 days. Single transgenic D2 mice that do not express Dkk1 were also fed with doxycycline for 14 days and used as controls. No significant differences of resting membrane potential (zero current potential) were observed between D1- and D2-MSNs or following Dkk1 expression (control D1-MSN, -73.7 ± 1.53 mV; iDkk1 D1-MSN, -75.0 ± 0.97 mV; control D2-MSN, -75.8 ± 1.49 mV; iDkk1 D2-MSN, -75.8 ± 0.88 mV). These data were in accordance with analyses of electrical properties of the cells, which showed no significant difference in estimated membrane capacitance (control D1-MSN, 25.9 ± 1.76 pF; iDkk1 D1-MSN, 23.7 ± 0.98 pF; control D2-MSN, 25.4 ± 1.15 pF; iDkk1 D2-MSN, 22.0 ± 0.62 pF). Recorded cells were then filled with Neurobiotin to visualize their dendritic arborization to allow quantification of their size and complexity (**Figure 2B**).

Once we had established our ability to identify and record from different neurons in the striatum, we next investigated possible functional changes in inhibitory synaptic function by recording miniature postsynaptic currents (mIPSCs) in MSNs when Dkk1 was induced. mIPSCs were recorded on D2-MSNs (GFP labeled) and D1-MSNs (GFP-negative cells, *post hoc* labeled with Neurobiotin and assessed for morphology). We found that Dkk1 did not affect the amplitude of the mIPSCs in either population (**Figure 2C**, upper panel). In contrast, a significant decrease in the frequency of mIPSCs (∼50%) was observed in D2-MSNs (GFP labeled) whereas no changes were recorded from D1-MSNs (**Figure 2C**). For both classes of neurons, Dkk1 expression did not affect mIPSC current kinetics (weighted tau decay: D1-MSN, 18.5 ± 0.91 ms; control D2-MSN, 20.1 ± 0.99 ms; iDkk1 D1-MSN, 20.1 ± 1.00 ms; iDkk1 D2-MSN, 19.3 ± 0.67 ms). These results reveal that deficiency in Wnt signaling affected inhibitory synaptic transmission in a subpopulation of neurons in the dorsal striatum, the D2-MSNs.

We next interrogated the possibility that Dkk1 affects the frequency of mIPSCs in the D2R-neurons by affecting dendritic arborizations. The morphology of recorded D2R-GFP cells in control and Dkk1 expressing mice was quantified by Sholl analyses. However, no significant differences were observed in dendritic arborization (number of dendritic branches) or in the total dendritic length (**Figure 2D**), suggesting that Dkk1 affected the frequency of mIPSCs in D2-MSN neurons without inducing without inducing changes in dendritic arborization. We found that the membrane capacitance was the same in the presence or absence of Dkk1. Previous studies have shown that dendritic morphology is correlated with changes in membrane capacitance (Matsumura et al., 2018). These results are consistent with our finding that Dkk1 does not affect dendritic morphology.

The Loss of Inhibitory Synapses Is Reversible

It is well documented that in several neurodegenerative diseases, synapses are lost at early stages (Scheff et al., 2006; Shankar and Walsh, 2009; Milnerwood and Raymond, 2010; Soukup et al., 2018), but it remains poorly understood if synapse number and function can be fully restored after substantial synapse degeneration. We recently found that excitatory synapse loss in the hippocampus triggered by induced Dkk1 expression can be fully reversed by reactivation of Wnt signaling (Marzo et al., 2016). These findings led us to investigate whether turning off Dkk1 expression could restore the number of inhibitory synapse to that of control levels. For these experiments, we induced Dkk1 expression for 14 days using doxycycline (ON period) followed by the withdrawn of doxycycline, for 2 weeks (iDkk1 ON–OFF) (**Figure 3A**), as previously done in the hippocampus (Marzo et al., 2016). As shown in **Figure 1**, induction of Dkk1 expression for 2 weeks did not affect the number of vGAT presynaptic terminals (**Figures 3B,C**) but significantly reduced the number of postsynaptic Gephyrin puncta and therefore the number of GABAergic synapses, as measured by the co-localization of vGAT and Gephyrin (**Figures 3B,C**). Upon cessation of Dkk1 expression for 2 weeks, the numbers of Gephyrin puncta and inhibitory synapses were restored to control levels (**Figures 3B,C**). These results demonstrate that inhibitory synapse number recovers after restoring Wnt signaling in the adult striatum.

Decreased Dopaminergic Synapse Number Is Reversible Upon Dkk1 Termination

A striking defect induced by Dkk1 in the dorsal striatum is the loss of dopaminergic receptors (Galli et al., 2014). We next examined whether withdrawal of Dkk1 after synapse degeneration affects the number of D1R and D2R receptor

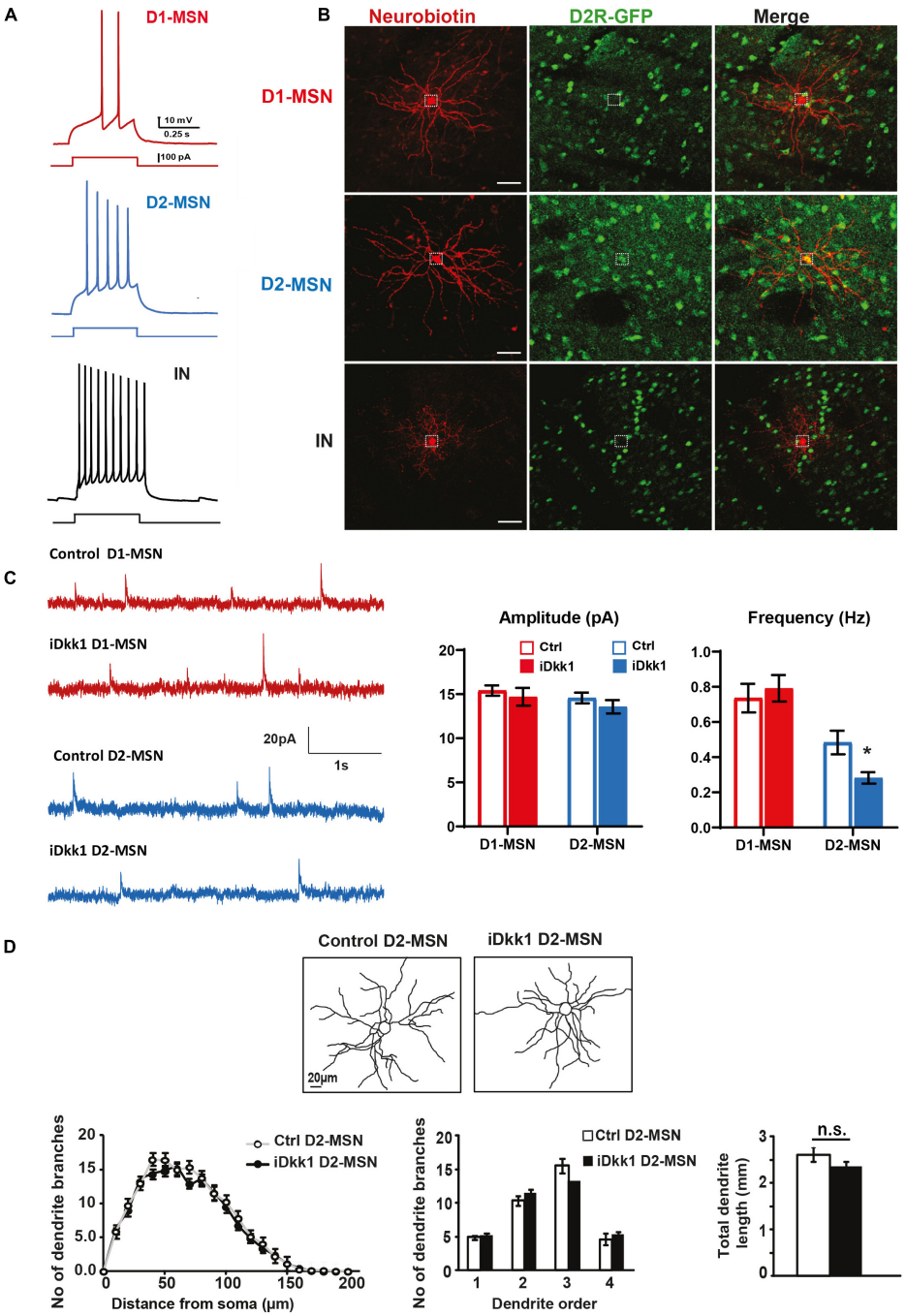

FIGURE 2 | Dkk1 decreases the frequency of mIPSCs only in D2-MSNs, without affecting their morphology. **(A)** Resting membrane potential (Vm) was similar in all conditions. Holding currents were adjusted to set a membrane potential of −70 mV, and these recordings were thus performed at rest. Representative traces showing action potentials (AP) elicited with a 500-ms current step of 100 pA. D1-MSNs (red) show a low firing rate. In contrast, D2-MSNs (blue) and interneurons (black, IN) are highly excitable. IN and D1-MSNs were distinguished based on their morphology and their AP firing patterns. **(B)** Confocal images of Neurobiotin-filled neurons in D2-iDkk1 mice. EGFP-labeled D2-MSNs were filled with Neurobiotin and show a large dendritic arbor. EGFP-negative neurons reveal either extensive branching (D1-MSNs) or small dendritic arbors (INs). The dashed circles represent a neuronal cell body. The scale bar represents 40 µm. **(C)** Representative traces of mIPSCs from D1-MSN (top traces) and D2-MSNs (lower traces) as indicated from control mice and from iDkk1 mice after induction of Dkk1 expression. mIPSC amplitude was not affected by Dkk1 in D1-MSNs or D2-MSNs (top panel). In contrast, the frequency of mIPSC is reduced only in D2-MSNs after induction of Dkk1 but not in D1-MSNs (lower panel). N = 17–21 cells recorded from four animals per condition; $^*p < 0.05$, two-way ANOVA with interaction followed by Tukey's *post hoc* tests. **(D)** Reconstruction of Neurobiotin-filled D2-MSNs (left panels). Sholl analysis (number of intersections), quantification of dendritic branches per dendritic order (1st, 2nd, 3rd, and 4th order) (repeated measure one-way ANOVA), and total length of dendrites (*t*-test) showed that Dkk1 does not affect D2-MSN dendritic morphology. N = 15 cells were evaluated from seven animals of each genotype.

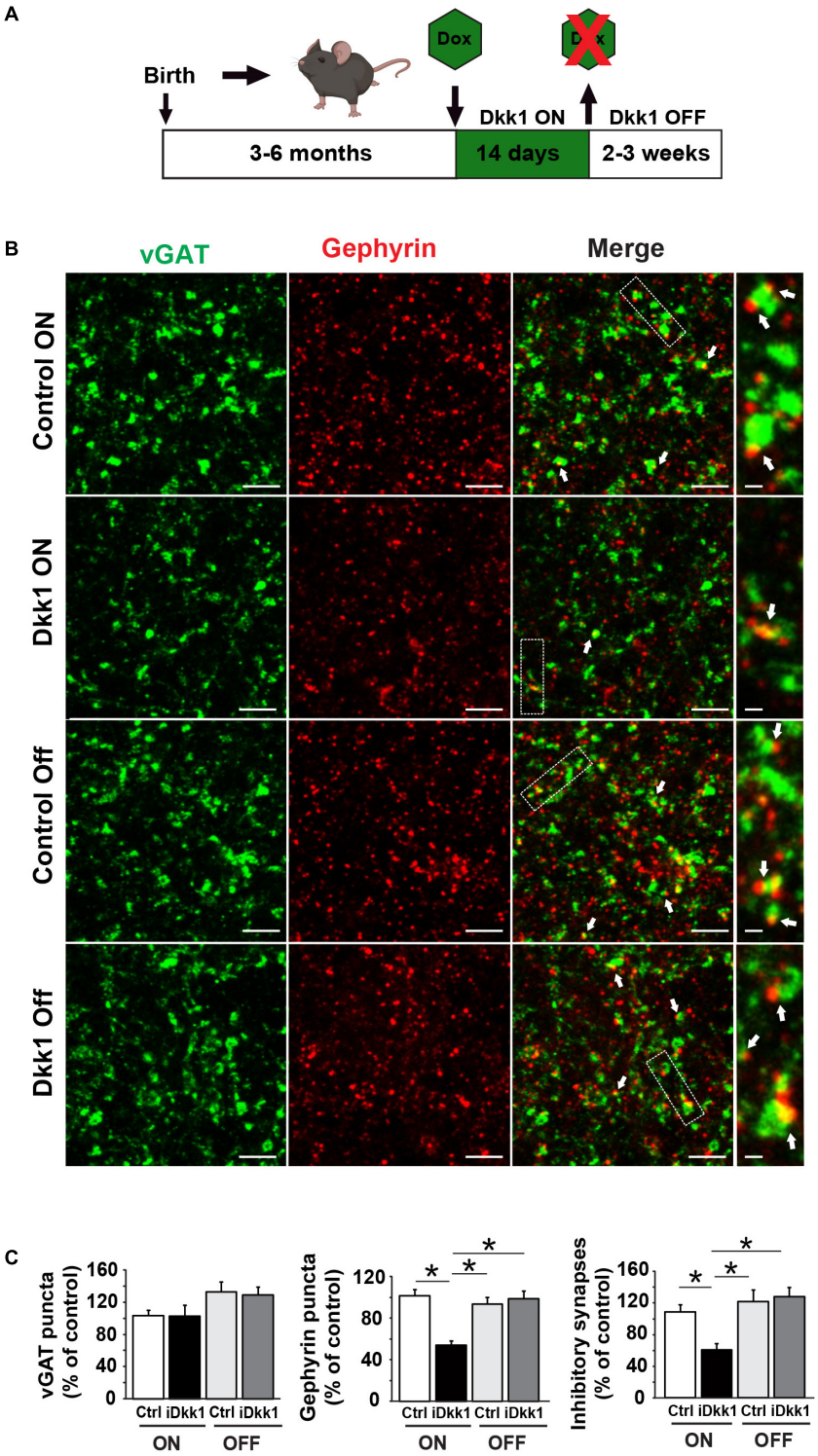

FIGURE 3 | Cessation of Dkk1 expression leads to full recovery of inhibitory synapse number. **(A)** Schematic diagram of the iDkk1 ON–OFF model. Three- to six-month adult mice were fed with doxycycline food (green hexagon) for 14 days, which induced the expression of Dkk1. Doxycycline feeding, and therefore induced Dkk1 expression, was then stopped for 2–3 weeks before using the animals for experiments. **(B)** Confocal images show a reduction in the number of inhibitory synapses based on the co-localization (white arrows) of pre-synaptic vGAT (green) and postsynaptic Gephyrin (red) puncta after induction of Dkk1 following doxycycline (iDkk1 ON) when compared to control mice exposed to doxycycline (Control ON). Synapse number recovered after cessation of Dkk1 expression (iDkk1 OFF). The scale bars represent 2 μm; Dashed boxes correspond to enlarged areas depicted on the right-most panels and scale bars represent 0.3 μm. **(C)** Quantification of the number of synapses based on the co-localization of pre- and postsynaptic markers. *$p < 0.05$, Kruskal–Wallis.

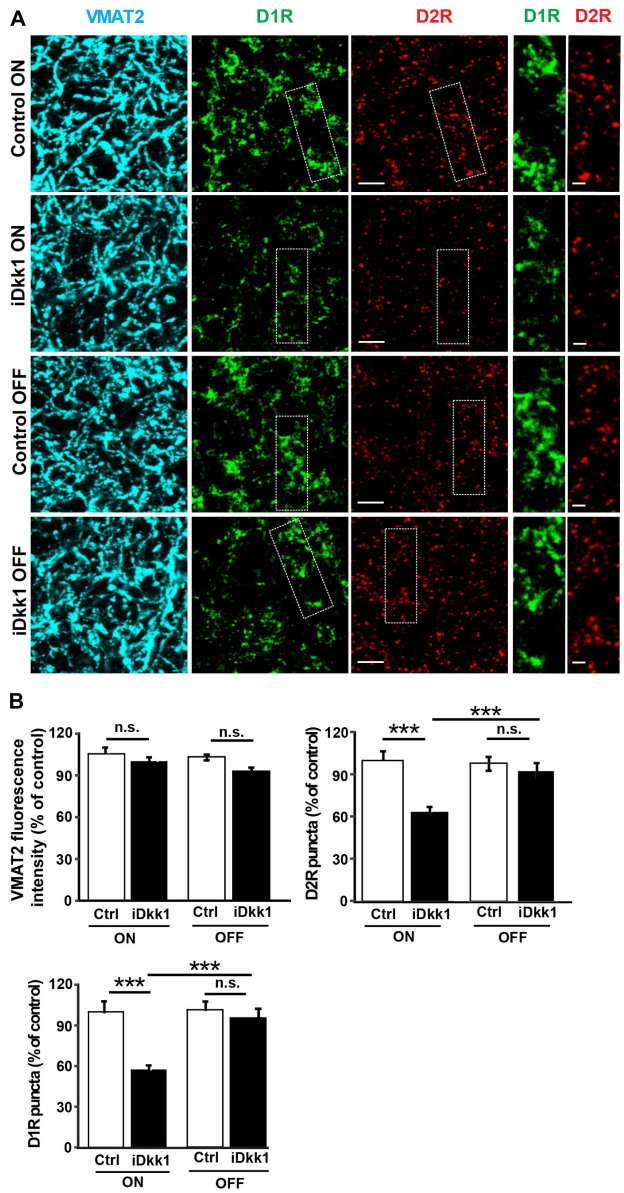

FIGURE 4 | Dopaminergic receptor cluster number is restored when Dkk1 expression is turned off. **(A)** Confocal images from the adult striatum reveal no change in dopaminergic afferents labeled with VMAT2 (blue) following induction of Dkk1 (iDkk1 ON) when compared to control mice exposed to doxycycline (Control ON). In contrast, the numbers of D1R (green)- and D2R-labeled puncta (red) decreased in the presence of Dkk1 (iDkk1 ON) but were restored with cessation of Dkk1 expression (iDkk1 OFF). The scale bars represent 2.5 μm; dashed squares are enlarged on the side and the scale bars represent 0.5 μm. **(B)** Quantification of the VMAT2 intensity and D1R- and D2R-labeled puncta number relative to the control show that the number of D1R- and D2R-labeled puncta fully recovered after turning off Dkk1 expression. $N = 5$ mice per group; $^{***}p < 0.001$, Kruskal–Wallis.

clusters. We first induced Dkk1 expression for 2 weeks (ON) in the striatum of iDkk1 mice and evaluated endogenous D1R and D2R receptor clusters and dopaminergic axon terminals labeled with an antibody against the vesicular monoamine transporter 2 (VMAT2). Dkk1 did not induce axon terminal degeneration as determined by VMAT2-labeled processes (**Figure 4A**) as we previously showed (Galli et al., 2014). In contrast, Dkk1 expression triggered a 40% loss in D1R- and D2R-labeled puncta (**Figures 4A,B**). Conversely, termination of Dkk1 expression resulted in the full recovery of the number of D1R and D2R receptor clusters to control levels (**Figures 4A,B**). Together, these studies showed that deficient Wnt signaling triggers the loss of dopaminergic and GABAergic synapses in the striatum but cessation of Dkk1 expression results in the full regeneration of these synapses.

D1R Recovery Correlates With Normal Amphetamine-Induced Locomotion After Dkk1 Cessation

Dopamine innervation to the dorsal striatum is essential for motor control. Potentiation of dopamine signaling by psychostimulants like amphetamine increases locomotion through D1Rs (Xu et al., 1994; Natarajan and Yamamoto, 2011). Indeed, the decrease in D1R and D2R expression in the striatum upon induction of Dkk1 for 2 weeks correlates with the inability of amphetamine to increase locomotion in iDkk1 mice (Galli et al., 2014). As termination of Dkk1 expression induces the recovery in the number of D1R clusters (**Figure 4**), we predicted that iDkk1 mice that had been taken off doxycycline feeding would respond normally to amphetamine. Indeed, amphetamine exposure significantly increased locomotion in control mice. The iDkk1 ON–OFF mice (**Figure 3A**) responded to amphetamine in a similar manner to control mice injected with amphetamine (**Figure 5A**). Given our previous finding that induction of Dkk1 results in the lack of response to amphetamine (Galli et al., 2014), our results here suggest that the response to the psychostimulant was fully restored following the cessation of Dkk1 expression.

Restoration of Wnt Signaling Leads to Normal Motor Coordination

We have previously shown that induced expression of Dkk1 in the adult brain altered normal striatum-regulated behavior, such as motor coordination and learning, evaluated by the performance of animals on the accelerating rotarod (Galli et al., 2014). Although the accelerating rotarod tests striatal function (Dang et al., 2006; Yin et al., 2009), it also assesses cerebellar function (Shiotsuki et al., 2010; Woo et al., 2018). As Dkk1 expression is driven by the CaMKII promoter (**Figure 1**), which is not expressed in the adult cerebellum (Mansuy et al., 1998), the defects in the rotarod are mainly due to the impact of Dkk1 on striatal function. The defect in the rotarod exhibited by iDkk1 mice is probably directly linked to loss of dopaminergic receptor clusters. Given the recovery of synapse number and the response to amphetamine in iDkk1 mice following cessation of Dkk1 expression, we decided to test the latency to fall in these animals when placed on the accelerating rotarod. We observed that upon termination of Dkk1 expression, iDkk1 mice performed well on the rotarod during the first day, when animals were naïve to the task, and also throughout days 2–4 in a similar manner to control animals (**Figure 5B**). Both iDkk1 and control mice exhibited

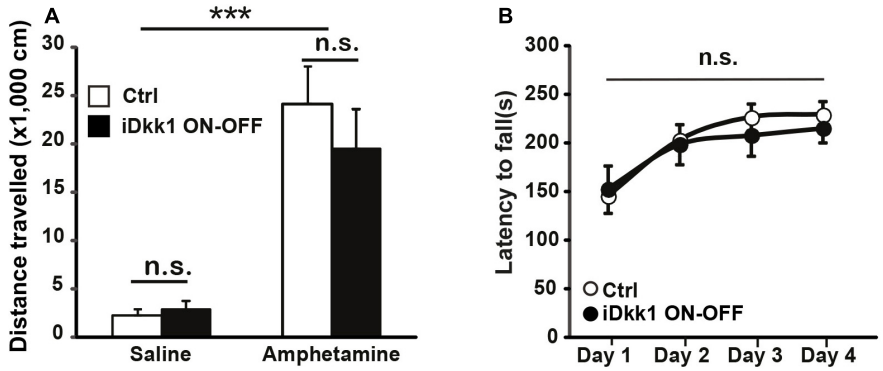

FIGURE 5 | Behavioral defects are reversed by cessation of Dkk1 expression. **(A)** Intraperitoneal injection of amphetamine (2 mg/kg) increases the traveled distance in the open field; ***$p < 0.001$, two-way ANOVA. However, no differences were observed between control and iDkk1 ON–OFF mice ($p > 0.05$) by two-way ANOVA. $N = 4$–5 mice per group. **(B)** Performances on the accelerating rotarod are identical between control and iDkk1 mice following cessation of Dkk1 expression (iDkk1 ON–OFF); $p > 0.05$, repeated measures one-way ANOVA. $N = 8$ mice per group.

similar improvement between sessions (**Figure 5B**), suggesting that both sets of animals have the same ability to learn. Thus, cessation of Dkk1 expression following synapse degeneration results in the full recovery of striatum function.

DISCUSSION

We previously showed that blockade of endogenous Wnts through the inducible expression of Dkk1 results in the substantial loss of excitatory and dopaminergic synapses in the adult striatum without affecting cell viability (Galli et al., 2014). In the current study, we demonstrate that Wnt signaling also plays an important role in inhibitory synapse integrity in the adult striatum. Indeed, we show for the first time that Dkk1 affects the function of D2-MSN GABAergic synapses. Importantly, reactivation of the Wnt signaling pathway after significant synapse loss results in the normal number of GABAergic and dopaminergic synapses, normal motor coordination and learning, and response to amphetamine regarding motor activity.

Studies have demonstrated that Wnt signaling is required for synapse integrity in several areas of the adult brain. Induced expression of Dkk1 in the adult hippocampus triggers the loss of 40% of excitatory synapses. However, inhibitory synapses are unaffected, suggesting that Dkk1 does not target inhibitory synapses in the hippocampus (Marzo et al., 2016). In the striatum, in contrast, induced Dkk1 expression resulted in a significant decrease in the number of inhibitory synapses. Importantly, patch-clamp recordings revealed that Dkk1 expression significantly decreased the frequency of mIPSCs in D2R-expressing MSNs, but it does not seem to affect GFP-negative neurons representing mostly D1R-expressing MSNs. D2-MSNs are part of the indirect pathway, which is one of the two main outputs of the striatum and is often described as the "no go" pathway as it inhibits thalamo-cortical activation (Bamford et al., 2018). *In vivo* optogenetic excitation of indirect-pathway MSNs in mice leads to a parkinsonian state, characterized by increased freezing, bradykinesia, and decreased locomotor activity (Kravitz et al., 2010). Thus, our finding that Dkk1 reduced inhibitory transmission in D2-MSN neurons suggests a higher activity in these neurons. However, we previously reported that 50% of excitatory corticostriatal synapses are lost after Dkk1 induction (Galli et al., 2014), which could balance for the loss of inhibitory inputs onto MSNs of the indirect pathway. Thus, further studies are required to determine the effect of Dkk1 on the direct or indirect pathway at the network level.

What are the mechanisms underlying the difference in the susceptibility of inhibitory synapses in the hippocampus and the striatum and also between D1-MSNs and D2-MSNs? Dkk1 antagonizes Wnt signaling by binding to the Wnt co-receptor, the low-density lipoprotein receptor-related protein 6 (LRP6), therefore preventing the formation of the Wnt–Fz–LRP6 complex and the subsequent activation of the Wnt signaling cascade (Mao et al., 2001; Buechler and Salinas, 2018). Given that inhibitory synapses differ between brain regions and between neuronal types (Kubota et al., 2016), it is possible that inhibitory synapses in the hippocampus and striatum, or between D1-MSNs and D2-MSNs, express a different level of LRP6 or other Wnt receptors at the cell surface, making some of these synapses more susceptible to Dkk1 than others. Further studies are required to determine the mechanisms that lead to this different susceptibility to Dkk1.

Deficiency in Wnt signaling has been linked to neurodegenerative diseases. In particular, increasing evidence suggests that deficiency in canonical Wnt signaling could contribute to synapse degeneration in Alzheimer's disease (Purro et al., 2012; Liu et al., 2014; Marzo et al., 2016). However, links between Wnt signaling and PD/HD are beginning to emerge. First, proteomic analyses of dopamine neurons from the rotenone-induced PD model reveals deficits in Wnt signaling (Stephano et al., 2018). Second, gain of function of Wnt4 is protective in a model of PD in the fly (Wu et al., 2019). Third, several genes linked to PD have been shown to interact with Wnt components or modulate Wnt signaling (Rawal et al., 2009; Berwick and Harvey, 2014). Of particular interest is the leucine-rich repeat kinase 2 (LRRK2), a serine/threonine kinase

linked to familial PD, which interacts with several components of the Wnt pathway such as LRP6 and Dishevelled (Dvl) (Sancho et al., 2009; Berwick and Harvey, 2012). Importantly, familial LRRK2 mutations exhibit decreased Wnt signaling probably due to defects in the interaction with Wnt components (Berwick and Harvey, 2012). Furthermore, the vacuolar protein sorting protein 35 (Vps35), an essential retromer subunit, regulates Wnt secretion (Belenkaya et al., 2008) and has been linked to autosomal dominant late-onset PD (Zimprich et al., 2011). Finally, polymorphisms in certain Wnt signaling components including Gsk3β have been linked to PD (Berwick and Harvey, 2014). However, a link between Wnt signaling and HD is less clear. For example, a mutant huntingtin has been linked to β-catenin degradation (Godin et al., 2010) and HD Research Crossroad database showed Wnt signaling as a possible target in HD (Kalathur et al., 2012). Our finding that Wnt deficiency affects inhibitory synapses in D2-MSNs is interesting because these neurons are particularly affected in dopamine depletion PD models (Day et al., 2006) and are vulnerable in human HD and in mouse models of HD (Albin et al., 1992; Andre et al., 2011a,b; Cepeda et al., 2013). Moreover, deficient Wnt signaling in the striatum triggers synapse degeneration and motor defects (Galli et al., 2014) as observed in PD and HD. Together, these findings suggest a potential link between dysfunction of Wnt signaling and PD and HD.

Although a link between Wnt signaling in PD and HD has not been established, our studies demonstrate that deficiency in Wnt signaling leads to the loss of excitatory, dopaminergic, and inhibitory synapses in the striatum (Galli et al., 2014). Notably, our results show that activation of the Wnt pathway by withdrawal of Dkk1 expression in iDkk1 mice after substantial synapse degeneration results in the restoration of inhibitory and dopaminergic synapse number to control levels. Consistently with recovery of synapse number, motor learning and coordination as well as the response to amphetamine were normal after Dkk1 cessation. Thus, reactivation of the Wnt pathway could be used as an approach to restore whole circuit function in the adult striatum even after significant functional defects.

This study provides new insights into the role of Wnt signaling in the maintenance of synaptic connections in the striatum. Induced Dkk1 expression triggers the degeneration of 40% of inhibitory GABAergic synapses in the adult striatum. However, electrophysiological recordings revealed that Dkk1 affects GABAergic synapse function on D2R-MSNs. Importantly, cessation of Dkk1 expression after substantial synapse degeneration in the adult striatum results in the recovery of inhibitory and dopaminergic synapses, motor coordination, and the ability to respond to amphetamine. Thus, reactivation of the Wnt signaling pathway promotes the restoration of functional neuronal circuits in the adult striatum. These findings suggest the exciting possibility that modulation of this prominent signaling pathway could provide a viable therapeutic approach for protection or recovery of neuronal circuits in PD and/or HD.

DATA AVAILABILITY STATEMENT

The raw data supporting the conclusions of this article will be made available by the authors, without undue reservation.

ETHICS STATEMENT

All animal procedures were conducted according to the Animals Scientific Procedures Act UK (1986) and in compliance with the ethical standards at University College London (UCL).

AUTHOR CONTRIBUTIONS

PS conceived the overall project, guided the project, and provided the funding. AG contributed to the design and analyses of the electrophysiology experiments. SG performed the cell biology and behavioral experiments. SS performed the electrophysiology experiments and analyses of dendritic arborization. TD analyzed the electrophysiology data and helped in the preparation of figures. All authors participated in the design of experiments, interpretation of data, and writing of the manuscript.

FUNDING

This work was supported by funding from MRC (MR/M014045/1 and MR/M024083/1) and Parkinson's UK (G-1204).

ACKNOWLEDGMENTS

We would like to thank Marina Podpolny for helping with the breeding and genotyping of transgenic mice, Aude Marzo for her input on the interpretation of the data, and members of our lab for insightful discussions on the results and comments on our manuscript. The D2R-GFP mice were obtained from the Jackson Laboratory, which were deposited by Prof. N. Heintz.

SUPPLEMENTARY MATERIAL

The Supplementary Material for this article can be found online at: https://www.frontiersin.org/articles/10.3389/fnsyn.2021.670467/full#supplementary-material

REFERENCES

Albin, R. L., Reiner, A., Anderson, K. D., Dure, L. S. IV, Handelin, B., Balfour, R., et al. (1992). Preferential loss of striato-external pallidal projection neurons in presymptomatic Huntington's disease. *Ann. Neurol.* 31, 425–430. doi: 10.1002/ana.410310412

Andre, V. M., Cepeda, C., Fisher, Y. E., Huynh, M., Bardakjian, N., Singh, S., et al. (2011a). Differential electrophysiological changes in striatal output neurons in

Huntington's disease. *J. Neurosci.* 31, 1170–1182. doi: 10.1523/JNEUROSCI.3539-10.2011

Andre, V. M., Fisher, Y. E., and Levine, M. S. (2011b). Altered Balance of activity in the striatal direct and indirect pathways in mouse models of Huntington's disease. *Front. Syst. Neurosci.* 5:46. doi: 10.3389/fnsys.2011.00046

Bamford, N. S., Wightman, R. M., and Sulzer, D. (2018). Dopamine's effects on corticostriatal synapses during reward-based behaviors. *Neuron* 97, 494–510. doi: 10.1016/j.neuron.2018.01.006

Belenkaya, T. Y., Wu, Y., Tang, X., Zhou, B., Cheng, L., Sharma, Y. V., et al. (2008). The retromer complex influences Wnt secretion by recycling wntless from endosomes to the trans-Golgi network. *Dev. Cell* 14, 120–131. doi: 10.1016/j.devcel.2007.12.003

Berwick, D. C., and Harvey, K. (2012). LRRK2 functions as a Wnt signaling scaffold, bridging cytosolic proteins and membrane-localized LRP6. *Hum. Mol. Genet.* 21, 4966–4979. doi: 10.1093/hmg/dds342

Berwick, D. C., and Harvey, K. (2014). The regulation and deregulation of Wnt signaling by PARK genes in health and disease. *J. Mol. Cell Biol.* 6, 3–12. doi: 10.1093/jmcb/mjt037

Budnik, V., and Salinas, P. C. (2011). Wnt signaling during synaptic development and plasticity. *Curr. Opin. Neurobiol.* 21, 151–159. doi: 10.1016/j.conb.2010.12.002

Buechler, J., and Salinas, P. C. (2018). Deficient Wnt signaling and synaptic vulnerability in Alzheimer's disease: emerging roles for the LRP6 receptor. *Front. Synaptic. Neurosci.* 10:38. doi: 10.3389/fnsyn.2018.00038

Caricasole, A., Copani, A., Caraci, F., Aronica, E., Rozemuller, A. J., Caruso, A., et al. (2004). Induction of Dickkopf-1, a negative modulator of the Wnt pathway, is associated with neuronal degeneration in Alzheimer's brain. *J. Neurosci.* 24, 6021–6027. doi: 10.1523/JNEUROSCI.1381-04.2004

Cazorla, M., Shegda, M., Ramesh, B., Harrison, N. L., and Kellendonk, C. (2012). Striatal D2 receptors regulate dendritic morphology of medium spiny neurons via Kir2 channels. *J. Neurosci.* 32, 2398–2409. doi: 10.1523/JNEUROSCI.6056-11.2012

Cepeda, C., Galvan, L., Holley, S. M., Rao, S. P., Andre, V. M., Botelho, E. P., et al. (2013). Multiple sources of striatal inhibition are differentially affected in Huntington's disease mouse models. *J. Neurosci.* 33, 7393–7406. doi: 10.1523/JNEUROSCI.2137-12.2013

Cheng, H. C., Ulane, C. M., and Burke, R. E. (2010). Clinical progression in Parkinson disease and the neurobiology of axons. *Ann. Neurol.* 67, 715–725. doi: 10.1002/ana.21995

Chu, E. Y., Hens, J., Andl, T., Kairo, A., Yamaguchi, T. P., Brisken, C., et al. (2004). Canonical WNT signaling promotes mammary placode development and is essential for initiation of mammary gland morphogenesis. *Development* 131, 4819–4829. doi: 10.1242/dev.01347

Dang, M. T., Yokoi, F., Yin, H. H., Lovinger, D. M., Wang, Y., and Li, Y. (2006). Disrupted motor learning and long-term synaptic plasticity in mice lacking NMDAR1 in the striatum. *Proc. Natl. Acad. Sci. U.S.A.* 103, 15254–15259. doi: 10.1073/pnas.0601758103

Day, M., Wang, Z., Ding, J., An, X., Ingham, C. A., Shering, A. F., et al. (2006). Selective elimination of glutamatergic synapses on striatopallidal neurons in Parkinson disease models. *Nat. Neurosci .9*, 251–259. doi: 10.1038/nn1632

Elliott, C., Rojo, A. I., Ribe, E., Broadstock, M., Xia, W., Morin, P., et al. (2018). A role for APP in Wnt signalling links synapse loss with beta-amyloid production. *Transl. Psychiatry* 8, 179. doi: 10.1038/s41398-018-0231-6

Galli, S., Lopes, D. M., Ammari, R., Kopra, J., Millar, S. E., Gibb, A., et al. (2014). Deficient Wnt signalling triggers striatal synaptic degeneration and impaired motor behaviour in adult mice. *Nat. Commun.* 5:4992. doi: 10.1038/ncomms5992

Gerfen, C. R. (1992). The neostriatal mosaic: multiple levels of compartmental organization in the basal ganglia. *Annu. Rev. Neurosci.* 15, 285–320. doi: 10.1146/annurev.ne.15.030192.001441

Gertler, T. S., Chan, C. S., and Surmeier, D. J. (2008). Dichotomous anatomical properties of adult striatal medium spiny neurons. *J. Neurosci.* 28, 10814–10824. doi: 10.1523/JNEUROSCI.2660-08.2008

Gittis, A. H., Nelson, A. B., Thwin, M. T., Palop, J. J., and Kreitzer, A. C. (2010). Distinct roles of GABAergic interneurons in the regulation of striatal output pathways. *J Neurosci* 30, 2223–2234. doi: 10.1523/JNEUROSCI.4870-09.2010

Godin, J. D., Poizat, G., Hickey, M. A., Maschat, F., and Humbert, S. (2010). Mutant huntingtin-impaired degradation of beta-catenin causes neurotoxicity in Huntington's disease. *EMBO J.* 29, 2433–2445. doi: 10.1038/emboj.2010.117

Gong, S., Zheng, C., Doughty, M. L., Losos, K., Didkovsky, N., Schambra, U. B., et al. (2003). A gene expression atlas of the central nervous system based on bacterial artificial chromosomes. *Nature* 425, 917–925. doi: 10.1038/nature02033

Janezic, S., Threlfell, S., Dodson, P. D., Dowie, M. J., Taylor, T. N., and Potgieter, D. (2013). Deficits in dopaminergic transmission precede neuron loss and dysfunction in a new Parkinson model. *Proc. Natl. Acad. Sci. U.S.A.* 110, E4016–E4025. doi: 10.1073/pnas.1309143110

Kalathur, R. K., Hernández-Prieto, M. A., and Futschik, M. E. (2012). Huntington's disease and its therapeutic target genes: a global functional profile based on the HD Research crossroads database. *BMC Neurol* 12:47. doi: 10.1186/1471-2377-12-47

Koos, T., and Tepper, J. M. (1999). Inhibitory control of neostriatal projection neurons by GABAergic interneurons. *Nat. Neurosci.* 2, 467–472. doi: 10.1038/8138

Koos, T., Tepper, J. M., and Wilson, C. J. (2004). Comparison of IPSCs evoked by spiny and fast-spiking neurons in the neostriatum. *J. Neurosci.* 24, 7916–7922. doi: 10.1523/JNEUROSCI.2163-04.2004

Kravitz, A. V., Freeze, B. S., Parker, P. R., Kay, K., Thwin, M. T., Deisseroth, K., et al. (2010). Regulation of parkinsonian motor behaviours by optogenetic control of basal ganglia circuitry. *Nature* 466, 622–626. doi: 10.1038/nature09159

Kreitzer, A. C., and Malenka, R. C. (2008). Striatal plasticity and basal ganglia circuit function. *Neuron* 60, 543–554. doi: 10.1016/j.neuron.2008.11.005

Kubota, Y., Karube, F., Nomura, M., and Kawaguchi, Y. (2016). The diversity of cortical inhibitory synapses. *Front. Neural Circuits* 10:27. doi: 10.3389/fncir.2016.00027

Lee, H. J., Weitz, A. J., Bernal-Casas, D., Duffy, B. A., Choy, M., Kravitz, A. V., et al. (2016). Activation of direct and indirect pathway medium spiny neurons drives distinct brain-wide responses. *Neuron* 91, 412–424. doi: 10.1016/j.neuron.2016.06.010

Liu, C. C., Tsai, C. W., Deak, F., Rogers, J., Penuliar, M., Sung, Y. M., et al. (2014). Deficiency in LRP6-mediated Wnt signaling contributes to synaptic abnormalities and amyloid pathology in Alzheimer's disease. *Neuron* 84, 63–77. doi: 10.1016/j.neuron.2014.08.048

Mansuy, I. M., Winder, D. G., Moallem, T. M., Osman, M., Mayford, M., Hawkins, R. D., et al. (1998). Inducible and reversible gene expression with the rtTA system for the study of memory. *Neuron* 21, 257–265.

Mao, B., Wu, W., Li, Y., Hoppe, D., Stannek, P., Glinka, A., et al. (2001). LDL-receptor-related protein 6 is a receptor for Dickkopf proteins. *Nature* 411, 321–325. doi: 10.1038/35077108

Marzo, A., Galli, S., Lopes, D., McLeod, F., Podpolny, M., Segovia-Roldan, M., et al. (2016). Reversal of synapse degeneration by restoring wnt signaling in the adult hippocampus. *Curr. Biol.* 26, 2551–2561. doi: 10.1016/j.cub.2016.07.024

Matsumura, R., Yamamoto, H., Hayakawa, T., Katsurabayashi, S., Niwano, M., and Hirano-Iwata, A. (2018). Dependence and homeostasis of membrane impedance on cell morphology in cultured hippocampal neurons. *Sci. Rep.* 8:9905. doi: 10.1038/s41598-018-28232-0

Milnerwood, A. J., and Raymond, L. A. (2010). Early synaptic pathophysiology in neurodegeneration: insights from Huntington's disease. *Trends Neurosci.* 33, 513–523. doi: 10.1016/j.tins.2010.08.002

Natarajan, R., and Yamamoto, B. K. (2011). The Basal Ganglia as a Substrate for the Multiple Actions of Amphetamines. *Basal Ganglia* 1, 49–57. doi: 10.1016/j.baga.2011.05.003

Nusse, R., and Clevers, H. (2017). Wnt/beta-catenin signaling, disease, and emerging therapeutic modalities. *Cell* 169, 985–999. doi: 10.1016/j.cell.2017.05.016

Odeh, F., Leergaard, T. B., Boy, J., Schmidt, T., Riess, O., and Bjaalie, J. G. (2011). Atlas of transgenic Tet-Off Ca2+/calmodulin-dependent protein kinase II and prion protein promoter activity in the mouse brain. *Neuroimage* 54, 2603–2311. doi: 10.1016/j.neuroimage.2010.11.032

Picconi, B., Piccoli, G., and Calabresi, P. (2012). Synaptic dysfunction in Parkinson's disease. *Adv. Exp. Med. Biol.* 970, 553–572. doi: 10.1007/978-3-7091-0932-8_24

Purro, S. A., Dickins, E. M., and Salinas, P. C. (2012). The secreted Wnt antagonist Dickkopf-1 is required for amyloid beta-mediated synaptic loss. *J. Neurosci.* 32, 3492–3498. doi: 10.1523/JNEUROSCI.4562-11.2012

Rawal, N., Corti, O., Sacchetti, P., Ardilla-Osorio, H., Sehat, B., Brice, A., et al. (2009). Parkin protects dopaminergic neurons from excessive Wnt/beta-catenin signaling. *Biochem. Biophys. Res. Commun.* 388, 473–478. doi: 10.1016/j.bbrc.2009.07.014

Reiner, A., Albin, R. L., Anderson, K. D., D'Amato, C. J., Penney, J. B., and Young, A. B. (1988). Differential loss of striatal projection neurons in Huntington disease. *Proc. Natl. Acad. Sci. U.S.A.* 85, 5733–5737. doi: 10.1073/pnas.85.15.5733

Rosi, M. C., Luccarini, I., Grossi, C., Fiorentini, A., Spillantini, M. G., Prisco, A., et al. (2010). Increased Dickkopf-1 expression in transgenic mouse models of neurodegenerative disease. *J. Neurochem.* 112, 1539–1551. doi: 10.1111/j.1471-4159.2009.06566.x

Sancho, R. M., Law, B. M., and Harvey, K. (2009). Mutations in the LRRK2 Roc-COR tandem domain link Parkinson's disease to Wnt signalling pathways. *Hum. Mol. Genet.* 18, 3955–3968. doi: 10.1093/hmg/ddp337

Scheff, S. W., Price, D. A., Schmitt, F. A., and Mufson, E. J. (2006). Hippocampal synaptic loss in early Alzheimer's disease and mild cognitive impairment. *Neurobiol. Aging* 27, 1372–1384. doi: 10.1016/j.neurobiolaging.2005.09.012

Schindelin, J., Arganda-Carreras, I., Frise, E., Kaynig, V., Longair, M., Pietzsch, T., et al. (2012). Fiji: an open-source platform for biological-image analysis. *Nat. Methods* 9, 676–682. doi: 10.1038/nmeth.2019

Schirinzi, T., Madeo, G., Martella, G., Maltese, M., Picconi, B., Calabresi, P., et al. (2016). Early synaptic dysfunction in Parkinson's disease: insights from animal models. *Mov. Disord* 31, 802–813. doi: 10.1002/mds.26620

Sellers, K. J., Elliott, C., Jackson, J., Ghosh, A., Ribe, E., Rojo, A. I., et al. (2018). Amyloid beta synaptotoxicity is Wnt-PCP dependent and blocked by fasudil. *Alzheimers Dement* 14, 306–317. doi: 10.1016/j.jalz.2017.09.008

Shankar, G. M., and Walsh, D. M. (2009). Alzheimer's disease: synaptic dysfunction and Abeta. *Mol. Neurodegener.* 4:48. doi: 10.1186/1750-1326-4-48

Sherman-Gold, R. (1993). *The Axon Guide for Electrophysiology and Biophysics*. Foster City, CA: Axon Instruments.

Shiotsuki, H., Yoshimi, K., Shimo, Y., Funayama, M., Takamatsu, Y., Ikeda, K., et al. (2010). A rotarod test for evaluation of motor skill learning. *J. Neurosci. Methods* 189, 180–185. doi: 10.1016/j.jneumeth.2010.03.026

Soukup, S. F., Vanhauwaert, R., and Verstreken, P. (2018). Parkinson's disease: convergence on synaptic homeostasis. *EMBO J.* 37, e98960. doi: 10.15252/embj.201898960

Stephano, F., Nolte, S., Hoffmann, J., El-Kholy, S., von Frieling, J., Bruchhaus, I., et al. (2018). Impaired Wnt signaling in dopamine containing neurons is associated with pathogenesis in a rotenone triggered Drosophila Parkinson's disease model. *Sci. Rep.* 8:2372. doi: 10.1038/s41598-018-20836-w

Surmeier, D. J., Ding, J., Day, M., Wang, Z., and Shen, W. (2007). D1 and D2 dopamine-receptor modulation of striatal glutamatergic signaling in striatal medium spiny neurons. *Trends Neurosci.* 30, 228–235. doi: 10.1016/j.tins.2007.03.008

Taverna, S., Canciani, B., and Pennartz, C. M. (2007). Membrane properties and synaptic connectivity of fast-spiking interneurons in rat ventral striatum. *Brain Res.* 1152, 49–56. doi: 10.1016/j.brainres.2007.03.053

Taverna, S., Ilijic, E., and Surmeier, D. J. (2008). Recurrent collateral connections of striatal medium spiny neurons are disrupted in models of Parkinson's disease. *J. Neurosci.* 28, 5504–5512. doi: 10.1523/JNEUROSCI.5493-07.2008

Wang, Z., Kai, L., Day, M., Ronesi, J., Yin, H. H., Ding, J., et al. (2006). Dopaminergic control of corticostriatal long-term synaptic depression in medium spiny neurons is mediated by cholinergic interneurons. *Neuron* 50, 443–452. doi: 10.1016/j.neuron.2006.04.010

Woo, J., Min, J. O., Kang, D. S., Kim, Y. S., Jung, G. H., Park, H. J., et al. (2018). Control of motor coordination by astrocytic tonic GABA release through modulation of excitation/inhibition balance in cerebellum. *Proc. Natl. Acad. Sci. U.S.A.* 115, 5004–5009. doi: 10.1073/pnas.1721187115

Wu, W., Han, Y., Fan, X., Li, Q., and Sun, L. (2019). Protective mechanism of Wnt4 gene on Parkinson's disease (PD) transgenic Drosophila. *Int. J. Neurosci.* 129, 703–714. doi: 10.1080/00207454.2018.1557168

Xu, M., Hu, X. T., Cooper, D. C., Moratalla, R., Graybiel, A. M., White, F. J., et al. (1994). Elimination of cocaine-induced hyperactivity and dopamine-mediated neurophysiological effects in dopamine D1 receptor mutant mice. *Cell* 79, 945–955.

Yin, H. H., Mulcare, S. P., Hilario, M. R., Clouse, E., Holloway, T., Davis, M. I., et al. (2009). Dynamic reorganization of striatal circuits during the acquisition and consolidation of a skill. *Nat. Neurosci.* 12, 333–341. doi: 10.1038/nn.2261

Zimprich, A., Benet-Pages, A., Struhal, W., Graf, E., Eck, S. H., Offman, M. N., et al. (2011). A mutation in VPS35, encoding a subunit of the retromer complex, causes late-onset Parkinson disease. *Am. J. Hum. Genet.* 89, 168–175. doi: 10.1016/j.ajhg.2011.06.008

Conflict of Interest: The authors declare that the research was conducted in the absence of any commercial or financial relationships that could be construed as a potential conflict of interest.

frontiers in Synaptic Neuroscience

ORIGINAL RESEARCH
published: 15 July 2021
doi: 10.3389/fnsyn.2021.695964

Plasticity of GluN1 at Ventral Hippocampal Synapses in the Infralimbic Cortex

*Yesenia Castillo-Ocampo[1], María Colón[1], Anixa Hernández[1], Pablo Lopez[1], Yamil Gerena[2] and James T. Porter[1]**

[1] Department of Basic Sciences, Ponce Research Institute, Ponce Health Sciences University, Ponce, Puerto Rico,
[2] Department of Pharmacology and Toxicology, School of Medicine, University of Puerto Rico, San Juan, Puerto Rico

Although the infralimbic cortex (IL) is not thought to play a role in fear acquisition, recent experiments found evidence that synaptic plasticity is occurring at ventral hippocampal (vHPC) synapses in IL during auditory fear acquisition as measured by changes in the *N*-methyl-D-aspartate (NMDA) receptor-mediated currents in male rats. These electrophysiological data suggest that fear conditioning changes the expression of NMDA receptors on vHPC-to-IL synapses. To further evaluate the plasticity of NMDA receptors at this specific synapse, we injected AAV particles expressing channelrhodopsin-EYFP into the vHPC of male and female rats to label vHPC projections with EYFP. To test for NMDA receptor changes in vHPC-to-IL synapses after fear learning, we used fluorescence-activated cell sorting (FACS) to quantify synaptosomes isolated from IL tissue punches that were positive for EYFP and the obligatory GluN1 subunit. More EYFP+/GluN1+ synaptosomes with greater average expression of GluN1 were isolated from male rats exposed to auditory fear conditioning (AFC) than those exposed to context and tones only or to contextual fear conditioning (CFC), suggesting that AFC increased NMDA receptor expression in males. In a second experiment, we found that pairing the tones and shocks was required to induce the molecular changes and that fear extinction did not reverse the changes. In contrast, females showed similar levels of EYFP+/GluN1+ synaptosomes in all behavioral groups. These findings suggest that AFC induces synaptic plasticity of NMDA receptors in the vHPC-to-IL projection in males, while female rats rely on different synaptic mechanisms.

Keywords: NMDA receptor, GluN1, fear conditioning, rat, synaptosomes, sex difference, synaptic plasticity, channelrhodopsin

OPEN ACCESS

Edited by:
Hansen Wang,
University of Toronto, Canada

Reviewed by:
Serena M. Dudek,
National Institute of Environmental Health Sciences (NIEHS), United States
Nadia Lunardi,
University of Virginia, United States
Linnaea Ostroff,
University of Connecticut, United States
Rosalina Fonseca,
New University of Lisbon, Portugal

****Correspondence:***
James T. Porter
jporter@psm.edu

Received: *15 April 2021*
Accepted: *25 June 2021*
Published: *15 July 2021*

Citation:
Castillo-Ocampo Y, Colón M, Hernández A, Lopez P, Gerena Y and Porter JT (2021) Plasticity of GluN1 at Ventral Hippocampal Synapses in the Infralimbic Cortex. Front. Synaptic Neurosci. 13:695964. doi: 10.3389/fnsyn.2021.695964

INTRODUCTION

Contextual and auditory fear conditioning (AFC) in rodents mimics fear-related behavior in humans (LeDoux, 2000; Phelps and LeDoux, 2005). Using this animal model, researchers identified the interconnected fear circuit with the amygdala as the central structure for fear expression. The intensity of the fear generated by amygdala outputs is attenuated by projections from the infralimbic cortex (IL) (Bloodgood et al., 2018; Bukalo et al., 2021). Abundant evidence

Abbreviations: vHPC, ventral hippocampus; IL, infralimbic cortex; FACS, fluorescence-activated cell sorting; ANOVA, analysis of variance; NMDAR, *N*-methyl-D-aspartate receptor; PTSD, post-traumatic stress disorder.

suggests that IL plays a central role in fear extinction memory (Chang and Maren, 2010; Milad and Quirk, 2012; Do-Monte et al., 2015; Marek et al., 2018; Tao et al., 2020). Furthermore, contextual and temporal information from the ventral hippocampus (vHPC) determines when IL inhibits fear expression which provides contextual specificity of fear extinction recall (Corcoran et al., 2005; Sierra-Mercado et al., 2011; Marek et al., 2018).

In contrast to the central role of IL in fear extinction, initial studies suggested that fear acquisition did not affect IL and IL activity did not affect fear learning (Milad and Quirk, 2002; Burgos-Robles et al., 2007). However, subsequent research has found evidence that fear acquisition alters the intrinsic excitability of IL neurons (Santini et al., 2008, 2012; Song et al., 2015; Soler-Cedeño et al., 2016; Bloodgood et al., 2018). Furthermore, pharmacologically reducing IL excitability increased fear learning (Santini and Porter, 2010), suggesting that ongoing IL neuronal activity during fear learning was impeding acquisition. Consistent with the rodent studies, recent human studies also found that fear learning alters activity in the ventral medial prefrontal cortex (vmPFC) which is considered to be homologous to the rodent IL (Fullana et al., 2016; Harrison et al., 2017; Dunsmoor et al., 2019) and people with vmPFC lesions show impaired fear acquisition (Battaglia et al., 2020). Taken together these studies suggest that associative fear learning induces plasticity in the homologous structures, the rodent IL, and the human vmPFC.

The acquisition of AFC does not appear to induce widespread synaptic plasticity in IL (Pattwell et al., 2012; Sepulveda-Orengo et al., 2013). In fact, these independent studies found that synaptic plasticity in IL occurs exclusively after fear extinction rather than fear acquisition. However, examination of ventral hippocampal (vHPC) synapses labeled with channelrhodopsin in IL suggests that fear acquisition induces more restricted plasticity at specific synapses in IL (Soler-Cedeño et al., 2019). This study found less *N*-methyl-D-aspartate (NMDA) receptor-mediated current at vHPC-to-IL synapses after AFC in male rats. The finding of less current suggests that AFC reduces the expression of NMDA receptors at vHPC-to-IL synapses in male rats. To address this possibility and determine whether females also show similar synaptic plasticity, we labeled vHPC synapses with AAV expression of channelrhodopsin-EYFP in both sexes and isolated synaptosomes from IL tissue punches after contextual fear conditioning (CFC) and AFC. Since NMDA receptors are composed of two obligatory GluN1 subunits (Paoletti et al., 2013), we decided to quantify GluN1 expression as a relative measure of total NMDA receptor (NMDAR) expression. From the general synaptosome population, vHPC-to-IL synaptosomes were identified and analyzed by fluorescence-activated cell sorting (FACS) for the expression of GluN1. Our results show that associative learning (tone with shock) induces an increase in GluN1 at vHPC-to-IL synaptosomes in males. In contrast, CFC did not affect GluN1 expression. In addition, neither CFC nor AFC induced changes in GluN1 expression in the females, suggesting that this synaptic plasticity is sex-dependent.

MATERIALS AND METHODS

Labeling Ventral Hippocampal Synapses With EYFP

Male and female Sprague–Dawley rats (P30) received infusions of an AAV5 vector (1.0 μL per hemisphere) that promotes channelrhodopsin-2 (ChR) and enhanced yellow fluorescent protein expression driven by the glutamatergic neuron-specific CaMKIIα promoter [AAV-CaMKIIα-hChR2(H134R)-EYFP; University of North Carolina at Chapel Hill Vector Core Services]. A titer of 10^{11} particles was infused into the vHPC with a 5-μL Hamilton syringe using the following stereotactic coordinates (−5.50 mm AP; ±4.50 mm ML; −7.0 mm DV). After a recovery of at least 2 months for optimal expression of ChR-EYFP, the rats were arbitrarily assigned to different experimental groups. Every animal used in experiments 1 and 2 expressed ChR-EYFP for tracing vHPC-to-IL projections, since this protein is trafficked to the axon terminals. We did not use the ChR-EYFP for optogenetic stimulation. After sacrifice, we took images with either an epifluorescence Olympus BX60 microscope or a NikonC2+ confocal microscope of random samples to confirm that EYFP expression was restricted to the vHPC and EYFP-labeled axons were visible in IL (**Supplementary Figure 5**).

Behavioral Groups for Experiment 1

Adult male and female rats (P90) were divided into three groups and placed in operant chambers (Ugo Basile) with three frosted white sides, a clear front, and a metal grid floor to provide electric foot shocks. The exposure group (EXPO) was exposed to the chambers for the same length of time without receiving any electric foot shocks. Animals were not habituated to the conditioning chambers. The CFC group was allowed to explore the chamber for 2 min to establish baseline movement of each animal in that context. Then, this group received five electric foot shocks (0.7 mA) spaced 2 min apart. The AFC group received six tones (Hz, 80 dB, 30 s) with an interval of 120 s between tones. Tones 2–6 were paired with a mild electrical foot shock (conditioned stimulus, CS, 0.44 mA, 0.5 s) beginning at the end of each tone. The next day, all rats were placed back into the same training context to test their recall memory. The AFC group received two tones, and the EXPO and CFC groups only received context exposure.

Behavioral Groups for Experiment 2

Adult male (P90, P180, and P330) and female (P90) rats were divided into three groups and placed in operant chambers (Ugo Basile). The older ages in the male group were caused by unexpected delays. Animals were not habituated to the conditioning chambers. On day 1, the AFC and extinction (EXT) groups received six tones (Hz, 80 dB, 30 s) with an interval of 120 s between tones. Tones 2–6 were paired with an electrical foot shock (conditioned stimulus, CS, 0.44 mA, 0.5 s) beginning at the end of each tone. On day 1, the control pseudoconditioned (PSUEDO) group received the six auditory tones unpaired with electric foot shocks and then five rapid electric foot shocks immediately before removing them from the

conditioning chamber to control for tone and shock exposure without inducing conditioned inhibition. On day 2, the PSEUDO and AFC groups remained in their home cages and the EXT group received two sessions of 15 tones (30 s duration, 2 min interval between tones) separated by 1 h. The third day, all groups were placed back into the same training context and were given two tones to test their recall memory.

Synaptosome Isolation

All behaviors and sacrifices were done during the morning. Immediately after recall, the animals received an overdose of 1.0 mL of pentobarbital mixed with phenytoin sodium (Euthanasia-III, MED-PHARMEX Inc., Pomona, CA, United States). After brain extraction, the brains were coronal cut into 1 mm slices with a brain matrix (BS-A 6000C, BrainTree Scientific, Inc.). IL tissue punches (1.5 mm) from IL were taken from each rat. Tissue punches were homogenized, and protein extraction was performed to extract synaptic proteins using the Syn-PER Synaptic Protein Extraction Reagent (cat no. 87793, Thermo Scientific) with phosphatase and protease inhibitors to avoid the degradation of proteins (P5726-5ML, Sigma and P2714-1BTL, Sigma). After homogenization, the samples were centrifuged for 10 min at 3,600 rpm at 4°C. The supernatant was centrifuged a second time at 11,400 rpm for 20 min at 4°C and the supernatant was discarded, and the pellet was kept. Meanwhile, antibodies against an extracellular epitope of rat GluN1 (cat no. AGC-001, Alomone Lab Co.) were conjugated with Alexa Fluor 647 following the manufacturer's instructions (Antibody Labeling Kit, cat no. A20186, Ex/Em 650/668). Before using the antibodies on the experimental samples, each batch of labeled antibody was tested to ensure the detection of GluN1 on synaptosomes from a naïve rat with appropriate fluorescence. The antibody was diluted (1:100) in 5% bovine serum albumin (BSA) in PBS and incubated with the synaptosomes for 1 h on ice. Then, the synaptosomes were washed once with 600 uL of 5% BSA in PBS and centrifuged for 5 min at 5,400 rpm at 4°C to wash away unbound antibody. The supernatant was discarded and the pellet was suspended in 400 uL of 0.5% paraformaldehyde, protected from light, and stored at 4°C.

FACS

Once the vHPC-to-IL synapses were labeled with AAV-mediated expression of EYFP and synaptosomes were isolated from IL tissue punches, EYFP-expressing synaptosomes were identified *via* FACS. First, we identified the appropriate size gate for our FACS machine (BD FACSAria I; BD Biosciences, San Jose, CA, United States) with fluorescent beads of 1, 2, and 4 μm diameters. Synaptosomes fall within this size range (Gylys et al., 2004; Evans, 2015) and larger particles are more likely to have intact presynaptic and postsynaptic membranes (Gylys et al., 2004). Then, synaptosomes from IL tissue punches were selected using these size limits and vHPC-to-IL synaptosomes were identified by EYFP fluorescence. Next, the expression of GluN1 by the EYFP+ population of synaptosomes was determined by detecting Alexa Fluor 647 which was conjugated to the anti-GluN1 antibody (Alexa Fluor 645 Antibody Labeling Kit, cat no. A20186). The gate for EYFP that represents the channelrhodopsin from the virus was established by comparing the detection of fluorescence in the 488 nm wavelength in synaptosomes from an animal that was not injected with the viral vector with synaptosomes from an AAV-injected animal. Similarly, synaptosomes from a rat that did not express EYFP were incubated with the conjugated anti-GluN1 antibody and the detectible fluorescence at 645 nm was compared to unlabeled synaptosomes to set the gate for detection of GluN1+ synaptosomes. To measure the mean fluorescence intensity of GluN1 immunolabeling for each rat, we generated a histogram of the double-positive EYFP+/GluN1+ synaptosomes in FlowJo software. Markers were placed to at the beginning and the end of the histogram, and the mean, median, and mode of the GluN1 fluorescence intensity were automatically calculated by FlowJo. The forward scatter of the double-positive EYFP+/GluN1+ synaptosomes was measured in FlowJo as an estimate of relative difference in the size of the synaptosomes. The side scatter of the double-positive EYFP+/GluN1+ synaptosomes was measured in FlowJo as an estimate of relative difference in the internal complexity (i.e., granularity and internal structures) of the synaptosomes.

Recent studies found that it is important to consider the potential contribution of aggregates of two or more synaptosomes in flow cytometry experiments (Biesemann et al., 2014; Hobson and Sims, 2019). These articles demonstrate that under proper conditions, the contribution of aggregates can be reduced to insignificant levels. To determine the contribution of aggregates in our samples, we isolated IL synaptosomes, separated them into two tubes, and incubated each sample with a different antibody conjugated to a different fluorophore. After immunolabeling, the samples were fixed, mixed together, and analyzed by FACS. As shown in **Supplementary Figure 1**, the FACS analysis found negligible amounts of double-positive synaptosomes which would represent aggregates of individually labeled synaptosomes. These data suggest that our experimental process generates minimal aggregates which do not contribute significatively to our results.

Statistical Analysis

In experiment 1, contextual fear was measured in the CFC group as the percent of time spent freezing during the 60 s before the shock in the CFC group and during the equivalent period in the EXPO group during training on day 1 with ANY-maze software (Ugo Basile, Italy). During recall, the freezing during 2 min in the conditioning context was measured as contextual fear in the CFC and EXPO groups. In the PSEUDO group, contextual fear was measured as freezing during 30 s before the first tone in the conditioning chamber during recall. In the PSEUDO, AFC, and EXT groups, auditory fear was measured as the percent of time spent freezing during each 30 s tone of training and recall with ANY-maze software. Behavioral data acquired on day 1 in experiments 1 and 2 were analyzed by repeated-measures two-way analysis of variance (ANOVA) followed by Tukey *post hoc* test (Graphpad Prism version 9.1.0, San Diego, CA, United States). The two trials of fear recall were averaged and compared by one-way ANOVA followed by Tukey *post hoc* test by treatment and sex (Graphpad Prism). Significance was set at $p \leq 0.05$. The raw data obtained from the BD FACSAria I

(BD Biosciences, San Jose, CA, United States) were filtered by size and EYFP expression using FlowJo 2 (BD Life Sciences, Becton, Dickinson & Company). The resulting EYFP+ population of synaptosomes was subsequently analyzed for immunolabeling of GluN1 in FlowJo. The fluorescence intensity histograms were generated by selecting the EYFP+/GluN1+ synaptosomes in quadrant 2 and analyzing them in FlowJo. A similar number of EYFP+/GluN1+ IL synaptosomes were detected and analyzed in both sexes [males: 7170 ± SEM: females: 8814 ± SEM; U (648, 528) = 203, $p = 0.08$]. The data were categorized as non-parametric by Shapiro–Wilk. Statistical analysis was performed with Kruskal–Wallis non-parametric test followed by Dunn's multiple comparison test (Graphpad Prism version 9.1.0, San Diego, CA, United States). Significance was set at $p \leq 0.05$. The investigators were not completely blinded to the treatment group. However, most of the samples were identified by a rat ID# and run by a FACS technician who was blinded to the treatment. The resulting data were then analyzed in FlowJo and saved as a PDF before the results were separated into treatment groups.

RESULTS

Fear-Related Behaviors for Experiment 1

Male and female rats were injected with an AAV vector to induce expression of channelrhodopsin and EYFP in vHPC neurons. After waiting 2 months for optimal expression and transport of the EYFP to the axon terminals of the vHPC neurons, rats (P90) were arbitrarily divided into three groups. The three experimental groups were designed to test whether contextual or AFC changes NMDA receptor expression at vHPC synapses in IL (**Figure 1**). The CFC group ($n = 9$ females and 9 males) received five foot shocks in the conditioning chamber, the exposure group (EXPO, $n = 9$ females and 9 males) was placed in the conditioning chamber and did not receive foot shocks, and the AFC group ($n = 6$ females and 8 males) received one habituation tone and five tones paired with a foot shock (**Figures 1A,B**, respectively). The female and male rats in the CFC and AFC groups showed a gradual increase in freezing during the behavioral protocol, indicating that the groups acquired contextual and auditory

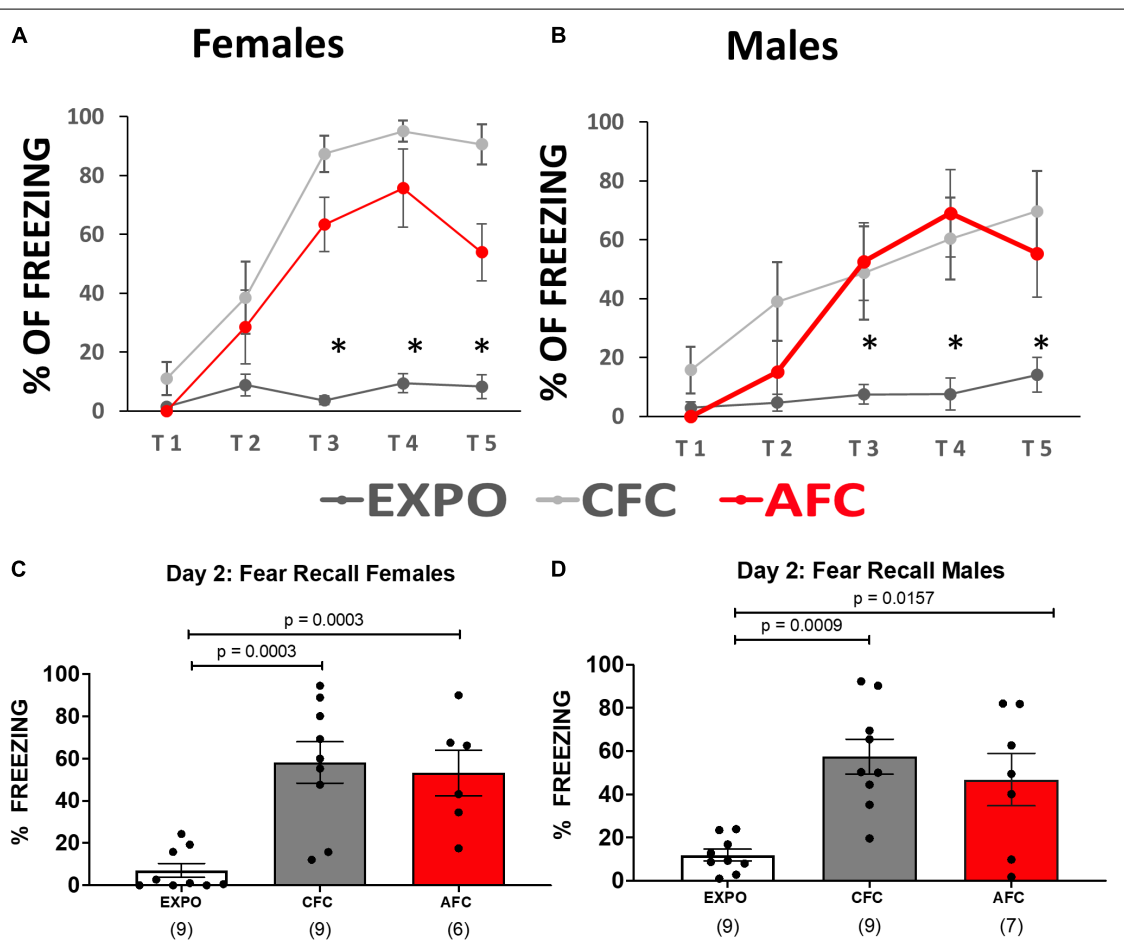

FIGURE 1 | Female and male rats acquired contextual and auditory fear. **(A,B)** Fear responses during training in the exposure, CFC, and AFC females and males, respectively. Asterisk denotes trials in which the CFC and AFC groups show more freezing than the exposure group ($p \leq 0.05$). **(C,D)** Long-term memory on day 2 of female and male groups showing freezing to the context in the EXPO and CFC groups and to the tone in the AFC group. Sample sizes are indicated below each bar in parentheses.

fear, respectively (**Figures 1A,B** and **Supplementary Statistical Table**). In contrast, the EXPO group maintained a low level of freezing throughout.

The following day the long-term memory was analyzed by measuring freezing during the first minute in the conditioning context in the EXPO and CFC groups or during two tones in the AFC group. Both females and males showed similar patterns of learning fear context per group (**Figures 1C,D**). Both the male [$F(2,22) = 3.954$, $p = 0.0341$] and female groups [$F(2,21) = 3.608$, $p = 0.0450$] showed different levels of freezing to the tones. The CFC (male, $p = 0.0009$; female, $p = 0.0003$) and AFC (male, $p = 0.0157$; female, $p = 0.0029$) groups showed more freezing than the EXPO groups, indicating that male and female rats recalled their fear learning from the previous day.

AFC Increases GluN1 Expression at vHPC-to-IL Synaptosomes

After the fear recall on day 2, the animals were sacrificed, brain slices were cut, and tissue punches were extracted from IL. The samples were homogenized, and synaptosomes were isolated by centrifugation and incubated with an antibody against an extracellular epitope of GluN1 (cat no. AGC-001, Alomone Lab Co.). Labeled synaptosomes were then analyzed by FACS. **Figure 2** shows the filters applied to the FACS data to measure GluN1 expression on vHPC-to-IL synaptosomes. First, the results were filtered by size to select the particles within the 1–4 μm size range of synaptosomes (**Figure 2A**). Then vHPC synaptosomes were identified by EYFP expression (**Figure 2C**) which was not found in synaptosomes from rats that did not receive viral injections (**Figure 2B**) confirming the capacity to detect the EYFP expressed in vHPC axon terminals. Finally, the double-positive synaptosomes (EYFP+/GluN1+) were identified to measure GluN1 expression (**Figures 2D,E**). A histogram shows that synaptosomes expressing EYFP could be separated from synaptosomes not expressing EYFP (**Figure 2F**).

Next, we analyzed the expression of EYFP+/GluN1+ synaptosomes in IL tissue from the different behavioral groups. **Figure 3A** shows that fear acquisition affected the expression of GluN1 on EYFP+ vHPC-to-IL synaptosomes in males. The

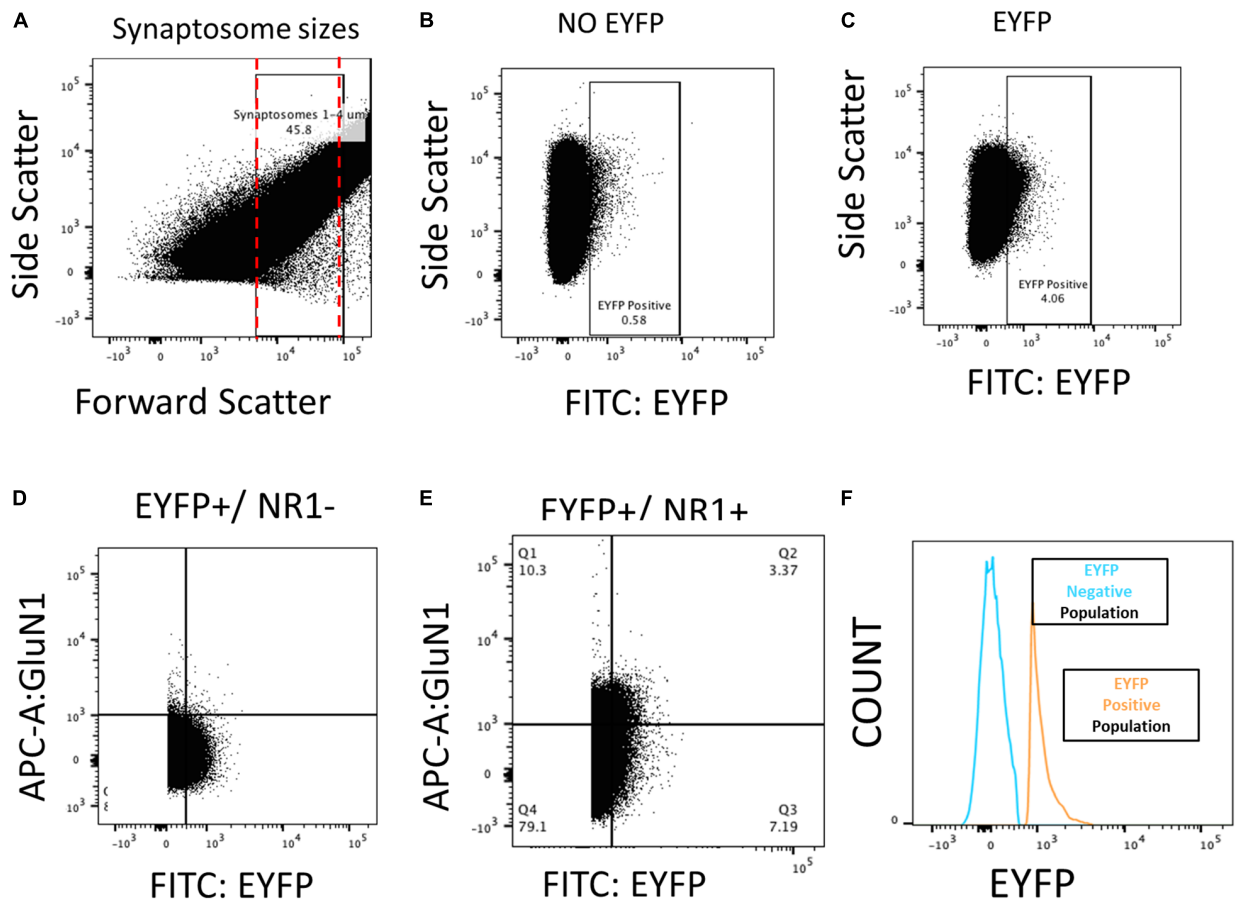

FIGURE 2 | FACS analysis of the NMDA subunit GluN1 on vHPC-to-IL synaptosomes from male and female rats. **(A)** Particles between 1 and 4 μm were selected as synaptosomes after isolation from IL tissue and used for subsequent analysis. **(B)** Rats without virus (NO EYFP) had a low percentage of synaptosomes in the EYFP+ quadrant. **(C)** Rats injected with the EYFP-expressing virus into the VHPC showed abundant expression of EYFP+ synaptosomes isolated from IL tissue. **(D)** EYFP+/GluN1– samples that lacked the antibody against GluN1 show no expression in GluN1+ quadrants. **(E,F)** EYFP+/GluN1+ samples show abundant detection of EYFP+/GluN1+ synaptosomes, indicating that we could isolate and quantify GluN1 expression in VHPC-to-IL synaptosomes.

expression of GluN1 on EYFP+ vHPC-to-IL synaptosomes varied in the male groups [$H(2,22) = 9.166$, $p = 0.0102$; **Figure 3A**]. The male AFC group showed more EYFP+/GluN1+ synaptosomes than in the EXPO ($p = 0.0234$) or CFC groups ($p = 0.0214$) suggesting that AFC increases NMDA receptor expression at vHPC-to-IL synapses. The CFC group expressed similar levels to the EXPO group ($p > 0.9999$), suggesting that the contextual fear acquisition was insufficient to induce the change.

To explore whether the increase in the number of EYFP+/GluN1+ synaptosomes was caused by synaptogenesis or an increase in NMDA receptors in existing vHPC-to-IL synapses, we compared histograms of the fluorescence intensity of GluN1 labeled EYFP+ synaptosomes in the EXPO, CFC, and AFC groups of male rats (**Figures 3B,C**). We found that AFC histograms were shifted to the right compared to the EXPO and CFC histograms producing a difference in the mean fluorescent

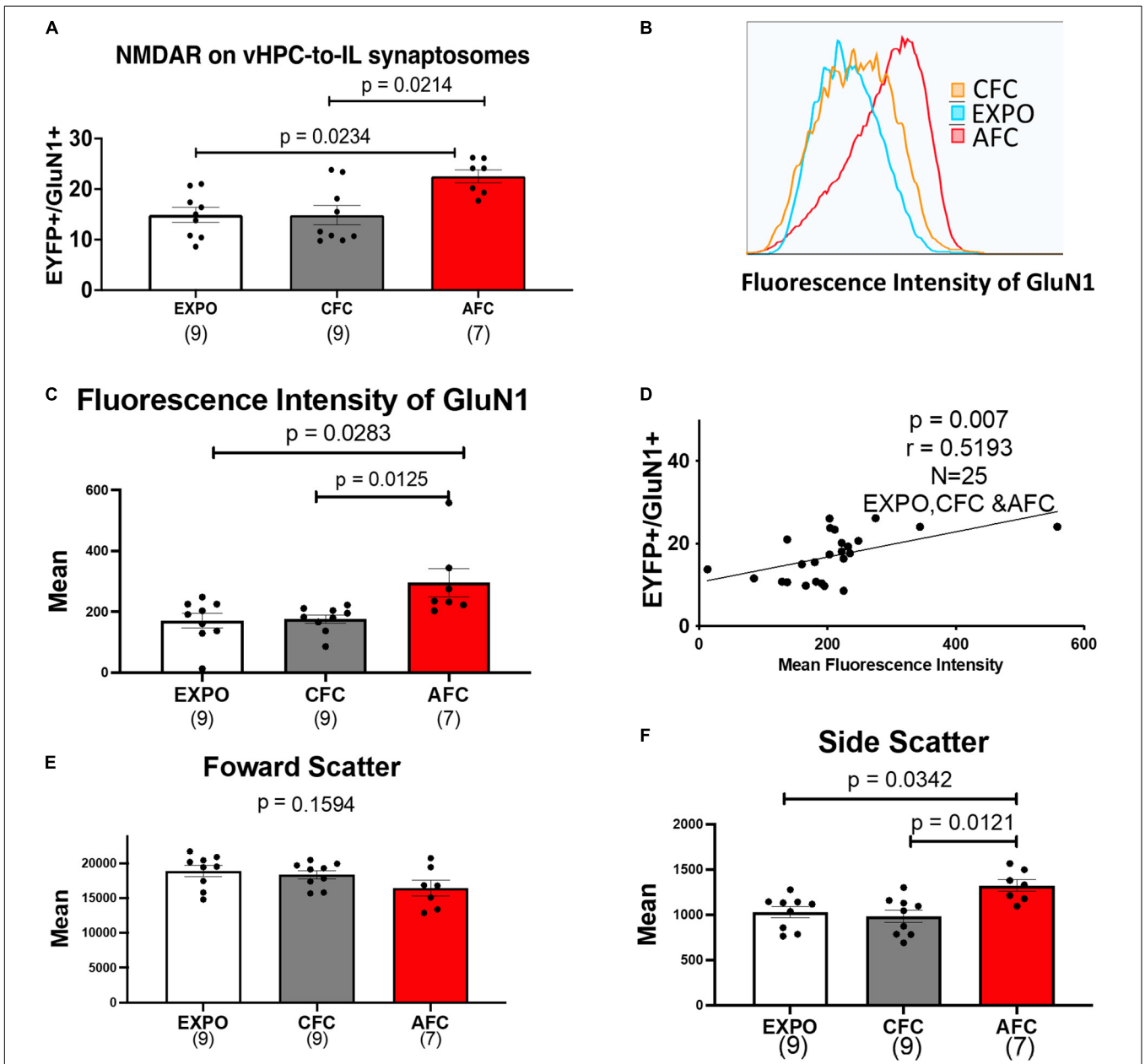

FIGURE 3 | AFC increases the number of NMDARS on VHPC-to-IL synaptosomes in males. **(A)** Relative levels of EYFP+/GluN1+ synaptosomes in male behavioral groups. **(B)** Representative histogram of the fluorescence intensity of GluN1 on EYFP+/GluN1+ synaptosomes from a single sample from the Exposure, CFC, and AFC male groups. **(C)** Mean fluorescence intensity of GluN1 on EYFP+/GluN1+ synaptosomes in male groups. **(D)** Correlation between the levels of EYFP+/GluN1+ synaptosomes and the mean fluorescence intensity of GluN1 in the male samples. **(E)** Mean forward scatter of the EYFP+/GluN1+ synaptosomes in the male groups. **(F)** Mean side scatter of the EYFP+/GluN1+ synaptosomes in the male groups. Sample sizes are indicated below each bar.

intensity of GluN1 on EYFP+ vHPC-to-IL synaptosomes in the male groups [$H(2,22) = 9.625$, $p = 0.0081$]. The mean of the AFC group was greater than the EXPO ($p = 0.0283$) and the CFC group ($p = 0.0125$). These data suggest that AFC increased the number of NMDARs at vHPC-to-IL synapses rather than simply increasing the number of vHPC-to-IL synapses. Furthermore, we found a correlation between the number of EYFP+/GluN1+ synaptosomes and the mean GluN1 fluorescence intensity ($r = 0.5193$, $p = 0.0078$; **Figure 3D**).

The observed increase in NMDA receptors on synaptosomes could occur if AFC increased the size of the synapses. To test this possibility, we analyzed the forward scatter of the EYFP+/GluN1+ synaptosomes since larger synaptosomes would produce more forward scatter. We found that the forward scatter was similar in all groups, suggesting that the synaptosomes are similar in size and that fear learning did not increase the size of the vHPC-to-IL synapses [$H(2,22) = 3.673$, $p = 0.1594$; **Figure 3E**]. However, the side scatter did vary among groups [$H(2,22) = 9.485$, $p = 0.0087$; **Figure 3F**]. We observed an increase in the side scatter of the AFC group compared to the EXPO ($p = 0.0342$) and CFC groups ($p = 0.0121$), suggesting that fear learning increased the intracellular complexity of the vHPC-IL synaptosomes.

In contrast to the male groups, we found similar GluN1 expression in all female behavioral groups suggesting that fear acquisition does not alter NMDA receptors at vHPC-to-IL synapses in females [$H(2,22) = 1.609$, $p = 0.44$; **Figure 4A**]. The histograms of the fluorescence intensity of GluN1 labeled EYFP+ synaptosomes were also similar in the EXPO, CFC, and AFC groups of female rats (**Figure 4B**). Although we found that the mean fluorescent intensity of GluN1 on EYFP+ vHPC-to-IL synaptosomes was different in the female groups [$H(2,22) = 7.951$, $p = 0.0188$], the only difference was between the AFC and CFC groups ($p = 0.0161$; **Figure 4C**). The mean of the EXPO group was similar to the CFC ($p = 0.3190$) and the AFC group ($p = 0.6195$), suggesting that neither contextual nor auditory fear acquisition altered GluN1 expression on vHPC-to-IL synaptosomes in the females. Furthermore, we found no correlation between the number of EYFP+/GluN1+ synaptosomes and the mean GluN1 fluorescence intensity ($r = 0.08$, $p = 0.1065$; **Supplementary Figure 2**). We also examined whether the GluN1 expression in females varied with the estrous cycle that was determined by vaginal smears at the time of sacrifice on day 2. We found no difference in mean fluorescent intensity of GluN1 labeled EYFP+ synaptosomes across the estrous cycle of the rats [$H(2,22) = 0.5232$, $p = 0.7869$; **Figure 4D**]. The number of EYFP+/GluN1+ synaptosomes did not also vary across the estrous cycle [$H(2,22) = 9.624$, $p = 0.2$; **Supplementary Figure 2C**]. This suggests that cyclic changes in estrogen and other reproductive hormones did not alter the NMDA receptor expression on the vHPC-to-IL synapses.

The forward scatter of the EYFP+/GluN1+ synaptosomes was similar in all female groups, suggesting that the synaptosomes are similar in size and that fear learning did not change the size of the vHPC-to-IL synapses in females [$H(2,22) = 0.1231$, $p = 0.9403$; **Figure 4E**]. As in males, we observed an increase in the side scatter of the AFC group compared to the CFC group ($p = 0.0370$) and the EXPO group ($p = 0.0387$), suggesting that auditory fear learning changed the intracellular complexity of the vHPC-IL synaptosomes [$H(2,22) = 6.605$, $p = 0.0368$; **Figure 4F**]. To explore the possibility that the females and males had different basal levels of GluN1 expression at this synapse, we compared the GluN1 expression in the EXPO group of both sexes. The female and male EXPO groups expressed similar levels of GluN1, suggesting that both sexes express similar basal levels of GluN1 (Mann–Whitney U = 23, $p = 0.14$).

Fear Behavior for Experiment II

Our initial experiment suggests that AFC increases the expression of NMDARs at vHPC-to-IL synapses of male rats. To determine if this synaptic plasticity required associative learning and whether fear extinction could reverse the synaptic changes, we repeated our experiments with a different cohort of rats. We divided male and female rats into three different behavioral groups, pseudoconditioning (PSEUDO), AFC, and extinction (EXT) (**Figure 5C**). Due to unexpected delays, the male rats were different ages (P90, P180, and P330) at the beginning of the behavioral training. As in the previous experiment, rats received injections of AAV into the vHPC to express ChR-EYFP at least 2 months before behavioral training. On day 1, the PSEUDO groups ($n = 11$ males and 12 females) received six tones and then five quick foot shocks immediately before being removed from the conditioning chamber to control for tone and shock exposure without inducing conditioned inhibition (**Figures 5A,B**). On day 1, the AFC groups ($n = 9$ males and 6 females) and the EXT groups ($n = 15$ males and 12 females) received one habituation tone and five tones paired with a foot shock. Both female and male rats in the AFC and EXT groups showed a gradual increase in freezing on day 1, indicating that they acquired fear to the tone (**Supplementary Statistical Table**). In contrast, the PSEUDO group that did not receive paired tones and shocks presented a low level of freezing to the tone (**Figures 5A,B**). On day 2, the EXT groups received two sessions of 14 tones without foot shocks in the conditioning context with 1 h between sessions.

On day 3, we tested the long-term memory of all three groups by exposing the rats to two tones in the conditioning context. In the males, the groups showed different levels of freezing to the tones [$F(2,32) = 2.245$, $p = 0.0012$; **Figure 6A**]. The AFC group only showed a trend of higher freezing than the PSEUDO group, since the unpaired PSEUDO group showed freezing during the tone ($p = 0.1571$). To determine if the PSEUDO group was freezing to the tone or to the context, we compared freezing during the 30 s before the first tone (contextual fear) to the freezing during each of the two recall tones (**Supplementary Figure 3A**). The rats froze similar amounts during the pretone and tone exposure periods [$F(2,27) = 0.7582$, $p = 0.4782$], suggesting that the PSEUDO males were actually showing contextual fear during the tone. The EXT group showed less freezing than the AFC group indicating good recall of fear extinction ($p = 0.0009$).

Next we analyzed the expression of GluN1 on vHPC-to-IL synaptosomes in the male groups and found a trend of a difference in the groups [$H(2,32) = 4.526$, $p = 0.1040$; **Supplementary Figure 3B**]. Since we used male rats from

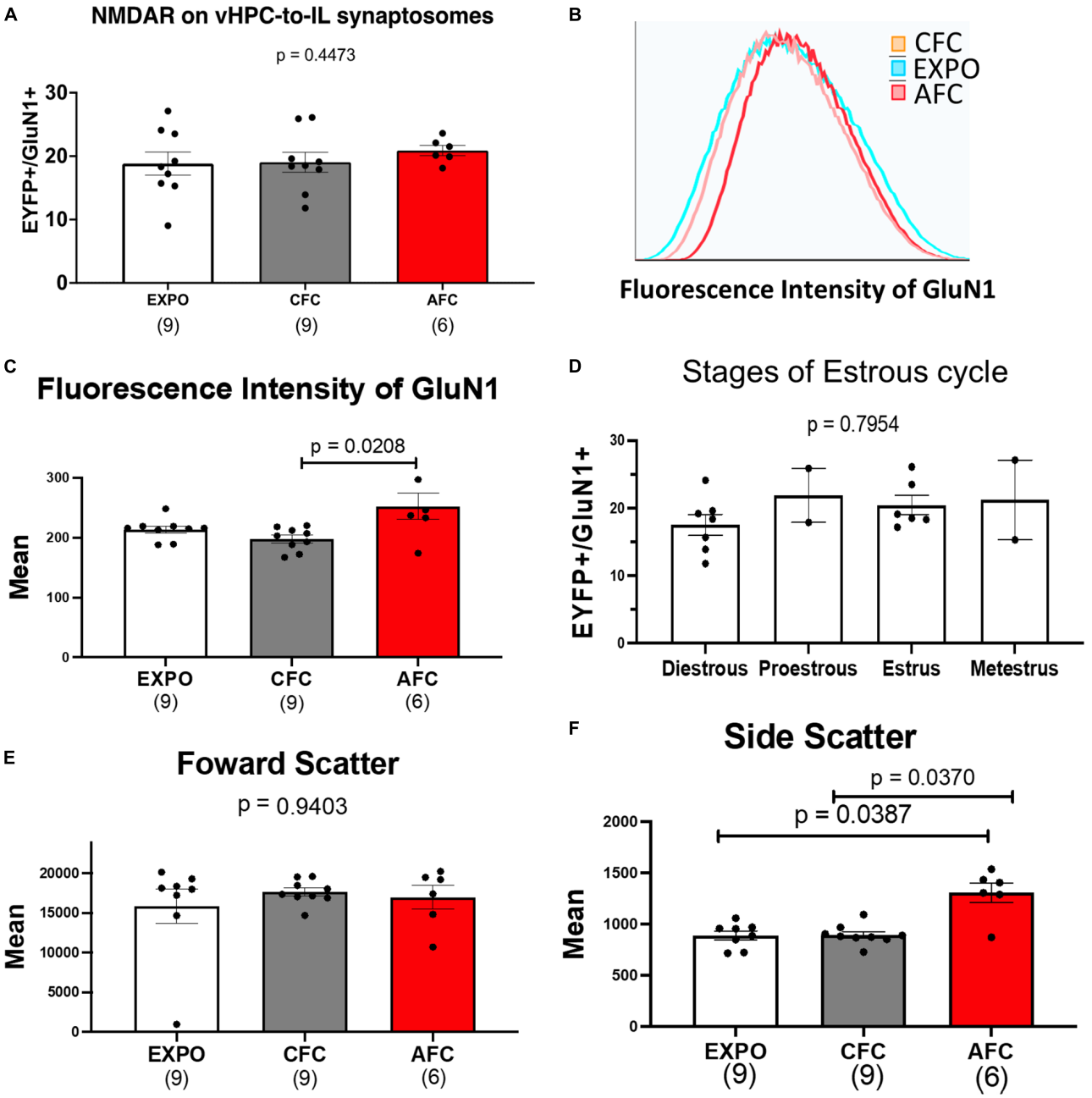

FIGURE 4 | AFC does not alter GluN1 expression at vHPC-IL synaptosomes in females. **(A)** Relative levels of EYFP+/GluN1+ synaptosomes in female behavioral groups. **(B)** Representative histogram of the fluorescence intensity of GluN1 on EYFP+/GluN1+ synaptosomes from a single sample from the EXPO, CFC, and AFC female groups. **(C)** Mean fluorescence intensity of GluN1 on EYFP+/GluN1+ synaptosomes in female groups. **(D)** Mean fluorescence intensity of GluN1 on EYFP+/GluN1+ synaptosomes across the estrous cycle. **(E)** Mean forward scatter of the EYFP+/GluN1+ synaptosomes in the female groups. **(F)** Mean side scatter of the EYFP+/GluN1+ synaptosomes in the female groups. Sample sizes are indicated below each bar.

P90, P180, and P330 in this experiment (**Figure 5C**), any learning-induced changes could be obscured by changes due to aging or time of ChR-EYFP expression. Therefore, we tested whether the expression of GluN1 at vHPC-to-IL synaptosomes varied with age in the male PSEUDO group which serves as our baseline group. As shown in **Supplementary Figure 3C**, the number of EYFP+/GluN1+ synaptosomes trended to be higher [$H(2,9) = 5.182$, $p = 0.0684$] and the fluorescent intensity of GluN1 immunolabeling increased in older male rats [$H(2,9) = 7.03$, $p = 0.0142$]. The side scatter of the EYFP+/GluN1+ synaptosomes also increased with age [$H(2,9) = 7.477$, $p = 0.0062$], but the forward scatter remained constant across ages [$H(2,9) = 1.417$, $p = 0.5238$]. To adjust for the effect of age, we normalized the EYFP+/GluN1+ expression

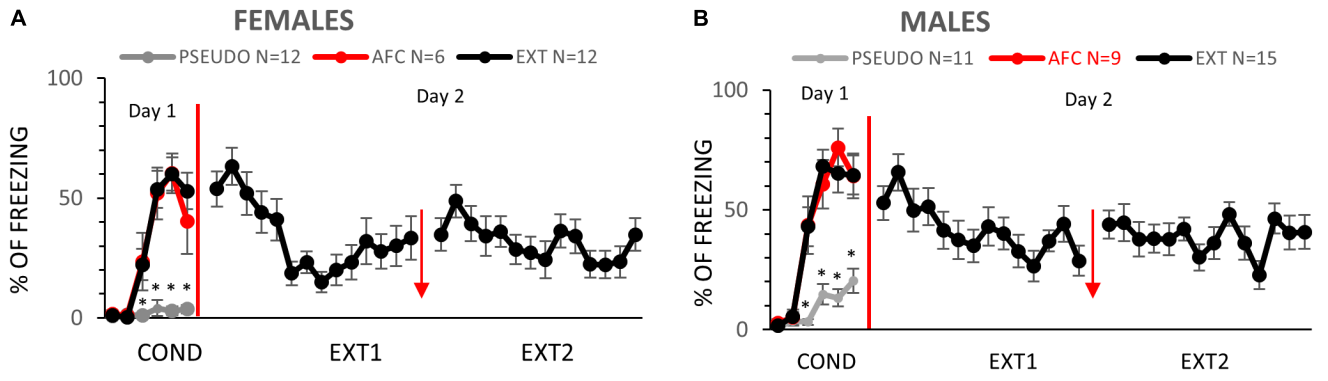

C

Groups	Total animals	Ages
PSEUDO	22 (10 M, 12 F)	M: 4 P90, 3 P180, 4 P330. F: P90
COND	15 (9 M, 6 F)	M: 2 P90, 3 P180, 4 P330. F: P90
EXT	27 (15 M, 12 F)	M: 8 P90, 3 P180, 4 P330. F: P90

FIGURE 5 | Females and males learn AFC and fear extinction. **(A,B)** Fear responses during training in the PSEUDO, AFC, and EXT female and male groups, respectively. Red arrow indicates 1 h break between extinction sessions. **(C)** Distribution of animals by age and sex in experiment 2. * Denotes trials in which the AFC and EXT groups show more freezing than the PSEUDO group ($p \leq 0.05$).

and GluN1 fluorescent intensity to the average of the PSEUDO group of the same age (**Figures 6B,C**). We separated the male groups by age and then normalized all data from P90 male animals to the average of the P90 PSEUDO group, all data from the P180 animals to the average of the P180 PSEUDO group, and all the data from P330 animals to the average of the P330 PSEUDO group. Then we combined the normalized data into the PSEUDO, AFC, and Ext groups. We found that the normalized EYFP+/GluN1+ expression [$H(2,32) = 7.182$, $p = 0.0276$] and GluN1 fluorescent intensity [$H(2,32) = 6.201$, $p = 0.0450$] varied among groups. To test whether associative learning was required for the changes in GluN1 expression, we compared the male PSEUDO and AFC groups. The results show that the AFC group expressed more EYFP+/GluN1+ synaptosomes than the PSEUDO group ($p = 0.0235$; **Figure 6B**). The AFC group also showed greater fluorescent intensity of GluN1 immunolabeling than the PSEUDO group ($p = 0.0470$; **Figure 6C**). These data suggest that synapses from vHPC-to-IL had more NMDARs after AFC. Therefore, the increase in GluN1 expression at vHPC-to-IL synapses observed in experiment 1 was replicated in this new group of rats, suggesting that the findings are robust. Even though the PSEUDO group showed similar levels of freezing during the tones as the AFC group, the PSEUDO group showed fewer EYFP+/GluN1+ synaptosomes than the AFC group. This suggests that the GluN1 expression was altered by the tone-shock pairing rather than the increase in fear *per se*.

The increased expression of GluN1 could contribute to the encoding of the AFC memory. To further examine this possibility, we compared GluN1 expression in the male AFC groups from experiments 1 and 2 to their fear level during recall. We found that the freezing at recall did not correlate with GluN1 expression, suggesting that the increase in NMDA receptors may not encode fear memory *per se* ($r = -0.0097$, $p = 0.9727$, $N = 15$; **Figure 6D**). Furthermore, the freezing to the last tone of conditioning on day 1 did not also correlate with GluN1 expression ($r = 0.1$, $p = 0.7$, $N = 15$).

Next, we compared the AFC and EXT groups to determine if extinction reversed the increase of NMDAR. The molecular assessment shows that the AFC and EXT groups expressed similar levels of EYFP+/GluN1+ synaptosomes ($p = 0.5080$; **Figure 6B**) and GluN1 immunofluorescence ($p > 0.9999$; **Figure 6C**). This suggests that EXT reduced the conditioned fear behavior without reversing the increase in GluN1 at vHPC-to-IL synapses induced by AFC in males. In addition, we analyzed forward and side scatter of the EYFP+/GluN1+ synaptosomes. PSEUDO, AFC, and EXT groups had similar values of forward [$H(2,32) = 1.882$, $p = 0.3901$] and side scatter [$H(2,32) = 0.2840$, $p = 0.8676$], suggesting that the synaptosomes were similar in size and complexity (**Figures 6E,F**).

Although we did not see any changes in GluN1 expression in the females in experiment 1, we also compared the GluN1 expression on vHPC-to-IL synaptosomes in female PSEUDO, AFC, and EXT groups (**Figure 7**). In the females, the groups showed similar levels of freezing to the tones [$F(2,27) = 0.4872$, $p = 0.1440$; **Figure 7A**). As with the males, the PSEUDO group showed abundant freezing during the recall tones which obscured any effect of AFC. To determine if the female PSEUDO group was freezing to the tone or to the context, we compared freezing during the 30 s before the first tone (contextual fear) to the freezing during each of the two recall tones (**Supplementary Figure 4A**). The female rats froze less during the pretone than during the second ($p = 0.0112$) tone exposure period, suggesting that the PSEUDO females were actually showing fear to the tone. Therefore, the PSEUDO protocol appears to have induced

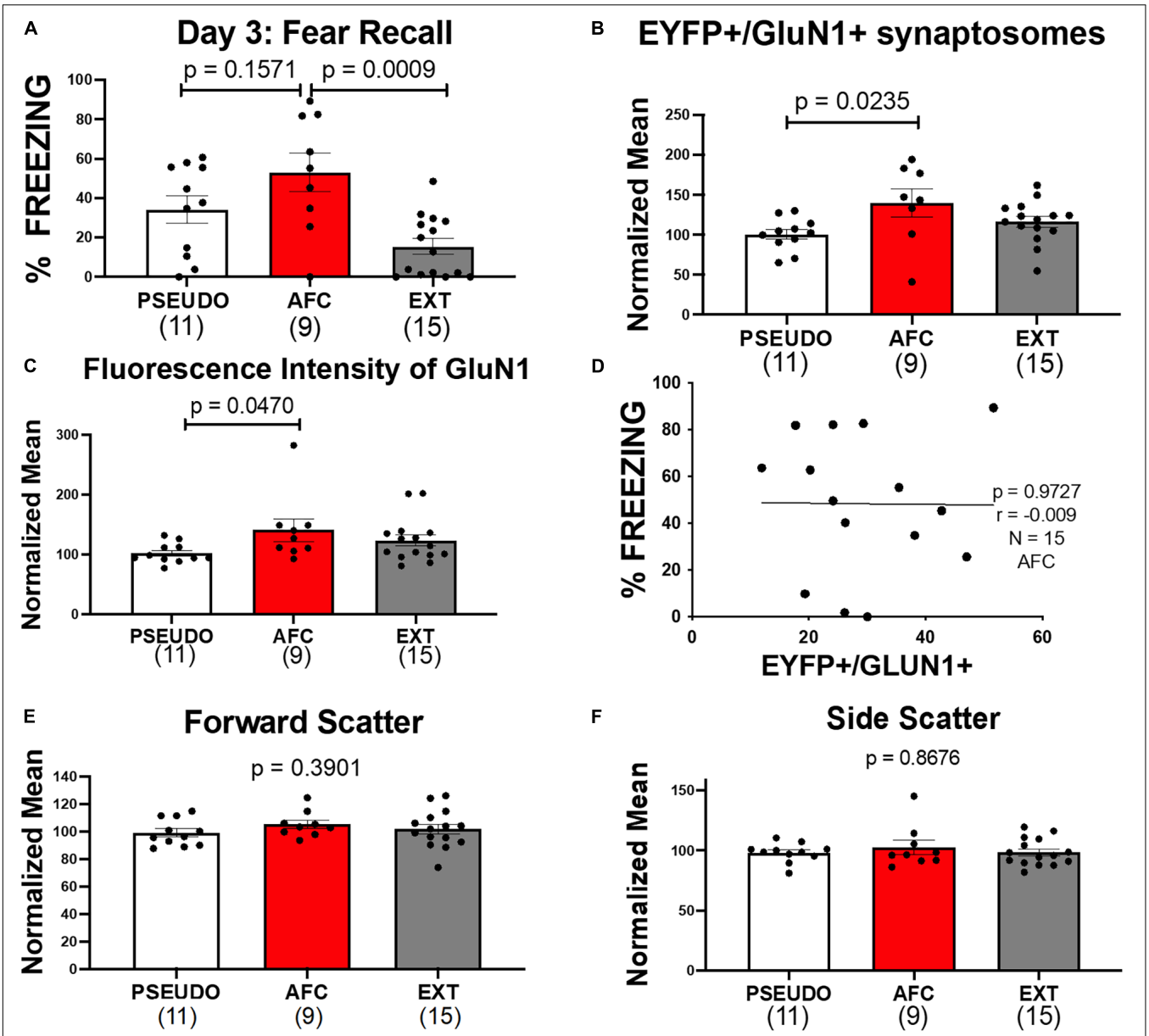

FIGURE 6 | Associative fear learning increases NMDARS on VHPC-to-IL synaptosomes in male rats. **(A)** Fear recall in the male groups. **(B)** Levels of EYFP+/GluN1+ synaptosomes normalized to the mean of the PSEUDO group of the corresponding age in the male groups. **(C)** Mean fluorescence intensity of GluN1 on EYFP+/GluN1+ synaptosomes in male groups normalized to the mean of the PSEUDO group of the corresponding age. **(D)** Graph comparing the levels of EYFP+/GluN1+ synaptosomes and the % freezing during recall of the males in the AFC groups in experiments 1 and 2. **(E,F)** Forward scatter and side scatter of EYFP+/GluN1+ synaptosomes in male groups normalized to the mean of the PSEUDO group of the corresponding age.

AFC in some of the female rats. In addition, the AFC and EXT groups showed similar levels of freezing suggesting poor extinction recall in the females.

Consistent with the results of experiment 1, we did not find any differences in EYFP+/GluN1+ expression [$H(2,27) = 2.274$, $p = 0.3207$; **Figure 7B**], GluN1 fluorescent intensity [$H(2,27) = 4.639$, $p = 0.0983$; **Figure 7C**], forward scatter [$H(2,27) = 0.6699$, $p = 0.7154$; **Figure 7D**], or side scatter [$H(2,27) = 0.6097$, $p = 0.7372$; **Figure 7E**]. However, the lack of behavioral differences among the female groups may have obscured any difference in GluN1 expression. Therefore, we also tested whether removing three animals from the PSEUDO group and one animal from the EXT group that exhibited freezing above 40% to create a behavior difference among the groups would similarly create a difference in GluN1 expression. As shown in **Supplementary Figure 4**, removing these animals created a behavioral difference among the groups but did not show any difference in GluN1 expression among the female groups. These data further suggest that fear learning does not alter NMDAR at the vHPC-to-IL synapse in females.

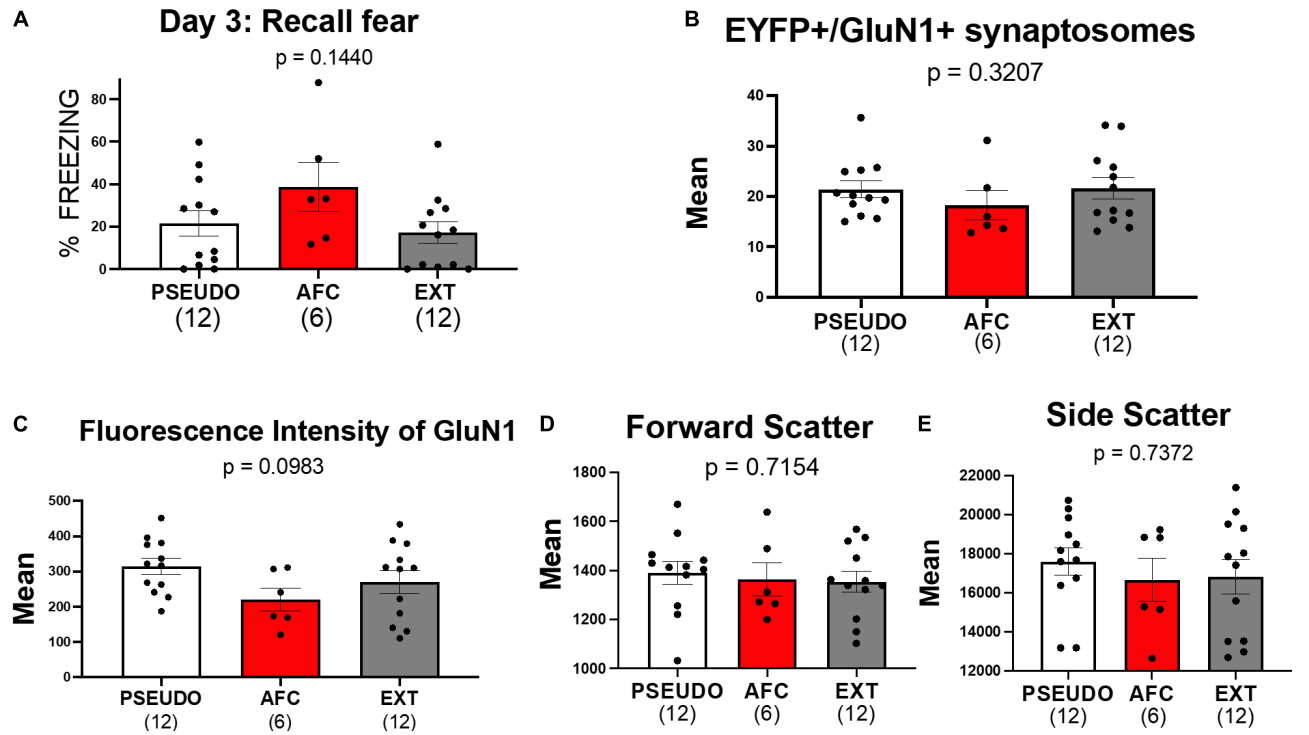

FIGURE 7 | Associative fear learning does not increase NMDAR on vHPC-to-IL synaptosomes in female rats. **(A)** Fear recall in the female groups. **(B)** Levels of EYFP+/GluN1+ synaptosomes in the female groups. **(C–E)** Mean fluorescence intensity of GluN1, forward scatter, and side scatter of EYFP+/GluN1+ synaptosomes in female groups.

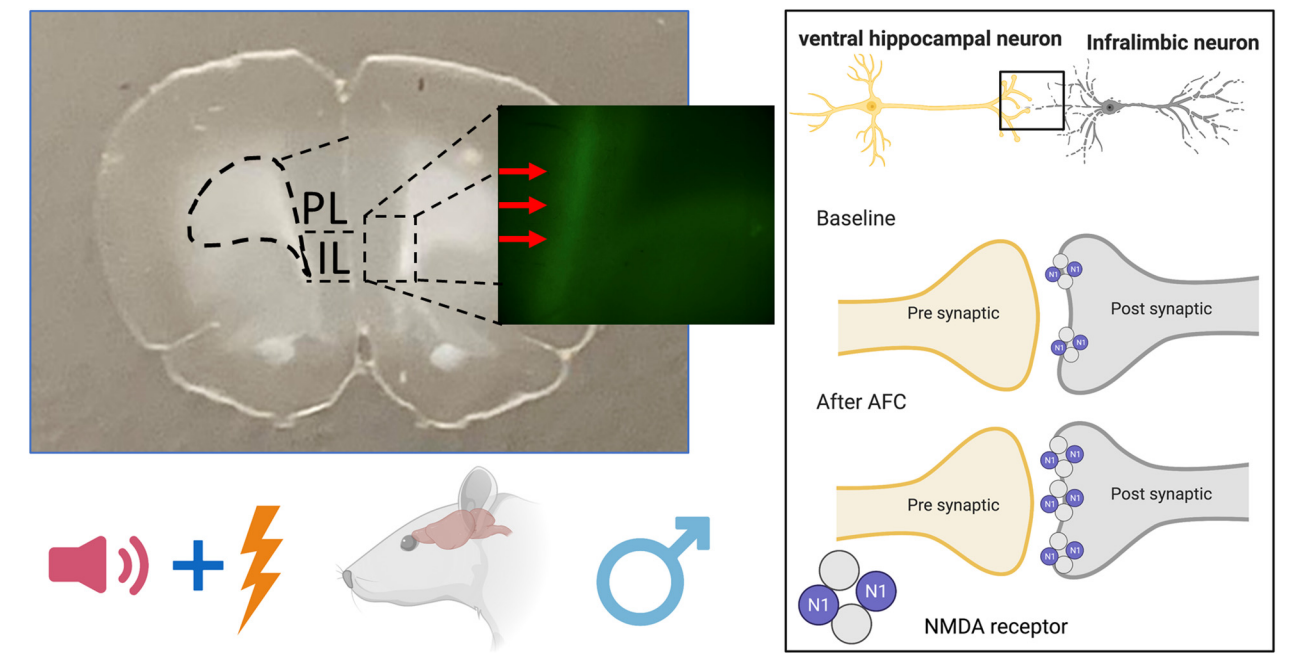

FIGURE 8 | Schematic diagram of NMDAR changes after auditory fear conditioning in male rat brain. Associative fear learning increases NMDAR on ventral hippocampal projections to the infralimbic cortex.

DISCUSSION

Scientists frequently employ the AAV expression of ChR-EYFP to determine the role of specific neuronal projections in behavior. In this study, we used FACS analysis of ChR-EYFP-labeled vHPC-to-IL synaptosomes to detect changes in GluN1 expression induced by fear conditioning. Our main finding is that AFC increased GluN1 expression at this synapse in males compared to EXPO and CFC, suggesting that the tone-shock pairing induced the change (**Figure 8**). In further support, male rats in the PSEUDO group that received unpaired tones and shocks did not exhibit the increase in GluN1 at vHPC-to-IL synaptosomes. In addition, the increase in GluN1 expression was not reversed by extinction. In contrast to the males, the females did not show differences in GluN1 expression at this synapse after any fear paradigm, suggesting that this is a sex-dependent form of synaptic plasticity induced by AFC in IL.

Our findings extend previous research showing that AFC induces synapse-dependent synaptic plasticity in IL of male rodents (Pattwell et al., 2012; Sepulveda-Orengo et al., 2013; Soler-Cedeño et al., 2019). In contrast to the electrophysiological finding of less NMDAR current after AFC reported earlier (Soler-Cedeño et al., 2019), we observed an increase in the fraction of vHPC-to-IL synaptosomes that expressed detectable levels of the obligatory GluN1 subunit of NMDAR after AFC. This increase in NMDAR at vHPC-to-IL synapses required the animal to learn the association of the cue and the shock, since neither CFC nor unpaired tones and shocks were sufficient to produce the change. The mean fluorescence intensity of GluN1 on the vHPC-to-IL synaptosomes also increased after AFC, suggesting that the associative learning led to more NMDARs at these synapses. The increase in the number of NMDARs occurred without an increase in synapse size, since the forward scatter of the synaptosomes did not change. However, the side scatter of the synaptosomes also increased after AFC suggesting a change in the intracellular organelles of the synaptosomes (Biesemann et al., 2014).

The vast majority of previous studies have used only male rodents to examine molecular mechanisms underlying fear learning (Zinebi et al., 2003; Burgos-Robles et al., 2007; Pattwell et al., 2012; Paoletti et al., 2013; Sepulveda-Orengo et al., 2013; Soler-Cedeño et al., 2019). Therefore, we also examined whether fear acquisition induces similar plasticity in females. In contrast to the plasticity observed in males, the females did not show any differences in the fraction of EYFP+/GluN1+ synaptosomes, GluN1 fluorescence intensity, or side scatter. Since we included females at different stages of the estrous cycle, it is possible that variability in the measurements could obscure any differences. However, the lack of strong correlation with the estrous stage argues against this possibility. The females did learn similar levels of conditioned fear to the tones. These data imply sex differences in the molecular mechanisms that encode auditory fear learning that warrants further study. Furthermore, this raises the possibility that many of the previous identified molecular mechanisms of fear acquisition and extinction may not apply to females.

The increase in NMDAR at vHPC-to-IL synaptosomes after associative fear learning does not seem to encode fear *per se*. First, the levels of GluN1 did not correlate with fear recall or fear acquisition. Second, the changes in GluN1 were not reversed by fear extinction, although fear extinction did reduce fear expression. Third, in spite of receiving unpaired tones and shocks, the PSEUDO group showed fear to the tone during recall that was similar to the fear expressed by the AFC group but only the AFC group showed the increase in GluN1 on the vHPC-to-IL synaptosomes. Taken together, these findings suggest that although learning the association between tone and shock is required to create these molecular changes, the changes do not encode the conditioned fear.

More NMDAR in vHPC-to-IL after AFC could produce a number of physiological consequences. The increase of NMDAR could enhance calcium influx into the dendritic spines to facilitate subsequence learning or memory formation. For example, animals might acquire more robust extinction memories due to more calcium influx through NMDAR during extinction learning. Consistent with this, increased NMDARs in IL synapses are associated with enhanced synaptic plasticity and increased fear extinction memory (Abumaria et al., 2011). In addition, animals with good fear extinction recall show more NMDAR-dependent bursts of action potentials in IL the day of extinction learning and blocking NMDAR in IL during extinction learning impairs the long-term extinction memory (Burgos-Robles et al., 2007). Furthermore, researchers found that stimulating NMDARs with D-cycloserine, a partial agonist at the glycine binding site of NMDARs, can enhance fear extinction in rodents (Richardson et al., 2004) and humans (Morrison and Ressler, 2014). Therefore, the literature highlights the importance of NMDARs for fear extinction and supports the possibility that the increase in NMDARs on the vHPC-to-IL synapses could contribute to fear extinction in the males.

Whole-cell recordings of optically stimulated vHPC synapses in IL found less synaptic NMDA current in layer V pyramidal neurons after AFC in males (Soler-Cedeño et al., 2019). Therefore, we expected to observe a reduction in the NMDARs on the vHPC-to-IL synaptosomes. In contrast, our results show increased NMDAR. Several possibilities could reconcile these apparently conflicting results. One possibility is that AFC might cause less vHPC activation of NMDA currents in IL neurons through dynamic changes in NMDAR subunit composition or phosphorylation state instead of a reduction in the relative amount of NMDAR (Lopez de and Sah, 2003; Zinebi et al., 2003; Abumaria et al., 2011; Lussier et al., 2015). The electrophysiological study measured the NMDAR current during the decay phase rather than at the peak to reduce AMPAR current contamination. Therefore, a shift toward faster decaying NMDAR-mediated currents could produce an apparent reduction in NMDA current. For example, a shift toward more GluN2A, which has faster decay kinetics, could produce less current even with more NMDARs (Lopez de and Sah, 2003; Gray et al., 2011; Paoletti et al., 2013). Alternatively, the diminished NMDA current could be caused

by the lateral movement of NMDA receptors to the edges of the synapse which could be detected on the synaptosomes in spite of being less activated by the synaptic release of glutamate (Paoletti et al., 2013; Lussier et al., 2015). Another possibility is that both presynaptic and postsynaptic NMDA receptors were detected on the synaptosomes, but only postsynaptic receptors were assessed with the electrophysiology. However, we do not think that there were significant levels of presynaptic GluN1 in our sample, since the vast majority of GluN1 was found on the largest synaptosomes (**Supplementary Figure 2A**). It is also important to note that the synaptosomes include vHPC synapses onto both pyramidal and GABAergic neurons from all cortical areas, whereas the electrophysiological studies were restricted to vHPC synapses onto layer V pyramidal neurons of IL. Given the strong feedforward inhibition produced by vHPC projections to IL (Marek et al., 2018), it is possible that synapses onto GABAergic neurons contribute substantially to our results. Although the mechanism behind the previously observed reduction in NMDAR current remains to be determined, the analysis of GluN1 on vHPC-to-IL synaptosomes suggests that the reduction is not due to reduced expression of NMDARs.

CONCLUSION

In summary, the use of ChR-EYFP combined with FACS allowed us to identify an increase in NMDARs specifically at the vHPC-to-IL synapse. This molecular change required the pairing of tones and shocks and occurred only in male rats. Our findings further indicate that fear acquisition alters IL physiology in male rats. The lack of similar synaptic plasticity in the females highlights the need to validate whether molecular changes identified in males also apply to females.

DATA AVAILABILITY STATEMENT

The raw data supporting the conclusions of this article will be made available by the authors, without undue reservation.

ETHICS STATEMENT

The animal study was reviewed and approved by the institutional animal care and use committee.

AUTHOR CONTRIBUTIONS

YC-O, YG, and JP designed the research, analyzed the data, and wrote the manuscript. YC-O, MC, AH, and PL performed the research. All authors contributed to the article and approved the submitted version.

FUNDING

This work was supported by the RCMI BRAIN and MAGIC Cores (NIMHHD U54 MD007579), R15 MH116345, and R01NS099036 from the National Institutes of Health.

SUPPLEMENTARY MATERIAL

The Supplementary Material for this article can be found online at: https://www.frontiersin.org/articles/10.3389/fnsyn.2021.695964/full#supplementary-material

REFERENCES

Abumaria, N., Yin, B., Zhang, L., Li, X. Y., Chen, T., Descalzi, G., et al. (2011). Effects of elevation of brain magnesium on fear conditioning, fear extinction, and synaptic plasticity in the infralimbic prefrontal cortex and lateral amygdala. *J. Neurosci.* 31, 14871–14881. doi: 10.1523/jneurosci.3782-11.2011

Battaglia, S., Garofalo, S., di Pellegrino, G., and Starita, F. (2020). Revaluing the role of vmPFC in the acquisition of pavlovian threat conditioning in humans. *J. Neurosci.* 40, 8491–8500. doi: 10.1523/jneurosci.0304-20.2020

Biesemann, C., Grønborg, M., Luquet, E., Wichert, S. P., Bernard, V., Bungers, S. R., et al. (2014). Proteomic screening of glutamatergic mouse brain synaptosomes isolated by fluorescence activated sorting. *EMBO J.* 33, 157–170. doi: 10.1002/embj.201386120

Bloodgood, D. W., Sugam, J. A., Holmes, A., and Kash, T. L. (2018). Fear extinction requires infralimbic cortex projections to the basolateral amygdala. *Transl. Psychiatry* 8:60.

Bukalo, O., Nonaka, M., Weinholtz, C. A., Mendez, A., Taylor, W. W., and Holmes, A. (2021). Effects of optogenetic photoexcitation of infralimbic cortex inputs to the basolateral amygdala on conditioned fear and extinction. *Behav. Brain Res.* 396:112913. doi: 10.1016/j.bbr.2020.112913

Burgos-Robles, A., Vidal-Gonzalez, I., Santini, E., and Quirk, G. J. (2007). Consolidation of fear extinction requires NMDA receptor-dependent bursting in the ventromedial prefrontal cortex. *Neuron* 53, 871–880. doi: 10.1016/j.neuron.2007.02.021

Chang, C. H., and Maren, S. (2010). Strain difference in the effect of infralimbic cortex lesions on fear extinction in rats. *Behav. Neurosci.* 124, 391–397. doi: 10.1037/a0019479

Corcoran, K. A., Desmond, T. J., Frey, K. A., and Maren, S. (2005). Hippocampal inactivation disrupts the acquisition and contextual encoding of fear extinction. *J. Neurosci.* 25, 8978–8987. doi: 10.1523/jneurosci.2246-05.2005

Do-Monte, F. H., Manzano-Nieves, G., Quiñones-Laracuente, K., Ramos-Medina, L., and Quirk, G. J. (2015). Revisiting the role of infralimbic cortex in fear extinction with optogenetics. *J. Neurosci.* 35, 3607–3615. doi: 10.1523/jneurosci.3137-14.2015

Dunsmoor, J. E., Kroes, M. C. W., Li, J., Daw, N. D., Simpson, H. B., and Phelps, E. A. (2019). Role of human ventromedial prefrontal cortex in learning and recall of enhanced extinction. *J. Neurosci.* 39, 3264–3276. doi: 10.1523/jneurosci.2713-18.2019

Evans, G. J. O. (2015). The synaptosome as a model system for studying synaptic physiology. *Cold Spring Harb. Protoc.* 2015, 421–424.

Fullana, M. A., Harrison, B. J., Soriano-Mas, C., Vervliet, B., Cardoner, N., Àvila-Parcet, A., et al. (2016). Neural signatures of human fear conditioning: An updated and extended meta-analysis of fMRI studies. *Mol. Psychiatry* 21, 500–508. doi: 10.1038/mp.2015.88

Gray, J. A., Shi, Y., Usui, H., During, M. J., Sakimura, K., and Nicoll, R. A. (2011). Distinct modes of AMPA receptor suppression at developing synapses by GluN2A and GluN2B: Single-Cell NMDA receptor subunit deletion in Vivo. *Neuron* 71, 1085–1101. doi: 10.1016/j.neuron.2011.08.007

Gylys, K. H., Fein, J. A., Yang, F., and Cole, G. M. (2004). Enrichment of presynaptic and postsynaptic markers by size-based gating analysis of synaptosome

preparations from rat and human cortex. *Cytometry* 60A, 90–96. doi: 10.1002/cyto.a.20031

Harrison, B. J., Fullana, M. A., Via, E., Soriano-Mas, C., Vervliet, B., Martínez-Zalacaín, I., et al. (2017). Human ventromedial prefrontal cortex and the positive affective processing of safety signals. *Neuroimage* 152, 12–18. doi: 10.1016/j.neuroimage.2017.02.080

Hobson, B. D., and Sims, P. A. (2019). Critical analysis of particle detection artifacts in synaptosome flow cytometry. *Eneuro*. 6:ENEURO.0009-19.2019. doi: 10.1523/ENEURO.0009-19.2019

LeDoux, J. E. (2000). Emotion circuits in the brain. *Annu. Rev. Neurosci.* 23, 155–184. doi: 10.1146/annurev.neuro.23.1.155

Lopez de, A., and Sah, P. (2003). Development and subunit composition of synaptic NMDA receptors in the amygdala: NR2B synapses in the adult central amygdala. *J. Neurosci.* 23, 6876–6883. doi: 10.1523/jneurosci.23-17-06876.2003

Lussier, M. P., Sanz-Clemente, A., and Roche, K. W. (2015). Dynamic regulation of N -Methyl-d-aspartate (n.d.) and α-Amino-3-hydroxy-5-methyl-4-isoxazolepropionic Acid (AMPA) receptors by posttranslational modifications. *J. Biol. Chem.* 290, 28596–28603. doi: 10.1074/jbc.r115.652750

Marek, R., Jin, J., Goode, T. D., Giustino, T. F., Wang, Q., Acca, G. M., et al. (2018). Hippocampus-driven feed-forward inhibition of the prefrontal cortex mediates relapse of extinguished fear. *Nat. Neurosci.* 21, 384–392. doi: 10.1038/s41593-018-0073-9

Milad, M. R., and Quirk, G. J. (2002). Neurons in medial prefrontal cortex signal memory for fear extinction. *Nature* 420, 70–74. doi: 10.1038/nature01138

Milad, M. R., and Quirk, G. J. (2012). Fear extinction as a model for translational neuroscience: ten years of progress. *Annu. Rev. Psychol.* 63, 129–151. doi: 10.1146/annurev.psych.121208.131631

Morrison, F. G., and Ressler, K. J. (2014). From the neurobiology of extinction to improved clinical treatments. *Depress Anxiety* 31, 279–290. doi: 10.1002/da.22214

Paoletti, P., Bellone, C., and Zhou, Q. (2013). NMDA receptor subunit diversity: impact on receptor properties, synaptic plasticity and disease. *Nat. Rev. Neurosci.* 14, 383–400. doi: 10.1038/nrn3504

Pattwell, S. S., Duhoux, S., Hartley, C. A., Johnson, D. C., Jing, D., Elliott, M. D., et al. (2012). Altered fear learning across development in both mouse and human. *Proc. Natl. Acad. Sci. U S A* 109, 16318–16323. doi: 10.1073/pnas.1206834109

Phelps, E. A., and LeDoux, J. E. (2005). Contributions of the amygdala to emotion processing: From animal models to human behavior. *Neuron* 48, 175–187. doi: 10.1016/j.neuron.2005.09.025

Richardson, R., Ledgerwood, L., and Cranney, J. (2004). Facilitation of fear extinction by D-Cycloserine: theoretical and clinical implications. *Learn. Mem.* 11, 510–516. doi: 10.1101/lm.78204

Santini, E., and Porter, J. T. (2010). M-type potassium channels modulate the intrinsic excitability of infralimbic neurons and regulate fear expression and extinction. *J. Neurosci.* 30, 12379–12386. doi: 10.1523/jneurosci.1295-10.2010

Santini, E., Quirk, G. J., and Porter, J. T. (2008). Fear conditioning and extinction differentially modify the intrinsic excitability of infralimbic neurons. *J. Neurosci.* 28, 4028–4036. doi: 10.1523/jneurosci.2623-07.2008

Santini, E., Sepulveda-Orengo, M., and Porter, J. T. (2012). Muscarinic receptors modulate the intrinsic excitability of infralimbic neurons and consolidation of fear extinction. *Neuropsychopharmacology* 37, 2047–2056. doi: 10.1038/npp.2012.52

Sepulveda-Orengo, M. T., Lopez, A. V., Soler-Cedeno, O., and Porter, J. T. (2013). Fear extinction induces mGluR5-mediated synaptic and intrinsic plasticity in infralimbic neurons. *J. Neurosci.* 33, 7184–7193. doi: 10.1523/jneurosci.5198-12.2013

Sierra-Mercado, D., Padilla-Coreano, N., and Quirk, G. J. (2011). Dissociable roles of prelimbic and infralimbic cortices, ventral hippocampus, and basolateral amygdala in the expression and extinction of conditioned fear. *Neuropsychopharmacology* 36, 529–538. doi: 10.1038/npp.2010.184

Soler-Cedeño, O., Cruz, E., Criado-Marrero, M., and Porter, J. T. (2016). Contextual fear conditioning depresses infralimbic excitability. *Neurobiol. Learn. Mem.* 130, 77–82. doi: 10.1016/j.nlm.2016.01.015

Soler-Cedeño, O., Torres-Rodríguez, O., Bernard, F., Maldonado, L., Hernández, A., and Porter, J. T. (2019). Plasticity of NMDA receptors at ventral hippocampal synapses in the infralimbic cortex regulates cued fear. *eNeuro* 6:ENEURO.0354-18.2019. doi: 10.1523/ENEURO.0354-18.2019

Song, C., Ehlers, V. L., and Moyer, J. R. (2015). Trace fear conditioning differentially modulates intrinsic excitability of medial prefrontal cortex-basolateral complex of amygdala projection neurons in infralimbic and prelimbic cortices. *J. Neurosci.* 35, 13511–13524. doi: 10.1523/jneurosci.2329-15.2015

Tao, Y., Cai, C. Y., Xian, J. Y., Kou, X. L., Lin, Y. H., Qin, C., et al. (2020). Projections from infralimbic cortex to paraventricular thalamus mediate fear extinction retrieval. *Neurosci. Bull.* 37, 229–241. doi: 10.1007/s12264-020-00603-6

Zinebi, F., Xie, J., Liu, J., Russell, R. T., Gallagher, J. P., McKernan, M. G., et al. (2003). NMDA currents and receptor protein are downregulated in the amygdala during maintenance of fear memory. *J. Neurosci.* 23, 10283–10291. doi: 10.1523/jneurosci.23-32-10283.2003

Conflict of Interest: The authors declare that the research was conducted in the absence of any commercial or financial relationships that could be construed as a potential conflict of interest.

frontiers in Synaptic Neuroscience

BRIEF RESEARCH REPORT
published: 27 January 2022
doi: 10.3389/fnsyn.2021.804898

Blast-Induced Mild Traumatic Brain Injury Alterations of Corticotropin-Releasing Factor Neuronal Activity in the Mouse Hypothalamic Paraventricular Nucleus

Sarah Simmons[1†], Ludovic D. Langlois[1†], Mario G. Oyola[2], Shawn Gouty[1], T. John Wu[2] and Fereshteh S. Nugent[1]**

[1]Department of Pharmacology and Molecular Therapeutics, Uniformed Services University of the Health Sciences, Bethesda, MD, United States, [2]Department of Gynecologic Surgery and Obstetrics, Uniformed Services University of the Health Sciences, Bethesda, MD, United States

OPEN ACCESS

Edited by:
Marco Atzori,
Autonomous University of San Luis Potosí, Mexico

Reviewed by:
Jeremy Borniger,
Stanford University, United States
Boris Heifets,
Stanford University, United States

***Correspondence:**
Fereshteh S. Nugent
fereshteh.nugent@usuhs.edu
T. John Wu
tao-yiao.wu@usuhs.edu

[†]These authors share first authorship

Received: 29 October 2021
Accepted: 27 December 2021
Published: 27 January 2022

Citation:
Simmons S, Langlois LD, Oyola MG, Gouty S, Wu TJ and Nugent FS (2022) Blast-Induced Mild Traumatic Brain Injury Alterations of Corticotropin-Releasing Factor Neuronal Activity in the Mouse Hypothalamic Paraventricular Nucleus. Front. Synaptic Neurosci. 13:804898. doi: 10.3389/fnsyn.2021.804898

Blast-induced mild traumatic brain injury (mbTBI) is the most common cause of TBI in US service members and veterans. Those exposed to TBI are at greater risk of developing neuropsychiatric disorders such as posttraumatic stress disorder, anxiety and depressive disorders, and substance use disorders following TBI. Previously, we have demonstrated that mbTBI increases anxiety-like behaviors in mice and dysregulates stress at the level of corticotropin-releasing factor (CRF) neurons in the paraventricular nucleus (PVN). To expand on how mTBI may dysregulate the stress axis centrally, here PVN CRF neuronal activity was evaluated using whole cell-patch clamp recordings in hypothalamic slices from sham and mbTBI adult male CRF:tdTomato mice 7 days post-injury. We found that mbTBI generally did not affect the neuronal excitability and intrinsic membrane properties of PVN CRF neurons; this injury selectively increased the frequency of spontaneous neuronal firing of PVN CRF neurons localized to the dorsal PVN (dPVN) but not ventral PVN (vPVN). Consistently, mbTBI-induced dPVN CRF hyperactivity was associated with pre- and post-synaptic depression of spontaneous GABAergic transmission onto dPVN CRF neurons suggesting that mbTBI-induced GABAergic synaptic dysfunction may underlie dPVN CRF neuronal hyperactivity and increases in dPVN CRF signaling. The present results provide the first evidence for mbTBI-induced alterations in PVN CRF neuronal activity and GABAergic synaptic function that could mediate hypothalamic CRF dysregulation following mbTBI contributing to stress psychopathology associated with blast injury.

Keywords: traumatic brain injury, blast injury, CRF, paraventricular nucleus, PVN, electrophysiology, neuronal activity, GABAergic synaptic transmission

INTRODUCTION

Traumatic brain injury (TBI) accounts for almost 3 million hospitalizations or admissions into the emergency room in the United States with the incidence rate increasing annually (Taylor et al., 2017; GBD 2016 Traumatic Brain Injury and Spinal Cord Injury Collaborators, 2019). Blast waves are one cause of TBI, and although they are most frequently experienced by active military personnel, civilians may also suffer from blast TBIs (Hicks et al., 2010; Helmick et al., 2015; Bowen et al., 2016). Among the non-fatal injuries, most TBIs continue to be a major source of long-lasting disabilities including impairments in cognition, mood/emotional regulation, and social interactions following mTBI and contribute to the inability of affected individuals to carry out routine daily activities and to maintain important social relationships and employment (Silver et al., 2009; Wong et al., 2013; Greer et al., 2020). Additionally, up to 30% of TBI patients experience neuroendocrine dysfunction (Lieberman et al., 2001; Krahulik et al., 2010; Molaie and Maguire, 2018; Hoffman and Taylor, 2019) with a high incidence of stress axis [also known as the hypothalamic-pituitary-adrenal (HPA) axis] dysregulation with accompanying behavioral deficits (Krahulik et al., 2010; Hoffman and Taylor, 2019).

One of the major neuromodulatory stress systems that is responsive to mTBI and has a significant influence on stress-related neuronal responses and affective states, is the hypothalamic PVN CRF (also known as corticotropin releasing hormone, CRH) system (Fox et al., 2016; Kosari-Nasab et al., 2019; McCorkle et al., 2021). In addition to peripheral CRF endocrine signaling, recent studies suggest that central actions of CRF neurons may play an important role in regulating mood and stress modulation of behaviors. For example, it has been shown that biphasic responses of PVN CRF neuronal activity can mediate opposing behaviors of approaching appetitive stimuli or escaping from aversive stimuli (Kim et al., 2019). Importantly, PVN CRF neurons can regulate complex behaviors in a changing environment following stress and shift innate defensive strategies (Füzesi et al., 2016; Daviu et al., 2020).

Previously, we have shown that blast-induced mild TBI (mbTBI)-induced neuroendocrine deficits and anxiety-like behaviors across both male and female mice include dysregulation of CRF pathways in the HPA axis (neuroendocrine-projecting PVN CRF neurons) but also in extrahypothalamic regions (non-neuroendocrine-projecting PVN CRF projections; Russell et al., 2018a,b). Using the early response gene c-Fos immunoreactivity, as a marker for neuronal activation and retrograde Fluoro-Gold (FG) labeling of neuroendocrine- vs. non-neuroendocrine-projecting CRF neurons of the PVN, we demonstrated that the central and peripheral CRF pathways are susceptible to mbTBI in both male and female mice 7–10 days after the blast injury. mbTBI increased restraint stress-induced corticosterone in males while decreasing in females. mbTBI diminished the percentage of restraint-activated (c-Fos+) PVN CRF neurons in male mice while increasing in females. However, when PVN CRF projection neurons were distinguished using FG staining, we observed that mbTBI only decreased c-Fos+ immunoreactivity in PVN non-neuroendocrine CRF neurons of females in response to restraint stress without any alterations in males (Russell et al., 2018a). This suggest sex-specific modulation of PVN CRF neurons by mbTBI across different projection-specific populations of PVN CRF neurons. Additionally, CRFR2 but not CRFR1 expression was affected by mbTBI in both sexes with distinct anatomical patterns of CRFR2 gene expression in stress-related PVN limbic projections (Russell et al., 2018b). Although these initial studies demonstrate that CRF stress responses from the PVN may be altered by mbTBI, it remains unclear how mbTBI dysregulates PVN CRF neuronal function in distinct anatomical and functional sub regions of the PVN. To address this, we recorded the depolarization induced neuronal excitability and spontaneous activity of CRF neurons in ventral and dorsal sub-regions of the male mouse PVN (vPVN and dPVN). We have found that mbTBI selectively increases spontaneous CRF neuronal activity within the dPVN without any significant alteration in PVN CRF neuronal excitability across dPVN and vPVN subregions. Given that the activity of distinct CRF neurons in these anatomical subregions of the PVN is shown to be differentially modulated by some of the neurotransmitters and bioactive substances (Mukai et al., 2020) and mediates endocrine vs. non-neuroendocrine components of PVN CRF signaling (Russell et al., 2018a,b), our data suggest that mbTBI-induced persistent dPVN CRF dysfunction may primarily contribute to stress-related psychopathology following mbTBI.

METHODS

Animals

Seven- to 9-week-old CRF:tdTomato male mice with the C57BL/6J background were generated as previously described (Russell et al., 2018a) by crossing B6(Cg)-Crh$^{tm(cre)Zjh}$/J(CRF-IRES-Cre; RRID: IMSR_JAX:012704; stock no. 012704; The Jackson Laboratory) mice and B6.Cg-Gt(ROSA) 26Sor$^{tm14(CAG-tdTomato)Hze}$/J (Ai14; RRID: IMSR_JAX:007914; stock no. 007914; The Jackson Laboratory) mice. The mice were same-sex housed, 2–3 per cage, and maintained at 22°C to 25°C, 50% humidity, on a 12-h light:12-h dark cycle (lights on at 0100 h) with *ad libitum* access to food and water. Mice were randomly assigned to sham or mbTBI experimental group. All animal procedures were carried out in accordance with the guidelines established by the National Institute of Health (NIH) and approved by the Uniformed Services University Institutional Animal Care and Use Committee.

mbTBI

Mice were exposed to mbTBI under isoflurane anesthesia using the Advanced Blast Simulator (ABS; ORA Inc., Fredericksburg, VA) under isoflurane anesthesia, as previously described (Russell et al., 2018a). The ABS consisted of the driver chamber (sealed with Valmex FR 1000 PVDF lacquer 7269 membrane (Mehler Texnologies GmbH, Rheinstrasse, Germany), the transition section, and the test chamber. Increased pressure (by compressed air) in the driver chamber ruptured the acetate/mesh seal, which

results in blast wave traveling through the transition section to the test chamber. The mean pressure of the blast wave was ∼19 psi (19 ± 0.4 psi). Sham animals were anesthetized but were not exposed to the blast injury. Immediately after sham or injury procedures, mice were observed for righting reflex (sham = 50.6 ± 7.6 s vs. ABS = 83.4 ± 0.8 s, $p < 0.05$) and returned to the home cage for recovery. Sham and mbTBI mice were euthanized for slice preparation and electrophysiology 7 days post-injury.

Slice Preparation

For all electrophysiology experiments, mice were anesthetized with isoflurane, decapitated, and brains were quickly dissected and placed into ice-cold artificial cerebrospinal fluid (ACSF) containing (in mM): 126 NaCl, 21.4 $NaHCO_3$, 2.5 KCl, 1.2 NaH_2PO_4, 2.4 $CaCl_2$, 1.0 $MgSO_4$, 11.1 glucose, and 0.4 ascorbic acid and saturated with 95% O_2–5% CO_2. Briefly, coronal hypothalamic slices containing PVN were cut at 250 μm and incubated in above prepared ACSF at 34°C for at least 1 h prior to electrophysiological experiments. For patch clamp recordings, slices were then transferred to a recording chamber and perfused with ascorbic-acid free ACSF at 28°C.

Electrophysiology

Voltage-clamp whole-cell recordings were performed from dPVN and vPVN CRF:tdTomato neurons using patch pipettes (3–6 MOhms) and a patch amplifier (MultiClamp 700 B) under infrared-differential interference contrast microscopy. For all experiments, PVN CRF neurons were identified by the presence of tdTomato fluorescence which is a reliable indicator for CRF+ neurons within the PVN of CRF:tdTomato mice (Wamsteeker Cusulin et al., 2013). The anatomical boundary between dPVn and vPVN was defined by the mediolateral line through the dorsal edge of the third ventricle (3 V) as previously described (Mukai et al., 2020) and shown in a representative image of a hypothalamic PVN slice prepared from a CRF:tdTomato male mouse in **Figure 1A**. Data acquisition and analysis were carried out using DigiData 1440A, pCLAMP 10 (Molecular Devices), Clampfit, and Mini Analysis 6.0.3 (Synaptosoft, Inc.). Signals were filtered at 3 kHz and digitized at 10 kHz.

To assess PVN CRF spontaneous neuronal activity/excitability in intact synaptic transmission, cells were patch clamped with potassium-gluconate based internal solution (130 mM K-gluconate, 15 mM KCl, 4 mM adenosine triphosphate (ATP)–Na+, 0.3 mM guanosine triphosphate (GTP)–Na+, 1 mM EGTA, and 5 mM HEPES, pH adjusted to 7.28 with KOH, osmolarity adjusted to 275–280 mOsm) in slices perfused with ACSF. Electrophysiological recordings of neuronal excitability, membrane properties, and GABAergic transmission were performed as previously described (Authement et al., 2018; Simmons et al., 2020). During neuronal excitability recordings in current-clamp mode, action potential (AP) generation was assessed in response to increasingly depolarizing current steps ranging from +10 to +100pA (+10 pA ea. step) while cells were kept at −67 to −70 mV with manual direct current injection between pulses. Current steps were 5 s in duration with 25 s inter-stimulus intervals. The number of APs induced by depolarization at each intensity was counted and averaged for each experimental group at each step. Resting membrane potential (RMP) was assessed immediately after achieving whole-cell patch configuration in current clamp recordings. The hyperpolarization-activated cation current (Ih) recordings were performed in voltage-clamp in response to stepping cells from −50 mV to −100 mV (700 ms duration). Input resistance (Rin) was measured at −50 pA step (5 s duration) and calculated by dividing the change in voltage response by the current-pulse amplitude and presented as MΩ. AP threshold, fast after-hyperpolarizations (fAHP), and medium after-hyperpolarizations (mAHP) were assessed using clampfit and measured from the first AP at the current step that was sufficient to generate the first AP/s. Spontaneous neuronal activity and AP firing patterns were assessed in both cell-attached recordings in voltage-clamp mode at $V = 0$ mV and whole cell recording in current-clamp mode at $I = 0$ pA for the duration of ∼1 min recording. The criteria used for designating tonic activity was set to ≥3 APs across each recording. Nearly all PVN neurons are tonically active regardless of subregion or treatment. The

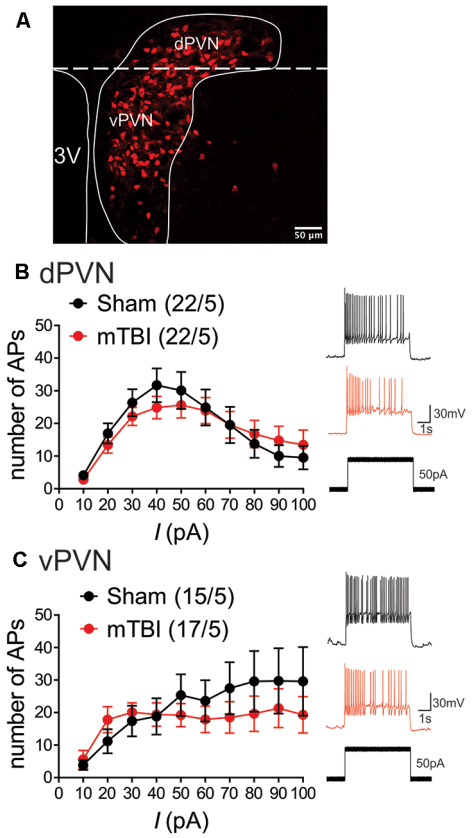

FIGURE 1 | mbTBI does not alter PVN CRF neuronal excitability. **(A)** Representative image showing the expression of the red fluorescent protein TdTomato in the PVN of the CRF;TdTomato mouse. Overlay is a schematic outline of the PVN labeled as the dorsal (d) PVN and ventral (v) PVN. Average number of action potentials generated across depolarizing current steps in Sham (black) and mTBI (red) mice and representative traces in response to 50 pA stimulation across **(B)** dPVN and **(C)** vPVN CRF neurons. Group numbers presented in graph as neurons/mice.

number of APs was counted over 1 min, and spike frequency was calculated.

Whole-cell recordings of $GABA_AR$-mediated spontaneous inhibitory postsynaptic currents (sIPSC) were performed in ACSF perfused with AP-V (50 uM), DNQX (10 μM), and glycine receptor inhibitor (strychnine, 1 μM). Patch pipettes were filled with KCl internal solution (125 mM KCl, 2.8 mM NaCl, 2 mM $MgCl_2$, 2 mM ATP Na+, 0.3 mM GTP-Na+, 0.6 mM EGTA, and 10 mM HEPES, pH adjusted to 7.28 with KOH, osmolarity adjusted to 275–280 mOsm). For sIPSCs, CRF neurons were voltage-clamped at −70 mV and recorded over 10 sweeps, each lasting 50 s. The cell series resistance was monitored through all the experiments and if this value changed by more than 10% or greater than 25 MΩ, data were not included.

Statistics

Values are presented as means ± SEM. The threshold for significance was set at $^*p < 0.05$ for all analyses. All statistical analyses of data were performed using Graphpad, Prism 9.2. For all electrophysiological data, n represents the number of recorded cells/mice. Two-way ANOVA was used across each subregion of PVN to compare neuronal excitability between sham and mbTBI across current injection. Mini Analysis software was used to detect and measure sIPSCs using preset detection parameters of IPSCs with an amplitude cutoff of 5 pA. Differences between sham and mbTBI mean and cumulative probabilities of sIPSC amplitude, charge transfer, tau decay, and frequency were analyzed using 2-tailed unpaired Student's-*t*-tests and Kolmogorov-Smirnov tests (KS, $\alpha = 0.05$), respectively.

RESULTS

mTBI Does Not Alter PVN CRF Neuronal Excitability and Intrinsic Membrane Properties Independent of the Anatomical Locations of CRF Neurons

Given our prior observations suggesting region-specific PVN CRF dysregulation, we first investigated the effects of mbTBI on PVN CRF depolarization-induced neuronal excitability and intrinsic membrane properties in intact synaptic transmission from dPVN and vPVN CRF neurons in PVN slices from sham and mbTBI male adult CRF:tdTomato mice 7 days post-injury (**Figure 1** and **Table 1**). We found that mbTBI did not affect neuronal excitability of dPVN or vPVN CRF neurons (**Figure 1B**: dPVN, n = 22/5 per group, 2-way ANOVA, effect of mbTBI: $F_{(1, 420)} = 0.28$, $P = 0.59$; effect of current: $F_{(9, 420)} = 8.03$, $P < 0.0001$; mbTBIxcurrent interaction: $F_{(9, 420)} = 0.47$, $P = 0.89$; **Figure 1C**: vPVN, n = 15–17/5/group, 2-way ANOVA, effect of mbTBI: $F_{(1, 300)} = 2.11$, $P = 0.14$; effect of current: $F_{(9, 300)} = 2.32$, $P < 0.05$; mbTBIxcurrent interaction: $F_{(9, 300)} = 0.55$, $P = 0.83$). Also we found that the effects of mbTBI on intrinsic properties were negligible where mbTBI did not significantly alter RMPs, Rin, AP threshold, mAHPs although we observed a significant reduction of fAHP amplitudes only in vPVN CRF neurons (**Table 1**, vPVN: fAHPs, unpaired Student's t-test, $t_{(29)} = 2.37$, $P < 0.05$). Note that all of CRF neurons were tonically active and fired close to their AP thresholds. Given that the more negative RMPs in the mouse PVN are reported in CRFR1 neurons within the dPVN that are exclusively GABAergic and are rarely found to be CRF positive (Jiang et al., 2018), we believe that the CRF neurons recorded here are a different population that exhibit more positive RMPs. Our observation of unusually more depolarized RMPs for CRF neurons are also consistent with what we have observed in other spontaneously active neurons when firing in tonic mode such as lateral habenula or ventral tegmental area dopamine neurons (Shepard et al., 2020; Langlois et al., 2021). However, we acknowledge that our measurements of RMPs are always made immediately after achieving whole-cell patch configuration in current clamp recordings while the evaluation of true RMPs of spontaneously active neurons requires spike silencing. Curiously, we also found that the Ih currents recorded from PVN CRF neurons in mTBI animals, in general, had smaller amplitudes compared to those from sham animals but only Ih currents of dPVN CRF neurons recorded from mbTBI mice showed a statistically significant difference in the amplitudes in comparison to those from sham animals (**Table 1**, dPVN: Ih currents, unpaired Student's t-test, $t_{(26)} = 2.42$, $P < 0.05$).

Of note, we noticed a significant phenotypic difference between dPVN vs. vPVN CRF neuronal excitability of sham animals in response to depolarization where dPVN CRF neurons exhibited spike-frequency adaptation and higher AP thresholds compared to those from vPVN CRF neurons. In other words, while dPVN CRF neurons exhibited depolarization-induced blockade of AP generation in response to larger depolarizing

TABLE 1 | mbTBI had negligible impact on intrinsic membrane properties of PVN CRF neurons.

	dPVN		vPVN	
Property	**Sham**	**mTBI**	**Sham**	**mTBI**
RMP	−40.9 ± 1.5, n21	−40.8 ± 1.4, n22	−42.8 ± 1.1, n16	−41.7 ± 1.3, n16
Rin	780.6 ± 97.3, n20	834.3 ± 54.45, n21	781.7 ± 85.49, n15	793.3 ± 72.22, n16
AP Threshold	−31.1 ± 0.6, n18	−32.7 ± 0.8, n21	−34.4 ± 1.1, n14	−32.6 ± 0.8, n16
fAHP	−18.2 ± 1.2, n18	−17.3 ± 1.0, n21	−17.5 ± 0.9, n15	−14.1 ± 1.2, n16 $^*P < 0.05$
mAHP	−43.2 ± 1.5, n18	−44.5 ± 1.5, n21	−40.0 ± 1.5, n15	−41.9 ± 1.8, n16
Ih	−20.3 ± 5.3, n13	−7.9 ± 1.2, n15 $^*P < 0.05$	−17.2 ± 5.4, n13	−9.1 ± 1.4, n14

*Table shows the intrinsic membrane and AP properties across dPVN and vPVN CRF neurons in sham and mTBI. Unpaired Student's t-test, *p < 0.05 noted for the statistical significance in comparisons between sham and mbTBI mice.*

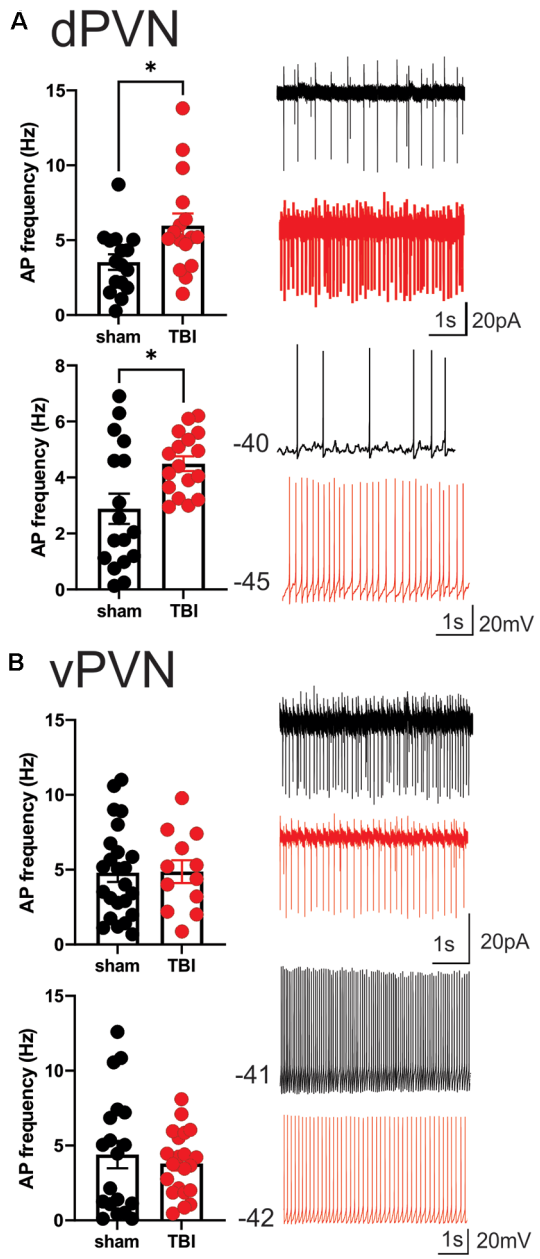

FIGURE 2 | mbTBI increases spontaneous activity of dPVN CRF neurons. Representative traces, and comparison of action potential (AP) frequency under voltage-clamp (top, $V = 0$) cell-attached recordings and current clamp (bottom, $I = 0$) whole-cell recordings across sham (black) and mTBI (red) mice in **(A)** dPVN and **(B)** vPVN CRF neurons. $n = 12–24/5$/Group. Unpaired Student's t-test, $^*p < 0.05$.

step currents that could be due to inactivation of Na+ channels with somatic depolarization, vPVN CRF neurons with lower AP thresholds maintained high frequency firing and negligible spike frequency adaptation (**Table 1**, AP threshold, unpaired Student's t-test, $t_{(30)} = 2.69$, $P < 0.05$; comparisons from sham animals in **Figure 1**: $n = 15–22/5$ per group, 2-way ANOVA, effect of PVN subregion: $F_{(1, 140)} = 6.55$, $P < 0.05$; effect of current: $F_{(9, 140)} = 0.71$, $P = 0.69$; PVN subregion × current interaction: $F_{(9, 140)} = 1.26$, $P = 0.26$).

mTBI Increases dPVN but Not vPVN CRF Spontaneous Neuronal Activity

The measurements of neuronal excitability are performed in response to artificial depolarization of neurons. Therefore, to assess the spontaneous activity of PVN CRF neurons without any manipulation, we recorded cell-attached voltage clamp and whole cell current clamp recordings of spontaneous neuronal activity in dPVN and vPVN neurons in PVN slices from sham and mbTBI male adult CRF:tdTomato mice 7 days post-injury. In general, we found that CRF PVN neurons are tonically active and mbTBI did not change the number of spontaneously active neurons. However, we found that only dPVN but not vPVN CRF neurons of mbTBI mice exhibited higher mean AP firing frequency compared to those from sham mice in both voltage clamp (**Figure 2A**, Student's t-test, $t_{(30)} = 2.53$, $p < 0.05$) and current clamp recordings (**Figure 2B**, Student's t-test, $t_{(32)} = 2.67$, $p < 0.05$) suggesting that mbTBI selectively induces dPVN hyperactivity.

mbTBI Decrease Spontaneous GABAergic Synaptic Transmission Onto dPVN CRF Neurons

Given that mbTBI increase dPVN neuronal activity, we then tested the effects of mbTBI on spontaneous GABAergic neurotransmission onto dPVN neurons from sham and mbTBI male adult CRF:tdTomato mice 7 days post-injury (**Figure 3**). Although we did not find any significant change in the group mean sIPSC amplitude (**Figure 3B**), charge transfer (**Figure 3C**), or frequency (**Figure 3D**) following mbTBI, we observed a significant leftward shift of the cumulative probability (CP) of sIPSC amplitude (**Figure 3B**, KS test, $p < 0.001$) and charge transfer (**Figure 3C**, KS test, $p < 0.0001$) as well as a significant rightward shift of the CP of sIPSC inter-event interval (**Figure 3D**, KS test, $p < 0.0001$) following mbTBI suggesting that mbTBI-induced reduction of spontaneous GABAergic neurotransmission onto dPVN CRF neurons. Note that the group mean and CP of sIPSC Tau decay did not alter by mbTBI (**Figure 3D**).

DISCUSSION

Previously, we showed that mbTBI may induce functional CRF dysregulation within neuroendocrine and non-neuroendocrine PVN CRF pathways (Russell et al., 2018a,b). As a follow up to previous studies, we were interested in a functional profile of the CRF neuronal subpopulations using electrophysiology in slice preparations from sham and mbTBI male adult CRF:TdTomato mice. We found that although mbTBI did not affect the overall neuronal excitability of dPVN and vPVN CRF neurons and its effects on intrinsic membrane properties of PVN CRF neurons were negligible, it selectively resulted in an increase in the spontaneous firing frequency of dPVN CRF neurons. dPVN CRF hyperactivity was also associated with decreased spontaneous GABAergic neurotransmission suggesting that mbTBI-induced

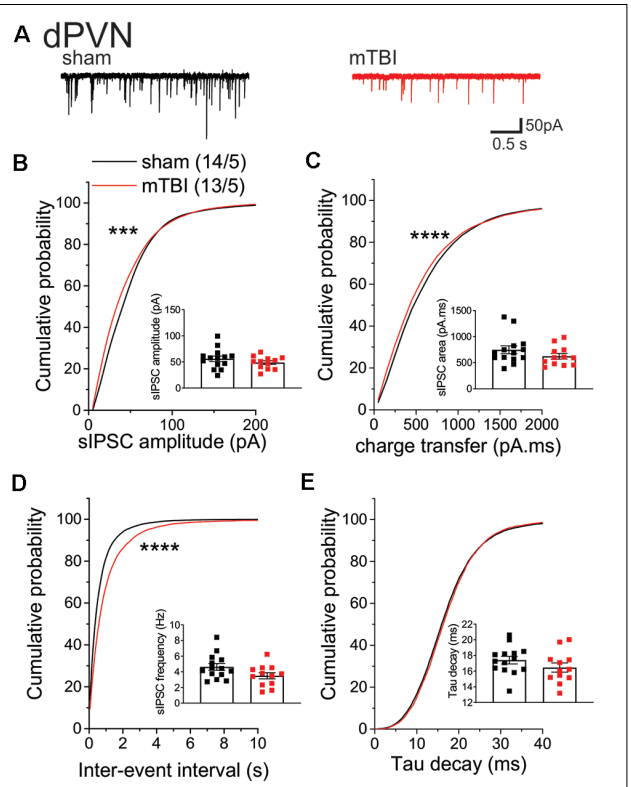

FIGURE 3 | mbTBI significantly decreased spontaneous $GABA_AR$-mediated synaptic transmission onto dPVN CRF neurons. **(A)** Representative traces of sham (black) and mTBI (red) spontaneous IPSPs (sIPSPs). Cumulative probability (CP) curves and group mean scatter dot-plot of sIPSPs **(B)** amplitude, **(C)** charge transfer, **(D)** inter-event interval (IEI) and **(E)** Tau decay. KS test for cumulative distribution curves, $^{***}p < 0.001$, $^{****}p < 0.0001$. Group neuron/mice numbers noted in **(B)** are identical across other sIPSP graphs.

GABAergic dysfunction could underlie the increased dPVN CRF signaling.

The parvocellular PVN CRF neurons mediate the physiological and behavioral stress responses of the HPA axis by releasing CRF into the median eminence which acts on the pituitary to release adrenocorticotropic hormone (ACTH). ACTH subsequently activates the synthesis and secretion of glucocorticoids, such as corticosterone from the adrenal glands to mediate stress responses. In addition to neuroendocrine PVN CRF neurons mostly located in the vPVN, the non-neuroendocrine, preautonomic dPVN CRF neurons project to the brainstem and spinal cord, and control sympathetic activity (Jiang et al., 2018; Mukai et al., 2020) and may be involved in mood regulation and behavioral flexibility in response to stressors, rewarding and aversive stimuli (Füzesi et al., 2016; Kim et al., 2019; Daviu et al., 2020). Therefore, our results suggest that mbTBI-induced dysregulation of non-neuroendocrine CRF pathways from the dPVN may primarily promote anxiety-like behaviors following mbTBI. We also found that mbTBI decreased spontaneous GABAergic-transmission onto dPVN CRF neurons which is most likely presynaptic in nature (less GABA release) which could support dPVN CRF hyperactivity following mbTBI. It is interesting to note that the blast injury in our paradigm did not affect glial numbers within the PVN and there was no change in Iba1+ and GFAP+ cells in the PVN of sham and mbTBI mice (data not shown) suggesting that mbTBI alters GABAergic inputs to the PVN rather than a direct insult to the PVN. Interestingly, a subpopulation of PVN parvocellular neurons in rats engage in a CRF feedback loop. These neurons express CRFR1 as well as CRF responsive HCN channels. CRF potentiates HCN channel activity and Ih currents and increases the neuronal activity of these PVN neurons (Qiu et al., 2005). A later study used CRF- and CRFR1-cre transgenic mouse lines with optogenetics circuit mapping and monosynaptic tracing provided compelling evidence for the existence of intra-PVN local CRF signaling where PVN CRF neurons form synaptic connections onto preautonomic CRFR1-expressing neurons within the PVN (Jiang et al., 2018). The almost exclusive GABAergic nature of this subset of PVN CRFR1 neurons within the dPVN is rarely found to be CRF positive and allows for a local PVN inhibitory feedback. Therefore, these GABAergic CRFR1 neurons form a microcircuit within the dPVN and may respond to the local release of CRF from PVN CRF neurons and in turn inhibit the activity of PVN CRF neurons. Interestingly, the ablation of PVN CRFR1 neurons also causes HPA axis hyperactivity (Jiang et al., 2018) suggesting that this subset of PVN neurons provide an important inhibitory synaptic braking mechanism to prevent PVN CRF hyperexcitability. Therefore, it is possible that mbTBI may remove the intrinsic inhibitory GABAergic feedback from PVN CRFR1 neurons onto dPVN CRF neurons. Specifically, mbTBI-induced decreases in presynaptic GABA release that is evident from our sIPSC recordings in dPVN CRF neurons may indicate that mbTBI results in a loss of these intrinsic GABAergic neurons or decreases their neuronal firing although we cannot exclude the possible alteration of extrinsic GABAergic synaptic inputs to PVN CRF neurons such as the median preoptic nucleus and the posterior bed nucleus of the stria terminalis by mbTBI (Bains et al., 2015). Our finding of mbTBI-induced suppression of amplitude and charge transfer of sIPSCs may also indicate that mbTBI could alter or induce postsynaptic GABAergic plasticity in dPVN CRF neurons. However, the reduction of the frequency of large sIPSCs that are AP-driven can generally impact both inter-event interval and amplitude distribution of sIPSCs, therefore mbTBI-induced changes in GABAergic transmission are most likely presynaptic in nature rather than a change in $GABA_AR$ conductance. PVN CRF neurons receive both glutamatergic and GABAergic synaptic inputs although the proportion of fast GABAergic synaptic transmission onto PVN CRF neurons is substantially higher than other brain regions suggesting that GABAergic inhibition mediated by $GABA_ARs$ and plasticity at GABAergic synapses onto PVN CRF neurons plays an important role in PVN CRF neuronal activity and restraining baseline HPA axis CRF signaling (Bains et al., 2015). Given that mbTBI-induced glutamatergic synaptic dysfunction in PVN CRF neurons is also likely to occur, it would be worthwhile to investigate input-specific glutamatergic and GABAergic plasticity and the shift in the excitation/inhibition balance across specific PVN populations. Interestingly, we

also found that mbTBI decreases Ih currents in dPVN CRF neurons which may be a homeostatic response to dPVN CRF hyperactivity following mbTBI or an indication of intrinsic plasticity. We acknowledge that our present results in male mice set a good foundation for future mbTBI studies in females where we expect to find sex- and subregion-specific differences in PVN CRF neuronal activity. Overall, our data suggest that mbTBI has differential effects on distinct neuroanatomical CRF pathways where it induces persistent GABAergic synaptic dysfunction in dPVN CRF neurons to promote dPVN CRF hyperactivity thereby selectively increasing hypothalamic as well as extrahypothalamic CRF signaling and promoting anxiety-like behaviors. Given the emerging role of extrahypothalamic PVN CRF signaling, our future studies will also consider central PVN CRF projections to stress-related brain circuits that may contribute to stress psychopathology associated with this model of mTBI.

DATA AVAILABILITY STATEMENT

The original contributions presented in the study are included in the article, further inquiries can be directed to the corresponding author/s.

ETHICS STATEMENT

The animal study was reviewed and approved by Uniformed Services University Institutional Animal Care and Use Committee.

AUTHOR CONTRIBUTIONS

FN and TJW were responsible for the study concept and design. SS, LL, MO, and SG contributed to the acquisition of animal data. LL, FN, and SS assisted with data analysis and interpretation of findings. FN, SS, LL, and TJW wrote the manuscript. All authors critically reviewed content and approved final version of manuscript for submission. All authors contributed to the article and approved the submitted version.

FUNDING

This work was supported by the National Institute of Neurological Disorders and Stroke (NIH/NINDS) Grant#R21 NS120628 (FN), and Center for Neuroscience and Regenerative Medicine and Office of Naval Research (TJW). The opinions and assertions contained herein are the private opinions of the authors and are not to be construed as official or reflecting the views of the Uniformed Services University of the Health Sciences or the Department of Defense or the Government of the United States. The funding agency did not contribute to writing this article or deciding to submit it.

ACKNOWLEDGMENTS

We acknowledge Drs. Yeonho Kim and Amanda Fu at the USUHS Pre-Clinical Modeling and Behavior Core for supporting the studies.

REFERENCES

Authement, M. E., Langlois, L. D., Shepard, R. D., Browne, C. A., Lucki, I., Kassis, H., et al. (2018). A role for corticotropin-releasing factor signaling in the lateral habenula and its modulation by early-life stress. *Sci. Signal.* 11:eaan6480. doi: 10.1126/scisignal.aan6480

Bains, J. S., Cusulin, J. I., and Inoue, W. (2015). Stress-related synaptic plasticity in the hypothalamus. *Nat. Rev. Neurosci.* 16, 377–388. doi: 10.1038/nrn3881

Bowen, L. N., Moore, D. F., and Okun, M. S. (2016). Is blast injury a modern phenomenon?: early historical descriptions of mining and volcanic traumatic brain injury with relevance to modern terrorist attacks and military warfare. *Neurologist* 21, 19–22. doi: 10.1097/NRL.0000000000000068

Daviu, N., Füzesi, T., Rosenegger, D. G., Rasiah, N. P., Sterley, T.-I., Peringod, G., et al. (2020). Paraventricular nucleus CRH neurons encode stress controllability and regulate defensive behavior selection. *Nat. Neurosci.* 2, 398–410. doi: 10.1038/s41593-020-0591-0

Füzesi, T., Daviu, N., Wamsteeker Cusulin, J. I., Bonin, R. P., and Bains, J. S. (2016). Hypothalamic CRH neurons orchestrate complex behaviours after stress. *Nat. Commun.* 7:11937. doi: 10.1038/ncomms11937

Fox, L. C., Davies, D. R., Scholl, J. L., Watt, M. J., and Forster, G. L. (2016). Differential effects of glucocorticoid and mineralocorticoid antagonism on anxiety behavior in mild traumatic brain injury. *Behav. Brain Res.* 312, 362–365. doi: 10.1016/j.bbr.2016.06.048

GBD 2016 Traumatic Brain Injury and Spinal Cord Injury Collaborators (2019). Global, regional and national burden of traumatic brain injury and spinal cord injury, 1990–2016: a systematic analysis for the global burden of disease study 2016. *Lancet Neurol.* 18, 56–87. doi: 10.1016/S1474-4422(18)30415-0

Greer, N., Sayer, N. A., Spoont, M., Taylor, B. C., Ackland, P. E., MacDonald, R., et al. (2020). Prevalence and severity of psychiatric disorders and suicidal behavior in service members and veterans with and without traumatic brain injury: systematic review. *J. Head Trauma Rehabil.* 35, 1–13. doi: 10.1097/HTR.0000000000000478

Helmick, K. M., Spells, C. A., Malik, S. Z., Davies, C. A., Marion, D. W., and Hinds, S. R. (2015). Traumatic brain injury in the US military: epidemiology and key clinical and research programs. *Brain Imaging Behav.* 9, 358–366. doi: 10.1007/s11682-015-9399-z

Hicks, R. R., Fertig, S. J., Desrocher, R. E., Koroshetz, W. J., and Pancrazio, J. J. (2010). Neurological effects of blast injury. *J. Trauma* 68, 1257–1263. doi: 10.1097/TA.0b013e3181d8956d

Hoffman, A. N., and Taylor, A. N. (2019). Stress reactivity after traumatic brain injury: implications for comorbid post-traumatic stress disorder. *Behav. Pharmacol.* 30, 115–121. doi: 10.1097/FBP.0000000000000461

Jiang, Z., Rajamanickam, S., and Justice, N. J. (2018). Local corticotropin-releasing factor signaling in the hypothalamic paraventricular nucleus. *J. Neurosci.* 38, 1874–1890. doi: 10.1523/JNEUROSCI.1492-17.2017

Kim, J., Lee, S., Fang, Y.-Y., Shin, A., Park, S., Hashikawa, S. B., et al. (2019). Rapid, biphasic CRF neuronal responses encode positive and negative valence. *Nat. Neurosci.* 22, 576–585. doi: 10.1038/s41593-019-0342-2

Kosari-Nasab, M., Sadeghi, T., Bashiri, H., Shokouhi, G., and Salari, A. A. (2019). The blockade of corticotropin-releasing factor 1 receptor attenuates anxiety-related symptoms and hypothalamus-pituitary-adrenal axis reactivity in mice with mild traumatic brain injury. *Behav. Pharmacol.* 30, 220–228. doi: 10.1097/FBP.0000000000000450

Krahulik, D., Zapletalova, J., Frysak, Z., and Vaverka, M. (2010). Dysfunction of hypothalamic-hypophysial axis after traumatic brain injury in adults. *J. Neurosurg.* 113, 581–584. doi: 10.3171/2009.10.JNS09930

Langlois, L. D., Berman, R. Y., Shepard, R. D., Simmons, S. C., Tsuda, M. C., Gouty, S., et al. (2021). Potentiation of glutamatergic synaptic transmission onto lateral habenula neurons following early life stress and intravenous morphine self-administration in rats. *Addict. Biol.* 27:e13064. doi: 10.1111/adb.13064

Lieberman, S. A., Oberoi, A. L., Gilkison, C. R., Masel, B. E., and Urban, R. J. (2001). Prevalence of neuroendocrine dysfunction in patients recovering from traumatic brain injury. *J. Clin. Endocrinol. Metab.* 86, 2752–2756. doi: 10.1210/jcem.86.6.7592

McCorkle, T. A., Barson, J. R., and Raghupathi, R. (2021). A role for the amygdala in impairments of affective behaviors following mild traumatic brain injury. *Front. Behav. Neurosci.* 15:601275. doi: 10.3389/fnbeh.2021.601275

Molaie, A. M., and Maguire, J. (2018). Neuroendocrine abnormalities following traumatic brain injury: an important contributor to neuropsychiatric sequelae. *Front. Endocrinol.* 9:176. doi: 10.3389/fendo.2018.00176

Mukai, Y., Nagayama, A., Itoi, K., and Yamanaka, A. (2020). Identification of substances which regulate activity of corticotropin-releasing factor-producing neurons in the paraventricular nucleus of the hypothalamus. *Sci. Rep.* 10:13639. doi: 10.1038/s41598-020-70481-5

Qiu, D. L., Chu, C. P., Shirasaka, T., Tsukino, H., Nakao, H., Kato, K., et al. (2005). Corticotrophin-releasing factor augments the I(H) in rat hypothalamic paraventricular nucleus parvocellular neurons *in vitro*. *J. Neurophysiol.* 94, 226–234. doi: 10.1152/jn.01325.2004

Russell, A. L., Handa, R. J., and Wu, T. J. (2018a). Sex-dependent effects of mild blast-induced traumatic brain injury on corticotropin-releasing factor receptor gene expression: potential link to anxiety-like behaviors. *Neuroscience* 392, 1–12. doi: 10.1016/j.neuroscience.2018.09.014

Russell, A. L., Richardson, M. R., Bauman, B. M., Hernandez, I. M., Saperstein, S., Handa, R. J., et al. (2018b). Differential responses of the HPA axis to mild blast traumatic brain injury in male and female mice. *Endocrinology* 159, 2363–2375. doi: 10.1210/en.2018-00203

Shepard, R. D., Langlois, L. D., Authement, M. E., and Nugent, F. S. (2020). Histone deacetylase inhibition reduces ventral tegmental area dopamine neuronal hyperexcitability involving AKAP150 signaling following maternal deprivation in juvenile male rats. *J. Neurosci. Res.* 98, 1457–1467. doi: 10.1002/jnr.24613

Silver, J. M., McAllister, T. W., and Arciniegas, D. B. (2009). Depression and cognitive complaints following mild traumatic brain injury. *Am. J. Psychiatry* 166, 653–661. doi: 10.1176/appi.ajp.2009.08111676

Simmons, S. C., Shepard, R. D., Gouty, S., Langlois, L. D., Flerlage, W. J., Cox, B. M., et al. (2020). Early life stress dysregulates kappa opioid receptor signaling within the lateral habenula. *Neurobiol. Stress* 13:100267. doi: 10.1016/j.ynstr.2020.100267

Taylor, C. A., Bell, J. M., Breiding, M. J., and Xu, L. (2017). Traumatic brain injury-related emergency department visits, hospitalizations and deaths - united states, 2007 and 2013. *MMWR Surveill. Summ.* 66, 1–16. doi: 10.15585/mmwr.ss6609a1

Wamsteeker Cusulin, J. I., Füzesi, T., Watts, A. G., and Bains, J. S. (2013). Characterization of corticotropin-releasing hormone neurons in the paraventricular nucleus of the hypothalamus of Crh-IRES-Cre mutant mice. *PLoS One* 8:e64943. doi: 10.1371/journal.pone.0064943

Wong, E. C., Schell, T. L., Jaycox, L. H., Marshall, G. N., Tanielian, T., and Miles, J. N. (2013). Mental health treatment experiences of U.S. service members previously deployed to Iraq and Afghanistan. *Psychiatr. Serv.* 64, 277–279. doi: 10.1176/appi.ps.201200240

Conflict of Interest: The authors declare that the research was conducted in the absence of any commercial or financial relationships that could be construed as a potential conflict of interest.

Publisher's Note: All claims expressed in this article are solely those of the authors and do not necessarily represent those of their affiliated organizations, or those of the publisher, the editors and the reviewers. Any product that may be evaluated in this article, or claim that may be made by its manufacturer, is not guaranteed or endorsed by the publisher.

frontiers | Frontiers in Synaptic Neuroscience

ORIGINAL RESEARCH
published: 24 May 2022
doi: 10.3389/fnsyn.2022.859278

Ameliorative Potential of Hot Compress on Sciatic Nerve Pain in Chronic Constriction Injury-Induced Rat Model

*Kwan-Yu Chan[1†], Wen-Ching Tsai[1†], Chien-Yi Chiang[2†], Meei-Ling Sheu[3,4,5], Chih-Yang Huang[2,6,7,8,9], Yi-Ching Tsai[10], Chia-Yun Tsai[11], Chia-Jung Lu[12], Zih-Ping Ho[13] and De-Wei Lai[11]**

[1] Department of Rehabilitation, Chang Bing Show Chwan Memorial Hospital, Changhua, Taiwan, [2] Cardiovascular and Mitochondrial Related Disease Research Center, Hualien Tzu Chi Hospital, Buddhist Tzu Chi Medical Foundation, Hualien, Taiwan, [3] Institute of Biomedical Sciences, National Chung Hsing University, Taichung, Taiwan, [4] Rong Hsing Research Center for Translational Medicine, National Chung Hsing University, Taichung, Taiwan, [5] Department of Medical Research, Taichung Veterans General Hospital, Taichung, Taiwan, [6] Department of Medical Laboratory Science and Biotechnology, Asia University, Taichung, Taiwan, [7] Graduate Institute of Biomedical Sciences, China Medical University, Taichung, Taiwan, [8] Center of General Education, Buddhist Tzu Chi Medical Foundation, Tzu Chi University of Science and Technology, Hualien, Taiwan, [9] Department of Medical Research, China Medical University Hospital, China Medical University, Taichung, Taiwan, [10] Immunomedicine Group, Department of Molecular Biology and Cell Research, Chang Bing Show Chwan Memorial Hospital, Changhua, Taiwan, [11] Experimental Animal Center, Department of Molecular Biology and Cell Research, Chang Bing Show Chwan Memorial Hospital, Changhua, Taiwan, [12] Neurodiagnostic center, Chang Bing Show Chwan Memorial Hospital, Changhua, Taiwan, [13] Department of Medical Research, Chang Bing Show Chwan Memorial Hospital, Changhua, Taiwan

OPEN ACCESS

Edited by:
Carl R. Lupica,
National Institute on Drug Abuse (NIH), United States

Reviewed by:
Kathleen Vincent,
Massachusetts General Hospital and Harvard Medical School, United States
Kerui Gong,
University of California, San Francisco, United States

***Correspondence:**
De-Wei Lai
deweilai123@gmail.com;
14700@cbshow.org.tw

[†] These authors have contributed equally to this work and share first authorship

Received: 21 January 2022
Accepted: 25 March 2022
Published: 24 May 2022

Citation:
Chan K-Y, Tsai W-C, Chiang C-Y, Sheu M-L, Huang C-Y, Tsai Y-C, Tsai C-Y, Lu C-J, Ho Z-P and Lai D-W (2022) Ameliorative Potential of Hot Compress on Sciatic Nerve Pain in Chronic Constriction Injury-Induced Rat Model. Front. Synaptic Neurosci. 14:859278. doi: 10.3389/fnsyn.2022.859278

Hot compress modalities are used to ameliorate pain despite prevalent confusion about which modality should be used and when. Most recommendations for hot compresses are based on empirical experience, with limited evidence to support its efficacy. To obtain insight into the nerve transmission mechanism of hot compresses and to identify the nerve injury marker proteins specifically associated with sciatic nerve pain, we established a rat model of chronic constriction injury (CCI) and performed mechanical allodynia, electrophysiology, and histopathological analysis. All CCI rats exhibited geometric representation of the affected hind paw, which indicated a hyper-impact on both mechanical gait and asymmetry of gait on day 28. The CCI model after 28 days of surgery significantly reduced compound muscle action potential (CMAP) amplitude, but also significantly reduced latency. Administration of hot compress for 3 weeks (heated at 40–42°C, cycle of 40 min, and rest for 20 min, three cycles each time, three times per week) significantly increased the paw withdrawal thresholds in response to stimulation by Von Frey fibers and reversed the CCI-induced reduced sciatic functional index (SFI) scores. Hot compress treatment in the CCI model improved CMAP amplitude and latency. The S100 protein expression level in the CCI+Hot compression group was 1.5-fold higher than in the CCI group; it dramatically reduced inflammation, such as tumor necrosis factor alpha and CD68 expression in nerve injury sites. Synaptophysin (Syn) expression in the CCI+Hot compression group was less than threefold in the CCI group at both nerve injury sites and brain (somatosensory cortex

and hippocampus). This finding indicates that local nerve damage and inflammation cause significant alterations in the sensorimotor strip, and hot compress treatment could significantly ameliorate sciatic nerve pain by attenuating Syn and inflammatory factors from local pathological nerves to the brain. This study determines the potential efficacy and safety of hot compress, and may have important implications for its widespread use in sciatic nerve pain treatment.

Keywords: hot compress, chronic constriction injury, compound muscle action potential, synaptophysin, somatosensory cortex, hippocampus

INTRODUCTION

Sciatic nerve pain affects a significant amount of the population worldwide. The common symptoms include widespread leg pain, paralysis, and related disabilities. Several synonyms exist for sciatica, such as lumbar radiculopathy, ischias, intervertebral disk disease, and nerve root entrapment. Patients usually receive treatment in primary care; however, a small percentage of the patients are referred to secondary care institutions and may eventually undergo surgery (Jacobs et al., 2011; Jensen et al., 2019). It is worth noting that approximately 90% of sciatica cases are caused by herniated discs and compression of the nerve root. Other causes include lumbar spinal stenosis and tumors (Valat et al., 2010). The common conservative treatments for sciatica include rehabilitation, massage, hot compresses, or corsets (including drug injection therapy) (Dahm et al., 2010; Dehghan and Farahbod, 2014; Lewis et al., 2015; Ropper and Zafonte, 2015). However, the molecular mechanisms underlying most conservative treatments remain unclear. Therefore, it is imperative to clarify sciatica with hot compress treatment and the molecular mechanisms involved in this research.

The conservative treatment of sciatica is mainly aimed at reducing pain through analgesics or reducing the nerve root pressure. Several studies have reported that conservative treatment may be limited in the natural course of sciatica or alleviating symptoms in some patients. Sciatica management includes drug and non-drug methods (Vroomen et al., 2000). The most common medications include non-steroidal anti-inflammatory drugs (NSAIDs) or acetaminophen. However, for some types of pain (e.g., acute low back pain), skeletal muscle relaxants/antispasticity drugs, antidepressants, corticosteroid injections (for back pain with radiculopathy), and opioids (for otherwise intractable pain) may be appropriate (Chou and Huffman, 2007; Pinto et al., 2012; Witenko et al., 2014; Machado et al., 2017). The non-pharmacological treatment strategy is to reduce the pain and related edema, while also promoting nerve repair to promote the restoration of normal function and activity (Jacobs et al., 2011; Savage et al., 2015). In this case, hot compresses are often used. However, involvement of the molecular mechanisms though moderate hot compress treatment conditions remain unclear.

Hot compresses may be associated with pain relief. Traditionally, a surface heat of 40–45°C treats the application site to a depth of approximately 1 cm; additionally, surface heating has been used in different forms (e.g., hot water bottles, towels, or bottles) to relieve menstrual cramps (Harris, 1938; Jo and Lee, 2018). Moreover, local hot compresses can promote blood circulation, eliminate local blood and body fluid retention, and reduce congestion and swelling, thereby reducing the pain caused by nerve compression (Petrofsky et al., 2013). In addition, synaptophysin (Syn) is widely distributed and plays a role in synaptic transmission, and may mediate the sciatic nerve pain induced by inflammation by acting on presynaptic Syn in the spinal cord dorsal horn neurons (Chou et al., 2002; Sommer and Kress, 2004; Zelenka et al., 2005). However, the molecular mechanisms involved in the regulation of hot compresses to reduce sciatic nerve pain are still not fully understood.

Our previous studies reported that chronic constriction injury (CCI) of the sciatic nerve model represents an advance in the study of neuropathic pain because the location of loose chromic gut ligatures on the rat sciatic nerve elicited behavior that seems analogous to that of humans with neuropathic pain (Chiang et al., 2014; Sheu et al., 2021). This study used the CCI rat model to explore information about hot compresses (non-pharmacological treatments) and the molecular mechanisms of nerve injury improvement. Furthermore, we determined the mechanism responsible for the effect of hot compress application in the CCI animal model by examining nerve repair and inflammation improvement, as well as the expression of S100, Syn, and TNFα at the injury site. The present study aimed to observe hot compress mediated treatment on injured hindlimbs following CCI sciatic nerve injury in a rat model to delineate the possible hot compress regulated mechanisms and therefore, determine the beneficial applications to patients with peripheral nerve injury.

MATERIALS AND METHODS

Animals

In this study, 8–10 weeks old Sprague-Dawley rats weighing 250–300 g were kept in ventilated, humidity- and temperature-controlled rooms with a 12 h light/dark cycle. Soft bedding and sufficient food and water were provided. All the experiments were approved by the Animal Care and Use Committee of the Chang Bing Show Chwan Memorial Hospital. All efforts were made to minimize the number of animals used and their suffering.

Animal Groups and Sciatic Nerve Surgery

The CCI surgery was modified from the description by Bennett and Xie's (1988) CCI model. These animals were

randomly assigned to five groups with a total of 40 animals, which were grouped into normal, sham, CCI, CCI+Hot compression, and hot compress alone groups, respectively. The CCI model was established in a manner similar to the method described by Chiang et al. (2014). Briefly, the right sciatic nerve was exposed and dissected from the surrounding connective tissue. Two ligatures of the 3-0 chromic gut were loosely ligated around the sciatic nerve without changing the morphology of the nerve. A sham surgery was performed by exposing the sciatic nerve without ligation. The surgical wound was closed in layers using 4-0 suture lines. All surgical procedures were performed under anesthesia with 4% isoflurane for induction, and 1–2% isoflurane for maintenance.

Hot Compress Treatment

After 1 week of CCI surgery, the animals in the CCI+Hot compression, and hot compression groups were treated with a hot pack. These animals were anesthetized with 1% isoflurane, laid on a hot pack, and heated at 40–42°C with their right hind limb. The treatments were performed for a cycle of 40 min and rest for 20 min, three cycles each time, three times per week (execution begins at 1:00 p.m. on Monday, Wednesday, and Friday) for three consecutive weeks. The sham and CCI alone groups also performed the anesthesia process simultaneously.

Electrophysiological Measurement

Electrical stimulation was performed using a Medelec Synergy electromyography (Oxford Instrument Medical Ltd., Surrey, United Kingdom). Three weeks after the hot compress treatment, all the animal groups were investigated for compound muscle action potential (CMAP) voltage before the animals were euthanized. After the animals were anesthetized with Zoletil 50 (40 mg/kg, i.p., Virbac), recording electrodes (Ambu A/S, Ballerup, Denmark) were fixed on the lateral and back sides, and real-time monitoring revealed that the R MEDIAN was a stable straight line before every operation. Electrical stimulation was performed through the right sciatic nerve.

Mechanical Allodynia (Von Frey Test)

In this experiment, the animals were individually placed in small cages with frames and placed for 5 min prior to the test for adaptation. A Von Frey filament was applied to touch the hind paw ipsilaterally until it bent for 5 s. The filaments were applied range from 0.008 to 300 g; if the animal withdrew or shook the hind paws in at least four out of the five applications, it was considered as a positive response. The first step of "up-down" Von Frey method (Dixon, 1980; Deuis et al., 2017) is to estimate the response to filaments close to 50% withdrawal threshold. If there is no response, the next tested with a higher force filament; on the contrary, if there is positive response, the next tested with lower force filament. This continues until at four reads are archived after the first convert response. Calculation of the 50% threshold were detected though least six responses around the threshold.

Sciatic Functional Index

The sciatic functional index (SFI) assessment method was modified from the description by Bain et al. (1989). Briefed method described following that a dark walking track of dimensions, 10 cm wide, 15 cm high, 50 cm long was prepared, and a paper strip of equal length and width was placed at the bottom of the track. The rat hind paws were soaked in red ink, and their hind footprints were clearly recorded. After the experiment, the strip was left to dry to measure the parameters. The factors for SFI included the print length (PL), toe spread (TS), and intermediary toe spread (ITS).The SFI value was calculated by the formula as follows: SFI = −38.3 (EPL−NPL)/NPL + 109.5(ETS−NTS)/NTS + 13.3(EIT−NIT)/NIT−8.8. EPL, experimental print length; NPL, normal print length; ETS, experimental toe spread; NTS, normal toe spread; EIT, experimental intermediary toe spread; NIT, intermediary toe spread. SFI = 0 and −100 indicate normal and complete dysfunctions, respectively. All the groups were assessed four weeks after the hot compress treatment.

Immunohistochemical Analysis

At day 28 after the hot compress treatment, the animals were anesthetized. The sciatic nerves and brain (brain cortex and hippocampus) were immediately removed, placed in 4% paraformaldehyde for 4 h, and then transferred to 30% sucrose at 4°C overnight. Each dissected tissue was embedded in a paraffin block and sectioned into 8 μ for sciatic nerves and 10 μm-thick sections for brain The tissue sections were deparaffinized and rehydrated through a series of xylene and ethanol washes, and antigen retrieval was performed in citrate buffer. The sections were then permeabilized with 0.2% Triton X-100 in PBS, blocked with PBS containing 1% bovine serum albumin (BSA), and stained with primary and secondary antibodies. These sections were subjected to immunohistochemical examination with anti-NGF (Chemicon, 1:250 dilution), anti-CD68 (Chemicon, 1:50 dilution), anti-TNFα (Abcam, 1:50 dilution), anti-synaptophysin (Abcam, 1:50 dilution), and anti-S100 (Thermo, 1:50 dilution) for the detection of inflammatory cells, inflammatory cytokines, small neurosecretory vesicles, and Schwann cells. Subsequently, the sections were washed and incubated overnight with secondary goat anti-mouse IgG-HRP (Thermo, 1:500 dilution). The staining was visualized using 3,3-diaminobenzidine (DAB). Analysis of IHC staining intensity using ImageJ, and selected highlight stained section tissues site were measured for each section of sciatic nerve (least 10 field/group). All experiments were performed least triplicates.

Statistical Analysis

The quantification was done by assistant blind to the experimental condition. The data are expressed as mean ± SD. The statistical analysis was performed as described previously (Liu et al., 2021). Statistical comparisons between groups were made using two-way ANOVA (time × withdrawal threshold), with Bonferroni's *post hoc* test for comparison between groups in Von Frey test model; statistical analysis on overall treatment effects compare with CCI were made by one-way ANOVA with

Dunnett's *post hoc* test. The statistical significance was set at a p-value < 0.05.

RESULTS

Pain Hypersensitivity Induced by Chronic Constriction Injury Surgery

After CCI surgery, we examined the development of neuropathic pain-like behaviors using mechanical allodynia tests and evaluated the SFI. The pain behaviors were investigated on days 0 (the day of surgery) and 3, 5, 7, 14, 21, and 28 after CCI (**Figure 1A**). In our measurements obtained from CCI rats, the paw withdrawal threshold to mechanical stimuli was significantly reduced to 5.8 ± 0.4 g ($p < 0.001$) on day 3 and further reduced to 3.2 ± 0.5 g ($p < 0.001$) on day 7, compared with the pain threshold measured in the sham group (14.8 ± 0.8 g) (**Figure 1B**). In addition, all the CCI rats exhibited a geometric representation of the affected hind paw, which was indicated by a significantly lower SFI than that measured in the sham group or normal control on day 28 (**Figure 1C**). The pain had a hyper-impact on both mechanical and asymmetric gaits for at least 4 weeks after CCI (**Figures 1B,C**).

Distal Digital Nerve Electrophysiology

The patterns of digital nerve activity varied as a function of the stimulus intensity and distal recording site (**Figure 2A**). The longest onset latency of the rats that responded to motor nerve stimulation was 10 ms; therefore, we set the onset latency of the rats that did not respond to the motor nerve stimulation at 10 ms. The intensity evaluated (20 ms, 5 mV) uniquely activated low-threshold axons, resulting in a composite response (**Figure 2B**). The CMAPs of the involved sciatic nerve were of attenuated amplitude of voltage and latency peak in the CCI groups (an amplitude of 1.5 ± 0.3 mV, latency 2.0 ± 0.08 ms) at 28 days post-injury in comparison with the sham groups (an amplitude of 6.4 ± 0.7 mV, latency 2.6 ± 0.05 ms), whereas no significant change was observed in the normal groups(an amplitude of 6.7 ± 0.5 mV, latency 2.7 ± 0.02 ms) (**Figures 2C,D**).Our data showed that the CCI model after 28 days of surgery not only showed a significant reduction in the CMAP amplitude, but also significantly reduced the latency.

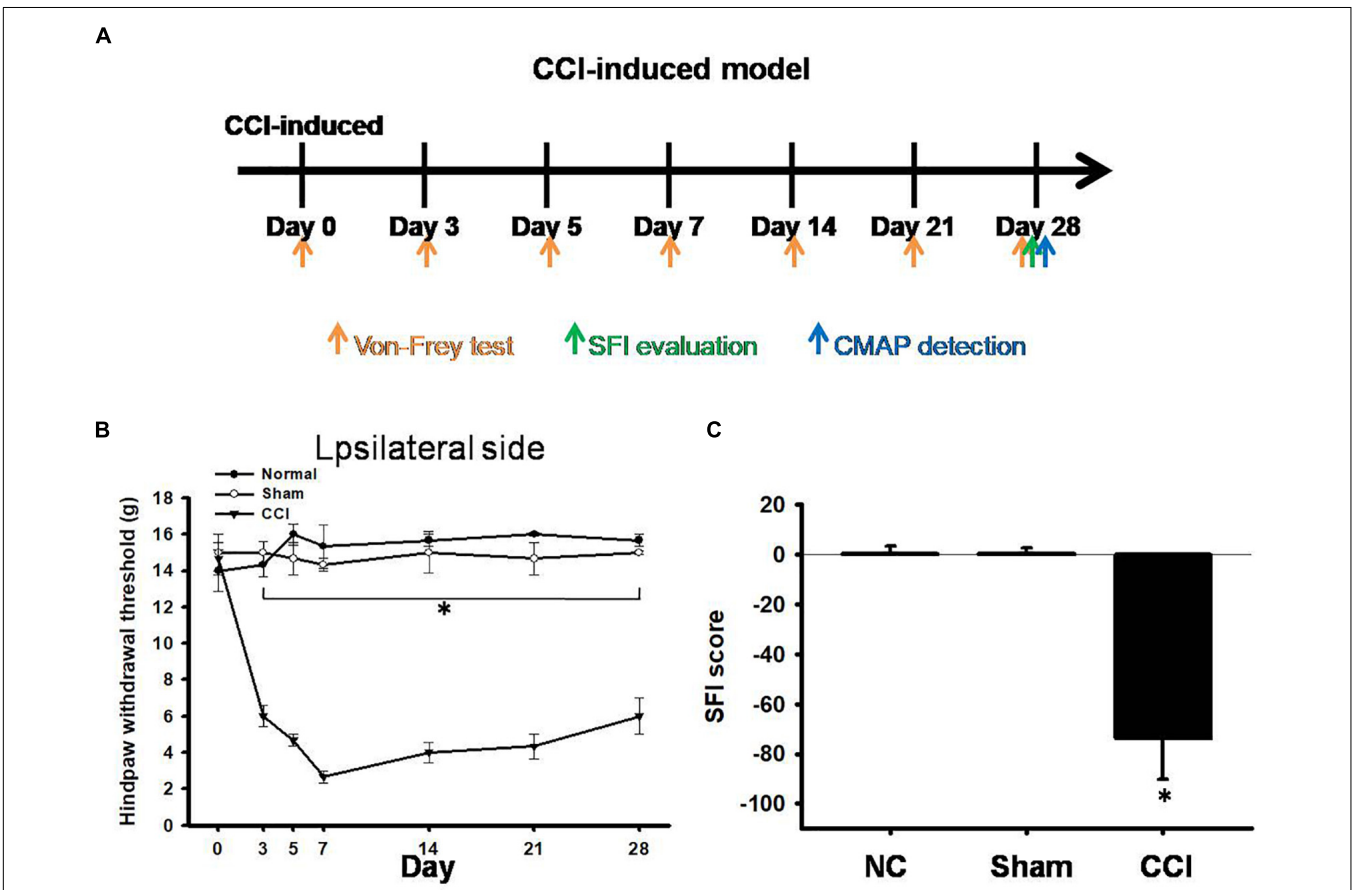

FIGURE 1 | Pain hypersensitivity in chronic constriction injury (CCI) rats. **(A)** Schematic view of the establishment of neuropathic pain animal model. **(B)** Thresholds for hindpaw withdrawal responses to Von Frey filament stimulation on the ipsilateral site in the normal, sham, and CCI groups, two-way ANOVA with Bonferroni *post hoc* test. **(C)** Determination of the sciatic functional index (SFI) in the normal, sham, and CCI groups, the data was analyzed by one-way ANOVA with *post hoc* Dunnett's test. *$p < 0.001$ was considered significant as compared with the CCI group, $n = 8$.

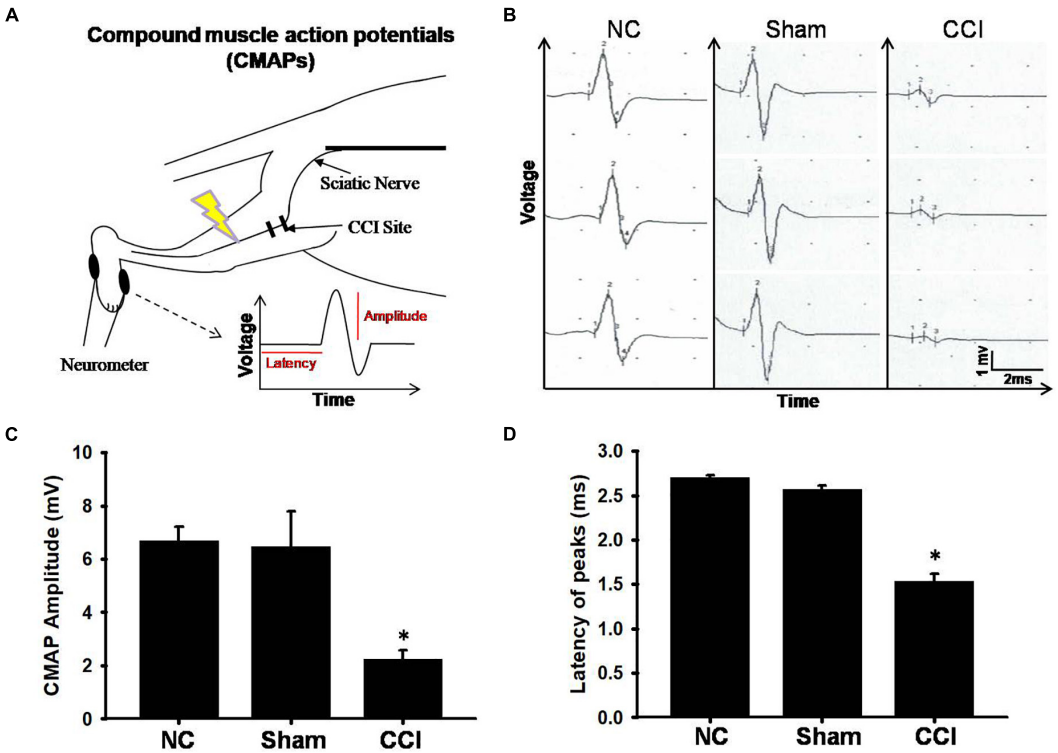

FIGURE 2 | Electrophysiological findings for each group. **(A)** The schematic of electrode positions for electrophysiological recording neurometer segments of the digital nerve with respect to stimulation. **(B)** Representative spontaneous voltage recorded from involved plantar muscles from different groups. The scale bars represent 1 mV and 2 ms. **(C)** Amplitude and **(D)** latency of compound muscle action potential (CMAP). The vertical dash lines indicate the latencies for the marked amplitude (mV). The horizontal dash lines denote the latency time (ms) of activity in stimuli interval. Data were analyzed by one-way ANOVA with *post hoc* Dunnett's test. *$p < 0.001$ was considered significant as compared with the sham group, $n = 8$.

Effect of Hot Compress Treatment on Behavioral Parameters in Chronic Constriction Injury Induced Neuropathic Pain

Behavioral changes, including mechanical allodynia, were significant in rats with CCI of the sciatic nerve by day 0, 3, 5, 7, 14, 21, and 28 compared to the sham groups. Additionally, the hot compress groups were treated on the 7th day after CCI surgery with a cycle of 40 min and rest for 20 min, three cycles each time, three times per week for three consecutive weeks, and the period of pain behavior was also investigated in the hot compress groups (**Figure 3A**). The administration of a hot compress cycle for 3 weeks significantly increased the paw withdrawal thresholds in response to stimulation by Von Frey fibers (**Figure 3B**) and reversed the CCI-induced reduction in the SFI scores (**Figure 3C**). The group treated with hot compress alone showed no mechanical allodynia or footprint deficits.

Hot Compress Improved Electrophysiological Response After Chronic Constriction Injury Surgery

We also investigated the CMAP amplitude and latency. A lower CMAP amplitude has been previously associated with pain perception. To further confirm the associations between hot compression and neuropathic pain, we determined the CMAP amplitude and latency in the CCI model undergoing hot compress treatment (**Figure 4A**), which showed that the hot compress alone group did not show significant changes in the CMAP amplitude and latency. However, we found that the hot compress was successful in attenuating the CMAP amplitude and latency in the CCI model (**Figures 4B,C**). Therefore, we recognized that the hot compress treatment in the CCI model improved the CMAP amplitude and latency.

Effect of Hot Compress on Histomorphological Alteration of Nerve System in Chronic Constriction Injury Model

H&E staining of the sciatic nerve showed an organized cellular structure (**Figures 5A**i–iv). In the CCI group, sciatic nerve injury was associated with various types of nerve damage as well as an increase in the cellular structure, infiltration, increase in intracellular spaces, and disorganized edema pattern because of the damage; the red arrow indicates cellular spaces and the yellow arrow indicates inflammatory cell infiltration (**Figure 5A**ii) compared with the sham group (**Figure 5A**i). Treatment with hot compress reversed the constriction-induced

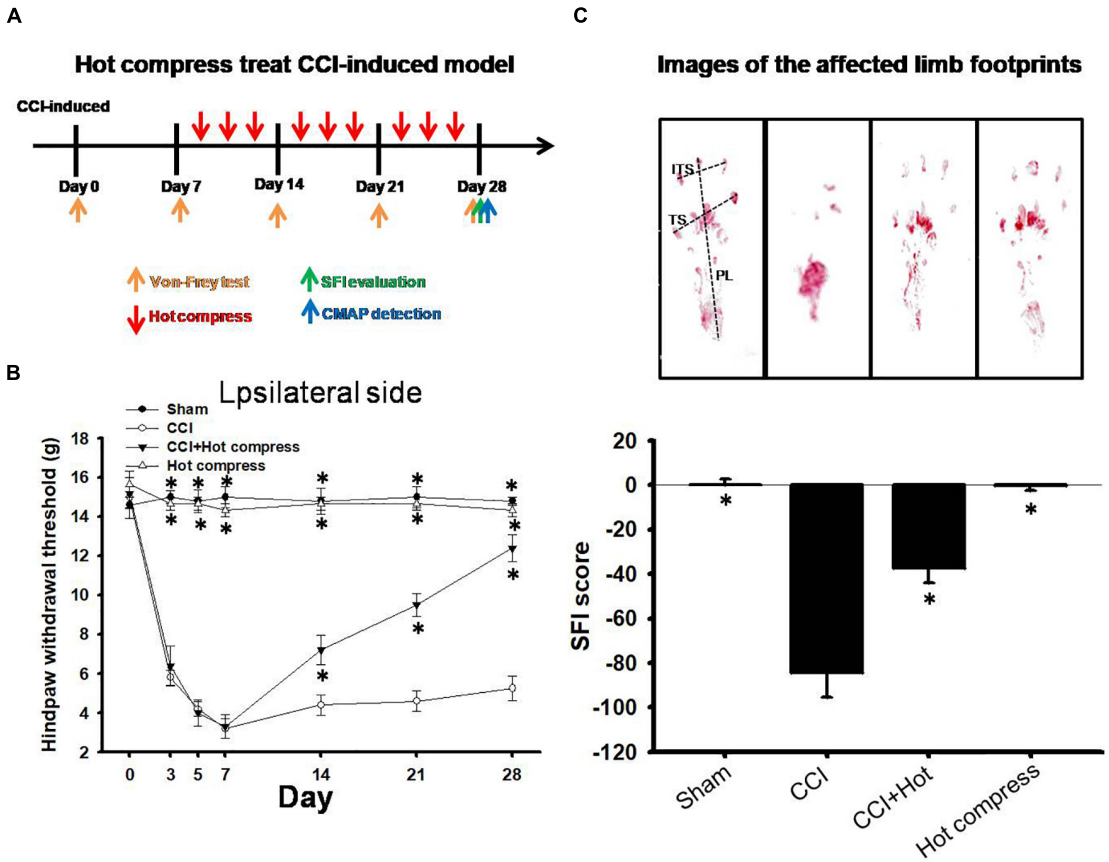

FIGURE 3 | Hot compress may relieve CCI-induced neuropathic pain. **(A)** Schematic view of hot compress treatment process. **(B)** Thresholds for hindpaw withdrawal responses to the Von Frey filament stimulation on the ipsilateral site in sham, CCI, CCI + hot compress, and hot compress alone groups. Two-way ANOVA with Bonferroni *post hoc* test. **(C)** Footprints and determination of the sciatic functional index (SFI) in sham, CCI, CCI + hot compress, and hot compress alone groups, the data were analyzed by one-way ANOVA with *post hoc* Dunnett's test. *$p < 0.001$ was considered significant as compared with the CCI group, $n = 8$. The factors for SFI included the print length (PL), toe spread (TS), and intermediary toe spread (ITS).

pathological changes (**Figure 5A**iii). The hot compress alone group showed no pathological cellular structures. In the sciatic nerve system, S100 protein is a valuable marker that can be used to identify myelinating Schwann cells, which is correlated with the expression of inflammatory cytokines and inflammatory cell deposition, such as TNFα and CD68. In this study, we found that the CCI group showed significantly reduced expression of S100 protein compared to the sham group. The S100 protein expression level in the CCI+Hot compression group was 1.5-fold higher than that in the CCI group ($F = 139.6$; df = 39, $p < 0.001$), and the hot compress alone group had no effect (**Figures 5A**v–viii). The trends of decreased S100 protein expression were reciprocal with increased TNFα expression and CD68 deposition. The TNFα expression level in the CCI group was more than fivefold of that of the sham group. In contrast, the CCI+Hot compression group showed significantly decreased TNFα expression compared to the CCI group ($F = 113.5$; df = 43, $p < 0.001$) (**Figures 5A**ix–xii). The CD68 expression level in the CCI group was twofold higher than that in the sham group. Additionally, the CCI+Hot compression group showed a dramatic reduction in CD68 expression compared to the CCI group ($F = 31.34$; df = 46, $p < 0.001$) (**Figures 5A**xiii–xvi). No significant difference in the TNFα and CD68 expression was found in the hot compress alone group. Syn expression within the dorsal root ganglion is highly correlated with the severity of neuropathic pain. Syn was highly expressed in the CCI group and significantly increased compared with the sham, CCI+Hot compression, and hot compress alone groups (**Figures 5A**xvii–xx). The Syn expression level in the CCI+Hot compression group was less than threefold in the CCI group ($F = 46.36$; df = 41, $p < 0.001$). The quantitative expression of S100, Syn, TNFα, and CD68 in the different groups, respectively (**Figure 5B**).

Effect of Hot Compress on Histomorphological Alteration of Hippocampus and Somatosensory Cortex in Chronic Constriction Injury Model

Synaptophysin and TNFα expression within the brain hippocampus CA3 (HPC) and somatosensory cortex (SSC) reflect the brain plasticity response to CCI injury. In this study,

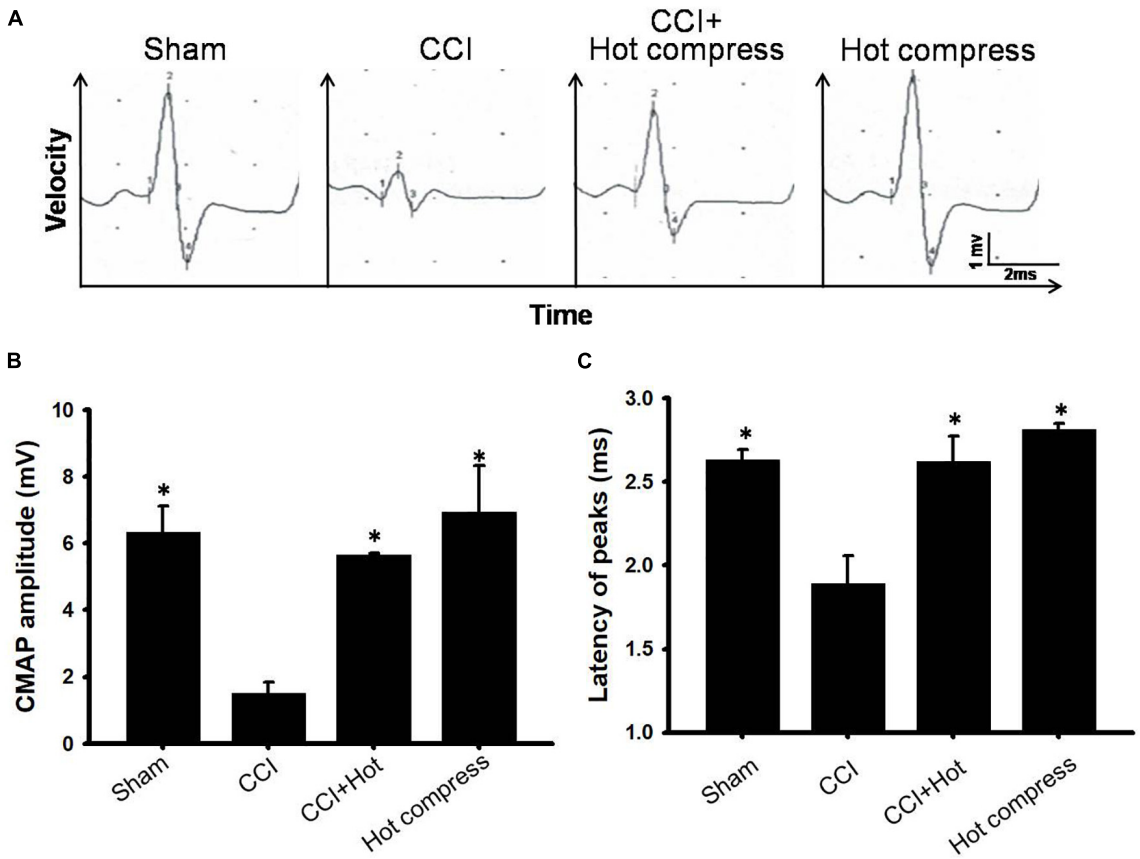

FIGURE 4 | The effects of hot compress on a peak-to-peak amplitude and latency of the compound muscle action potentials (CMAPs) of the rat sciatic nerve. Panel **(A)** showed representative CMAPs tracings for sham, CCI, CCI+Hot compression, hot compress alone groups on the postoperative day 28. **(B)** The quantification of the hot compress effect on peak-to-peak amplitude and **(C)** latency is shown, respectively. Data were analyzed by one-way ANOVA with *post hoc* Dunnett's test. $^*p < 0.001$ was considered significant as compared with the CCI group, $n = 8$.

decreased levels of Syn and TNFα expression were noted in the CCI + hot compression group than in the CCI group (**Figures 6A,B**). The synexpression levels in the HPC in the CCI group were threefold higher than those in the sham group and more than twofold higher than that in the CCI + hot compression group ($F = 16.87$; df = 43, $p < 0.001$), and SSC ($F = 50.73$; df = 43, $p < 0.001$). The TNFα expression level in the CCI group was twofold higher than that in the sham group and 1.7-fold higher than in the CCI + hot compression group ($F = 13.49$; df = 42, $p < 0.05$), respectively. Significant differences were found for TNFα expression within the SSC between the CCI and sham groups and between the CCI and CCI + hot compression groups. However, there was no significant difference in the expression of TNFα within the hippocampus in the CCI and sham groups and between the CCI and CCI + hot compression groups. Increased Syn expression within the sensorimotor strip indicates the responsiveness to peripheral nerve neuropathic injury. In this study, the increased intensity of evoked potential proportionally increased in the CCI group. The quantitative expression of Syn and TNFα in SSC and HPC from different groups are shown in **Figures 6C,D**. This finding indicates that local nerve damage and inflammation causes significant alterations in the sensorimotor strip, and hot compression treatment could significantly ameliorate the sciatic nerve pain by attenuating highly sensitive sensorimotor strips from local pathologic nerves (**Figure 7**).

DISCUSSION

Sciatic nerve pain is caused by a herniated disc and compression of the nerve root, leading to abnormal spontaneous and induced pain. Currently, the most conservative treatments for sciatica include rehabilitation, massage, hot compresses, and corsets (Kim et al., 2015). However, there is limited evidence to support the efficacy of specific modalities and the nerve transmission mechanisms involved in hot compression. In this study, we aimed to explore the effect of hot compression on neuropathic pain and its underlying mechanisms.

The exposure conditions are critical in hot compress treatments. Previous studies have reported that a heat exposure of >42°Cleads to nerve hyper-sensitivity through the release of CGRP in rat sciatic nerve axons in an *in vitro* model (Sauer et al., 2001; Ren et al., 2018). In addition, the axonal

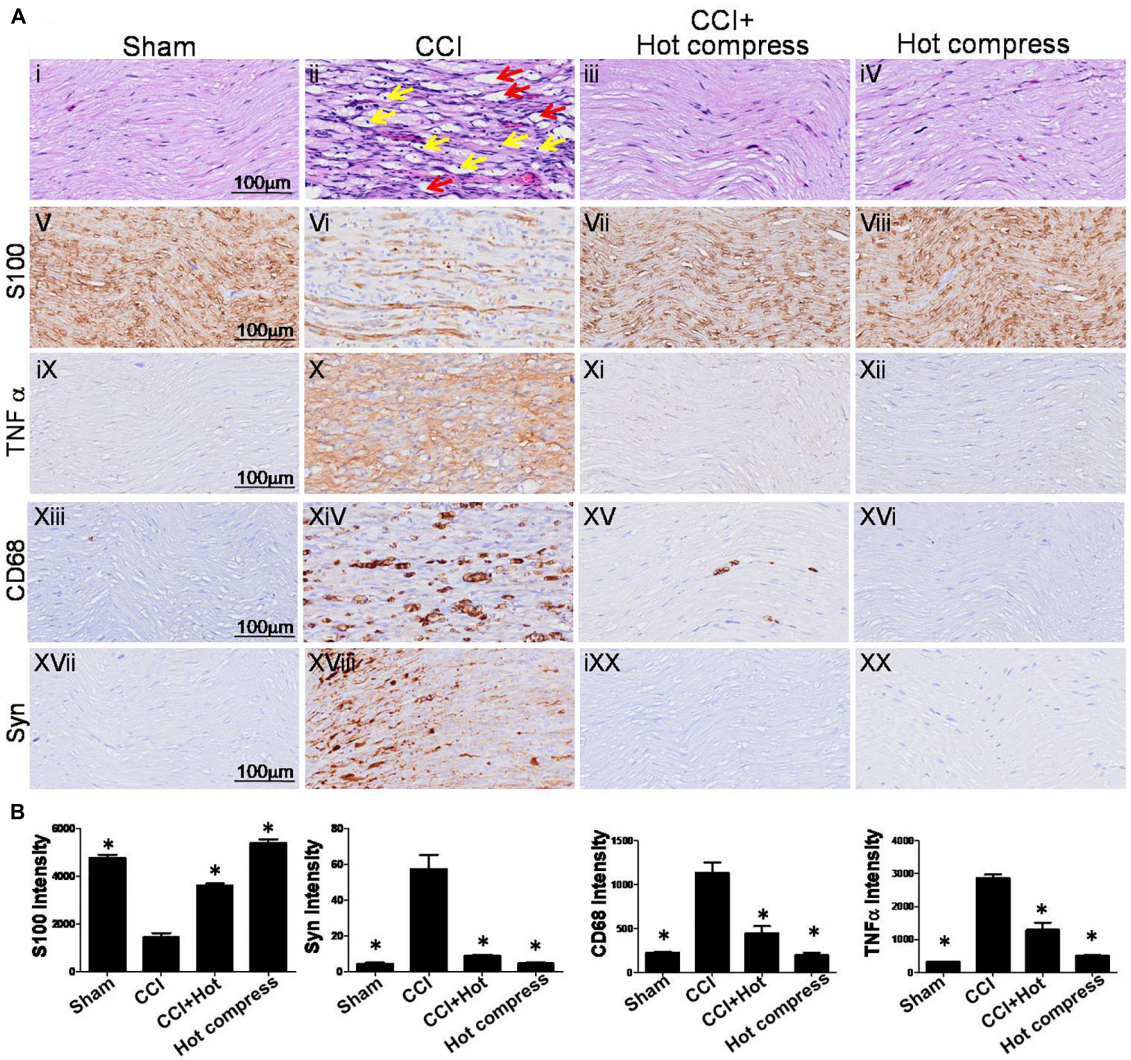

FIGURE 5 | Histological examinations of rat sciatic nerve on the 28th day. **(A)** Through (i–iv) H&E staining and (v–xx) immuno-histopathological (IHC) staining over the distal end of the nerve in the different groups. Tissue sections from peripheral nervous were stained by IHC with anti-S100 antibody, which indicate location of Schwann cells and anti-CD68 antibody indicate microglia. (i) The sham group showed an organized cellular pattern without edema and infiltration. (ii) The CCI group showed worse cellular changes, the red arrow indicated cellular spaces, and the yellow arrow indicated inflammatory cell infiltration, (iii) the CCI + hot compress group showed minimal infiltration and cellular edema, (iv) the hot compress alone group not pathological effects. (v–viii) S100 and (xvii–xx) Syn immunoreactivity is seen for nerve injury markers in different groups and nerve pathology was confirmed. For (ix–xii) TNFα and (xiii–xvi) CD68, immunoreactivity is also seen localizing to the nerve inflammation dysphonic site. **(B)** A quantitative analysis of expression level of S100, Syn, TNFα, and CD68 in the different groups. Data were analyzed by one-way ANOVA with *post hoc* Dunnett's test. *$p < 0.001$ was considered significant as compared with the CCI group, $n = 8$. Bar, 100 μm.

thermal responsiveness, when sensitized, also contributes to neuropathic pain following nerve injury or inflammation. Our data support that local hot compress (40–42°C) of the affected area 7 days after surgery in the CCI animal model can effectively reduce the inflammation and restore nerve sensitivity. In fact, some studies utilizing CCI models have found that the initial skin temperature of the affected limb initially increased in the course of 3–5 days, and finally decreased after 28–30 days (Wakisaka et al., 1991; Kim et al., 2012). Such findings have been attributed to autonomic mediation, such as denervation-induced supersensitivity to catecholamines and concomitant reduction of sympathetic vasoconstrictor outflow. Therefore, our study reported that moderate hot compression starting a week after the injury can effectively attenuate the infiltration of inflammatory factors in the affected area, which implies that periodic and continuous hot compression promotes vasoconstriction, and blood circulation contributes to nerve acceleration to the recovery phase. Furthermore, a recent study reported that a physical squeezing-induced nerve injury model produced large changes in the CMAP amplitude prior to large changes in the conduction velocity (Stecker et al., 2008; Fidancı and Öztürk, 2021). Therefore, we used CMAP electrophysiological testing to evaluate the therapeutic effects of hot compress treatment in the CCI model. This result shows that the CCI model reduced the

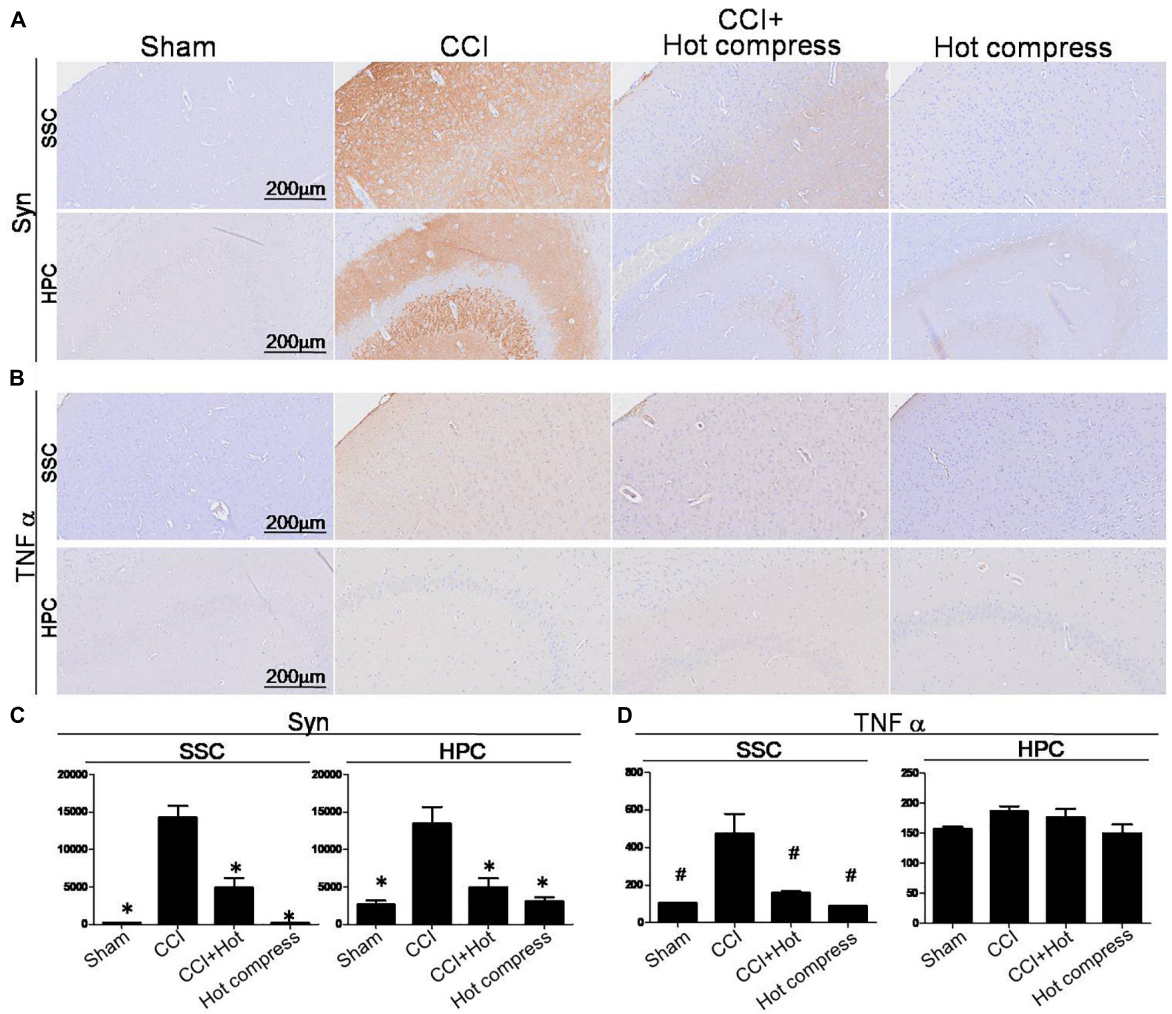

FIGURE 6 | Histological examinations of Syn and TNFα expression over the SSC and HPC regions in the brain on the 28th day. IHC staining for **(A)** Syn and **(B)** TNF-α, **(A)** quantitative analysis of the expression level of Syn in the brain SSC (left) and HPC (right), and **(D)** quantitative analysis of the expression level of TNFα over the SSC (left) and HPC (right). Somatosensory cortex, SSC; hippocampus (CA3), HPC. Data were analyzed by one-way ANOVA with *post hoc* Dunnett's test. $^{*}p < 0.001$, $^{\#}p < 0.05$ was considered significant as compared with the CCI group, $n = 8$. Bar, 100 μm.

CMAP amplitude and latency of time, while the hot compress treatment group effectively reversed the CMAP amplitude and latency of time.

Peripheral nerve pain is caused by the emergence and persistence of spontaneous activity of primary afferent neurons, which promotes the secondary and persistent increase in the excitability of the sensory circuit of the spinal dorsal horn, including sciatic nerve pain. In addition, especially long-term pain, the synthesis of more presynaptic vesicle protein release Syn in the nerve damage area will increase, which is related to the primary afferent C fibers (several of which are nociceptors) and the superficial spinal cord dorsal (Crair and Malenka, 1995; Sandkühler and Liu, 1998). The excitatory synaptic transmission between angular neurons is involved, and is a key factor for the long-term enhancement of synapses at thalamocortical synapses (Chou et al., 2002; Chen et al., 2009). In our study, we found that the hot compress treatment group can effectively reduce the expression of Syn in the nerve compression area or in the cerebral cortex area, which implies that hot compression attenuated sciatic nerve pain through reduced Syn. Furthermore, the expression of S100 proteins is observed to occur mostly in the Schwann cells in the peripheral nervous system. S-100 is one of the most useful markers for definitively characterizing nerve damage. Our results showed that hot compression can effectively restore the nerve cells at the location of the nerve injury, including increasing the expression of S100; thus, we cannot exclude the possibility that it can restore the injured nerve microenvironment under moderate hot compress treatment conditions, including microglia cells and Schwann cells.

Proinflammatory cytokines, including TNFα and IL-1β induce pain, and their inhibitors that relieve pain have been extensively researched (Schäfers and Sommer, 2007). The development of hyperalgesia despite the loosely placed ligature around the sciatic nerve in the CCI model without actual mechanical

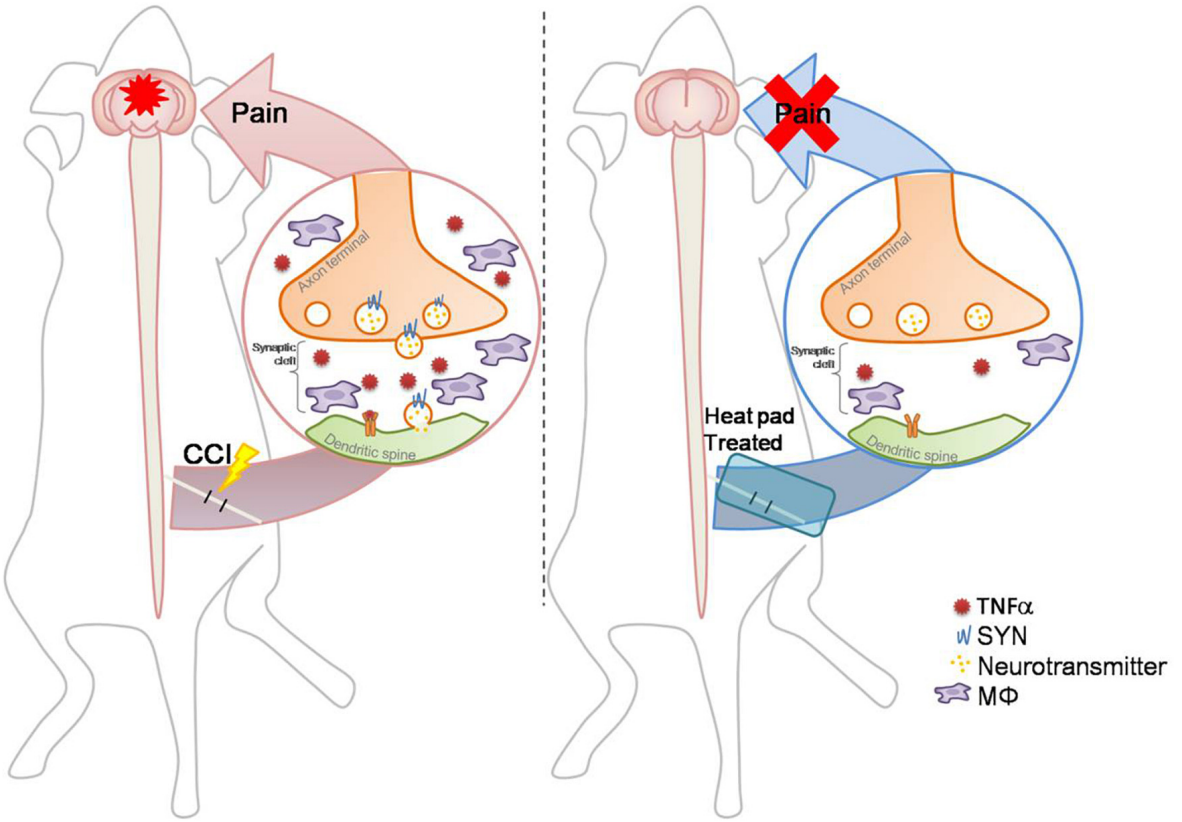

FIGURE 7 | Schematic diagram: a conditional hot compress regulates the crosstalk between the inflammatory factors and synaptic transmission signals. The CCI-induced nerve injury increases TNFα and Syn levels and increases immune cell infiltration. The hot compress inhibits inflammatory factors and Syn to attenuate mechanical allodynia and abnormal electrophysiological responses, and exerts an effective analgesic effect on CCI-induced neuropathic pain through neuroendocrine cells to the brain mediation for inhibiting sciatic nerve pain.

damage indicates that the development of neuropathic pain is mainly associated with inflammation and the released mediators, rather than nerve injury. Additionally, peripheral nerve injury also leads to the activation of peripheral (Schwann cells) and central (microglia and astrocyte) glial cells and begins to secrete proinflammatory cytokines, including TNFα, IL-1β, and PGE2 (Zelenka et al., 2005). These positive feedback loops between inflammatory mediators and glial activation and between glia and neurons lead to the further enhancement and maintenance of neuropathic pain (Ignatowski et al., 1999). In our current study, we demonstrated that moderate hot compresses can dramatically reduce inflammatory factors, both in the location of the nerve injury and the brain. Moreover, the pain relief effect of hot compresses may be enhanced by increasing the blood circulation and reducing the inflammatory factors. However, we also found that the macrophage marker protein CD68 is also significantly reduced, which implies that the hot compress treatment may also partially regulate switching of the M1/M2 phenotype of macrophages and act as a trigger or accelerator of auxiliary tissue repair (Nakagawa et al., 2018), which is a topic worthy of further elucidation. Endogenous tissue repair and regeneration in the nerve injury that critical step is to managing inflammatory response (Franco and Fernández-Suárez, 2015; Wynn and Vannella, 2016; Li et al., 2018). In the brain, the somatosensory cortex and hippocampus are responsible for the registration of physical pain (Yang and Chang, 2019). In particular, neurogenesis contributes to learning and memory and may trigger the development of chronic pain (Apkarian et al., 2016). Some studies have reported that the levels of biologically active TNFα are increased in the locus coeruleus and hippocampus at day 8 arrival maximum and following recovery to normal, which corresponds to the development of hyperalgesia in the CCI model (Covey et al., 2000). This is consistent with the results of our study. However, the CCI model showed higher TNFα expression in the somatosensory cortex than the sham group, while the hot compress treatment relieved TNFα expression in the CCI model. These results imply that the hot compress treatment on the affected area not only reduces inflammation in the affected area, but also effectively reduces the inflammatory factors secreted to the brain. Taken together, we recognized that moderate hot compresses may effectively improve sciatic nerve pain and inhibit inflammation caused by Syn and immune cell infiltration. Moreover, the scope of hot compress treatment is not only regulated by the affected area; however, it is also closely related to the plasticity of the brain through nerve conduction.

CONCLUSION

In summary, we demonstrate the potential efficacy and safety of hot compresses in the treatment of sciatic nerve pain, and confirmed that hot compresses may significantly improve sciatic nerve pain by reducing Syn and inflammatory factors from local pathological nerves to the brain. This target regulatory molecular pathway may enhance our understanding of the mechanisms related to hot compress therapy, which may help to use hot compress therapy in a wider range of neuropain diseases and have important significance in assisting different neuropathic therapies.

DATA AVAILABILITY STATEMENT

The original contributions presented in the study are included in the article/supplementary material, further inquiries can be directed to the corresponding author.

ETHICS STATEMENT

The animal study was reviewed and approved by the Chang Bing Show Chwan Memorial Hospital.

AUTHOR CONTRIBUTIONS

K-YC, W-CT, C-YC, and D-WL conceived and designed the experiments. C-JL and C-YH supported CMAP technical assistance. Y-CT, C-YT, and Z-PH performed most of the experiments and analyzed the data. K-YC, M-LS, and D-WL made intellectual contributions and contributed to the writing and revision of the manuscript. All authors agreed to be accountable for all aspects of the work, ensuring integrity and accuracy.

FUNDING

This work was supported by research grants from Chang Bing Show Chwan Memorial Hospital (BRD-109037 and BRD-108023) and part of the Ministry of Science and Technology, Taiwan, R.O.C. (MOST 110-2314-B-758-001).

ACKNOWLEDGMENTS

We thank the core facility at the animal center of Chang Bing Show Chwan Memorial Hospital, Changhua, Taiwan.

REFERENCES

Apkarian, A. V., Mutso, A. A., Centeno, M. V., Kan, L., Wu, M., Levinstein, M., et al. (2016). Role of adult hippocampal neurogenesis in persistent pain. *Pain* 157, 418–428. doi: 10.1097/j.pain.0000000000000332

Bain, J. R., Mackinnon, S. E., and Hunter, D. A. (1989). Functional evaluation of complete sciatic, peroneal, and posterior tibial nerve lesions in the rat. *Plast. Reconstr. Surg.* 83, 129–138. doi: 10.1097/00006534-198901000-00024

Bennett, G. J., and Xie, Y. K. (1988). A peripheral mononeuropathy in rat that produces disorders of pain sensation like those seen in man. *Pain* 33, 87–107. doi: 10.1016/0304-3959(88)90209-6

Chen, Y., Balasubramanyan, S., Lai, A. Y., Todd, K. G., and Smith, P. A. (2009). Effects of sciatic nerve axotomy on excitatory synaptic transmission in rat substantia gelatinosa. *J. Neurophysiol.* 102, 3203–3215. doi: 10.1152/jn.00296.2009

Chiang, C. Y., Sheu, M. L., Cheng, F. C., Chen, C. J., Su, H. L., Sheehan, J., et al. (2014). Comprehensive analysis of neurobehavior associated with histomorphological alterations in a chronic constrictive nerve injury model through use of the CatWalk XT system. *J. Neurosurg.* 120, 250–262. doi: 10.3171/2013.9.jns13353

Chou, A. K., Muhammad, R., Huang, S. M., Chen, J. T., Wu, C. L., Lin, C. R., et al. (2002). Altered synaptophysin expression in the rat spinal cord after chronic constriction injury of sciatic nerve. *Neurosci. Lett.* 333, 155–158. doi: 10.1016/s0304-3940(02)00575-x

Chou, R., and Huffman, L. H. (2007). Medications for acute and chronic low back pain: a review of the evidence for an American Pain Society/American College of Physicians clinical practice guideline. *Ann. Intern. Med.* 147, 505–514. doi: 10.7326/0003-4819-147-7-200710020-00008

Covey, W. C., Ignatowski, T. A., Knight, P. R., and Spengler, R. N. (2000). Brain-derived TNFalpha: involvement in neuroplastic changes implicated in the conscious perception of persistent pain. *Brain Res.* 859, 113–122. doi: 10.1016/s0006-8993(00)01965-x

Crair, M. C., and Malenka, R. C. (1995). A critical period for long-term potentiation at thalamocortical synapses. *Nature* 375, 325–328. doi: 10.1038/375325a0

Dahm, K. T., Brurberg, K. G., Jamtvedt, G., and Hagen, K. B. (2010). Advice to rest in bed versus advice to stay active for acute low-back pain and sciatica. *Cochrane Database Syst. Rev.* CD007612. doi: 10.1002/14651858.CD007612.pub2

Dehghan, M., and Farahbod, F. (2014). The efficacy of thermotherapy and cryotherapy on pain relief in patients with acute low back pain, a clinical trial study. *J. Clin. Diagn. Res.* 8, LC01–LC4. doi: 10.7860/jcdr/2014/7404.4818

Deuis, J. R., Dvorakova, L. S., and Vetter, I. (2017). Methods used to evaluate pain behaviors in rodents. *Front. Mol. Neurosci.* 10:284. doi: 10.3389/fnmol.2017.00284

Dixon, W. J. (1980). Efficient analysis of experimental observations. *Annu. Rev. Pharmacol. Toxicol.* 20, 441–462. doi: 10.1146/annurev.pa.20.040180.002301

Fidancı, H., and Öztürk, Ý (2021). The relationship between nerve conduction studies and neuropathic pain in sciatic nerve injury due to intramuscular injection. *Korean J. Pain* 34, 124–131. doi: 10.3344/kjp.2021.34.1.124

Franco, R., and Fernández-Suárez, D. (2015). Alternatively activated microglia and macrophages in the central nervous system. *Prog. Neurobiol.* 131, 65–86. doi: 10.1016/j.pneurobio.2015.05.003

Harris, W. (1938). Sciatica and its treatment. *Br. Med. J.* 2, 1245–1247. doi: 10.1136/bmj.2.4067.1245

Ignatowski, T. A., Covey, W. C., Knight, P. R., Severin, C. M., Nickola, T. J., and Spengler, R. N. (1999). Brain-derived TNFalpha mediates neuropathic pain. *Brain Res.* 841, 70–77. doi: 10.1016/s0006-8993(99)01782-5

Jacobs, W. C., van Tulder, M., Arts, M., Rubinstein, S. M., van Middelkoop, M., Ostelo, R., et al. (2011). Surgery versus conservative management of sciatica due to a lumbar herniated disc: a systematic review. *Eur. Spine J.* 20, 513–522. doi: 10.1007/s00586-010-1603-7

Jensen, R. K., Kongsted, A., Kjaer, P., and Koes, B. (2019). Diagnosis and treatment of sciatica. *BMJ* 367:l6273. doi: 10.1136/bmj.l6273

Jo, J., and Lee, S. H. (2018). Heat therapy for primary dysmenorrhea: a systematic review and meta-analysis of its effects on pain relief and quality of life. *Sci. Rep.* 8:16252. doi: 10.1038/s41598-018-34303-z

Kim, E. J., Choi, Y. D., Lim, C. Y., Kim, K. H., and Lee, S. D. (2015). Effect of heating and cooling combination therapy on patients with chronic low back pain: study protocol for a randomized controlled trial. *Trials* 16:285. doi: 10.1186/s13063-015-0800-4

Kim, M. S., Seo, D. H., Lim, M. H., Kim, T. U., Lee, S. J., and Hyun, J. K. (2012). Skin temperature changes following sciatic nerve injury in rats. *J. Neurotrauma* 29, 2738–2747. doi: 10.1089/neu.2012.2414

Lewis, R. A., Williams, N. H., Sutton, A. J., Burton, K., Din, N. U., Matar, H. E., et al. (2015). Comparative clinical effectiveness of management strategies for sciatica: systematic review and network meta-analyses. *Spine J.* 15, 1461–1477. doi: 10.1016/j.spinee.2013.08.049

Li, J., Tan, J., Martino, M. M., and Lui, K. O. (2018). Regulatory T-cells: potential regulator of tissue repair and regeneration. *Front. Immunol.* 9:585. doi: 10.3389/fimmu.2018.00585

Liu, S. C., Sheu, M. L., Tsai, Y. C., Lin, Y. C., Chang, C. W., and Lai, D. W. (2021). Attenuation of *in vitro* and *in vivo* melanin synthesis using a Chinese herbal medicine through the inhibition of tyrosinase activity. *Phytomedicine* 95:153876. doi: 10.1016/j.phymed.2021.153876

Machado, G. C., Maher, C. G., Ferreira, P. H., Day, R. O., Pinheiro, M. B., and Ferreira, M. L. (2017). Non-steroidal anti-inflammatory drugs for spinal pain: a systematic review and meta-analysis. *Ann. Rheum Dis.* 76, 1269–1278. doi: 10.1136/annrheumdis-2016-210597

Nakagawa, T., Hiraga, S. I., Mizumura, K., Hori, K., Ozaki, N., and Koeda, T. (2018). Topical thermal therapy with hot packs suppresses physical inactivity-induced mechanical hyperalgesia and up-regulation of NGF. *J. Physiol. Sci.* 68, 629–637. doi: 10.1007/s12576-017-0574-4

Petrofsky, J., Berk, L., Bains, G. I., Khowailed, A., Hui, T., Granado, M., et al. (2013). Moist heat or dry heat for delayed onset muscle soreness. *J. Clin. Med. Res.* 5, 416–425. doi: 10.4021/jocmr1521w

Pinto, R. Z., Maher, C. G., Ferreira, M. L., Ferreira, P. H., Hancock, M., Oliveira, V. C., et al. (2012). Drugs for relief of pain in patients with sciatica: systematic review and meta-analysis. *BMJ* 344:e497. doi: 10.1136/bmj.e497

Ren, H., Jin, H., Jia, Z., Ji, N., and Luo, F. (2018). Pulsed radiofrequency applied to the sciatic nerve improves neuropathic pain by down-regulating the expression of calcitonin gene-related peptide in the dorsal root ganglion. *Int. J. Med. Sci.* 15, 153–160. doi: 10.7150/ijms.20501

Ropper, A. H., and Zafonte, R. D. (2015). Sciatica. *N. Engl. J. Med.* 372, 1240–1248. doi: 10.1056/NEJMra1410151

Sandkühler, J., and Liu, X. (1998). Induction of long-term potentiation at spinal synapses by noxious stimulation or nerve injury. *Eur. J. Neurosci.* 10, 2476–2480. doi: 10.1046/j.1460-9568.1998.00278.x

Sauer, S. K., Reeh, P. W., and Bove, G. M. (2001). Noxious heat-induced CGRP release from rat sciatic nerve axons *in vitro*. *Eur. J. Neurosci.* 14, 1203–1208. doi: 10.1046/j.0953-816x.2001.01741.x

Savage, N. J., Fritz, J. M., Kircher, J. C., and Thackeray, A. (2015). The prognostic value of electrodiagnostic testing in patients with sciatica receiving physical therapy. *Eur. Spine J.* 24, 434–443. doi: 10.1007/s00586-014-3469-6

Schäfers, M., and Sommer, C. (2007). Anticytokine therapy in neuropathic pain management. *Expert Rev. Neurother.* 7, 1613–1627. doi: 10.1586/14737175.7.11.1613

Sheu, M. L., Shen, C. C., Tsou, H. K., Yang, M. Y., Su, H. L., Sheehan, J., et al. (2021). Dual regeneration of muscle and nerve by intramuscular infusion of mitochondria in a nerve crush injury model. *Neurosurgery* 89, E49–E59. doi: 10.1093/neuros/nyab105

Sommer, C., and Kress, M. (2004). Recent findings on how proinflammatory cytokines cause pain: peripheral mechanisms in inflammatory and neuropathic hyperalgesia. *Neurosci. Lett.* 361, 184–187. doi: 10.1016/j.neulet.2003.12.007

Stecker, M. M., Baylor, K., and Chan, Y. M. (2008). Acute nerve compression and the compound muscle action potential. *J. Brachial Plex. Peripher. Nerve Inj.* 3:1. doi: 10.1186/1749-7221-3-1

Valat, J. P., Genevay, S., Marty, M., Rozenberg, S., and Koes, B. (2010). Sciatica. *Best Pract. Res. Clin. Rheumatol.* 24, 241–252. doi: 10.1016/j.berh.2009.11.005

Vroomen, P. C., de Krom, M. C., Slofstra, P. D., and Knottnerus, J. A. (2000). Conservative treatment of sciatica: a systematic review. *J. Spinal Disord.* 13, 463–469. doi: 10.1097/00002517-200012000-00001

Wakisaka, S., Kajander, K. C., and Bennett, G. J. (1991). Abnormal skin temperature and abnormal sympathetic vasomotor innervation in an experimental painful peripheral neuropathy. *Pain* 46, 299–313. doi: 10.1016/0304-3959(91)90113-c

Witenko, C., Moorman-Li, R., Motycka, C., Duane, K., Hincapie-Castillo, J., Leonard, P., et al. (2014). Considerations for the appropriate use of skeletal muscle relaxants for the management of acute low back pain. *P T* 39, 427–435.

Wynn, T. A., and Vannella, K. M. (2016). Macrophages in tissue repair, regeneration, and fibrosis. *Immunity* 44, 450–462. doi: 10.1016/j.immuni.2016.02.015

Yang, S., and Chang, M. C. (2019). Chronic pain: structural and functional changes in brain structures and associated negative affective states. *Int. J. Mol. Sci.* 20:3130. doi: 10.3390/ijms20133130

Zelenka, M., Schäfers, M., and Sommer, C. (2005). Intraneural injection of interleukin-1beta and tumor necrosis factor-alpha into rat sciatic nerve at physiological doses induces signs of neuropathic pain. *Pain* 116, 257–263. doi: 10.1016/j.pain.2005.04.018

Conflict of Interest: The authors declare that the research was conducted in the absence of any commercial or financial relationships that could be construed as a potential conflict of interest.

Publisher's Note: All claims expressed in this article are solely those of the authors and do not necessarily represent those of their affiliated organizations, or those of the publisher, the editors and the reviewers. Any product that may be evaluated in this article, or claim that may be made by its manufacturer, is not guaranteed or endorsed by the publisher.

Frontiers in
Synaptic Neuroscience

Synthesizing knowledge on various aspects of synapses

Part of a popular neuroscience journal series which advances our understanding of the synaptic structure, function, plasticity and alterations in disease.

Discover the latest Research Topics

See more →

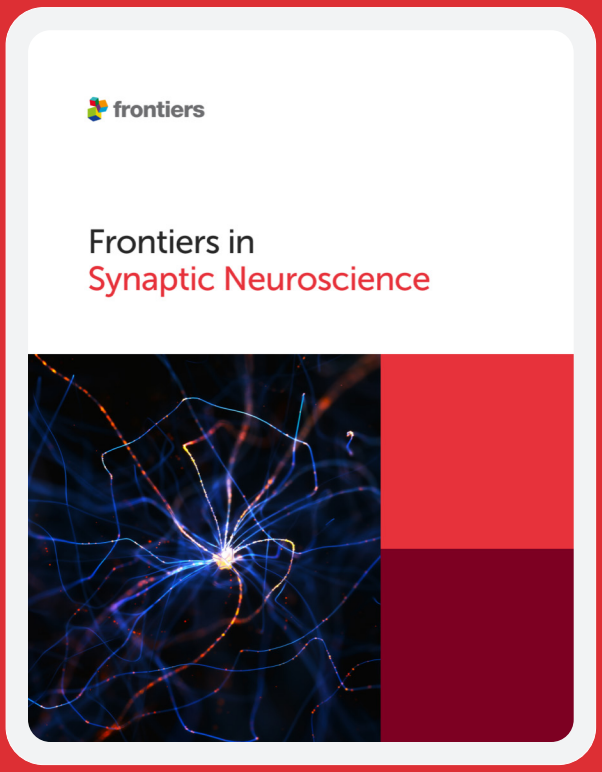

Frontiers

Avenue du Tribunal-Fédéral 34
1005 Lausanne, Switzerland
frontiersin.org

Contact us

+41 (0)21 510 17 00
frontiersin.org/about/contact